Ollscoil na hÉireann, Corcaigh

National University of Ireland, Cork

Novel Surface Enhanced Raman Spectroscopy (SERS) Sensors

Thesis presented by

Yuqing Yang

for the degree of

Doctor of Philosophy

University College Cork

Tyndall National Institute

Head of School/Department: Dr Fatima Gunning

Supervisor(s): Dr Pierre Lovera and Dr Alan O'Riordan

2022

Abstract.

Surface Enhanced Raman Spectroscopy (SERS)-based sensors and devices offer rapid, cost-effective, highly selective, and sensitive detection of various chemicals in water. This thesis explores the SERS principle, substrate fabrication methods, functionalization techniques, and their applications. It also addresses the limitations of SERS sensing devices, including cross-contamination during application and challenges in fabrication reproducibility.

The fabricated sensors were based on Ag-Gum Arabic nanostructures for the detection of 2,4-D in Chapter 2, Ag-Corn Starch nanostructures for MCPA in Chapter 3, and Ag NPs/ss-DNA in Chapter 3. The nanoparticles were synthesized using an electrochemical deposition method, which enables tailoring of the nanoparticle structure by adjusting parameters such as deposition time, precursor concentrations, and applied voltage. This method is straightforward and repeatable, making the sensor fabrication process highly reproducible.

In Chapters 2 and 3, no significant changes in Raman signal intensities were observed as the analyte concentrations increased, contrary to what would typically be expected with SERS effects. Instead, a slight increase in the ratio between two peaks of the Raman spectra was noted. This may be attributed to a local increase in pesticide concentration caused by the polysaccharide polymer layers of Gum Arabic and Corn Starch. Although changes in the ratio between two peaks were detectable as the concentration increased, quantification was not feasible due to the low slope obtained and the inadequacy of the experimental procedure, which involved oversampling. Additionally, the recorded spectra for the two pesticides were very similar, rendering selectivity unachievable.

For the E. coli O157 ss-DNA SERS sensor, neither Gum Arabic nor Corn Starch was used. Instead, a two-thiol functionalization method was employed for the development of the Ag nanoparticle SERS ss-DNA sensor. This ss-DNA SERS sensor demonstrated good linearity, selectivity, and relatively fast detection compared to other sensors or methods used for ss-DNA detection.

Declaration.

This is to certify that the work I am submitting is my own and has not been submitted for another degree, either at University College Cork or elsewhere. All external references and sources are clearly acknowledged and identified within the contents. I have read and understood the regulations of University College Cork concerning plagiarism and intellectual property.

Yuqing Yang

May 2022

Abbreviations and Acronyms.

2,4-D	2,4-Dichlorophenoxyacetic acid
CS	corn starch
EF	enhancement factor
GA	gum arabic
MCPA	2-methyl-4-chlorophenoxyacetic acid
MB	methylene blue
NP	nanoparticles
STEC	shiga toxin-producing escherichia coli
SERS	surface enhanced raman spectroscopy

Acknowledgement.

Thank my supervisors, Pierre Lovera and Alan O'Riordan for hiring me to carry out Ph.D. research work in a flexible environment and in a multi-discipline project, AQUASENSE Marie-Curie ITN project. Tyndall National Institute, where I worked, offered me a research platform with freedom and kindness, where there are many excellent people and many smiles. It is also a precious experience to share with all my project partners in the AQUASENSE project. Thank you for the perfect project meeting arrangement through which we were able to communicate our research progress and difficulties.

Chapter 1. Surface Enhanced Raman Spectroscopy: applications in agriculture and food safety

The sections detailing Surface Enhanced Raman Scattering has been published in *Photonics* 2021, *8*(12), 568; https://doi.org/10.3390/photonics8120568;

The section regarding electrochemical deposition for SERS substrate fabrication is in Sensing Technologies for Real Time Monitoring of Water Quality, Chapter 4, Willy.

Contribution: Conceptualization, Y.Y. and N.C.; data curation, Y.Y. and N.C.; writing-original draft preparation, Y.Y. and N.C.; writing-review and editing, A.O. and P.L.; visualization, Y.Y. and N.C.; supervision, A.O. and P.L.; project administration, A.O. and P.L.; funding acquisition, A.O. and P.L. All authors have read and agreed to the published version of the manuscript.

Abstract: Recent global warming has resulted in shifting of weather patterns and led to intensification of natural disasters and upsurges in pests and diseases. As a result, global food systems are under pressure and need adjustments to meet the change-often by using pesticides. Unfortunately, such pesticides are harmful for human and the environment, and as a result, need to be controlled. Traditional detection methods currently used are time consuming in terms of sample preparation, are high cost, and instrumentation is typically not portable. Surface Enhanced Raman Scattering (SERS) technology has emerged as an attractive candidate for rapid, high sensitivity and high selectivity detection of contaminants relevant to the food industry and environmental monitoring. In this chapter, the principles of SERS as well as recent SERS substrate fabrication methods are first discussed. Following this, their development and applications for agrifood safety is reviewed, with focus on detection of dye molecules, melamine in food products, and the detection of different classes of pesticides such as organophosphate and neonicotinoids.

Keywords: Surface Enhanced Raman Scattering (SERS), fabrication, application, agriculture, food safety.

1, Introduction.

Climate change is manifesting itself with increased temperatures more favorable to the spread of pests and diseases. This has resulted in more challenging food production, as well as higher number of foodborne disease outbreaks. To try to protect yield and ensure food safety, farmers have little choice other than treating their crop with a range of pesticides.[1] Unfortunately, there are more and more reports showing that these phytosanitary products are harmful to human, but also lead to the loss of biodiversity, accumulation in soil and have deleterious effects on indigenous microbiome.[2] As a

result, it is necessary to monitor biological and chemical contamination in food systems throughout the whole food chain.

Traditional detection of pesticides in food and agriculture systems are mainly based on methods such as chromatography techniques coupled with mass spectrometry.[3] These methods are time consuming and high cost. Therefore, implementation of new portable technologies is needed to provide pesticide usage monitoring and enforcing of regulation.

In this regard, Surface Enhanced Raman Spectroscopy (SERS) has attracted a lot of attention as it has the potential to address most of these requirements. The advantages of SERS include ultrasensitive detection, fast turnover, in-situ sampling, low cost, and the suitability for large-scale screening. Sensors based on SERS have been shown to provide real time data on soil nutrients in research level[4-5], monitor water run-off and contaminants in water supplies [6], and also detect pesticide residues in food [7-8]. The technique has also found applications in a wide range of sectors including: material, forensic, biological, food safety and electrochemical fields,[9-13,14-19] with the most common chemical contaminants being within environmental and food sectors, such as pesticides, adulterants, antibiotics and illegal drugs and illegal food dyes. The drawback of SERS technology, disadvantages of different SERS substrate fabrication methods, SERS substrate functionalization limitation will be discussed in the end of each section.

In this chapter, we review the main SERS substrate fabrication methods and bring a special focus on applications for the detection of hazardous chemicals in both food and agriculture, together with its limitations.

2, Raman spectroscopy and Surface Enhanced Raman Scattering (SERS).

Raman spectroscopy was first discovered in 1928 by Sir Chandrasekhara Venkata Raman.[20] It was observed that when monochromatic light excited a molecule, the majority of light was elastically scattered - this is Rayleigh scattering where $E_{incident} = E_{scattered}$, but also a small fraction of photons was inelastically scattered - this corresponds to Raman scattering where $E_{incident} \neq E_{scattered}$. When $E_{scattered} < E_{incident}$, this effect is called a Stokes shift and when $E_{scattered} > E_{incident}$, it is an anti-Stoke shift. The energy difference between $E_{incident}$ and $E_{scattered}$ relates to the rotational and vibrational mode of the molecule. As a result, a Raman spectrum provides the fingerprint of this molecule. Figure 1.1 shows an energy diagram for the two types of scattering.[21] Each peak in a Raman spectrum corresponds to a different vibrational mode of the bonds of the molecule under investigation. The light sources used for Raman instrument are lasers ranging from near ultraviolet, visible, to near-infrared. [22-23] Different laser light sources will result in different Raman spectra for the same material.[24] Near-infrared excitation wavelength (>780nm) is better for fluorescence reduction in Raman spectroscopy.[25] Raman spectroscopy is important in analytical chemistry as it allows testing samples in water environment, where Infrared (IR) Spectroscopy is sensitive to water and is not suitable for water sample.[26] Raman technology bridges fundamental physics and chemistry as well. Raman spectroscopy is widely used to characterize the orientation, defects, number of layers, and doping of different materials, enabling standardization and quality control.[27] Raman spectroscopy peak features varies for powder/thin film/thick film/solution status for the same chemical.[28] Different Raman instruments from different lab could have different spectroscopy peak features.[29] However, Raman scattering efficiency is very low, with typically only 1 in 10^8 incident photons being Raman scattered.[30] This leads to low LOD/LOQ in analytical application, making Raman spectroscopy suitable only for crystal/powder/high concentration

solution.[31] For example, Raman spectroscopy can only detect TNT in soil with LOD 1.9 ± 0.4% by mass,[32] or detect amino acids at 3 g/100 ml in H_2O.[33] Fortunately, the efficiency of this scattering can be increased by using nanostructured plasmonic metals in a technique known as Surface Enhanced Raman Spectroscopy (SERS).

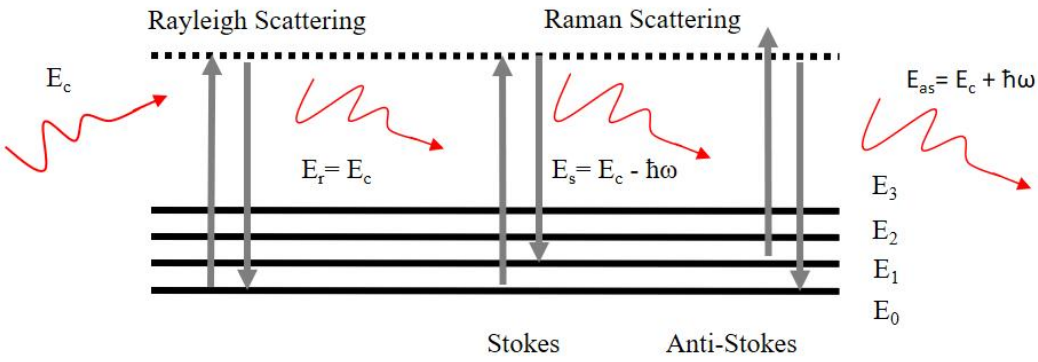

Figure 1.1: Schematics of energy levels of a molecule for Rayleigh and Raman Scattering. [34] Rayleigh scattering: $E_{incident} = E_{scattered}$, Raman scattering: $E_{incident} \neq E_{scattered}$. When $E_{scattered} < E_{incident,}$ it is called a Stokes shift and when $E_{scattered} > E_{incident,}$ it is an anti-Stoke shift.

SERS effects were first observed by Fleischman *et al.* in 1974, when acquiring Raman spectra of pyridine on electrochemically roughened silver. [35] In SERS, monochromatic laser light sources are used to excite plasmons in nanostructured metallic surfaces (Au, Ag, Cu, etc.). The SERS enhancement includes both electromagnetic enhancement and chemical enhancement. The first enhancement is based on an electromagnetic enhancement [36-37] due to localized surface plasmons, while the second originates from chemical resonant energy charge transfer. [35, 38-40] The enhancement factor (EF) typically reaches 10^6, which drastically improves the sensitivity of the plasmonic based device.

2.1. Localized Surface Plasmon Resonance (LSPR) - Electromagnetic Enhancement.

When monochromatic light excites a metallic nanostructure, the free electrons on its surface oscillate. This collective oscillation is known as Localized Surface Plasmon Resonance (LSPR). [41] The excited LSPR makes a molecule located at the proximity of the surface highly polarizable and forms a large electric field on the surface. This electric field induces dipole moments in a molecule on the surface of nanostructures, and sequentially produces Raman enhancement. These large, localised electromagnetic fields present around the nanostructures or in nano-gaps between closely-spaced nanostructures are known as "hot spots",[42] see Figure 1.2. The Raman signal of the molecule is enhanced if the wavelength of the incident light is in resonance with the plasmon mode of the nanostructure. LSPR enhancement depends on the size, shape, composition, orientation and local electric field of the nanostructure. This will be discussed in the next section.

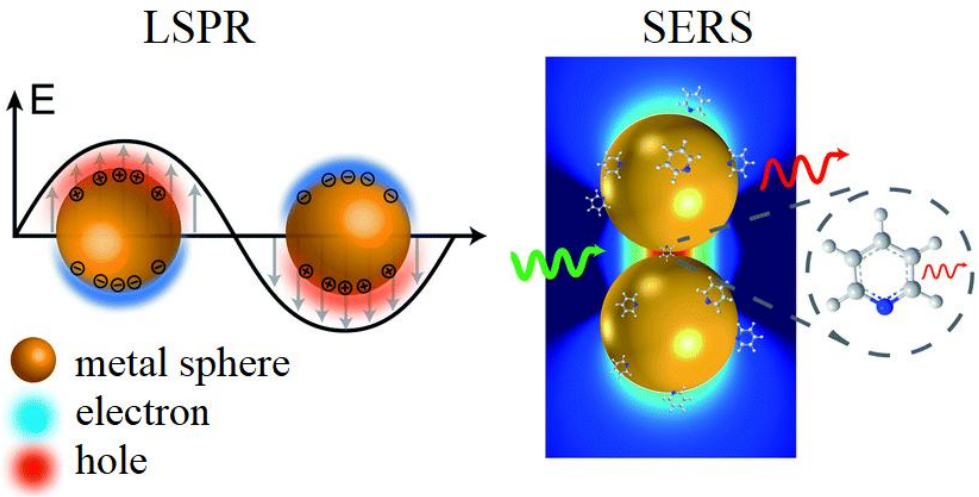

Figure 1.2 **:** Left: Localized Surface Plasmon Resonance (LSPR). Right: Plasmonic effects: Electric Field around two nanoparticles and the presence of a SERS "hotspot". (permission from the Royal Society of Chemistry.)[43]

2.2. Chemical enhancement.

The chemical mechanism of SERS do not rely on the EM environment (e.g. plasmon excitation).[44] The origins of the chemical enhancement is based on the change in polarisability of molecule adsorbed to a metal surface. Upon excitation by the incident monochromatic laser light, charge transfer occurs between the molecule and the metal.[45] In this process, some form the metal-molecule bond.[44] It is generally estimated that the chemical effect contributes to a factor of 10^2 of the total SERS enhancement.

A SERS spectrum will typically display different features compared to a normal Raman spectrum.[46] Usually, a normal Raman spectrum provides more peak information as a SERS spectrum has less and broader peaks.[43] As a result, SERS is less good for identification of analytes compared to normal Raman as it provides less peak information.

2.3. Enhancement Factor (EF).

The enhancement factor (EF) depends on molecular adsorption on plasmonic surface, as well as the morphology, roughness and homogeneity of this surface and the laser wavelength, etc. The calculation of the enhancement factor is $\mathrm{EF} = \frac{I_{SERS}}{N_{SERS}} \cdot \frac{N_{RS}}{I_{RS}}$,[47] where I_{SERS} is the SERS signal, I_{RS} is the normal Raman signal obtained under the same experimental conditions as the SERS signal, but without the SERS substrate, N_{SERS} is the number of molecules excited in SERS and N_{RS} is the number of molecules excited in classical Raman.

Experimental values of EFs are typically in the range of 10^4 to 10^6. However, electromagnetic "hotspots" are claimed to have provided massive enhancements of between 10^{11} to 10^{14} orders of magnitude of the SERS signal.[48] And it is key to a single

molecule detection, which may be achieved from selective excitation of single molecules.[49] By tuning the excitation laser wavelength, an optimized SERS signal can be achieved. This is called surface enhanced resonance Raman spectroscopy (SERRS),[50] where the excitation wavelength matches both the plasmon and the molecular electronic resonance.[47] For example, Litti et al. used gold nanostructures functionalized with SERRS labels and with antibodies to link the tumor cells, and in a further step, to identify tumor cells.[51] SERRS increased SERS signal intensity in this research as it has both localized surface plasmon resonance of the plasmonic nanostructures, and with the reporter molecules.

2.4. Limitations of SERS technology.

SERS is a non-destructive technique to identify chemicals with good sensitivity, and is not water sensitive, thus is attractive for bio application and application in food or environment industry. However, SERS technology itself has its own limitations. Firstly, SERS effects are limited by the availability of plasmonic materials. Traditional SERS effective materials are noble metal nano particles, e.g. silver nano particle, gold nano particles, or copper nano particles. Recently, new SERS materials have emerged such as Mxene,[52] or composite materials such as noble nano particles with graphene.[53] Secondly, the Raman instrument will affect the measurement results – this includes the choice of laser excitation wavelength and detectors. When the laser wavelength is tuned to the peak of the Plasmon resonance, this would lead to high enhancements and has been shown experimentally. For the detector, a long-pass or notch filter is used to absorb or reflect any Rayleigh scattering while allowing for transmission of the Raman signal.[54] Hence, it is hard to compare SERS performance for different devices across different

laboratories.[47] Finally, high-resolution handheld Raman instrument need more effort to be developed, and this block the way for minimized SERS device development.

3, Fabrication of SERS-active substrates.

The SERS substrate plays a crucial role as the electromagnetic enhancement is related to the material, size, shape of the nano particles, and the distance between the nano particles. Solís et al. used [55] state-of-the-art electromagnetic computation methods to produce predictive simulations for a variety of nanoparticle-based SERS substrates with different shapes. SERS substrates need nanostructured metallic surfaces with well-defined distances in the region of 10-100 nm between nano clusters.[56] By decreasing the distance between the nanostructures, while keeping the other parameters the same, the electric field becomes more localized and concentrated, and the corresponding SERS intensity signal increases accordingly. An example of this was discussed by Lee *et al*. where the distance between metallic clusters was decreased from 30 nm to 10 nm, and an intensity increase of over 200-fold was observed.[57] Particle size and morphology will also affect the final SERS intensity.[58] Peter *et al*. synthesized a group of gold nano particles with different sizes, and studied their SERS intensity towards MBA detection.

They found that the SERS intensity increased with the increase of the nano particles size from 20-100 nm. The SERS intensity of the adsorbed MBAs is detectable for particle sizes larger than 50 nm, and it increases with particle size, while the SERS signal is not detectable within the detection limit for particle sizes smaller than 50 nm. Njoki *et al*. studied the correlation between optical and spectroscopic properties of gold nanoparticles and their diameters (10-100 nm) in solution. They found that that the particle size was related to the surface Plasmon (SP) resonance band properties as well as the surface-enhanced Raman scattering (SERS) spectroscopic properties. The

wavelength of the SP bands λmax (519 to 569 nm) displays a gradual increase with gold particle size, this trend was fitted by a polynomial cubic curve. This correlation is also compared to the simulation results based on Mie theory, the experimental results agreed with theory studies.[58] There are two fundamentally different approaches to the development of SERS-active nanostructures with "hotspots": bottom-up assembly and top-down fabrication have been used.[59]

3.1. Bottom-up Assembly.

Bottom-up approaches refer to the fabrication of nanostructures by chemical synthesis[60-61], colloid aggregation[56, 62], electrochemical deposition[63-67], and self-assembly.[68-70] These methods have been used to fabricate a variety of nanostructures ranging from a few nanometers to a few hundred nanometers in size. Metal nanoparticles can be synthesised chemically at low cost with tailored geometries such as nanoparticles,[71-72] nanowires,[73-74], nanospheres,[71, 75-76] nanorods,[77-80] nanotubes,[81-82] nanotriangles,[83] nano flower[84], nano-urchins,[85] and nanoshells,[86-87] see Figure 1.3. Besides pure metallic nanoparticles, composite materials such as bimetallic or hybrid nanostructures[88], Graphene Oxide / Au nanostars, [89], SiO_2@TiO_2@Ag[90] etc. and other composite material based on molecular imprint (MIP) have also attracted research attention [84, 90-93] and have been reviewed recently.[94]

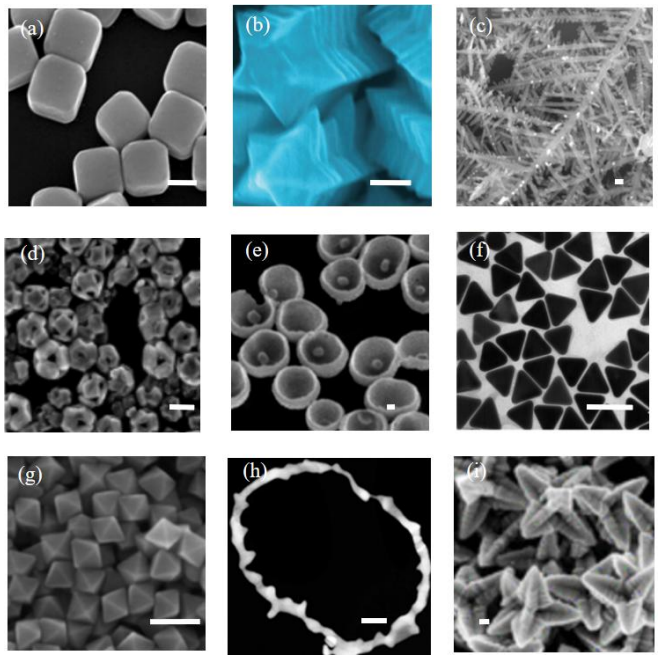

Figure 1.3: TEM/SEM images of (a) Ag/ Au nanocubes, [95] (b) GO/Au nanostars, [89] (c) Ag nanodendrides, [64] (d) Au nanocages, [96] (e) Au nanobowls with Au seed inside,[97] (f) gold nanotriangles, [98](g) Gold octahedrals, [99] (h) Au nano ring, [100] and (i) gold hollow stars [101]. Scale bar: 100 nm.

Metal NPs such as gold or silver are the most common materials used in SERS studies.[102-103] The most common fabrication of SERS substrates are gold (Au) and silver (Ag) colloids with diameters between 10 and 100 nm, as they yield the greatest enhancements at their "hot spots".

For example, they can be presented in a suspension or sol-gel in the presence of the analyte of interest.[104-106] The nanostructures, together with the analyte suspension, can then be drop-casted onto a substrate to generate enhanced Raman signal for the analytes. The disadvantage of this method is that the nanoparticle suspensions must be mixed with the analyte solution for SERS applications, which means it requires sample preparation.[107-108] However, this drawback was addressed by Yang *et al.*, who grew Ag nanoshells on thiol-modified silica NPs, and deposited them directly on apple skin for

analysis [109]. Although there is a greater enhancement observed with these substrates, it is hard to obtain a homogeneous surface to get uniform enhancement, as it is hard to control the size of the nano particles and the distance between them. Nano particles could appear abnormal aggregation, during Raman measurements, nano particles could move their positions as well. Additionally, they have limitations for field analysis due to their complex sample preparation steps and requirement for additional drying time. In contrast, solid based devices may be more suited for portable and remote sensing, i.e. NPs that are immobilised on a solid substrate.[110-113] For example, Fan *et al.* fabricated self-assembled Ag NPs onto glass slides by using 3-mercaptopropyltrimethoxysilane (3-MPTMS).[113] This transformation stabilizes the Ag NPs, avoids the usual aggregation process and produces reliable SERS active substrates. Yu *et al.* fabricated silver colloidal nanoparticles for SERS analysis and injected them to a filter membrane, thus entrapping them inside. The filter therefore was used as the solid portable substrate. It demonstrated 1-2 orders of magnitude better SERS enhancement than the typical approach.[114] In addition, Shiohara *et al.* fabricated gold nanostars and deposited them onto a polydimethylsiloxane (PDMS) platform for SERS evaluation. They used back side illumination for the detection of selected pesticide on fruit skin. The transparent substrate allows SERS detection through backside excitation and facilitating practical implementation.[115]

Other supports also add additional functionalities to SERS devices. Optical fiber-based SERS sensors have in this regard generated steady interest as a versatile means of extending SERS for portable field applications.[79] There is also a growing interest in the fabrication of flexible SERS substrates. These substrates are ultra-low cost, disposable, easy to use and highly suitable for on-site sensing applications. Polavarapu *et al.* fabricated SERS substrates by directly writing on paper using a pen filled with

plasmonic nanoparticle inks such as gold nanospheres, silver nanospheres and gold nanorods to detect thiabendazole.[116] These simple substrates were able to detect pesticide down to 20 ppb. This approach shows portable, cost effective fabrication of efficient SERS substrates at the point of care. The SERS ink cartridges fixed in a pen might be used in the real world application. Lee *et al.* also fabricated SERS paper substrates impregnated with gold nanorods by dip coating.[117] This SERS substrate can contact with 1,4-BDT directly and more efficient in sample collection comparing to rigid substrates as paper fibrous offer a 3D structure for easy catch and transport of targeted analytes to the electromagnetic hot spots in the paper. They demonstrated detection limit of analyte (140 pg spread over 4 cm2) by simply swabbing the surface. This highly efficient and cost-effective SERS substrate brings SERS-based device closer to real-world applications. Chen *et al.* combined adhesive tape and SERS activity of Au nanoparticles to fabricate a "SERS tape" substrate. The Au particles were deposited onto the sticky side of the tape that was used to extract pesticides from different kinds of fruit and vegetable peels.[118] This proof-of-concept SERS tape has been used for various pesticide residues such as thiram, parathion-methyl, and chlorpyrifos on complex surfaces including cucumber, green vegetable, apple and orange. However, the tape can easily lose its adhesion ability after the application of colloidal gold nanoparticles. These flexible sensors fabricated by different methods dramatically improve the portability, feasibility as well as sample collection efficiency of SERS detection for pollutants as a promising technique for both laboratory and field-based detection[119]. However, the availability of a handheld Raman instrument is a key factor for portable SERS devices. For the application in the real world, developed SERS sensors should have good selectivity to avoid cross contamination.

Overall, bottom up assemblies have shown very high enhancement but they often give inconsistent performance. This is mainly because of a lack of structural uniformity over the entire area of the substrate, which could result in poor reproducibility and inhomogeneity, as different size, shape, composition, orientation and local dielectric of the plasmonic structures have different enhancement factors as mentioned before. The arrangements of the aggregates on the nanostructured surface are also hard to control.

3.2. Top-down Synthesis.

Top-down approaches for nanofabrication are scalable and highly reproducible. Top-down approaches include lithography techniques (electron-beam (E-beam)[120-122] and nanoimprint lithography [123-124]), laser etching together with film deposition (sputtering, metal evaporation, atomic layer deposition),[125-126] templating (using anodic aluminium oxide [81], porous polymer (Polyester(PS),[127] masks or molds[73]), and inkjet printing.[128]

E-beam and nanoimprint lithography are fabrication methods used to create patterns with dimension down to 10 nm. In E-beam lithography, the photon resist is crosslinked after being exposed to an electron beam. The exposed resist can then be washed away, leaving only the unexposed resist on the substrate. A noble metal layer is then evaporated onto the whole substrate and the unexposed polymer is then removed together with its metal over-layer, leaving only the metal pattern on the substrate. SERS substrates with various geometries such as nanoparticle dimers have been fabricated using E-beam lithography, see Figure 1.4 (a-e).

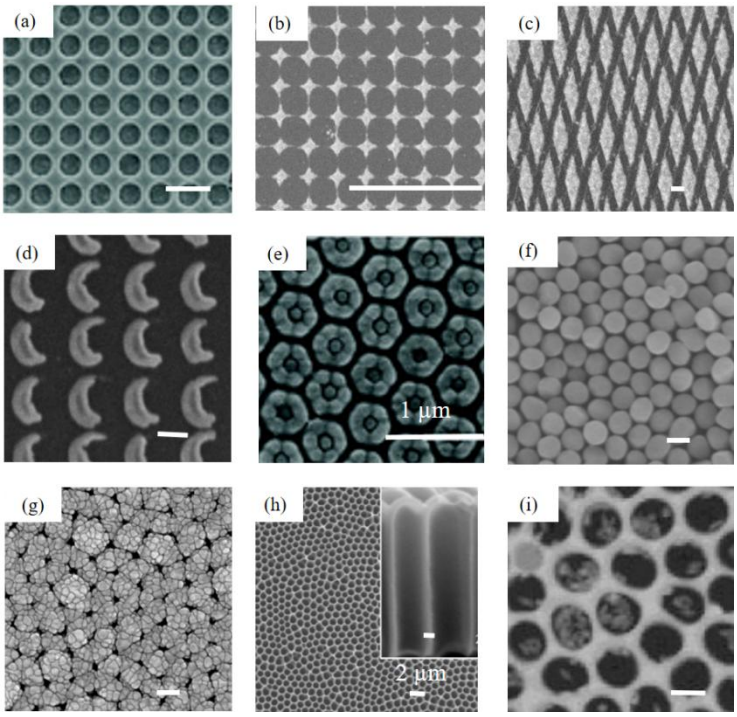

Figure 1.4: TEM or SEM images of top down approaches including E-beam fabricated (a) gold nanodisks,[121] (b) Au star-like arrays,[129] (c) Au diamond shaped structures,[129] (d) Ag nanocrescent structures,[130] (e) Ag nano-crown arrays;[131] AAO templated structures: (f) Ag-nanorods via metal deposition,[132] (g) Nano-flower like Ag/AAO, [133] (h) Au nano-island @ Ag-frustum arrays, [134] and (i) Au nanobipyramids self-assembled onto the AAO substrate.[135] Scale bars: 100 nm unless indicated otherwise.

Besides, Hu *et al*. fabricated polymer nanofinger structures on Si wafers using nanoimprint lithography, and coated the nanofingers with 70 nm of gold by E-beam evaporation, followed by exposure to solvent, inducing a leaning or self-closing of the nanowires, creating hot spots.[136] The fabricated arrays of electromagnetically coupled Ag nanoparticles on Si, could increase Raman efficiency by controlling the inter-particle separation between Ag nanoparticles. These substrates showed high SERS enhancement with good control and reproducibility. However, lithography based

methods, although extremely tuneable and scalable, suffer from high cost, slow throughput, and are time consuming.

Laser-induced fabrication of SERS substrates has attracted research attention as it is scalable and cost-effective.[122] See Figure 1.5. The fabrication of laser-induced SERS substrates always involves two steps. Firstly, fabrication of a nano/micro patterned substrate using ultra-fast laser pulses followed by physical vapor deposition (PVD) to deposite the metal layer on the nano/micro patterned substrates in order to get plasmonic structures. Yang *et al*. used a nanosecond pulsed laser (1064 nm, pulse duration (τ) (full width at half maximum, FWHM) 5 ns, pulse repetition rate (PRR) 100 kHz, spot size ~ 20 μm and laser ablation speed (ν) 100 mm/s.) ablation system to create micropatterns and generate different size nanoparticles.[137] The ablated Si surfaces were then deposited with Ag by electron beam evaporation. The enhancement factor of the fabricated substrates was estimated to be ~5.5×10^6.

Diebold *et al*. fabricated Ag SERS substrate using a femtosecond laser (100 fs pulses at a repetition rate of 1 kHz, 800 nm center wavelength) structuring process.[125] This pulse train was frequency-doubled to a center wavelength of 400 nm through a thin $BiBO_3$ crystal. They used an n-type silicon wafer as the substrate. These laser pulses had an average fluence of 10 kJ/m^2 at the surface of a silicon wafer. A thermal deposition at a rate of 0.15 nm/s onto the structured silicon with different thicknesses of 10, 30, 60, 80, 100, and 200 nm was undertaken to get the optimized Ag nanostructure sizes for enhanced SERS performance. Similarly, Indrė Aleknavičienė *et al*. fabricated fast and scalable SERS substrates at low cost using ultrashort-pulse laser-induced (280 fs, 100 kHz, 350-380 nJ) plasma-assisted ablation (LIPAA) of soda-lime glass. The fabrication speed was as fast as 150 mm/s.[138] After the amorphous nanostructure formation on the glass surface, deposition of a 170 nm silver layer by vacuum

deposition (around 100 nm in diameter, forming 1-3 μm size dendrimers) was applied to the glass substrate. This SERS substrate achieved an average enhancement factor (EF) of 3.0×10^5 evaluated using thiophenol.

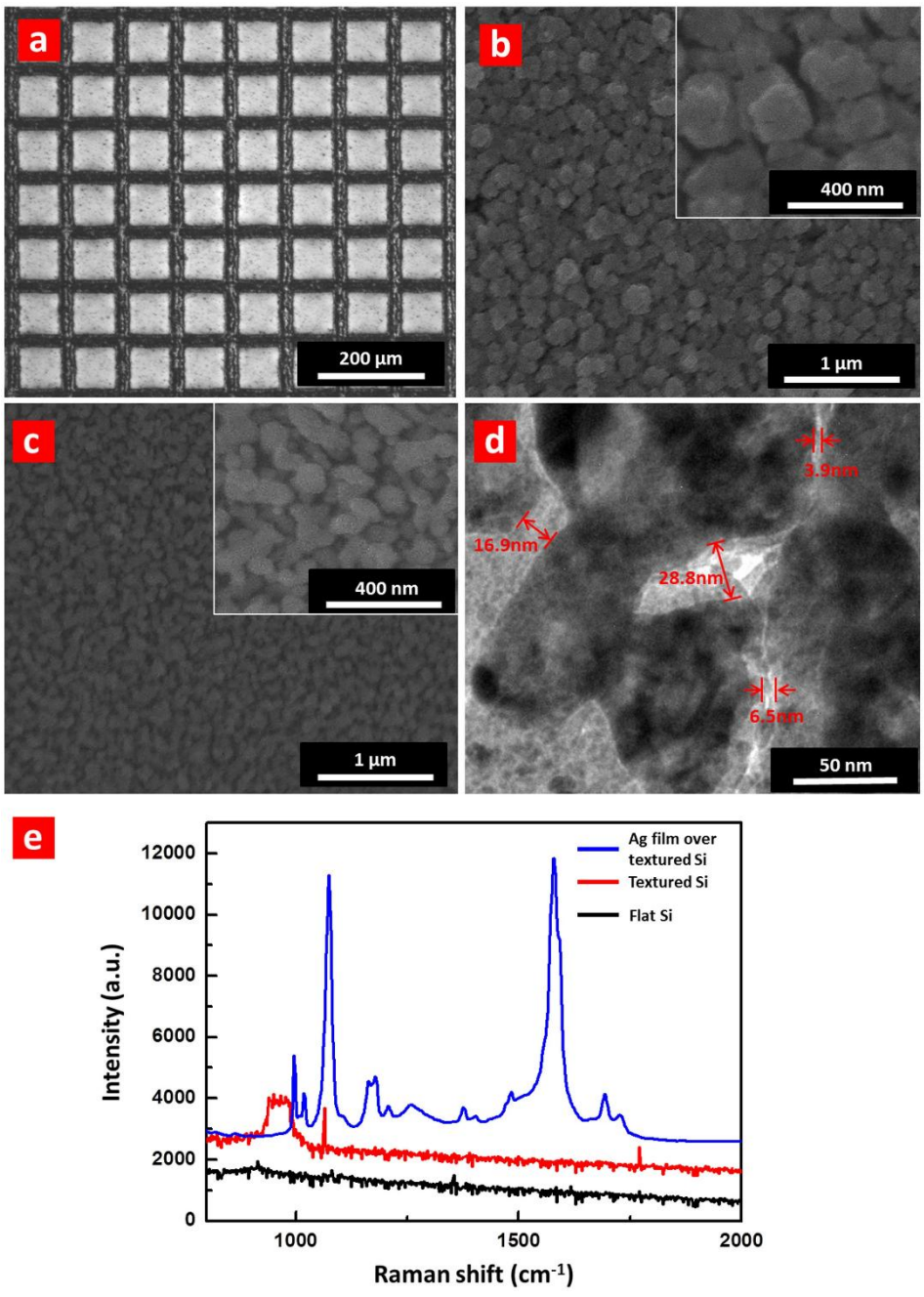

Figure 1.5: (a) Microscope image of the microsquare array made by laser etching on Si surface. Laser ablation at laser fluences of (b) 21.0 and (c) 14.3 J/cm^2 (τ = 5 ns, PRR = 100 kHz, laser spot size ~ 20 μm, ν = 100 mm/s). (d) TEM image of the small nanogaps

in between the nanoparticles. (e) The SERS spectra of 4-methylbenzenethiol molecules adsorbed on flat Si surface (500x magnification), textured Si surfaces (500x magnification) and Ag film over the textured Si.

Inkjet printing combined with electrochemical deposition is more convenient than e-beam lithography in terms of time and cost, and allows larger area fabrication at the same time. Inkjet printing method can be used either on solid substrate or on flexible substrate. [47, 119, 128, 139-149] However, the choices of ink for inkjet printing are currently limited.

SERS substrates fabricated by templating methods is another widely used approach and has been demonstrated by a number of groups, see Figure 1.4 (f) to (i). Kleinman *et al*. have studied substrates based on colloidal Polystyrene (PS) capped by silver. These substrates showed high enhancement and have been used to demonstrate sensing of analytes such as glucose.[150] Another very popular method is to use Anodised Aluminium Oxide (AAO) as a template to produce nanotubes.[151] Aluminium foil is anodised in acid to create nanopores which are then used as a template to fabricate SERS substrates. Metals can be pulsed electrodeposited inside the template channels,[132] or deposited via electron beam evaporation. [152-153] Alternatively, polymers can be employed to template the AAO. Lovera *et al*. fabricated super hydrophobic PS nanotubes by wetting commercial AAO filters and depositing silver onto the resulting PS nanotube structures.[81] Similarly, Wang *et al*. patterned polymethyl methacrylate (PMMA) on a honeycomb-like AAO template and deposited Ag onto the polymer to create Ag "nano-crown" arrays.[131] Other templates used for the fabrication of nanowires and nanotubes for SERS substrates include Polycarbonate membranes (PCM),[154-156] Polystyrene microspheres (PSM)[157-159] and nano-channel glasses. Charconnet *et al.*

fabricated superlattices by templated self-assembly of gold nanoparticles on a flexible support, with tunable lattice-plasmon resonances through macroscopic strain. They found that the highest SERS performance was achieved by matching the lattice plasmon mode to the excitation wavelength, by post-assembly fine-tuning of long-range structural parameters.[160] The above substrates fabricated with "top-down" methods are manufactured reproducibly with high throughput, but often produced weaker signals than 'bottom-up' method, due to larger distance between the nano structures and smaller surface density for nanoparticles that contribute to SERS signal. It involves also the use of expensive equipment and/or complex procedures. Combination of bottom-up and top-down fabricate method could increase the Raman intensity by creating a rougher and more homogeneous plasmonic surface.[161]

3.3. Fabrication of effective SERS substrates by electrochemical deposition.

3.3.1. Introduction to Electrochemistry.

The standard three-electrode electrochemical cell is the most used in electrochemistry workstation. It includes a working electrode (WE), a reference electrode (RE) and a counter electrode (CE) immersed in the same electrolytic solution. The working electrode is where the chemical reaction occurs. The materials used for working electrodes are typically gold, carbon, silver and platinum, etc. If the reaction is a reduction, the electrode is cathode; if it is an oxidation reaction the electrode is called anode.[162] The counter electrode (CE) acts as a supply of electrons (source/sink of electrons) to the working electrode for the redox reaction. Usually, the CE is at least ten times larger than the WE so that it will not be a limiting factor in the kinetics of the electrochemical process. The reference electrode provides a stable known potential for the electrochemical system.[162] Reliable RE include the standard hydrogen electrode, saturated calomel electrode, the silver/ silver chloride electrode and platinum pseudo-

reference. One of most widely used of these electrodes is the Ag/AgCl electrode. Electrochemical methods are used to determine the redox reaction in the system. There are four main types of electrochemical techniques: voltammetric, potentiometric, coulometric and impedimetric techniques.

The relation between the Gibbs free energy (ΔG) and the potential applied to the electrode can be written as:

$$\Delta G = -nFE^0$$

where, n is the number of electrons involved in the reaction, F is Faraday's constant (96485 C.mol^{-1}) and E^0 is the standard cell potential. Standard thermodynamics says that the actual free energy change is related to ΔG^0, the free energy change under standard conditions (1 atm, 298K):

$$\Delta G = \Delta G^0 + RT \ln Q$$

where, R is the standard gas constant (8.314 J.mol^{-1}.K^{-1}), T is temperature (K) and Q is the reaction quotient which is the function of the activities or concentrations of the chemical species involved in a chemical reaction. This equation relates Gibbs free energy to the concentration of the oxidized and reduced species and it can be combined with:

$$E = E^0 - \frac{RT}{nF} \ln \frac{Red}{Ox}$$

where, *Red* and *Ox* are the concentrations (mol.cm^{-3}) of the reduced and oxidized forms of a redox couple, respectively. This is known as the Nernst equation.

Cyclic voltammetry is the most used electrochemical technique; the Randles-Sevcik equation describes the effect of scan rate on the peak current i_p in cyclic voltammetry:

$$i_p = 0.4463 nF AC \left(\frac{nF\nu D}{RT}\right)^{\frac{1}{2}}$$

Where i_p is the current maximum in amps, n is the number of electrons transferred in the redox event (usually 1), A is the electrode area (cm^2), F is the Faraday constant (C/mol), D is the diffusion coefficient (cm^2/s), C is the concentration (mol/cm^3), v is the scan rate (V/s), R is the gas constant (JK^{-1} mol^{-1}), T is the temperature (K).

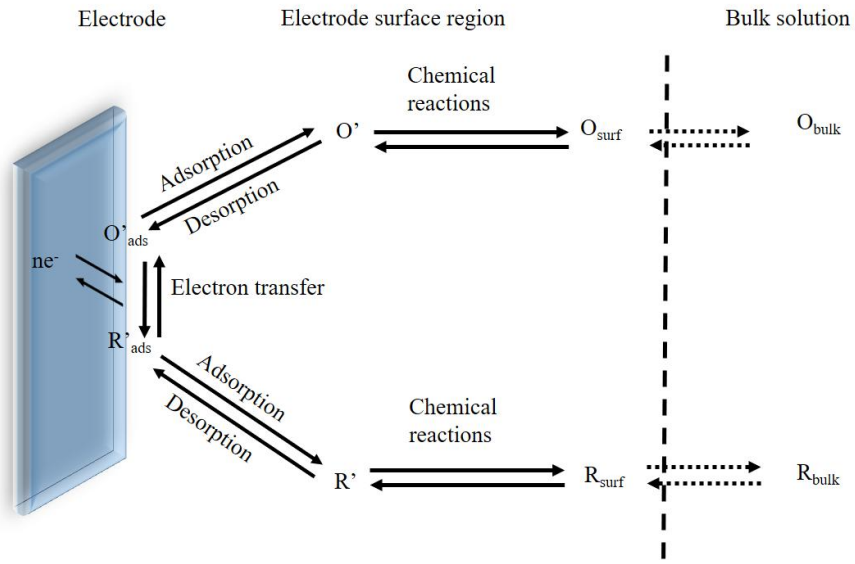

Figure 1.6 Demonstration of mass transfer, electron transfer at the electrode surface, chemical reactions preceding or following the electron transfer process.

In the redox reaction $O + ne^- \rightarrow R$, the current (or electrode reaction rate) is governed by the rates of processes, mass transfer, electron transfer at the electrode surface, chemical reactions preceding or following the electron transfer (Figure 1.6). As well as other surface reactions, such as adsorption, desorption, or crystallization (electrodeposition). The rate constants for some of these processes (e.g., electron transfer at the electrode surface or adsorption) depends upon the potential. When a steady-state current is obtained, the rates of all reaction steps in a series are the same.

3.3.2. Fabrication of SERS substrates by electrochemical methods.

There are several methods to fabricate the SERS substrates as mentioned above, including chemical and physical processes. Chemical methods encompass chemical synthesis[60], colloidal method[56], electrodeposition[63-66], etc. Physical method relate to electron-beam lithography[120-122], inkjet printing [128, 142-148, 163-164], template method[73], etc. Both methods have advantages and disadvantages. For chemical methods, synthesis metallic nanostructures can be readily achieved, but spreading the nanocluster homogeneously on the substrate is difficult and it is also hard to control the distance between adjacent nano clusters. For the physical method, it is easy to get periodic substrate with plasmonic nanostructures, but the process is complex, time-consuming and sometimes expensive. For inkjet printing, the choices for the substrate and ink are limited.

Amongst these different fabrication methods, electrochemical based ones are more cost effective compared to electron-beam (E-Beam) lithography, and offer a wider choice of substrates and plasmonic material compared to inkjet method. The morphology and the shape of the plasmon structures can be controlled through control of the deposition time, deposition voltage, and concentration of the precursor solvent.

For electrochemical method in SERS substrate fabrication, Wang *et al.* used electrochemically roughened nano-Au film as the SERS substrate, which had high reproducibility and good stability for the detection of organic pollutants.[90] Li *et al.* electrodeposited a high density of ZnO-nanorods onto polystyrene microspheres, then Ag-nanoparticles (Ag-NPs) were formed onto the surface of each ZnO-nanorod through electrochemical deposition, resulting in an ordered hierarchical Ag/ZnO hybrid arrays.[165] Wu *et al.* used ammonia reduction nitridation and electrochemical deposition method to deposit Au nanoparticles on TiN surfaces to form the Au/TiN composite as effective SERS substrate.[166] Lu *et al.* reported on the

electrochemical deposition method for fabricating super hydrophobic flexible SERS substrates based on 3D Ag nanodendrites (Ag NDs)/carbon fiber cloth. This micro/nanostructures substrate could easily obtain ultra-wet surfaces.[167] Zavatski *et al.* deposited copper on porous aluminum oxide using electrochemical method and protected the metal nanostructure's surface from oxidation by covering the surface with polyethylene glycol and silver.[168] Lu *et al.* synthesized hierarchical flower-like gold microstructures on a flexible PET film substrate through electrochemical deposition method.[169]

SERS signals will be affected by the background noise from the environment. Besides, some pesticides do not have strong interaction with the metallic SERS substrate surface. As in electrochemical sensing field, functionalization can overcome these shortcoming in some SERS detection.[170]

3.4 Summary of advantages and disadvantages for SERS substrates fabrication.

There are several ways to fabricate SERS substrates including bottom-up synthesis (chemical synthesis related process) and top-down synthesis (electron-beam (E-beam) lithography, laser etching together with film deposition), templating and inkjet printing. Each of them has its own advantages and disadvantages. For chemical synthesis, it is not easy to control the distance between the nano particles (especially for self-assembly chemical method) and sometimes nano particles are easy to aggregate; most of the time, it is needed to shift the nano particles to a supporting substrate for analytes detection with drying process involved. If the distance in between the NPs are not controlled, the enhancement factor (EF) from site to site will be different and this will lead to poorly repeatable SERS signal on a single SERS substrate - the SERS device will show a big error bar in quantification process. Apart from that, this fabrication method could show

poor reproducibility across different SERS substrates. For E-beam lithography or nanoimprint, the fabrication of SERS substrates is quite reproducible, however, the nano gaps in between the nano particles are usually large compared to the other fabrication methods. This large nano gap will lead to poor detection limit in SERS application. For laser assisted fabrication method, the choices of supporting substrates and SERS active materials are limited. The supporting materials are usually silicon and glass, while the SERS active material is gold. Electrochemical synthesis or the other fabrication method combined is a good candidate for SERS sensor/device fabrication, as it enables to control the morphology, size, nano gap of the NPs, by controlling the deposition parameters such as deposition time, voltage, precursor concentrations. Besides, it does not need high temperature or high vacuum environment, which will provide a more reproducible fabrication process.

4, Chemical functionalization of SERS substrates.

SERS substrates without functionalization have limitations when dealing with real samples, e.g. strong background noise from the environment (i.e. Raman signals coming from other non-targeted molecules present in the sample (contamination)); or dealing with macro molecular such as DNA/proteins, which would block the SERS signal. For this reason, functionalization of SERS substrates is often undertaken to improve the selectivity or sensitivity in identifying the specific target analyte, which could lower detection time and limit of detection (LOD).[170] The most widely used functionalization method is the attachment of self-assembled monolayer (SAM) of thiols to silver or gold metallic nano structures. Functional groups along the thiol are used to physisorb or chemically bind the analyte of interest to the substrate, thereby pre-concentrating the analyte at the surface leading to a subsequent increase in sensitivity.

The thiol attaches to the metal nano structure surface owing to the strong affinity of sulphur with metals. However, the mechanism for the thiol group binding to the metal surface is not totally understood yet. One theory is that the thiol moieties chemisorb to planar gold surfaces, with the loss of hydrogen during the formation of the bond.[171] In 2003, Meirav Cohen-Atiya *et al*. studied adsorption of thiols on different metal surfaces by potentiometric measurements.[172] This adsorption process involves several complex steps including negative charge transfer, discharge through a reduction process. These steps related to the metal, the surface state of the metal, and the end functional groups in thiols. In 2014, Xue *et al*. used AFM to study the force between Au NPs and thiols under different experimental condition including oxidized Au surface and reduced Au surface with different pH effects. They stated that the bond between Au and thiol is a covalent bond.[173] In 2019, Inkpen and colleagues suggested that in gold-thiol SAMs prepared from solution deposition of dithiols, the gold-sulfur coupling had a physisorbed character, by both experiment and density functional theory (DFT) calculation.[174] Henrik Grönbeck *et al*. suggested the role of the thiol chain length must be considered when accessing the stability of monolayer systems on surfaces and clusters.[175] The formation of the Metal-S bond was not always very strong and the attachment of the thiol to the metal surface often happens in a few seconds. In order to obtain a homogeneous thiol self-assembly layer, longer incubation times, typically 24 hours, are required. Thiol concentration can affect binding results. For example, Levin et al. functionalized Au nano shell by self-assembly of pMA using different concentrations. As the concentration increased, the intensity of the spectral features increase rapidly and reached a asymptotically saturation coverage at high pMA concentrations.[176] The spacing between functional thiols (that attract targeted analytes) can be adjusted by adding different kind of thiols (that do not interact with targeted

analytes). Some bio-sensors based on thiolated single stand-DNA[177] or thiolated anti-body[178] have been used to detect DNA/RNA/antigen in environment, while thiol-aptamers are also used for DNA detection, see Figure 1.7.

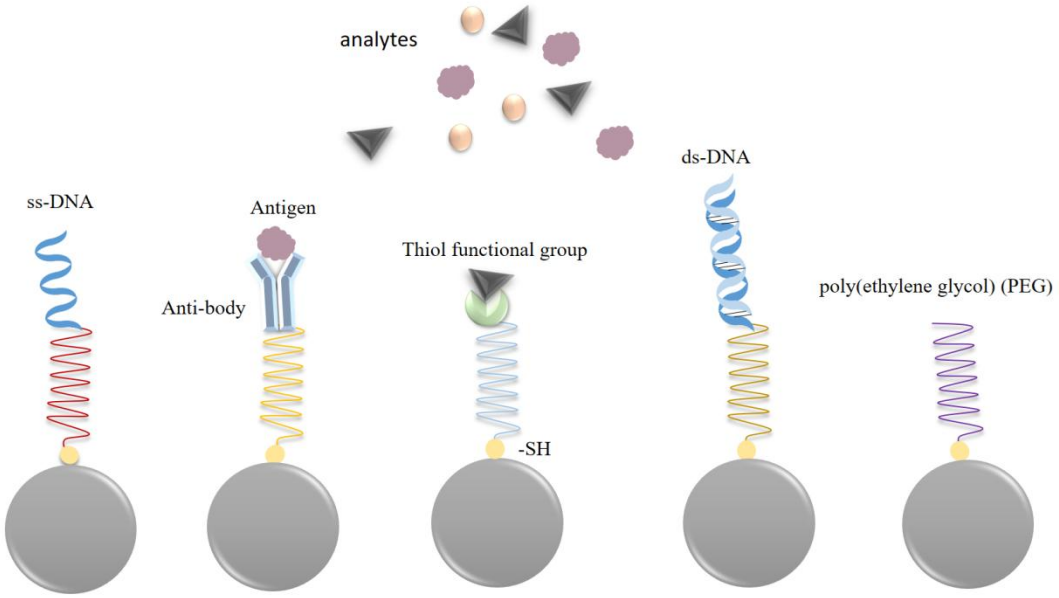

Figure 1.7**:** Different functionalisation thiols applied to metal nanoparticles : thiol-ss-DNA，thiol- anti-body, thiol-ds-DNA, thiol-PEG.

The interaction between antibody and antigen is considered strong due to the presence of forces or interactions such as hydrophobic interactions, hydrogen bonds, van der Waals forces or ionic bonds.[179] Functionalization of SERS substrates with antibodies has gained much interest in recent years because of the significant level of sensitivity and selectivity that can be achieved with them.[180] Aptamers are single stranded DNA sequences that can be designed to capture specific chemicals. Thiolated aptamers conjugated onto metal nano structures can capture and combine with the targeted chemicals to get surface enhanced Raman spectra. Sensors based on aptamers and SERS have been used for detecting pesticides, DNAs, RNAs, uranyl, biotoxin, pathogen,

hazard foodborne etc.[140, 181-185] He *et al.* presented an aptamer-based assay for the determination of fumonisin B1 (FB1), this SERS platform was based on platinum-coated gold nanorod (AuNR) and DNA sequences. In the absence of FB1, the aptamer and its cDNA associate, SERS signal at 1366 cm^{-1} decreased linearly in the 10-500 pg/mL concentration range. Besides, the assay was applied to the determination of FB1 contents in spiked corn samples.[140] He *et al.* fabricated aptamer-modified ZnO-Ag hybrids arrays by colloidal crystals templating method to determine UO_2^{2+} with a LOD of 7.2×10^{-13} M achieved, which is nearly five orders below the EPA-defined maximum contaminant level.[181] Huang et al. synthesized core-satellite surface-enhanced Raman scattering (SERS) biosensor towards biotoxin detection with a LOD of 0.83 fg/mL. DNA aptamer induced specific target recognition; this research method can also be used in ultrasensitive detection of other targets, e.g., DNAs, RNAs, and other molecules that have corresponding DNA aptamers. [182] Wang *et al.* used antibody-antigen-aptamer hetero sandwich structures surface-enhanced Raman scattering (SERS) immunoassay to detect total prostate specific antigens (tPSA) with a detection limit of 0.94 fg/mL and have successfully tested real serum samples from clinical patients which was consistent with clinical test results.[183] Wang *et al.* constructed a novel SERS biosensor combining target-responsive DNA hydrogel for sensitive detection of AFP. The aptamer in DNA hydrogel can specifically recognize AFP and accurately control the release of immunoglobulin G (IgG) encapsulated in hydrogel. This method has a wide detection linear range (50 pg/mL to 0.5 μg/mL) and a detection limit down to 50 pg/mL due to the ultrahigh sensitivity of the SERS biosensor.[184] Gold/silver nanoparticles modified with polyethylene glycol (thiol-PEG) provide a capping system that stabilizes the antibody and avoid the reticular endothelial system. For example, Chen *et al.* applied self-assembly of thiolated polyethylene glycol (PEG)-modified Au nanoparticles (NPs) into

a closely packed particle film for the production of reproducible, highly active surface-enhanced Raman scattering (SERS) substrate. This 2D particle film produces large, reproducible SERS signal by using 4-mercaptobenzoic acid as a SERS model molecule, reaching a detection limit of 1×10^{-11} M.[186]

5, Summary of advantages and disadvantages for SERS substrates functionalization.

Surface functionalization can improve selectivity and sometimes sensitivity of a SERS device, especially in real environment application where there are many different chemical species. For some molecules that do not have active interaction towards SERS substrate (i.e. noble metal nano particles), surface functionalization could help trap targeted analytes to nano particle surface, thus, getting effective Raman signal and detection. For example, a metal-organic frame network is widely used as a functionalization approach.[187] Benzene, nitrobenzene, toluene, or 2,6-di-*tert*-butylpyridine do not have active interaction to nano particles, but metal-organic framework (MOF) film traps targets at the nano particles surface, allowing the unique Raman spectrum of each molecule to be recognized. The choices for SERS surface functionalization are limited. Molecules used for SERS functionalization are SH-functionalized molecules, 4-Mercaptobenzoic acid, Thiophenol, N, NH*x* functionalized molecules (Adenine), and these molecules form an adsorbate on the metallic surface through S or N binding. Dye molecules, such as methylene blue, crystal violet, or rhodamine 6G have also been used, as they provide very high Raman cross-sections because of resonant enhancement, even if with lower affinity to the surface through electrostatic interaction.[47]

SERS surface functionalization usually takes more than 24 hours to finalize. Functional molecule orientation on SERS substrate surfaces varies and this can result in poor repeatability of SERS signal. Another drawback of functionalization in SERS application is that SERS signal comes from not only analytes but also functional layer and this makes data analysis more difficult; the variation generated in functionalization step will also lead to variation in quantification for SERS devices, e.g. the variation of thiols bonding/chemical bonding in functionalization steps will lead to different baseline for the developed SERS device.

6, SERS sensor application.

SERS sensors are reported to be fast, ultra-sensitive, selective and have been widely used in agriculture and food analytical research for pesticides monitoring, ss-DNA detection, bacteria detection, etc. in literature. A variety of SERS substrates have been used for the detection of pesticide in fruit surface, soil and food matrix, with low LOD reported. The detection steps typically involve the SERS substrate preparation, sample preparation (for soil, fruit juice, food matrix, etc.), Raman measurements and data analysis.

The final detection results of SERS signal in SERS application will be affected by surface binding of molecule on the SERS surface, molecule orientation on surfaces, adsorption state, etc. Also, different molecule orientation will affect the intensity or spectrum feature of SERS signal.[188-189]

Marshallet al. synthesized silver nanoparticle with different nano gaps and assembled them to an extended silver film, for single molecule Surface-Enhanced Raman Scattering (SERS) spectroscopy. They found that the SERS signal is strongly dependent on the particle size and the molecule orientation in between the nano gap. Finite

Difference Time Domain (FDTD) simulations have been used to support the experimental results as well in this research.[188] Sun et al. used a molecular template (MT) on the SERS substrates with self-assembly probe molecules on silver nano particles to improve the detection sensitivity. This SERS platform reached a good limit of detection (LOD) of SERS by controlling molecular orientations.[189] This method is an efficient, accurate, and simple method.

Molecular structure will also result in different EF, for example, Morton et al found that the enhancement of SERS for does not increase pyridine ring, as more charge is transferred from the pyridine ring to the cluster. However, the magnitude of chemical enhancement is governed by the energy difference between the lowest unoccupied energy level (LUMO) of the molecule and the highest occupied energy level (HOMO) of the metal. This trend has been verified by considering substituted benzenethiols, small molecules, and silver clusters of different sizes. The results indicate that molecules that show significant stabilization of the HOMO-LUMO gaps (such as those that readily accept π-backbonding) most likely to have strong chemical enhancement. This provided theory for designing new molecules which exhibit high chemical enhancements. However, it is still very challenge to describe the magnitude of the Raman enhancements using electronic structure methods such as DFT accurately, as they probably underestimate the energy gap.[190]

Several molecule such as SH-functionalized molecules,[191-192] 4-MBA,[193] Rhodamine 6G,[194] crystal violet[195] etc. have strong Raman response and are often used as Raman reporter. Marques *et al*. studied 4-Mercaptobenzoic acid (4-MBA) adsorbate by connecting it to Ag surface through a thiolate-Ag bonding that was able to trigger a self-

assembly process of Ag NPs. This process is driven by cooperative hydrogen bonds between the carboxylic groups of 4-MBA located in different nanoparticles pH=4. UV-Vis and DFT-based calculation of the model complex [AgNP-(4-MBA)$_2$-AgNP] help to understand the self-assembled complex formation through the comparison of calculated and experimental SERS spectra.[196] Madzharova *et al*. obtained surface-enhanced hyper Raman scattering (SEHRS) spectra (excited off-resonance at a wavelength of 1064 nm) and surface-enhanced Raman scattering (SERS) spectra excited at 785 nm or at 633 nm, from thiophenol, benzyl mercaptan, and phenylethyl mercaptan and from the three isomers 2-aminothiophenol (2-ATP), 3-aminothiophenol (3-ATP), and 4-aminothiophenol (4-ATP). The SEHRS spectra show a different interaction of thiophenol, benzyl mercaptan, and phenylethyl mercaptan with silver and gold nanostructures, with the support of Density functional theory (DFT) calculations. Besides, 2-ATP, 3-ATP, and 4-ATP show a different interaction with gold nanostructures that was found to depend on pH.[192] Those SERS reporter molecules contain sulfur atom(s) or nitrogen atom(s), this will help the molecule to have better affinity to nano metal particles and gain a better SERS signal.

Two pesticides Organophosphates (OP) and Neonicotinoids detection by SERS are widely studied, most OP contains sulfur atoms and Neonicotinoids contains nitrogen atom (s) or both. Silver/Au and sulfur/nitrogen atoms are larger in size. They have less charge states and can be easily polarized. Covalent bonds form between Au/Ag and sulfur/nitrogen atoms.

6.1. Pesticides detection.

Organophosphates (OP) represent the largest class of pesticides, making up to 50% of the neurotoxic agents in chemical pesticides.[197] Most OP usage is agricultural, since the Environmental Protection Agency banned their residential use in 2001.[198] However, their human and animal toxicity still make them a societal health and environmental concern.[199-201] Moreover, small amounts (in the order of ng/L for example) is detectable in food and drinking water by gas chromatography-mass spectrometry (GC-MS).[202-205] It is possible to detect OP pesticides by using SERS and most of OP pesticides contains sulfur atoms that have good affinity to SERS metal nano particle surface. Hou *et al.* showed an *in situ* SERS method, using commercially available gold nanoparticle colloids, to detect organophosphates isocarbophos and phorate, and neonicotinoid imidacloprid, on different plant surfaces.[206] Similarly, Bianhua *et al.* reported on the use of silver-coated gold bimetallic nanoparticles for *in situ* detection of a range of pesticides on fruit peels without further sample preparation.[207] In this research, different pesticides were distinguished by their 'fingerprint'. Both of these techniques demonstrated limits of detection (LOD) below the required maximum residue levels (MRL). However, these colloidal based solutions as described above are not ideal for portable applications while solid SERS substrates that can be prepared in advance are more suitable. For example, Chen *et al.* used "SERS tape" to extract OP pesticides (thiram, chlorpyrifos, methyl parathion) from different kinds of fruit and vegetable peels.[208] The tape is placed onto the surface of the produce and peeled off for SERS analysis. This is non-invasive and requires no sample or substrate preparation. Additionally, Li *et al.* have created a 'smart dust' that easily spreads over a probed surface for *in-situ* SERS measurements.[209] This method requires no preparation or particle aggregation/concentration on the substrate. Their shell-isolated nanoparticles are used to analyse residues of OP pesticide parathion, on a fresh orange. They present

comparable results between a normal Raman and a portable Raman, demonstrating the substrates potential use in-field. Those methods were able to detect pesticides down to a low limit, however, it is hard to quantify targeted pesticides. In real application, it is possible to get Raman signal also from other molecule and get cross contamination.

Table 1: Organophosphates (OP) detection by SERS in food industry and environment monitoring.

Organophosphates (matrix)		SERS substrate	LOD (reported)	LOD (converted)
Phosmet 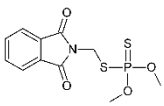	Ooling tea[210]	Ag NPs	0.1 mg/kg	0.3 µmol/L
	fruit or vegetable peels[140]	Snowflake-like Au NPs	0.032 ng/cm^{-2}	100 nmol/L
	fruit[211]	multi-walled carbon nanotubes	0.5 mg/kg	1.5 µmol/L
	paddy water[212]	Au nanorods	0.25mg/L	7.5 µmol/L
	fruit skin[213]	polyurethane-Ag NPs	0.6 µg/mL	1.8 µmol/L
	Plant Surfaces[214]	polyurethane micelle/ Ag NP	0.08 g/mL	240 µmol/L
	pesticides residue[215]	Au NP coated ZrO_2 nanofiber	10^{-8} M	10^{-8} mol/L
	Orange[216]	Au NPs decorated glycidyl methacrylate-ethylene dimethacrylate material	1 µg/L	3 nmol/L

Parathion-methyl 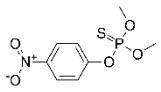	fruit or vegetable peels[217]	Snowflake-like Au NPs	0.026 ng/cm	0.099 nmol/L
	peach[218]	Au@Ag NP	0.001 mg/kg	3.8 nmol/L
	solvent[219]	Ag NP decorated ZnO-nanorods	10^{-8} M	10^{-8} M
Malathion 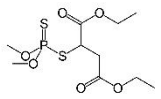	solvent[220]	Au NP	1 ppm	3 μM/L
	solvent[221]	nanoporous structure	12 ppb	36 nMol/L
	solvent[222]	nanostructured Ag	10 nM	10 nM
Chlorpyrifos 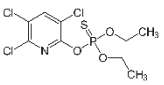	tomato surface[223]	Ag colloid	10^{-9} mol/L	10^{-9} mol/L
	soil[224]	Au NP	10 ppm	28.6 μMol/L
	fruits[225]	Ag NP	10 ng/ml	28.6 nMol/L

Neonicotinoids usually contains nitrogen atom(s) and are a more recent and relatively powerful class of insecticide. Since the introduction of imidacloprid in 1991, they have been the fastest-growing class of insecticides in modern crop protection,[226] representing almost 17% of the global market.[227] Typical detection methods of neonicotinoids are based on enzyme linked immuno-sorbent assays (ELISA),[228-229] HPLC- or GC- mass spectrometry,[230-234] surface plasmon resonance,[235] and fluorescence spectroscopy,[236]

none of which are suitable for field analysis. Neonicotinoids are extremely effective against herbivorous insects,[237] while having perceived low toxicity to mammals, birds, and fish.[238] This has led to their widespread uptake for use on a variety of crops. However, concerns have been raised recently about environmental impact affecting the homing capacity of honey bees, resulting in global colony collapse of the pollinator population.[2, 239] Consequently, the European Union enforced a temporary ban (Dec 2013)[240] reducing the MRL of neonicotinoids to between 0.01 to 3 mg/kg for many fruits and vegetables.[230, 241]

Research regarding detection of neonicotinoids by SERS thus show wide interest. Cao *et al.* synthesized three types of AuNP/MOF (metal-organic framework) composite to investigate the interaction between acetamiprid and the bridging molecules of the MOFs. Acetamiprid in this case was used to evaluate the characteristics of the SERS substrates. LODs of 0.02 μM, 0.009 μM, and 0.02 μM were achieved for the three composites, which could satisfy the requirement of detection according to the MRLs of acetamiprid.[242] However, these metal-organic framework SERS sensors have poor reproducibility. Yang *et al.* used SERS to evaluate the penetration behaviors of 4 pesticides (acetamiprid, thiabendazole, ferbam and phosmet) in a variety of fresh produce matrices. They used a pesticide/ AgNP complex deposited onto the external surfaces of different fresh produce and measured the penetration depth of the complex using SERS.[243] Although the results are promising, this method requires complex sample preparation with the pesticide and AgNP, including washing steps, and is not ideal for farm-side analysis. On the other hand, Wijaya *et al.* employed silver dendrites for SERS-based detection of acetamiprid in apple juice and from swabs of the apple surface.[244] This method does not need pre-treatment for the apple juice samples and the use of the swab is non-invasive to the fruit. This method therefore has the potential to be used for on-site pesticide detection.

However, selectivity study has not been carried out in this study, it is hard to avoid cross contaminations in real environment.

6.2. Shortcomings and challenges of SERS device development.

SERS device is used to identify or further quantify an unknown sample. All challenges stated in section 2.4, 3.4, 4.1 for SERS are valid also for SERS device development. First, high-resolution handheld or portable Raman instrument development is difficult and limit SERS application in real outdoor environment, SERS devices with good performance are only available in laboratory level. Second, SERS substrates with good repeatability and reproducibility are made by E-beam lithography, and such substrates have lower EF comparing to SERS substrate made by the other approaches, e.g. chemical synthesis or electrochemical deposition, etc. While repeatability and reproducibility are important for SERS quantification, usually, ten measurements are recommend and taken in a single SERS substrate for quantification. Reproducibility is essential to retain the same sensitivity/ LOD for the developed SERS device, also, reproducibility is an important parameter for application and mass production, though standard addition method could be used to minimize the difference between different SERS devices. Machine learning and artificial intelligence has been used to help increase the accuracy, reliability and sensitivity in SERS.[245] In real environment application, cross-contamination is another factor to consider, sample pre-treatments or surface functionalization for SERS substrate can help improve selectivity of SERS device and avoid the impact from contaminant appeared in the real sample. Last, SERS signal reading and data analysis is important and is one of the most difficult part for SERS study. As in most of the cases, it is hard to precisely determine the adsorption site of analytes on nano particle surface.[246] In summary, SERS devices are

widely studied in lab/research level, comparing to MS and HPLC technologies, there are still problems to be solved until SERS devices can be used in industry. SERS devices is good for tracing ultra-low concentration analyte while MS/HPLC can help accurate quantification.

7. Scope and organization of this thesis.

This thesis used electrochemical deposition method to fabricate SERS substrate on a micro chip platform that were fabricated through photolithography method. With portable potentiostats, it is possible to fabricate these SERS substrates anywhere with a PC. The SERS substrate fabrication process takes usually tens of seconds with tens of micro liter of silver precursor. Fabrication of SERS substrate by electrochemical deposition on the micro chip platform is fast, simple and relatively environment friendly compared to other fabrication methods such as E-beam lithography, inkjet printing, chemical synthesis, etc.. By controlling the electrochemical deposition parameters such as voltage, deposition time, precursor concentrations, it is possible to tailor the morphology of the SERS substrates. Through optimization of the electrochemical deposition process and parameters, SERS substrates with relatively good detection ability were chosen for further analytes detection study.

Silver nanoparticles are commonly used SERS substrate and show good SERS performance as discussed in many research studies. In this thesis, Ag nanoparticles based SERS sensors were used to detect different chemicals in water environment. By using the micro sensor chip and electrochemical deposition method, it is possible to develop Ag nanoparticles based SERS sensors using the strong electric field generated at gold micro bands. Electrochemical deposition parameters are relatively controllable and do not require tuning of the temperature, which is of benefit for SERS sensor mass

production. For SERS sensor quantification, it is essential to have homogeneously distributed nanoparticles and nanogaps to gain small standard deviation in between different Raman measurements. SERS substrate fabrication optimization process is necessary to reach this goal.

In Chapter 2, silver-gum Arabic (Ag-GA) substrates were synthesized and optimized by electrochemical deposition method. Gum Arabic was used to help synthesis of the silver nano particles, acting as a silver nano particle shape monitoring agent. Importantly, it also helped to capture and concentrate 2,4-D pesticides.

By changing the concentration of $AgNO_3$, Gum Arabic, the deposition time, and the deposition voltage, the optimized deposition parameters were used for Ag-GA SERS sensor fabrication and for 2,4-D detection. The performance of this AG-GA SERS sensor was good and reach EU pesticides restriction limit requirement (0.1 ppb). For Chapter 2, real river water samples were used to verify the developed sensors, the results showed that the contamination in both river water or mineral water did not interrupt the detection of 2,4-D by this Ag-GA substrate.

Similarly, in Chapter 3, Silver-Corn Starch (Ag-CS) SERS substrates were fabricated and optimized. Cornstarch and gum Arabic are both polysaccharide and share similar chemical properties, CS has more -OH group compared to GA, while CS does not contain protein and GA contains protein. CS acted as a functional layer that helped to capture and concentrate MCPA pesticide to the nano particles surface. With the knowledge and conclusions gained in Chapter 2, the optimization process was easier in Chapter 3 and the sensor performance improved, in terms of detection ability. What is more, in Chapter 3, data analysis method changed and it turned to be more suitable for this research, without baseline subtraction.

In Chapter 4, functionalized Ag nanoparticles SERS substrate were used for ss-DNA detection from bacteria STEC, two thiols including thiol-ss-probe-DNA and $HS(CH_2)_6OH$ were used for SERS sensor functionalization with $HS(CH_2)_6OH$ used to block the Ag SERS surface to avoid unwanted attachment of target-ss-DNA and Raman reporter, methylene blue. The sensitivity of this ss-DNA SERS sensor is competitive with existing SERS sensors, besides, this SERS sensor has good selectivity towards different bacteria.

All in all, this thesis showed the development of three SERS substrates, which were fast in fabrication, have relative short response time and are easy to operate. For SERS substrates in Chapter 2 and 3, the sensitivity were not ideal and they did not have selectivity towards different chemicals. These SERS substrates showed similar properties as non-molecular imprint SERS substrates, and molecular imprint can help to improve the performance of the devices. However, chemical synthesis (high temperature) was only used in MIP for SERS research so far, it has not been used by electrochemical deposition fabrication method for MIP SERS sensors. For sensor in Chapter 4, the ss-DNA SERS sensor showed good sensitivity and selectivity, though standard addition method should be used in real situation for quantification, as the baseline for each sensor would be different.

Reference.

1. Food Agriculture Organisation *The future of food and agriculture – Trends and challenges*; United Nations Rome, 2017.
2. Henry, M.; Beguin, M.; Requier, F.; Rollin, O.; Odoux, J.-F.; Aupinel, P.; Aptel, J.; Tchamitchian, S.; Decourtye, A., A common pesticide decreases foraging success and survival in honey bees. *Science* **2012,** *336* (6079), 348-350.
3. Stachniuk, A.; Fornal, E., Liquid Chromatography-Mass Spectrometry in the Analysis of Pesticide Residues in Food. *Food Analytical Methods* **2016,** *9* (6), 1654-1665.
4. Gong, T. X.; Huang, Y. F.; Wei, Z. J.; Huang, W.; Wei, X. B.; Zhang, X. S., Magnetic assembled 3D SERS substrate for sensitive detection of pesticide residue in soil. *Nanotechnology* **2020,** *31* (20).
5. Guselnikova, O.; Postnikov, P.; Elashnikov, R.; Miliutina, E.; Svorcik, V.; Lyutakov, O., Metal-organic framework (MOF-5) coated SERS active gold gratings: A platform for the selective detection of organic contaminants in soil. *Analytica Chimica Acta* **2019,** *1068*, 70-79.
6. Krafft, B.; Tycova, A.; Urban, R. D.; Dusny, C.; Belder, D., Microfluidic device for concentration and SERS-based detection of bacteria in drinking water. *Electrophoresis*.
7. Xu, Y.; Kutsanedzie, F. Y. H.; Hassan, M.; Zhu, J. J.; Ahmad, W.; Li, H. H.; Chen, Q. S., Mesoporous silica supported orderly-spaced gold nanoparticles SERS-based sensor for pesticides detection in food. *Food Chemistry* **2020,** *315*.
8. Zhu, C. H.; Zhao, Q. S.; Meng, G. W.; Wang, X. J.; Hu, X. Y.; Han, F. M.; Lei, Y., Silver nanoparticle-assembled micro-bowl arrays for sensitive SERS detection of pesticide residue. *Nanotechnology* **2020,** *31* (20).
9. Grubisha, D. S.; Lipert, R. J.; Park, H.-Y.; Driskell, J.; Porter, M. D., Femtomolar Detection of Prostate-Specific Antigen: An Immunoassay Based on Surface-Enhanced Raman Scattering and Immunogold Labels. *Analytical Chemistry* **2003,** *75* (21), 5936-5943.
10. Fan, M.; Andrade, G. F. S.; Brolo, A. G., A review on the fabrication of substrates for surface enhanced Raman spectroscopy and their applications in analytical chemistry. *Analytica Chimica Acta* **2011,** *693* (1–2), 7-25.

11. Justin, L. A.; Jeremy, D. D.; Ralph, A. T.; Yiping, Z., Current Progress on Surface-Enhanced Raman Scattering Chemical/Biological Sensing. In *Functional Nanoparticles for Bioanalysis, Nanomedicine, and Bioelectronic Devices Volume 2*, American Chemical Society: 2012; Vol. 1113, pp 235-272.

12. Xie, W.; Schlucker, S., Medical applications of surface-enhanced Raman scattering. *Physical Chemistry Chemical Physics* **2013,** *15* (15), 5329-5344.

13. Willets, K. A., Probing nanoscale interfaces with electrochemical surface-enhanced Raman scattering. *Current Opinion in Electrochemistry* **2019,** *13*, 18-24.

14. Craig, A. P.; Franca, A. S.; Irudayaraj, J., Surface-Enhanced Raman Spectroscopy Applied to Food Safety. In *Annual Review of Food Science and Technology, Vol 4*, Doyle, M. P.; Klaenhammer, T. R., Eds. 2013; Vol. 4, pp 369-380.

15. Fan, C.; Hu, Z. Q.; Mustapha, A.; Lin, M. S., Rapid detection of food- and waterborne bacteria using surface-enhanced Raman spectroscopy coupled with silver nanosubstrates. *Appl Microbiol Biot* **2011,** *92* (5), 1053-1061.

16. Zhang, Y.; Huang, Y.; Zhai, F.; Du, R.; Liu, Y.; Lai, K., Analyses of enrofloxacin, furazolidone and malachite green in fish products with surface-enhanced Raman spectroscopy. *Food Chemistry* **2012,** *135* (2), 845-850.

17. Cialla, D.; Marz, A.; Bohme, R.; Theil, F.; Weber, K.; Schmitt, M.; Popp, J., Surface-enhanced Raman spectroscopy (SERS): progress and trends. *Analytical and Bioanalytical Chemistry* **2012,** *403* (1), 27-54.

18. Granger, J. H.; Schlotter, N. E.; Crawford, A. C.; Porter, M. D., Prospects for point-of-care pathogen diagnostics using surface-enhanced Raman scattering (SERS). *Chemical Society Reviews* **2016,** *45* (14), 3865-3882.

19. Jarvis, R. M.; Goodacre, R., Characterisation and identification of bacteria using SERS. *Chemical Society Reviews* **2008,** *37* (5), 931-936.

20. Raman, C. V.; Krishnan, K. S., A new type of secondary radiation (Reprinted from Nature, vol 121, pg 501-502, 1928). *Curr Sci India* **1998,** *74* (4), 381-381.

21. Laserna, J., *Modern Techniques in Raman Spectroscopy*. John Wiley and Sons: 1996.

22. Kalantar-zadeh, K.; Fry, B., *Nanotechnology-enabled sensors*. Springer Science & Business Media: 2007.

23. Settle, F. A., *Handbook of instrumental techniques for analytical chemistry*. Prentice Hall PTR: 1997.

24. Zhu, J.; Wang, Q., Excitation wavelength dependence of Raman scattering and substrate dependence on hydrogenated silicon-based thin film. *Physica B: Condensed Matter* **2018,** *545*, 315-322.

25. Ye, J.; Li, J.; Lu, M.; Qi, X.; Li, B.; Wei, H.; Li, Y.; Zou, M., Dual-wavelength excitation combined Raman spectroscopy for detection of highly fluorescent samples. *Applied optics* **2021,** *60* (23), 6918-6927.

26. Chon, B.; Xu, S.; Lee, Y. J., Compensation of Strong Water Absorption in Infrared Spectroscopy Reveals the Secondary Structure of Proteins in Dilute Solutions. *Analytical Chemistry* **2021,** *93* (4), 2215-2225.

27. Li, Z.; Deng, L.; Kinloch, I. A.; Young, R. J., Raman spectroscopy of carbon materials and their composites: Graphene, nanotubes and fibres. *Progress in Materials Science* **2023,** *135*, 101089.

28. Nochi, M.; Ozaki, Y.; Sato, H., Water-induced conformational changes in the powder and film of ε-poly(L)lysine studied by infrared and Raman spectroscopy. *Spectrochimica Acta Part A: Molecular and Biomolecular Spectroscopy* **2021,** *260*, 119900.

29. Mi, T.; Wang, J. J.; McCague, C.; Bai, Y., Application of Raman Spectroscopy in the study of the corrosion of steel reinforcement in concrete: A critical review. *Cement and Concrete Composites* **2023,** *143*, 105231.

30. Gardiner, D. J., *Practical Raman Spectroscopy*. Spinger-Verlag: 1989.

31. Das, R. S.; Agrawal, Y. K., Raman spectroscopy: Recent advancements, techniques and applications. *Vibrational Spectroscopy* **2011,** *57* (2), 163-176.

32. Schlack, T. R.; Beal, S. A.; Corriveau, E. J.; Clausen, J. L., Detection Limits of Trinitrotoluene and Ammonium Nitrate in Soil by Raman Spectroscopy. *ACS Omega* **2021,** *6* (25), 16316-16323.

33. Zhu, G.; Zhu, X.; Fan, Q.; Wan, X., Raman spectra of amino acids and their aqueous solutions. *Spectrochimica Acta Part A: Molecular and Biomolecular Spectroscopy* **2011,** *78* (3), 1187-1195.

34. Jablonski, A., Efficiency of anti-Stokes fluorescence in dyes. *Nature* **1933,** *131* (3319), 839.

35. Fleischmann, M.; Hendra, P. J.; McQuillan, A. J., Raman spectra of pyridine adsorbed at a silver electrode. *Chemical Physics Letters* **1974,** *26* (2), 163-166.

36. Gersten, J. I., The effect of surface roughness on surface enhanced Raman scattering. *The Journal of Chemical Physics* **1980,** *72* (10), 5779-5780.

37. Gersten, J.; Nitzan, A., Electromagnetic theory of enhanced Raman scattering by molecules adsorbed on rough surfaces. *The Journal of Chemical Physics* **1980,** *73* (7), 3023-3037.

38. Moskovits, M., Surface-enhanced spectroscopy. *Reviews of Modern Physics* **1985,** *57* (3), 783-826.

39. Otto, A.; Mrozek, I.; Grabhorn, H.; Akemann, W., Surface-enhanced Raman scattering. *Journal of Physics: Condensed Matter* **1992,** *4* (5), 1143.

40. Stiles, P. L.; Dieringer, J. A.; Shah, N. C.; Duyne, R. P. V., Surface-Enhanced Raman Spectroscopy. *Annual Review of Analytical Chemistry* **2008,** *1* (1), 601-626.

41. Hutter, E.; Fendler, J. H., Exploitation of Localized Surface Plasmon Resonance. *Advanced Materials* **2004,** *16* (19), 1685-1706.

42. Camden, J. P.; Dieringer, J. A.; Wang, Y.; Masiello, D. J.; Marks, L. D.; Schatz, G. C.; Van Duyne, R. P., Probing the Structure of Single-Molecule Surface-Enhanced Raman Scattering Hot Spots. *Journal of the American Chemical Society* **2008,** *130* (38), 12616-12617.

43. Pérez-Jiménez, A. I.; Lyu, D.; Lu, Z.; Liu, G.; Ren, B., Surface-enhanced Raman spectroscopy: benefits, trade-offs and future developments. *Chemical Science* **2020,** *11* (18), 4563-4577.

44. Langer, J.; Jimenez de Aberasturi, D.; Aizpurua, J.; Alvarez-Puebla, R. A.; Auguié, B.; Baumberg, J. J.; Bazan, G. C.; Bell, S. E. J.; Boisen, A.; Brolo, A. G.; Choo, J.; Cialla-May, D.; Deckert, V.; Fabris, L.; Faulds, K.; García de Abajo, F. J.; Goodacre, R.; Graham, D.; Haes, A. J.; Haynes, C. L.; Huck, C.; Itoh, T.; Käll, M.; Kneipp, J.; Kotov, N. A.; Kuang, H.; Le Ru, E. C.; Lee, H. K.; Li, J.-F.; Ling, X. Y.; Maier, S. A.; Mayerhöfer, T.; Moskovits, M.; Murakoshi, K.; Nam, J.-M.; Nie, S.; Ozaki, Y.; Pastoriza-Santos, I.; Perez-Juste, J.; Popp, J.; Pucci, A.; Reich, S.; Ren, B.; Schatz, G. C.; Shegai, T.; Schlücker, S.; Tay, L.-L.; Thomas, K. G.; Tian, Z.-Q.; Van Duyne, R. P.; Vo-Dinh, T.; Wang, Y.; Willets, K. A.; Xu, C.; Xu, H.; Xu, Y.; Yamamoto, Y. S.; Zhao, B.; Liz-Marzán, L. M., Present and Future of Surface-Enhanced Raman Scattering. *ACS Nano* **2020,** *14* (1), 28-117.

45. Dao, D. Q.; Truong, D. H.; Nguyen, T. L. A.; Ngo, T. C.; An, N. T. T.; Huy, B. T., Insight into SERS Chemical Enhancement Mechanism of Fungicide Thiram Adsorbed on Silver Nanoparticles. *Journal of Cluster Science* **2022,** *33* (6), 1-15.

46. Mishra, N.; Liu, M.; Fang, Y.; Kulkarni, S., Study of adsorption behavior of aminothiophenols on gold nanorods using surface-enhanced Raman spectroscopy. *Journal of Nanophotonics* **2011,** *5*, 053513.

47. Bell, S. E. J.; Charron, G.; Cortés, E.; Kneipp, J.; de la Chapelle, M. L.; Langer, J.; Procházka, M.; Tran, V.; Schlücker, S., Towards Reliable and Quantitative Surface-Enhanced Raman Scattering (SERS): From Key Parameters to Good Analytical Practice. *Angewandte Chemie International Edition* **2020,** *59* (14), 5454-5462.

48. Weaver, M. J.; Zou, S.; Chan, H. Y. H., Peer Reviewed: The New Interfacial Ubiquity of Surface-Enhanced Raman Spectroscopy. *Analytical Chemistry* **2000,** *72* (1), 38 A-47 A.

49. Almehmadi, L. M.; Curley, S. M.; Tokranova, N. A.; Tenenbaum, S. A.; Lednev, I. K., Surface Enhanced Raman Spectroscopy for Single Molecule Protein Detection. *Scientific Reports* **2019,** *9* (1), 12356.

50. Nicolson, F.; Jamieson, L. E.; Mabbott, S.; Plakas, K.; Shand, N. C.; Detty, M. R.; Graham, D.; Faulds, K., Surface enhanced resonance Raman spectroscopy (SERRS) for probing through plastic and tissue barriers using a handheld spectrometer. *Analyst* **2018,** *143* (24), 5965-5973.

51. Litti, L.; Colusso, A.; Pinto, M.; Ruli, E.; Scarsi, A.; Ventura, L.; Toffoli, G.; Colombatti, M.; Fracasso, G.; Meneghetti, M., SERRS multiplexing with multivalent nanostructures for the identification and enumeration of epithelial and mesenchymal cells. *Scientific Reports* **2020,** *10* (1), 15805.

52. He, Z.; Rong, T.; Li, Y.; Ma, J.; Li, Q.; Wu, F.; Wang, Y.; Wang, F., Two-Dimensional TiVC Solid-Solution MXene as Surface-Enhanced Raman Scattering Substrate. *ACS Nano* **2022,** *16* (3), 4072-4083.

53. Srichan, C.; Ekpanyapong, M.; Horprathum, M.; Eiamchai, P.; Nuntawong, N.; Phokharatkul, D.; Danvirutai, P.; Bohez, E.; Wisitsoraat, A.; Tuantranont, A., Highly-Sensitive Surface-Enhanced Raman Spectroscopy (SERS)-based Chemical Sensor using 3D Graphene Foam Decorated with Silver Nanoparticles as SERS substrate. *Scientific Reports* **2016,** *6* (1), 23733.

54. Sharma, B.; Frontiera, R. R.; Henry, A.-I.; Ringe, E.; Van Duyne, R. P., SERS: Materials, applications, and the future. *Materials Today* **2012,** *15* (1), 16-25.

55. Solís, D. M.; Taboada, J. M.; Obelleiro, F.; Liz-Marzán, L. M.; García de Abajo, F. J., Optimization of Nanoparticle-Based SERS Substrates through Large-Scale Realistic Simulations. *ACS Photonics* **2017,** *4* (2), 329-337.

56. Bell, S. E.; McCourt, M. R., SERS enhancement by aggregated Au colloids: effect of particle size. *Physical Chemistry Chemical Physics* **2009,** *11* (34), 7455-7462.

57. Lee, S. J.; Guan, Z.; Xu, H.; Moskovits, M., Surface-Enhanced Raman Spectroscopy and Nanogeometry: The Plasmonic Origin of SERS. *The Journal of Physical Chemistry C* **2007,** *111* (49), 17985-17988.

58. Njoki, P. N.; Lim, I. I. S.; Mott, D.; Park, H.-Y.; Khan, B.; Mishra, S.; Sujakumar, R.; Luo, J.; Zhong, C.-J., Size Correlation of Optical and Spectroscopic Properties for Gold Nanoparticles. *The Journal of Physical Chemistry C* **2007,** *111* (40), 14664-14669.

59. Lancaster, C. A.; Scholl, W. E.; Ticknor, M. A.; Shumaker-Parry, J. S., Uniting Top-Down and Bottom-Up Strategies Using Fabricated Nanostructures as Hosts for Synthesis of Nanomites. *The Journal of Physical Chemistry C* **2020,** *124* (12), 6822-6829.

60. Banholzer, M. J.; Millstone, J. E.; Qin, L.; Mirkin, C. A., Rationally designed nanostructures for surface-enhanced Raman spectroscopy. *Chemical Society Reviews* **2008,** *37* (5), 885-897.

61. Pan, X.-T.; Liu, Y.-Y.; Qian, S.-Q.; Yang, J.-M.; Li, Y.; Gao, J.; Liu, C.-G.; Wang, K.; Xia, X.-H., Free-Standing Single Ag Nanowires for Multifunctional Optical Probes. *ACS Applied Materials & Interfaces* **2021,** *13* (16), 19023-19030.

62. Xu, K.-X.; Chen, X.; Huang, Z.; Chen, Z.-N.; Chen, J.; Sun, J.-J.; Fang, Y.; Li, J.-F., Ligand-Free Fabrication of Ag Nanoassemblies for Highly Sensitive and Reproducible Surface-Enhanced Raman Scattering Sensing of Antibiotics. *ACS Applied Materials & Interfaces* **2021,** *13* (1), 1766-1772.

63. Choi, S.; Jeong, H.; Choi, K. H.; Song, J. Y.; Kim, J., Electrodeposition of triangular Pd rod nanostructures and their electrocatalytic and SERS activities. *ACS Appl Mater Interfaces* **2014,** *6* (4), 3002-7.

64. Ge, D.; Wei, J.; Ding, J.; Zhang, J.; Ma, C.; Wang, M.; Zhang, L.; Zhu, S., Silver Nano-Dendrite-Plated Porous Silicon Substrates Formed by Single-Step

Electrochemical Synthesis for Surface-Enhanced Raman Scattering. *ACS Applied Nano Materials* **2020,** *3* (3), 3011-3018.

65. Jeong, H.; Kim, J., Electrodeposition of nanoflake Pd structures: structure-dependent wettability and SERS activity. *ACS Appl Mater Interfaces* **2015,** *7* (13), 7129-35.

66. Raveendran, J.; Stamplecoskie, K. G.; Docoslis, A., Tunable Fractal Nanostructures for Surface-Enhanced Raman Scattering via Templated Electrodeposition of Silver on Low-Energy Surfaces. *ACS Applied Nano Materials* **2020,** *3* (3), 2665-2679.

67. Longoni, M.; Zalaffi, M. S.; de Ferri, L.; Stortini, A. M.; Pojana, G.; Ugo, P., Surface Enhanced Raman Spectroscopy With Electrodeposited Copper Ultramicro-Wires With/Without Silver Nanostars Decoration. *Nanomaterials* **2021,** *11* (2), 518.

68. Grzelczak, M.; Vermant, J.; Furst, E. M.; Liz-Marzán, L. M., Directed Self-Assembly of Nanoparticles. *ACS Nano* **2010,** *4* (7), 3591-3605.

69. Zhu, S.; Fan, C.; Wang, J.; He, J.; Liang, E., Self-assembled Ag nanoparticles for surface enhanced Raman scattering. *Optical Review* **2013,** *20* (5), 361-366.

70. Gao, T.; Wang, Y.; Wang, K.; Zhang, X.; Dui, J.; Li, G.; Lou, S.; Zhou, S., Controlled synthesis of homogeneous Ag nanosheet-assembled film for effective SERS substrate. *ACS Appl Mater Interfaces* **2013,** *5* (15), 7308-14.

71. Zhang, L., Self-assembly Ag nanoparticle monolayer film as SERS Substrate for pesticide detection. *Applied Surface Science* **2013,** *270* (0), 292-294.

72. Hepel, M.; Zhong, C.-J., *Functional Nanoparticles for Bioanalysis, Nanomedicine, and Bioelectronic Devices Volume 2*. American Chemical Society: 2012; Vol. 1113, p 0.

73. Lee, S. J.; Morrill, A. R.; Moskovits, M., Hot Spots in Silver Nanowire Bundles for Surface-Enhanced Raman Spectroscopy. *Journal of the American Chemical Society* **2006,** *128* (7), 2200-2201.

74. Zheng, G.; Patolsky, F.; Cui, Y.; Wang, W. U.; Lieber, C. M., Multiplexed electrical detection of cancer markers with nanowire sensor arrays. *Nature Biotechnology* **2005,** *23* (10), 1294-1301.

75. Tang, J.; Zhao, Q.; Zhang, N.; Man, S.-Q., Facile fabrication of large-area and uniform silica nanospheres monolayer for efficient surface-enhanced Raman scattering. *Applied Surface Science* **2014,** *308* (0), 247-252.

76. Li, W.; Camargo, P. H. C.; Lu, X.; Xia, Y., Dimers of Silver Nanospheres: Facile Synthesis and Their Use as Hot Spots for Surface-Enhanced Raman Scattering. *Nano Letters* **2009,** *9* (1), 485-490.

77. Martín, A.; Pescaglini, A.; Schopf, C.; Scardaci, V.; Coull, R.; Byrne, L.; Iacopino, D., Surface-Enhanced Raman Scattering of 4-Aminobenzenethiol on Au Nanorod Ordered Arrays. *The Journal of Physical Chemistry C* **2014,** *118* (24), 13260-13267.

78. Martin, A.; Wang, J. J.; Iacopino, D., Flexible SERS active substrates from ordered vertical Au nanorod arrays. *RSC Advances* **2014,** *4* (38), 20038-20043.

79. Xie, Z.; Tao, J.; Lu, Y.; Lin, K.; Yan, J.; Wang, P.; Ming, H., Polymer optical fiber SERS sensor with gold nanorods. *Optics Communications* **2009,** *282* (3), 439-442.

80. Oh, M. K.; Shin, Y. S.; Lee, C. L.; De, R.; Kang, H.; Yu, N. E.; Kim, B. H.; Kim, J. H.; Yang, J. K., Morphological and SERS Properties of Silver Nanorod Array Films Fabricated by Oblique Thermal Evaporation at Various Substrate Temperatures. *Nanoscale Res Lett* **2015,** *10* (1), 962.

81. Lovera, P.; Creedon, N.; Alatawi, H.; Mitchell, M.; Burke, M.; Quinn, A. J.; O'Riordan, A., Low-cost silver capped polystyrene nanotube arrays as super-hydrophobic substrates for SERS applications. *Nanotechnology* **2014,** *25* (17), 175502.

82. Lovera, P.; Creedon, N.; Alatawi, H.; O'Riordan, A., *Metal capped polystyrene nanotubes arrays as super-hydrophobic substrates for SERS applications*. SPIE: 2014; Vol. 9129.

83. Walker, D. A.; Browne, K. P.; Kowalczyk, B.; Grzybowski, B. A., Self-Assembly of Nanotriangle Superlattices Facilitated by Repulsive Electrostatic Interactions. *Angewandte Chemie International Edition* **2010,** *49* (38), 6760-6763.

84. Kumar-Krishnan, S.; Esparza, R.; Pal, U., Controlled Fabrication of Flower-Shaped Au-Cu Nanostructures Using a Deep Eutectic Solvent and Their Performance in Surface-Enhanced Raman Scattering-Based Molecular Sensing. *ACS Omega* **2020,** *5* (7), 3699-3708.

85. Liu, Z.; Yang, Z.; Peng, B.; Cao, C.; Zhang, C.; You, H.; Xiong, Q.; Li, Z.; Fang, J., Highly Sensitive, Uniform, and Reproducible Surface - Enhanced Raman Spectroscopy from Hollow Au - Ag Alloy Nanourchins. *Advanced Materials* **2014,** *26* (15), 2431-2439.

86. Yang, M.; Alvarez-Puebla, R. n.; Kim, H.-S.; Aldeanueva-Potel, P.; Liz-Marzá n, L. M.; Kotov, N. A., SERS-Active Gold Lace Nanoshells with Built-in Hotspots. *Nano Letters* **2010,** *10* (10), 4013-4019.

87. Barbillon, G., Applications of Shell-Isolated Nanoparticle-Enhanced Raman Spectroscopy. *Photonics* **2021,** *8* (2), 46.

88. Barbillon, G.; Ivanov, A.; Sarychev, A. K., Hybrid Au/Si Disk-Shaped Nanoresonators on Gold Film for Amplified SERS Chemical Sensing. *Nanomaterials* **2019,** *9* (11), 1588.

89. Vigderman, L.; Zubarev, E. R., Starfruit-Shaped Gold Nanorods and Nanowires: Synthesis and SERS Characterization. *Langmuir* **2012,** *28* (24), 9034-9040.

90. Li, H.; Wang, Y.; Li, Y.; Zhang, J.; Qiao, Y.; Wang, Q.; Che, G., Fabrication of pollutant-resistance SERS imprinted sensors based on SiO2@TiO2@Ag composites for selective detection of pyrethroids in water. *Journal of Physics and Chemistry of Solids* **2020,** *138*, 109254.

91. Krishnan, S. K.; Chipatecua Godoy, Y., Deep Eutectic Solvent-Assisted Synthesis of Au Nanostars Supported on Graphene Oxide as an Efficient Substrate for SERS-Based Molecular Sensing. *ACS Omega* **2020,** *5* (3), 1384-1393.

92. Zhu, C.; Meng, G.; Huang, Q.; Huang, Z.; Chu, Z., Au Hierarchical Micro/Nanotower Arrays and Their Improved SERS Effect by Ag Nanoparticle Decoration. *Crystal Growth & Design* **2011,** *11* (3), 748-752.

93. Subramanian, B.; Theriault, G.; Robichaud, J.; Tchoukanova, N.; Djaoued, Y., Large-area crack-free Au-SiO2 2D inverse opal composite films: Fabrication and SERS applications. *Mater. Chem. Phys.* **2020,** *244*, 9.

94. Barbillon, G., Latest Novelties on Plasmonic and Non-Plasmonic Nanomaterials for SERS Sensing. *Nanomaterials* **2020,** *10* (6), 1200.

95. Sun, Y.; Xia, Y., Shape-controlled synthesis of gold and silver nanoparticles. *Science* **2002,** *298* (5601), 2176-2179.

96. Chen, J.; McLellan, J. M.; Siekkinen, A.; Xiong, Y.; Li, Z.-Y.; Xia, Y., Facile Synthesis of Gold−Silver Nanocages with Controllable Pores on the Surface. *Journal of the American Chemical Society* **2006,** *128* (46), 14776-14777.

97. Ye, J.; Van Dorpe, P.; Van Roy, W.; Borghs, G.; Maes, G., Fabrication, Characterization, and Optical Properties of Gold Nanobowl Submonolayer Structures. *Langmuir* **2009,** *25* (3), 1822-1827.

98. Kuttner, C.; Mayer, M.; Dulle, M.; Moscoso, A.; López-Romero, J. M.; Förster, S.; Fery, A.; Pérez-Juste, J.; Contreras-Cáceres, R., Seeded Growth Synthesis of Gold Nanotriangles: Size Control, SAXS Analysis, and SERS Performance. *ACS Applied Materials & Interfaces* **2018,** *10* (13), 11152-11163.

99. Li, C.; Shuford, K. L.; Chen, M.; Lee, E. J.; Cho, S. O., A Facile Polyol Route to Uniform Gold Octahedra with Tailorable Size and Their Optical Properties. *ACS Nano* **2008,** *2* (9), 1760-1769.

100. Nguyen, P.-D.; Zhang, X.; Su, J., One-Step Controlled Synthesis of Size-Tunable Toroidal Gold Particles for Biochemical Sensing. *ACS Applied Nano Materials* **2019,** *2* (12), 7839-7847.

101. Qiu, Y. H.; Ding, S. J.; Lin, Y. J.; Chen, K.; Yang, D. J.; Ma, S.; Li, X.; Lin, H. Q.; Wang, J.; Wang, Q. Q., Growth of Au Hollow Stars and Harmonic Excitation Energy Transfer. *ACS Nano* **2020,** *14* (1), 736-745.

102. Maier, S. A.; Brongersma, M. L.; Kik, P. G.; Meltzer, S.; Requicha, A. A.; Atwater, H. A., Plasmonics—a route to nanoscale optical devices. *Advanced Materials* **2001,** *13* (19), 1501-1505.

103. Alvarez-Puebla, R.; Liz-Marzán, L. M.; García de Abajo, F. J., Light Concentration at the Nanometer Scale. *The Journal of Physical Chemistry Letters* **2010,** *1* (16), 2428-2434.

104. Aroca, R.; Alvarez-Puebla, R.; Pieczonka, N.; Sanchez-Cortez, S.; Garcia-Ramos, J., Surface-enhanced Raman scattering on colloidal nanostructures. *Advances in Colloid and Interface Science* **2005,** *116* (1-3), 45-61.

105. Lee, P. C.; Meisel, D., Adsorption and surface-enhanced Raman of dyes on silver and gold sols. *The Journal of Physical Chemistry* **1982,** *86* (17), 3391-3395.

106. Rivas, L.; Sanchez-Cortes, S.; García-Ramos, J. V.; Morcillo, G., Mixed Silver/Gold Colloids: A Study of Their Formation, Morphology, and Surface-Enhanced Raman Activity. *Langmuir* **2000,** *16* (25), 9722-9728.

107. Faulds, K.; Littleford, R. E.; Graham, D.; Dent, G.; Smith, W. E., Comparison of Surface-Enhanced Resonance Raman Scattering from Unaggregated and Aggregated Nanoparticles. *Analytical Chemistry* **2004,** *76* (3), 592-598.

108. Schopf, C.; Martín, A.; Burke, M.; Jones, D.; Pescaglini, A.; O'Riordan, A.; Quinn, A. J.; Iacopino, D., Au nanorod plasmonic superstructures obtained by a

combined droplet evaporation and stamping method. *Journal of Materials Chemistry C* **2014,** *2* (18), 3536-3541.

109. Yang, J.-K.; Kang, H.; Lee, H.; Jo, A.; Jeong, S.; Jeon, S.-J.; Kim, H.-I.; Lee, H.-Y.; Jeong, D. H.; Kim, J.-H., Single-step and rapid growth of silver nanoshells as SERS-active nanostructures for label-free detection of pesticides. *ACS Applied Materials & Interfaces* **2014,** *6* (15), 12541-12549.

110. Aroca, R. F.; Goulet, P. J. G.; dos Santos, D. S.; Alvarez-Puebla, R. A.; Oliveira, O. N., Silver Nanowire Layer-by-Layer Films as Substrates for Surface-Enhanced Raman Scattering. *Analytical Chemistry* **2005,** *77* (2), 378-382.

111. Freeman, R. G.; Grabar, K. C.; Allison, K. J.; Bright, R. M.; Davis, J. A.; Guthrie, A. P.; Hommer, M. B.; Jackson, M. A.; Smith, P. C.; Walter, D. G., Self-assembled metal colloid monolayers: an approach to SERS substrates. *Science* **1995,** *267* (5204), 1629-1632.

112. Wang, Z.; Pan, S.; Krauss, T. D.; Du, H.; Rothberg, L. J., The structural basis for giant enhancement enabling single-molecule Raman scattering. *Proceedings of the National Academy of Sciences* **2003,** *100* (15), 8638-8643.

113. Fan, M.; Brolo, A. G., Silver nanoparticles self assembly as SERS substrates with near single molecule detection limit. *Physical Chemistry Chemical Physics* **2009,** *11* (34), 7381-7389.

114. Yu, W. W.; White, I. M., A simple filter-based approach to surface enhanced Raman spectroscopy for trace chemical detection. *Analyst* **2012,** *137* (5), 1168-1173.

115. Shiohara, A.; Langer, J.; Polavarapu, L.; Liz-Marzan, L. M., Solution processed polydimethylsiloxane/gold nanostar flexible substrates for plasmonic sensing. *Nanoscale* **2014,** *6* (16), 9817-9823.

116. Polavarapu, L.; La Porta, A.; Novikov, S. M.; Coronado-Puchau, M.; Liz-Marzan, L. M., Pen-on-Paper Approach Toward the Design of Universal Surface Enhanced Raman Scattering Substrates. *Small* **2014,** *10* (15), 3065-3071.

117. Lee, C. H.; Tian, L.; Singamaneni, S., Paper-based SERS swab for rapid trace detection on real-world surfaces. *ACS Applied Materials & Interfaces* **2010,** *2* (12), 3429-3435.

118. Chen, J. M.; Huang, Y. J.; Kannan, P.; Zhang, L.; Lin, Z. Y.; Zhang, J. W.; Chen, T.; Guo, L. H., Flexible and Adhesive Surface Enhance Raman Scattering Active Tape

for Rapid Detection of Pesticide Residues in Fruits and Vegetables. *Analytical Chemistry* **2016,** *88* (4), 2149-2155.

119. Restaino, S. M.; White, I. M., A critical review of flexible and porous SERS sensors for analytical chemistry at the point-of-sample. *Anal Chim Acta* **2019,** *1060*, 17-29.

120. Kahl, M.; Voges, E.; Kostrewa, S.; Viets, C.; Hill, W., Periodically structured metallic substrates for SERS. *Sensors and Actuators B: Chemical* **1998,** *51* (1–3), 285-291.

121. Yu, Q.; Guan, P.; Qin, D.; Golden, G.; Wallace, P. M., Inverted Size-Dependence of Surface-Enhanced Raman Scattering on Gold Nanohole and Nanodisk Arrays. *Nano Letters* **2008,** *8* (7), 1923-1928.

122. Wu, T.; Lin, Y.-W., Surface-enhanced Raman scattering active gold nanoparticle/nanohole arrays fabricated through electron beam lithography. *Applied Surface Science* **2018,** *435*, 1143-1149.

123. Krishnamoorthy, S.; Krishnan, S.; Thoniyot, P.; Low, H. Y., Inherently Reproducible Fabrication of Plasmonic Nanoparticle Arrays for SERS by Combining Nanoimprint and Copolymer Lithography. *ACS Applied Materials & Interfaces* **2011,** *3* (4), 1033-1040.

124. Robinson, C.; Justice, J.; Petäjä, J.; Karppinen, M.; Corbett, B.; O'Riordan, A.; Lovera, P., Nanoimprint Lithography–Based Fabrication of Plasmonic Array of Elliptical Nanoholes for Dual-Wavelength, Dual-Polarisation Refractive Index Sensing. *Plasmonics* **2019,** *14* (4), 951-959.

125. Diebold, E. D.; Mack, N. H.; Doorn, S. K.; Mazur, E., Femtosecond Laser-Nanostructured Substrates for Surface-Enhanced Raman Scattering. *Langmuir* **2009,** *25* (3), 1790-1794.

126. Atanasov, P. A.; Nedyalkov, N. N.; Nikov, R. G.; Fukata, N.; Jevasuwan, W.; Subramani, T.; Hirsch, D.; Rauschenbach, B., SERS analyses of thiamethoxam assisted by Ag films and nanostructures produced by laser techniques. *Journal of Raman Spectroscopy* **2018,** *49* (3), 397-403.

127. Xueyan Bian, J. X., Jing Yang, Ka-lam Chiu, Shouxiang Jiang, Flexible Ag SERS substrate for non-destructive and rapid detection of toxic materials on irregular surface. *Surfaces and Interfaces* **2021,** *23* (2468-0230).

128. Li, L.; Yang, S. Y.; Duan, J. L.; Huang, L.; Xiao, G. N., Fabrication and SERS performance of silver nanoarrays by inkjet printing silver nanoparticles ink on the gratings of compact disc recordable. *Spectrochimica Acta Part a-Molecular and Biomolecular Spectroscopy* **2020,** *225*.

129. Huebner, U.; Boucher, R.; Schneidewind, H.; Cialla, D.; Popp, J., Microfabricated SERS-arrays with sharp-edged metallic nanostructures. *Microelectronic Engineering* **2008,** *85* (8), 1792-1794.

130. Li, K.; Clime, L.; Cui, B.; Veres, T., Surface enhanced Raman scattering on long-range ordered noble-metal nanocrescent arrays. *Nanotechnology* **2008,** *19* (14), 145305.

131. Wang, Y.; Wang, Y.; Wang, H.; Cong, M.; Xu, W.; Xu, S., Surface-enhanced Raman scattering on a hierarchical structural Ag nano-crown array in different detection ways. *Physical Chemistry Chemical Physics* **2015,** *17* (2), 1173-1179.

132. Huang, Z.; Meng, G.; Huang, Q.; Chen, B.; Zhu, C.; Zhang, Z., Large‐area Ag nanorod array substrates for SERS: AAO template‐assisted fabrication, functionalization, and application in detection PCBs. *Journal of Raman Spectroscopy* **2013,** *44* (2), 240-246.

133. Shi, G.; Wang, M.; Zhu, Y.; Yan, X.; Pan, S.; Zhang, A., Nanoflower-like Ag/AAO SERS platform with quasi-photonic crystal nanostructure for efficient detection of goat serum. *Current Applied Physics* **2019,** *19* (11), 1276-1285.

134. Wang, J. Y.; Zhang, J. Y.; Wang, J.; Fang, G. Z.; Liu, J. F.; Wang, S., Fluorescent peptide probes for organophosphorus pesticides detection. *J. Hazard. Mater.* **2020,** *389*, 8.

135. Lin, B.; Kannan, P.; Qiu, B.; Lin, Z.; Guo, L., On-spot surface enhanced Raman scattering detection of Aflatoxin B1 in peanut extracts using gold nanobipyramids evenly trapped into the AAO nanoholes. *Food Chemistry* **2020,** *307*, 125528.

136. Hu, M.; Ou, F. S.; Wu, W.; Naumov, I.; Li, X.; Bratkovsky, A. M.; Williams, R. S.; Li, Z., Gold Nanofingers for Molecule Trapping and Detection. *Journal of the American Chemical Society* **2010,** *132* (37), 12820-12822.

137. Yang, J., Li, J., Du, Z, Laser Hybrid Micro/nano-structuring of Si Surfaces in Air and its Applications for SERS Detection. *Scientific Reports* **2014,** *4*, 6657.

138. Indrė Aleknavičienė, E. P., Martynas Talaikis, Marija Jankunec, Gediminas Račiukaitis, Low-cost SERS substrate featuring laser-ablated amorphous nanostructure. *Applied Surface Science* **2022,** *571* (0169-4332).

139. Li, L.; Yang, S.; Duan, J.; Huang, L.; Xiao, G., Fabrication and SERS performance of silver nanoarrays by inkjet printing silver nanoparticles ink on the gratings of compact disc recordable. *Spectrochim Acta A Mol Biomol Spectrosc* **2020,** *225*, 117598.

140. He, D. Y.; Wu, Z. Z.; Cui, B.; Xu, E. B., Aptamer and gold nanorod-based fumonisin B1 assay using both fluorometry and SERS. *Microchimica Acta* **2020,** *187* (4).

141. Yu, B.; Ge, M.; Li, P.; Xie, Q.; Yang, L., Development of surface-enhanced Raman spectroscopy application for determination of illicit drugs: Towards a practical sensor. *Talanta* **2019,** *191*, 1-10.

142. D'Apuzzo, F.; Sengupta, R. N.; Overbay, M.; Aronoff, J. S.; Rogacs, A.; Barcelo, S. J., A Generalizable Single-Chip Calibration Method for Highly Quantitative SERS via Inkjet Dispense. *Analytical Chemistry* **2020,** *92* (1), 1372-1378.

143. Joshi, P.; Santhanam, V., Inkjet-Based Fabrication Process with Control over the Morphology of SERS-Active Silver Nanostructures. *Industrial & Engineering Chemistry Research* **2018,** *57* (15), 5250-5258.

144. Kumar, A.; Santhanam, V., Paper swab based SERS detection of non-permitted colourants from dals and vegetables using a portable spectrometer. *Analytica Chimica Acta* **2019,** *1090*, 106-113.

145. Li, L.; Xiao, G. N., Research Progress of Preparing Surface-Enhanced Raman Scattering Active Substrates by Printing Technologies. *Spectroscopy and Spectral Analysis* **2019,** *39* (11), 3326-3332.

146. Micciche, C.; Arrabito, G.; Amato, F.; Buscarino, G.; Agnello, S.; Pignataro, B., Inkjet printing Ag nanoparticles for SERS hot spots. *Analytical Methods* **2018,** *10* (26), 3215-3223.

147. Oravec, M.; Sasinkova, V.; Tomanova, K.; Gal, L.; Parciova, S.; Huck, C. W., In-situ surface-enhanced Raman scattering and FT-Raman spectroscopy of black prints. *Vibrational Spectroscopy* **2018,** *94*, 16-21.

148. Weng, G. J.; Yang, Y.; Zhao, J.; Zhu, J.; Li, J. J.; Zhao, J. W., Preparation and SERS performance of Au NP/paper strips based on inkjet printing and seed mediated growth: The effect of silver ions. *Solid State Communications* **2018,** *272*, 67-73.

149. Yu, W. W.; White, I. M., Inkjet-printed paper-based SERS dipsticks and swabs for trace chemical detection. *Analyst* **2013,** *138* (4), 1020-1025.

150. Kleinman, S. L.; Frontiera, R. R.; Henry, A.-I.; Dieringer, J. A.; Van Duyne, R. P., Creating, characterizing, and controlling chemistry with SERS hot spots. *Physical Chemistry Chemical Physics* **2013,** *15* (1), 21-36.

151. Martin, C. R., Nanomaterials: a membrane-based synthetic approach. *Science* **1994,** *266* (5193), 1961-1966.

152. Ruan, C.; Eres, G.; Wang, W.; Zhang, Z.; Gu, B., Controlled Fabrication of Nanopillar Arrays as Active Substrates for Surface-Enhanced Raman Spectroscopy. *Langmuir* **2007,** *23* (10), 5757-5760.

153. Dickey, M. D.; Weiss, E. A.; Smythe, E. J.; Chiechi, R. C.; Capasso, F.; Whitesides, G. M., Fabrication of Arrays of Metal and Metal Oxide Nanotubes by Shadow Evaporation. *ACS Nano* **2008,** *2* (4), 800-808.

154. Batista, E. A.; dos Santos, D. P.; Andrade, G. F. S.; Sant'Ana, A. C.; Brolo, A. G.; Temperini, M. L. A., Using Polycarbonate Membranes as Templates for the Preparation of Au Nanostructures for Surface-Enhanced Raman Scattering. *Journal of Nanoscience and Nanotechnology* **2009,** *9* (5), 3233-3238.

155. Penn, M. A.; Drake, D. M.; Driskell, J. D., Accelerated Surface-Enhanced Raman Spectroscopy (SERS)-Based Immunoassay on a Gold-Plated Membrane. *Analytical Chemistry* **2013,** *85* (18), 8609-8617.

156. Wigginton, K. R.; Vikesland, P. J., Gold-coated polycarbonate membrane filter for pathogen concentration and SERS-based detection. *Analyst* **2010,** *135* (6), 1320-1326.

157. Piao, L.; Park, S.; Lee, H. B.; Kim, K.; Kim, J.; Chung, T. D., Single Gold Microshell Tailored to Sensitive Surface Enhanced Raman Scattering Probe. *Analytical Chemistry* **2010,** *82* (1), 447-451.

158. Wang, J. J.; Zhou, F.; Duan, G. T.; Li, Y.; Liu, G. Q.; Su, F. H.; Cai, W. P., A controlled Ag-Au bimetallic nanoshelled microsphere array and its improved surface-enhanced Raman scattering effect. *RSC Advances* **2014,** *4* (17), 8758-8763.

159. Zhao, Y. H.; Luo, W. Q.; Kanda, P.; Cheng, H. W.; Chen, Y. Y.; Wang, S. P.; Huan, S. Y., Silver deposited polystyrene (PS) microspheres for surface-enhanced Raman spectroscopic-encoding and rapid label-free detection of melamine in milk powder. *Talanta* **2013,** *113*, 7-13.

160. Charconnet, M.; Kuttner, C.; Plou, J.; García-Pomar, J. L.; Mihi, A.; Liz-Marzán, L. M.; Seifert, A., Mechanically Tunable Lattice-Plasmon Resonances by Templated Self-Assembled Superlattices for Multi-Wavelength Surface-Enhanced Raman Spectroscopy. *Small Methods n/a* (n/a), 2100453.

161. Krishnamoorthy, S.; Krishnan, S.; Thoniyot, P.; Low, H. Y., Inherently reproducible fabrication of plasmonic nanoparticle arrays for SERS by combining nanoimprint and copolymer lithography. *ACS Appl Mater Interfaces* **2011,** *3* (4), 1033-40.

162. Bard, A. J.; Faulkner, L. R.; Leddy, J.; Zoski, C. G., *Electrochemical methods: Fundamentals and Applications*. Wiley New York, 1980; Vol. 2.

163. Chisanga, M.; Linton, D.; Muhamadali, H.; Ellis, D. I.; Kimber, R. L.; Mironov, A.; Goodacre, R., Rapid differentiation of Campylobacter jejuni cell wall mutants using Raman spectroscopy, SERS and mass spectrometry combined with chemometrics. *Analyst* **2020,** *145* (4), 1236-1249.

164. Lan, L. L.; Hou, X. Y.; Gao, Y. M.; Fan, X. C.; Qiu, T., Inkjet-printed paper-based semiconducting substrates for surface-enhanced Raman spectroscopy. *Nanotechnology* **2020,** *31* (5).

165. Li, Z. B.; Zhang, L. J.; He, X.; Chen, B. S., Urchin-like ZnO-nanorod arrays templated growth of ordered hierarchical Ag/ZnO hybrid arrays for surface-enhanced Raman scattering. *Nanotechnology* **2020,** *31* (16).

166. Wu, Z. G.; Liu, Y. M.; Wu, M. M.; Chen, Y.; Chen, Y. N.; Xian, H. H.; Wang, X. P.; Wei, H. Y., Preparation and Surface Enhanced Raman Spectroscopy of Au/TiN Composite Films. *Spectroscopy and Spectral Analysis* **2020,** *40* (2), 420-426.

167. Lu, S. C.; You, T. T.; Yang, N.; Gao, Y. K.; Yin, P. G., Flexible SERS substrate based on Ag nanodendrite-coated carbon fiber cloth: simultaneous detection for multiple pesticides in liquid droplet. *Analytical and Bioanalytical Chemistry* **2020,** *412* (5), 1159-1167.

168. Zavatski, S.; Redko, S.; Bandarenka, H., Shelf Life Improvement of SERS-Active Substrates Based on Copper and Porous Aluminum Oxide. *International Journal of Nanoscience* **2019,** *18* (3-4).

169. Lu, S. C.; You, T. T.; Gao, Y. K.; Yang, N.; Zhang, C. M.; Yin, P. G., Rapid fabrication of three-dimensional flower-like gold microstructures on flexible substrate for SERS applications. *Spectrochimica Acta Part a-Molecular and Biomolecular Spectroscopy* **2019,** *212*, 371-379.

170. Klutse, C. K.; Mayer, A.; Wittkamper, J.; Cullum, B. M., Applications of Self-Assembled Monolayers in Surface-Enhanced Raman Scattering. *Journal of Nanotechnology* **2012,** *2012*, 319038.

171. Frederik Tielens, E. S., AuS and SH Bond Formation/Breaking during the Formation of Alkanethiol SAMs on Au(111): A Theoretical Study. *The Journal of Physical Chemistry C 114* (20), 9444-9452.

172. Meirav Cohen-Atiya, D. M., Studying thiol adsorption on Au, Ag and Hg surfaces by potentiometric measurements. *Journal of Electroanalytical Chemistry* **2003,** *550–551*, 267-276.

173. Xue, Y.; Li, X.; Li, H.; Zhang, W., Quantifying thiol–gold interactions towards the efficient strength control. *Nature Communications* **2014,** *5* (1), 4348.

174. Michael S. Inkpen, Z. F. L., Haixing Li, Luis M. Campos, Jeffrey B. Neaton & Latha Venkataraman, Non-chemisorbed gold–sulfur binding prevails in self-assembled monolayers. *Nature Chemistry* **2019,** *11*, 351–358.

175. Henrik Grönbeck, A. C., and Wanda Andreoni, Thiols and Disulfides on the Au(111) Surface: The Headgroup−Gold Interaction. *Journal of the American Chemical Society* **2000,** *122* (16), 3839–3842.

176. Levin, C. S.; Bishnoi, S. W.; Grady, N. K.; Halas, N. J., Determining the Conformation of Thiolated Poly(ethylene glycol) on Au Nanoshells by Surface-Enhanced Raman Scattering Spectroscopic Assay. *Analytical Chemistry* **2006,** *78* (10), 3277-3281.

177. Yang, E. L.; Li, D.; Yin, P. K.; Xie, Q. Y.; Li, Y.; Lin, Q. Y.; Duan, Y. X., A novel surface-enhanced Raman scattering (SERS) strategy for ultrasensitive detection of bacteria based on three-dimensional (3D) DNA walker. *Biosensors & Bioelectronics* **2021,** *172*.

178. Agnieszka Kamińska, K. W., Aneta Kowalska, Evelin Witkowska, Tomasz Szymborski, Anna Janeczek , Jacek Waluk SERS-based Immunoassay in a Microfluidic System for the Multiplexed Recognition of Interleukins from Blood Plasma: Towards Picogram Detection. *Scientific Reports* **2017,** *7*, 10656.

179. Oss, C. J. v., Antibody–Antigen Intermolecular Forces. *Encyclopedia of Immunology (Second Edition)* **1998**, 163-167.

180. Kamińska, A.; Winkler, K.; Kowalska, A.; Witkowska, E.; Szymborski, T.; Janeczek, A.; Waluk, J., SERS-based Immunoassay in a Microfluidic System for the Multiplexed Recognition of Interleukins from Blood Plasma: Towards Picogram Detection. *Scientific Reports* **2017,** *7* (1), 10656.

181. He, X.; Zhou, X.; Liu, Y.; Wang, X. L., Ultrasensitive, recyclable and portable microfluidic surface-enhanced raman scattering (SERS) biosensor for uranyl ions detection. *Sensors and Actuators B-Chemical* **2020,** *311*.

182. Huang, D. D.; Chen, J. M.; Ding, L.; Guo, L. H.; Kannan, P.; Luo, F.; Qiu, B.; Lin, Z. Y., Core-satellite assemblies and exonuclease assisted double amplification strategy for ultrasensitive SERS detection of biotoxin. *Analytica Chimica Acta* **2020,** *1110*, 56-63.

183. Wang, J. R.; Xia, C.; Yang, L.; Li, Y. F.; Li, C. M.; Huang, C. Z., DNA Nanofirecrackers Assembled through Hybridization Chain Reaction for Ultrasensitive SERS Immunoassay of Prostate Specific Antigen. *Analytical Chemistry* **2020,** *92* (5), 4046-4052.

184. Wang, Q.; Hu, Y. J.; Jiang, N. J.; Wang, J. J.; Yu, M.; Zhuang, X. M., Preparation of Aptamer Responsive DNA Functionalized Hydrogels for the Sensitive Detection of alpha-Fetoprotein Using SERS Method. *Bioconjugate Chemistry* **2020,** *31* (3), 813-820.

185. Zhou, S. S.; Lu, C.; Li, Y. Z.; Xue, L.; Zhao, C. Y.; Tian, G. F.; Bao, Y. M.; Tang, L. H.; Lin, J. H.; Zheng, J. K., Gold Nanobones Enhanced Ultrasensitive Surface-Enhanced Raman Scattering Aptasensor for Detecting Escherichia coil O157:H7. *Acs Sensors* **2020,** *5* (2), 588-596.

186. Chen, Q.; Wu, Q.; Zhang, Q.; Hu, J., Surface-Enhanced Raman Scattering from Self-Assembled Film of Thiolated Peg-Modified Gold Nanoparticles. *Journal of Applied Spectroscopy* **2017,** *84* (3), 407-412.

187. Kreno, L. E.; Greeneltch, N. G.; Farha, O. K.; Hupp, J. T.; Van Duyne, R. P., SERS of molecules that do not adsorb on Ag surfaces: a metal–organic framework-based functionalization strategy. *Analyst* **2014,** *139* (16), 4073-4080.

188. Marshall, A. R. L.; Stokes, J.; Viscomi, F. N.; Proctor, J. E.; Gierschner, J.; Bouillard, J.-S. G.; Adawi, A. M., Determining molecular orientation via single molecule SERS in a plasmonic nano-gap. *Nanoscale* **2017,** *9* (44), 17415-17421.

189. Sun, C.; Chen, T.; Ruan, W.; Zhao, B.; Cong, Q., Controlling the orientation of probe molecules on surface-enhanced Raman scattering substrates: A novel strategy to improve sensitivity. *Analytica Chimica Acta* **2017,** *994*, 65-72.

190. Morton, S. M.; Jensen, L., Understanding the Molecule−Surface Chemical Coupling in SERS. *Journal of the American Chemical Society* **2009,** *131* (11), 4090-4098.

191. Hong, Y.; Wang, R.; Jiang, Z.; Cong, Z.; Song, H., Rapid SERS Detection of Thiol-Containing Natural Products in Culturing Complex. *International journal of analytical chemistry* **2020,** *2020*, 9271236.

192. Madzharova, F.; Heiner, Z.; Kneipp, J., Surface-Enhanced Hyper Raman Spectra of Aromatic Thiols on Gold and Silver Nanoparticles. *The Journal of Physical Chemistry C* **2020,** *124* (11), 6233-6241.

193. Wang, K.; Li, J., Reliable SERS detection of pesticides with a large-scale self-assembled Au@4-MBA@Ag nanoparticle array. *Spectrochimica Acta Part A: Molecular and Biomolecular Spectroscopy* **2021,** *263*, 120218.

194. de Barros, A.; Shimizu, F. M.; de Oliveira, C. S.; Sigoli, F. A.; dos Santos, D. P.; Mazali, I. O., Dynamic Behavior of Surface-Enhanced Raman Spectra for Rhodamine 6G Interacting with Gold Nanorods: Implication for Analyses under Wet versus Dry Conditions. *ACS Applied Nano Materials* **2020,** *3* (8), 8138-8147.

195. Chen, H.; You, T.; Jiang, L.; Gao, Y.; Yin, P., Creating dynamic SERS hotspots on the surface of pH-responsive microgels for direct detection of crystal violet in solution. *RSC Advances* **2017,** *7* (52), 32743-32748.

196. Marques, F. C.; Alves, R. S.; dos Santos, D. P.; Andrade, G. F. S., Surface-enhanced Raman spectroscopy of one and a few molecules of acid 4-mercaptobenzoic in AgNP enabled by hot spots generated by hydrogen bonding. *Physical Chemistry Chemical Physics* **2022,** *24* (44), 27449-27458.

197. Zaim, M.; Jambulingam, P. *Global insecticide use for vector-borne disease control*; World Health Organization: 2007.

198. Kozawa, K.; Aoyama, Y.; Mashimo, S.; Kimura, H., Toxicity and actual regulation of organophosphate pesticides. *Toxin Reviews* **2009,** *28* (4), 245-254.

199. Rosenstock, L.; Keifer, M.; Daniell, W. E.; McConnell, R.; Claypoole, K.; Group, P. H. E. S., Chronic central nervous system effects of acute organophosphate pesticide intoxication. *The Lancet* **1991,** *338* (8761), 223-227.

200. Eskenazi, B.; Bradman, A.; Castorina, R., Exposures of children to organophosphate pesticides and their potential adverse health effects. *Environmental Health Perspectives* **1999,** *107* (Suppl 3), 409.

201. Stephens, R.; Spurgeon, A.; Calvert, I. A.; Beach, J.; Levy, L. S.; Harrington, J.; Berry, H., Neuropsychological effects of long-term exposure to organophosphates in sheep dip. *The Lancet* **1995,** *345* (8958), 1135-1139.

202. Fries, E.; Püttmann, W., Occurrence of organophosphate esters in surface water and ground water in Germany. *Journal of Environmental Monitoring* **2001,** *3* (6), 621-626.

203. Karalliedde, L.; Eddleston, M.; Murray, V., *The global picture of organophosphate insecticide poisoning*. World Scientific: 2001; p 431-471.

204. Banks, K. E.; Hunter, D. H.; Wachal, D. J., Chlorpyrifos in surface waters before and after a federally mandated ban. *Environment International* **2005,** *31* (3), 351-356.

205. Pogačnik, L.; Franko, M., Determination of organophosphate and carbamate pesticides in spiked samples of tap water and fruit juices by a biosensor with photothermal detection. *Biosensors and Bioelectronics* **1999,** *14* (6), 569-578.

206. Hou, R.; Pang, S.; He, L., In situ SERS detection of multi-class insecticides on plant surfaces. *Analytical Methods* **2015,** *7* (15), 6325-6330.

207. Liu, B.; Han, G.; Zhang, Z.; Liu, R.; Jiang, C.; Wang, S.; Han, M.-Y., Shell Thickness-Dependent Raman Enhancement for Rapid Identification and Detection of Pesticide Residues at Fruit Peels. *Analytical Chemistry* **2012,** *84* (1), 255-261.

208. Chen, J.; Huang, Y.; Kannan, P.; Zhang, L.; Lin, Z.; Zhang, J.; Chen, T.; Guo, L., Flexible and Adhesive Surface Enhance Raman Scattering Active Tape for Rapid Detection of Pesticide Residues in Fruits and Vegetables. *Analytical Chemistry* **2016,** *88* (4), 2149-2155.

209. Li, J. F.; Huang, Y. F.; Ding, Y.; Yang, Z. L.; Li, S. B.; Zhou, X. S.; Fan, F. R.; Zhang, W.; Zhou, Z. Y.; Wu, D. Y.; Ren, B.; Wang, Z. L.; Tian, Z. Q., Shell-isolated nanoparticle-enhanced Raman spectroscopy. *Nature* **2010,** *464* (7287), 392-395.

210. Chen, X.; Wang, D. H.; Li, J.; Xu, T. T.; Lai, K. Q.; Ding, Q.; Lin, H. T.; Sun, L.; Lin, M. S., A spectroscopic approach to detect and quantify phosmet residues in Oolong tea by surface-enhanced Raman scattering and silver nanoparticle substrate. *Food Chemistry* **2020,** *312*.

211. Jiang, L.; Gu, K. J.; Liu, R. Y.; Jin, S. Z.; Wang, H. Q.; Pan, C. P., Rapid detection of pesticide residues in fruits by surface-enhanced Raman scattering based on modified QuEChERS pretreatment method with portable Raman instrument. *Sn Applied Sciences* **2019,** *1* (6).

212. Weng, S. Z.; Zhu, W. X.; Dong, R. L.; Zheng, L.; Wang, F., Rapid Detection of Pesticide Residues in Paddy Water Using Surface-Enhanced Raman Spectroscopy. *Sensors* **2019,** *19* (3).

213. Kang, Y.; Wu, T.; Chen, W. C.; Li, L.; Du, Y. P., A novel metastable state nanoparticle-enhanced Raman spectroscopy coupled with thin layer chromatography for determination of multiple pesticides. *Food Chemistry* **2019,** *270*, 494-501.

214. Kang, Y.; Li, L.; Chen, W. C.; Zhang, F. Y.; Du, Y. P.; Wu, T., Rapid In Situ SERS Analysis of Pesticide Residues on Plant Surfaces Based on Micelle Extraction of Targets and Stabilization of Ag Nanoparticle Aggregates. *Food Analytical Methods* **2018,** *11* (11), 3161-3169.

215. Lee, H.; Liao, J. D.; Sivashanmugan, K.; Liu, B. H.; Fu, W. E.; Chen, C. C.; Chen, G. D.; Juang, Y. D., Gold Nanoparticle-Coated ZrO2-Nanofiber Surface as a SERS-Active Substrate for Trace Detection of Pesticide Residue. *Nanomaterials* **2018,** *8* (6).

216. Wang, X.; Du, Y. P.; Zhang, H.; Xu, Y.; Pan, Y. C.; Wu, T.; Hu, H. L., Fast enrichment and ultrasensitive in-situ detection of pesticide residues on oranges with surface-enhanced Raman spectroscopy based on Au nanoparticles decorated glycidyl methacrylate-ethylene dimethacrylate material. *Food Control* **2014,** *46*, 108-114.

217. Huang, D. D.; Zhao, J. C.; Wang, M. L.; Zhu, S. H., Snowflake-like gold nanoparticles as SERS substrates for the sensitive detection of organophosphorus pesticide residues. *Food Control* **2020,** *108*.

218. Yaseen, T.; Pu, H. B.; Sun, D. W., Rapid detection of multiple organophosphorus pesticides (triazophos and parathion-methyl) residues in peach by SERS based on core-shell bimetallic Au@Ag NPs. *Food Additives and Contaminants Part a-Chemistry Analysis Control Exposure & Risk Assessment* **2019,** *36* (5), 762-778.

219. Tang, F.; Zhang, M. Z.; Li, Z. B.; Du, Z. F.; Chen, B. S.; He, X.; Zhao, S. Y., Hexagonally arranged arrays of urchin-like Ag-nanoparticle decorated ZnO-nanorods grafted on PAN-nanopillars as surface-enhanced Raman scattering substrates. *Crystengcomm* **2018,** *20* (25), 3550-3558.

220. Dowgiallo, A. M., Trace level pesticide detection utilizing gold nanoparticles and surface enhanced Raman spectroscopy (SERS). In *Synthesis and Photonics of Nanoscale Materials Xvi*, Kabashin, A. V.; Dubowski, J. J.; Geohegan, D. B., Eds. 2019; Vol. 10907.

221. Yazdi, S. H.; White, I. M., A nanoporous optofluidic microsystem for highly sensitive and repeatable surface enhanced Raman spectroscopy detection. *Biomicrofluidics* **2012,** *6* (1).

222. Fathi, F.; Lagugne-Labarthet, F.; Pedersen, D. B.; Kraatz, H. B., Studies of the interaction of two organophosphonates with nanostructured silver surfaces. *Analyst* **2012,** *137* (19), 4448-4453.

223. Ma, P.; Wang, L. Y.; Xu, L.; Li, J. Y.; Zhang, X. D.; Chen, H., Rapid quantitative determination of chlorpyrifos pesticide residues in tomatoes by surface-enhanced Raman spectroscopy. *European Food Research and Technology* **2020,** *246* (1), 239-251.

224. Dowgiallo, A. M.; Guenther, D. A., Determination of the Limit of Detection of Multiple Pesticides Utilizing Gold Nanoparticles and Surface-Enhanced Raman Spectroscopy. *Journal of Agricultural and Food Chemistry* **2019,** *67* (46), 12642-12651.

225. Tang, J. S.; Chen, W. W.; Ju, H. X., Rapid detection of pesticide residues using a silver nanoparticles coated glass bead as nonplanar substrate for SERS sensing. *Sensors and Actuators B-Chemical* **2019,** *287*, 576-583.

226. Elbert, A.; Haas, M.; Springer, B.; Thielert, W.; Nauen, R., Applied aspects of neonicotinoid uses in crop protection. *Pest Management Science* **2008,** *64* (11), 1099-1105.

227. Jeschke, P.; Nauen, R., Neonicotinoids—from zero to hero in insecticide chemistry. *Pest Management Science* **2008,** *64* (11), 1084-1098.

228. Lee, J. K.; Ahn, K. C.; Park, O. S.; Kang, S. Y.; Hammock, B. D., Development of an ELISA for the Detection of the Residues of the Insecticide Imidacloprid in Agricultural and Environmental Samples. *Journal of Agricultural and Food Chemistry* **2001,** *49* (5), 2159-2167.

229. Watanabe, E.; Baba, K.; Eun, H.; Miyake, S., Application of a commercial immunoassay to the direct determination of insecticide imidacloprid in fruit juices. *Food Chemistry* **2007,** *102* (3), 745-750.

230. Ferrer, I.; Thurman, E. M.; Fernández-Alba, A. R., Quantitation and Accurate Mass Analysis of Pesticides in Vegetables by LC/TOF-MS. *Analytical Chemistry* **2005,** *77* (9), 2818-2825.

231. Obana, H.; Okihashi, M.; Akutsu, K.; Kitagawa, Y.; Hori, S., Determination of Acetamiprid, Imidacloprid, and Nitenpyram Residues in Vegetables and Fruits by High-Performance Liquid Chromatography with Diode-Array Detection. *Journal of Agricultural and Food Chemistry* **2002,** *50* (16), 4464-4467.

232. Liu, S.; Zheng, Z.; Wei, F.; Ren, Y.; Gui, W.; Wu, H.; Zhu, G., Simultaneous Determination of Seven Neonicotinoid Pesticide Residues in Food by Ultraperformance Liquid Chromatography Tandem Mass Spectrometry. *Journal of Agricultural and Food Chemistry* **2010,** *58* (6), 3271-3278.

233. Aguera, A.; Almansa, E.; Malato, S.; Maldonado, M.; Fernandez-Alba, A., Evaluation of photocatalytic degradation of imidacloprid in industrial water by GC-MS and LC-MS. *Analysis* **1998,** *26* (7), 245-251.

234. Navalón, A.; González-Casado, A.; El-Khattabi, R.; Vilchez, J. L.; Fernández-Alba, A. R., Determination of imidacloprid in vegetable samples by gas chromatography–mass spectrometry. *Analyst* **1997,** *122* (6), 579-581.

235. Ding, X.; Zhang, W.; Cheng, D.; He, J.; Yang, K.-L., Oligopeptides functionalized surface plasmon resonance biosensors for detecting thiacloprid and imidacloprid. *Biosensors and Bioelectronics* **2012,** *35* (1), 271-276.

236. Vílchez, J. L.; Valencia, M. C.; Navalón, A.; Molinero-Morales, B.; Capitán-Vallvey, L. F., Flow injection analysis of the insecticide imidacloprid in water samples with photochemically induced fluorescence detection. *Analytica Chimica Acta* **2001,** *439* (2), 299-305.

237. Nauen, R.; Bretschneider, T., New modes of action of insecticides. *Pesticide Outlook* **2002,** *13* (6), 241-245.

238. Tomizawa, M.; Casida, J. E., Neonicotinoid insecticide toxicology: mechanisms of selective action. *Annual Review of Pharmacology and Toxicology* **2005,** *45*, 247-268.

239. Whitehorn, P. R.; O'Connor, S.; Wackers, F. L.; Goulson, D., Neonicotinoid pesticide reduces bumble bee colony growth and queen production. *Science* **2012,** *336* (6079), 351-352.

240. European Commission, Commission Implementing Regulation (EU) No 485/2013 of 24 May 2013 amending Implementing Regulation (EU) No 540/2011, as regards the conditions of approval of the active substances clothianidin, thiamethoxam and imidacloprid, and prohibiting the use and sale of seeds treated with plant protection products containing those active substances. *Official Journal of the European Union* **2013,** *139*, 12-14.

241. European Food Safety Authority, The 2014 European Union Report on Pesticide Residues in Food. *EFSA Journal* **2016,** *14* (10), e04611-n/a.

242. Cao, X. L.; Hong, S. H.; Jiang, Z. J.; She, Y. X.; Wang, S. S.; Zhang, C.; Li, H.; Jin, F.; Jin, M. J.; Wang, J., SERS-active metal-organic frameworks with embedded gold nanoparticles. *Analyst* **2017,** *142* (14), 2640-2647.

243. Yang, T.; Zhao, B.; Hou, R.; Zhang, Z.; Kinchla, A. J.; Clark, J. M.; He, L., Evaluation of the Penetration of Multiple Classes of Pesticides in Fresh Produce Using Surface-Enhanced Raman Scattering Mapping. *J Food Sci* **2016,** *81* (11), T2891-t2901.

244. Wijaya, W.; Pang, S.; Labuza, T. P.; He, L. L., Rapid Detection of Acetamiprid in Foods using Surface-Enhanced Raman Spectroscopy (SERS). *Journal of Food Science* **2014,** *79* (4), T743-T747.

245. Zhou, H.; Xu, L.; Ren, Z.; Zhu, J.; Lee, C., Machine learning-augmented surface-enhanced spectroscopy toward next-generation molecular diagnostics. *Nanoscale Advances* **2023,** *5* (3), 538-570.

246. Brem, S.; Schlücker, S., Surface-Enhanced Raman Spectroscopy and Density Functional Theory Calculations of a Rationally Designed Rhodamine with Thiol Groups at the Xanthene Ring. *The Journal of Physical Chemistry C* **2017,** *121* (28), 15310-15317.

Chapter 2. 2,4-dichlorophenoxyacetic acid (2,4-D) Pesticide Detection using Electrochemically Prepared Silver-Gum Arabic Nanocluster Substrates

This work has been published in *Sensor and Actuator B: chemical.* Volume 364, 1 August 2022, 131851. https://doi.org/10.1016/j.snb.2022.131851.

Author Contributions: Y.Y. (Yuqing Yang) undertook experimental results, including the Raman data analysis and manuscript preparation. P.L. (Pierre Lovera) was responsible for supervising and data analysis & manuscript preparation, and A. O'R. (Alan O'Riordan) was responsible for supervising and manuscript preparation.

Abstract: In this work, we investigated a method to detect 2,4-D pesticide in water environments, using Silver-Gum Arabic (Ag-GA) electrochemically co-deposited substrates. This electrochemical synthesis yields high nanoparticle density and homogeneous substrates (area: 40 µm x 20 µm) with as little as 2 µL of $AgNO_3$ and Gum Arabic mixed solution, using a portable potentiostat. Different morphologies, including Ag-GA spherical nanoparticles and nano dendrites, were synthesized by tuning the deposition parameters. The initial intention was to use the SERS effect to detect 2,4-D. However, no significant change in peak intensity was observed as the analyte concentration increased, contrary to what is typically expected with SERS. Consequently, the sensor did not perform as designed. A change in the peak ratio was observed over a wide range of 2,4-D concentrations, but the slope was very low. This suggests that the detection principle might rely on the local concentration of 2,4-D within the Gum Arabic layer, as more material accumulates with increasing concentrations. It should be noted that the experimental method involved oversampling, a flawed analytical practice that rendered quantification of 2,4-D impossible.

Keywords: Ag-Gum Arabic substrate, electrochemical deposition, 2,4-dichlorophenoxyacetic acid (2,4-D) pesticide detection.

With the world population predicted to reach 9.8 billion by 2050, it is necessary to increase food production accordingly.[1] Unfortunately, crops face numerous threats from insects, diseases, and competing weeds. Therefore, pesticides are widely used to protect crops and increase yield simultaneously. Among these, 2,4-dichlorophenoxyacetic acid (2,4-D, $C_8H_6Cl_2O_3$) is a phenoxy herbicide extensively applied in agriculture to control weeds in corn and grain fields.[2] Unfortunately, there is growing evidence that 2,4-D is harmful to both human health and the environment.[3-4] To prevent or minimize the

negative impacts of the use of pesticides, the European Union has regulated their use and provided strict guidelines for their application. For example, a maximum residue limit (MRL) of 0.1 ppb (parts per billion) for individual pesticides has been established.[5] However, despite these precautions, pesticides can still leach from the ground into water and runoff into nearby water bodies.[6] 2,4-D in particular has good solubility in water and traces above the MRL have been found in rivers and drinking water.[7] To this end, it is necessary to monitor 2,4-D pesticides and possibly prevent pollution events. The most common method currently used to detect 2,4-D in the environment is by applying chromatography to purify the small molecule, followed by mass spectrometry (HLC-MS) to qualitatively identify the herbicides.[8] Unfortunately, this method is time-consuming and requires high-end equipment operated by skilled personnel in dedicated laboratories. To tackle this challenge, numerous methods have been investigated in recent years for simpler 2,4-D detection, including platforms based on electrochemistry,[9] fluorescence,[10] chemiluminescence[11], etc. Among them, optical detection based on surface-enhanced Raman spectroscopy (SERS) has shown tremendous potential.[8, 12]

SERS is an ultra-sensitive technique that is capable of providing a spectral fingerprint of the analytes under investigation. SERS is mostly based on the enhanced Raman signal by noble metallic nano structures that can generate a strong electromagnetic field with the excitation at a certain laser wavelength, such as Ag, Au, and Cu, which is also named Localized Surface Plasmon Resonance (LSPR).[13-14] The excited LSPR generates a large electric field on the metal surface and this electric field induces dipole moments in a molecule on the surface of nanostructures, and gains an enhanced Raman signal. These strong, localized electromagnetic fields present in nano-gaps between nanostructures are known as “hot spots”.[15] The enhanced Raman signals are composed

of an electromagnetic enhancement[16] and a chemical enhancement.[17] The electromagnetic enhancement contributes to 10^{11}-10^{13} the magnitude of the SERS signal while the chemical enhancement contributes only by a factor of ~10^2.[18] The magnitude of the SERS enhancement depends on the morphology,[19] the size of the metallic nano particles,[20] the gap size between the metallic nano particles,[21] the measurement environment, as well as the wavelength of the laser excitation source.[22-25]

Because of the simplicity of operation and sensitivity in detection, SERS has been used for trace detection of 2,4-D pesticides[26] including SERS substrates based on hollow Au@Ag nano-snowflake particles functionalized with 4-MBA/2,4-D antigen,[12] citrate functionalized AgNPs on cellulose paper,[27] silver NPs with molecular imprint polymers (MIP)[28] and highly roughened surface flower-like Ag NPs.[29] In particular, SERS substrates based on well-ordered AuNPs inside mesostructured silica channels have been used to detect 2,4-D, with a limit of detection (LOD) down to 0.79 ppt (parts per trillion) achieved.[30] These methods require either (i) an incubation time of more than 1 h, (ii) a pre-treatment step by mixing the solution with ethanol, or (iii) a waiting time to allow the 2,4-D solution to dry on the SERS substrate. To quickly determine pesticides such as 2,4-D directly in water samples without any pre-treatment remains a key challenge.

SERS substrates are commonly fabricated through chemical synthesis,[31-32] electron beam (E-beam) lithography,[33] laser assisted fabrication, or templating method.[34-36] For chemical methods, though size and morphology controllable nano particles are available, drop-casting of the nano particles onto a substrate, paper, glass or silica, etc. is still required.[37-47] The distance between the nano particles is hard to control. This in turn leads to difficulties in the quantification of target analyte, as for quantification in SERS, data points for each analytes concentration for linear calibration are the average of more

than three measurements in more than three locations on a SERS substrate (usually ten spectra are measured in ten different locations). Another significant issue with the use of nanoparticles is that they could be removed or lifted after application of analyte solution, again resulting in quantification inaccuracy. Most research papers that reported on chemical synthesis fabrication methods for effective SERS substrates carry out experiments in a dry environment (i.e., the solution was dropped casted and allowed to dry) instead of a water environment, with the drying time usually lasting for 30 minutes to one hour.[38-39, 41-42, 44] Besides that, for some research using paper SERS substrates and chemically synthesized nano particles as effective SERS substrates, the background Raman signal from a paper substrate could affect the target analyte Raman signal readout. Laser-assisted fabrication methods, combining laser etching on glass/silica substrates for nano patterns and followed by metal layer deposition, have limited choices for the morphology of the nano patterns and plasmonic materials.[48-50] The templating method entails several steps and has a higher likelihood of fabrication failure.[35, 51] These methods are either time-consuming or involve complex steps. High throughput, low cost, and reproducible fabrication of SERS substrates are still elusive.

Electrochemical methods allow morphology, size, nano gap controllable deposition of nano structures and can achieve a high Enhancement Factor. There are several papers relating to the deposition of metallic materials only. For instance, Xia et al. [52] synthesized Ag nanosheets with a nanogap smaller than 10 nm by environmentally friendly electrochemical deposition and this method achieved high reproducibility. [43] Wang et al. used electrochemically roughened nano-Au film to detect environmental pollutant *p*-nitrophenol (PNP). Chen et al. [53] prepared pyramid-shaped silver nanostructures by electrochemical deposition as an effective and reusable SERS substrate. Zong et al.[45] synthesized a gold nanostructure on microelectrodes in

microchips by gold electroplating and used it for SERS characterization by R6G. Cheng et al.[54] electrochemically synthesized branched metallic nanostructures and evaluated them by SERS using DTTCI as the analyte. Those researcheres demonstrated the fabrication of effective SERS substrate by electrochemical method, but none of them used SERS substrates as an analytical sensor, until Dao[55] used electrochemical deposition of Ag nanoparticles on Si surface to detect and quantify fungicide difenoconazole in a dry environment, achieving a LOD = 0.023 ppm (0.56 nM). In our work, we used electrodeposition of composite materials and showed their Raman-based sensing abilities towards 2,4-D. As 2,4-D does not contain either N or S in its chemical structure, its interaction with the silver surface, and consequently a SERS signal, will be weak, as discussed in Chapter 1. In this work, the Gum Arabic coating helped concentrate the pesticide at the surface of the nanostructure and allowed for its Raman-based detection.

We report on the rapid and reproducible fabrication of Silver-Gum Arabic (Ag-GA) SERS substrates by electrochemical deposition. This electrochemical deposition is based on SiO_2/Si chips that were fabricated following a standard photolithography process. The electrochemical method produced a SERS substrate with an area of 40 µm x 20 µm and required less than 10 s for preparation, with 2 µL of a non-toxic solvent. This is an environment-friendly, efficient, high throughput, and scalable SERS substrates fabrication method. The fabricated samples are used for herbicide 2,4-D detection directly in aqueous solutions, with detection down to 1 pM reported without the need for sample preparation.

Gum Arabic was selected as it is a branched hetero-polysaccharide containing protein and carbohydrate groups and is a biodegradable, non-toxic, and easily available biopolymer.[56-57] Polysaccharide materials have been used for the removal of heavy

metals,[58] pesticides, and pollutants in polluted water bodies,[59-60] because of their great adsorption ability towards different chemicals.[61] Gum Arabic has also been used for green chemical synthesis of silver nano particles.[62-64] During this process, Gum Arabic acts as a reducing agent to reduce silver ions, subsequently forming Ag-GA NPs.[64] In this work, an electrochemical deposition method was used to fabricate Ag-GA SERS substrates. Gum Arabic is a conductive biopolymer that is also widely used as a raw material for composite conductive materials studies.[65-67] Besides, its viscosity changes significantly with the change in Gum Arabic solution concentration, and this property allows it to act as a shape-controlling agent in Ag NPs electrochemical deposition. The size and morphology of the silver nanoparticles were tailored by controlling electrochemical deposition parameters such as deposition time, deposition voltage, and precursor concentration. During the electrochemical deposition process, silver ions are electrochemically reduced, and then combined with Gum Arabic monomers to form Ag-GA nanoclusters, which deposit on the chip surface in the vicinity of the electrodes, see schematic in Figure 2.1. The electrochemical approach greatly accelerated the $Ag^{+} \rightarrow Ag$ process compared to the natural reducing process by the Gum Arabic alone.[63] In addition, tailoring deposition parameters enabled not only the formation of size and morphology of the Ag-GA nanoclusters but also the regular distributed gap pattern in between the nanoclusters, to be engineered.

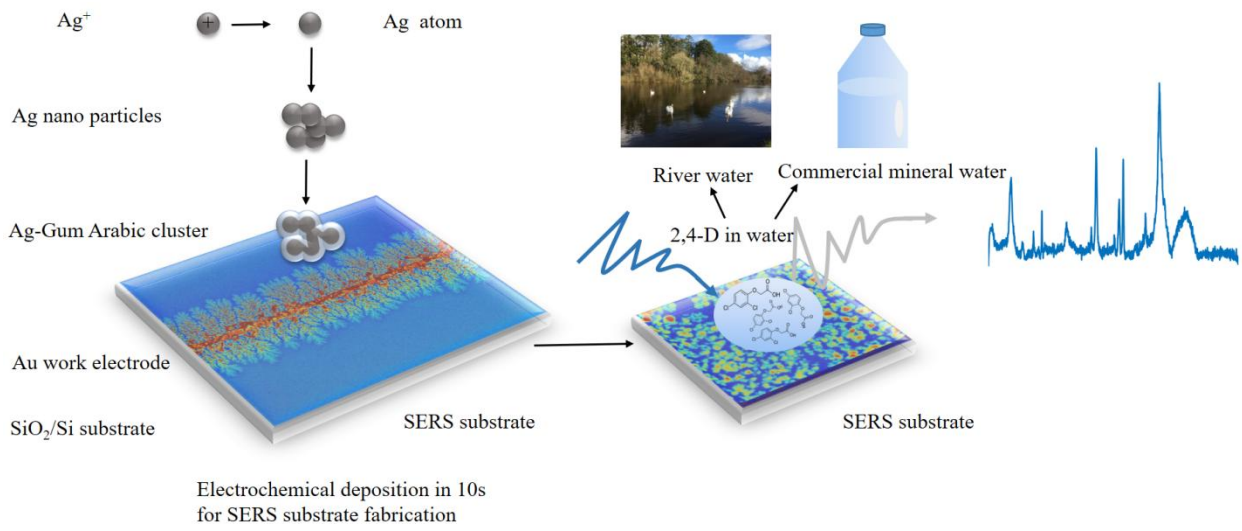

Figure 2.1: Schematic of Ag-GA SERS substrate deposition by electrochemistry and detection of 2,4-D in water environment.

1. Experimental section.

1.1. Materials.

$AgNO_3$ was purchased from Sigma-Aldrich (Ireland), CAS number: 7761-88-8, 99.99% trace metals basis. 2,4-D was purchased from Sigma-Aldrich (Ireland), CAS number: 94-75-7, ≥95%, crystalline. Gum Arabic was purchased from both Sigma Aldrich (CAS number: 9000-01-5) and from Amazon.co.uk (food catalog, see details in SI section 4.). Volvic natural mineral water was purchased from a local shopping market (its composition details are in SI). The real river sample was collected from the local river Lee, Cork, Ireland. The analyses and data collection were carried out on the same day as the collection. Samples were prepared using ultra-pure Mili-Q water (18.2 $M\Omega \cdot cm^{-1}$, Mili-Q). Electrochemical depositions were undertaken with an Ivium pocketSTAT handheld potentiostat (Scan range: ±30mA/±10V, size: 16x6.7x1.9 cm, weight: 300, applicable scan rates: 1 µV/s to 10,000 V/s) operating under computer control (software: Iviumsoft). DI water and 2,4-D analyte used in this research were stored in new colorless Eppendorf AG PCR tubes (mL range) from Sigma-Aldrich

(Ireland), and $AgNO_3$ solution was contained in a new centrifuge tube from Sigma-Aldrich (Ireland).

For 2,4-D serial dilution preparation, 0.0088 g of 2,4-D powder was dissolved in 20 mL of DI water, giving a concentration of 2 mM. 100 µL of this 2mM 2,4-D solution was then diluted in 900 µL of DI water to obtain a 0.2 mM solution. Further dilutions were obtained by using the same approach.

Most Raman-related research typically uses acid-washed glassware to minimize risks associated with contamination.[68] In this research, the solutions were stored in plasticware. Such materials have been used for highly sensitive detection of analytes using LC-MS. Additionally, many publications report on the integration of SERS substrates with PDMS fluidic cells, achieving sensitive detection of MB at nM concentrations. For example, with the wide application of SERS in 3-D printing, new device designs have emerged. Zhang et al. used a 3-D printed PDMS channel to contain noble nanoparticles and analytes for SERS measurement and were able to detect MB down to 10 nM.[69] Pu et al. also reviewed SERS application combined with PDMS microfluidic devices.[70]

1.2. Microelectrode Fabrication on Si/SiO_2 chip.

SERS sensors were fabricated on four-inch silicon wafer substrates with a 300 nm layer of thermally grown silicon dioxide as previously described.[71] 34 individual SiO_2/Si chips were produced on each silicon wafer, with a chip size of 1 cm (width) x 1.7 cm (length) x 0.1 cm (thickness). For the chip fabrication process, briefly, the working electrodes were patterned using photolithography and physical vapor deposition (PVD) (50 nm of Au, with 10 nm of Ti adhesion layer) followed by a lift-off step. A second optical lithographic and metal deposition process (Au 100 nm/Ti 10 nm)

was undertaken to define micro-SD pin-out, interconnection tracks, as well as the on-chip counter electrode (500 µm wide × 6 mm long). A third lithographic step was employed to define the Pt (Pt 100 nm/ Ti 10 nm) on-chip reference electrode (500 µm wide × 6 mm long). Finally, 500 nm of Plasma-enhanced chemical vapor deposition (PECVD) Si_3N_4 was blanket deposited on the whole wafer. Openings over the working/counter/reference electrodes and the electrical contacts were defined by lithography and dry etching process. See SI Figure S1.

1.3. Synthesis of Gum Arabic Coated Ag (Ag-GA) nanoclusters.

The SERS substrates were prepared using different concentrations (1pM, 0.1 nM, 10 nM, 200 nM, 600 nM, 2µM, 6µM, 0.02mM, 0.2mM) of Gum Arabic and 5 mM $AgNO_3$ solutions after the optimization process. The Gum Arabic solutions were prepared by dissolving Gum Arabic powder in DI water. This solution was mixed by hand with a glass rod at ambient temperature to allow Gum Arabic to dissolve in DI water completely. For the electrochemical deposition step, Gum Arabic and $AgNO_3$ solutions were mixed with a 1:1 ratio, and a small aliquot (2 µL) was dropped on a chip surface to cover a working electrode, the on-chip pseudo reference and counter electrodes. $AgNO_3$ and Gum Arabic solutions were mixed just before the SERS substrate fabrication, as given enough time, $AgNO_3$ and Gum Arabic would chemically react to form Ag-Gum Arabic nanoparticles (See SI Figure S2). Electrochemical deposition was undertaken with an Ivium pocketSTAT handheld potentiostat using the parameters presented in Table 1 (below). After the application of voltage, the Ag-GA substrate is prepared by electrochemical deposition. The sensor chip bearing Ag-GA nano particles was then rinsed under flowing DI water several times. Lastly, the Ag-GA substrate was visually dried under a nitrogen flow for several seconds before Raman measurements.

For each 2,4-D Raman detection measurement, Ag-GA samples were freshly prepared and used immediately, as Ag can easily oxidize in air (GA has a porous structure that adsorbs water to the surface that could accelerate the oxidation process). Chapter 3 discusses a method to store this type of sensor.

1.4. Microscopic and SEM characterization.

Microscopic images of the fabricated Ag-GA substrates were acquired with a Renishaw InVia Raman microscope with a 50 x (NA 0.75) objective. SEM characterization was undertaken with a FEI Quanta 650, the acceleration voltage used was 10 KV, and the spot size was 2.5 nm. Secondary electrons were used for SEM.

1.5. Raman measurements.

Raman spectra were acquired with a Renishaw InVia microscope (confocal, software: Renishaw's WiRE™ 3.4 (Windows®-based Raman Environment), spectral resolution: 0.3 cm^{-1} (FWHM), spatial resolution (lateral): 0.25 µm, spatial resolution (axial) < 1 µm) equipped with a 514 nm Ag ion laser (model number: stellar-pro), a 2400 l/mm(vis) grating and Renishaw CCD detector (1024 pixel × 256 pixel). For the measurements, the SERS sensor chips were placed in a dedicated holder, as shown in SI Figure S3 (C-D). A 10 µL aliquot of 2,4-D solution was dropped over the Ag-GA SERS substrate and covered with a cover glass slide. All measurements were acquired using a 20x objective (LEICA, NA 0.4, lateral resolution of ~688 nm, and an axial resolution of ~6875 nm) with the smallest and brightest laser spot adjusted to focus on the measurement surface. All the spectra presented herein were averaged from ten measurements obtained at different random points on the substrate, except for the repeatability study, where 25 measurements were employed. For the first (lowest) concentration in different 2,4-D concentration detection experiments, the 2,4-D spectrum was obtained after half an hour.

All spectra were obtained using a laser power of 0.07 mW[1] and an integration time of 10 s with one measurement/spectrum for each spot. The Ag-GA substrate area was around 40 µm x 20 µm and the laser spot size was around 1-2 µm.

1.6. Sampling methodology.

The same substrate was used for Raman measurements of different concentrations of 2,4-D solutions. The measurement was first undertaken with a low 2,4-D concentration. After the measurements of this low concentration were done, the analyte solution was removed with a small piece of cleanroom wipe (SUPERIOR Polycellulose wipes purchased from Sigma-Aldrich (Ireland) from the edge of the droplet (care was taken not to touch the SERS substrate itself). The next concentration of 2,4-D solution were applied (it was observed that the solution did not visually dry during our experiments). This method ensured that the Ag-GA substrate was consistent across all 2,4-D concentrations. This methodology was used by Sharipov et al. to detect bisphenol A and bisphenol S, using a molecular imprint paper-based SERS sensor.[72]

1.7. Data Analysis.

All spectra were corrected using the baseline subtraction algorithm described by Schulze et al.[73] The false color map was generated by Matlab R2018b-academic use. The baseline subtraction process was shown in SI Figure S5. The linear fitting was done by Origin™ (OriginPro 2016).

2. Results and discussion.

2.1. Ag-GA substrate Fabrication.

[1] The laser power was checked daily by using a reference Si calibration chip shown in SI Figure S4.

A microband sensor is presented in Figure 2.2. The sensor chips were originally developed for electrochemical-based sensing applications.[71, 74] The detailed chip circuit design is presented in SI Figure S3 (E). The chips had a micro-SD pin-out for easy electrical plug-and-play connectivity to the potentiostat (see SI Figure S3 (A-B)). Each chip had six working electrodes that may be individually addressed. In the present work, the electrodes employed were single Au micro bands (1 µm wide, 45 µm long, 50 nm high). These were selected as the high current densities, observed at ultra microelectrodes, enabled the formation of nanoclusters emanating away from the band. A small aliquot -for example, only 2 µL- of the mixed GA/$AgNO_3$ solution was required for one substrate fabrication on the chip. Considering the SiO_2/Si chips can be mass-produced with high throughput and the electrodeposition process took only 10 seconds, the present approach was efficient, scalable, and environmentally friendly. Figure 2.2 (B) shows the SEM image of a Ag-GA structure electrodeposited on a micro-band electrode. The nanoclusters were strongly attached to the chip surface, were stable, and allowed hundreds of Raman measurements to be undertaken without any degradation of the substrate being observed.

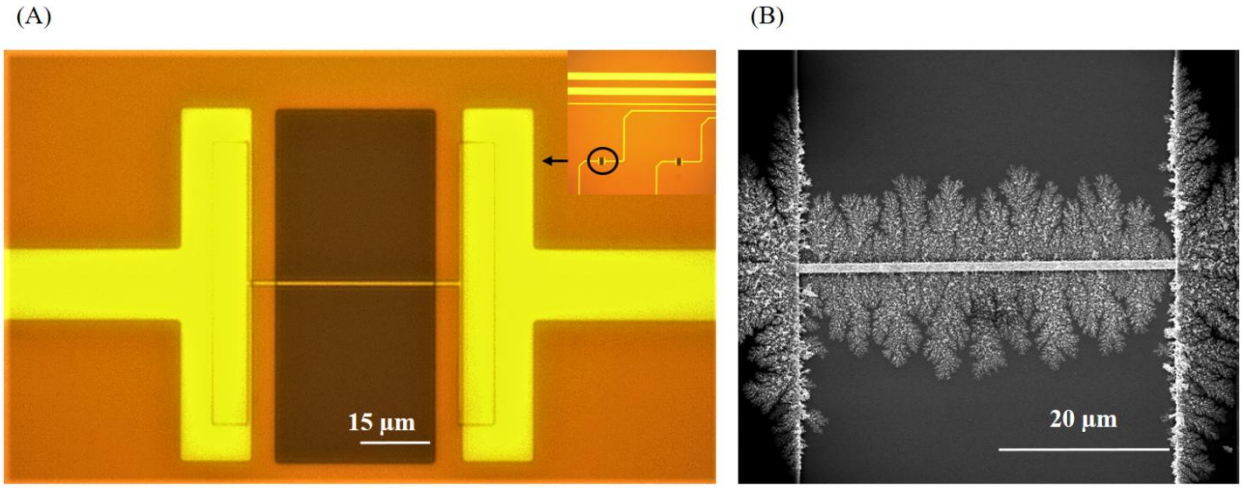

Figure 2.2 (A) Microscope image showing a micro-band working electrode on the chip (20x under a microscope); Insert: three electrodes system for electrochemical deposition

(2.5x under a microscope). (B) SEM image of a microelectrode after Ag-GA electrodeposition

3. Electrodeposition process and sample characterization.

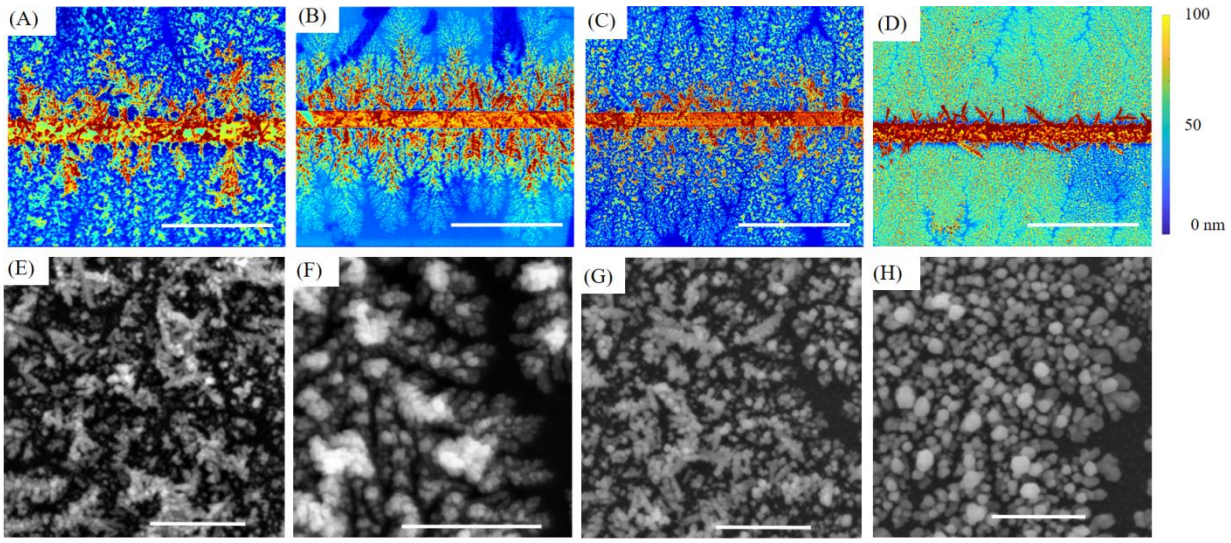

Figure 2.3 (A - D) False color maps from SEM images for structure one to structure four by Matlab 2018, scale bar: 5 μm; the color bar at 0 nm is the SiO_2/Si reference surface. (E-H) SEM images of nanostructures for structure one to structure four. Scale bars: 500 nm.

Figure 2.3 (A-D) shows SEM images of four Ag-GA nanostructures prepared using different experimental parameters as described in Table 1. The relationship between the deposition current (nA) and time (s) is shown in SI Figure S6 (A). The deposition current shows a linear relationship with deposition time, and the maximum current for the four Ag-GA substrates were 70 nA, 60 nA, 90 nA, and 120 nA, respectively. The false color maps in Figure 2.3 (A-D) show different Ag-GA substrate structures. False color maps indicated the nanocluster space distribution across the chip surfaces, as well as the 3-D nature of the deposited nanocluster structures. The color bar indicates the distance of the nanocluster from the SiO_2/Si substrate, the deep blue color (color bar

value at 0 nm) is the SiO_2/Si reference surface; the nanoclusters that present light green color are around 50 nm in height, which is around the same height as the working electrode. The higher the number in the color bar, the further the nanoclusters are away from SiO_2/Si substrate. The nanoclusters that showed a yellow color were ~ 100 nm away from SiO_2/Si surface while the nanoclusters that showed a red color were more than 100 nm away from the SiO_2/Si reference surface. Optical images are presented in Figure S6 (C) and Original SEM images are presented in SI Figure S7 (A-D). Figure 2.3 (E-H) shows high-resolution SEM images of nanoclusters for the four structures. Ag-GA nano dendrite structures formed in Figure 2.3 (E-G) labelled structure S_1, S_2, S_3, while round-shape Ag-GA nano particles growth was observed in Figure 2.3 (H), labelled structure S_4. The size of the Ag-GA nano particles in structure S_4 was estimated to be in the range of 50-70 nm, see SI Figure S8. For structures S_1 and S_3, Ag-GA nano dendrites growth on the surface of SiO_2 was observed to be orthogonal to the chip's surface - see also SEM image tilted at 35 ^{o} in SI Figure S9 that showed the isolated growth of the nanoclusters on SiO_2. By comparison, for structure S_2, the Ag-GA nano dendrites grew along the Au electrode and stacked together perpendicularly to the chip surface.

Nanoclusters and nanogap formation may be explained by the interplay between mass transport (diffusion and electron migration) of Ag ions and passivation by Gum Arabic. After mixing with Gum Arabic, the resistance of the mixed solution is higher than $AgNO_3$ alone. This was inferred by the recordings of the electrical current when using solutions with and without Gum Arabic, see SI Figure S6 (A) and Figure S10 (A). Using the same deposition parameter as S_4 (-0.2 V, 2 s; -0.8 V, 8 s), the maximum deposition current was about 2 μA without Gum Arabic, while it was around 120 nA after mixing $AgNO_3$ with Gum Arabic. The reduction of Ag ions to Ag atoms reaction

happened on the substrate emanating away from the electrodes due to the strong electric field. Ag-GA nano structure formed immediately and stacked on the SiO_2/Si substrate. The formation of Ag-GA nanoclusters further affected the electric field distribution and helped the formation of nanogaps in between the nanoclusters.[75] As different concentrations of Gum Arabic solutions had different resistances, it was observed that the resistance increased as the concentration of Gum Arabic increased within certain Gum Arabic concentrations.[76] According to Ohm's law, $J = \sigma E$, where J is the current density, σ is the electrical conductivity, and E is the electric field, different concentrations of Gum Arabic solutions resulted in different electrical conductivity for the mixed silver precursor solutions, which further resulted in different current densities in the electrochemical system. Thus, there were different Ag-GA nanostructures formed with different Gum Arabic concentrations when the other deposition parameters were maintained (see structures 1, 3, 4 and SI Figure S11 (A-E)). The applied voltage also affected the growth pattern and growth direction of the Ag-GA nano particles (see structures 1, 2 and SI Figure S11 (M-O)). The detailed discussion is presented in SI. In conclusion, by adjusting the concentration of $AgNO_3$ and Gum Arabic in the solution as well as the electrochemical deposition parameters such as applied voltage and deposition time, it is possible to engineer the size and morphology of the Ag-GA nano structures and the nano gap patterns in between the nano clusters. The homogeneously distributed, high density of nanostructures and nano gaps made these substrates good candidates for SERS applications.

Table 1 Electrochemical deposition parameters for the four structures.

Ag-GA substrate	[$AgNO_3$]	[Gum Arabic]	Applied potential and deposition time	Maximum current (nA)

S_1	5mM	2g/L	Step 1: -0.2 V, 2s; Step 2: -0.8 V, 8s.	70
S_2	5mM	2g/L	Step 1: -0.2 V, 2s; Step 2: -0.5 V, 8s; Step 3: -0.6 V, 2s.	60
S_3	5mM	1g/L	Step 1: -0.2 V, 2s; Step 2: -0.8 V, 8s.	90
S_4	5mM	0.5g/L	Step 1: -0.2 V, 2s; Step 2: -0.8 V, 8s.	120

4. Raman-based detection of 2,4-D pesticide.

4.1. 2,4-D detection in DI water.

In the present work, Gum Arabic (GA) was used for the synthesis of the Ag nanostructures, and different concentrations of GA allowed for the synthesis of various morphologies. The fabricated samples were then tested for the detection of 2,4-D. As previously mentioned, 2,4-D lacks Nitrogen or Sulfur atoms in its chemical structure, and as a result, its interaction with the sensor surface is expected to be weak. This observation was confirmed in our case, where 2,4-D did not yield a repeatable Raman signal on a sensor bearing Ag nanostructures alone (i.e., without GA), even at a very high concentration (1 mM), see SI Figure S12.

In this regard, GA may be capable of capturing and concentrating the target compound at the sensor surface, enabling its detection using Raman spectroscopy. Indeed, polysaccharides have previously been employed to interact with organic molecules, specifically pesticides[59]. Gum Arabic, in particular, has been utilized as a flavor carrier in the food industry,[77] but it has also found environmental remediation

applications due to its ability to interact with pollutants such as pesticides[59], antibiotic[78] or antifungal crystal violet dye[79].

GA consists of polysaccharides rich in galactose and arabinose, and a small protein fraction associated with these polysaccharides, see SI Figure S13. It contains a large amount of -OH, -O-, and -CH bonds as well as a small portion of -NH_2 and -SH groups associated with the protein.[80] Such functional groups may attract 2,4-D to the surface of the Ag-GA nano particles. For example, in the research of Hassanzadeh-Afruzi et al.,[78] the proposed interaction between levofloxacin Antibiotic and GA was through hydrogen bonding or electrostatic interaction of the carboxylic acid functional group (-COOH, -F) and -OH/-COOH of GA, as well as physical entrapment. Amino acid in protein can bind to 2,4-D and this has been studied by Forgács et al. using charge-transfer chromatography.[81] Similar interaction might occur for 2,4-D as depicted below in Figure 2.4.

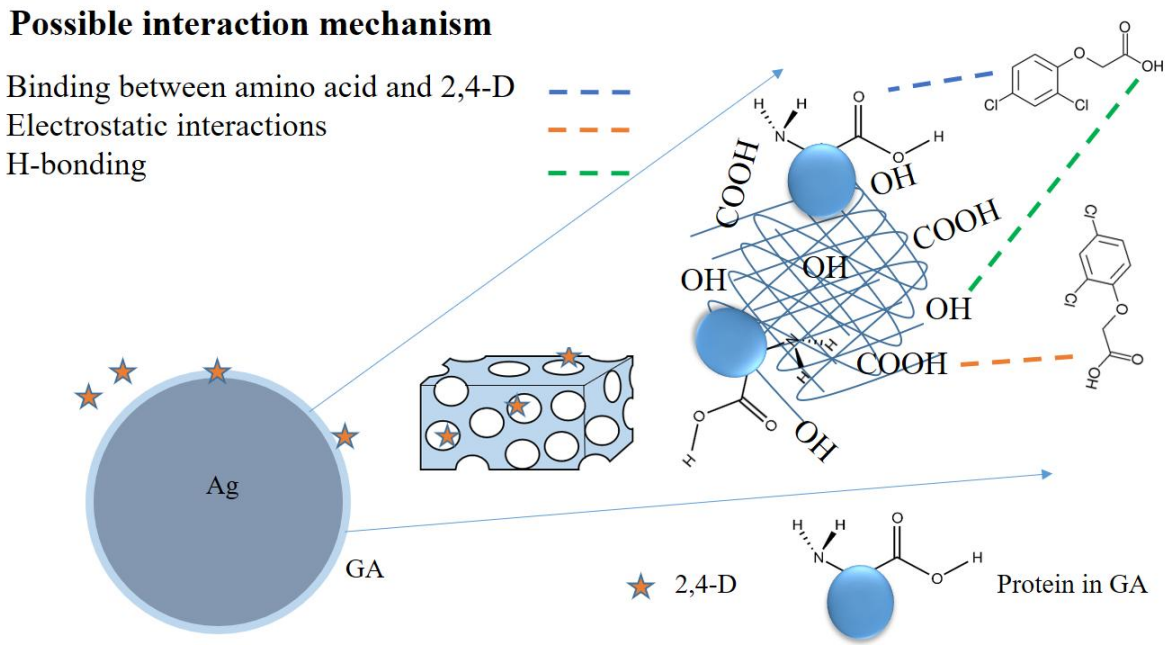

Figure 2.4: Possible interaction mechanism between GA layer and 2,4-D through amino acid, electrostatic interaction, and H-bonding.

Figure 2.5 (A) below depicts the experimental setup used to take the Raman spectra. Briefly, the sensor chip was placed in a designed chip holder. The size of the chip holder is the same as a microscope slide. After the application of the analyte solution on the sensor chip, Raman measurements were carried out after covering the sensor and analyte solution with a coverslip.

The initial Raman spectrum of bare Ag-Gum Arabic samples, acquired in air, exhibited peaks at 200cm^{-1} and two broad peaks at ~1400 cm^{-1} and ~1600 cm^{-1}, as shown in Figure 2.5. The peaks at ~200cm^{-1} can be assigned to silver nanoparticle.[82-83] After the application of DI water, the Raman intensity (a.u.) of the overall spectrum decreases from ~8000 to ~3000 Raman counts because of the water environment, see Figure 2.5 (B). The Raman signal in water is usually weaker than in a dry environment.[84]

The Si/SiO_2 peaks are not significant in these spectra because of the coverage of the Ag-GA nanostructures, which block the Si/SiO_2 peak signal. Additionally, the SERS signal from Ag-GA NP itself is much higher than that of the Si/SiO_2 peaks, making the Si/SiO_2 peaks at 520 cm^{-1} and 950 cm^{-1} [85, 86] (See SI Figure S4 for Raman spectrum of bare Si/SiO_2 chip) not shown in the spectrum.

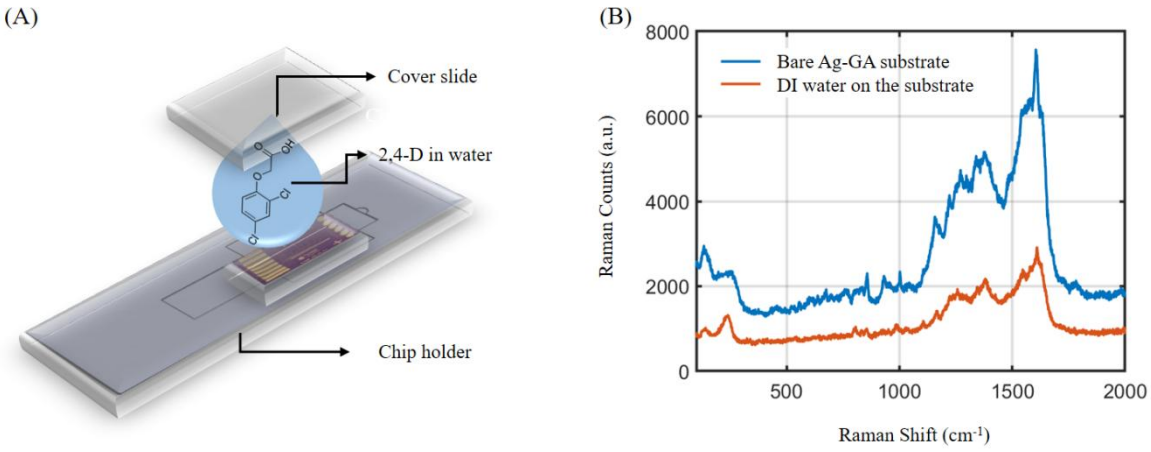

Figure 2.5: (A) Schematic illustration of the Raman measurement setup; (B) Raman spectrum of Ag-GA substrate before and after DI water application (without baseline subtraction).

Figure 2.6 (A) shows the Raman spectra of DI water and a 0.1nM 2,4-D solution after baseline correction. There are no clear peak features in the DI water spectrum of the Ag-GA substrate. On the contrary, after the application of the 2,4-D solution on the Ag-GA substrate, the spectrum shown in Figure 2.6 (B) immediately appeared, and clear peaks at 293 cm^{-1}, ~900 cm^{-1}, ~1098 cm^{-1}, ~1129 cm^{-1}, and 1400 cm^{-1} can be observed. These peaks were not observed in DI water, suggesting that the signal was generated because of the 2,4-D analyte.

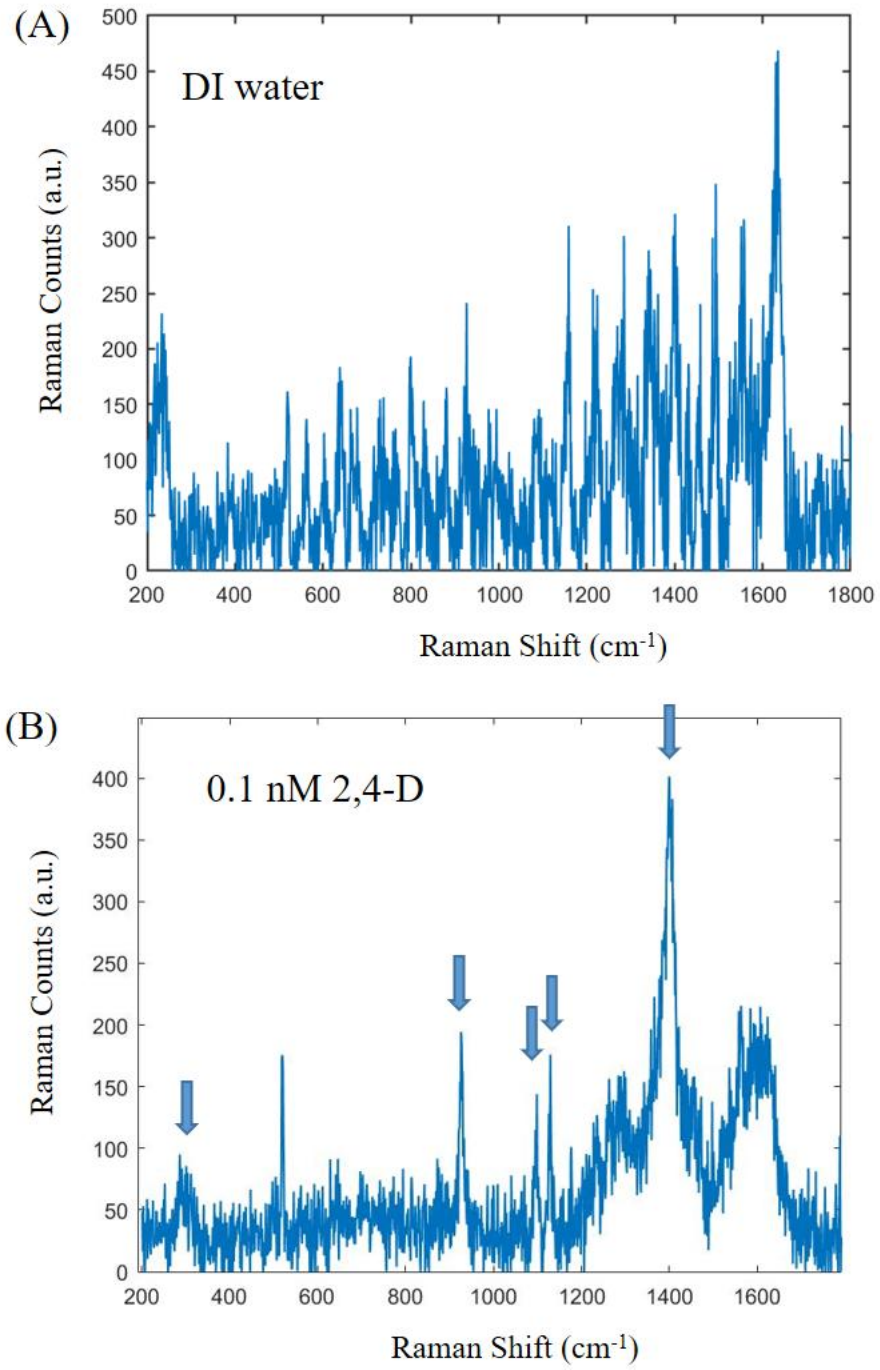

Figure 2.6: (A) Spectrum of deionized water as the reference (background corrected); (B) Spectrum of a 0.1 nM solution of 2,4-D on a S_4 Ag-GA substrate.

To attempt to assign the observed peaks to molecular vibration of 2,4-D, Raman spectra of 2,4-D powder were taken, see SI Figure S14. The solubility of 2,4-D in water is 900 mg/L (4 mM) and no normal Raman signal could be observed at this

concentration. However, Hua, Santos Costa, and Jia et al. reported SERS spectra of 2,4-D solution[87-89], see Table 2. For, 2,4-D powder, the Raman bands at 194, 413, 840, and 1105 cm^{-1} were assigned to in-plane vibrational modes involving C-Cl and C-O-C bonds.[87-88] The peak at 893 cm^{-1} was assigned to C-COO^- vibration and the peak at 1050 cm^{-1} to C-O vibration and Carbon ring vibration. And the peak at 1393 is CH_2 vibration.[89]

Table 2: 2,4-D Raman peak assignment in different states according to literature.[87-89]

2,4-D spectrum in this research	**2,4-D powder**	**2,4-D Raman peaks with Ag NPs in literature**	**Vibrational modes**
293	194, 413	422	δ(COC) + δ(CCl)
/	840	800	ν(CC)ring + ν(C–O) + ν(C–Cl)
927	893	/	ν(C–COO−)
1098	1050	/	ν(CC)ring + ν(CO) + δ(CH)ring
1129	1105	1178	ν(CC)ring + ν(C–Cl)

There seems to be some mismatch between some of the peaks recorded in our experiment and those of the 2,4-D powder/2,4-D SERS reported in the literature. Possible reasons are the difference in Raman spectra for the same compounds in different forms (i.e., crystal vs. solution), as discussed in Chapter 1, and the present experiment might have contributions from the GA layer.

To study the detection properties of the developed sensors in more detail, Raman spectra of diluted solutions of 2,4-D were acquired on different types of structures S_1-S_4.

Different structures exhibited varying response times to different concentrations of 2,4-D, as shown in Table 3 below. A change in the Raman spectrum was observed that for structures S_1-S_3 and 0.1 nM (0.0221 ppb) of 2,4-D within 30 minutes, as depicted in

SI Figure S15, while structure the spectral change occurred with a concentration as low as 1 pM (0.221 ppt) of 2,4-D within the same time frame for S_4. Structure S_4 exhibited immediate spectral changes for 0.1 nM 2,4-D as shown in Figure 2.6.

The difference in response time between lower and higher 2,4-D concentrations suggests that the observed peaks are indeed related to 2,4-D. The enhanced sensing capabilities of S_4 could be attributed to differences in morphology and size of the Ag-GA nanoparticles.[20, 90-91] The Raman signal also depends on the adsorption ability of the substrate and the total adsorbed amount of targeted analytes near the surface. Thus, the density of nanoparticles in one laser spot area also contributes to the difference in detection ability among these four structures.[92] In addition to the differences in morphology and nanoparticle size, S_4 exhibits a higher density of Ag-GA NPs and a narrower nanogap between nano clusters compared to the other three structures, as observed from the color maps in Figure 2.3 (A-D).

For S_4, it was observed that the lower the 2,4-D concentration used, the longer it took to obtain a Raman signal. SI Figure S16 shows the spectra acquired at different positions for S_4 within the first 30 minutes, revealing that the spectral features associated with the addition of 2,4-D only began to appear at the 13th spectrum (indicated by arrows). After the application of 2,4-D at 1 pM on the Ag-GA substrate, 2,4-D molecules likely interacted with the Ag-GA surfaces in various orientations. Gum Arabic, present on the surface of the sensor, possesses numerous functional groups (-OH, -COOH, -C-O-C-, and functional groups from proteins in Gum Arabic), interacting with water/2,4-D in diverse ways. These factors possibly collectively contributed to the spectrum features observed in SI Figure S16, before a repeatable 2,4-D spectrum features appeared.

Table 3: Comparison of response time and detection ability of S_1-S_4.

Structure type	Detection ability in 30 minutes	Response time for 0.1 nM
Structure 1	0.1 nM	30 minutes
Structure 2	0.1 nM	30 minutes
Structure 3	0.1 nM	30 minutes
Structure 4	0.001 nM	Immediately

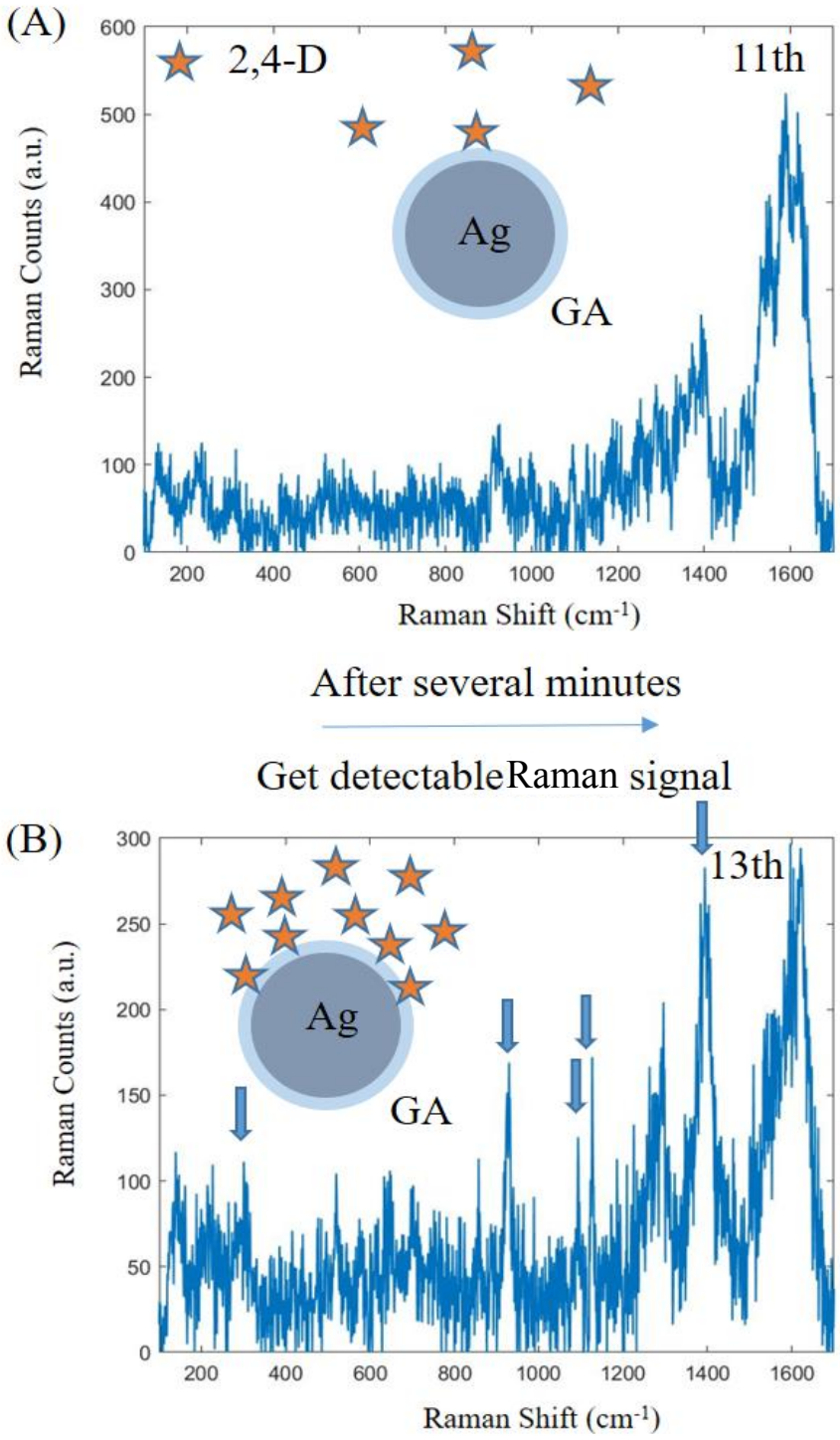

Figure 2.7.: Spectra acquired with S_4 and 1pM 2,4-D after (A) 11th measurement (16.5 minutes) and (B) 13th measurement (19.5 minutes). The inset shows schematics of 2,4-D diffusion near Ag-GA NPs surface.

This time dependence of the signal for 1 pM 2,4-D can also be explained by the fact that, at a low concentration of 2,4-D, it takes longer for the molecule to reach the Ag-GA surface because of diffusion.[93] Within the same time window (half an hour), at a higher concentration of 2,4-D (0.1 nM), more molecules interacted with the sensor surface, leading to faster acquisition of the Raman signal, as illustrated in the schematic in Figure 2.7.

S_4 was selected as the sample type for further study presented below due to its superior detection ability. Different concentrations of 2,4-D ranging from 1 pM to 0.2 mM in DI water were utilized for the 2,4-D detection study, as depicted in the spectra in Figure 2.8.

In the experiment involving S_4, an aliquot of the lowest 2,4-D concentration (1 pM) was applied to the sensor, and 10 spectra were acquired after the 2,4-D signal appeared, during a 30-minute incubation period. Subsequently, the solution was removed using a cleanroom wipe based on the capillary principle, and a solution with a higher 2,4-D concentration was applied onto the Ag-GA substrate, followed by the acquisition of 10 spectra. These steps were repeated for the remaining concentrations. This methodology was employed to study the concentration dependence on one substrate and thereby eliminate possible sample-to-sample variability. However, using only one sensor for a series of 2,4-D concentration tests is not a good analytical practice. If the 2,4-D molecules are trapped in the GA layers, more and more molecules are effectively added at each step, making quantification impossible. The 2,4-D concentrations used for incubation influence the results, but the outcome also depends, to some extent, on the previously used concentrations.

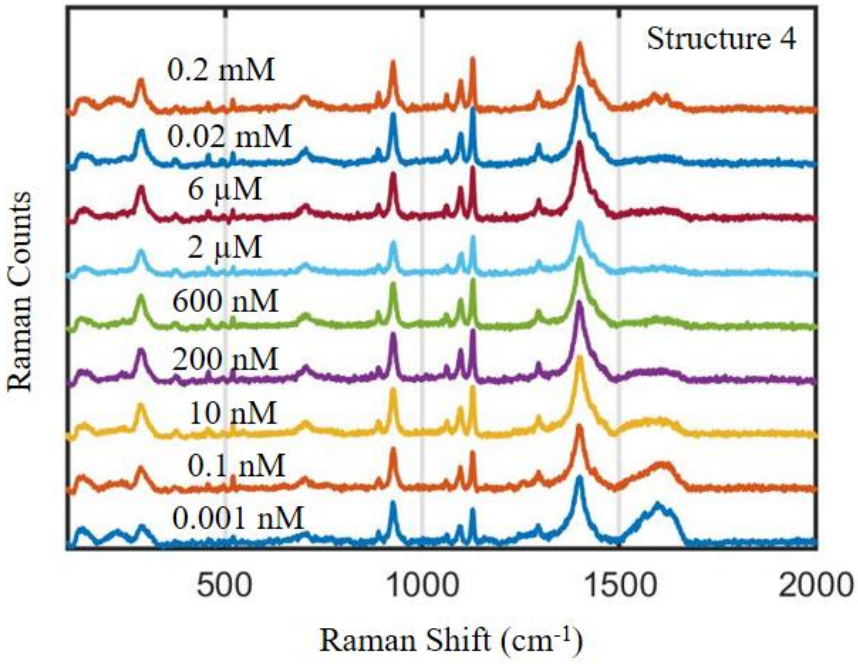

Figure 2.8.: Spectra of different 2,4-D concentrations ranging from 1 pM to 0.2 mM in DI water.

From the spectra in Figure 2.8, peaks of interest at ~293 cm^{-1}, ~900 cm^{-1}, 1400 cm^{-1}, and three sharp peaks at ~1130 cm^{-1} were observed for all the concentrations studied. However, when plotting the intensity of these peaks against Log[2,4-D]. There was no significant peak intensity change vs. [2,4-D], a big peak intensity changed would be expected in most of the SERS studies, as seen in SI Figure S17.

For all the raw data used in different 2,4-D concentration detection, the noise levels were similar for different 2,4-D concentrations, SI Figure S18. The 2,4-D concentration increase did not seem to affect much the spectra. This can be related to the interaction mechanism between 2,4-D and Gum Arabic. A possible mechanism is that the analyte molecules are trapped within the GA layer and remain confined thereafter. As discussed earlier, Gum Arabic possesses numerous functional groups (-OH, -COOH, -C-O-C-, and functional groups from proteins in Gum Arabic) and may interact with 2,4-D through hydrogen bonding or electrostatic interactions of the carboxylic acid functional

group (-COOH) and -OH/-COOH of GA, as well as physical entrapment. To further understand the interaction mechanism between 2,4-D and Gum Arabic, the Langmuir diffusion model and Raman counts vs. time experiments at one concentration could be further studied, but this is not within the scope of this study.[94]

However, while there is no definite dependence of single peak intensity vs. Log[2,4-D], further analysis reveals slight changes in the spectra with concentration. For example, Figure 2.9 (A) shows spectra recorded at 0.1 nM and 0.02 mM, normalized against the peak at 1400 cm^{-1}. Figure 2.9 (B, C) indicate changes in the normalized intensity of the peaks at 290 cm^{-1} and 1130 cm^{-1}. The broad peak near 1600 cm^{-1} also decreases due to the overall coverage of 2,4-D molecules as the concentration increases, as seen in Figure 2.9 (D).

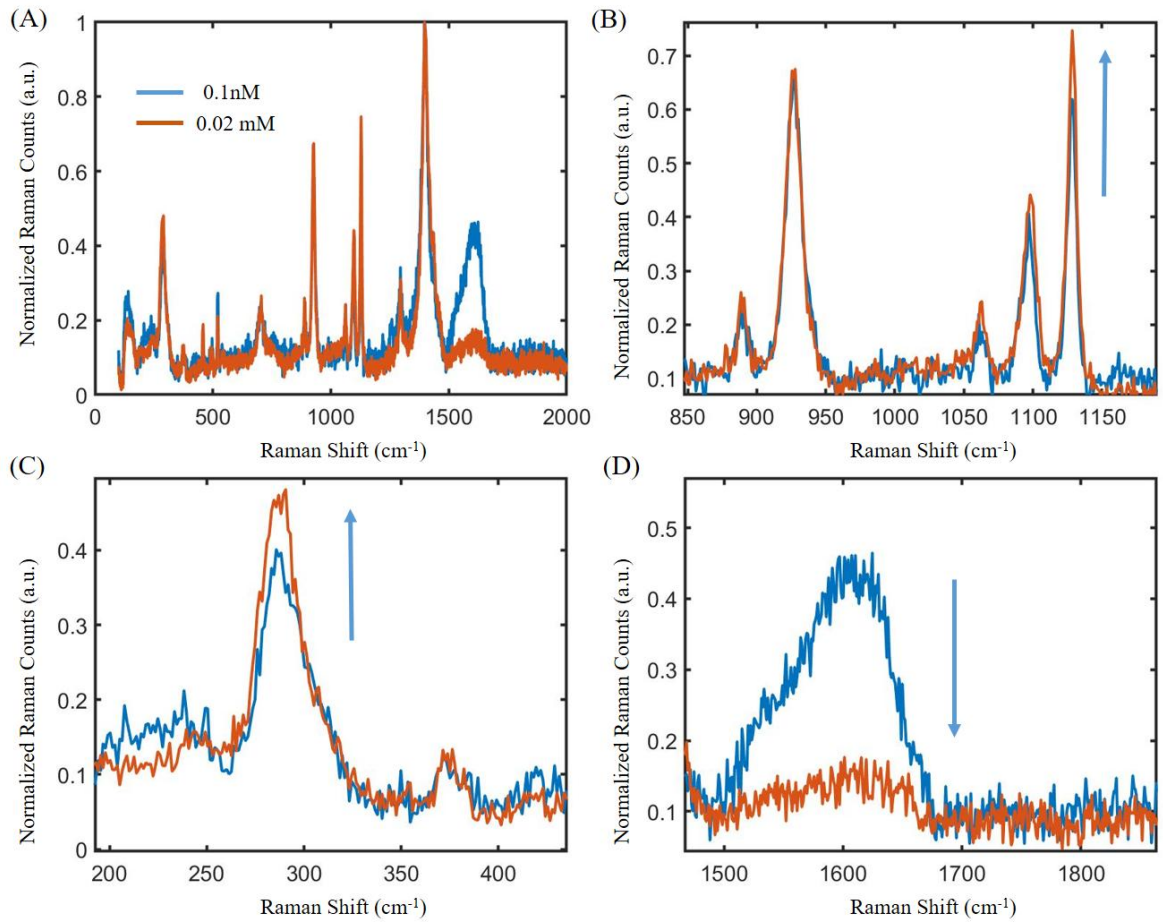

Figure 2.9: (A) Comparison between normalized 2,4-D spectra of structure 4 of 0.1 nM and 0.02 mM at 1400 cm^{-1} in calibration section for S_4; (B, C) Peak 293 cm^{-1} and 1130 cm^{-1} increased; (D) peak around 1600 cm^{-1} decreased.

The peak at 1400 cm^{-1} could be related to the characteristic peak for the Gum Arabic layer, [95] while the peaks at 1130 cm^{-1} and 293 cm^{-1} can be related to 2,4-D (Peak 1130 cm^{-1} is related to ν(CC)ring + ν(C–Cl), and peak 293 cm^{-1} is δ(COC) + δ(CCl), see table 2). The peak ratio could thus reflect the interaction between 2,4-D and GA.

Figure 2.10 shows the trend lines for peak ratio $I_{927cm^{-1}/1400\ cm^{-1}}$, $I_{298cm^{-1}/1400\ cm^{-1}}$, $I_{1130cm^{-1}/1400\ cm^{-1}}$, $I_{1098cm^{-1}/1400\ cm^{-1}}$ vs. Log[2,4-D]. As can be seen, there is no correlation for peak ratio $I_{927cm^{-1}/1400\ cm^{-1}}$, $I_{1098cm^{-1}/1400\ cm^{-1}}$ vs. Log[2,4-D]. However, the peak ratios $I_{298cm^{-1}/1400\ cm^{-1}}$ and $I_{1130cm^{-1}/1400\ cm^{-1}}$ increased with Log[2,4-D]. The peak ratio $I_{1130cm^{-1}/1400\ cm^{-1}}$ was used for further study.

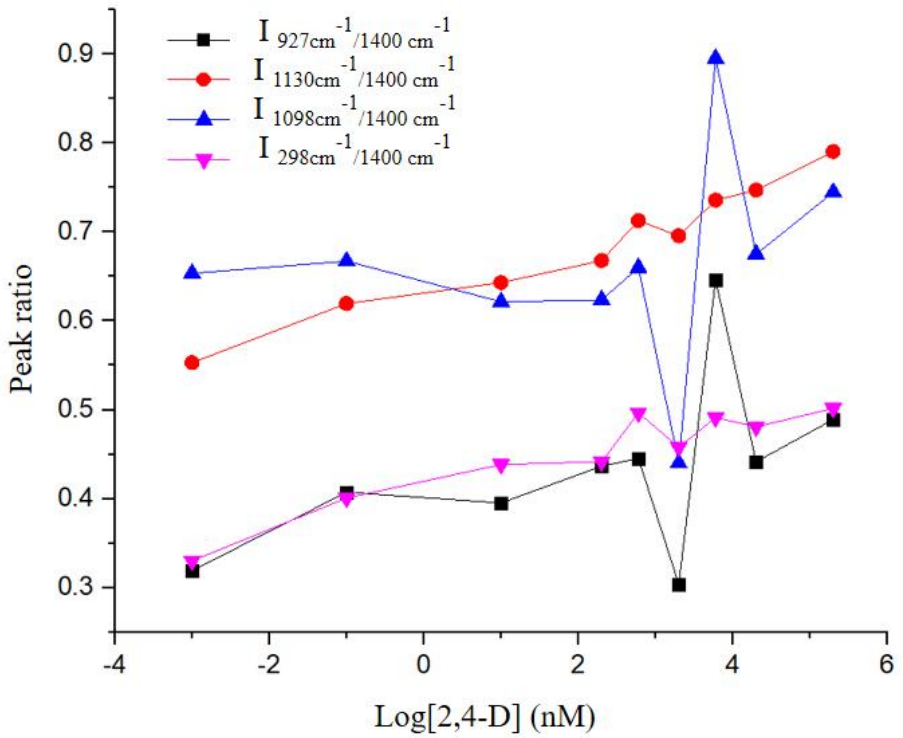

Figure 2.10: peak ratio $I_{927cm^{-1}/1400\ cm^{-1}}$, $I_{298cm^{-1}/1400\ cm^{-1}}$, $I_{1130cm^{-1}/1400\ cm^{-1}}$, $I_{1098cm^{-1}/1400\ cm^{-1}}$ vs Log[2,4-D].

Though there is time dependence for the 2,4-D signal to show up, the peak ratio $I_{1130\ cm\text{-}1}$ / $I_{1400\ cm\text{-}1}$ did not show any kinetic trend before the 2,4-D signal at low concentration (1 pM) appeared, as shown in SI Figure S19. The value of peak ratio $I_{1130\ cm\text{-}1}$ / $I_{1400\ cm\text{-}1}$ is in the range of 0.3-1 at 1 pM 2,4-D in 30 minutes, the peak ratio is thus only valid after the 2,4-D signal is shown for analysis.

To assess the error bar of the developed sensor, the repeatability for S_4 (with 2,4-D concentration at 2 μM) at 25 random points on a Ag-GA substrate is shown in Figure 2.11 (A), while the repeatability for S_1-S_3 is displayed in SI Figure S21-23. Data are also presented in another format in SI Figure S23. The Standard Deviations (SDs) of S_1-S_4 for $I_{1130\ cm\text{-}1}$ / $I_{1400\ cm\text{-}1}$ were 0.07, 0.06, 0.08, and 0.07, respectively, with an RSD range 9-12%, as seen in SI Figure S 20-22 (B) and Figure 2.11 (B). This level of variation is typical in nanostructure-based sensor calibration studies, where the Relative Standard Deviation (RSD) for repeatability studies is around ~10%.[96-97]

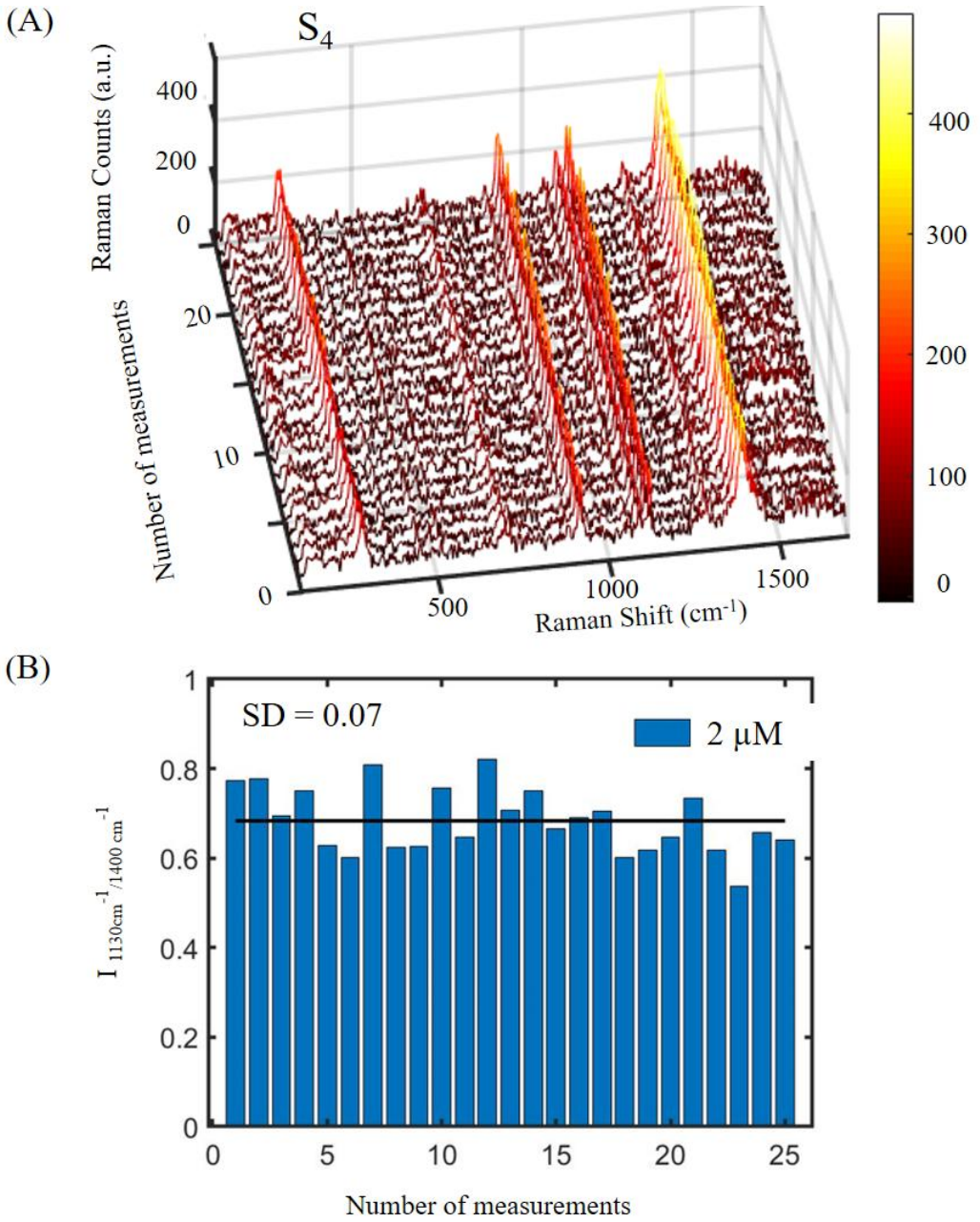

Figure 2.11 (A) Color waterfall spectra of 25 random positions for 2 μM 2,4-D on a S_4 Ag-GA substrate, the color bar stands for Raman intensity (a.u.). (B) Histogram I_{1130} cm^{-1} / I_{1400} cm^{-1} at 25 different random points, the SDs were 0.07 for the peak ratio.

The peak ratio I_{1130} cm^{-1}/I_{1400} cm^{-1} vs. [2,4-D] is depicted in Figure 2.12 (A). At low concentrations (1 pM), this ratio is 0.55 and increases as the concentration rises, reaching 0.75 at higher concentrations. Similar results for S_1-S_3 are illustrated in SI Figure S24-26 (A). Similar results were also observed by using commercial GA, see SI

section 5. This increase in the peak ratio could describe the sequential loading of the GA layer with the 2,4-D molecules applied. Upon incubation in the lowest concentration (1 pM), the GA layer is loaded with the target analyte, which is reflected in the appearance of peaks in the initial Raman spectrum. Once this initial loading has occurred, the GA layer's functional group that can interact with 2,4-D becomes mostly filled, and further loading becomes more challenging and slower, eventually reaching saturation. In the range of 2,4-D concentrations studied for S_4, a fit of $y = 0.6296 + 0.0266\log_{10}(x)$, with an $R^2 = 0.9530$ was obtained, between $I_{1130\ cm\text{-}1} / I_{1400\ cm\text{-}1}$ and $\log_{10}$ [2,4-D] (in nM), shown in Figure 2.12 (B).

The low slope indicated a low sensitivity of the sensor and reflects the slow loading of 2,4-D on the GA layer after the initial incubation. The RSD of error bars for $I_{1130\ cm\text{-}1} / I_{1400\ cm\text{-}1}$ against the logarithm of the concentrations of the 2,4-D ranged from 4-14% (SDs range from 0.038 to 0.129). This, conjugated with the low slope, implies that the sensor cannot be used for calibration or quantification. The initial peak ratio value varies among different Ag-GA sensors at the same 2,4-D concentration due to variability in sensor fabrication. This is the reason to use the substrate for the concentration sequence, otherwise, it is not able to see the trend of the Raman intensity vs. 2.4-D concentration, given that the change of the Raman intensity was not significant with the change of 2,4-D concentration. This calibration approach, however, is not a good analytical practice in general. In most of the situations, a single substrate was used for a single concentration. The sampling method has been discussed also in experimental section 1.6.

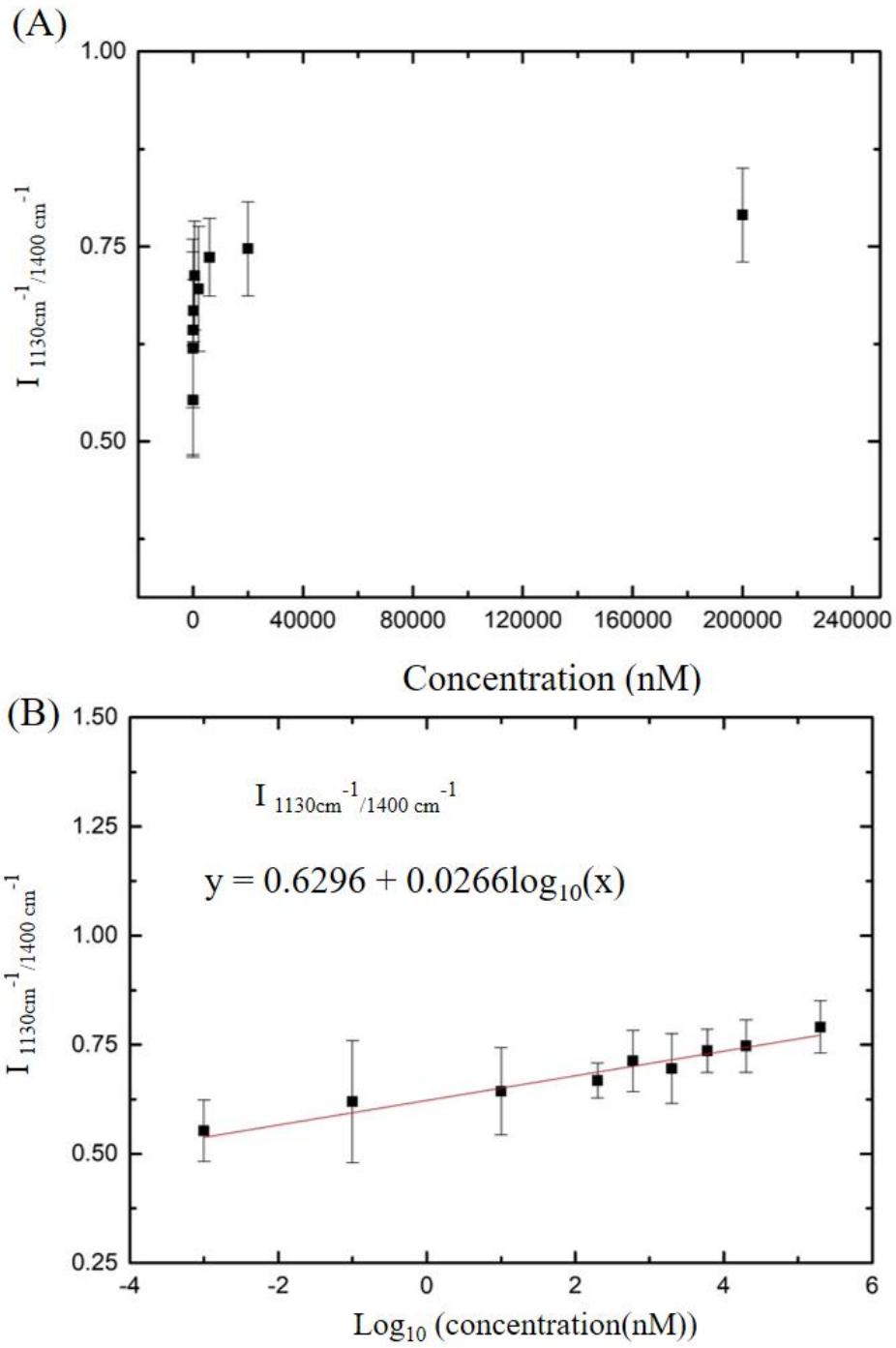

Figure 2.12: (A) I_{1130} cm^{-1} / I_{1400} cm^{-1} vs Concentration (in nM) for a S_4 substrate. (B) Fitting line for I_{1130} cm^{-1} / I_{1400} cm^{-1} vs log(concentration (in nM)) for a S_4 substrate. The error bars were obtained from the standard deviation (SD) of ten measurements at random points.

For the majority of SERS-related sensors or SERS studies, the signal change (or peak intensity change) is usually significant with changes in the concentrations of analytes as there is a strong interaction with the SERS surface itself - especially for Raman-active analytes such as methylene blue, crystal violet, etc., that contain -S or -N atoms. With surface functionalization methods, it is possible to capture analytes close to the SERS surface to benefit from enhanced signals. The binding between the functionalized SERS substrate and analytes can occur through biochemical processes such as DNA binding or antigen-antibody binding, as mentioned in Chapter 1. Another popular method nowadays to detect organic molecules is to use the molecular imprint (MIP) method.[28] This method uses polymer as a matrix and targeted analytes as embedded templates. The targeted analyte is trapped inside the polymer matrix. After removing the template by chemical washing, 'holes' in the shape of the targeted analyte are left in the matrix, and these 'holes' can selectively host the targeted analytes again.

This allows the MIP-based SERS substrate to detect targeted analytes with better capacity as well as better selectivity compared to the non-imprint molecular (NIP) method, which does not create extra tailored 'holes' for detection. For example, Hua et al. found that the adsorption capacity of the MIP SERS substrate is double that of the NIP SERS substrate for 2,4-D detection.[28] Many sensing research projects involve MIPs using enabling technologies other than SERS, such as fluorescence or electrochemical sensors. Elamin et al. developed a new electrochemical sensor based on a MIP nanocomposite using overoxidized polypyrrole and copper nanoparticles for the detection of sulfadiazine. From their experimental results, the signal change was 2.5, from 2.5 to 5.0 for NIP, while for MIP, the range was from 7.5 to 22 with a change of 14.5 at the same concentration range of sulfadiazine.[98] He et al. compared the fluorescence spectra of SiO_2@CDs&NBD@MIP and SiO_2@CDs&NBD@NIP with the

addition of the indicated concentrations of CNP. For MIP, the signal change ranged from 1.1 to 1.5 with a change of 0.4 (slope: 0.005), while for NIP, the signal change ranged from 1.05 to 1.10 with a change of 0.05 (slope: 0.001).[99]

Chemical synthesis used for MIP SERS sensors typically requires high-temperature conditions to enable crosslinking or other binding between the polymer matrix and targeted analyte monomers. In the study by Marti et al.[28] for 2,4-D detection, the mixed chemicals were capped and heated at 45 °C for 4 hours and then at 60 °C for 2 hours in a water bath. Lu et al. used clean wafers and placed them in a 1% (v/v) APTES anhydrous ethanol solution at 80 °C for 6 hours for the amination process to obtain the MIP template,[100] They further applied Ag-Au NPs on the wafer to detect colorectal cancer biomarkers.

In this research, electrochemical co-deposition was used for Ag-GA NPs synthesis. There was no need to use a high temperature during this process, and the fabrication took no more than ten minutes, including preparation and electrochemical deposition operations. However, for electrochemical deposition, high temperature is not available in preparing the NPs, MIP is thus not available for current experimental conditions.

The experimental results in the present research are consistent with NIP sensor research, although the result (the slope) was not as good as MIP SERS sensors. For NIP sensors and the Ag-GA SERS sensor in this research, the slope is low. However, this is a characteristic of this type of sensor based on NIP, as it has less hosting capacity than MIP sensors.[100-101] Furthermore, the error bar in this research is large, which, combined with the low slope, makes the result not ideal in terms of sensor performance. Similar results were also presented in the research of Marques et al.[38], where they used a paper-based SERS sensor to screen tetracycline (TET) in milk. From the results, the error bar is large and the slope is small over a wide [TET] range, making this sensor not ideal for

TET quantification in real-world applications. However, their research offers a one-step, simple screening of TET in milk under 0.01 ppm with low cost, and the results showed a linear trend between peak ratio and Ln [TET].

In this research, again, one SERS substrate was used for all concentrations under study, rather than employing one SERS substrate for each 2,4-D concentration. The advantage of this approach is that it maintained consistent experimental conditions across all 2,4-D concentrations, thereby limiting the potential experimental errors arising from different SERS substrates.[102-103] The disadvantage of this approach however is that the calculated detection limit will not be accurate and it prevents quantification. In this sense, using the same substrate for calibration is a poor analytical practice. The detection limit claimed in this research was based on experimental data (lowest 2,4-D concentration that has a Raman signal), not calculated data.

4.2. 2,4-D detection in real samples.

The effect of different matrices on the sensor performance was studied, by spiking both commercial mineral water and river water samples with known 2,4-D concentrations. The mineral composition of the commercial mineral water is shown in Table S1 in SI. As S_4 was able to detect 2,4-D at 0.1 nM immediately, it was chosen for a real sample study. Ten measurements were undertaken for each concentration on a S_4 Ag-GA substrate. The experiments were repeated three times on three individual substrates. The error bar was calculated using data from the standard deviation (SD) of the three replicates across the three substrates and shows that the interaction of the sensor with 2,4-D in the presence of different ions remains largely unaffected.

The reference spectrum for mineral water is shown in Figure 2.13 (A), the interference peaks near 1000 cm^{-1} are probably due to the interaction between Gum

Arabic and SO_4^{2-} present in mineral water.[104] From 0.15 nM to 1.5 μM of 2,4-D used, see Figure 2.14, a plot was obtained: $y = 0.5865 + 0.0329\log_{10}(x)$, where x is the peak ratio $I_{1130\ cm\text{-}1} / I_{1400\ cm\text{-}1}$, with a $R^2 = 0.9804$. See Figure 2.13 (B), similar results were obtained for river water, in the concentration range of 0.015 nM to 1.5 μM, a plot of $y = 0.6456 + 0.0180\log_{10}(x)$, with $R^2 = 0.9681$ was obtained. The slope of 2,4-D in mineral water is higher than in DI water. It is possible that ions in mineral water aided the penetration of 2,4-D into the GA layer.

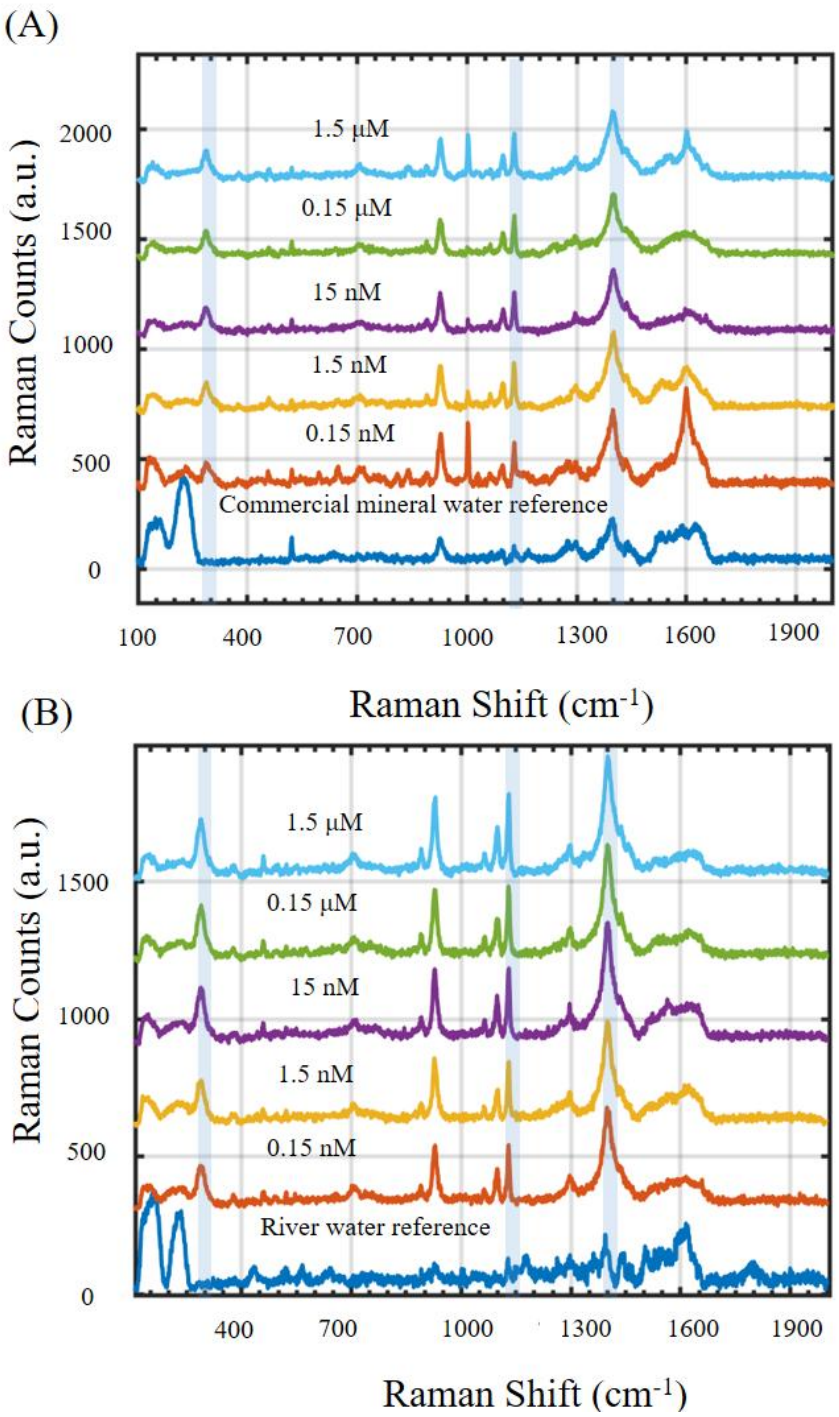

Figure 2.13: Spectra for real sample (A) commercial mineral water; (B) river water on S_4 Ag-GA substrates at concentrations 0.15 nM, 1.5 nM, 15 nM, 0.15 μM, 1.5 μM, and the spectra for reference water samples, spectra offset for clarity.

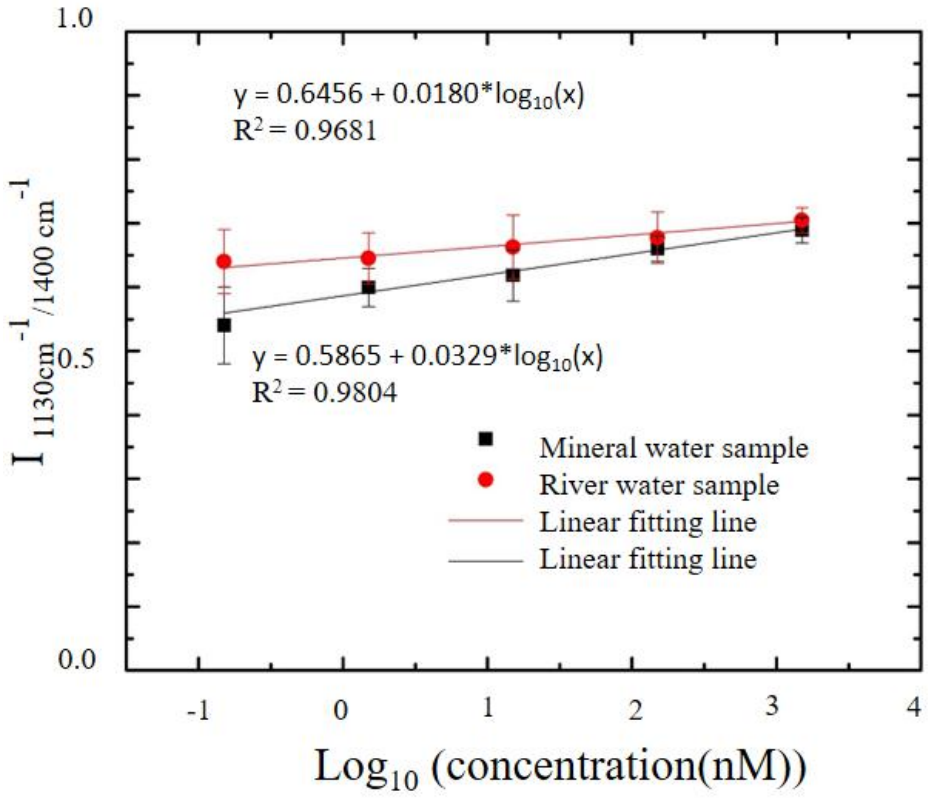

Figure 2.14: Linear calibration lines for 2,4-D in both river water and mineral real samples. Each data point was from the average of three sensor chips, and the error bar was the SD of these three data. For each sensor at a certain 2,4-D concentration for each water sample, ten spectra were obtained.

5. Conclusions.

In summary, proof-of-concept Ag-Gum Arabic nanocluster-based substrates were prepared using an electrochemical deposition method. This fabrication method was environmentally friendly, efficient, and simple. The analyte 2,4-D does not contain an -S or -N atom and does not generate a strong SERS signal on the silver nanoparticle surface. Instead, it interacts with the gum Arabic layer, helping to get a consistently readable Raman signal on the Ag-GA surface.

As the concentration of 2,4-D increased, a slight enhancement in signal was observed. However, the risk of rapid saturation became evident after multiple measurements at different 2,4-D concentrations. It is possible that there were insufficient binding sites for 2,4-D on the Ag-GA surface, similar to NIP sensors. The experimental method, which involved adding different 2,4-D concentrations to the same substrate, had shortcomings. Based on the results, the detection was not sensitive to changes in 2,4-D concentration, making quantification impossible. Nevertheless, the experimental data showed a signal at a low concentration of 1 pM 2,4-D.

Additionally, the design and method for Ag-GA substrate fabrication and noble nanoparticle synthesis could be completely changed, for example, by using MIP chemical synthesis. The 2,4-D antibody functionalization approach can be utilized based on the current silicon chip platform, although the antibody approach would increase the sensor development cost. Although limited by this Ag-GA sensor chip platform, this research somehow offers a simple way of fabricating Raman-based sensors. Different Ag-GA NPs produced by electrochemical deposition can also be used in other sensing applications, not limited to 2,4-D detection.

Reference.

1. Kumar-Krishnan, S.; Esparza, R.; Pal, U., Controlled Fabrication of Flower-Shaped Au-Cu Nanostructures Using a Deep Eutectic Solvent and Their Performance in Surface-Enhanced Raman Scattering-Based Molecular Sensing. *ACS Omega* **2020,** *5* (7), 3699-3708.
2. Ju, Z.; Liu, S.-S.; Xu, Y.-Q.; Li, K., Combined Toxicity of 2,4-Dichlorophenoxyacetic Acid and Its Metabolites 2,4-Dichlorophenol (2,4-DCP) on Two Nontarget Organisms. *ACS omega* **2019,** *4* (1), 1669-1677.
3. Carles, L., et al., Potential of preventive bioremediation to reduce environmental contamination by pesticides in an agricultural context: A case study with the herbicide 2,4-D. *Journal of Hazardous Materials* **2021,** *416*, 125740.
4. Prado, A. G. S.; Airoldi, C., Effect of the pesticide 2,4-D on microbial activity of the soil monitored by microcalorimetry. *Thermochimica Acta* **2000,** *349* (1), 17-22.
5. Health Service Executive, N. D. W. G., Pesticides in Drinking Water Frequently Asked Questions. **2018**.
6. Meftaul, I. M.; Venkateswarlu, K.; Dharmarajan, R.; Annamalai, P.; Megharaj, M., Movement and Fate of 2,4-D in Urban Soils: A Potential Environmental Health Concern. *ACS Omega* **2020,** *5* (22), 13287-13295.
7. Organization, W. H., 2,4-D in Drinking-water. Background document for development of WHO Guidelines for Drinking-water Quality. **2003**.
8. Meulenberg, E. P.; Stoks, P. G., Water quality control in the production of drinking water from river water. The application of immunological techniques for the detection of chlorophenoxy acid herbicides (2,4-D). *Analytica Chimica Acta* **1995,** *311* (3), 407-413.
9. Congur, G., Monitoring of glyphosate-DNA interaction and synergistic genotoxic effect of glyphosate and 2,4-dichlorophenoxyacetic acid using an electrochemical biosensor. *Environmental Pollution* **2021,** *271*, 116360.
10. Kumar, S.; Mehta, D.; Chaudhary, S.; Chaudhary, G. R., Pr@Gd2O3 nanoparticles: An effective fluorescence sensor for herbicide 2,4-dichlorophenoxyacetic acid. *Journal of Molecular Liquids* **2021,** *324*, 114712.
11. El-Maghrabey, M.; Suzuki, H.; Kishikawa, N.; Kuroda, N., A sensitive chemiluminescence detection approach for determination of 2,4-dinitrophenylhydrazine

derivatized aldehydes using online UV irradiation – luminol CL reaction. Application to the HPLC analysis of aldehydes in oil samples. *Talanta* **2021,** *233*, 122522.

12. Xu, Y.; Kutsanedzie, F. Y. H.; Hassan, M. M.; Zhu, J.; Li, H.; Chen, Q., Functionalized hollow Au@Ag nanoflower SERS matrix for pesticide sensing in food. *Sensors and Actuators B: Chemical* **2020,** *324*, 128718.

13. Langer, J., et al., Present and Future of Surface-Enhanced Raman Scattering. *ACS Nano* **2020,** *14* (1), 28-117.

14. Han, B.; Chen, L.; Jin, S.; Guo, S.; Park, J.; Yoo, H. S.; Park, J. H.; Zhao, B.; Jung, Y. M., Modulating Mechanism of the LSPR and SERS in Ag/ITO Film: Carrier Density Effect. *The Journal of Physical Chemistry Letters* **2021,** *12* (31), 7612-7618.

15. Peng, Y. S.; Cai, P.; Yang, L. L.; Liu, Y. Y.; Zhu, L. F.; Zhang, Q. Q.; Liu, J. J.; Huang, Z. R.; Yang, Y., Theoretical and Experimental Studies of Ti3C2 MXene for Surface-Enhanced Raman Spectroscopy-Based Sensing. *Acs Omega* **2020,** *5* (41), 26486-26496.

16. Ding, S.-Y.; You, E.-M.; Tian, Z.-Q.; Moskovits, M., Electromagnetic theories of surface-enhanced Raman spectroscopy. *Chemical Society Reviews* **2017,** *46* (13), 4042-4076.

17. Yu, X.; Cai, H.; Zhang, W.; Li, X.; Pan, N.; Luo, Y.; Wang, X.; Hou, J. G., Tuning Chemical Enhancement of SERS by Controlling the Chemical Reduction of Graphene Oxide Nanosheets. *ACS Nano* **2011,** *5* (2), 952-958.

18. Le Ru, E. C.; Blackie, E.; Meyer, M.; Etchegoin, P. G., Surface Enhanced Raman Scattering Enhancement Factors: A Comprehensive Study. *The Journal of Physical Chemistry C* **2007,** *111* (37), 13794-13803.

19. Li, M.; Qiu, Y.; Fan, C.; Cui, K.; Zhang, Y.; Xiao, Z., Design of SERS nanoprobes for Raman imaging: materials, critical factors and architectures. *Acta Pharmaceutica Sinica B* **2018,** *8* (3), 381-389.

20. Stamplecoskie, K. G.; Scaiano, J. C.; Tiwari, V. S.; Anis, H., Optimal Size of Silver Nanoparticles for Surface-Enhanced Raman Spectroscopy. *The Journal of Physical Chemistry C* **2011,** *115* (5), 1403-1409.

21. Guo, C.; Chen, X.; Ding, S.-Y.; Mayer, D.; Wang, Q.; Zhao, Z.; Ni, L.; Liu, H.; Lee, T.; Xu, B.; Xiang, D., Molecular Orbital Gating Surface-Enhanced Raman Scattering. *ACS Nano* **2018,** *12* (11), 11229-11235.

22. Mao, P.; Liu, C.; Favraud, G.; Chen, Q.; Han, M.; Fratalocchi, A.; Zhang, S., Broadband single molecule SERS detection designed by warped optical spaces. *Nature Communications* **2018,** *9* (1), 5428.

23. Zhu, W.; Crozier, K. B., Quantum mechanical limit to plasmonic enhancement as observed by surface-enhanced Raman scattering. *Nature Communications* **2014,** *5* (1), 5228.

24. Zhang, Y.; Gu, Y.; He, J.; Thackray, B. D.; Ye, J., Ultrabright gap-enhanced Raman tags for high-speed bioimaging. *Nature Communications* **2019,** *10* (1), 3905.

25. Liu, W., et al., Improved Surface-Enhanced Raman Spectroscopy Sensitivity on Metallic Tungsten Oxide by the Synergistic Effect of Surface Plasmon Resonance Coupling and Charge Transfer. *The Journal of Physical Chemistry Letters* **2018,** *9* (14), 4096-4100.

26. Creedon, N.; Lovera, P.; Moreno, J. G.; Nolan, M.; O'Riordan, A., Highly Sensitive SERS Detection of Neonicotinoid Pesticides. Complete Raman Spectral Assignment of Clothianidin and Imidacloprid. *The Journal of Physical Chemistry A* **2020,** *124* (36), 7238-7247.

27. Hassan, M. M., et al., Cellulose paper-based SERS sensor for sensitive detection of 2,4-D residue levels in tea coupled uninformative variable elimination-partial least squares. *Spectrochimica Acta Part A: Molecular and Biomolecular Spectroscopy* **2021,** *248* (1386-1425), 119198.

28. Hua, M. Z.; Feng, S.; Wang, S.; Lu, X., Rapid detection and quantification of 2,4-dichlorophenoxyacetic acid in milk using molecularly imprinted polymers-surface-enhanced Raman spectroscopy. *Food Chemistry* **2018,** *258*, 254-259.

29. Hassan, M. M., et al., Signal optimized rough silver nanoparticle for rapid SERS sensing of pesticide residues in tea. *Food Chemistry* **2021,** *338*, 127796.

30. Xu, Y., et al., Mesoporous silica supported orderly-spaced gold nanoparticles SERS-based sensor for pesticides detection in food. *Food Chemistry* **2020,** *315*, 126300.

31. Joseph, D.; Kwak, C. H.; Huh, Y. S.; Han, Y.-K., Synthesis of AuAg@Ag core@shell hollow cubic nanostructures as SERS substrates for attomolar chemical sensing. *Sensors and Actuators B: Chemical* **2019,** *281*, 471-477.

32. Li, Z. H., et al., Facile synthesis of Au nanoparticle-coated Fe3O4 magnetic composite nanospheres and their application in SERS detection of malachite green.

Spectrochimica Acta Part A: Molecular and Biomolecular Spectroscopy **2020,** *241*, 118532.

33. Petti, L., et al., A plasmonic nanostructure fabricated by electron beam lithography as a sensitive and highly homogeneous SERS substrate for bio-sensing applications. *Vibrational Spectroscopy* **2016,** *82*, 22-30.

34. Shi, G., et al., Nanoflower-like Ag/AAO SERS platform with quasi-photonic crystal nanostructure for efficient detection of goat serum. *Current Applied Physics* **2019,** *19* (11), 1276-1285.

35. Creedon, N. C.; Lovera, P.; Furey, A.; O'Riordan, A., Transparent polymer-based SERS substrates templated by a soda can. *Sensors and Actuators B: Chemical* **2018,** *259*, 64-74.

36. Lovera, P.; Creedon, N.; Alatawi, H.; Mitchell, M.; Burke, M.; Quinn, A. J.; O'Riordan, A., Low-cost silver capped polystyrene nanotube arrays as super-hydrophobic substrates for SERS applications. *Nanotechnology* **2014,** *25* (17), 175502.

37. Jiang, T.; Wang, X.; Tang, S.; Zhou, J.; Gu, C.; Tang, J., Seed-mediated synthesis and SERS performance of graphene oxide-wrapped Ag nanomushroom. *Scientific Reports* **2017,** *7* (1), 9795.

38. Marques, A.; Veigas, B.; Araújo, A.; Pagará, B.; Baptista, P. V.; Águas, H.; Martins, R.; Fortunato, E., Paper-Based SERS Platform for One-Step Screening of Tetracycline in Milk. *Scientific Reports* **2019,** *9* (1), 17922.

39. Parnsubsakul, A.; Ngoensawat, U.; Wutikhun, T.; Sukmanee, T.; Sapcharoenkun, C.; Pienpinijtham, P.; Ekgasit, S., Silver nanoparticle/bacterial nanocellulose paper composites for paste-and-read SERS detection of pesticides on fruit surfaces. *Carbohydrate Polymers* **2020,** *235*, 115956.

40. Rajapandiyan, P.; Yang, J., Photochemical method for decoration of silver nanoparticles on filter paper substrate for SERS application. *Journal of Raman Spectroscopy* **2014,** *45* (7), 574-580.

41. Siebe, H. S.; Chen, Q.; Li, X.; Xu, Y.; Browne, W. R.; Bell, S. E. J., Filter paper based SERS substrate for the direct detection of analytes in complex matrices. *Analyst* **2021,** *146* (4), 1281-1288.

42. Tegegne, W. A.; Su, W.-N.; Beyene, A. B.; Huang, W.-H.; Tsai, M.-C.; Hwang, B.-J., Flexible hydrophobic filter paper-based SERS substrate using silver nanocubes for sensitive and rapid detection of adenine. *Microchemical Journal* **2021,** *168*, 106349.

43. Wang, J.; Qiu, C.; Mu, X.; Pang, H.; Chen, X.; Liu, D., Ultrasensitive SERS detection of rhodamine 6G and p-nitrophenol based on electrochemically roughened nano-Au film. *Talanta* **2020,** *210*, 120631.

44. Xie, J.; Li, L.; Khan, I. M.; Wang, Z.; Ma, X., Flexible paper-based SERS substrate strategy for rapid detection of methyl parathion on the surface of fruit. *Spectrochimica Acta Part A: Molecular and Biomolecular Spectroscopy* **2020,** *231*, 118104.

45. Zong, X.; Zhu, R.; Guo, X., Nanostructured gold microelectrodes for SERS and EIS measurements by incorporating ZnO nanorod growth with electroplating. *Scientific Reports* **2015,** *5* (1), 16454.

46. Tezcan, T.; Hsu, C.-H., High-sensitivity SERS based sensing on the labeling side of glass slides using low branched gold nanoparticles prepared with surfactant-free synthesis. *RSC Advances* **2020,** *10* (56), 34290-34298.

47. Zhang, J.; He, L.; Chen, P.; Tian, C.; Wang, J.; Liu, B.; Jiang, C.; Zhang, Z., A silica-based SERS chip for rapid and ultrasensitive detection of fluoride ions triggered by a cyclic boronate ester cleavage reaction. *Nanoscale* **2017,** *9* (4), 1599-1606.

48. Liu, X.; Lebedkin, S.; Besser, H.; Pfleging, W.; Prinz, S.; Wissmann, M.; Schwab, P. M.; Nazarenko, I.; Guttmann, M.; Kappes, M. M.; Lemmer, U., Tailored Surface-Enhanced Raman Nanopillar Arrays Fabricated by Laser-Assisted Replication for Biomolecular Detection Using Organic Semiconductor Lasers. *ACS Nano* **2015,** *9* (1), 260-270.

49. Hoffmann, M.; Wackerow, S.; Abdolvand, A.; Zolotovskaya, S. A., High performance SERS platforms via parametric optimization of the laser-assisted photodeposition of silver and gold nanoparticles. *Opt. Mater. Express* **2021,** *11* (9), 3079-3098.

50. MacKenzie, M.; Chi, H.; Varma, M.; Pal, P.; Kar, A.; Paterson, L., Femtosecond laser fabrication of silver nanostructures on glass for surface enhanced Raman spectroscopy. *Scientific Reports* **2019,** *9* (1), 17058.

51. Sammi, H.; Nair, R. V.; Sardana, N., Recent advances in nanoporous AAO based substrates for surface-enhanced raman scattering. *Materials Today: Proceedings* **2021,** *41*, 843-850.

52. Xia, Y.; Wu, Y.; Hang, T.; Chang, J.; Li, M., Electrodeposition of High Density Silver Nanosheets with Controllable Morphologies Served as Effective and Reproducible SERS Substrates. *Langmuir* **2016,** *32* (14), 3385-3392.

53. Chen, S.; Liu, B.; Zhang, X.; Mo, Y.; Chen, F.; Shi, H.; Zhang, W.; Hu, C.; Chen, J., Electrochemical fabrication of pyramid-shape silver microstructure as effective and reusable SERS substrate. *Electrochimica Acta* **2018,** *274*, 242-249.

54. Cheng, Z.-Q.; Li, Z.-W.; Xu, J.-H.; Yao, R.; Li, Z.-L.; Liang, S.; Cheng, G.-L.; Zhou, Y.-H.; Luo, X.; Zhong, J., Morphology-Controlled Fabrication of Large-Scale Dendritic Silver Nanostructures for Catalysis and SERS Applications. *Nanoscale Research Letters* **2019,** *14* (1), 89.

55. Dao, T. C.; Luong, T. Q. N., Fabrication of uniform arrays of silver nanoparticles on silicon by electrodeposition in ethanol solution and their use in SERS detection of difenoconazole pesticide. *RSC Advances* **2020,** *10* (67), 40940-40947.

56. Street, C. A.; Anderson, D. M. W., Refinement of structures previously proposed for gum arabic and other acacia gum exudates. *Talanta* **1983,** *30* (11), 887-893.

57. Goff, H. D.; Guo, Q., The Role of Hydrocolloids in the Development of Food Structure. In *Handbook of Food Structure Development*, The Royal Society of Chemistry: 2020; pp 1-28.

58. Banerjee, S. S.; Chen, D. H., Fast removal of copper ions by gum arabic modified magnetic nano-adsorbent. *J Hazard Mater* **2007,** *147* (3), 792-9.

59. Sanchez, L. M.; Ollier, R. P.; Pereira, A. E. S.; Fraceto, L. F.; Alvarez, V. A., Pesticide removal from industrial effluents using biopolymeric materials. In *Biopolymer Membranes and Films*, de Moraes, M. A.; da Silva, C. F.; Vieira, R. S., Eds. Elsevier: 2020; pp 359-382.

60. Kee, Y. L.; Mukherjee, S.; Pariatamby, A., Effective remediation of phenol,2,4-bis(1,1-dimethylethyl) and bis(2-ethylhexyl) phthalate in farm effluent using Guar gum – A plant based biopolymer. *Chemosphere* **2015,** *136*, 111-117.

61. Riddell, G. L.; Davies, C. W., A Study of Gum Arabic, Part I. Viscosity and Adsorption Measurements. *The Journal of Physical Chemistry* **1931,** *35* (9), 2722-2731.

62. Chen, Z.; Ye, H.; Chen, Y.; Xu, J., Tuning the dispersity and sphericity of silver particles by wrapping mechanism using Arabic gum. *Materials Letters* **2021,** *293*, 129665.

63. Anwar, A.; Masri, A.; Rao, K.; Rajendran, K.; Khan, N. A.; Shah, M. R.; Siddiqui, R., Antimicrobial activities of green synthesized gums-stabilized nanoparticles loaded with flavonoids. *Scientific Reports* **2019,** *9* (1), 3122.

64. Song, J. E., et al., Hydrophobic Interactions Increase Attachment of Gum Arabic- and PVP-Coated Ag Nanoparticles to Hydrophobic Surfaces. *Environmental Science & Technology* **2011,** *45* (14), 5988-5995.

65. Bhakat, D.; Barik, P.; Bhattacharjee, A., Electrical conductivity behavior of Gum Arabic biopolymer-Fe3O4 nanocomposites. *Journal of Physics and Chemistry of Solids* **2018,** *112*, 73-79.

66. A, I.; K.S, S.; S, M.; K.S, R., Viscosity and thermal conductivity of dispersions of gum arabic capped MWCNT in water: Influence of MWCNT concentration and temperature. *Journal of the Taiwan Institute of Chemical Engineers* **2013,** *44* (3), 474-479.

67. Chabot, V.; Kim, B.; Sloper, B.; Tzoganakis, C.; Yu, A., High yield production and purification of few layer graphene by Gum Arabic assisted physical sonication. *Scientific Reports* **2013,** *3* (1), 1378.

68. Tian, L.; Su, M.; Yu, F.; Xu, Y.; Li, X.; Li, L.; Liu, H.; Tan, W., Liquid-state quantitative SERS analyzer on self-ordered metal liquid-like plasmonic arrays. *Nature Communications* **2018,** *9* (1), 3642.

69. Zhang, X.; Zhang, H.; Yan, S.; Zeng, Z.; Huang, A.; Liu, A.; Yuan, Y.; Huang, Y., Organic Molecule Detection Based on SERS in Microfluidics. *Scientific Reports* **2019,** *9* (1), 17634.

70. Pu, H.; Xiao, W.; Sun, D.-W., SERS-microfluidic systems: A potential platform for rapid analysis of food contaminants. *Trends in Food Science & Technology* **2017,** *70*, 114-126.

71. Seymour, I.; O'Sullivan, B.; Lovera, P.; Rohan, J. F.; O'Riordan, A., Elimination of Oxygen Interference in the Electrochemical Detection of Monochloramine, Using In Situ pH Control at Interdigitated Electrodes. *ACS Sensors* **2021,** *6* (3), 1030-1038.

72. Sharipov, M.; Ju, T. J.; Azizov, S.; Turaev, A.; Lee, Y.-I., Novel molecularly imprinted nanogel modified microfluidic paper-based SERS substrate for simultaneous detection of bisphenol A and bisphenol S traces in plastics. *Journal of Hazardous Materials* **2024,** *461*, 132561.

73. Schulze, H. G.; Foist, R. B.; Okuda, K.; Ivanov, A.; Turner, R. F. B., A Small-Window Moving Average-Based Fully Automated Baseline Estimation Method for Raman Spectra. *Appl. Spectrosc.* **2012,** *66* (7), 757-764.

74. Daly, R.; Narayan, T.; Shao, H.; O'Riordan, A.; Lovera, P., Platinum-Based Interdigitated Micro-Electrode Arrays for Reagent-Free Detection of Copper. *Sensors* **2021,** *21* (10).

75. Guler, M. T.; Bilican, I., Capacitive detection of single bacterium from drinking water with a detailed investigation of electrical flow cytometry. *Sensors and Actuators A: Physical* **2018,** *269*, 454-463.

76. D Bhakat, P. B. A. B., Electrical conductive properties of some composites of gum arabic bioplolymer and magnetite nanoparticles. *Indian Journal of Pure & Applied Physics* **2018,** *56*, 428-433.

77. Prasad, N.; Thombare, N.; Sharma, S. C.; Kumar, S., Gum arabic – A versatile natural gum: A review on production, processing, properties and applications. *Industrial Crops and Products* **2022,** *187*, 115304.

78. Hassanzadeh-Afruzi, F.; Esmailzadeh, F.; Heidari, G.; Maleki, A.; Nazarzadeh Zare, E., Arabic Gum-Grafted-Hydrolyzed Polyacrylonitrile@ZnFe2O4 as a Magnetic Adsorbent for Remediation of Levofloxacin Antibiotic from Aqueous Solutions. *ACS Omega* **2023,** *8* (7), 6337-6348.

79. Sharma, G.; Kumar, A.; Naushad, M.; Dhiman, P.; Thakur, B.; García-Peñas, A.; Stadler, F. J., Gum Acacia-Crosslinked-Poly(Acrylamide) Hydrogel Supported C3N4/BiOI Heterostructure for Remediation of Noxious Crystal Violet Dye. *Materials* **2022,** *15* (7), 2549.

80. Mariod, A. A., Chemical Properties of Gum Arabic. In *Gum Arabic*, Mariod, A. A., Ed. Academic Press: 2018; pp 67-73.

81. Forgács, E.; Cserháti, T.; Barta, I., The binding of amino acids to the herbicide 2,4-dichlorophenoxy acetic acid. *Amino acids* **2000,** *18* (1), 69-79.

82. Mabrouk, M.; Mansour, A.; Abdelhamid, A.; Abualnaja, K.; Mamoon, A.; Shabaan, W.; Matter, A.; Ayoub, H.; Farouk Basuony Abdelhamid, A.; Ayoub, H., Impact of aqueous exposure to silver nanoparticles on growth performance, redox status, non-specific immunity, and histopathological changes of Nile Tilapia, Oreochromis niloticus, challenged with Aeromonas hydrophila. *Aquaculture Reports* **2021**.

83. Joshi, N.; Jain, N.; Pathak, A.; Singh, J.; Prasad, R.; Upadhyaya, C., Biosynthesis of silver nanoparticles using Carissa carandas berries and its potential antibacterial activities. *Journal of Sol-Gel Science and Technology* **2018,** *86*.

84. Kim, S.; Byun, K. M.; Lee, S. Y., Influence of water content on Raman spectroscopy characterization of skin sample. *Biomed Opt Express* **2017,** *8* (2), 1130-1138.

85. Narayanan, S.; Kalidindi, S.; Schadler, L., Determination of unknown stress states in silicon wafers using microlaser Raman spectroscopy. *Journal of Applied Physics* **1997,** *82*.

86. Hrubý, J.; Vavrečková, Š.; Masaryk, L.; Sojka, A.; Navarro-Giraldo, J.; Bartoš, M.; Herchel, R.; Moncol, J.; Nemec, I.; Neugebauer, P., Deposition of Tetracoordinate Co(II) Complex with Chalcone Ligands on Graphene. *Molecules* **2020,** *25* (21), 5021.

87. Hua, M. Z.; Feng, S.; Wang, S.; Lu, X., Rapid detection and quantification of 2,4-dichlorophenoxyacetic acid in milk using molecularly imprinted polymers–surface-enhanced Raman spectroscopy. *Food Chemistry* **2018,** *258*, 254-259.

88. Santos Costa, J. C.; Ando, R. A.; Sant'Ana, A. C.; Rossi, L. M.; Santos, P. S.; Temperini, M. L. A.; Corio, P., High performance gold nanorods and silver nanocubes in surface-enhanced Raman spectroscopy of pesticides. *Physical Chemistry Chemical Physics* **2009,** *11* (34), 7491-7498.

89. Jia, J.; Jin, X.-Y.; Liu, Q.-L.; Liang, W.; Lin, M.-S.; Xu, H.-H., Preparation, Characterization and Intracellular Imaging of 2,4-Dichlorophenoxyacetic Acid Conjugated Gold Nanorods. *Journal of Nanoscience and Nanotechnology* **2016,** *16*, 4936-4942.

90. Shen, X. S.; Wang, G. Z.; Hong, X.; Zhu, W., Nanospheres of silver nanoparticles: agglomeration, surface morphology control and application as SERS substrates. *Physical Chemistry Chemical Physics* **2009,** *11* (34), 7450-7454.

91. Joseph, D.; Huh, Y. S.; Han, Y.-K., A top-down chemical approach to tuning the morphology and plasmon resonance of spiky nanostars for enriched SERS-based chemical sensing. *Sensors and Actuators B: Chemical* **2019,** *288*, 120-126.

92. Solís, D. M.; Taboada, J. M.; Obelleiro, F.; Liz-Marzán, L. M.; García de Abajo, F. J., Optimization of Nanoparticle-Based SERS Substrates through Large-Scale Realistic Simulations. *ACS Photonics* **2017,** *4* (2), 329-337.

93. Rodriguez-Ruiz, V.; Maksimenko, A.; Salzano, G.; Lampropoulou, M.; Lazarou, Y.; Agostoni, V.; Couvreur, P.; Gref, R.; Yannakopoulou, K., Positively charged cyclodextrins as effective molecular transporters of active phosphorylated forms of gemcitabine into cancer cells. *Scientific Reports* **2017,** *7*.

94. Zhao, X.; Zhang, H.; Li, W.; Li, X.; Fan, W.; Zhang, Y., Langmuir-diffusion model: Its modification and further application to glutinous rice flour particles. *Journal of Food Process Engineering* **2020,** *43* (9), e13470.

95. Vandenabeele, P.; Ortega-Avilès, M.; Castilleros, D. T.; Moens, L., Raman spectroscopic analysis of Mexican natural artists' materials. *Spectrochimica Acta Part A: Molecular and Biomolecular Spectroscopy* **2007,** *68* (4), 1085-1088.

96. Botta, R.; Rajanikanth, A.; Bansal, C., Silver nanocluster films for glucose sensing by Surface Enhanced Raman Scattering (SERS). *Sensing and Bio-Sensing Research* **2016,** *9*.

97. Chen, D.; Zhu, X.; Huang, J.; Wang, G.; Zhao, Y.; Chen, F.; Wei, J.; Song, Z.; Zhao, Y., Polydopamine@Gold Nanowaxberry Enabling Improved SERS Sensing of Pesticides, Pollutants, and Explosives in Complex Samples. *Analytical Chemistry* **2018,** *90* (15), 9048-9054.

98. Elamin, M. B.; Ali, S. M. A.; Essousi, H.; Chrouda, A.; Alhaidari, L. M.; Jaffrezic-Renault, N.; Barhoumi, H., An Electrochemical Sensor for Sulfadiazine Determination Based on a Copper Nanoparticles/Molecularly Imprinted Overoxidized Polypyrrole Composite. *Sensors* **2023,** *23* (3), 1270.

99. He, H.; Cao, M.; Hu, J.; Zhu, L.; Su, C.; Du, S.; Yang, J.; Tang, Y.; Chen, L., Fluorescent turn-on assay of C-type natriuretic peptide using a molecularly imprinted ratiometric fluorescent probe with high selectivity and sensitivity. *Microchimica Acta* **2020,** *187*.

100. Lu, Y.; Liu, Q.; Fu, B.; Li, P.; Xu, W., Label-free MIP-SERS biosensor for sensitive detection of colorectal cancer biomarker. *Talanta* **2023,** *258*, 124461.

101. Xu, Y.; Hassan, M.; Ali, S.; Li, H.; Chen, Q., SERS-based rapid detection of 2,4-dichlorophenoxyacetic acid in food matrices using molecularly imprinted magnetic polymers. *Microchimica Acta* **2020,** *187*.

102. Wu, H.; Niu, G.; Ren, W.; Jiang, L.; Zhao, J.; Quan, Y.; Ren, M. X.; Yu, W.; Zhang, Y.; Cao, X.; Liu, Y.; An, R.; Dai, L.; Wang, Z.; Zhao, L.; Xie, Z.; Zhao, G., Highly sensitive label-free detection of analytes at different scales using uniform

graphene-nanopyramids hybrid SERS system. *Sensors and Actuators B: Chemical* **2022,** *354*, 131205.

103. Shen, J.; Liu, G.; Zhang, W.; Shi, W.; Zhou, Y.; Yu, Z.; Mei, Q.; Zhang, L.; Huang, W., Design and Detection of Cyanide Raman Tag pH-Responsive SERS Probes. *Biosensors* **2023,** *13* (1), 21.

104. Niaura, G.; Malinauskas, A., Surface-enhanced Raman spectroscopy of ClO4- and SO42- anions adsorbed at a Cu electrode. *Journal of the Chemical Society, Faraday Transactions* **1998,** *94* (15), 2205-2211.

Supporting Information.

1. Chip fabrication process.

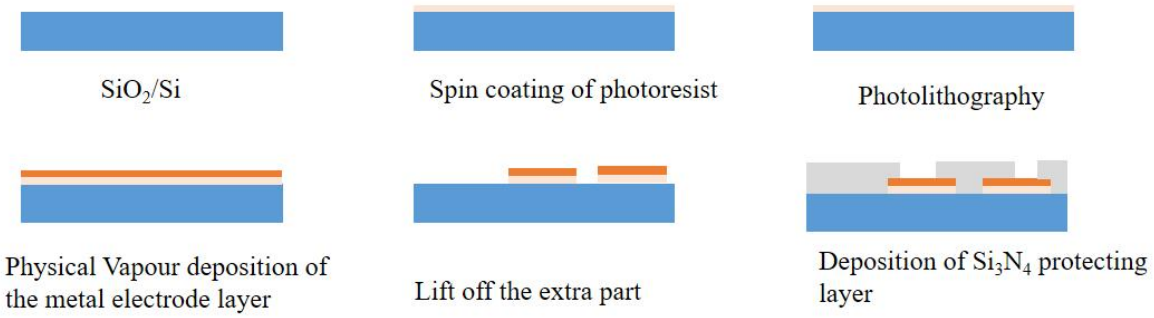

Figure S1: Chip fabrication process flow. Briefly, working electrodes, a reference electrode, a counter electrode, connecting wires, and contacting pads were patterned using photolithography and physical vapor deposition (PVD) followed by a lift-off step. Finally, Plasma-enhanced chemical vapor deposition (PECVD) Si_3N_4 was blanket deposited on the whole wafer, the openings were over the working/counter/reference electrodes, and the electrical contacts were defined by lithography and dry etching process.

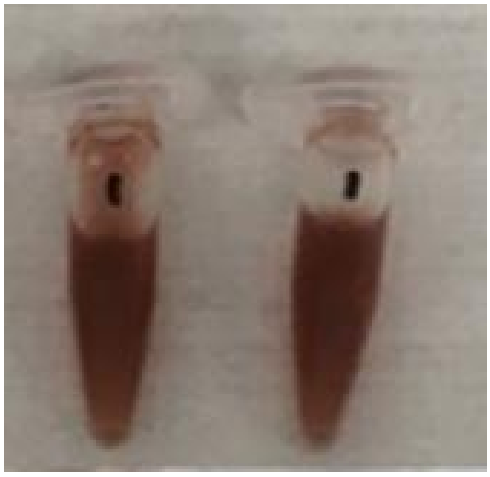

Figure S2: Given enough time, $AgNO_3$ and Gum Arabic would chemically react to form Ag-Gum Arabic nanoparticles.

2. Electrochemical deposition setup.

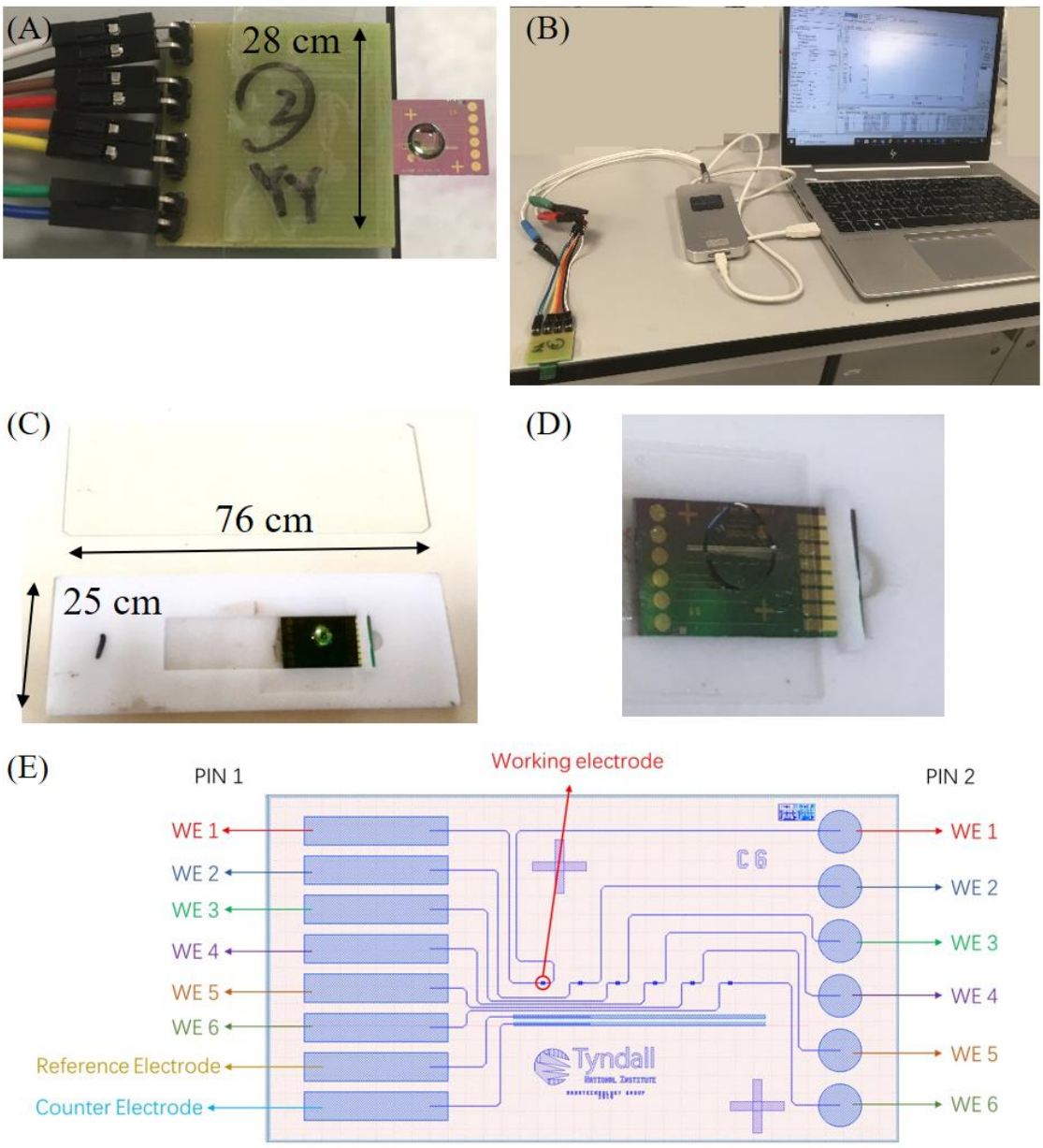

Figure S3: (A) Chip connector. (B) SERS substrate fabrication setup by electrochemical deposition. (C, D) Chip holder for Raman measurements in a water environment. (E) Chip design layout.

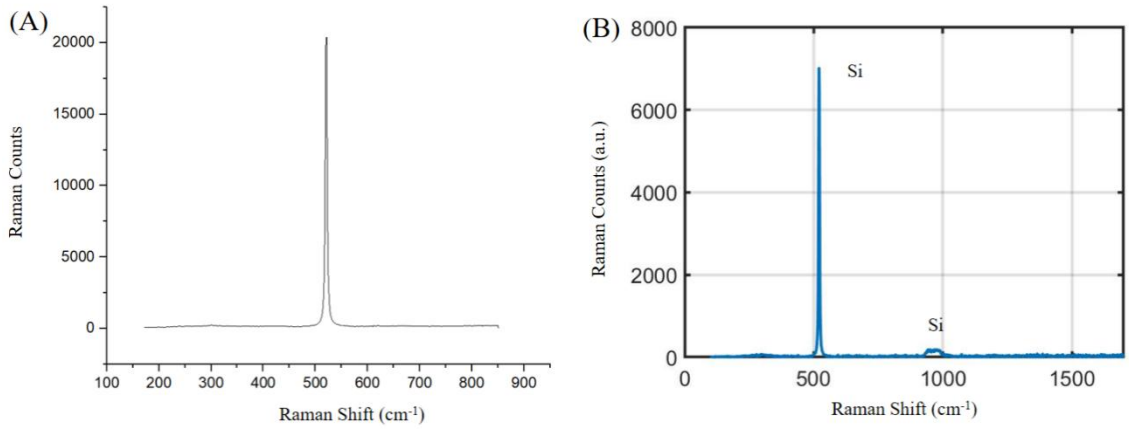

Figure S4: (A) Spectrum of Si chip used for daily laser power calibration by Raman counts (around 20000 a.u.), Raman peak at 520 cm^{-1}. Laser power: 0.7 mW, lens: 50x, exposure time: 1s. For laser power calibration, a daily check of this Si chip was carried out before experiments. The intensity should be tuned to remain around 20000 a.u and the peak should stay near 520 cm^{-1}. (B) Raman spectra of Si/SiO_2 sensor chip. Si: 520 cm^{-1}, 950 cm^{-1}. Laser power: 0.07 mW, exposure time: 10s, lens: 20x.

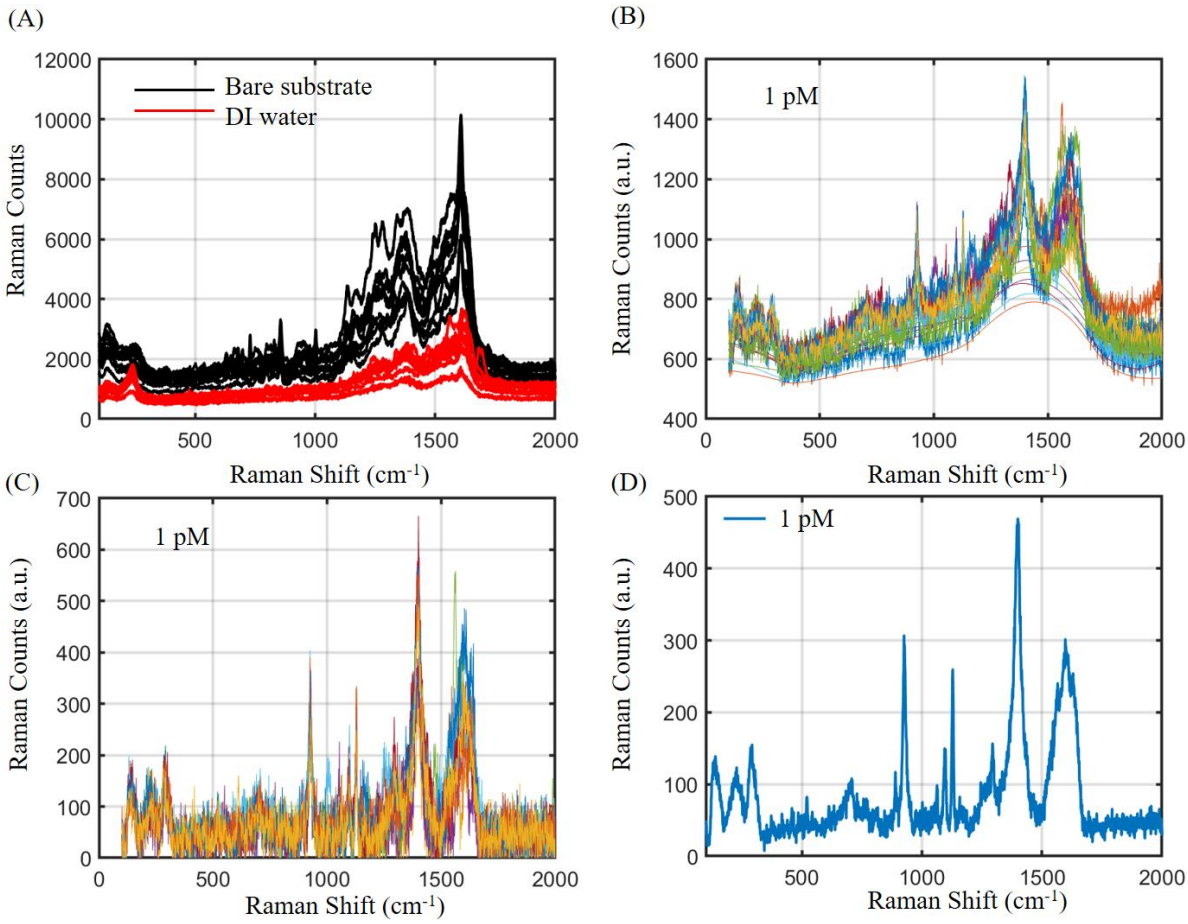

Figure S5: (A) bare substrate (in black) and substrate after application of DI water (in red). (B-D) Data processing by Matlab. (B) Raw data for 1 pM 2,4-D, the clean lines are the baseline for spectra and the background signal came from the Gum Arabic layer. (C) Spectra after baseline subtraction. (D) Average of the ten measurements in (B) for 1 pM 2,4-D.

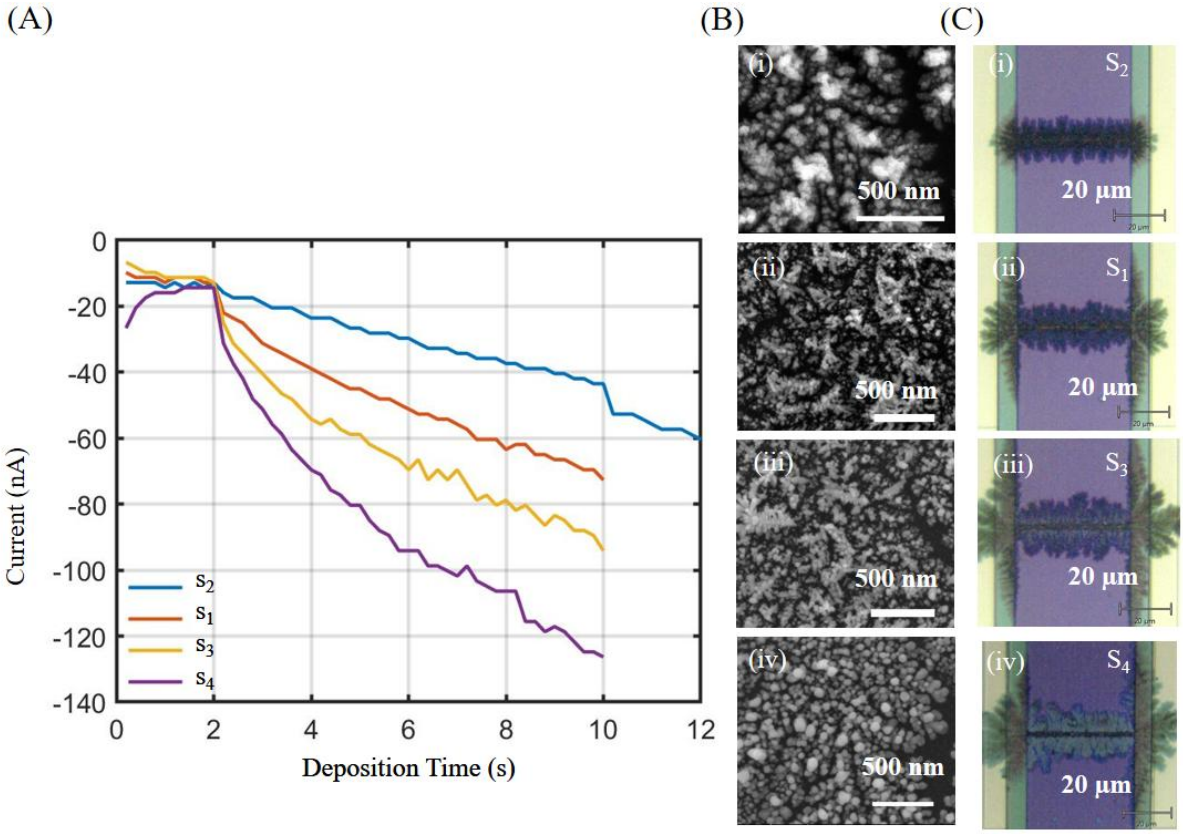

Figure S6: (A) Current (nA)-deposition time (s) graph for four Ag-GA nanostructures. On the same chip, for S_1-S_4, deposition current is around 70 nA, 60 nA, 90 nA, and 120 nA, respectively; (B) Corresponding SEM images for S_1-S_4. (C) Corresponding microscope (x50) images for S_1-S_4.

3. Optimization of the Ag-GA nano structure.

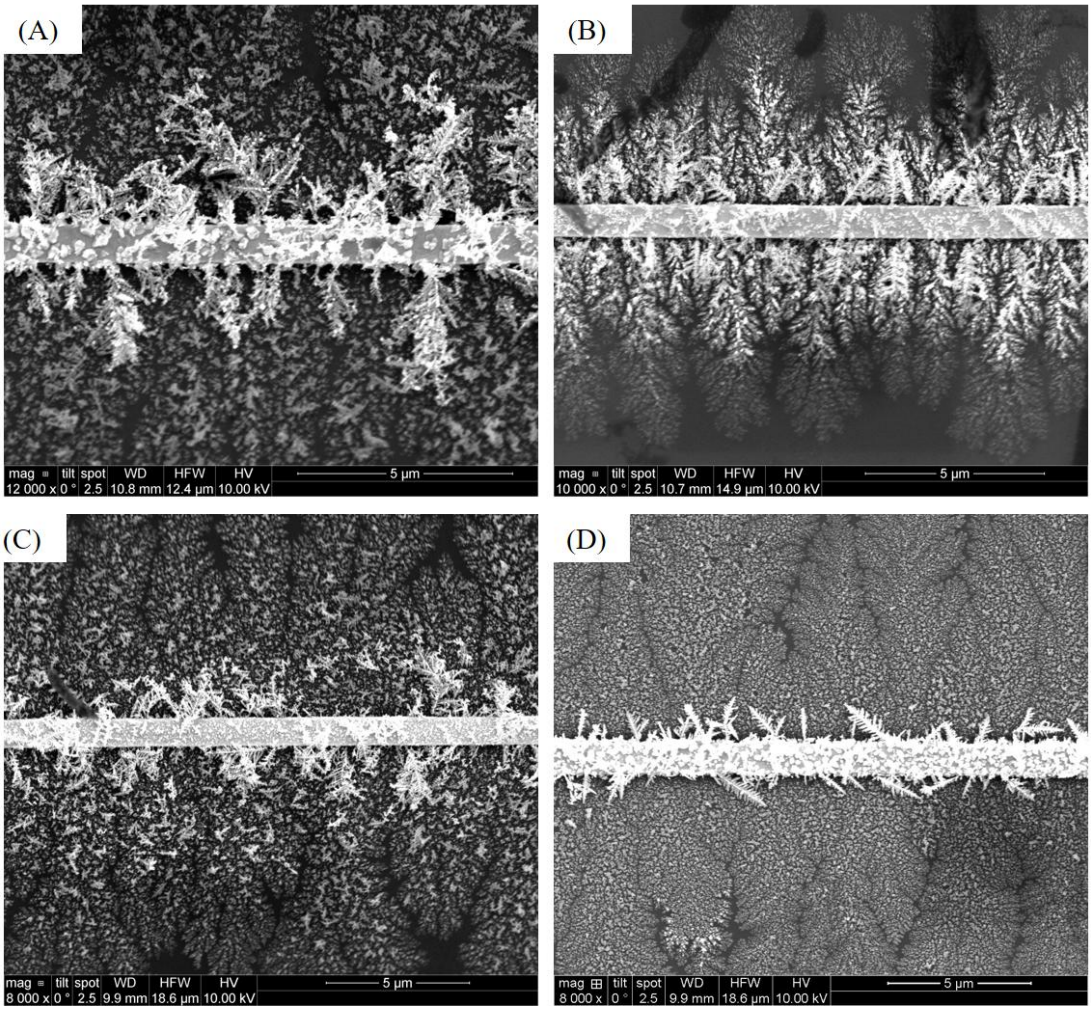

Figure S7: (A-D) SEM images of Ag-GA Nano structures S_1-S_4.

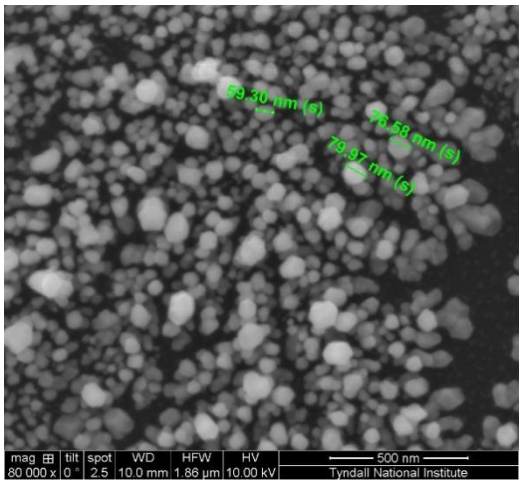

Figure S8: SEM image of Ag-GA SERS substrate S_4. SEM: 10 KV, spot size 2.5 nm. Particle size is indicated in the image. Scale bar: 500 nm.

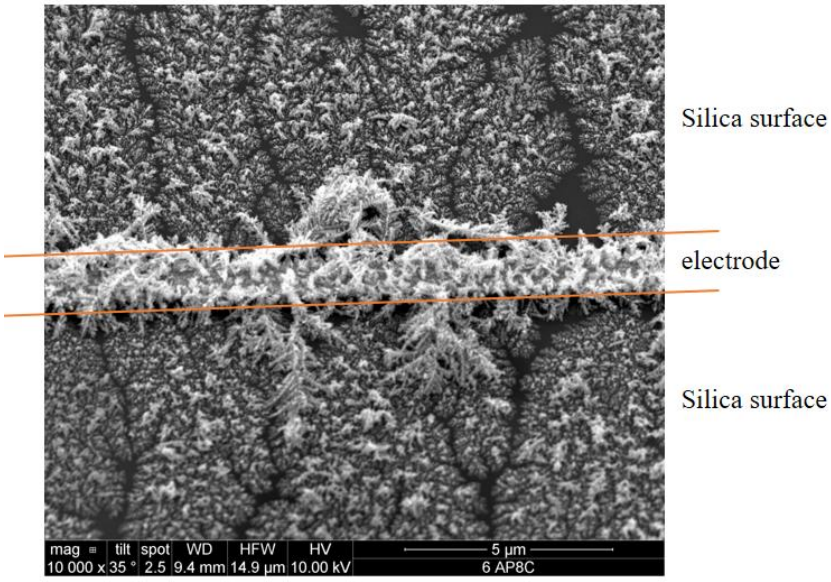

Figure S9: SEM image tilted at 35◦ that showed the isolated growth of the nanoclusters on SiO_2.

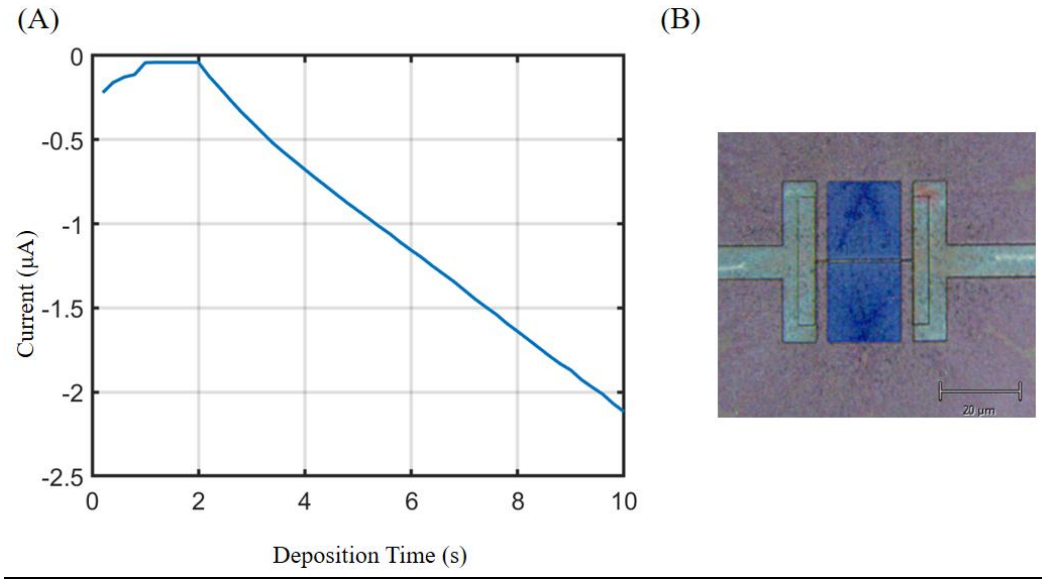

Figure S10: Current (µA)-time (s) graph for Ag deposition without Gum Arabic (5 mM $AgNO_3$).

To optimize the Ag-GA nano structure from an application point of view (detection ability and response time), and electrochemical deposit Ag-GA nano structures that

meet the requirements of a SERS device, different concentrations of $AgNO_3$, voltage settings, concentrations of Gum Arabic, deposition times were studied. With the sample voltage and deposition time (step 1: -0.2 V, 2 s; step 2: -0.8 V, 12 s; step 3: -1.2 V, 2 s), and the same concentration of $AgNO_3$ (5 mM), by tuning the concentration of Gum Arabic solution of 1 g/L, 2 g/L, 3 g/L, 10 g/L, 100 g/L, the volume and morphologies of the Ag NPs are different. As shown in **Figure S11 (A-E).** When the concentration of Gum Arabic is larger than 3 g/L, the silver nano particles tend to aggregate with smaller nano gaps in between, while when the concentration of Gum Arabic is below 3 g/L, the silver nano clusters distributed separately on the SiO_2/Si substrate with nano gap forming in between the silver nano clusters. For 1 g/L Gum Arabic solvent, the silver nanoparticles were decorated by small size nano dendrite on the top; For 2 g/L Gum Arabic solvent, the silver nanoparticles had thicker and larger size nano dendrite decoration on the top compared to 1 g/L Gum Arabic solvent. To study the dependence between deposition time and morphology, 2 g/L Gum Arabic solvent and 5 mM $AgNO_3$ solvent were used, voltage setting: setting 1: step 1: -0.2 V, 2 s; setting 2: step 1: -0.2 V, 2 s; step 2: -0.8 V, 8 s; setting 3: step 1: -0.2 V, 2 s; step 2: -0.8 V, 12 s; setting 4: step 1: -0.2 V, 2 s; step 2: -0.8 V, 16 s; As shown in **Figure S11 (F-I),** the deposition time increased, the nano dendrites grow bigger. With the same voltage setting (step1: -0.2 V, 2 s; step2: -0.5 V, 8 s; step3: -0.6 V, 2 s.) and the same Gum Arabic concentration (1g/L), different $AgNO_3$ concentration (1 mM, 5 mM, 0.5 M) was used to show the effect of the concentration of $AgNO_3$. As shown in **Figure S11 (J-L),** at low $AgNO_3$ concentration (1 mM), there was a thin layer of Ag-GA nano particles grow on the SiO_2/Si substrate; at $AgNO_3$ concentration of 5 mM, a thicker layer of Ag-GA nano particles grew on the SiO_2/Si substrate, as shown in **Figure S11 (J)**; at high $AgNO_3$ concentration (0.05 M), the Ag-GA dendrite tended to grow in 3D as shown in **Figure**

S11 (L). $AgNO_3$ concentration of 5 mM was the optimized parameter for this electrochemical platform. As shown in **Figure S11 (K)**, there was a dense coverage of Ag-GA nano particles providing numerous hotspots and the size of the nano particles had good resonance with the laser wavelength (514 nm). To determine the optimized deposition voltage, we used different voltage combinations at the same concentration of $AgNO_3$ (5 mM) and Gum Arabic (2 g/L). Combination 1: step1: -0.2 V, 2 s; step2: -0.5 V, 8 s; step3: -0.6 V, 2 s; combination 2: step1: -0.2 V, 2 s; E_2: -0.8 V, 8 s; E_3: -1.2 V, 2 s; combination 3: step1: -0.2 V, 2 s; step2: -1.2 V, 8 s; step3: -1.5 V, 2 s; as shown in **Figure S11 (M-O)**. At lower voltage combination (combination 1: step1: -0.2 V, 2 s; step2: -0.5 V, 8 s; step3: -0.6 V, 2 s), the Ag-Ga nano dendrites grow near the Au electrode; at voltage combination 2 (step1: -0.2 V, 2 s; step2: -0.8 V, 8 s; step3: -1.2 V, 2 s;), the Ag-Ga nano particles grew on the SiO_2/Si substrate with nano dendrites that were decorated on the top of the nano particles; At higher voltage combination (combination 3: step1: -0.2 V, 2 s; step2: -1.2 V, 8 s; step3: -1.5 V, 2 s), irregular growth of the Ag-GA particles occurs, this inhomogeneous growth of Ag-GA particles resulted in dramatically different Raman signal at different points during the 2,4-D detection process. In this electrochemical platform, a voltage below 1.2 V was used.

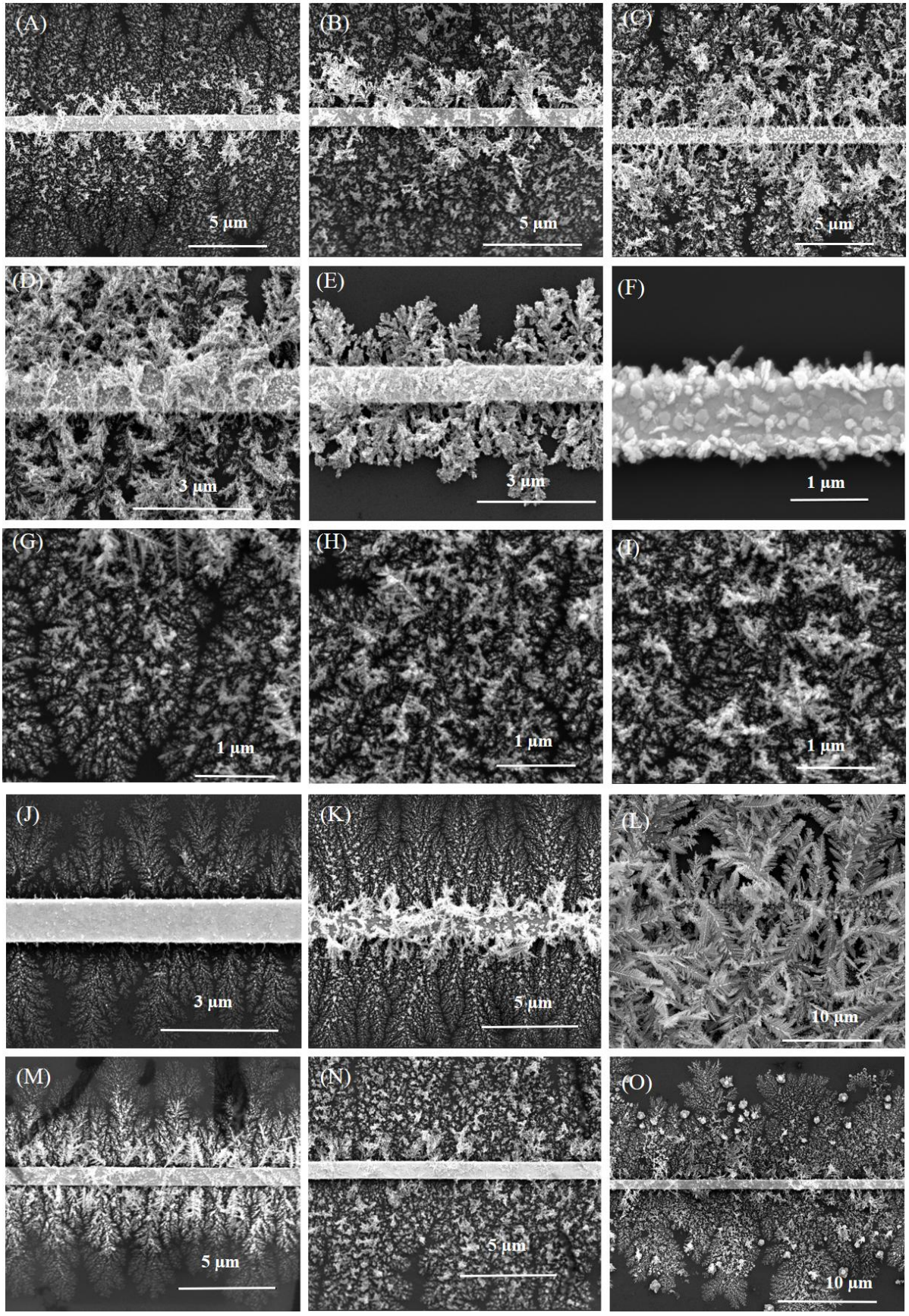
(A)
5 µm
(B)
5 µm
(C)
5 µm
(D)
3 µm
(E)
3 µm
(F)
1 µm
(G)
1 µm
(H)
1 µm
(I)
1 µm
(J)
3 µm
(K)
5 µm
(L)
10 µm
(M)
5 µm
(N)
5 µm
(O)
10 µm

Figure S11: SEM images of different deposition parameters. (A-E): different Gum Arabic concentration: 1 g/L, 2 g/L, 3 g/L, 10 g/L, 100 g/L; (F) deposition voltage at -0.2 V, 2 s; (G-I) E: -0.8 V, different deposition time: 8 s, 12 s, 16 s; (J-L) different $AgNO_3$ concentrations: 1 mM, 5 mM, 0.05 M. (M-O) different voltage settings which effected the growth pattern of the nano gaps. $AgNO_3$: Gum Arabic=1:1 in all the experiments. All the nanostructures have been electrochemically deposited at least 3 times.

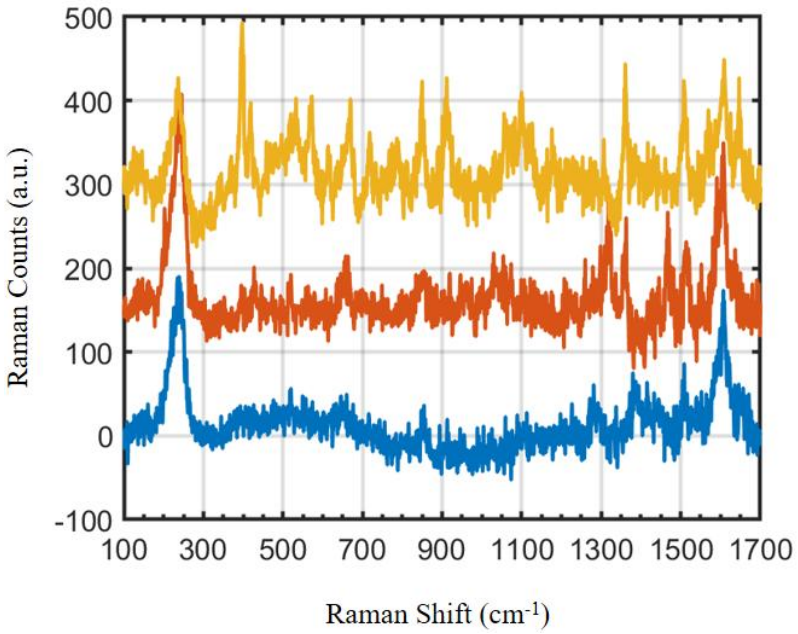

Figure S12: Spectra for 2,4-D at 1mM on bare silver nano particle SERS substrate, at three different locations. The silver nano particle was deposited by electrochemical synthesis, the electrochemical deposition curve is shown in Figure S10.

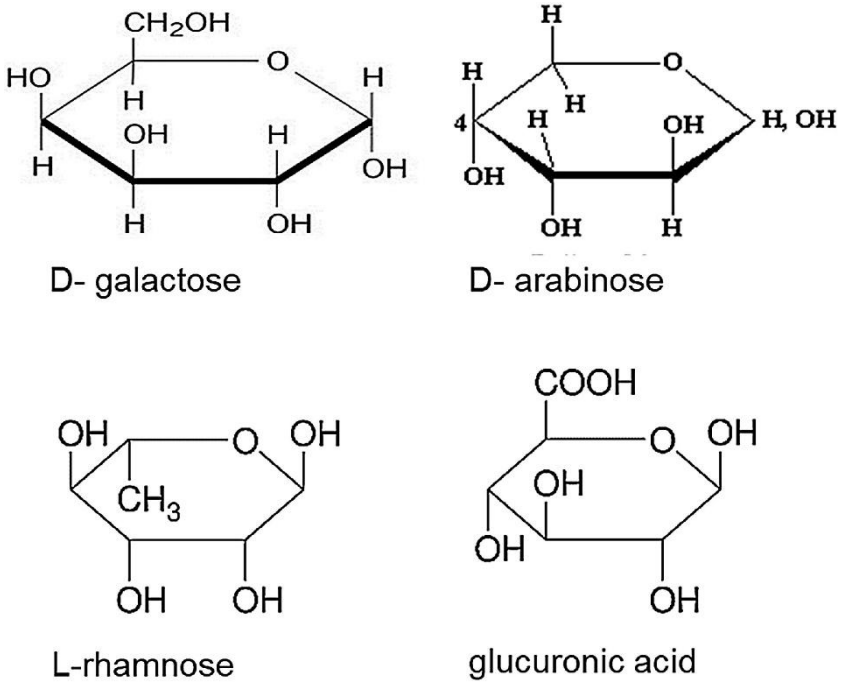

Figure S13: Chemical structures of Gum Arabic unit. Gum Arabic contains around 39-42% of galactose units, 24-27% of arabinose units, 12-16% of rhamnose units, 15-16% of glucuronic acid units, 1.5-2.4% of protein moieties, and 12-16% of moisture. These percentages are different with different gums depending on the acacia trees' ages or locations.[346]

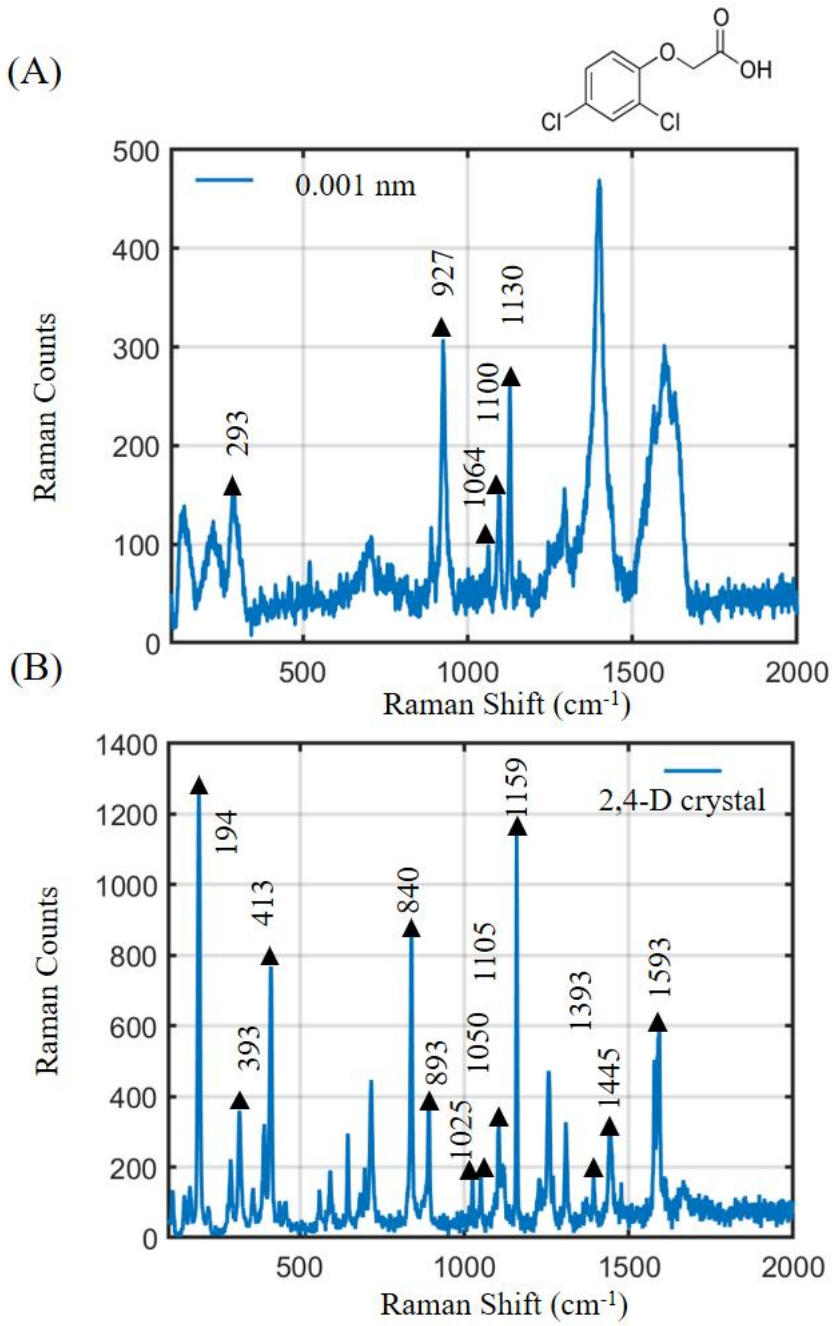

Figure S14: (A) Raman spectrum acquired with the sensor for 0.001 nM 2,4-D. (B) Raman spectrum for 2,4-D crystal. (laser power: 0.35 mW, exposure time: 30 s, 20x.).

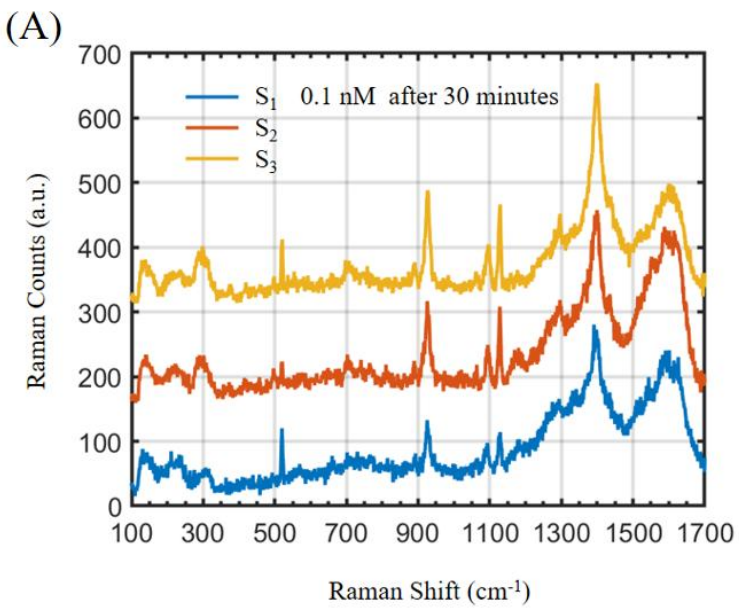

Figure S15: (A) Raman spectra for S_1-S_3 that were able to detect 2,4-D at 0.1 nM after 30 minutes. Peak around 520 cm^{-1} is from Si sensor substrate under Ag-GA nano structures. Si peak Raman signal intensity varies because of different coverage/nano gaps of Ag-GA nano structures at different measurement locations.

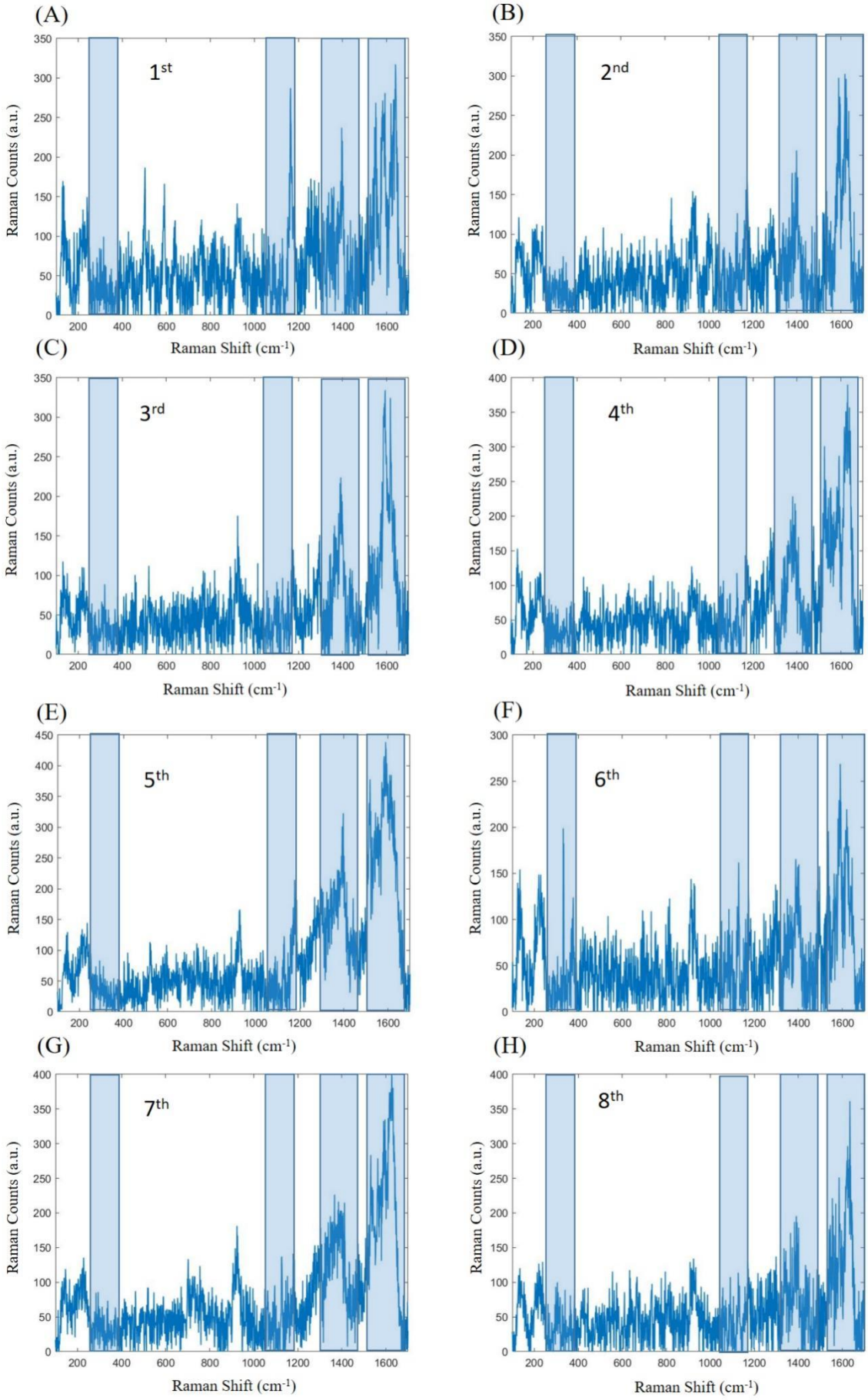
(A)
1st
(B)
2nd
(C)
3rd
(D)
4th
(E)
5th
(F)
6th
(G)
7th
(H)
8th
Raman Counts (a.u.)
Raman Shift (cm-1)

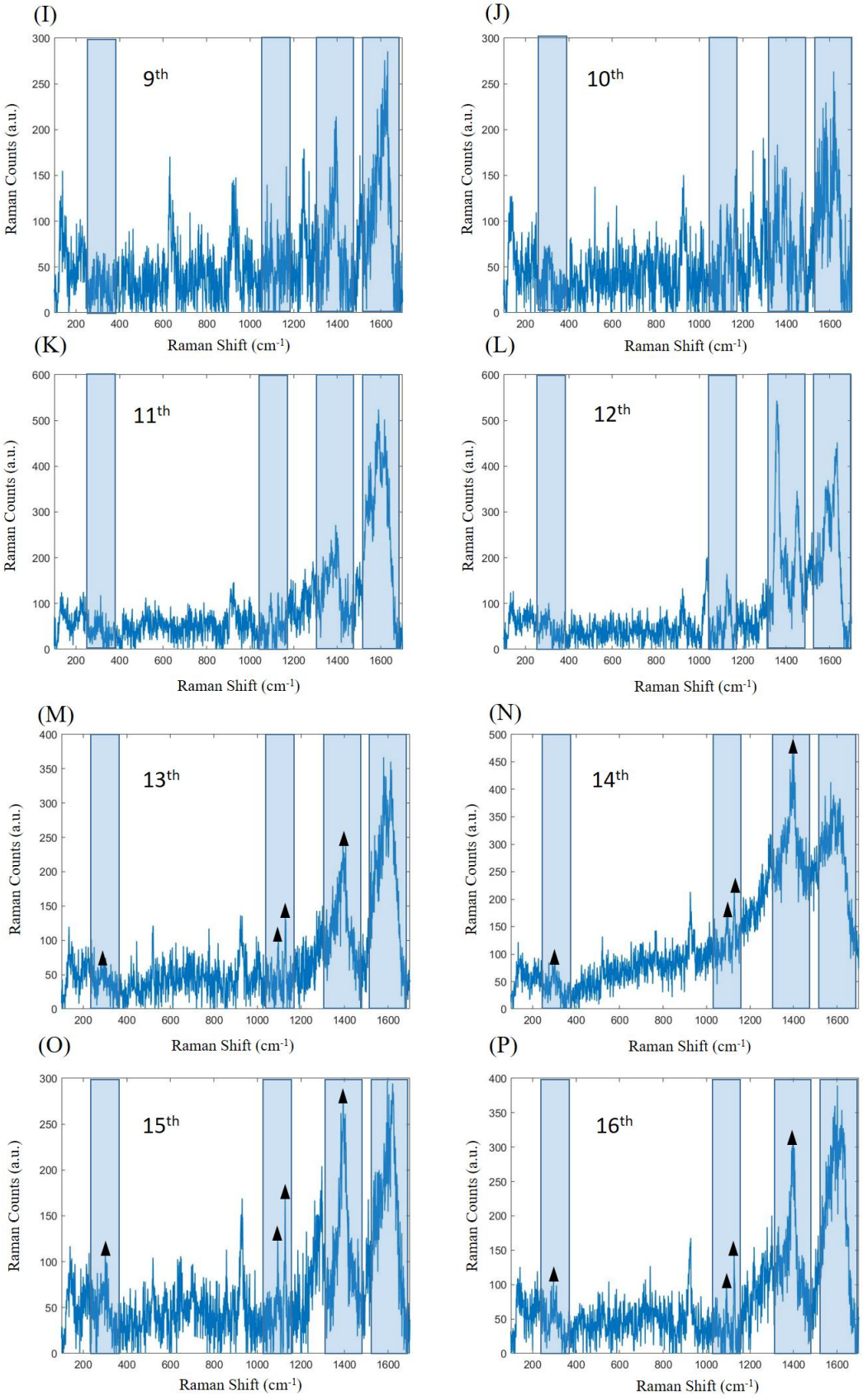
(I)
9th
(J)
10th
(K)
11th
(L)
12th
(M)
13th
(N)
14th
(O)
15th
(P)
16th
Raman Counts (a.u.)
Raman Shift (cm-1)

Figure S16: (A-P) The change of spectra before 2,4-D (1 pM) Raman signal appeared on the S_4 SERS substrate. (A-L) 1st -12th spectra. (M-P) 13th -16th spectra are for 2.4-D at 1 pM after around 30 minutes. Baselines have been subtracted for all spectra. It took around 1.5 minutes for each measurement.

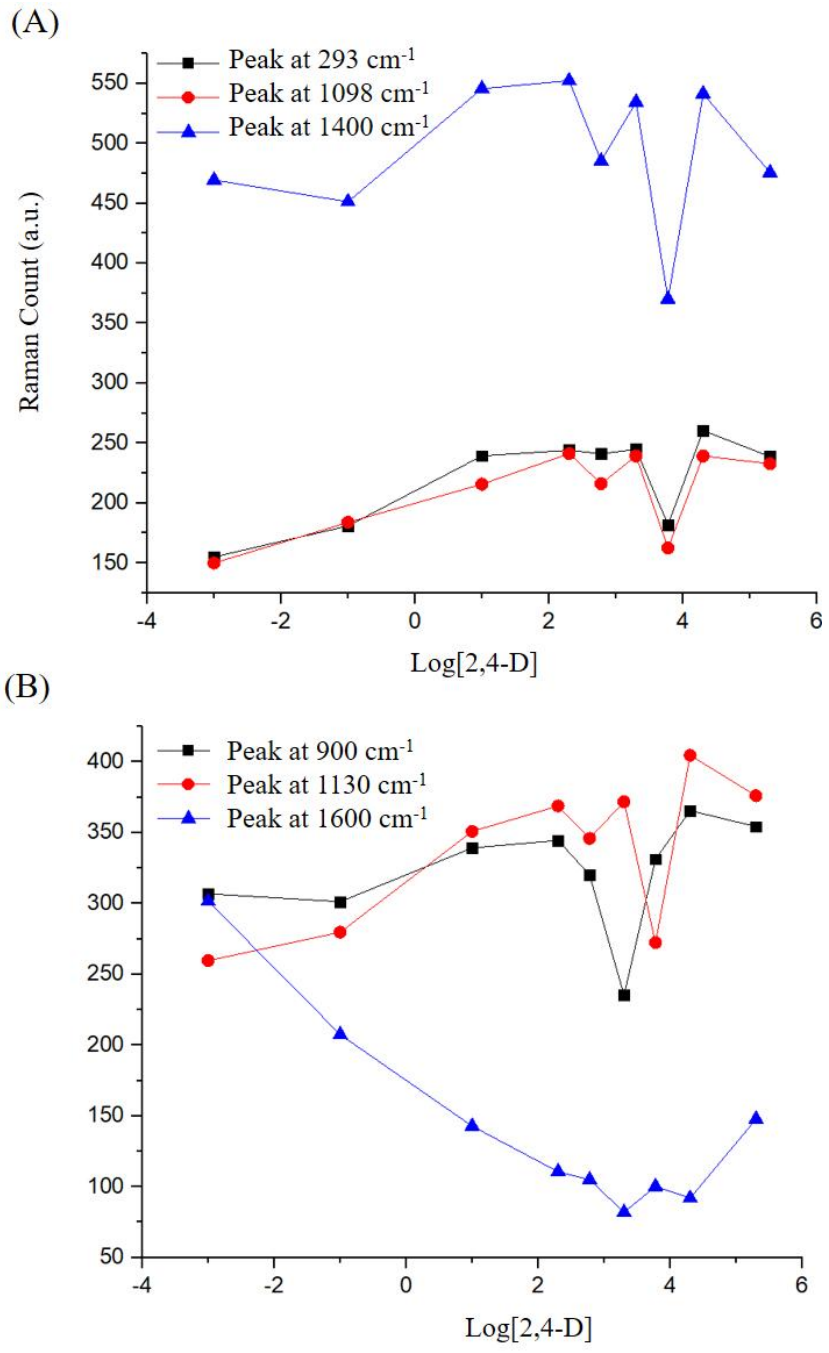

Figure S17: Singel peak intensity vs. Log[2,4-D].

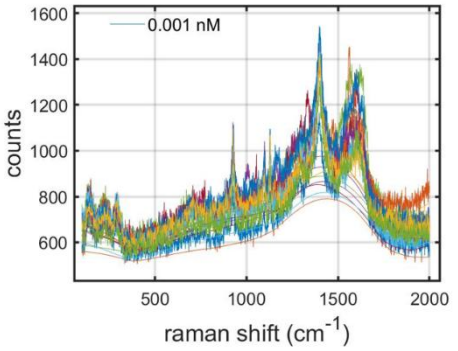
0.001 nM
counts
raman shift (cm-1)

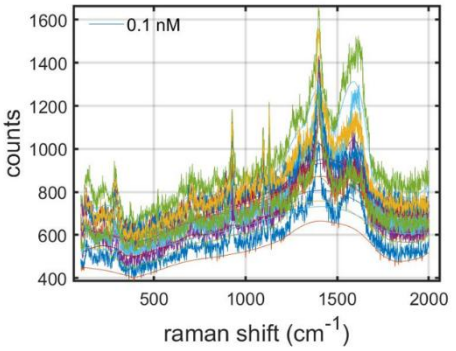
0.1 nM
counts
raman shift (cm-1)

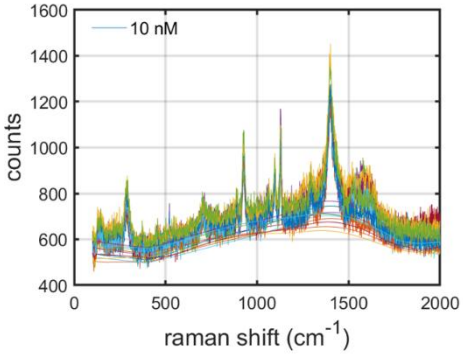
10 nM
counts
raman shift (cm-1)

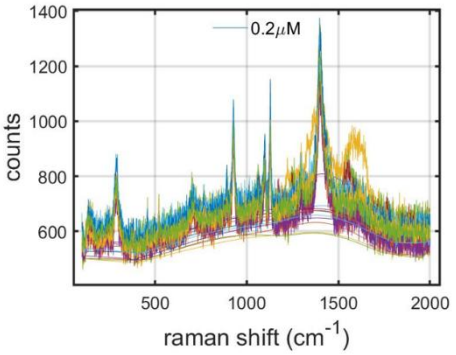
0.2μM
counts
raman shift (cm-1)

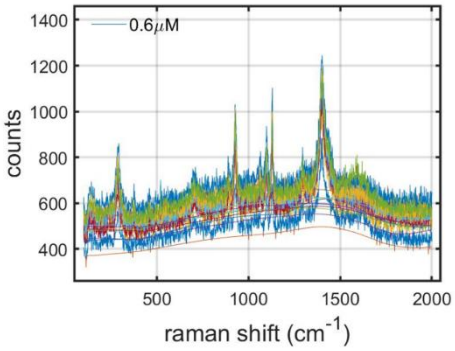
0.6μM
counts
raman shift (cm-1)

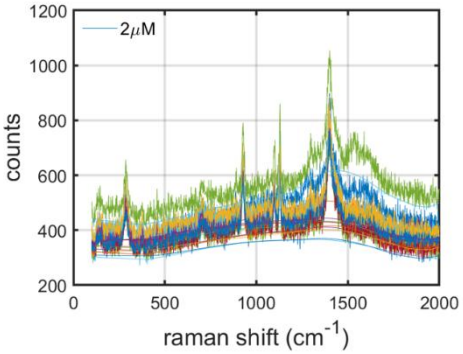
2μM
counts
raman shift (cm-1)

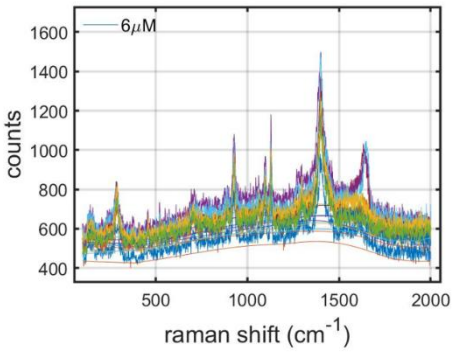
6μM
counts
raman shift (cm-1)

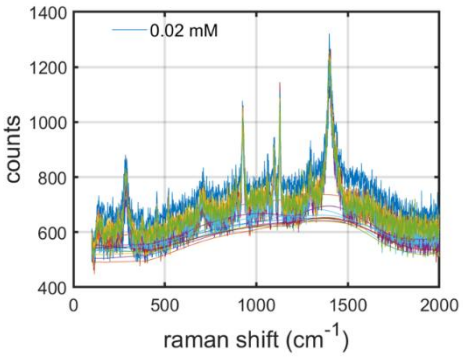
0.02 mM
counts
raman shift (cm-1)

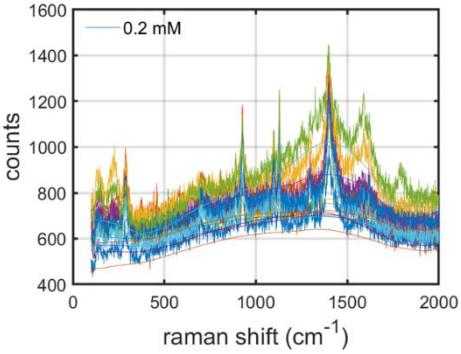
0.2 mM
counts
raman shift (cm-1)

Figure S18: Raw data in Figure 2.4. The spectra were for 2,4-D at different concentrations, and the smooth lines were subtracted from background signals in data analysis. Ten spectra were used for each concentration. At the lowest/first 2,4-D concentration, it took around 30 minutes to get the signal. It took 15 minutes in total to get all the data for each concentration.

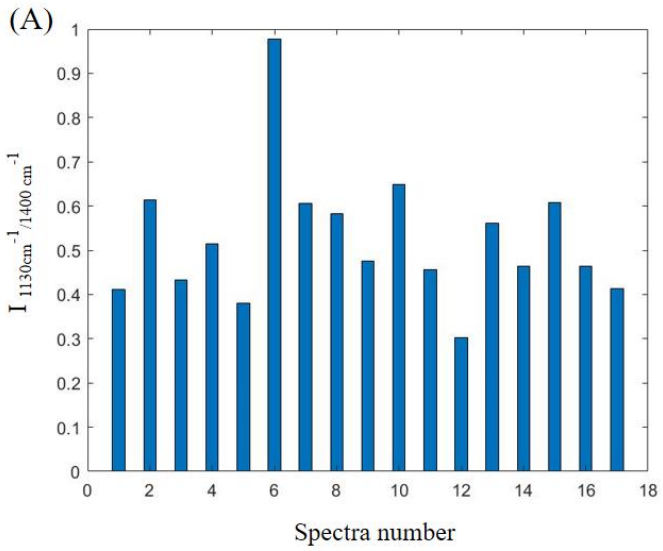

Figure S 19: (A) peak ratio $I_{1130\ cm\text{-}1}/I_{1400\ cm\text{-}1}$ changes with several continuous measurements in Figure S12.

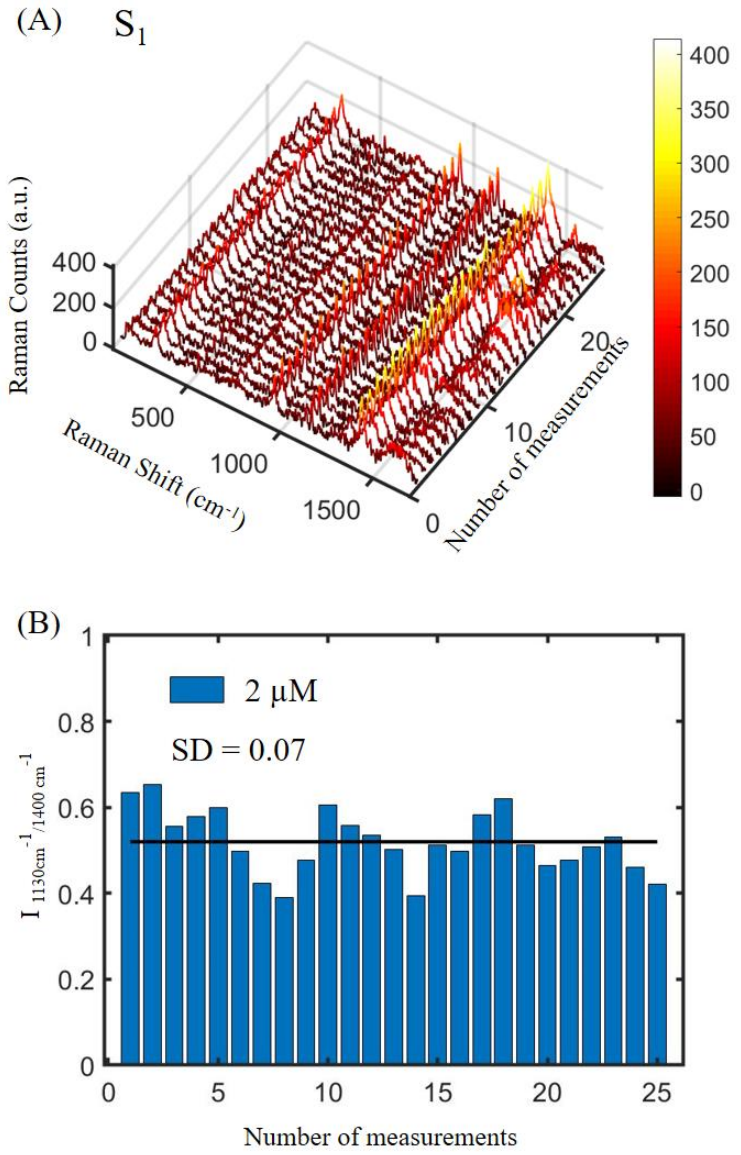

Figure S20 (A) Color waterfall spectra of 25 random points for 2 μM 2,4-D on a S_1 SERS substrate, the color bar stands for Raman intensity (a.u.). (B) Histogram of I_{1130} cm^{-1} / I_{1400} cm^{-1} at 25 different random points, the SD was 0.07 for the peak ratio.

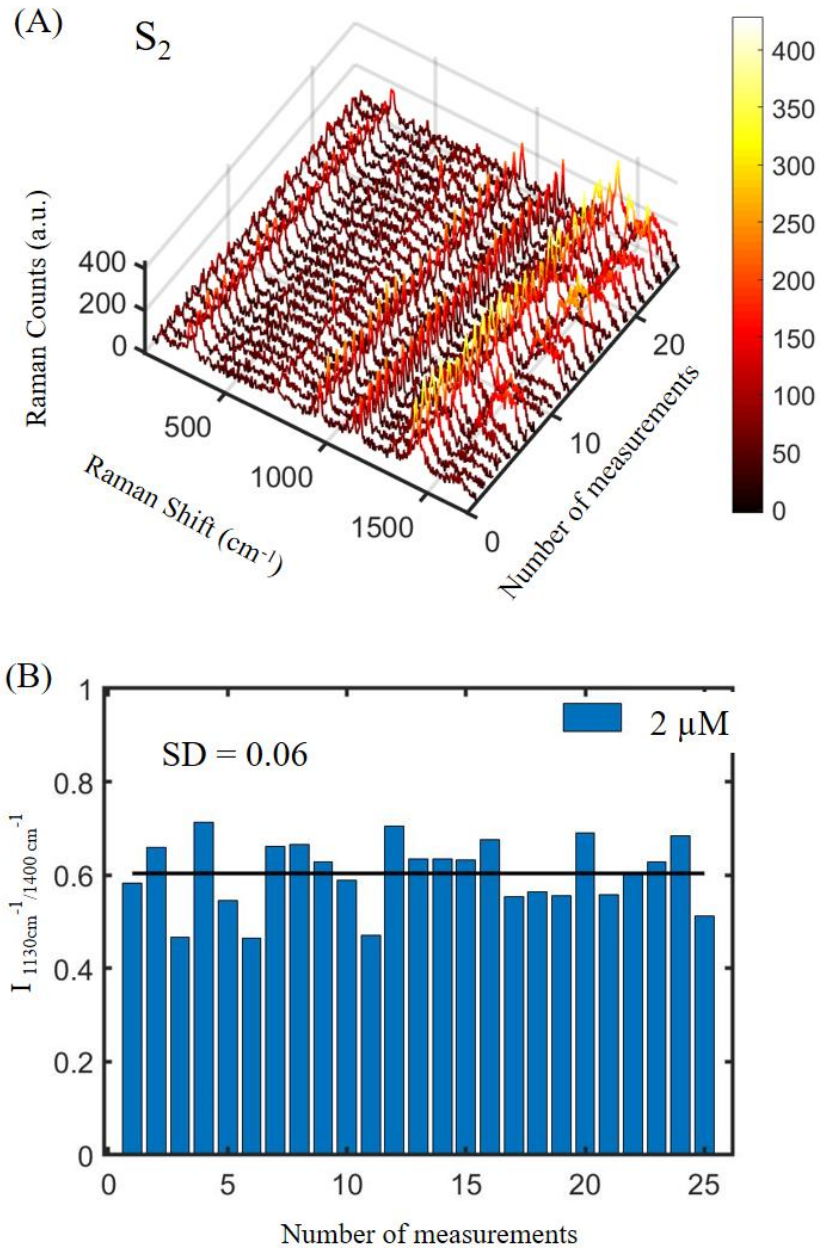

Figure S21 (A) Color waterfall spectra of 25 random points for 2 μM 2,4-D on a S_2 SERS substrate, the color bar stands for Raman intensity (a.u.). (B) Histogram of I_{1130} cm^{-1} / I_{1400} cm^{-1} at 25 different random points, the SD was 0.06 for the peak ratio.

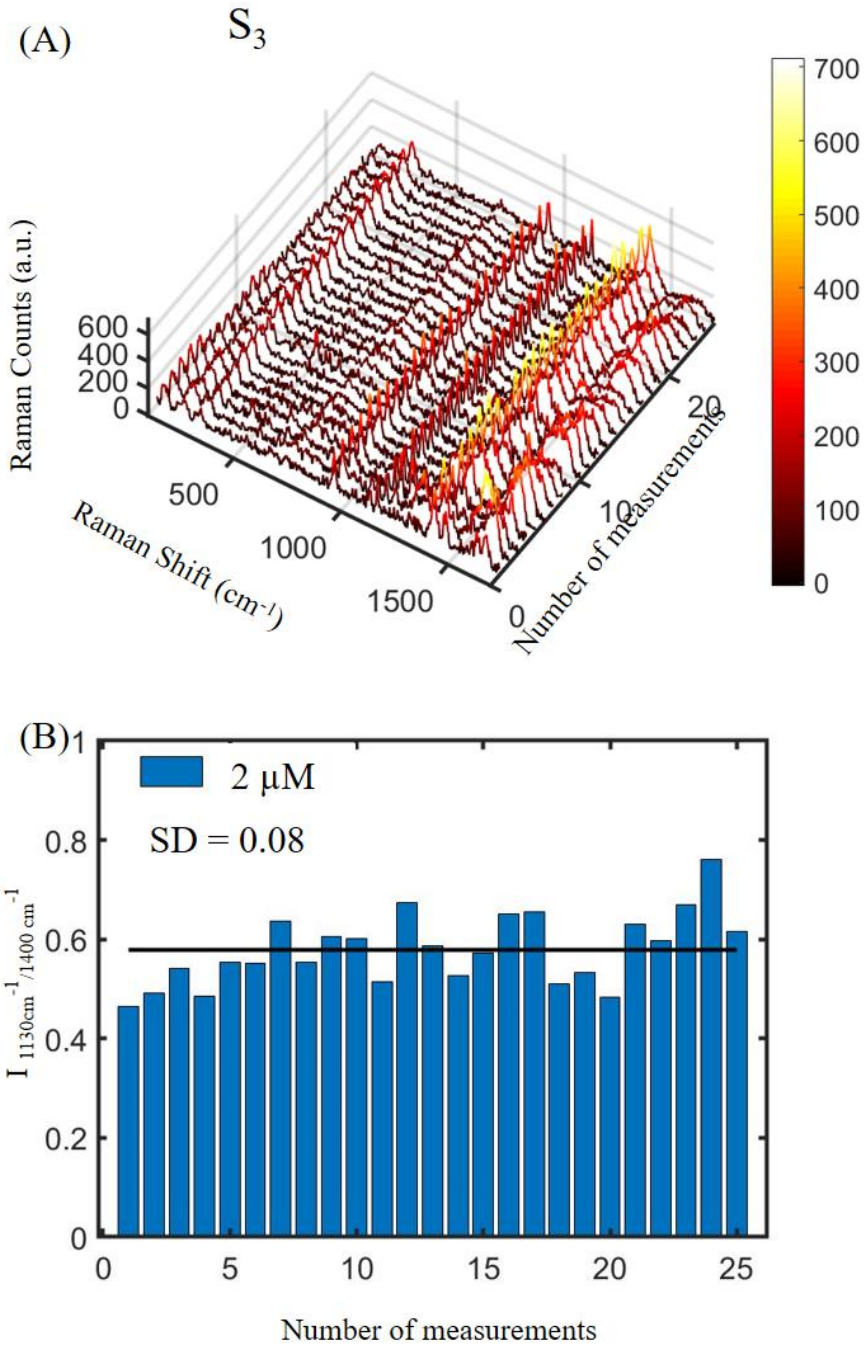

Figure S22 (A) Color waterfall spectra of 25 random points for 2 μM 2,4-D on a S_3 SERS substrate, the color bar stands for Raman intensity (a.u.). (B) Histogram of I_{1130} cm^{-1} / I_{1400} cm^{-1} at 25 different random points, the SD was 0.08 for the peak ratio.

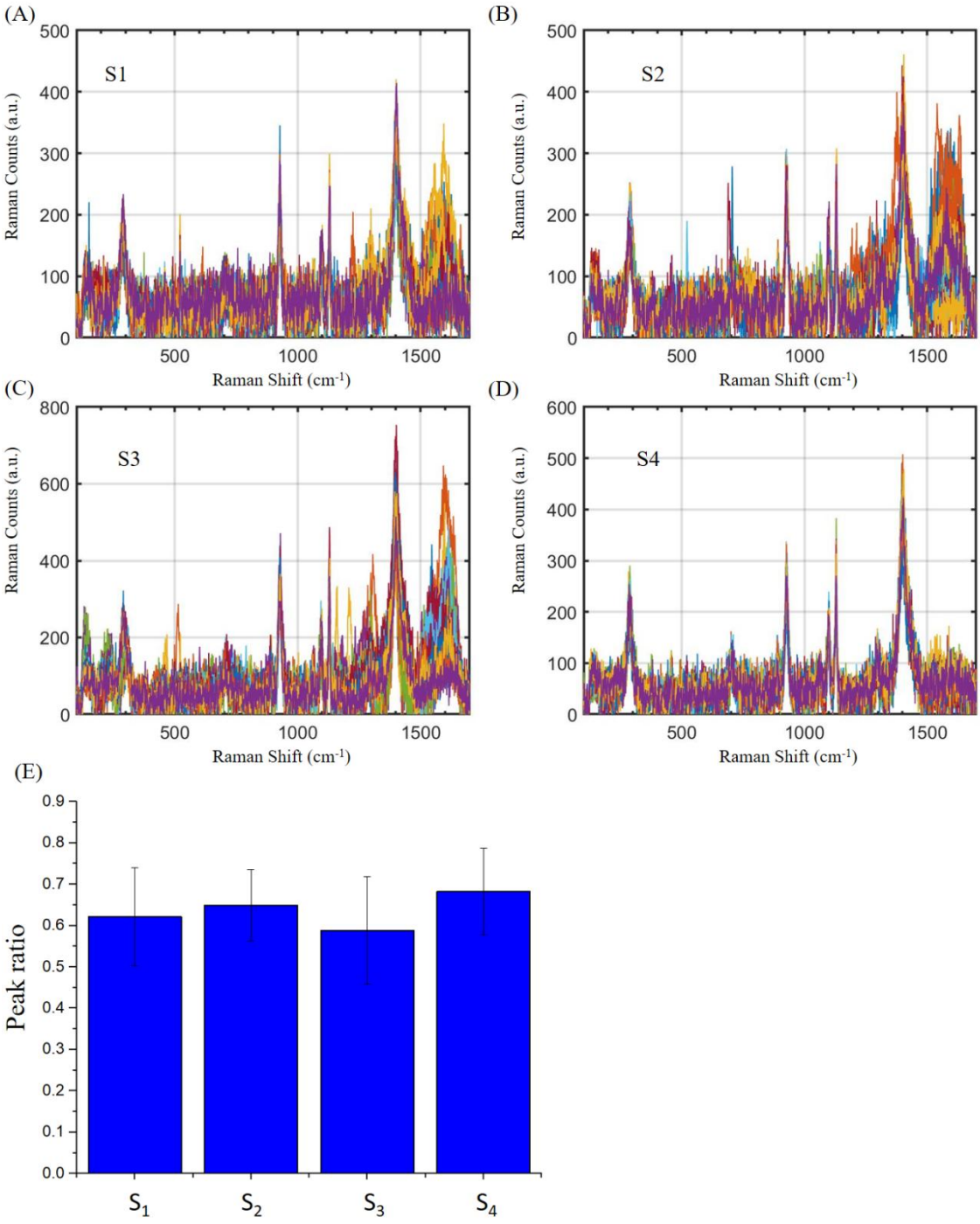

Figure S23: (A-D) Spectra of 25 random measurement points for 2 µM 2,4-D on S_1-S_4 SERS substrates in Figure S20-22 and Figure 2.11. (B) Mean and SD plot for peak ratio I_{1130} cm^{-1} / I_{1400} cm^{-1} at 25 different random measurement points in (A-D).

(A) Structure 1

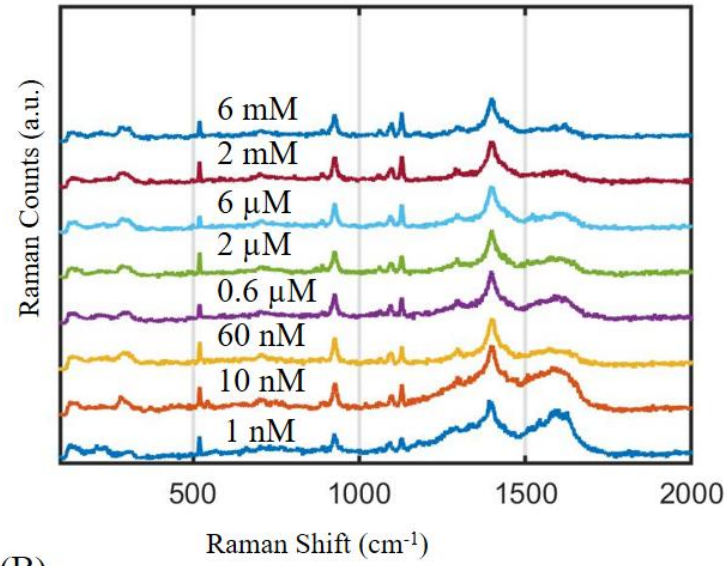

(B)

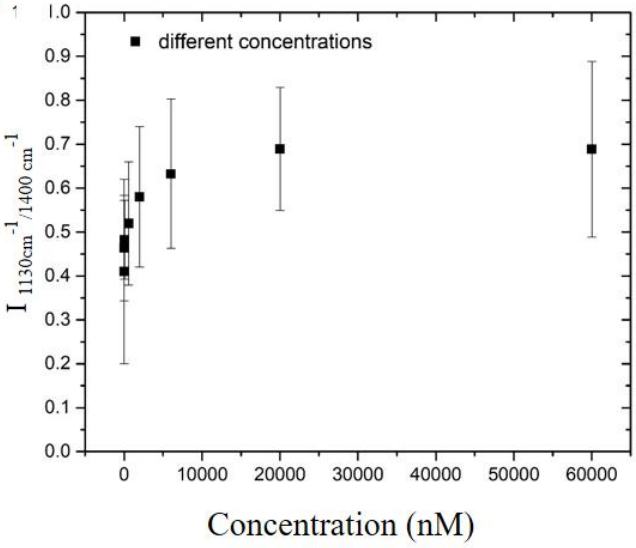

(C)

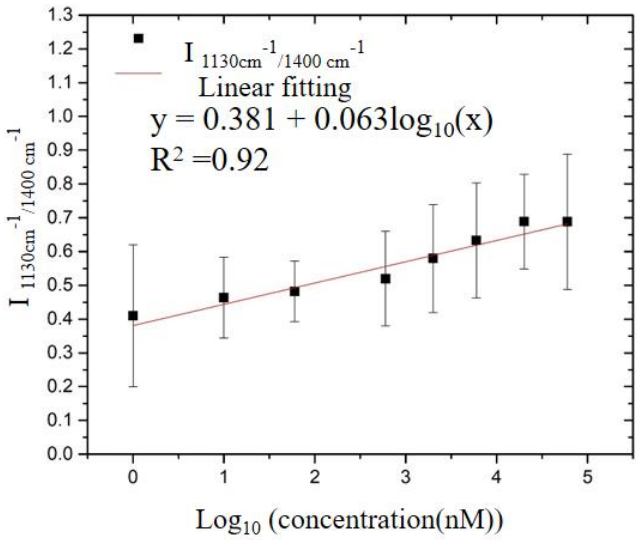

Figure S24: (A) Spectra of 2,4-D concentration from 1 nM to 6 mM, offset for clarity. (B) I_{1130} cm^{-1} / I_{1400} cm^{-1} vs. Concentration (in nM) for a S_1 substrate. (C) Fitting line for I_{1130} cm^{-1} / I_{1400} cm^{-1} vs. log(concentration (in nM)) for a S_1 substrate. The error bars were obtained from the standard deviation (SD) of ten measurements at random points.

(A)

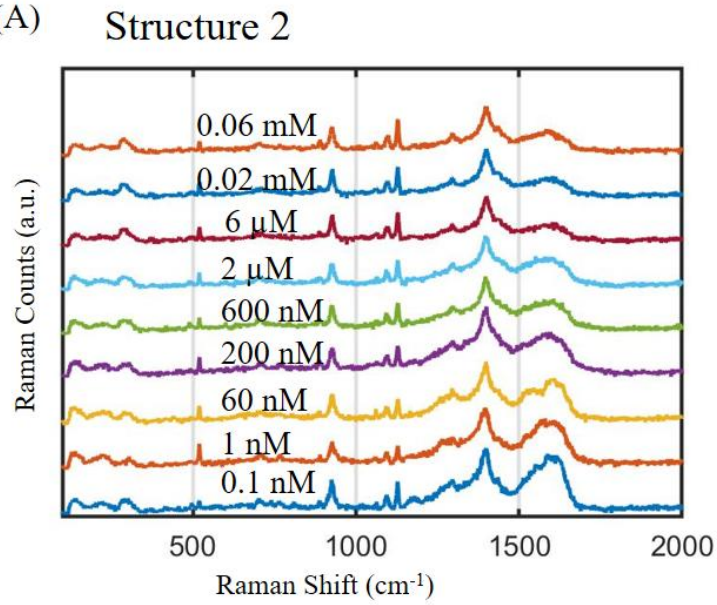
Structure 2
0.06 mM
0.02 mM
6 μM
2 μM
600 nM
200 nM
60 nM
1 nM
0.1 nM
Raman Counts (a.u.)
500
1000
1500
2000
Raman Shift (cm-1)

(B)

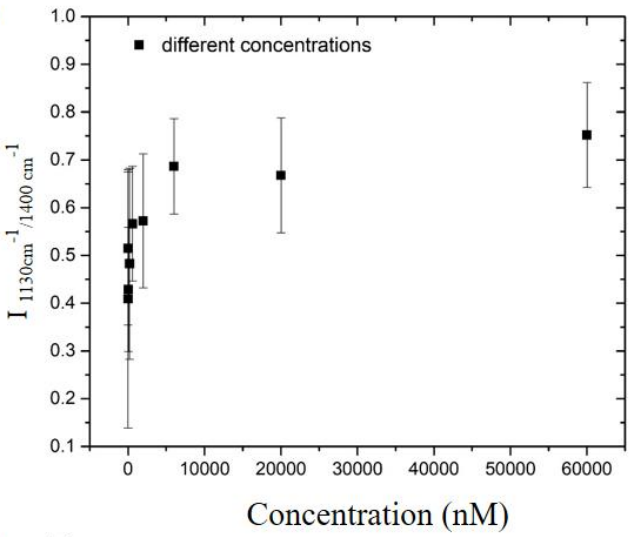
different concentrations
I 1130cm-1/1400 cm-1
0.1
0.2
0.3
0.4
0.5
0.6
0.7
0.8
0.9
1.0
0
10000
20000
30000
40000
50000
60000
Concentration (nM)

(C)

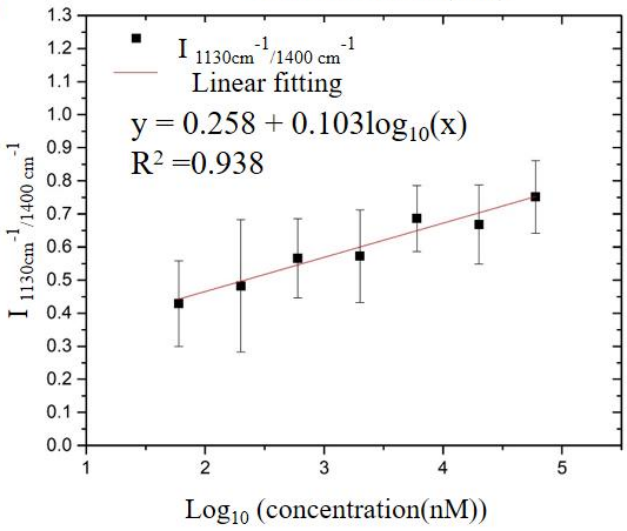
I 1130cm-1/1400 cm-1
Linear fitting
y = 0.258 + 0.103log10(x)
R2 =0.938
I 1130cm-1/1400 cm-1
0.0
0.1
0.2
0.3
0.4
0.5
0.6
0.7
0.8
0.9
1.0
1.1
1.2
1.3
1
2
3
4
5
Log10 (concentration(nM))

Figure S25: (A) Spectra of 2,4-D concentration from 0.1 nM to 0.06 mM, offset for clarity. (B) I_{1130} cm^{-1} / I_{1400} cm^{-1} vs. Concentration (in nM) for a S_2 substrate. (C) Fitting line for I_{1130} cm^{-1} / I_{1400} cm^{-1} vs. Log(concentration (in nM)) for a S_2 substrate. The error bars were obtained from the standard deviation (SD) of ten measurements at random points.

(A) Structure 3

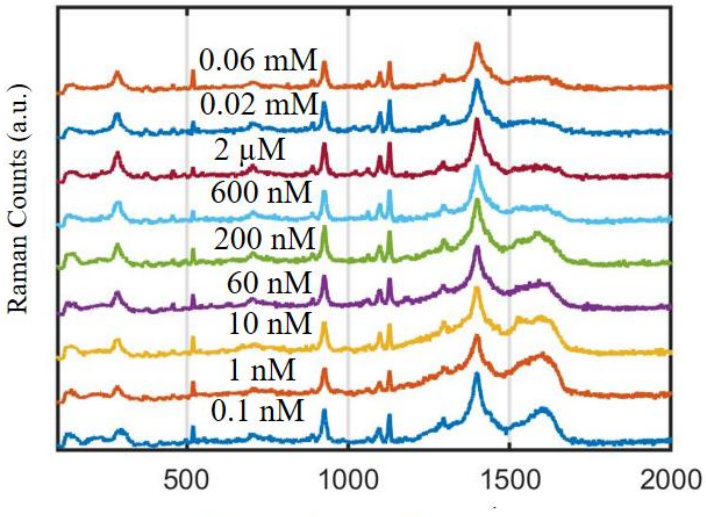

(B)

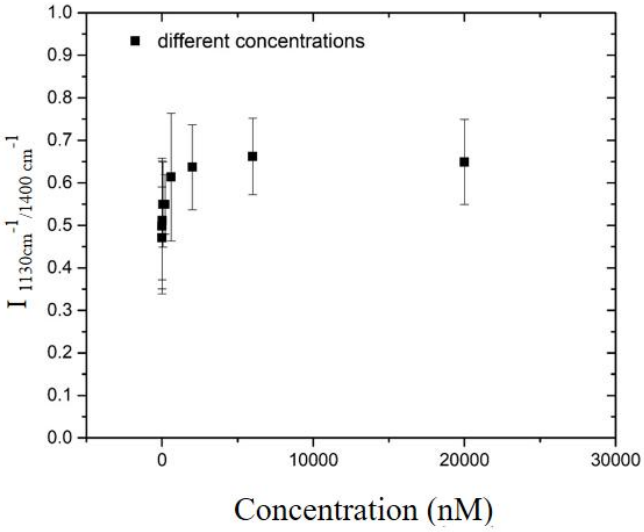

(C)

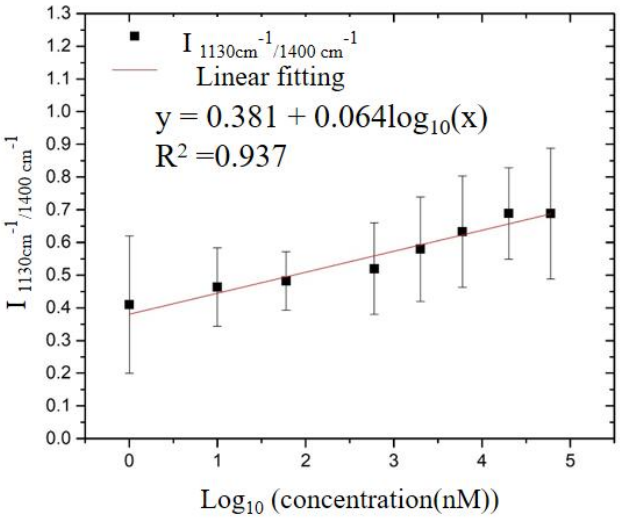

Figure S26: (A) Spectra of 2,4-D concentration from 0.1 nM to 0.06 mM, offset for clarity. (B) I_{1130} cm^{-1} / I_{1400} cm^{-1} vs. Concentration (in nM) for a S_3 substrate. (C) Fitting line for I_{1130} cm^{-1} / I_{1400} cm^{-1} vs. log(concentration (in nM)) for a S_3 substrate. The error bars were obtained from the standard deviation (SD) of ten measurements at random points.

4. Gum Arabic from Amazon: purchase information.

- Gum Arabic Powder-100g
- 100% Pure and Natural
- The soothing and anti-inflammatory properties of the gum from African trees, (notably the Acacia Arabica), are extracted to provide the Gum Arabic granules.
- These Gum Arabic granules are used as an emulsifying and thickening ingredient in cosmetics and beauty products.

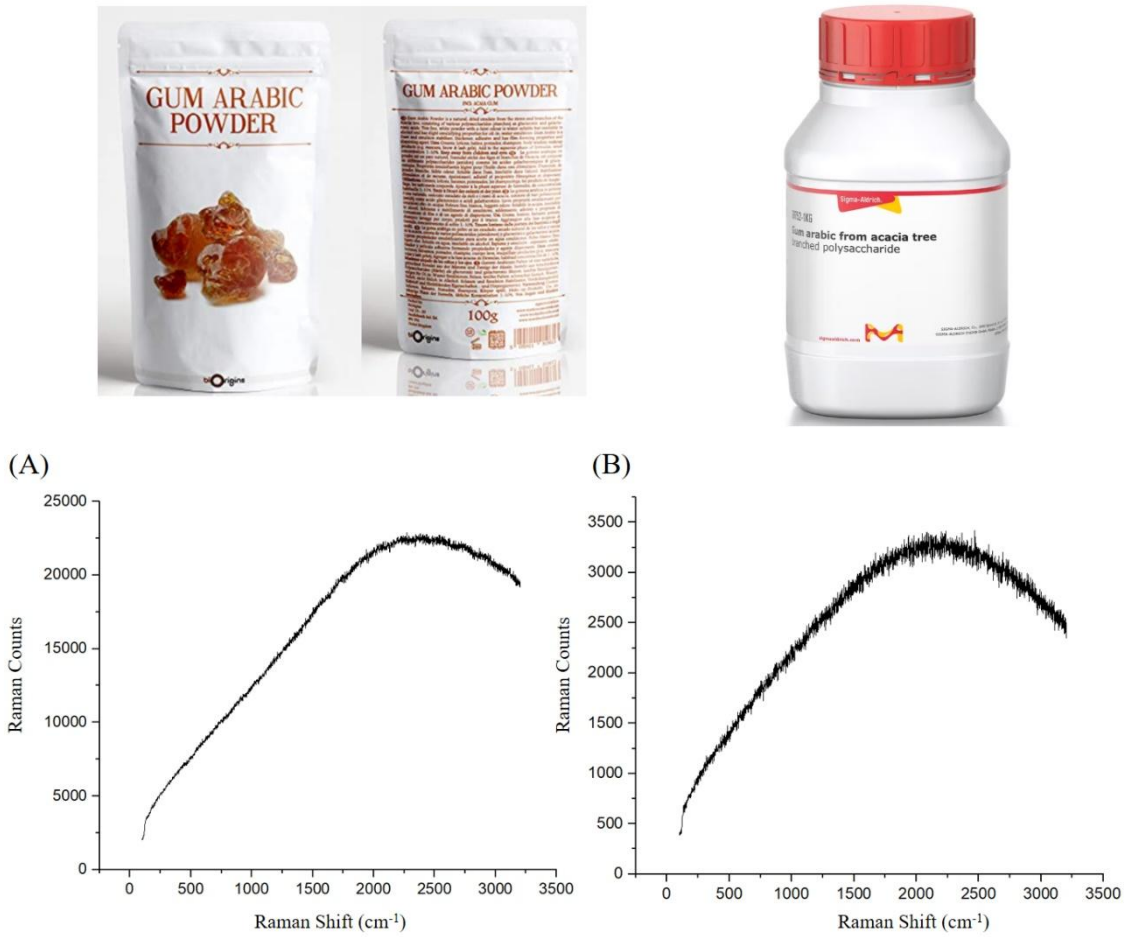

Figure S27: (A) Raman spectrum for Gum Arabic: Mystic Moments from Amazon. (B) Raman spectrum for Gum Arabic from Sigma Aldrich for comparison.

5. SERS substrate fabricated by commercial Gum Arabic.

The same experiment was also carried out by using the commercial Gum Arabic, similar peaks for detecting 2,4-D: 290 cm^{-1}, 926 cm^{-1}, 1128 cm^{-1}, and 1397 cm^{-1} show up. The deposition parameters (-0.2 V, 2 s; -0.8 V, 8 s; -1.2 V, 2 s; 5 mM $AgNO_3$; 20 g/L Gum Arabic) were different from the lab-used one because the type or quality of the gum Arabic was different. The SEM image of Ag-GA NPs is shown in Figure S28 (A).

Different concentrations from 1 nM to 0.06 mM were used for calibration, and ten spectra were taken for each concentration, the average of the ten spectra is shown in

Figure S28 (B), and all the raw data is shown in Figure S29. The logarithm trend for I_{1130} cm^{-1} / I_{1400} cm^{-1}, I I_{293} cm^{-1} / I_{1400} cm^{-1} vs. concentration (in nM) was shown in Figure S28 (C), The relation between I_{1130} cm^{-1} / I_{1400} cm^{-1} (y) and $\log_{10}$ (concentration (in nM)) (x) was $y = 0.51 + 0.04\log_{10}(x)$ with $R^2 = 0.99$. The relation between I_{290} cm^{-1} / I_{1400} cm^{-1} (y) and $\log_{10}$ (concentration (in nM)) (x) and was $y = 0.29 + 0.027\log_{10}(x)$ with $R^2 = 0.939$. (See Figure S28 (D)). The lowest concentration that had been detected by this SERS substrate was 1 nM. The repeatability of this SERS substrate for I_{1130} cm^{-1} / I_{1400} cm^{-1} is shown in Figure S28 (E), the RSD was 5%.

(A)

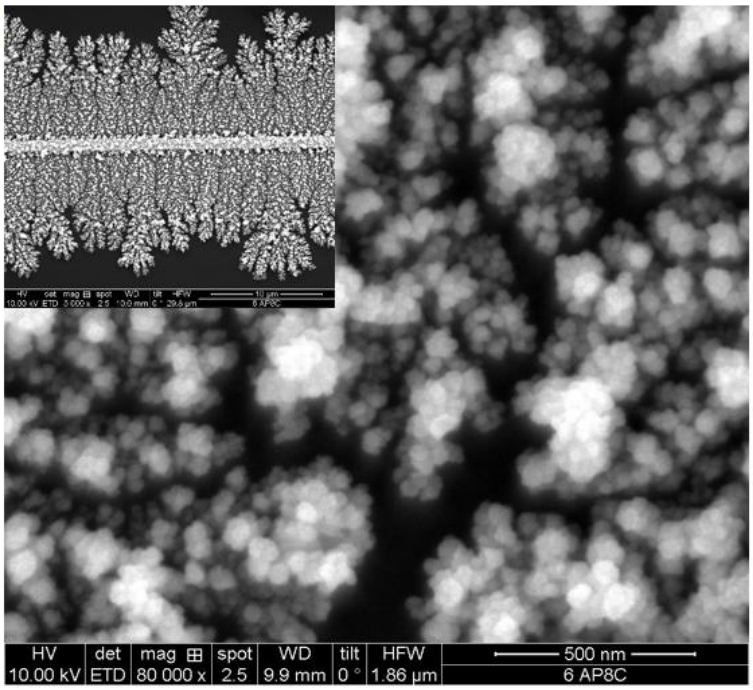
HV
10.00 kV
det
ETD
mag
80 000 x
spot
2.5
WD
9.9 mm
tilt
0 °
HFW
1.86 µm
500 nm
6 AP8C

(B)

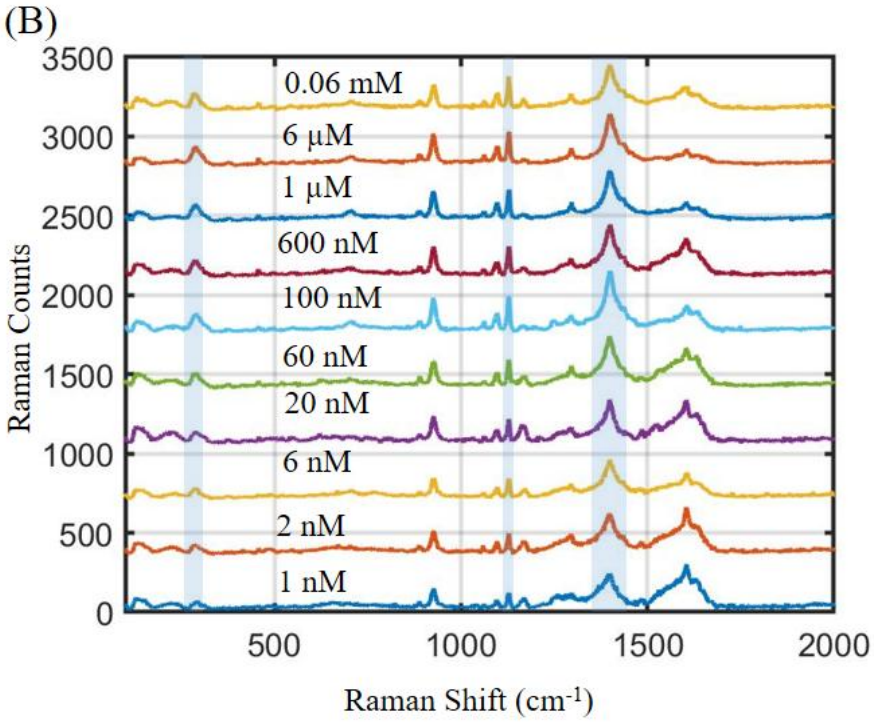
0.06 mM
6 µM
1 µM
600 nM
100 nM
60 nM
20 nM
6 nM
2 nM
1 nM
Raman Counts
0
500
1000
1500
2000
2500
3000
3500
500
1000
1500
2000
Raman Shift (cm-1)

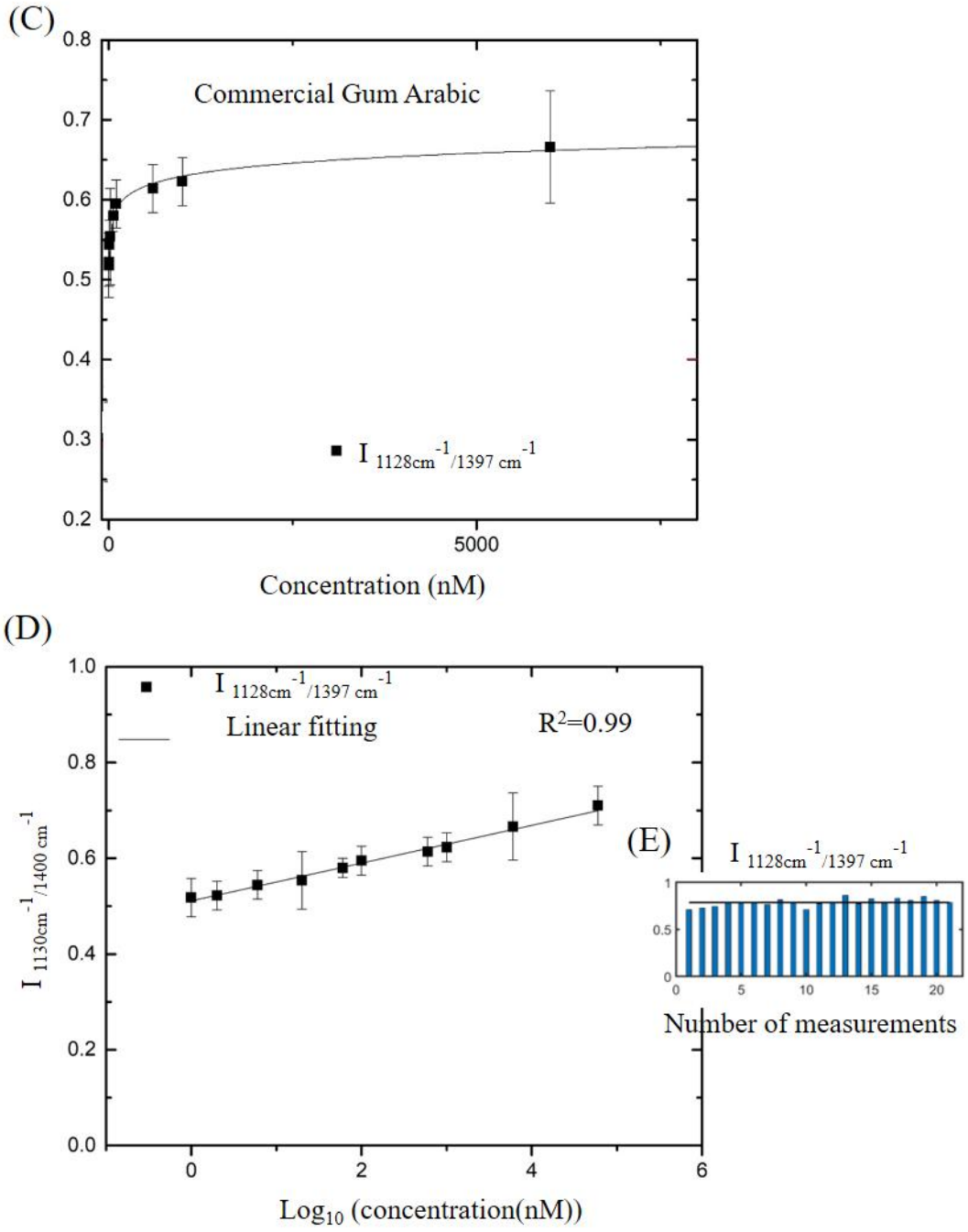

Figure S28: An Ag-GA SERS substrate that was fabricated by using commercial Gum Arabic, for 2,4-D detection. The deposition parameters (-0.2 V, 2 s; -0.8 V, 8 s; -1.2 V, 2 s; 5 mM $AgNO_3$; 20 g/L Gum Arabic). (A) SEM images for the Ag-GA nano structure; (B) Spectra of 2,4-D at different concentrations on SERS substrate from 1 nM to 0.06 mM. (C) logarithm trend for I_{1130} cm^{-1} / I_{1400} cm^{-1} vs. [2,4-D] (in nM); (D) Linear fitting

for I_{1130} cm^{-1} / I_{1400} cm^{-1} vs. Log[2,4-D] (in nM); The linear relation between I_{1130} cm^{-1} / I_{1400} cm^{-1} (y) and $\log_{10}$ ([2,4-D] (in nM)) (x) was $y = 0.51 + 0.04\log_{10}(x)$ with $R^2 = 0.99$. The error bar was from the standard deviation (SD) of ten measurements at random points on a SERS substrate. (E) The repeatability of the SERS substrate for 2,4-D at 1 μM at 20 different random points on a SERS substrate.

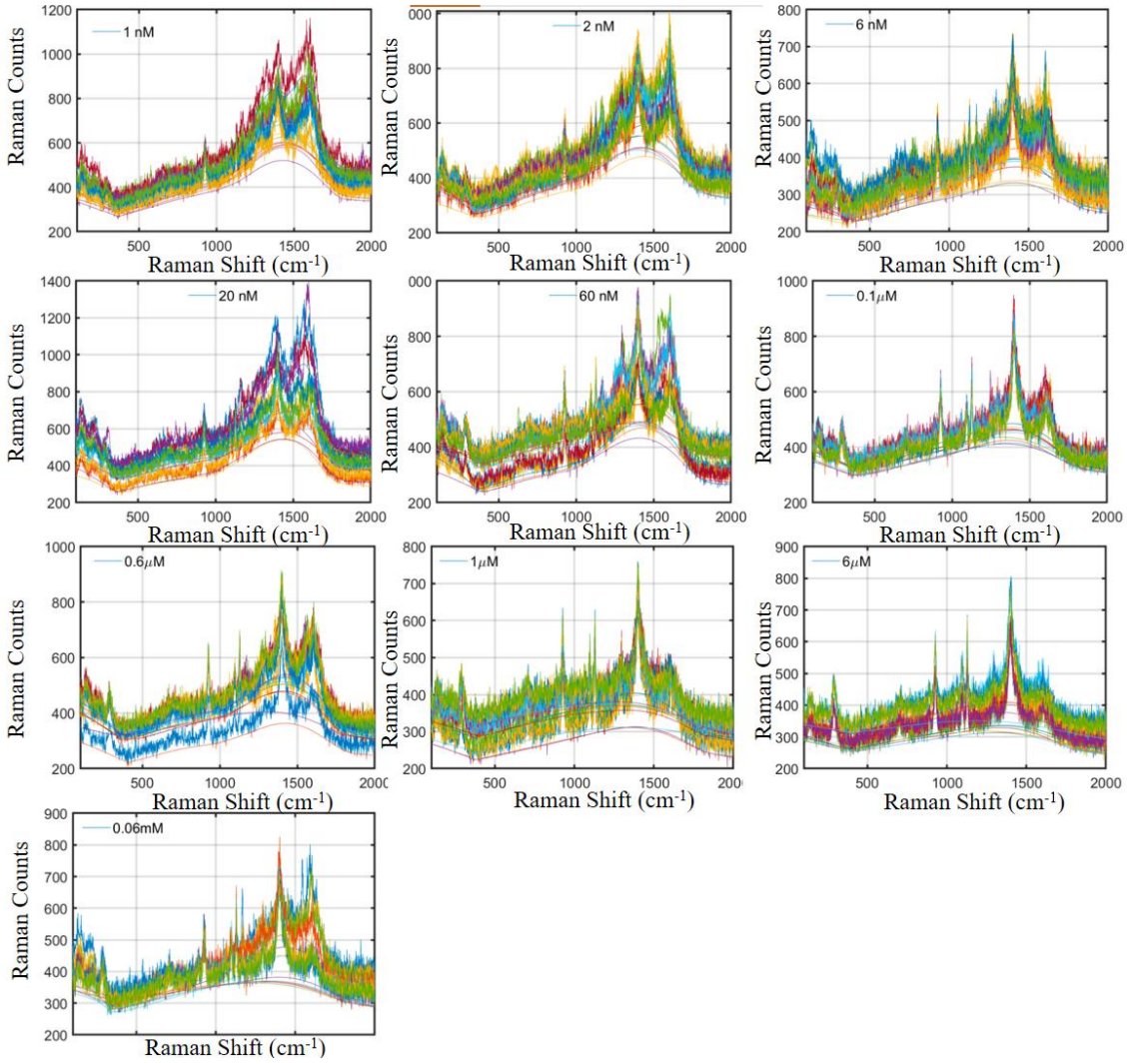

Figure S29: all raw data in Figure S23. The spectra were for 2,4-D at different concentrations and the smooth lines were subtracted background signals. Ten spectra were used for each concentration. At the lowest/first 2,4-D concentration, it took around

30 minutes to get the signal. It took 15 minutes in total to get all data for each concentration.

Table S1 Mineral composition of commercial mineral water.

Mineral water composition	mg/L	Mineral water composition	mg/L
Calcium (Ca^{2+})	12	Potassium (Pb^{+})	6
Sulphates (SO_4^{2-})	9	Silica (SiO_2)	32
Magnesium (Mg^{2+})	8	Chlorides (Cl^{-})	15
Sodium (Na^{+})	12	Nitrates (N^{3-})	7.3
Bicarbonates (HCO_3^{-})	74		

Reference.

1. Al-Baadani, H. H.; Al-Mufarrej, S. I.; Al-Garadi, M. A.; Alhidary, I. A.; Al-Sagan, A. A.; Azzam, M. M., The use of gum Arabic as a natural prebiotic in animals: A review. *Animal Feed Science and Technology* **2021,** *274*, 114894.

2. Xu, Y.; Kutsanedzie, F. Y. H.; Hassan, M. M.; Zhu, J.; Li, H.; Chen, Q., Functionalized hollow Au@Ag nanoflower SERS matrix for pesticide sensing in food. *Sensors and Actuators B: Chemical* **2020,** *324*, 128718.

3. Hassan, M. M.; Jiao, T.; Ahmad, W.; Yi, X.; Zareef, M.; Ali, S.; Li, H.; Chen, Q., Cellulose paper-based SERS sensor for sensitive detection of 2,4-D residue levels in tea coupled uninformative variable elimination-partial least squares. *Spectrochimica Acta Part A: Molecular and Biomolecular Spectroscopy* **2021,** *248*, 119198.

4. Hassan, M. M.; Zareef, M.; Jiao, T.; Liu, S.; Xu, Y.; Viswadevarayalu, A.; Li, H.; Chen, Q., Signal optimized rough silver nanoparticle for rapid SERS sensing of pesticide residues in tea. *Food Chemistry* **2021,** *338*, 127796.

5. Xu, Y.; Kutsanedzie, F. Y. H.; Hassan, M.; Zhu, J.; Ahmad, W.; Li, H.; Chen, Q., Mesoporous silica supported orderly-spaced gold nanoparticles SERS-based sensor for pesticides detection in food. *Food Chemistry* **2020,** *315*, 126300.

6. Hua, M. Z.; Feng, S.; Wang, S.; Lu, X., Rapid detection and quantification of 2,4-dichlorophenoxyacetic acid in milk using molecularly imprinted polymers–surface-enhanced Raman spectroscopy. *Food Chemistry* **2018,** *258*, 254-259.

7. Hassan, M. M.; Jiao, T. H.; Ahmad, W.; Yi, X.; Zareef, M.; Ali, S.; Li, H. H.; Chen, Q. S., Cellulose paper-based SERS sensor for sensitive detection of 2,4-D residue levels in tea coupled uninformative variable elimination-partial least squares. *SPECTROCHIMICA ACTA PART A-MOLECULAR AND BIOMOLECULAR SPECTROSCOPY* **2021,** *248*.

8. Xu, Y.; Hassan, M. M.; Ali, S.; Li, H.; Chen, Q., SERS-based rapid detection of 2,4-dichlorophenoxyacetic acid in food matrices using molecularly imprinted magnetic polymers. *Microchimica Acta* **2020,** *187* (8), 454.

9. Feng, X.; Zhang, G.; Chin, L. K.; Liu, A. Q.; Liedberg, B., Highly Sensitive, Label-Free Detection of 2,4-Dichlorophenoxyacetic Acid Using an Optofluidic Chip. *ACS Sensors* **2017,** *2* (7), 955-960.

10. Zhang, Z.; Ma, X.; Li, B.; Zhao, J.; Qi, J.; Hao, G.; Jianhui, R.; Yang, X., Fluorescence detection of 2,4-dichlorophenoxyacetic acid by ratiometric fluorescence imaging on paper-based microfluidic chips. *Analyst* **2020,** *145* (3), 963-974.

11. Xie, C.; Gao, S.; Guo, Q.; Xu, K., Electrochemical sensor for 2,4-dichlorophenoxy acetic acid using molecularly imprinted polypyrrole membrane as recognition element. *Microchimica Acta* **2010,** *169* (1), 145-152.

12. Peng, D. H.; Li, X.; Zhang, L. Z.; Gong, J. M., Novel visible-light-responsive photoelectrochemical sensor of 2,4-dichlorophenoxyacetic acid using molecularly imprinted polymer/BiOI nanoflake arrays. *ELECTROCHEMISTRY COMMUNICATIONS* **2014,** *47*, 9-12.

13. Shi, H. J.; Zhao, G. H.; Liu, M. C.; Zhu, Z. L., A novel photoelectrochemical sensor based on molecularly imprinted polymer modified TiO2 nanotubes and its highly selective detection of 2,4-dichlorophenoxyacetic acid. *ELECTROCHEMISTRY COMMUNICATIONS* **2011,** *13* (12), 1404-1407.

14. Liu, F. P.; Xu, Q.; Huang, W.; Zhang, Z. F.; Xiang, G.; Zhang, C. Z.; Liang, C. Y.; Lian, H.; Peng, J. Y., Green synthesis of porous graphene and its application for sensitive detection of hydrogen peroxide and 2,4-dichlorophenoxyacetic acid. *ELECTROCHIMICA ACTA* **2019,** *295*, 615-623.

15. Orooji, N.; Takdastan, A.; Yengejeh, R. J.; Jorfi, S.; Davami, A. H., A quick and inexpensive method to determine 2,4-dichlorophenoxyacetic acid residues in water samples by HPLC. *DESALINATION AND WATER TREATMENT* **2021,** *217*, 329-338.

16. de Amarante, O. P., Jr.; Brito, N. M.; Dos Santos, T. C.; Nunes, G. S.; Ribeiro, M. L., Determination of 2,4-dichlorophenoxyacetic acid and its major transformation product in soil samples by liquid chromatographic analysis. *Talanta* **2003,** *60* (1), 115-21.

Chapter 3. 2-methyl-4-chlorophenoxyacetic acid (MCPA) herbicide detection by electrochemically-deposited silver-cornstarch (Ag-CS) Surface Enhanced Raman Spectroscopy (SERS) substrate

Author Contributions: Y.Y. (Yuqing Yang) undertook experimental results including the Raman data analysis and manuscript preparation. P.L. (Pierre Lovera) and A. O'R. (Alan O'Riordan) were responsible for supervising and manuscript preparation.

Abstract: Surface Enhanced Raman Spectroscopy (SERS) has been widely used in the analytical sensing field in research. However, SERS substrate fabrication in a large scale for analytical applications is still a challenge. In this chapter, the electrochemical deposition method was used for Ag-Cornstarch substrate fabrication, which took three seconds for each SERS substrate deposition with precursors of $AgNO_3$ and cornstarch. After optimization of the Ag-Cornstarch nano structure by changing electrochemical deposition parameters, the Ag-CS structures were used for further SERS characterization and study. It was found that this Ag-Cornstarch nano structure was still active for Raman measurement after five weeks with a relative standard deviation RSD = 15% in Raman signal change. The SERS substrate has been used for Raman active molecular Methylene blue and 4-ATP test, where the Raman Enhancement Factor (EF) of this Ag-CS SERS substrate was estimated to be at 10^9 by using methylene blue (MB). For Ag-CS substrate, the RSD of 50 spectra at peak 1600 cm^{-1} was 6%. Detection of herbicide MCPA was undertaken using these substrates. Similar to Chapter 2, no change in Raman peak intensity was observed as the concentration of MCPA increased, suggesting that its detection was not based on strong SERS effects. As with 2,4-D, a slight increase in the peak ratio was observed with increasing concentrations. However, the experiment faced the same shortcomings as in Chapter 2 regarding the experimental protocol, rendering quantification impossible. Additionally, the spectra were very similar to those recorded in Chapter 2 for 2,4-D, making it impossible to discriminate between the two analytes due to a lack of selectivity.

Keywords: Ag-Cornstarch substrate, electrochemical deposition, MCPA pesticide detection.

1. Introduction.

MCPA is a phenoxy herbicide used for controlling broadleaf weeds in agriculture and has been used in cultures of cereals, flax, potatoes, rice, vines, and peas, It works by killing dicotyledonous but not monocotyledonous plants.[1] MCPA can run off from fields and reach nearby water bodies[2-3]. Its presence has even been found in drinking water.[4] Farmworker exposure has resulted in reversible anemia, digestive problems, muscular weakness, and slight liver damage.[5] It is therefore essential to monitor MCPA herbicide in the environment to prevent such pollution. Current technologies available for its detection are HPLC[6], electrochemical sensors[7], and fluorescence spectroscopy[8]. Recently, Surface Enhanced Raman Spectroscopy (SERS) has been shown to have good potential for the detection of pesticides.

Surface Enhanced Raman Spectroscopy is supported by plasmonic nanostructures that act as Raman signal amplifiers.[9] These plasmonic structures create 'hot spots' upon the excitation of laser,[10] which generate a strong electromagnetic field at the surface. Analyte molecules located in these 'hot spots' can benefit from enhanced Raman signals. The overall enhancement is made of an electromagnetic enhancement and a chemical enhancement,[11] where the chemical enhancement contributes to 10^2 of the total EF.[12] It has been reported that EF could reach 10^5-10^{12},[13] depending on plasmonic structure morphology and size,[14] the gap between plasmonic structures,[15] the excitation laser wavelength,[16] the adsorption state of analytes[17], etc. Plasmonic structures are made of noble metal nano particles and are usually fabricated by E-beam lithography,[18] electrochemical deposition,[19] chemical synthesis,[20] or templating methods[21]. However, mass production of the SERS structure is still challenging. E-beam lithography is time-consuming and not suitable for mass production; nanogaps are hard to control in the chemical synthesis method when applying nano particles on a supporting substrate; templating method involves several steps, which may cause a high failure rate.

Electrochemical methods allow mass production because of the easily controllable and repeatable experimental conditions, which do not require high temperature or high vacuum environment. As such, it has become a good candidate for SERS structure fabrication.

In this research, electrochemical deposition techniques were used for the fabrication of SERS substrates, with $AgNO_3$ and cornstarch gel solution used as precursors. Corn starch acted as a shape control and stabilization agent for silver nanoparticles.[22-23] As the MCPA molecules do not contain sulfur or nitrogen atoms they do not have strong interactions with silver nano particles surface as discussed in Chapter 1, and as such do not generate a SERS signal directly. The cornstarch biopolymer layer helps trap MCPA close to the Ag-CS nano structure surface and helps its Raman-based detection.

2. Experimental section.

2.1. Materials.

$AgNO_3$ (CAS number: 7761-88-8, 99.99% trace metals basis), 4-ATP, Methylene Blue, and 2-methyl-4-chlorophenoxyacetic acid (MCPA) (CAS number: 94-74-6, analytical standard) were purchased from Sigma-Aldrich, Ireland. 4-ATP was dissolved in ethanol and then diluted in DI water in series. Sealing film (BRAND® Seal-R-film™ Sealing Film) was purchased from Sigma-Aldrich, Ireland. Cornstarch (belbake, cornflour, 500g) was bought from the local supermarket (food standard). Deionized (DI) water was Milli-Q level (18.2 $M\Omega \cdot cm^{-1}$). The electrochemical depositions were performed with an Ivium pocketSTAT handheld potentiostat (Scan range: ±30mA/±10V, size: 16x6.7x1.9cm, weight: 300, applicable scan rates: 1 µV/s to 10,000 V/s) that was connected to a laptop (software: Iviumsoft). DI water and MCPA analyte used in this research were stored in new colorless Eppendorf AG PCR tubes (mL range) from

Sigma-Aldrich (Ireland). The$AgNO_3$ solution was contained in a new centrifuge tube from Sigma-Aldrich (Ireland). For MCPA solution preparation, 28.5 mg of MCPA powder was dissolved in 500 mL DI water to obtain a 0.285 mM solution. 100 µL of this 0.285 mM MCPA solution was then diluted with 900 µL of DI water to prepare a 28.5 µM MCPA solution. The other concentrations were prepared by using the same approach.

2.2 Fabrication of microelectrode on chip.

SERS sensors were fabricated on four-inch silicon wafer substrates with a 300 nm layer of thermally grown silicon dioxide as previously described.71 34 individual SiO2/Si chips were produced on each silicon wafer, with a chip size of 1 cm (width) x 1.7 cm (length) x 0.1 cm (thickness). For the chip fabrication process, briefly, the working electrodes were patterned using photolithography and physical vapor deposition (PVD) (50 nm of Au, with 10 nm of Ti adhesion layer) followed by a lift-off step. A second optical lithographic and metal deposition process (Au 100 nm/Ti 10 nm) was undertaken to define micro-SD pin-out, interconnection tracks, as well as the on-chip counter electrode (500 µm wide × 6 mm long). A third lithographic step was employed to define the Pt (Pt 100 nm/ Ti 10 nm) on-chip reference electrode (500 µm wide × 6 mm long). Finally, 500 nm of Plasma-enhanced chemical vapor deposition (PECVD) Si3N4 was blanket deposited on the whole wafer. Openings over the working/counter/reference electrodes and the electrical contacts were defined by lithography and dry etching process.

2.3 Fabrication of Ag-CS SERS substrate.

A cornstarch gel was prepared by microwave heating. This was found to be necessary as the untreated corn starch could not be dissolved in water. Briefly, 0.25g of cornstarch

powder was added to 20 mL DI water in a beaker and mixed with a glass rod. This was then heated in a microwave (900 W) for 1.5 minutes. After the microwave heating process, the cornstarch gel was transferred to a 20 mL centrifuge tube, with the cover on top, and this tube was placed quickly in cold water until it cooled down to ambient temperature for future usage.

SERS substrates were fabricated using 5 mM $AgNO_3$ solutions and the prepared cornstarch gel at the volume ratio 5:1 and 50:1. A small aliquot (2μL) was deposited on the chip surface to cover the three electrodes (working electrode, on-chip pseudo reference electrode, and counter electrode). Potentials of -0.6 eV and -0.5 eV were applied for three seconds for this sensor fabrication. The electrochemical deposition was undertaken with an Ivium pocketSTAT handheld potentiostat. The sensor substrates were then rinsed thoroughly in DI water and dried under a nitrogen flow for several seconds.

For storage, the SERS sensors were covered gently with several layers of sealing film to reduce the oxidation of Ag-CS NPs. These sealing film-covered SERS sensors were placed in a 20 mL centrifuge tube, which was filled with nitrogen. The centrifuge tube was sealed with sealing film to prevent the entrance of air and then stored in the fridge for future use.

2.4 Optical and SEM Characterization.

Optical micrographs of the fabricated samples were acquired with a Renishaw Raman system with a 20x lens (NA 0.4) objective. A FEI Quanta 650 was used for SEM characterization. The accelerating voltage used was 10 KV with a spot size of 2.5 nm. Secondary electrons were used for SEM.

2.5 Raman measurements.

The Raman spectra were acquired with a Renishaw InVia confocal microscope (software: Renishaw's WiRE™ 3.4 (Windows®-based Raman Environment), spectral resolution: 0.3 cm^{-1} (FWHM), spatial resolution (lateral): 0.25 μm, spatial resolution (axial) < 1 μm), which is equipped with a 514 nm Ar ion laser (model number: stellar-pro) and a 2400 l/mm(vis) grating) and Renishaw CCD detector (1024 pixels × 256 pixels). For Raman measurements, the sensors were placed in a dedicated holder that has been described in the previous chapter.[25] A 20 μL aliquot of MCPA solution was deposited on top of the sensor and covered with a cover glass slide. All the measurements were acquired using a 20x lens (LEICA, NA 0.4, lateral resolution of ~688 nm, and an axial resolution of ~6875 nm). All the spectra were from the average of ten times measurement at different random points with one measurement/spectrum for each spot (50 Raman measurements for reproducible study). The laser power was 0.07 mW[2] and the integration time was ten seconds. For Raman vs MCPA concentration experiments, different concentrations of MCPA from a lower concentration to a higher concentration, were used on the same Ag-CS SERS sensor. Once the Raman measurements at the lower concentration were finished, the solution was removed with a small piece of cleanroom wipe (SUPERIOR Polycellulose wipes purchased from Sigma-Aldrich (Ireland)) from the edge of the droplet (care was taken not touch the substrate itself) and the next concentration of MCPA solution applied. As in Chapter 2, this calibration method keeps the Ag-CS SERS substrate consistent across all MCPA concentrations. However, the limitation of this method is similar to Chapter 2, and the experimental method will affect the calculated Limit of Detection (LOD), and quantification.

[2] Laser power was calibrated by using a Si reference sample in a daily basis as described in Chapter 2.

2.6 Data Analysis.

The spectra for 4-ATP and MB were corrected using the baseline subtraction algorithm by Schulze et al. [26] using Matlab R2018b-academic. Origin™ (OriginPro 2016) was used for linear fitting.

3. Results and discussion.

3.1 Ag-CS SERS sensor fabrication, optimization, and SEM characterization.

During the electrochemical deposition process, the $Ag^+ + e^- \rightarrow Ag$ reaction occurred immediately, leading to the formation of Ag-CS nanoparticles. These Ag-CS nano particles then assemble near to the electrode on the silicon substrate. As the reaction occurs, the Ag-CS nano particles will further affect the electric field distribution.[27] This process helps with the formation of the nano gap in between the nano clusters. SEM images for Ag-CS SERS sensors are shown in Figure 3.1 together with the corresponding optical images at 50x (NA 0.75). Deposition parameters of -0.5V and 3 seconds were used for Figure 3.1 (A, B). Figure 3.1 (C, D) shows structures obtained with deposition parameters of -0.6 V for 3 seconds. For Figure 3.1 (A, C), a precursor ratio V_{AgNO3}:V_{CS} of 50:1 was used whereas a precursor ratio V_{AgNO3}:V_{CS} of 5:1 was used for Figure 3.1 (B, D). The current level is at hundreds of nA as shown in SI Figure S1. Comparing Figure 3.1 (A, B) and Figure 3.1 (C, D), one can see that, for the same deposition potential, the Ag-CS nano structure grew bigger with a higher precursor ratio V_{AgNO3}:V_{CS}. Because the total resistance for the precursor solution is smaller at a higher precursor ratio V_{AgNO3}: V_{CS}, the current density was higher for the same applied potential. Similarly, keeping the precursor ratio the same but increasing the deposition potential (Figure 3.1 (A, C) vs Figure 3.1 (B, D), results in higher current densities, and the Ag-CS nano structure spreads better in a bigger area.

Both parameters (deposition potential and precursor ratio) can be varied to synthesize Ag-CS nanoparticles. However, by looking at the optical images, localized aggregation of Ag-CS nano particles was observed in Figure 3.1 (A, B, D), which appeared black. In Figure 3.1 (A, B), the Ag-CS nano particle deposited mostly on the Au microelectrode, which means that these depositions depended on the electrode surface state, and were less controllable than the structures shown in Figure 3.1 (C) that grew on the silicon substrate. In addition, the structures shown in Figure 3.1 (C) were less likely to get interference from the Au electrodes (Au catalyst effect for example)[28], when doing SERS measurements. Considering both morphology homogeneity and surface area, the parameters used for structures shown in Figure 3.1 (C) were chosen for the SERS study, as it yielded a dense coverage of Ag-CS nanoparticles distributed on SiO_2/Si substrate with nano gaps. This optical image indicates that a thin layer of Ag-CS nano particles grew on each side of the Au electrode, and had a Khaki color under the microscope. For Raman measurements, the laser was focused on the SiO_2/Si substrate instead of the Au electrode.

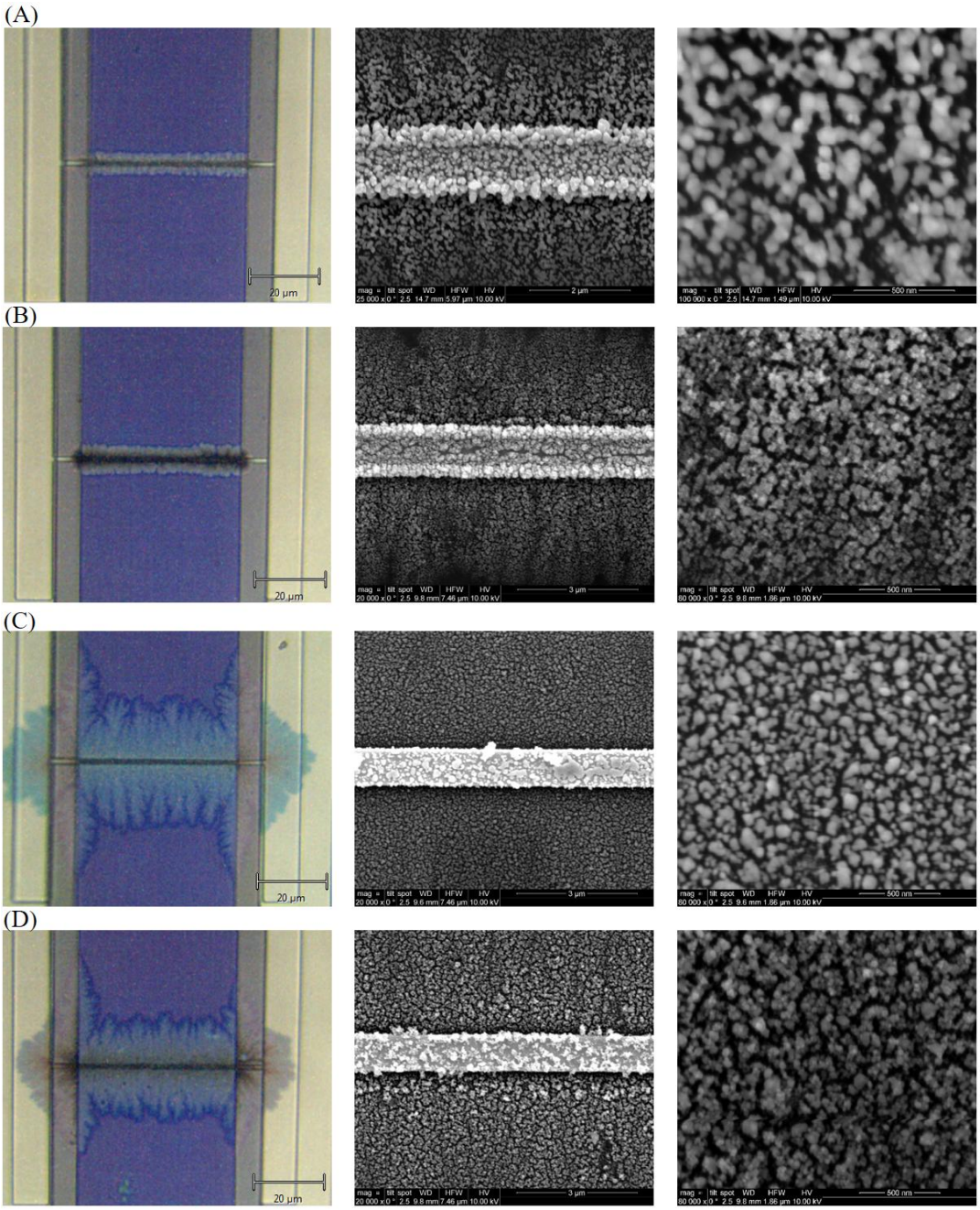

Figure 3.1: Optical and SEM images for different Ag-CS structures depending on different deposition parameters. (A) V_{AgNO3}:V_{CS}= 50:1, -0.5 V, 3 s; (B) V_{AgNO3}:V_{CS}= 5:1, -0.5 V, 3 s; (C) V_{AgNO3}:V_{CS}= 50:1, -0.6 V, 3 s; (D) V_{AgNO3}:V_{CS}= 5:1, -0.6 V, 3 s. All the depositions have been repeated at least 3 times.

3.2 SERS sensor characterization with 4-ATP and Methylene Blue (MB).

To evaluate the enhancement factor (EF) of this Ag-CS SERS sensor, 4-ATP and Methylene Blue (MB) were used for characterization. MB and 4-ATP are both widely used Raman reporters, with strong Raman responses. For instance, 4-ATP contains a thiol group that directly binds to the silver surface, resulting in a strong SERS signal. Figure 3.2 (A, C) show the spectra for 4-ATP and Methylene Blue at different concentrations. Regarding MB, the peak at 1625 cm^{-1} is attributed to the ring stretching C-C[29]. For 4-ATP, the peaks at 1075 and 1575 cm^{-1} are the vibrations of C-S and C-C, and the other three characteristic peaks at 1140, 1390, and 1435 cm^{-1} are assigned to the b2 modes of 4-ATP.[30] As can be seen in Figure 3.2, the peak intensities increase with the increase of analyte concentration. The corresponding linear fitting results are shown in Figure 3.2 (B, D). For 4-ATP, the linear relation between Raman counts (a.u.) and $\log_{10}$ [4-ATP (μM)] was $y = 4358.454 + 3375.131\log(x)$, with $R^2 = 0.9966$. The LOD was calculated to be 0.05 nM by the 3σ/M method, where σ is the standard deviation and M is the slope of the linear calibration. For MB, the linear relation between $\log_{10}$ (Raman counts (a.u.)) and $\log_{10}$[MB (μM)] was $\mathrm{Log}_{10}(y) = 4.350 + 0.460\log_{10}(x)$, with $R^2 = 0.9747$, and the LOD was calculated to be 0.39 μM. The enhancement factor was calculated based on the formula:

$$EF = I_{SERS} \cdot N_{bulk} / N_{SERS} \cdot I_{bulk} \quad \text{(Eq. 1)}$$

Where I_{SERS} is the SERS intensity; I_{bulk} is the Raman intensity; and N_{bulk} is the number of probed molecules contributing to normal Raman signals and determined under the same experimental conditions as in SERS measurements, but without SERS substrates. N_{SERS} is the number of targeted molecules adsorbed on SERS substrates and is related only to the molecular interaction with the SERS substrate surface.

The EF was calculated to be around 0.2×10^{10} for MB (0.05 μM). For 0.05 μM MB by SERS: $I_{SERS} = 5234$, $N_{SERS} = V_{MB\ effective\ for\ SERS} \cdot [MB]$, $V_{MB\ effective\ for\ SERS} = \pi \cdot r^2 \cdot 10^{-7}$,

where r is the laser spot radius (in μm); 10^{-7} is the estimated SERS effective height for MB solution (100 nm, assumed to be the SERS effective range, even if the total amount of MB that interact with Ag NPs surface could be smaller). For normal Raman at 1 mM MB concentration: I_{bulk}= 517, N_{bulk} = $V_{MB\ effective\ for\ Raman}$· [MB], $V_{MB\ effective\ for\ Raman}$ = $\pi \cdot r^2 \cdot h_{effective}$, where $h_{effective}$ is the effective height for MB drop on a SERS sensor for Raman measurement and was estimated to be 1 mm. EF = $5234 \cdot \pi \cdot r^2 \cdot 10^{-3}$ m·10^{-3} M/517· $\pi \cdot r^2 \cdot 10^{-7}$m·0.05·$10^{-6}$ M = 0.2 x10^{10}. The spectra of MB at 1 mM without SERS substrate and MB at 0.05 μM with SERS substrate are shown in SI Figure S2.

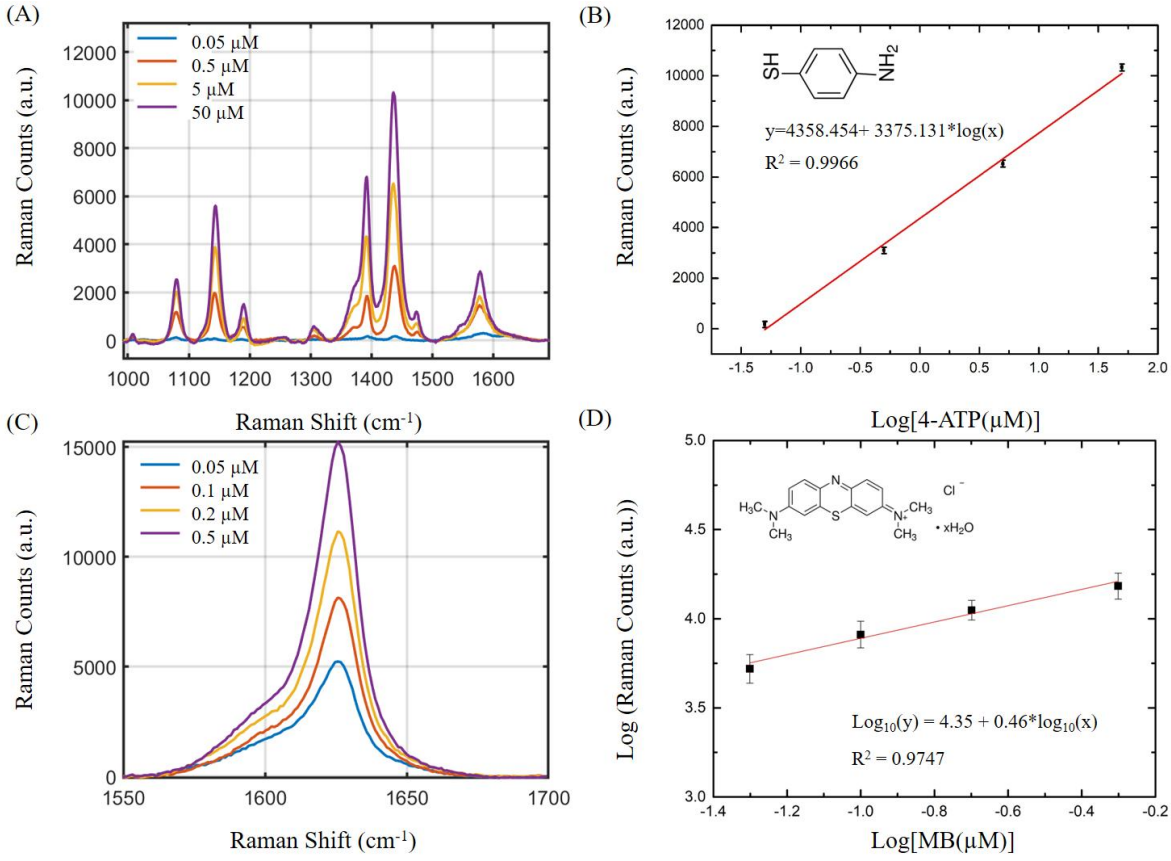

Figure 3.2: Ag-CS SERS sensor characterization by Raman reporter 4-ATP and Methylene Blue (MB). (A) Spectra for 4-ATP at different concentrations: 0.05 μM, 0.5 μM, 5μM, 50 μM; (B) Linear calibration for 4-ATP for the highest peak at 1440 cm^{-1};

(C) Spectra for Methylene Blue (MB) at different concentrations: 0.05 μM, 0.1 μM, 0.2 μM, 0.5 μM; (D) Linear calibration for 4-ATP for the highest peak at 1625 cm^{-1}.

3.3 Stability for the Ag-CS SERS substrate.

Starch is a polysaccharide composed of both amylose, a mostly linear polymer, and amylopectin, a highly branched polymer, see Figure 3.3. Both polymers are comprised of D-glucose with the primary difference between them being their linkages.[31] Amylose's subunits are linked mostly by α-(1→4). Amylopectin has subunits linked both by α-(1→4) and by α-(1→6), with about 95% of the glycosidic bonds being α-(1→4) linkages and roughly 5% being α-(1→6).[32] Corn Starch ($(C_6H_{10}O_5)_n$) contains -OH group, as well as -C-O-C-, $-CH_2-$ groups.[33]

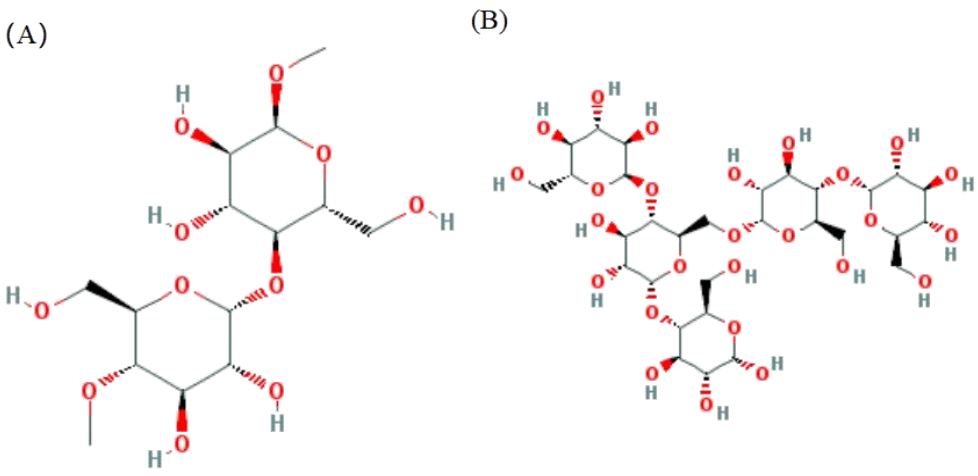

Figure 3.3: General structure of amylose and amylopectin.[31]

Ag-GA substrates were fabricated using electrodeposition of $AgNO_3$/corn starch solutions. The Raman spectra for these substrates on different chips are shown in Figure 3.4 and SI Figure S3. The spectra indicate that the fabrication method and peak feature for this Ag-CS substrate are repeatable, even if the intensity varies. There are currently

in the literature no reports focusing on Raman characterization of cooked corn starch (to interpret the spectrum). However, according to the peak assignment for corn starch powder, the peaks at ~800 and 1003 cm^{-1} could be assigned to C-O-C, C-O-H bending and -CO stretching, the peak at 1163 cm^{-1} could be assigned to C-O, C-C stretching and C-O-H bending, the peak at 1244 cm^{-1} could be assigned to C-C-H, O-C-H, C-O-H bending, the peak at 1379 cm^{-1} could be C-O-H bending, and the peak at 1600 cm^{-1} could be assigned to CH, CH2, C-O-H bending.[34-35] See Table 1. After the application of DI water, the -OH bonds have a good affinity to water[35]. This, combined with the weaker signal typically observed in the water environment, resulted in the spectrum in blue in Figure 3.4. Only two broad peaks at ~1400 cm^{-1} and ~1600 cm^{-1} can be seen with the peaks at ~800 and 1003 cm^{-1} disappearing and the peaks at 1163, and 1244 cm^{-1} decreasing.

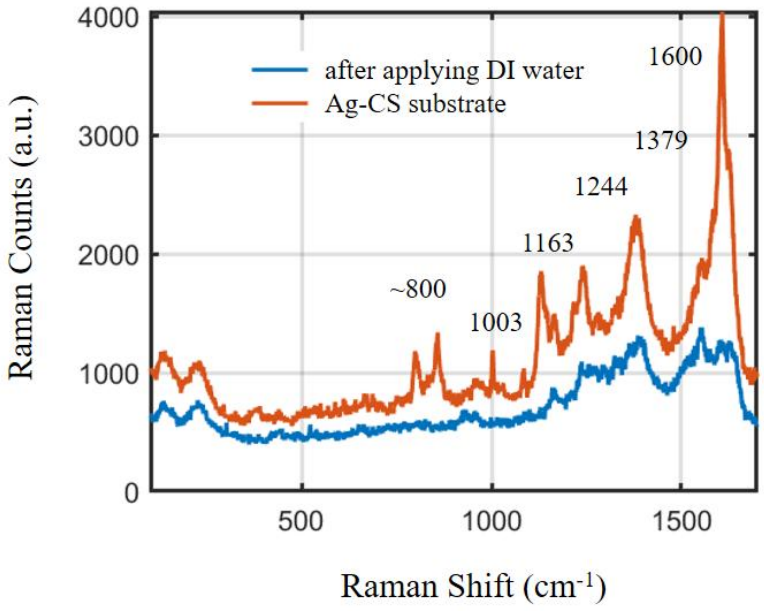

Figure 3.4: Raman spectra for Ag-CS SERS substrate in air (in orange) and after application of DI water (in blue).

Table 1: Corn Starch peak assignment.[34-35]

Raman Peak	Vibration
~800 and 1003 cm^{-1}	C-O-C, C-O-H bending and -CO stretching
1163 cm^{-1}	C-O, C-C stretching, and C-O-H bending
1244 cm^{-1}	C-C-H, O-C-H, C-O-H bending
1379 cm^{-1}	C-O-H bending
1600 cm^{-1}	CH, CH2, C-O-H bending

To study the stability of fabricated sensors that were stored in the fridge, Raman spectra were acquired in the air over five weeks, see Figure 3.5. The relative standard deviation (RSD) for the highest feature peak at 1600 cm^{-1} of the Ag-CS substrate is 15% during five weeks. Figure 3.5 (A) shows 40 spectra of bare Ag-CS substrate after 0/2/4/5 weeks (ten spectra for each experiment). The corresponding bar plot for the highest peak at 1600 cm^{-1} is shown in Figure 3.5 (B). All raw data are shown in SI Figure S4. The 5^{th} spectrum for week 0/2/4/5 is shown in SI Figure S5 (A). The peak features did not change after five weeks. The Raman counts of the highest peak at 1600 cm^{-1} for the ten measurements is shown in SI Figure S5 (B). There was only a slight decrease in the Raman signal after weeks and the peak features for Ag-CS remained. It is widely reported that Ag nanostructures can easily oxidize in air,[36-38] and the Ag-CS substrate storage method used here could overcome or limit this drawback, from the experimental data in this section. A small decrease in the Raman signal over the five weeks can be observed also in Figure 3.5 (B) and this might be due to the slight oxidation of the substrate every time a new measurement is undertaken (opening the sealing film and exposing it to air).

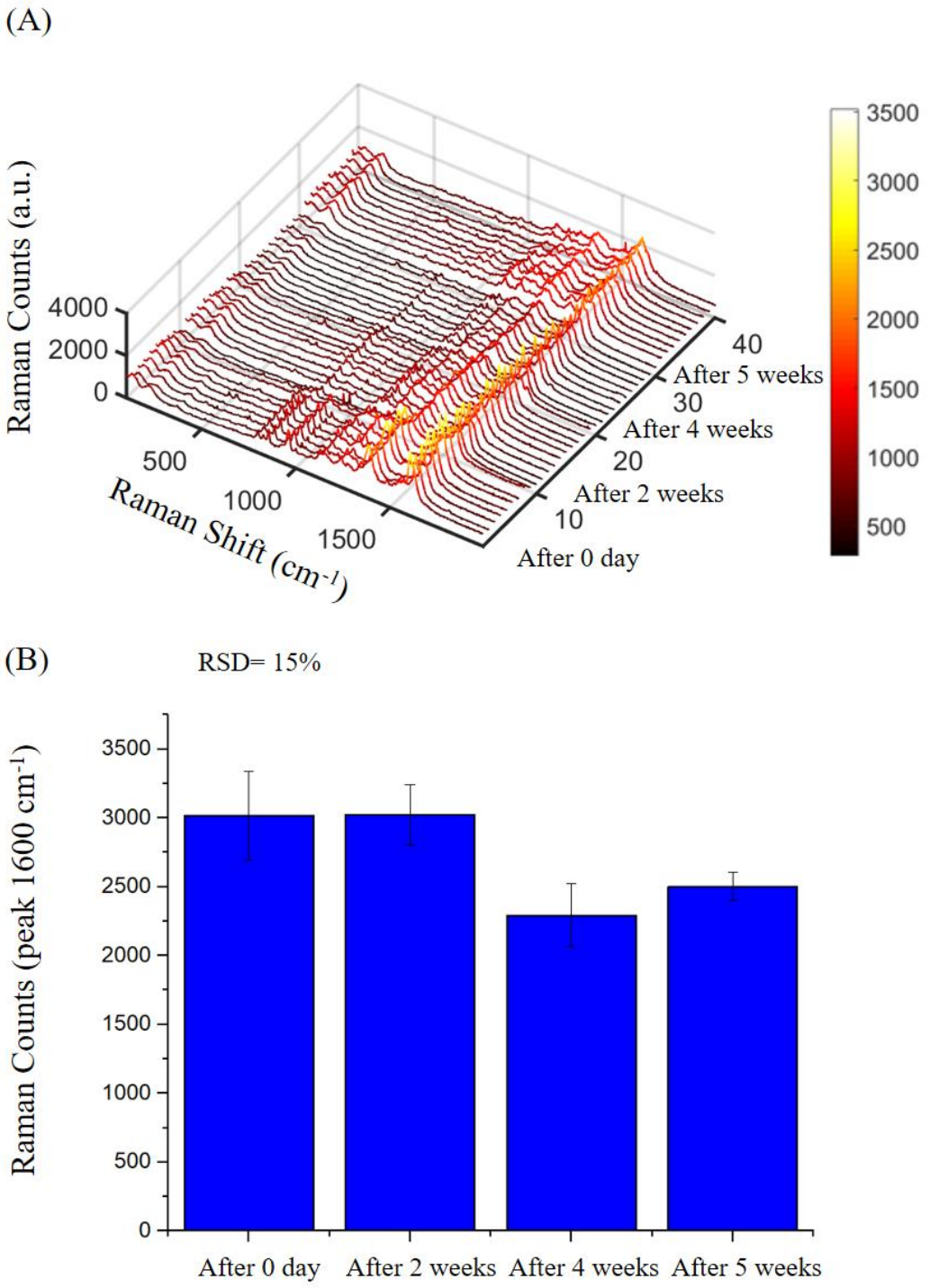

Figure 3.5: Stability study of the SERS substrate after zero days, two weeks, four weeks, and five weeks. (A) 40 spectra of bare Ag-CS SERS sensor after 0/2/4/5 weeks. See also SI Figure S4. (B) Corresponding bar plot of the peak at 1600 cm^{-1}, the overall RSD of these data was 15%. Ten spectra were taken for each experiment.

3.4 MCPA detection with Ag-CS substrate.

To see if the fabricated substrates could be used for the detection of MCPA, Raman spectra were recorded after incubation in 0.0285 nM MCPA solution, see Figure 3.6. The Raman spectrum after the application of DI water is also shown in Figure 3.6 for reference. For the spectrum acquired in the MCPA solution, new peaks at ~291 cm^{-1} and sharp peaks around ~928 cm^{-1}, ~1129 cm^{-1}, and 1400 cm^{-1} show up after the 2nd Raman measurement. In DI water, these peaks did not show, suggesting they were related to MCPA.

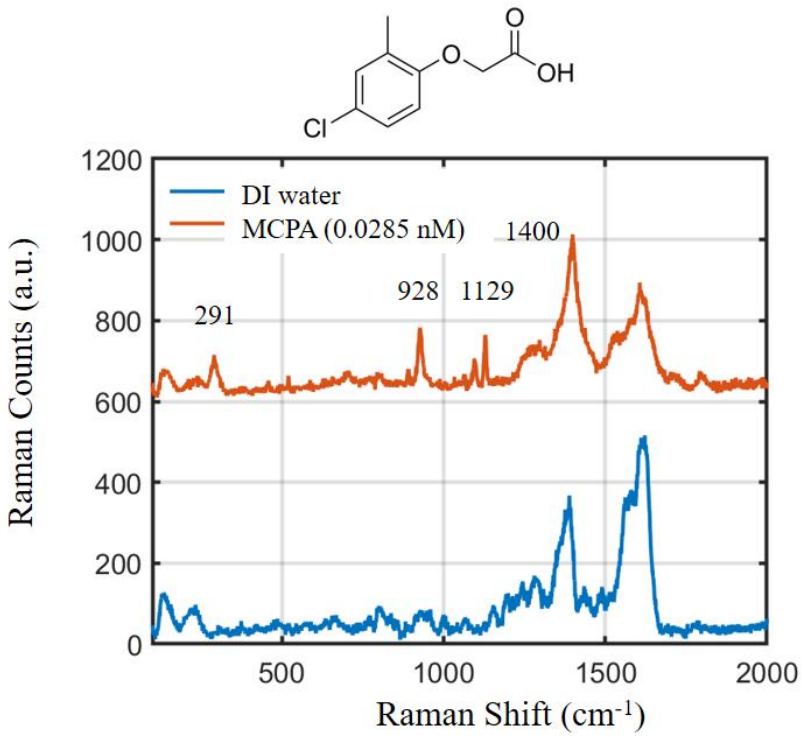

Figure 3.6: Raman spectra of Ag-CS substrate after application of DI water (bottom) and (top) after application of MCPA (0.0285 nM) solution.

The Raman spectrum of MCPA powder is shown in SI Figure S6. No peak assignment could be found in the literature for MCPA. Generally speaking, Raman spectra of a particular compound is sensitive to its state (e.g., powder or solution) as

well as the experimental conditions such as pH, etc. So for precise Raman peak assignment, it is necessary to use theoretical studies such as DFT (density functional theory) modeling to help the analysis.[39] Also, there are differences between SERS and Raman spectra for the same chemical, as discussed in Chapter 1. In the present study, we have tentatively assigned the observed peaks by comparing the spectrum with the one obtained with 2,4-D which has a very similar chemical structure, see Table 2. The peak at 291 cm^{-1} can be assigned to C-Cl and C-O-C bonds, the peak at 1129 cm^{-1} can be related to C-H_{ring} scissoring, and the peak at 927 cm^{-1} related to C-COO^- vibration.

As discussed in the introduction, MCPA does not have a strong affinity with the silver surface, and as a result, it is unlikely that the recorded spectra correspond to direct SERS of the molecule. However, it is possible that MCPA molecules enter the corn starch porous structure[40-41] and interact with its functional groups. For example, corn starch has -OH, -O-, and -CH bonds[33], and the -OH groups could interact with the -COOH group of MCPA through hydrogen bonding,[42] see schematics in Figure 3.7. This way, the CS layer can trap and concentrate the MCPA analyte close to the surface of the silver nanostructure. The measured signal is then a result of the local concentration of the target analyte at the surface of the Ag nanostructure. may benefit from enhanced Raman signal through electromagnetic enhancement.

Table 2: MCPA crystal Raman peak, and MCPA solution on Ag-CS substrate peak assignment, according to 2,4-D crystal vibration modes.

Peaks measured with MCPA solution in this research	MCPA powder	2,4-D SERS with Ag NPs peaks from literature	Tentative vibration modes (from 2,4-D molecule in solution)
291 cm^{-1}	205	422	δ(COC) + δ(CCl)

\	798	800	ν(CC)ring + ν(C–O) + ν(C–Cl)
927 cm^{-1}	927	/	ν(C–COO−)
1099 cm^{-1}	1083	/	ν(CC)ring + ν(CO) + δ(CH)ring
1129 cm^{-1}	1116	1178	ν(CC)ring + ν(C–Cl)

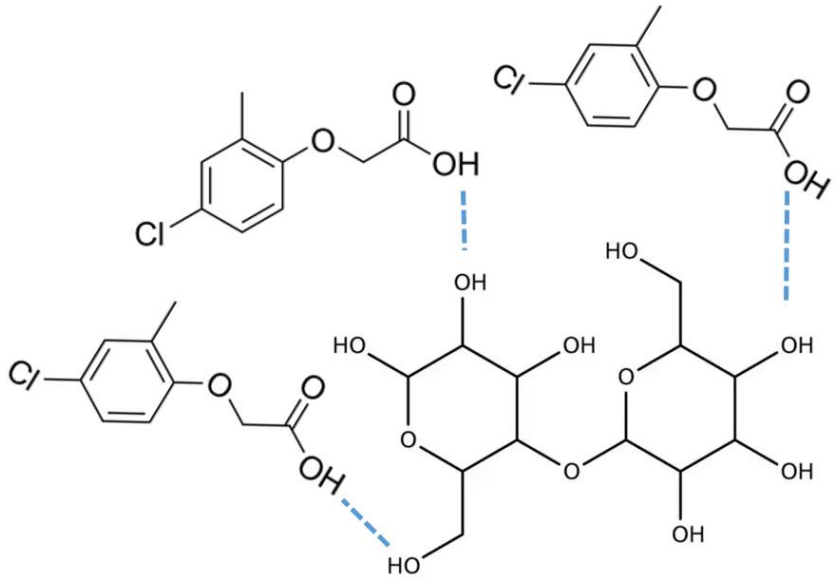

Figure 3.7: Possible interaction between MCPA and CS through hydrogen bond.

It can be observed that the spectra are similar to the ones obtained for 2,4-D in Chapter 2. SI Figure S7 in SI shows the spectra overlapped for MCPA and 2,4-D. A drawback of the present method is therefore that it is not possible to distinguish between the two molecules. The chemical structures of 2,4-D and MCPA are similar - they both have a benzene ring, -Cl atoms, and a side chain -O-CH_2-COOH. The only difference is that 2,4-D has one more -Cl in the benzene ring and MCPA has -CH_3 in the same position. Molecules with similar chemical structures often share the same Raman peak features in SERS studies, this has been approved by other research. For example, Zhou et al., observed that the SERS spectra of three antibiotics with similar chemical structures NFX, CIP, and OFX obtained with bare Ag NPs exhibited the same Raman spectra with peaks located in the region of 1394 ± 10 cm^{-1}.[43] Interestingly, they were

able to distinguish these chemicals structure by using 1-Mercapto-1-undecanol (MUO) modified Ag NPs (MUO @Ag NPs) SERS substrates.

Similarly, Lv et al. studied SERS spectra of the main fatty acid (FAs) in vegetable oils, oleic acid (OA), linoleic acid (LA), α-linolenic acid (ALA), all of them are simple molecules containing only -CH3, -CH2, and -COOH as functional groups and C=C, -C-C-, -C-H, O=C-, -OH, and C-O as chemical bonds. OA, LA, and ALA are fatty acids with 1, 2, and 3 C=C bonds, respectively. Their molecular formulas include the same number of carbon atoms and the same type of functional groups but different numbers of C=C bonds. Their SERS spectra were found to be similar.[44]

3.4.1 Evaluation of the repeatability of Ag-CS substrate towards MCPA detection.

To evaluate the repeatability of these substrates, a 0.285 nM MCPA solution was used and 50 Raman measurements were acquired at different random points on a sensor, see Figure 3.8 (A) with, and (B) without baseline subtraction. Some variations in terms of absolute intensities could be observed for the different peaks. For this reason, and similarly to Chapter 2, peak ratios were studied instead of single peaks.

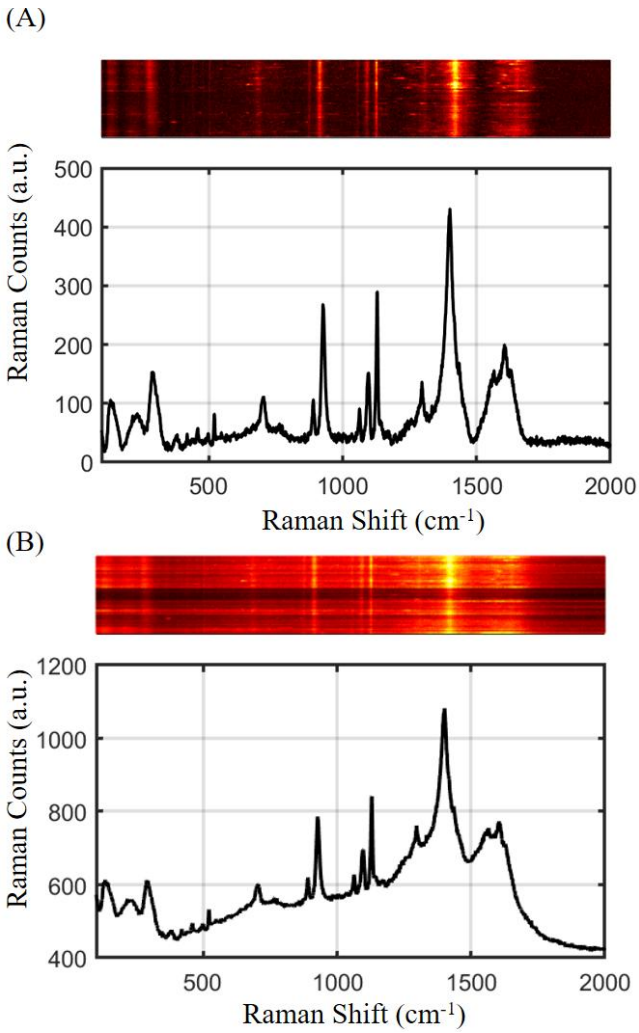

Figure 3.8: Repeatability study of the SERS substrate with 0.285nM MCPA at 50 different random points. Raman color maps and spectra (A) with baseline subtraction, (B) without baseline subtraction;

Figure 3.9 (A-B) shows data without baseline subtraction. The RSD of peak ratio $I_{291\ cm\text{-}1}$ / $I_{1400\ cm\text{-}1}$ and $I_{1129\ cm\text{-}1}$ / $I_{1400\ cm\text{-}1}$ of 50 measurements were 9% and 6% (the SD were 0.05 and 0.04), respectively. The same measurements with baseline subtraction are shown in SI Figure S8 and the RSD of peak ratio $I_{291\ cm\text{-}1}$ / $I_{1400\ cm\text{-}1}$ and $I_{1129\ cm\text{-}1}$ / $I_{1400\ cm\text{-}1}$ of 50 measurements were calculated to be 18% and 13% (the SD is 0.07 and 0.08), respectively.

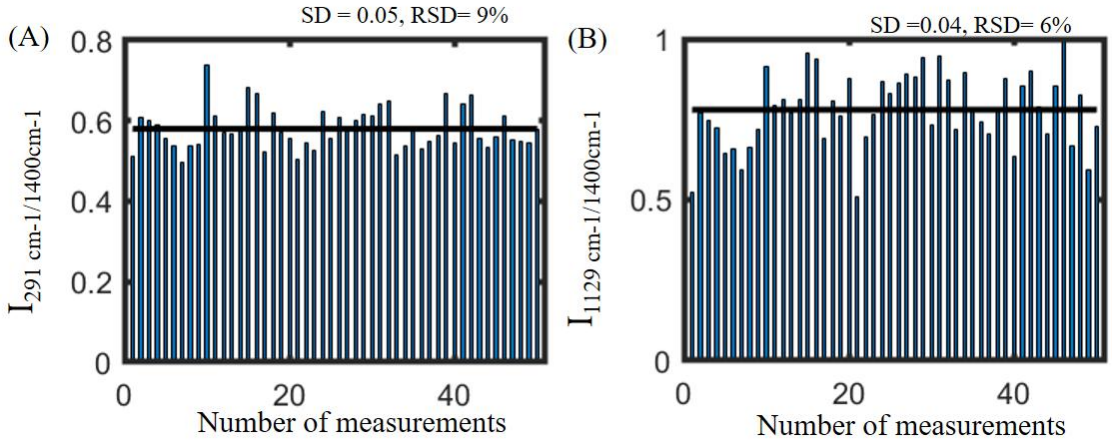

Figure 3.9: (A-D) Bar plot of 50 Raman measurements. The RSD at peak ratio $I_{291\ cm\text{-}1}$ / $I_{1400\ cm\text{-}1}$ and $I_{1129\ cm\text{-}1}$ / $I_{1400\ cm\text{-}1}$ of 50 measurements without baseline subtraction was 9% and 6% (the SD is 0.05 and 0.04), respectively.

3.4.2 Data analysis for different MCPA concentrations on an Ag-CS substrate, without baseline subtraction.

For data analysis in SERS, most research used Raman intensity vs. Log [analyte] for calibration[45-48]. Liu et al. used Raman intensity vs. [R6G] for linear calibration;[49] Meng et al. used sigmoid function to fit Log [BZA] vs. peak ratio.[50] Wang et al. used non-linear fitting for Raman intensity vs. Log[H1N1] and Log [HAdV].[51] These fittings were based on the data feature and the trend. Other advanced math models such as UVE-PLS[52-53] need specific requirements and modelling for SERS data and are out of the scope of this research. Besides, Xu et al. also did not subtract the baseline of Raman spectra for data analysis, for the detection of 2.4-D by using hollow Au and Ag-nanoflower.[54]

Upon the application of 28.5 fM MCPA on Ag-CS substrate, a similar spectrum as the one obtained for 0.285 nM appeared after the 2nd measurement, see SI Figure S9. The experiment for the detection of 28.5 fM MCPA on an Ag-CS substrate has been

repeated three more times, refer to SI Figure S10. The feature peak at 1600 cm^{-1} was not always sharp as depicted in SI Figure S10 and was not considered in the data analysis study. It is probably related to -CH2-OH for CS, [34-35] the orientation of the interaction between MCPA with -CH2-OH in CS surface varies in different detection locations. The other peaks such as 291 cm^{-1}, 1129 cm^{-1}, and 1400 cm^{-1}, kept the same feature in the repeated experiments and further studied in the following data analysis section.

In Chapter 2, the Raman spectrum changed with 2,4-D down to 1 pM in 30 minutes. The superior detection ability of the Ag-CS substrate towards MCPA in this chapter, compared to 2,4-D in Chapter 2, could be attributed to (i) the structure of CS vs. GA, as CS contains more -OH groups, which interact with more MCPA molecular close to the surface. (ii) It is also possible that the Ag-CS substrate has a thinner polymer layer than Ag-GA and that saturation is obtained faster.

Various concentrations ranging from 28.5 fM to 0.285 mM of MCPA (28.5 fM, 2.85 pM, 28.5 pM, 2.85 nM, 285 nM, 2.85 μM, 0.285 mM.) in DI water, were tested for the MCPA detection study, using the Ag-CS NPs substrate, see Figure 3.10. Each spectrum was calculated based on the average of ten spectra acquired from different spots on the substrate. The raw data are presented in SI Figure S11. The overall peak intensity decreased with the increase in MCPA concentration.

In this experiment, different MCPA concentrations were added to the same substrate. This made it impossible to quantify MCPA directly, as MCPA interacted with CS through hydrogen bonding. Besides, this was not good analytical practice. A single sensor should be used for a single MCPA concentration. However, this approach reduced the variation arising from different Ag-CS substrates. The same experiment was repeated, and the spectra are presented in SI section 1 Figure S12. The spectra without baseline subtraction are shown in Figure 3.10. The trend lines for Raman counts at

single peak 293 cm^{-1},1129 cm^{-1} and 1400 cm^{-1} Raman are shown in SI Figure S13(A). Combining this observation with the repeated experimental results shown in SI Figure S13 (B), it was noted that the trend lines for single peaks did not consistently follow the same pattern, and therefore, these single peaks could not be used directly for data analysis.

From the spectra in Figure 3.10, the recorded signal included both the Raman signal and background signal, the background signal could include background fluorescence.[55-56] Following the application of the analyte MCPA, the interaction between MCPA and CS, or the coverage of MCPA on the CS surface, could lead to a reduction in the background fluorescence signal from CS.

Data processing with baseline subtraction is shown in SI section 2.

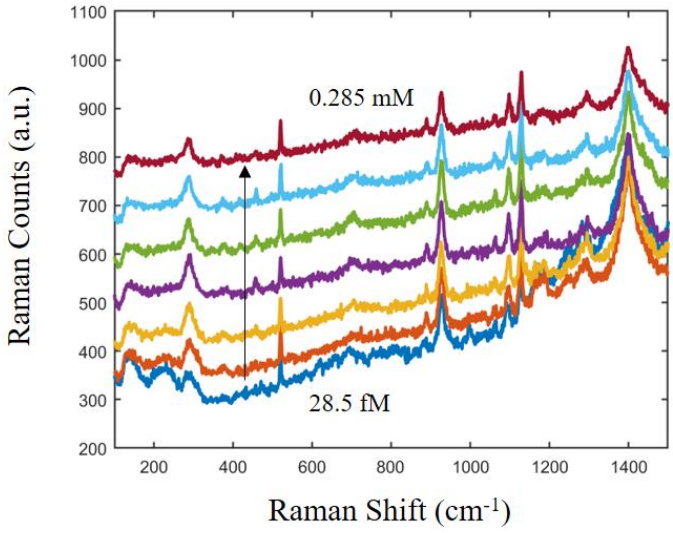

Figure 3.10: Spectra of different MCPA concentrations from 28.5 fM to 0.285 mM (28.5 fM, 2.85 pM, 28.5 pM, 2.85 nM, 285 nM, 2.85 µM, 0.285 mM.) without baseline subtraction.

Similar to Chapter 2, analysis using the peak ratios approach was undertaken. Figure 3.11 shows the plot of peak ratios $I_{291\ cm\text{-}1/1400cm\text{-}1}$ and $I_{1129\ cm\text{-}1/1400cm\text{-}1}$ against the

logarithm of the concentrations of the MCPA solution. The peak ratios $I_{291\ cm\text{-}1/1400cm\text{-}1}$ and $I_{1129\ cm\text{-}1/1400cm\text{-}1}$ increased with log [MCPA]. For $I_{1129\ cm\text{-}1/1400cm\text{-}1}$, the value changed from 0.68 to 0.88, and for $I_{291\ cm\text{-}1/1400cm\text{-}1}$, the value changed from 0.43 to 0.56. A repeated experiment and the peak ratio vs. log[MCPA] trend line are shown in SI Figure S14(A).

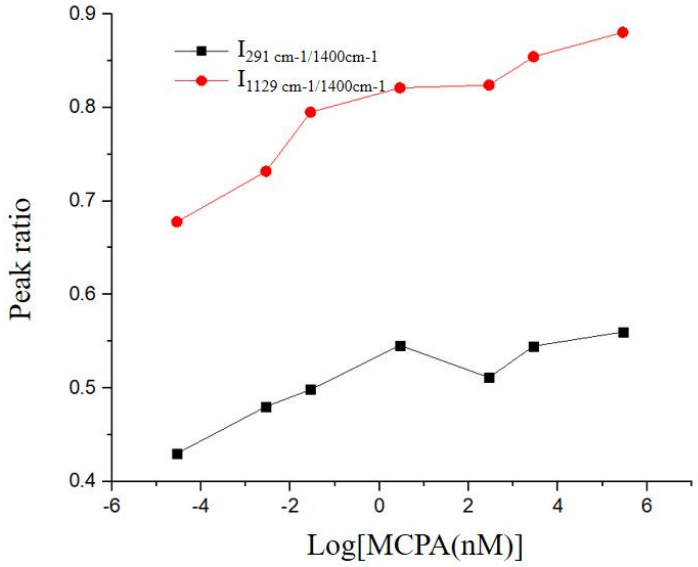

Figure 3.11: peak ratios vs. log[MCPA] from 28.5 fM to 0.285 mM.

The peak ratio $I_{1129\ cm\text{-}1/1400cm\text{-}1}$ was further studied for fitting, see Figure 3.12. A linear plot was obtained for $I_{1129\ cm\text{-}1/1400cm\text{-}1}$: y = 0.789 + 0.018log(x), R^2 = 0.90. Fitting for peak ratio $I_{291\ cm\text{-}1/1400cm\text{-}1}$ is shown in SI Figure S15 with R^2=0.748. A Raman signal was obtained for a concentration as low as 28.5 fM. However, quantification is not possible as the starting values are different for the same MCPA concentration on different Ag-CS substrates, this is related to fabrication variation. Also, adding more MCPA on the Ag-CS substrate will make the Raman signal increase regardless of the concentration. A similar fitting result is shown in SI Figure S14 (B) in the repeated experiment.

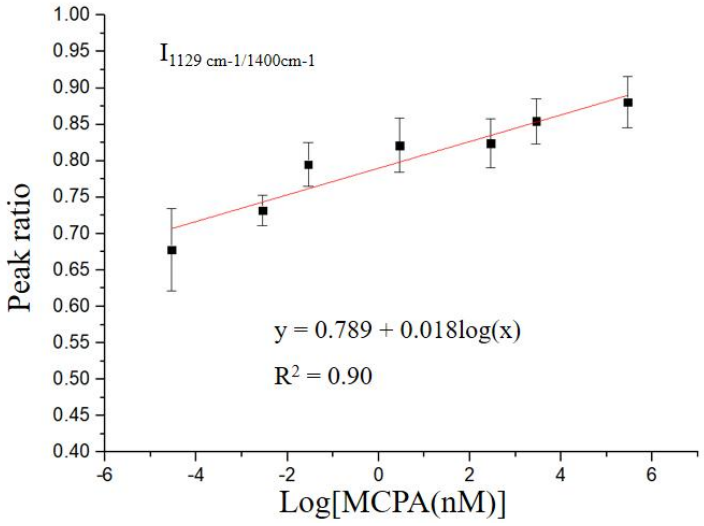

Figure 3.12: Fitting for peak ratios $I_{1129\ cm\text{-}1/1400cm\text{-}1}$vs. log [MCPA].

According to the fitting results, the peak ratio increased with log[MCPA]. The peaks at 293 cm^{-1} and 1129 cm^{-1} can be related to MCPA, where 293 cm^{-1} is δ(COC) and δ(C-Cl) vibration, and 1129 cm^{-1} is $\nu(CC)_{ring}$ and ν(C-Cl) of MCPA as discussed in Table 1. The peak at 1400 cm^{-1} is attributed to the C-O-H bending in the carbon ring of CS. The peak ratio reflects the interaction between MCPA and CS. Each -OH site in the carbon

ring of CS can interact with more than one MCPA molecule, and the signal increases with the addition of MCPA to the substrate.

Without baseline subtraction, the error bar/RSD was smaller compared to the ones in Chapter 2, this could be related to the detection principle. The overall signal is generated after the interaction between MCPA and Ag-CS SERS substrate. In particular, the background signal was related to Ag-CS NPs as well as the coverage of MCPA. It is thus reasonable to consider MCPA/Ag-CS as a whole in the data analysis section.

Similar to Chapter 2, this research used Ag-CS to attract MCPA to close to the silver surface and it constituted an indirect detection of MCPA where the CS layer helped capture and concentrate MCPA to gain an increased Raman signal. This approach can be viewed as non-imprinted polymer (NIP) and not molecular imprint (MIP), the latter method helps to gain better sensitivity and selectivity as discussed in Chapter 2.

4. Conclusion.

This research used the electrochemical deposition method for SERS sensor fabrication and this sensor was used to detect herbicides MCPA. These SERS sensors showed good performance towards 4-ATP and methylene blue detection and were able to detect concentrations down to 0.05 nM for 4-ATP and 0.39 µM for methylene blue. The EF was calculated to be at least 10^9 for 0.05 µM MB. This Ag-CS substrate showed a good SERS signal after five weeks with RSD = 15 %, after sealing with sealing film and storage in the fridge.

MCPA does not contain a -S or -N atom and as such does not have strong interaction with silver nanoparticles. Cornstarch on the other side may assist in attracting and concentrating MCPA closing to the Ag-CS surface. The detection principle is based on

the interaction between MCPA and the cornstarch function layer, similar to non-molecular imprint method. This Ag-CS sensor cannot quantify MCPA due to the sensor surface's low capacity to host MCPA and the experimental approach. Unlike the previous research in Chapter 2, no baseline subtraction was used for data analysis. This provided smaller error bars and better fitting results.

Nevertheless, this Ag-CS substrate does not exhibit selectivity towards any analyte in real-world applications, and not possible to use it for MCPA quantification. Although some analytes such as MB or 4-ATP have their characteristic peaks, there are other contaminants in the real world, resulting in the SERS signal originating from other chemicals. This sensor does not have selectivity. A possible way to overcome this problem is to use MIP functional layers.

Reference.

1. Morton, P. A.; Fennell, C.; Cassidy, R.; Doody, D.; Fenton, O.; Mellander, P.-E.; Jordan, P., A review of the pesticide MCPA in the land-water environment and emerging research needs. *WIREs Water* **2020,** *7* (1), e1402.

2. Glozier, N. E.; Struger, J.; Cessna, A. J.; Gledhill, M.; Rondeau, M.; Ernst, W. R.; Sekela, M. A.; Cagampan, S. J.; Sverko, E.; Murphy, C.; Murray, J. L.; Donald, D. B., Occurrence of glyphosate and acidic herbicides in select urban rivers and streams in Canada, 2007. *Environmental Science and Pollution Research* **2012,** *19* (3), 821-834.

3. Rippy, M. A.; Deletic, A.; Black, J.; Aryal, R.; Lampard, J.-L.; Tang, J. Y.-M.; McCarthy, D.; Kolotelo, P.; Sidhu, J.; Gernjak, W., Pesticide occurrence and spatio-temporal variability in urban run-off across Australia. *Water Research* **2017,** *115*, 245-255.

4. Morton, P. A.; Cassidy, R.; Floyd, S.; Doody, D. G.; McRoberts, W. C.; Jordan, P., Approaches to herbicide (MCPA) pollution mitigation in drinking water source catchments using enhanced space and time monitoring. *Science of The Total Environment* **2021,** *755*, 142827.

5. Manninen, A.; Kangas, J.; Klen, T.; Savolainen, H., Exposure of finnish farm workers to phenoxy acid herbicides. *Archives of Environmental Contamination and Toxicology* **1986,** *15* (1), 107-111.

6. Dickow, L. M.; Gerken, D. F.; Sams, R. A.; Ashcraft, S. M., Simultaneous Determination of 2,4-D and MCPA in Canine Plasma and Urine by HPLC with Fluorescence Detection Using 9-Anthryldiazomethane (ADAM). *Journal of Analytical Toxicology* **2001,** *25* (1), 35-39.

7. Rahemi, V.; Garrido, J. M. P. J.; Borges, F.; Brett, C. M. A.; Garrido, E. M. P. J., Electrochemical sensor for simultaneous determination of herbicide MCPA and its metabolite 4-chloro-2-methylphenol. Application to photodegradation environmental monitoring. *Environmental Science and Pollution Research* **2015,** *22* (6), 4491-4499.

8. Mueller, T. C.; Moorman, T. B.; Locke, M. A., Detection of Herbicides Using Fluorescence Spectroscopy. *Weed Science* **2017,** *40* (2), 270-274.

9. Sharma, B.; Frontiera, R. R.; Henry, A.-I.; Ringe, E.; Van Duyne, R. P., SERS: Materials, applications, and the future. *Materials Today* **2012,** *15* (1), 16-25.

10. Radziuk, D.; Moehwald, H., Prospects for plasmonic hot spots in single molecule SERS towards the chemical imaging of live cells. *Physical Chemistry Chemical Physics* **2015,** *17* (33), 21072-21093.

11. Langer, J.; Jimenez de Aberasturi, D.; Aizpurua, J.; Alvarez-Puebla, R. A.; Auguié, B.; Baumberg, J. J.; Bazan, G. C.; Bell, S. E. J.; Boisen, A.; Brolo, A. G.; Choo, J.; Cialla-May, D.; Deckert, V.; Fabris, L.; Faulds, K.; García de Abajo, F. J.; Goodacre, R.; Graham, D.; Haes, A. J.; Haynes, C. L.; Huck, C.; Itoh, T.; Käll, M.; Kneipp, J.; Kotov, N. A.; Kuang, H.; Le Ru, E. C.; Lee, H. K.; Li, J.-F.; Ling, X. Y.; Maier, S. A.; Mayerhöfer, T.; Moskovits, M.; Murakoshi, K.; Nam, J.-M.; Nie, S.; Ozaki, Y.; Pastoriza-Santos, I.; Perez-Juste, J.; Popp, J.; Pucci, A.; Reich, S.; Ren, B.; Schatz, G. C.; Shegai, T.; Schlücker, S.; Tay, L.-L.; Thomas, K. G.; Tian, Z.-Q.; Van Duyne, R. P.; Vo-Dinh, T.; Wang, Y.; Willets, K. A.; Xu, C.; Xu, H.; Xu, Y.; Yamamoto, Y. S.; Zhao, B.; Liz-Marzán, L. M., Present and Future of Surface-Enhanced Raman Scattering. *ACS Nano* **2020,** *14* (1), 28-117.

12. Liu, B.; Thielert, B.; Reutter, A.; Stosch, R.; Lemmens, P., Quantifying the Contribution of Chemical Enhancement to SERS: A Model Based on the Analysis of Light-Induced Degradation Processes. *The Journal of Physical Chemistry C* **2019,** *123* (31), 19119-19124.

13. Le Ru, E. C.; Blackie, E.; Meyer, M.; Etchegoin, P. G., Surface Enhanced Raman Scattering Enhancement Factors: A Comprehensive Study. *The Journal of Physical Chemistry C* **2007,** *111* (37), 13794-13803.

14. Boyack, R.; Le Ru, E. C., Investigation of particle shape and size effects in SERS using T-matrix calculations. *Physical Chemistry Chemical Physics* **2009,** *11* (34), 7398-7405.

15. Lee, D.; Yoon, S., Effect of Nanogap Curvature on SERS: A Finite-Difference Time-Domain Study. *The Journal of Physical Chemistry C* **2016,** *120* (37), 20642-20650.

16. Kleinman, S. L.; Sharma, B.; Blaber, M. G.; Henry, A.-I.; Valley, N.; Freeman, R. G.; Natan, M. J.; Schatz, G. C.; Van Duyne, R. P., Structure Enhancement Factor Relationships in Single Gold Nanoantennas by Surface-Enhanced Raman Excitation Spectroscopy. *Journal of the American Chemical Society* **2013,** *135* (1), 301-308.

17. He, S.; Chua, J.; Tan, E. K. M.; Kah, J. C. Y., Optimizing the SERS enhancement of a facile gold nanostar immobilized paper-based SERS substrate. *RSC Advances* **2017,** *7* (27), 16264-16272.

18. Yue, W.; Wang, Z.; Yang, Y.; Chen, L.; Syed, A.; Wong, K.; Wang, X., Electron-beam lithography of gold nanostructures for surface-enhanced Raman scattering. *Journal of Micromechanics and Microengineering* **2012,** *22* (12), 125007.

19. Jing, L.; Shi, Y.-e.; Cui, J.; Zhang, X.; Zhan, J., Hydrophobic gold nanostructures via electrochemical deposition for sensitive SERS detection of persistent toxic substances. *RSC Advances* **2015,** *5* (18), 13443-13450.

20. William, R. V.; Das, G. M.; Dantham, V. R.; Laha, R., Enhancement of Single Molecule Raman Scattering using Sprouted Potato Shaped Bimetallic Nanoparticles. *Scientific Reports* **2019,** *9* (1), 10771.

21. Sui, C.; Wang, K.; Wang, S.; Ren, J.; Bai, X.; Bai, J., SERS activity with tenfold detection limit optimization on a type of nanoporous AAO-based complex multilayer substrate. *Nanoscale* **2016,** *8* (11), 5920-5927.

22. Ortega, F.; García, M. A.; Arce, V. B., Nanocomposite films with silver nanoparticles synthesized in situ: Effect of corn starch content. *Food Hydrocolloids* **2019,** *97*, 105200.

23. Ortega-Arroyo, L.; Martin-Martinez, E. S.; Aguilar-Mendez, M. A.; Cruz-Orea, A.; Hernandez-Pérez, I.; Glorieux, C., Green synthesis method of silver nanoparticles using starch as capping agent applied the methodology of surface response. *Starch - Stärke* **2013,** *65* (9-10), 814-821.

24. Seymour, I.; O'Sullivan, B.; Lovera, P.; Rohan, J. F.; O'Riordan, A., Elimination of Oxygen Interference in the Electrochemical Detection of Monochloramine, Using In Situ pH Control at Interdigitated Electrodes. *ACS Sensors* **2021,** *6* (3), 1030-1038.

25. Yang, Y.; O'Riordan, A.; Lovera, P., Highly sensitive pesticide detection using electrochemically prepared Silver-Gum Arabic nanocluster SERS substrates. *Sensors and Actuators B: Chemical* **2022,** *364*, 131851.

26. Schulze, H. G.; Foist, R. B.; Okuda, K.; Ivanov, A.; Turner, R. F. B., A Small-Window Moving Average-Based Fully Automated Baseline Estimation Method for Raman Spectra. *Appl. Spectrosc.* **2012,** *66* (7), 757-764.

27. Shi, L.; Zhong, X.; Ding, H.; Yu, Z.; Jin, J.; Zhou, T.; Zhu, Y.; Liu, Z., Continuous separation of microparticles based on optically induced dielectrophoresis. *Microfluidics and Nanofluidics* **2022,** *26* (1), 6.

28. Hvolbæk, B.; Janssens, T. V. W.; Clausen, B. S.; Falsig, H.; Christensen, C. H.; Nørskov, J. K., Catalytic activity of Au nanoparticles. *Nano Today* **2007,** *2* (4), 14-18.

29. Li, C.; Huang, Y.; Lai, K.; Rasco, B. A.; Fan, Y., Analysis of trace methylene blue in fish muscles using ultra-sensitive surface-enhanced Raman spectroscopy. *Food Control* **2016,** *65*, 99-105.

30. Fu, H.; Bao, H.; Zhang, H.; Zhao, Q.; Zhou, L.; Zhu, S.; Wei, Y.; Li, Y.; Cai, W., Quantitative Surface-Enhanced Raman Spectroscopy for Field Detections Based on Structurally Homogeneous Silver-Coated Silicon Nanocone Arrays. *ACS Omega* **2021,** *6* (29), 18928-18938.

31. Karim, A. A.; Norziah, M. H.; Seow, C. C., Methods for the study of starch retrogradation. *Food Chemistry* **2000,** *71* (1), 9-36.

32. Cho, K.-Y.; Lim, S.-T., Preparation and Properties of Benzyl Corn Starches. *Starch - Stärke* **1998,** *50* (6), 250-257.

33. Mariod, A. A., Chemical Properties of Gum Arabic. In *Gum Arabic*, Mariod, A. A., Ed. Academic Press: 2018; pp 67-73.

34. Almeida, M. R.; Alves, R. S.; Nascimbem, L. B.; Stephani, R.; Poppi, R. J.; de Oliveira, L. F., Determination of amylose content in starch using Raman spectroscopy and multivariate calibration analysis. *Analytical and bioanalytical chemistry* **2010,** *397* (7), 2693-701.

35. Kittaka, S.; Yamaguchi, K.; Takahara, S., High physisorption affinity of water molecules to the hydroxylated aluminum oxide (001) surface. *Journal of colloid and interface science* **2012,** *368* (1), 552-7.

36. Michieli, N.; Pilot, R.; Russo, V.; Scian, C.; Todescato, F.; Signorini, R.; Agnoli, S.; Cesca, T.; Bozio, R.; Mattei, G., Oxidation effects on the SERS response of silver nanoprism arrays. *RSC Advances* **2017,** *7* (1), 369-378.

37. Matikainen, A.; Nuutinen, T.; Itkonen, T.; Heinilehto, S.; Puustinen, J.; Hiltunen, J.; Lappalainen, J.; Karioja, P.; Vahimaa, P., Atmospheric oxidation and carbon contamination of silver and its effect on surface-enhanced Raman spectroscopy (SERS). *Scientific Reports* **2016,** *6* (1), 37192.

38. Erol, M.; Han, Y.; Stanley, S. K.; Stafford, C. M.; Du, H.; Sukhishvili, S., SERS Not To Be Taken for Granted in the Presence of Oxygen. *Journal of the American Chemical Society* **2009,** *131* (22), 7480-7481.

39. Cañamares, M. V.; Chenal, C.; Birke, R. L.; Lombardi, J. R., DFT, SERS, and Single-Molecule SERS of Crystal Violet. *The Journal of Physical Chemistry C* **2008,** *112* (51), 20295-20300.

40. Wu, W.; Jiao, A.; Xu, E.; Chen, Y.; Jin, Z., Effects of Extrusion Technology Combined with Enzymatic Hydrolysis on the Structural and Physicochemical Properties of Porous Corn Starch. *Food and Bioprocess Technology* **2020,** *13* (3), 442-451.

41. Davoudi, Z.; Azizi, M. H.; Barzegar, M., Porous corn starch obtained from combined cold plasma and enzymatic hydrolysis: Microstructure and physicochemical properties. *International Journal of Biological Macromolecules* **2022,** *223*, 790-797.

42. Hassanzadeh-Afruzi, F.; Esmailzadeh, F.; Heidari, G.; Maleki, A.; Nazarzadeh Zare, E., Arabic Gum-Grafted-Hydrolyzed Polyacrylonitrile@ZnFe2O4 as a Magnetic Adsorbent for Remediation of Levofloxacin Antibiotic from Aqueous Solutions. *ACS Omega* **2023,** *8* (7), 6337-6348.

43. Zhou, S.; Hu, Z.; Zhang, Y.; Wang, D.; Gong, Z.; Fan, M., Differentiation and identification structural similar chemicals using SERS coupled with different chemometric methods: The example of fluoroquinolones. *Microchemical Journal* **2022,** *183*, 108023.

44. Lv, M.; Zhang, X.; Ren, H.; Liu, L.; Zhao, Y.; Wang, Z.; Wu, Z.; Liu, L.; Xu, H., A rapid method to authenticate vegetable oils through surface-enhanced Raman scattering. *Scientific Reports* **2016,** *6*, 23405.

45. Yue, X.; Su, Y.; Wang, X.; Li, L.; Ji, W.; Ozaki, Y., Reusable Silicon-Based SERS Chip for Ratiometric Analysis of Fluoride Ion in Aqueous Solutions. *ACS Sensors* **2019,** *4* (9), 2336-2342.

46. Castro-Grijalba, A.; Montes-García, V.; Cordero-Ferradás, M. J.; Coronado, E.; Pérez-Juste, J.; Pastoriza-Santos, I., SERS-Based Molecularly Imprinted Plasmonic Sensor for Highly Sensitive PAH Detection. *ACS Sensors* **2020,** *5* (3), 693-702.

47. Barbarin, I.; Politakos, N.; Serrano Cantador, L.; Cecilia, J. A.; Sanz, O.; Tomosvka, R., Tailoring of Textural Properties of 3D Reduced Graphene Oxide

Composite Monoliths by Using Highly Crosslinked Polymer Particles toward Improved CO2 Sorption. *ACS Applied Polymer Materials* **2022,** *4* (12), 9065-9075.

48. Yang, X.; Wang, S.; Wang, Y.; He, Y.; Chai, Y.; Yuan, R., Stimuli-Responsive DNA Microcapsules for SERS Sensing of Trace MicroRNA. *ACS Applied Materials & Interfaces* **2018,** *10* (15), 12491-12496.

49. Liu, X.; Dang, A.; Li, T.; Sun, Y.; Lee, T.-C.; Deng, W.; Wu, S.; Zada, A.; Zhao, T.; Li, H., Plasmonic Coupling of Au Nanoclusters on a Flexible MXene/Graphene Oxide Fiber for Ultrasensitive SERS Sensing. *ACS Sensors* **2023,** *8* (3), 1287-1298.

50. Meng, X.; Wang, Y.; Song, X.; Zhang, M.; Yu, J.; Qiu, L.; Lin, J.; Wang, X., Ag-Coated Ternary Layered Double Hydroxide as a High-Performance SERS Sensor for Aldehydes. *ACS Applied Materials & Interfaces* **2023,** *15* (41), 48818-48825.

51. Wang, C.; Wang, C.; Wang, X.; Wang, K.; Zhu, Y.; Rong, Z.; Wang, W.; Xiao, R.; Wang, S., Magnetic SERS Strip for Sensitive and Simultaneous Detection of Respiratory Viruses. *ACS Applied Materials & Interfaces* **2019,** *11* (21), 19495-19505.

52. Hassan, M. M.; Jiao, T.; Ahmad, W.; Yi, X.; Zareef, M.; Ali, S.; Li, H.; Chen, Q., Cellulose paper-based SERS sensor for sensitive detection of 2,4-D residue levels in tea coupled uninformative variable elimination-partial least squares. *Spectrochimica Acta Part A: Molecular and Biomolecular Spectroscopy* **2021,** *248*, 119198.

53. Wen, Y.; Wang, X.; Li, D.; Zhang, Q.; Deng, B.; Chen, Y., Rapid detection of phenytoin sodium by partial-least squares and linear regression models combined with surface-enhanced Raman spectroscopy. *Journal of Pharmaceutical and Biomedical Analysis* **2023,** *223*, 115160.

54. Xu, Y.; Kutsanedzie, F. Y. H.; Hassan, M. M.; Zhu, J.; Li, H.; Chen, Q., Functionalized hollow Au@Ag nanoflower SERS matrix for pesticide sensing in food. *Sensors and Actuators B: Chemical* **2020,** *324*, 128718.

55. Kotula, A. P.; Orski, S. V.; Brignac, K. C.; Lynch, J. M.; Heilala, B. M. J., Time-gated Raman spectroscopy of recovered plastics. *Marine Pollution Bulletin* **2022,** *181*, 113894.

56. Mazilu, M.; Luca, A. C. D.; Riches, A.; Herrington, C. S.; Dholakia, K., Optimal algorithm for fluorescence suppression of modulated Raman spectroscopy. *Opt. Express* **2010,** *18* (11), 11382-11395.

Supporting Information.

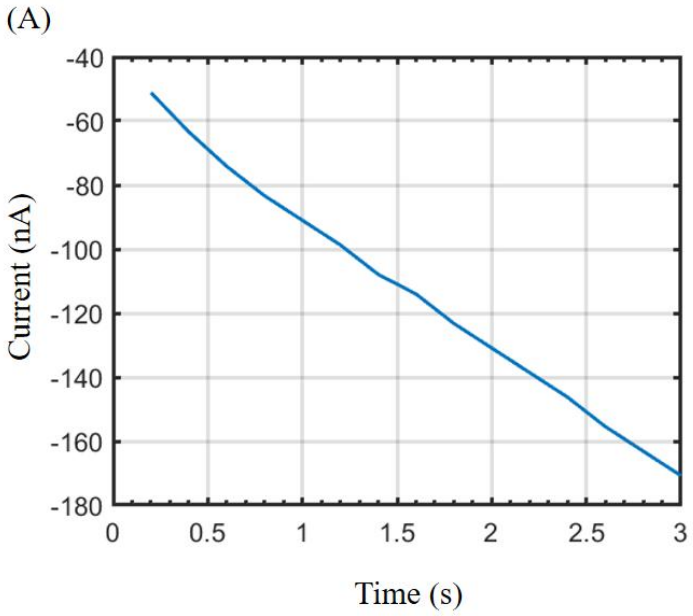

Figure S1: Current (nA)-time (s) plot for electrochemical deposition at -0.6 V voltage.

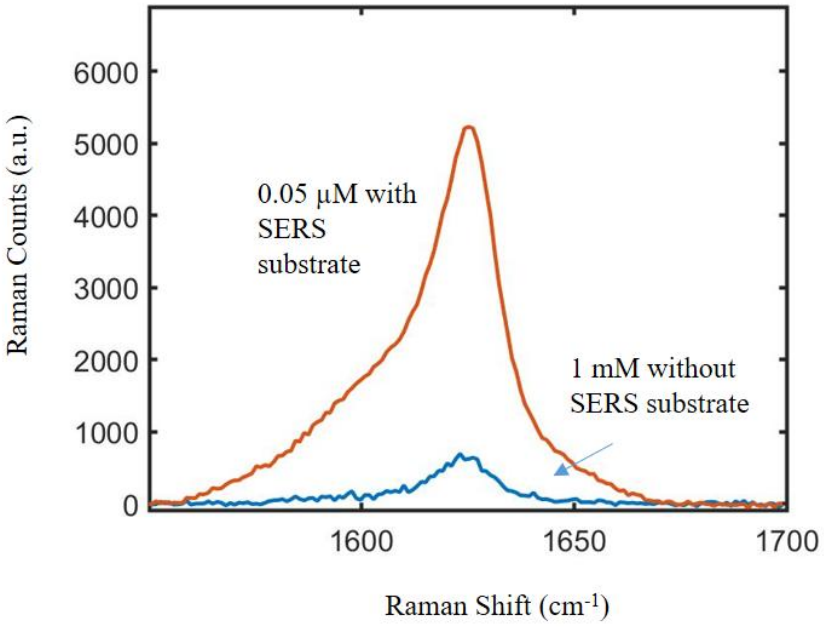

Figure S2: The spectra of MB at 1 mM without SERS substrate and MB at 0.05 µM with SERS substrate.

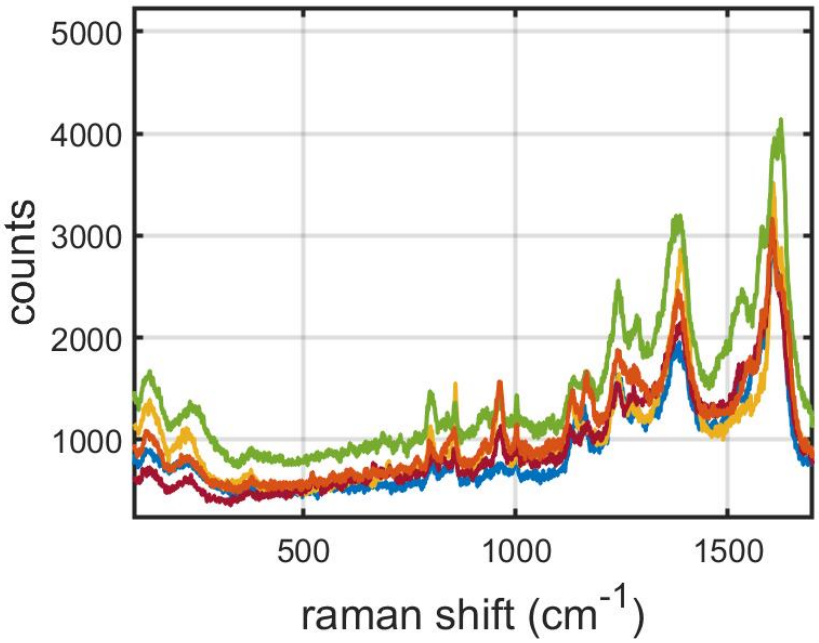

Figure S3: Ag-CS Raman spectra from five different chips.

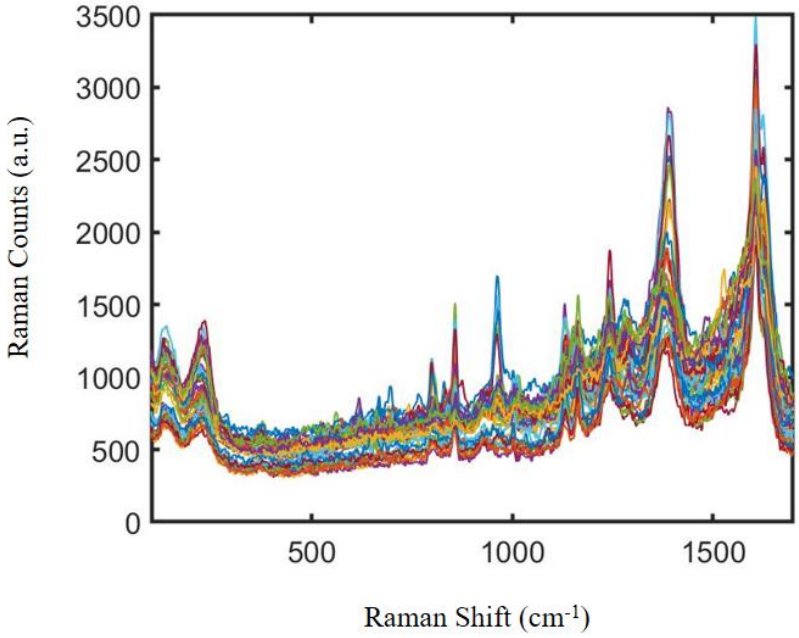

Figure S4: Raw data for stability study in Figure 3.3. 10 spectra were taken each week over five weeks.

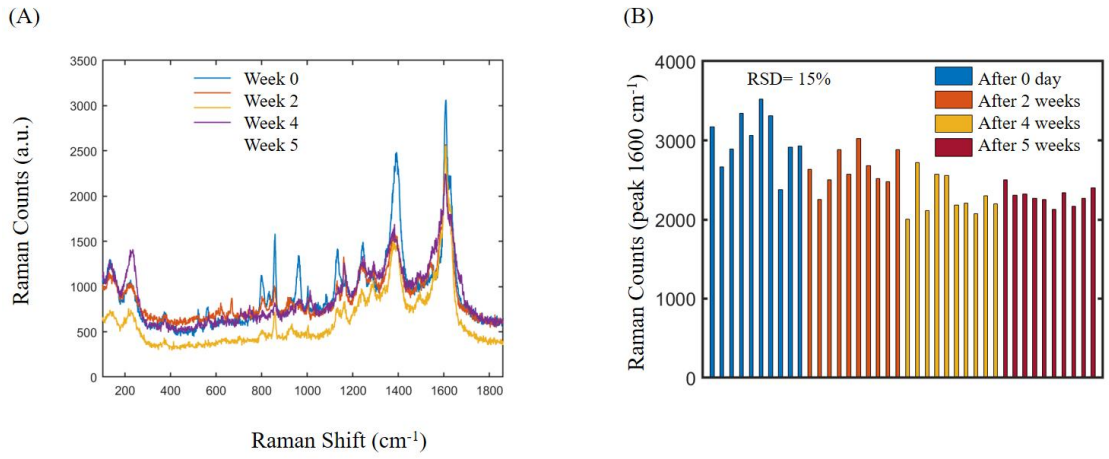

Figure S5: (A) spectrum of Ag-CS bare substrate in week 0/2/4/5 at 5th measurement. (B) a peak at 1600 cm^{-1} of ten spectra in week 0/2/4/5.

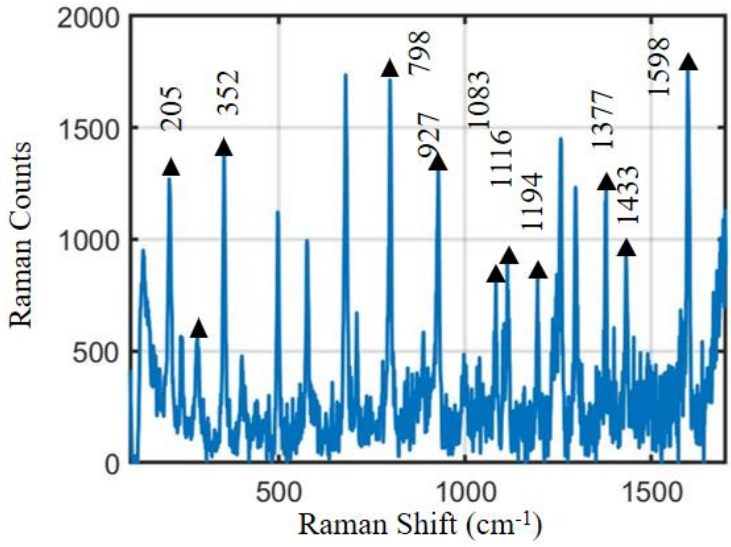

Figure S6: MCPA crystal Raman Spectrum (laser power: 0.35 mW, exposure time: 30 s, lens: 20x.).

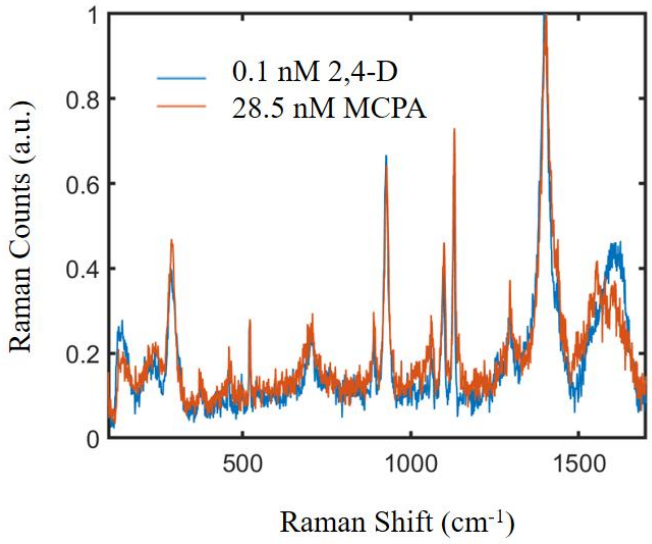

Figure S7: Comparison of the spectra of 2,4-D and MCPA.

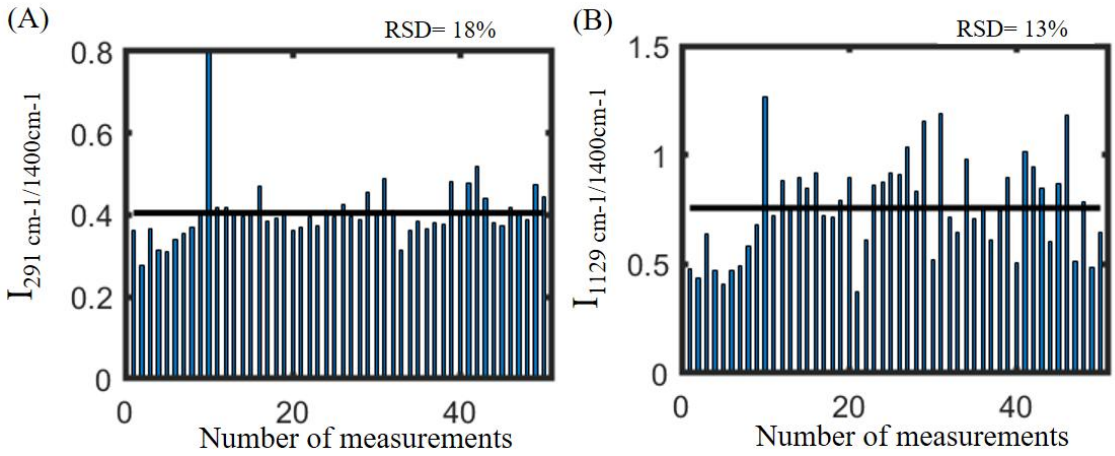

Figure S8: (A, B) shows data of peak ratio $I_{291\ cm\text{-}1}$ / $I_{1400\ cm\text{-}1}$, $I_{1129\ cm\text{-}1}$ / $I_{1400\ cm\text{-}1}$ after baseline subtraction. The RSD at peak ratio $I_{291\ cm\text{-}1}$ / $I_{1400\ cm\text{-}1}$, $I_{1129\ cm\text{-}1}$ / $I_{1400\ cm\text{-}1}$ of 50 measurements without baseline subtraction was 18%, 13% (the SD is 0.07 and 0.08).

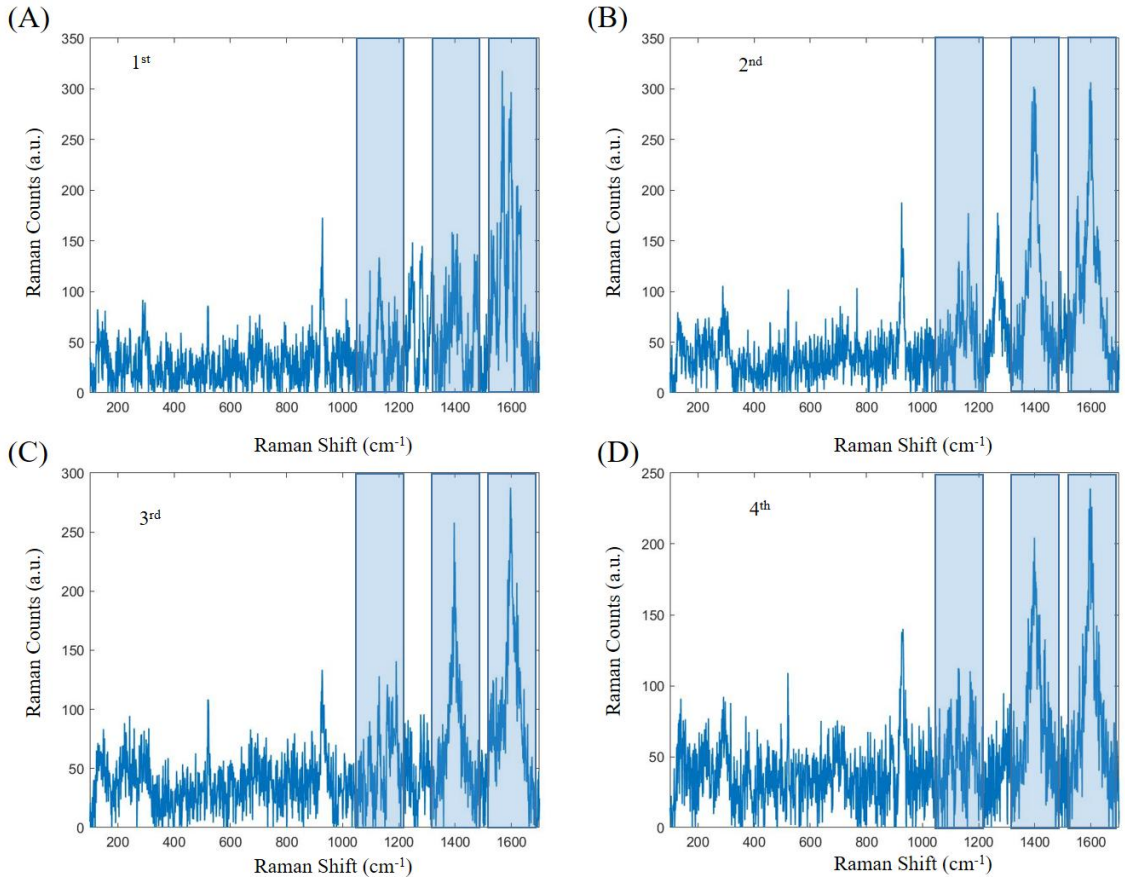

Figure S9: After the application of MCPA at 28.5 fM.

Figure S9 (A-D) shows data after baseline subtraction. The RSD at peak ratio $I_{291\ cm\text{-}1}$ / $I_{1400\ cm\text{-}1}$, $I_{291\ cm\text{-}1}$ / $I_{1600\ cm\text{-}1}$, $I_{1129\ cm\text{-}1}$ / $I_{1400\ cm\text{-}1}$, $I_{1129\ cm\text{-}1}$ / $I_{1600\ cm\text{-}1}$ of 50 measurements without baseline subtraction was 18%, 13%, 29%, 29% as shown in the bar plot Figure S9. Without baseline subtraction, the peak ratios showed better RSD values than with baseline subtraction for this research.

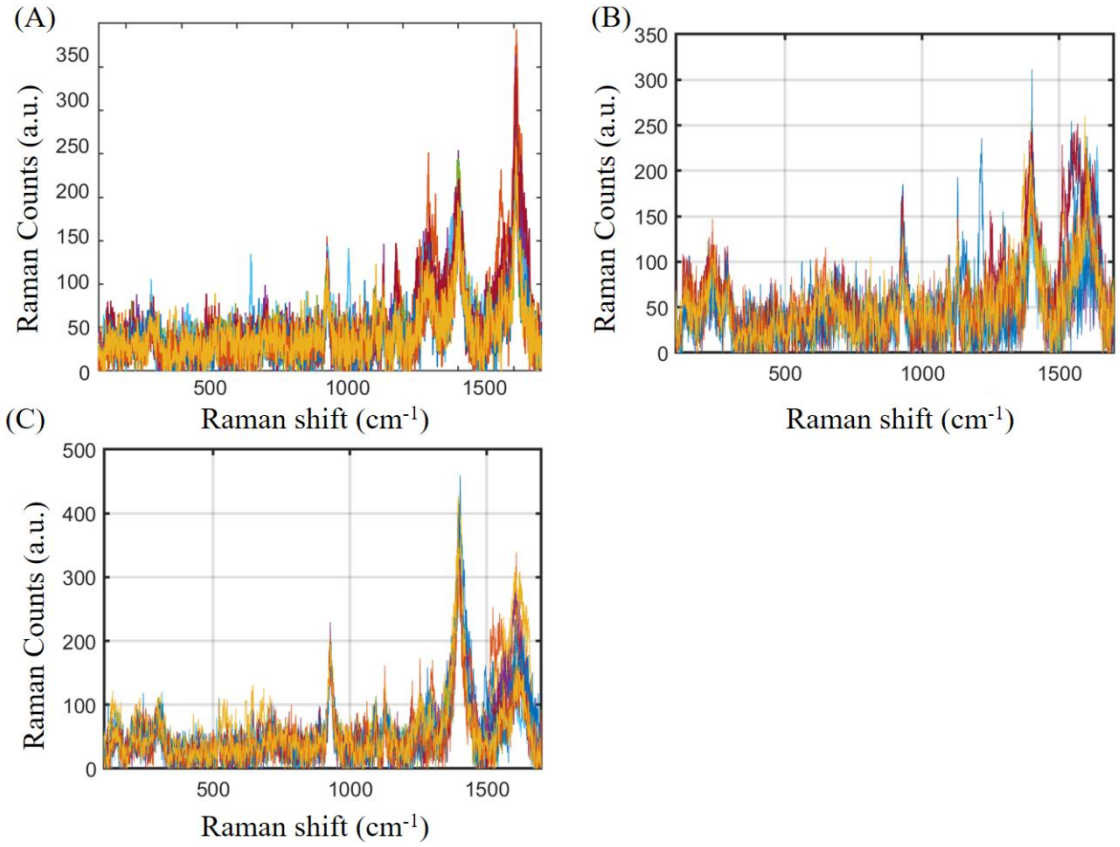

Figure S10: Three repeated experiments for 28.5 fM MCPA detection.

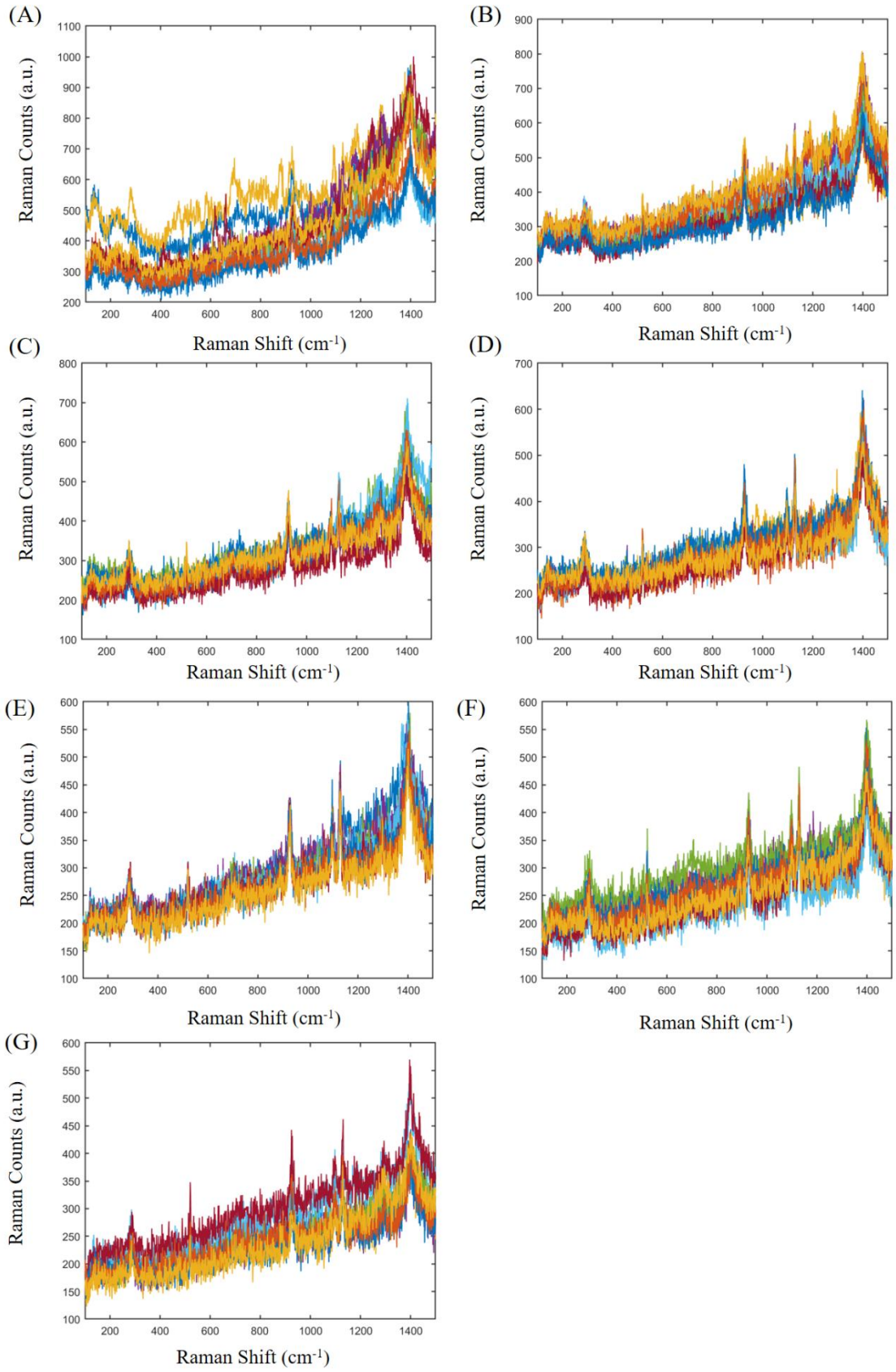
(A)
Raman Counts (a.u.)
Raman Shift (cm-1)
(B)
Raman Counts (a.u.)
Raman Shift (cm-1)
(C)
Raman Counts (a.u.)
Raman Shift (cm-1)
(D)
Raman Counts (a.u.)
Raman Shift (cm-1)
(E)
Raman Counts (a.u.)
Raman Shift (cm-1)
(F)
Raman Counts (a.u.)
Raman Shift (cm-1)
(G)
Raman Counts (a.u.)
Raman Shift (cm-1)

Figure S11: Raw data in Figure S5. (A-G) Raman spectra for different concentrations of MCPA from 28.5 fM to 0.285 mM ((28.5 fM, 2.85 pM, 28.5 pM, 2.85 nM, 0.285 µm, 2.85 µm, 0.285 mM). Ten spectra were taken for each concentration without baseline subtraction.

1, Repeat the experiment.

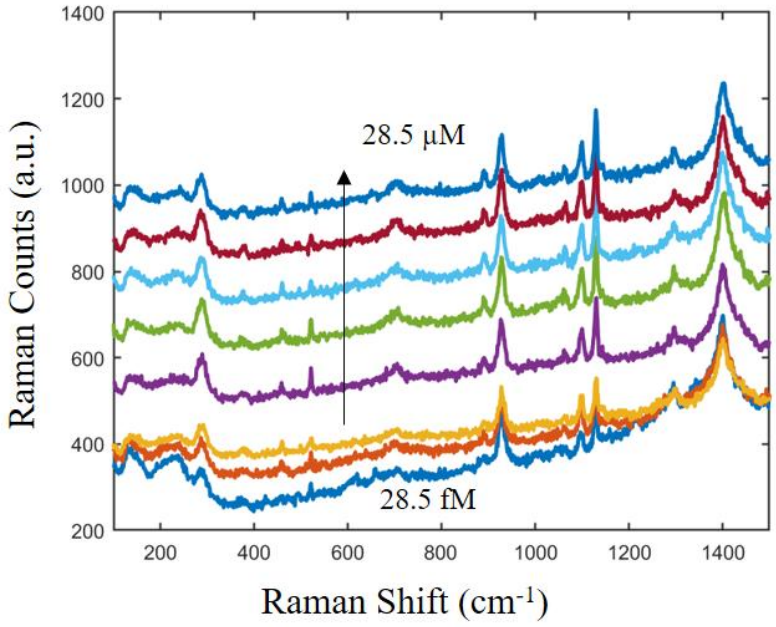

Figure S12: Repeated experiment as in section 3.4.2： Spectrum of different MCPA concentrations from 28.5 fM to 28.5 µM (28.5fM, 2.85 pM, 0.285 nM, 2.85 nM, 28.5 nM, 0.285µM, 28.5 µM.) without baseline subtraction.

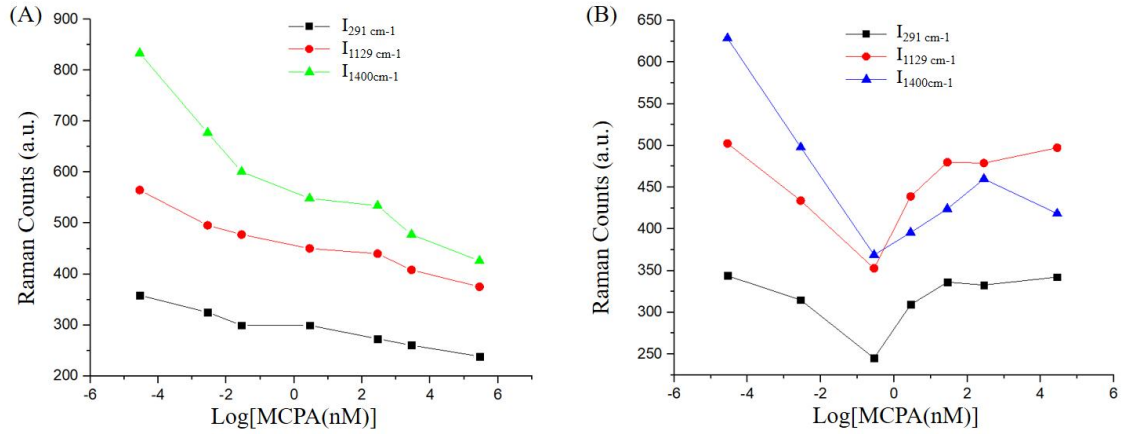

Figure S13: Trend line of Raman counts (a.u.) changes for single peaks 293 cm^{-1}, 1129 cm^{-1}, and 1400 cm^{-1} without baseline subtraction for spectra in (A) Figure 3.10 and (B) Figure S11.

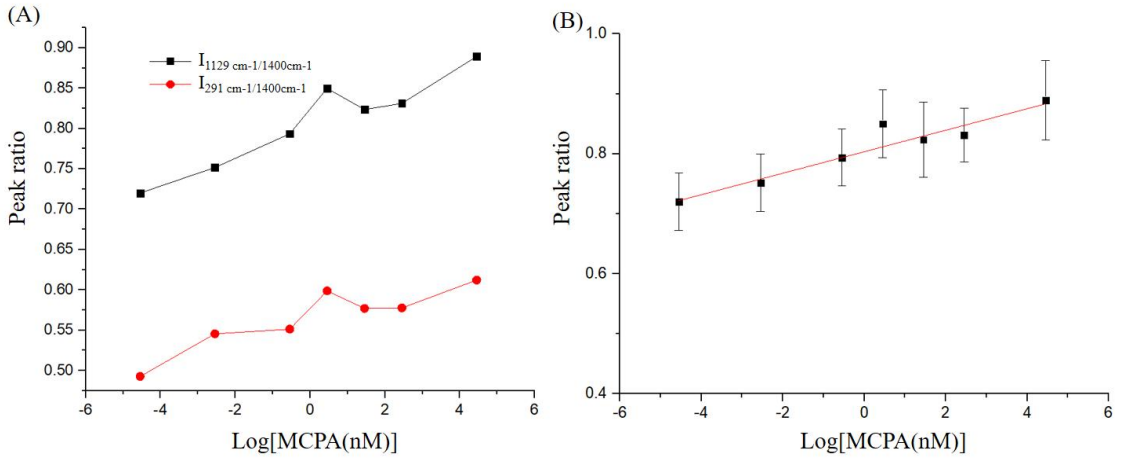

Figure S14: (A) peak ratios vs [MCPA] from 28.5 fM to 28.5 µM (28.5fM, 2.85 pM, 0.285 nM, 2.85 nM, 28.5 nM, 0.285µM, 28.5 µM.). (B) Fitting for peak ratio $I_{1129\ cm-1/1400cm-1}$: $y=0.7+0.032\log(x)$, $R^2= 0.98$.

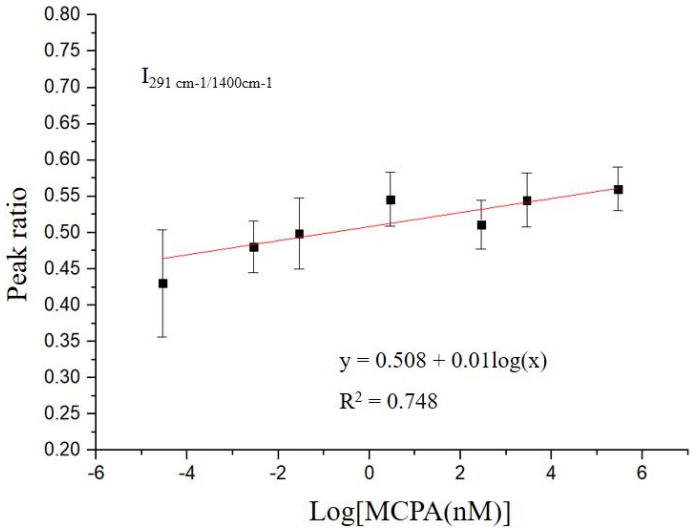

Figure S15: fitting for peak ratio $I_{291\ cm\text{-}1/1400cm\text{-}1}$ in section 3.4.2 without baseline subtraction: $y = 0.508 + 0.01\log(x)$, $R^2 = 0.748$.

2, Data analysis with baseline subtraction for different MCPA on an Ag-CS substrate.

As seen in Figure S16, different concentrations from 28.5 fM to 0.285 mM of MCPA in DI water were used for MCPA detection study by Ag-CS NPs substrate. Each spectrum was calculated based on the average of ten spectra acquired from different spots on the substrate. Raw data were shown in SI Figure S19. Similar to Chapter 2 in 2,4-D detection, the peaks of interest were peaks at 293 cm^{-1}, 1129 cm^{-1}, and 1400 cm^{-1}. They did not show dramatic change with the change of Log[MCPA].

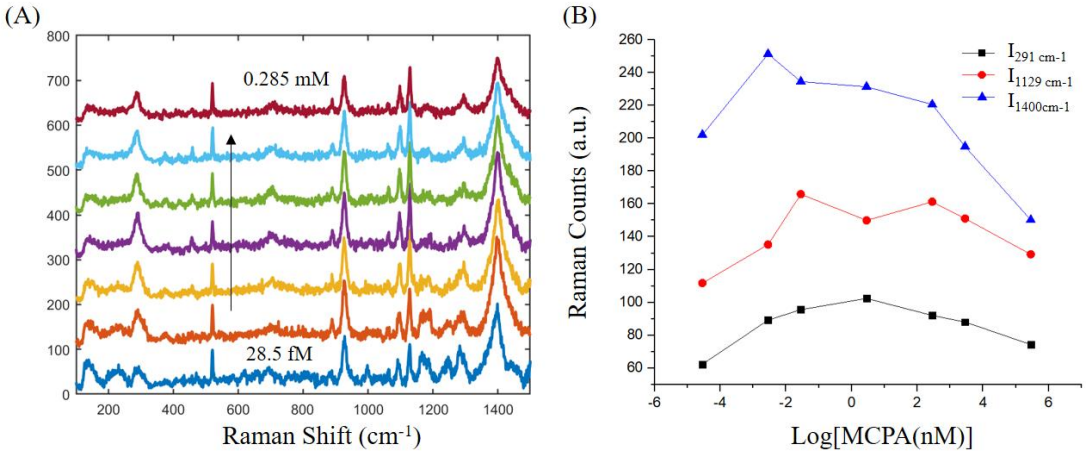

Figure S16: (A) Spectra after baseline subtraction for MCPA at different concentrations from 28.5 fM to 0.285 mM in DI water. (B) Single peak intensity changes with the change of log[MCPA].

See Figure S17 (A), when it comes to peak ratio, $I_{291\ cm\text{-}1/1400cm\text{-}1}$, $I_{1129\ cm\text{-}1/1400cm\text{-}1}$. The data points for peak ratios showed increasing trends with log [MCPA]. According to the fitting for $I_{1129\ cm\text{-}1/1400cm\text{-}1}$, $y=0.6626+0.3372\log(x)$, $R^2=0.7995$. See Figure S17 (B).; fitting for $I_{291\ cm\text{-}1/1400cm\text{-}1}$: $y = 0.403 + 0.015\log(x)$, $R^2 = 0.826$, see Figure S 18, where x is [MCPA] in nM, y is peak ratio $I_{1129cm\text{-}1/1400cm\text{-}1}$. The error bar for this fitting is large, as expected, and has been already discussed in in section 3.4.1.

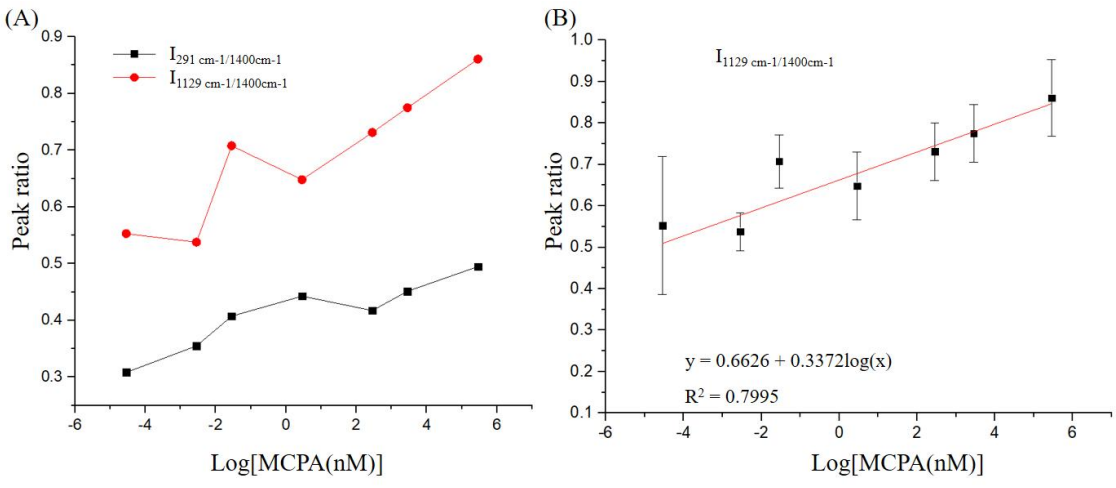

Figure S17: (A) Peak ratios vs Log [MCPA] from 28.5 fM to 0.285 mM; (B) fitting for peak ratio $I_{1129cm-1/1400cm-1}$ vs log [MCPA].

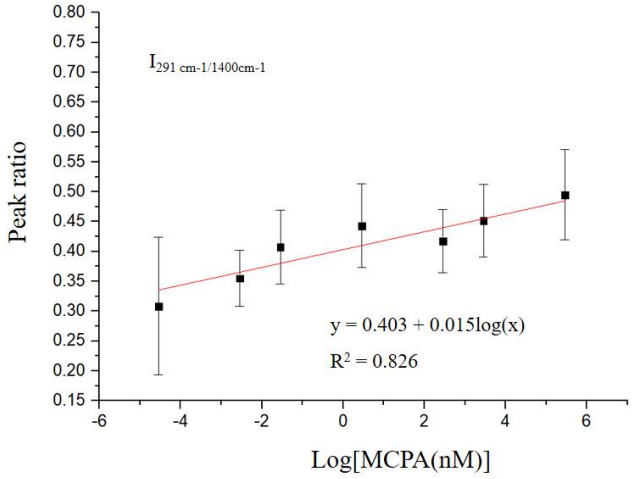

Figure S18: fitting for peak ratio $I_{291\ cm-1/1400cm-1}$ with baseline subtraction: y = 0.403 + 0.015log(x), R^2 = 0.826.

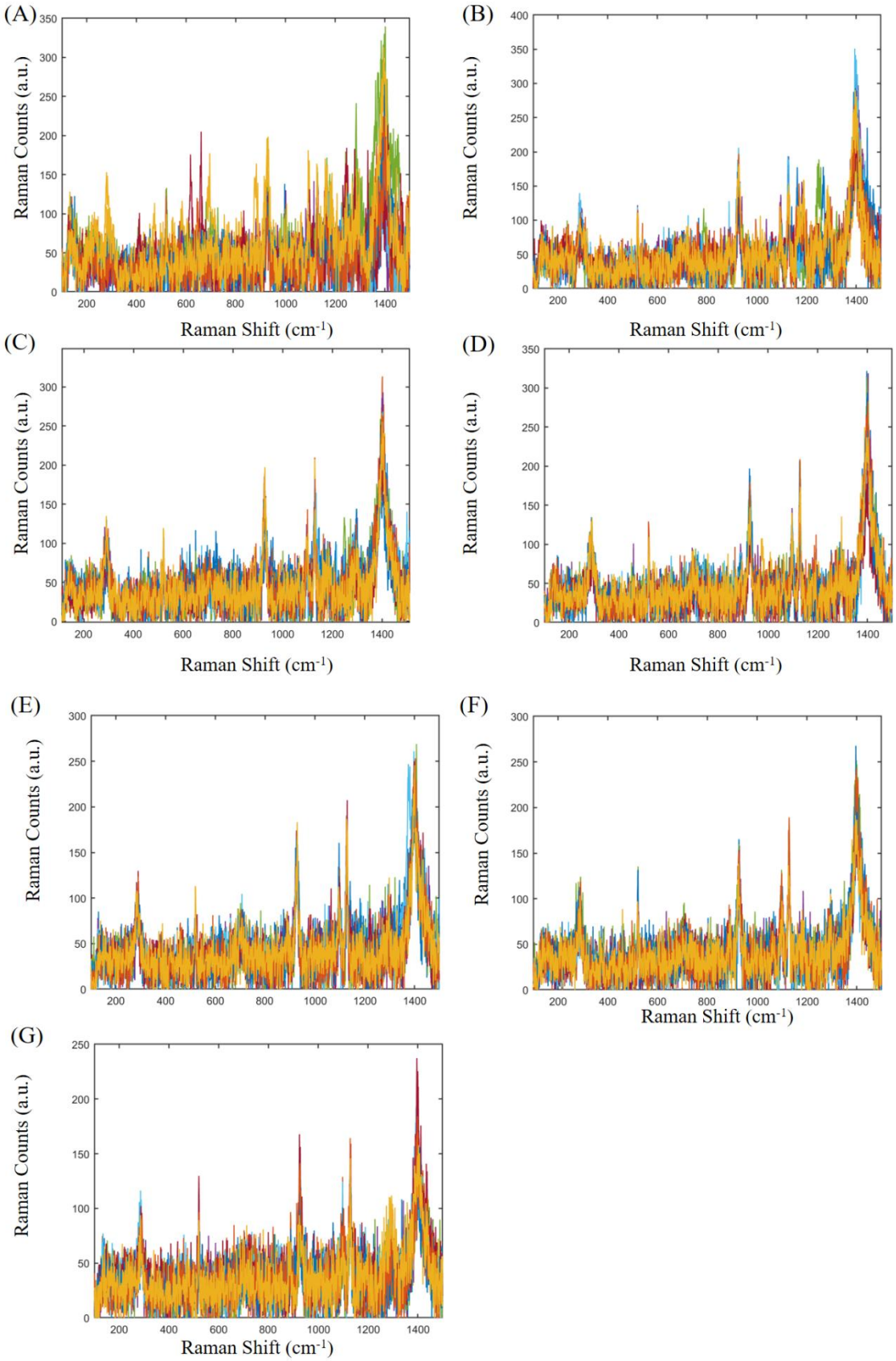
(A)
(B)
(C)
(D)
(E)
(F)
(G)
Raman Counts (a.u.)
Raman Shift (cm-1)

Figure S19: Raw data in Figure S5. (A-G) Raman spectra for different concentrations of MCPA from 28.5 fM to 0.285 mM ((28.5 fM, 2.85 pM, 28.5 pM, 2.85 nM, 0.285 μm, 2.85 μm, 0.285 mM). Ten spectra were taken for each concentration after baseline subtraction.

Chapter 4. Detection of *str2* from Shiga toxin-producing *Escherichia coli* (STEC) by a Surface Enhanced Raman Spectroscopy (SERS) sensor using recycled silicon chips

This work has been published in Sensor and Actuator Volume 373, 15 December 2022, 132618. https://doi.org/10.1016/j.snb.2022.132618.

Author Contribution: Y.Y. (Yuqing Yang) and L.A.W. (Luiza Adela Wasiewska) contributed equally to this research. Y.Y. was responsible for SERS experiments, analyze the data and writes the manuscript, L.A.W. was responsible for DNA part and contributed to intelligent suggestions, C.M.B (Catherine M. Burgess) and G.D (Geraldine Duffy) were responsible for DNA part and supervising, P.L. (Pierre Lovera) was responsible for supervising and SERS data analysis and A.O. (Alan O'Riordan) was responsible for supervising.

Abstract: In this research, a selective, cost-efficient, highly sensitive Ag nanostructure Surface Enhanced Raman Spectroscopy (SERS) sensor was developed as a methodological approach to rapidly detect a targeted-ss-DNA (*stx*2) in STEC (Shiga toxin-producing *Escherichia coli*). The Ag nanostructure-based SERS substrate was functionalized by two type of thiols: thiol-ss-DNA for bonding targeted-ss-DNA and 6-Mercapto-1-hexanol ($HS(CH_2)_6OH$) for blocking the Ag nanostructure surface. Methylene Blue (MB) was used as a Raman marker to quantify targeted-ss-DNA, as well as a model molecule to characterize the electrodeposited Ag nanostructure SERS substrate. Ag nanostructure SERS substrates showed good sensitivity and repeatability towards MB detection, with an experimental detection limit of 0.01 μM, RSD = 12.48% (at 45 different random points). More importantly, the Ag nanostructure/ss-DNA SERS substrate showed good selectivity towards STEC O157 *stx*2 targeted DNA, as well as good linearity and sensitivity towards its detection in a buffer solution, range from 1 aM to 100 pM. The SERS sensors were able to identify target DNA (*stx*2) in an STEC strain and the study showed proof of principle that SERS substrate has potential as a cost effective, highly selective, highly sensitive DNA and bacteria sensor without the aid of DNA amplification. With further development and validation, this methodological approach has the potential for use in the point-of-use detection for instance on a farm or in the food industry.

Key words: Shiga toxin-producing *Escherichia coli* (*E. coli*), DNA detection, SERS, surface enhanced Raman spectroscopy, thiol functionalized Ag nanostructure SERS substrate.

1. Introduction.

Shiga toxin-producing *Escherichia coli* (STEC) is a food-borne pathogen of significant public health concern because of the severity of illness it can cause. Infection with STEC can causes a spectrum of symptoms, ranging from diarrhea, bloody diarrhea, hemolytic uremic syndrome (HUS) to hemorrhagic colitis, and can even lead to death.[1]. The main source of STEC is animal fecal material, especially from ruminant animals, which then contaminates the food or water chain. The profile of STEC strains causing human illness has continued to evolve since it first emerged as a cause of human illness. This has included changes in understanding the role of serogroup and the presence/absence of particular genes (*stx* and *eae*) as indicators of STEC virulence potential. *E. coli* O157:H7 was the first serogroup implicated in STEC human infections (1980s). In the 2000s, further serogroups (*E. coli* O26, O103, O111 and O145) were linked to serious illness and became known as the 'top five' STEC serogroups. In 2011, the serogroup O104 was added to this group following a European outbreak linked to sprouted fenugreek seeds, becoming the 'top six'. Recent international epidemiological data has shown the profile of STEC strains associated with human illness, now includes many serogroups outside the traditional 'top six'. Thus, STEC detection methods are now moving from serogroup to virulence gene based detection methods as the most specific way to detect and identify STEC. A key virulence trait is the shiga toxin-producing gene(s) (*stx*) encoded by *stx*1 and *stx*2 with *stx*2 often reported in seriously ill patients.[2]

The most common ways to determine STEC are now based on PCR/ Real Time approaches[3-4] but emerging approaches include inductively coupled plasma mass spectrometry (ICP-MS),[5] solid phase cytometry (SPC) in conjunction with fluorescent

viability staining and culture methods.[6] For PCR and ICP-MS, the advantages are that the assays are extremely specific, sensitive, and cost-effective for each operation. However, ICP-MS equipment is expensive, time-consuming and they require trained personnel with years of experience. For SPC method, the assay is able to detect viable organisms but it consists of a multi-step process; it is limited to the ability to detect the fluorescent signal; in addition, additional steps are required for confirmation of *E. coli*.

Surface Enhanced Raman Spectroscopy (SERS) is emerging as a fast, ultra-sensitive, cost-effective, easy-operation technique,[7] used in a variety of sensing fields,[8] including DNA/bacterial sensors.[9-10] SERS is mostly based on Ag/Au/Cu noble nano structures as an effective SERS substrate.[11] The enhanced Raman signal originates from plasmonic phenomena at noble metal nano structures, and can be evaluated through the Enhancement Factor (EF). It is widely accepted that the overall enhancement is a combination of the so called chemical and electromagnetic enhancements.[12] For DNA or bacterial detection, SERS substrates need further functionalization steps to achieve selectivity.[13-14]

SERS substrates have been used for *E. coli* detection using Zn_2GeO_4 as the active material.[15] Srivastava, S. K. et al. used a nano biosensor chip,[16] with plasmonic nano sculptured thin films of silver on a silicon platform, functionalized with adsorbed 4-aminothiophenol molecules, then glutaraldehyde, to detect *E. coli* down to a concentration level of a single bacterium with an incubation time of four hours, but this approach lacks selectivity. Zhou, H. et al. reported on the detection of living bacteria in drinking water by SERS by coating the cell wall of the microorganisms with silver nanoparticles.[17] The total assay time was only 10 min with a reported limit of detection (LOD) of 2.5×10^2 cells mL^{-1} on a glass slide by using SERS mapping. Those methods

lacked a linear calibration between the bacterial concentration in buffer solution and Raman intensity, thus it is hard to define the bacterial concentration for an unknown sample. To solve this problem, Bi, L. et al. synthesized Au@Ag core-shell nanorod (Au@AgNR) tag SERS platform for ultrasensitive bacteria detection and antibiotic-susceptibility testing (AST),[18] with logarithm of *E. coli* concentration in a range of 10^7–10^2 CFU (colony forming unit) mL^{-1} with a LOD as low 10^2 CFU mL^{-1}. However, the incubation time for bacteria was three hours to gain readable Raman signals, which limited its application. Díaz-Amaya, S. et al. used aptameric DNA sequences conjugated to 4-aminothiophenol-gold nanoparticle complexes (4-ATP/Au) for the sensitive and highly specific detection of *E. coli* O157:H7 via SERS within 20 min.[19] Low concentrations of *E. coli* O157:H7 were detected (10^2 CFU mL^{-1}) with a linear range from 10^2-10^6 CFU mL^{-1} in both pure culture ($\sim 10^1$ CFU mL^{-1}) and ground beef samples ($\sim 10^2$ CFU mL^{-1}). However, in this research example, the Raman signal gained from Au NPs may have large standard deviation values in intensity, as this SERS substrate is inhomogeneous, especially after binding to *E. coli*.

Direct detection of bacteria via SERS suffers from either long incubation time, quantification difficulties, or lack of selectivity because of cell culture contamination. Another way is to detect the single stand DNA (ss-DNA) from STEC with the help of DNA amplification method such as PCR[20] or reporter/capture DNA.[21-25] This research demonstrates the use of SERS as an analytical approach for indirect detection of *stx*2 gene from STEC without the need for PCR amplification; by using thiol functionalized SERS substrates and Methylene Blue as a Raman marker. This analytical method is shown to be ultra-sensitive, highly selective towards targeted DNA, and could also be used for other ss-DNA relevant to cancer or infectious diseases.[26]

2. Materials and methods.

2.1. Chemicals.

$AgNO_3$, 6-Mercapto-1-hexanol ($HS(CH_2)_6OH$), Methylene Blue (MB), HEPES (4-(2-hydroxyethyl)-1-piperazineethanesulfonic acid) solution, KCl, NaCl were purchased from Sigma-Aldrich, Ireland. All solutions were prepared by diluting with ultra-pure Milli-Q water (18.2 $M\Omega \cdot cm^{-1}$). 1 mM stock solution of Methylene Blue (MB) was prepared by diluting with DI water in brown glass bottle, the bottle was stored in the fridge for further use (MB solution can usually be stored in the fridge for months). Buffers used for DNA dilutions was 0.1 M PBS, pH = 7.2 while MB for DNA detection was diluted in 0.2 M HEPES and 0.1 M KCl, pH = 7. 6-Mercapto-1-hexanol ($HS(CH_2)_6OH$) solution was prepared by diluting 100 mM to 10 mM in ethanol (EMSURE grade for analysis), then dilute to 5 mM through adding the same volume of DI water. Containers used for dilution are new colorless Eppendorf AG PCR tubes (mL range) from Sigma-Aldrich (Ireland).

All synthetic oligonucleotides were obtained from Sigma Aldrich Ireland in dried form. Upon arrival, they were diluted with sterile DI water to 100 µM and stored at -20°C in new PCR tubes. Targeted-ss-DNA was prepared by diluting targeted-ss-DNA solution (100 µM, 10 µL) in PBS buffer (990 µL) to 1 µM, and these steps were repeated to obtain different concentrations.

The probe sequence for *stx*2 detection was selected based on ISO/TS 13136:2012 standard. The probe was modified with thiols at the 5' end, enabling covalent attachment to the nanoparticles. Sequences used in this work are detailed below:

Table 2 DNA sequences used in this work.

Name	Sequence
*stx*2 probe	5’ [ThiC6] TCG TCA GGC ACT GTC TGA AAC TGC TCC 3’
*stx*2 target	5’ GGA GCA GTT TCA GAC AGT GCC TGA CGA 3’
Non-target	5’ TTAC ATA AGA ACG CCC ACT GAG ATC ATC CAG 3’

2.2. Equipment.

Electrochemical depositions were performed with an Ivium pocketSTAT handheld potentiostat connected to a computer. Raman spectra were acquired with a Renishaw InVia microscope equipped with a 514 nm Ar ion laser and CCD detector (1024 pixel × 256 pixel). All measurements were acquired using a 20x lens (NA 0.4, axial resolution: 0.58 μm).[3] Optical images were acquired with a Leica Mikroskopie & Systeme GmbH. SEM characterization was undertaken with a FEI Quanta 650 (the acceleration voltage = 10 KV, the spot size = 2.5 nm). Bransonic sonicator (Model M1800H-E) and thermocycles from applied biosystems by Thermo Fisher Scientific were used to treat the DNA extracted from bacterial sample before the measurement. For Raman measurements, the SERS sensor was placed in a chip holder.

2.3. Silicon chips fabrication.

The Au microelectrode Si/SiO_2 micro chip fabrication process has been shown in the other paper publish by our group.[27-28] Briefly, photoresist was deposited on SiO_2/Si substrate by spin coating. Then metal layers (Pt/Au) were deposited on the SiO_2/Si/photon resist layer by physical vapor deposition followed by a lift-off. Finally, a layer of Si_3N_4 was deposited to protect the conductive electrode, with the contact pads,

[3] Laser energy/Raman intensity was calibrated by using Si reference sample in a daily bases.

working electrodes, reference electrode, and counter electrode exposed using etching. The size for reference and counter electrodes are 500 μm wide × 6 mm long.

2.4. Ag nanostructure SERS substrate electrochemical synthesis on recycled chips.

In this research, we recycled chips previously used for electrochemical sensing as SERS substrates.[27, 29-30] The main advantages of using recycled chips is to reduce cost and increase sustainability. For the pre-used chips, the designed micro-band working electrodes were previously functionalized with a variety of materials for different sensing applications in the group, while counter and the reference electrodes were usually not functionalized and kept as pristine surfaces. These pristine electrodes were subsequently used as working electrodes for SERS substrate fabrication. In order to use recycled chips, several cleaning procedures were carried out prior to electrochemical deposition of Ag. First, the recycled chips were pre-treated by soaking in H_2O_2 (H_2O_2: DI water = 1: 20, overnight.); followed by thorough rinsing with DI water and drying them under nitrogen. This deposition for Ag nanostructure was undertaken by applying -0.1 V at 0.5 mM $AgNO_3$ solution (5 μL) for 10 seconds, the corresponding current (μA)-time (s) curve is shown in SI Figure S1 (C).

2.5. DNA sensor development.

DNA sensors were prepared by incubating in 1μM solution (0.1 M PBS buffer) of thiol modified probe DNA (50 μL) for 24 hours (Figure 4.1 (A, B)). Subsequently, the sensors were incubated in 50 μL of a 6-Mercapto-1-hexanol solution (5 mM) overnight to block unmodified surfaces and avoid non-specific binding (Figure 4.1 (C)). Sensor chips were rinsed with DI water and dried with nitrogen after thiol application. DNA detection was performed by incubating functionalized Raman substrates in 50 μM MB

that was diluted in 0.2 M HEPES buffer and 0.1 M KCl, pH = 7 for 10 minutes, prior to and after incubation with target DNA for 20 minutes. (Figure 4.1 (D, F)). After MB solution application (10 minutes), the solution was removed and Raman measurements were undertaken in a dry environment. After the application of thiol ss-DNA, the SERS surface was covered and only Si peak at 520 cm^{-1} was shown. Peaks at 707 cm^{-1} (O-H out of plane bending), 1011 cm^{-1} (C-C-C stretching) and 1086 cm^{-1} (C-O stretching) for 6-Mercapto-1-hexanol[31] appeared, see Figure 4.1 (C) after the second thiol application. There is no peak at 1625 cm^{-1} in Figure 4.1 (C), while the peak emerged after MB application in Figure 4.1 (D). In Figure 4.1 (F), after applying targeted ss-DNA, MB signal increased.

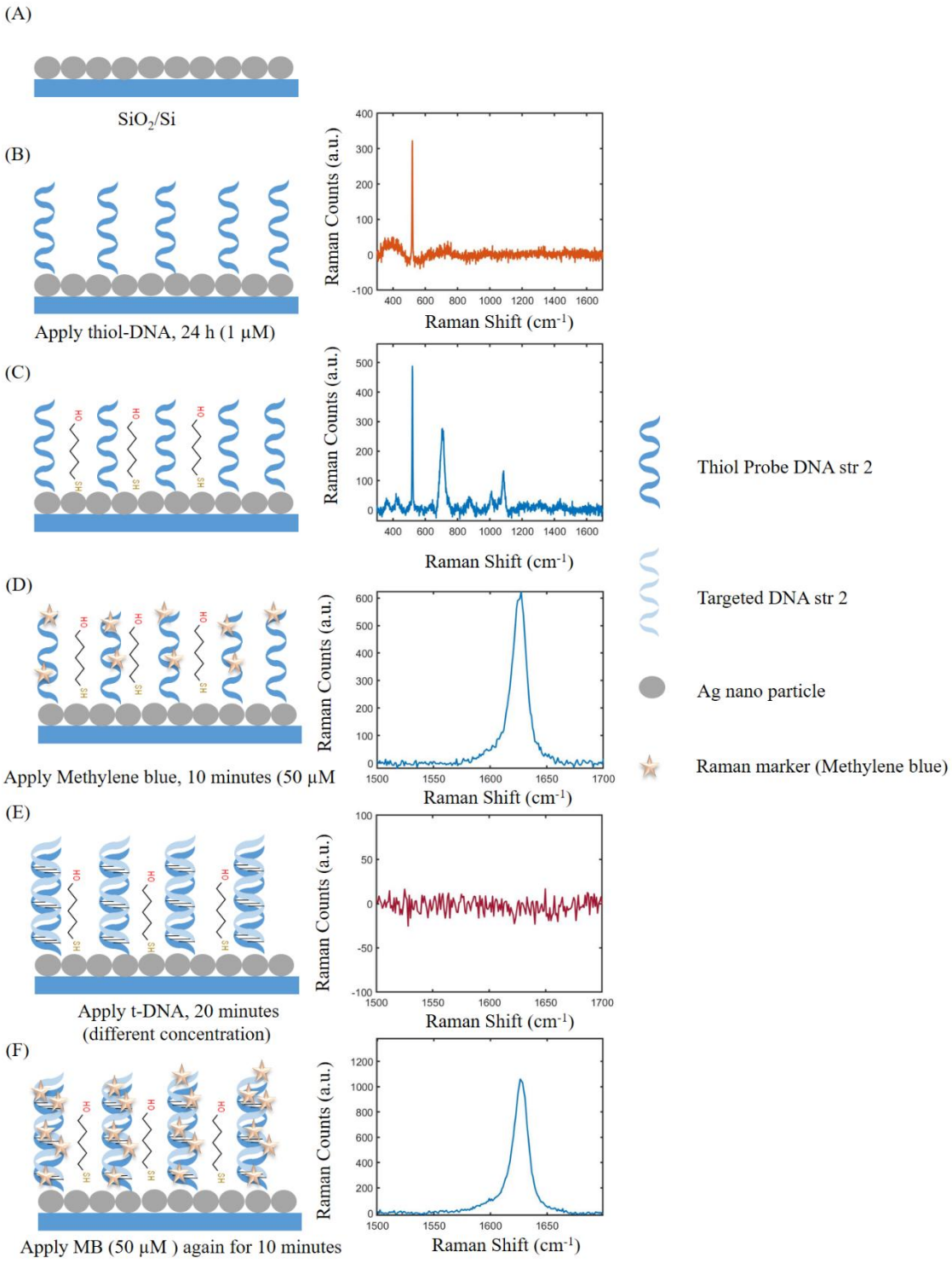

Figure 4.1: Illustration of the DNA sensor development process and the corresponding Raman spectra. (A) Ag nanostructure electrodeposition on SiO_2/Si substrate; (B)

Immobilisation of thiol modified probe DNA (50µL, 1µM) onto a SERS substrate and incubating for 24 hours. (C) Immobilisation of 6-Mercapto-1-hexanol (50µL, 5mM) in the free spaces between probe DNA; (D) MB binding ss-DNA on a functionalized SERS substrate (incubation time: 10 minutes); (E) Hybridization of target DNA to the ss-DNA modified SERS substrate for 20 minutes; (F) MB intercalation between the dsDNA (incubation time: 10 minutes). The integration time was 10s. The total time used for the first two spectra was 1.5 minutes, and the total time used for the last three spectra was 0.2 minutes.

2.6. Bacterial DNA extraction.

DNA was extracted from STEC O157 (ATCC35150), *Salmonella spp*. (SARB65) and *Staphylococcus aureus* (NCTC 8178). STEC O157 contained the *stx*2 gene while the other bacteria were used as negative samples to confirm the selectivity of the SERS sensor. The cultures were grown from culture collection stocks, which were stored on protective beads at -80°C. A single bead of each isolate was streaked on Tryptone Soy Agar (Oxoid, Fisher Scientific Ireland) and incubated overnight at 37 °C. An isolated colony was then placed in Tryptone Soy Broth and again incubated at 37 °C overnight. DNA was extracted from the resulting culture using a Qiagen DNeasy Blood and Tissue kit (Qiagen, Manchester, UK), and following the manufacturer's instructions. The DNA concentration was measured using a Qubit dsDNA BR Assay Kit (Thermo Fisher Scientific, Ireland) on a Qubit 4.0 fluorometer.

DNA samples were diluted five times in 0.1 M PBS buffer, pH = 7.2, sonicated for five minutes to break the long DNA strand and heated to 95 °C for two minutes to denature ds-DNA. Afterwards, the samples were rapidly cooled down on ice. 50 µL of

bacteria DNA were incubated on a prepared SERS sensor for 20 minutes at room temperature. After incubation, the sensor was washed with DI water (DI water was stored in a large polypropylene bottle (25L) for lab use and polypropylene bottle for daily use), followed by MB (50 μM) application for ten minutes, whereon Raman detection was performed.

2.7. Raman Measurements and Data Analysis.

All Raman measurements were acquired using a 20x lens (NA 0.4, lateral resolution of ~688 nm and an axial resolution of ~6875 nm). The test area was confined to a small localized area (60 x 60 μm approximately), as this deposited Ag nanostructure showed different SERS signal in different localized areas of the Pt/Au electrode as shown in SI Figure S1 (A, B). All the spectra presented herein were an averaged value of ten measurements obtained at different random points on a SERS substrate. For the repeatability study, 45 measurements were taken at different random points on a SERS substrate in a localized area. All Raman spectra were taken using a laser power of 0.07 mW with an integration time of ten seconds. In order to confine Raman measurements in the same area (60 μm x 60 μm), set up of the original point as (0, 0) at one end of Au macro electrode and the ruler window in the Renishaw system was used to mark the area, as shown in SI Figure S1 (A). The targeted ss-DNA detection was carried out in dry environment, while MB detection to characterize Ag nanostructure SERS substrate in section 3.1 was carried out in water environment. All spectra were corrected by subtracting the baseline using Matlab R2018b-academic use, which is shown in SI Figure S2 (A-C). The linear fitting was done by Origin™ (OriginPro 2016).

3. Results and discussion.

In this research, an electrode originally designed as a counter electrode (6 mm long) on a SiO_2/Si chip was used as a working electrode, see Figure 4.2 (A), and was used to electrochemically deposit Ag nanostructure. During electrochemical deposition (the electrochemical deposition set up is shown in Figure 4.2 (B), Ag nanostructure were formed on the SiO_2/Si substrate based on the edge effects of the strong electric field generated by edge discontinuities of the large Au electrode.[32] (Figure 4.2 (C)). In this electrochemical deposition process, a two electrodes system (working and counter electrode) was used (shown in Figure 4.2 (A)). In this electrochemical reaction, silver was reduced to Ag nanostructure through chemical reaction:

$$Ag^+ + e^- \rightarrow Ag$$

, also forming regular distributed nano gaps between Ag nanostructure during this process. Those Ag nanostructure grew on the SiO_2/Si substrates adjacent to the electrode, because of the strong electrical field distribution near the electrode edge. Figure 4.2 (D) shows the Raman measurement set-up with a chip holder.

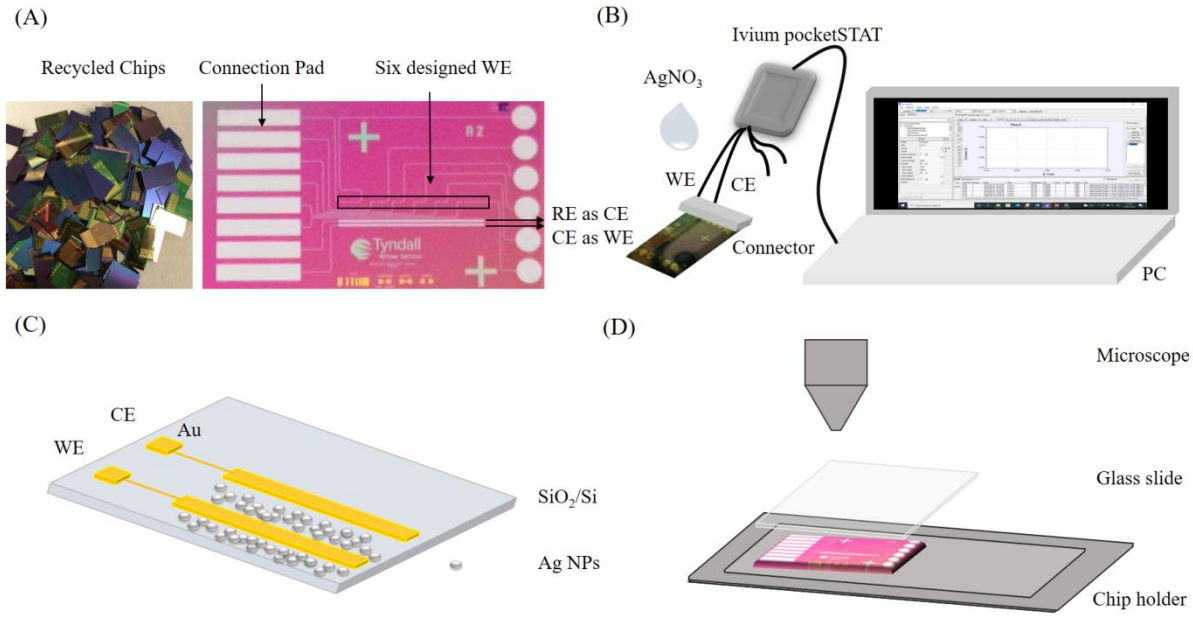

Figure 4.2: (A) Recycled chips and chip design for electrochemical deposition (chip size: 1.0 x 1.7 cm; and 0.1 cm in thickness, more information about this chip platform has been included in Chapter 2). In this research, six designed Au working electrode (micro band electrode) were not used, only designed Au reference and Au counter electrode (big electrode) were used for electrochemical deposition, designed reference electrode acted as counter electrode and designed counter electrode acted as working electrode. (B) Electrochemical deposition set up, only two big electrodes were used for electrochemical deposition; (C) Demonstration of Ag nanostructure deposition by electrochemical method along a Au counter electrode as designed; (D) Raman test platform with a chip holder for both dry and aqueous environments. Raman measurement were carried out on top of Ag nano structures shown in Figure (C).

3.1, Ag nanostructure SERS substrate characterization.

Optical micrographs of the fabricated samples acquired with a 20x objective are shown in SI Figure S1 (A). Ag nanostructure grew and spread on SiO_2/Si substrate

along the Pt/Au macro electrode (mm^2), presenting a flat thin Ag nanostructure layer. SEM images are shown in Figure 4.3 (A-B), the substrate exhibited a dense coverage of Ag nanostructures. The SERS signals at different locations within a localized area were found to be repeatable which is essential for DNA quantification, the repeatability has been proved by using MB as a Raman active analyte in section 3.2. For the quantification process, ten spectra from MB labelled hybridized DNA were taken and the average value was used for linear fitting; the error bars for quantification were from the standard deviation (SD) of those ten measurements.

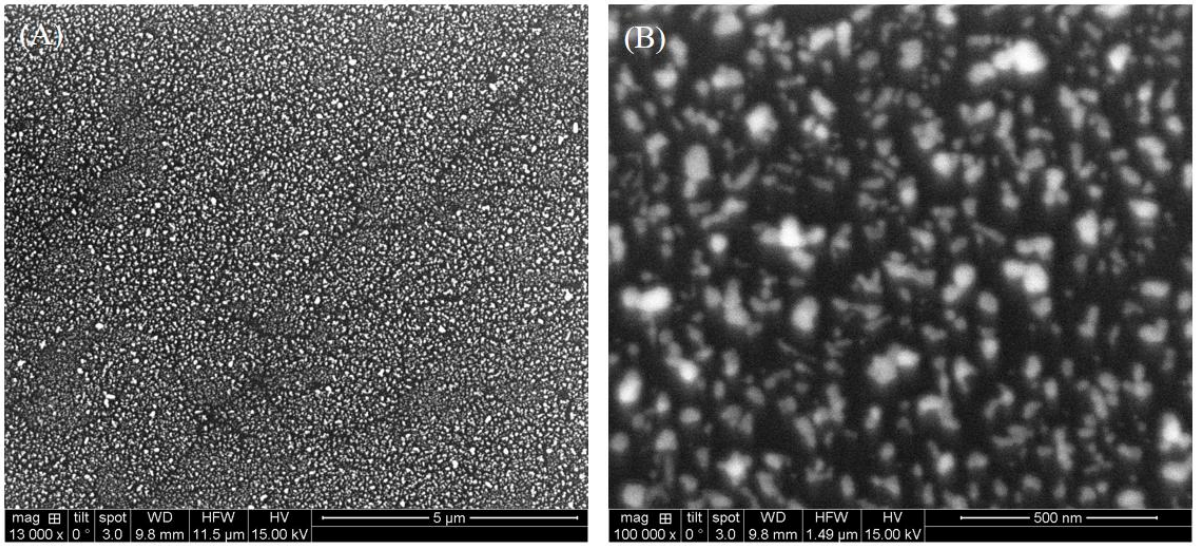

Figure 4.3: (A) SEM image for an Ag nanostructure SERS substrate (scale bar; five µm); (B) SEM image for an Ag nanostructure SERS substrate at a higher magnitude (scale bar; 500 nm).

3.2, Ag nanostructure SERS substrate characterized by Methylene Blue (MB).

To characterize the deposited Ag nanostructure SERS substrate, Methylene Blue (MB) was used as a model molecule as reported in previous research.[33] Figure 4.4 (A) presents the characteristic peak for MB located at 1625 cm^{-1}, associated with the

vibration mode of C-C ring stretching and C-N ring stretching.[34] 10 µL of MB solution at different concentrations was dropped on a SERS substrate, and then covered with a cover glass. The peak intensity increased with increased concentrations between 0.05 µM and 1 µM, as expected. The linear fitting is shown in Figure 4.4 (B), and exhibited a linear relation between logarithmic of Raman counts (y) and logarithmic of MB concentration (x, in µM): $y = 3.777+0.437\log_{10}x$, with an $R^2 = 0.9932$. The experimental LOD was 0.01 µM.

The enhancement factor was calculated to be around 10^{10} for 0.01 µM MB by using:

$$EF = I_{SERS} \cdot N_{bulk} / N_{SERS} \cdot I_{bulk} \quad \text{(Eq. 1)}$$

where I_{SERS} is SERS intensity; I_{bulk} is Raman intensity; N_{bulk} is determined under the same experimental conditions as in SERS measurements, but without SERS substrates; N_{SERS} is the number of targeted molecules adsorbed on SERS substrates, and it is related only to the molecular interaction with the SERS substrate surface. The detailed calculation is shown in SI.

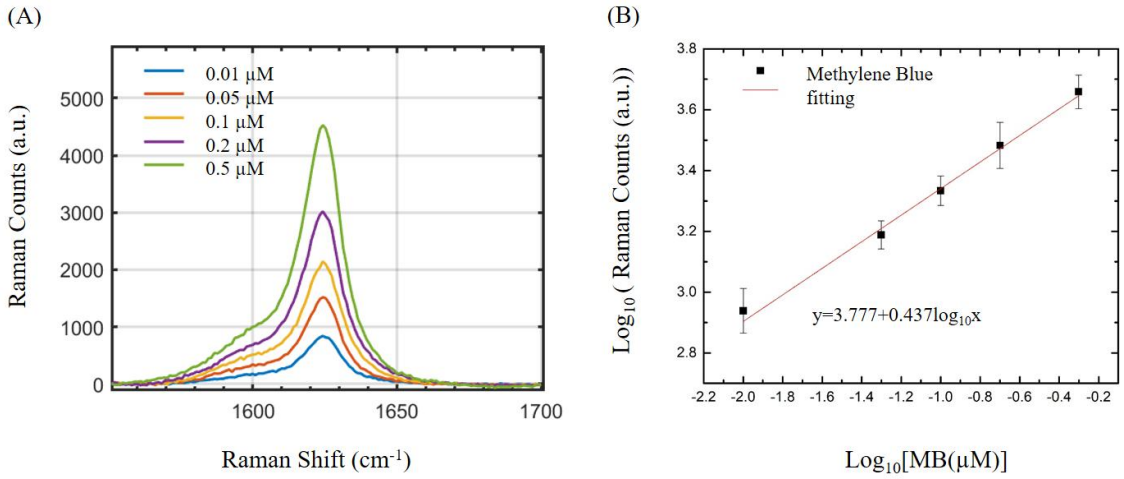

Figure 4.4: (A) Spectra of different concentrations of Methylene Blue (MB): 0.01 µM, 0.05 µM, 0.1 µM, 0.2 µM, 0.5 µM; from 1550 cm^{-1} to 1700 cm^{-1}, the characteristic is

located in 1625 cm^{-1} and a reference spectrum without MB. (B) Linear fitting for Log_{10} (Raman Counts) (y) VS Log_{10} ([MB] (x, in μM)) at different MB concentrations: $y = 3.777+0.437\log_{10}x$, where $R^2 = 0.9932$. The measurements for each MB concentration were taken at ten different random points on a Ag SERS substrate, the error bars were one SD (standard deviation) of these ten measurements.

The repeatability of this Ag SERS substrate was characterized by testing MB (0.1 μM) at 45 different points on a SERS substrate. The spectra are shown in Figure 4.5 (A), and the peak intensities at 1625 cm^{-1} for 45 points as a bar plot are shown in Figure 4.5 (B), with a SD=149.58. The sensitivity and reproducibility of SERS detection towards MB was attributed to the uniform distribution of the Ag nanostructure on the surface of SiO_2/Si substrate in a micrometer (μm) range.

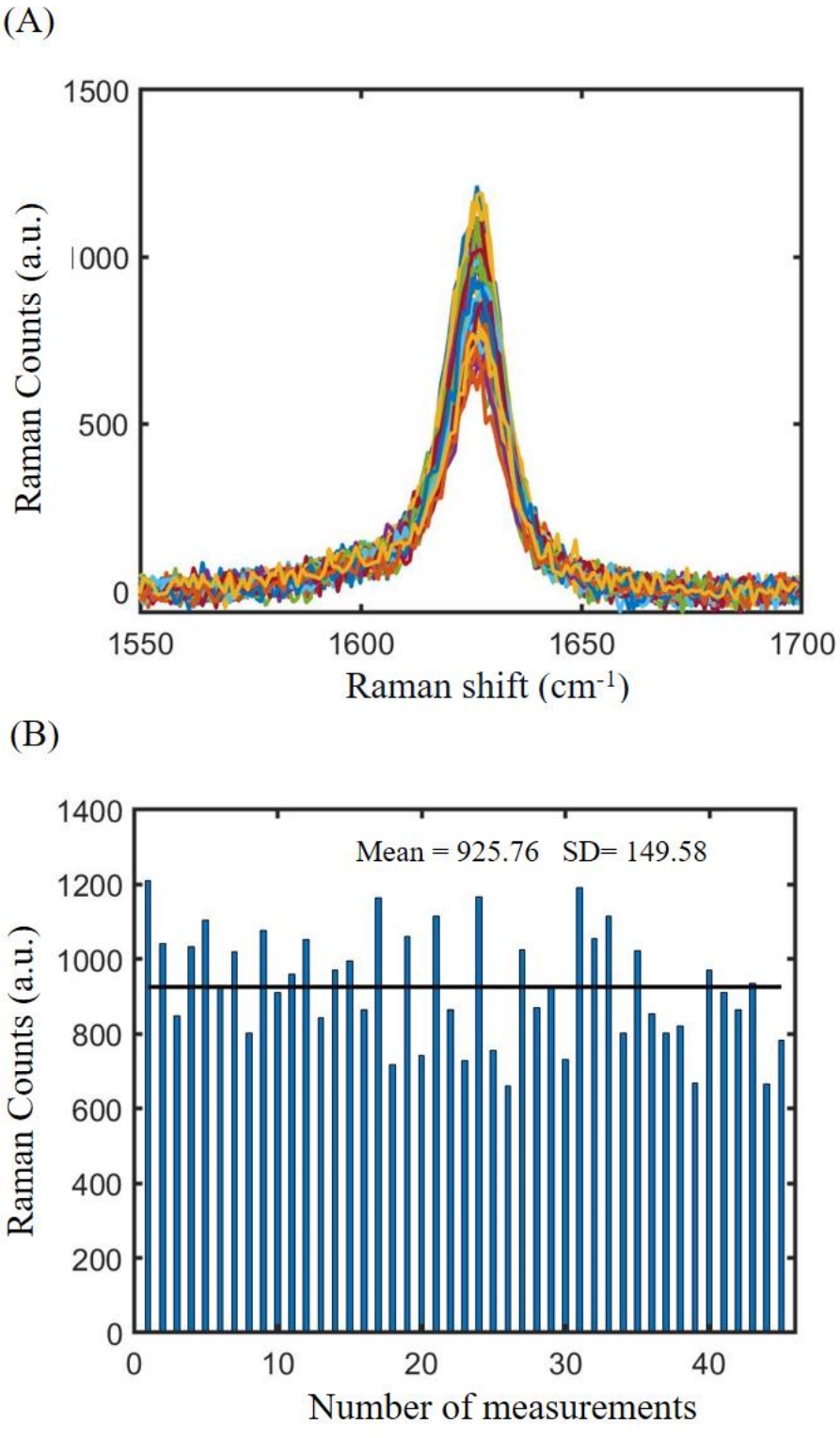

Figure 4.5: Repeatability study of an Ag nanostructure SERS substrate. (A) Spectra of MB at 0.1 μM from 45 different random points on a Ag nanostructure SERS substrate after baseline subtraction. (B) Bar plot of Raman intensity of the characteristic peak of

MB at 1625 cm^{-1} in (A) after baseline subtraction, with SD=149.58 for 45 different random points on an Ag nanostructure SERS substrate.

3.3, Detection of targeted DNA using SERS.

After two-step thiol functionalization, the corresponding Raman spectra are shown in SI Figure S3 (A), peak around 520 cm^{-1} showed Raman peak of Si, the overall Raman intensity for two thiols were weaker than Si and indicated good coverage of two thiols over Ag NPs surface. For thiol-ss-DNA, no obvious Raman peak showed from 300 cm^{-1}-1650 cm^{-1}. After application of $HS(CH_2)_6OH$, extra peaks appear at 706 cm^{-1}, 875 cm^{-1}, 1009 cm^{-1}, 1085 cm^{-1}. The peak at 706 cm^{-1} is assigned to O-H out of plane bending, the peaks at 875 cm^{-1} and 1009 cm^{-1} are assigned to C-C-C stretching, and the peak at 1100 cm^{-1} relates to C-O stretching of $HS(CH_2)_6OH$.[35]

MB was used as a Raman marker to provide stronger SERS signals in DNA detection, as shown in Figure 4.1 (D, F). MB can attach to DNA through electrostatic interaction where the negatively charged phosphate backbone of DNA (weak binding),[36] bind with guanine on single strand DNA[37] or intercalate between the double strand DNA (strong binding).[38] The higher the targeted ss-DNA concentration, the higher concentration of MB that is attached to DNA through electrostatic force; Also, MB shows different binding affinities towards ss-DNA and ds-DNA, as MB binds to ss-DNA by electrostatic force while it binds to ds-DNA by both intercalations and electrostatic interactions.[39-40] Thus, MB can be used to quantify targeted ss-DNA upon DNA hybridization. The ionic strength of the solution that would affect MB to ds-DNA binding efficiency.[41] Based on Kara et al., the MB intercalation mechanism between ds-DNA was preferred over the electrostatic interaction or binding with guanine on single

strand DNA at 10 mM NaCl.[42] In this research, DNA detection was undertaken by using 50 μM MB dissolved in 0.02 M HEPES buffer with 10 mM KCl to achieve a higher efficiency of intercalation.

To process SERS quantification of targeted DNA, MB (50 μM, 20 μL) was applied to the functionalized SERS substrate (Ag nanostructure/ss-DNA), and the initial MB Raman peak at 1625 cm^{-1} was shown due to MB interaction with ss-DNA. After the hybridization of the target DNA for 20 minutes (Figure 4.1 (E)), the MB was applied again and the peak was higher compared to ss-DNA due to intercalation between the ds-DNA (ds-DNAs).

To establish a linear calibration, different concentrations of target DNA were incubated on top of sensors for 20 minutes, followed by 10 minutes of incubation with MB and then Raman measurement. Linear quantification of this STEC bacteria DNA was based on MB signal difference (I_1-I_2/I_1) between the functionalized substrate (Ag nanostructure/thiol-ss-DNA) and the SERS substrate after binding of the target DNA, where the MB signal difference change reflect the concentration of target DNA hybridization in that 20 minutes incubation times. Using the initial signal (I_1) from functionalized SERS substrate as a reference resulted in a better linear fitting result, see SI Figure S4 (A-B). However, using peak intensity change (I_1-I_2/I_1) (with error bar calculated by coefficient of variation) resulted in smaller error bars in the linear fitting compared to using I_1 (error bar were from standard deviations),

This SERS sensor requires dense thiols coverage; otherwise, the Raman intensity changes, after the binding of targeted DNA, will not be obvious (MB signal difference (I_1-I_2/I_1) would be too small to see the difference between different targeted-ss-DNA concentrations). A way to check the successful binding of the thiols is through checking

initial Raman intensity of the functionalized SERS substrate (Ag nanostructure/ss-DNA). In our work, this usually ranges from several hundreds to a few thousands ($500<I<2000$, I is Raman counts (a.u.)); otherwise, we attribute values outside of this range to indicate unsuccessful thiols bonding ($I>2000$) or unsuccessful Ag nanostructure deposition ($I<500$). As bare Ag nanostructure surface is still exposed to air and contributes to higher Raman intensity ($I>2000$), or not enough Ag nanostructure contributed to enhanced Raman signal ($I<500$). The success rate of SERS sensor fabrication was 84.21% out of 19 sensors as shown in SI bar plot Figure S5. In real applications, SERS sensor calibration was undertaken using a standard addition method for unknown DNA samples, which is essential to get reliable results because of the initial Raman signal differences.

The SERS spectra at different concentrations of the target DNA are presented in Figure 4.6 (A), the intensity of the 1625 cm^{-1} peak increased with the increased concentrations of target DNA.

Figure 4.6 (B) shows the same experiment using non-target DNA, where little change in the intensity was observed. The spectra is shown in SI Figure S3 (C). For target DNA, the intensity change (before and after applying the targeted-DNA, I_2-I_1/I_1) ranged from 50 % to 350 %. The linear relation of the intensity change (before and after applying the targeted-DNA, I_1-I_2/I_1) and the logarithmic concentration of targeted DNA is shown in Figure 4.6 (B): $y = 0.3394\log_{10}x + 0.7530$, with $R^2 = 0.9972$, the LOD was calculated to be 0.4900 aM through 3σ/m method. For non-targeted DNA, the intensity change stayed around 0 % demonstrating the selectivity of this SERS sensor.

The explanation of this ultra-low detection ability for this SERS sensor is in section 3.4. Results from literature also proved the possibility of zmol or amol DNA detection.

For example, Li et al. synthesized DNA-functionalized single walled carbon nanotube (SWCNT)-Au platform where gold-coated SWCNT acts as an isolated micro electrode, this platform was able to detect lower than 10 zmol complimentary 10-base DNA, this is corresponded to having 6 DNA molecules in a 1 mL sample solution.[43] Shi et al. used two-dimensional carbon-coated molybdenum disulfide (2-D MoS_2@C) hollow nano rods combining with nucleic acid signal amplification strategies and DNA hexahedral nano framework to fabricate a novel self-powered biosensing platform for microRNA-199a detection. The nanomaterial is then applied on carbon cloth. This assay shows an extensive linear range of 0.0001-100 pM with a low detection limit of 4.94 amol/L.

Comparison between Ag-MB and Ag-ss-DNA/ds-DNA-MB was also discussed in section 3.4 and demonstrated in Figure 4.11. Figure 4.7-4.10 show four repeat experiments on four different chips for both higher concentrations and lower concentrations (Newly made targeted ss-DNA solutions for each experiments). For higher concentrations of targeted ss-DNA, I_1-I_2/I_1 vs Log_{10} ([t-DNA] (in pM)) showed linear trend (Figure 4.7). For lower concentration (Figure 4.8), there was no signal change for targeted ss-DNA at 0.1 aM and at 1 aM, MB SERS signal increased. Repeat experiments proved the possibility of this ultra-low (1 aM) target ss-DNA detection (Figure 4.8-4.10).

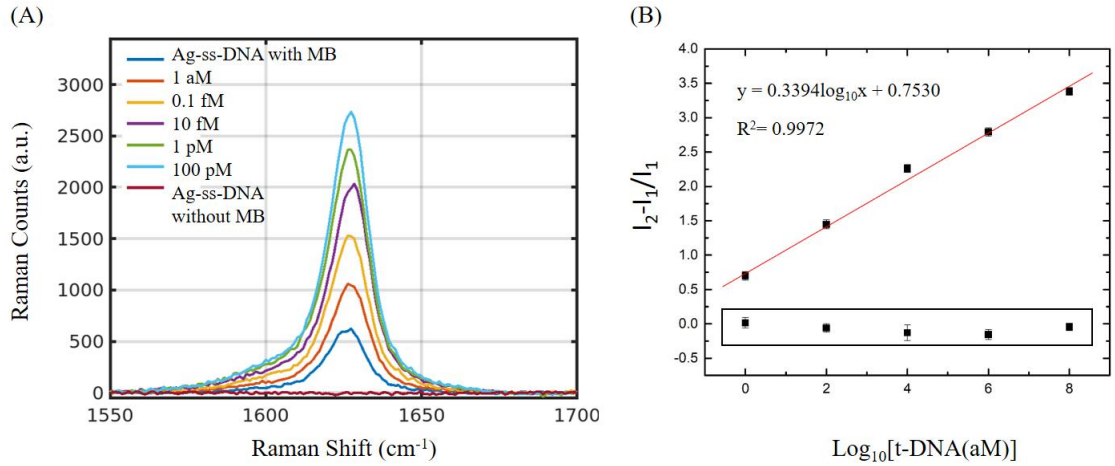

Figure 4.6: Targeted DNA (*stx*2) detection and linear calibration. (A) MB spectra after hybridization with different target DNA concentrations (i) 1 aM, (ii) 0.1 fM, (iii) 10 fM, (iv) 1 pM, and (v) 100 pM. And reference spectra of Ag-ss-DNA SERS substrate with and without MB. (B) Linear fitting for I_1-I_2/I_1 VS Log_{10} ([t-DNA] (in aM)) at different target DNA concentrations: $y = 0.3394\log_{10}x + 0.7530$, with $R^2 = 0.9972$. Data points in the box is non-targeted DNA, which do not show Raman intensity change with the change of non-targeted DNA concentrations. The measurements for each targeted/non-targeted DNA concentration were taken in ten different random points on the functionalized Ag nanostructure SERS substrate, the error bars were the SD (standard deviation) of these ten measurements. All raw data are shown in Figure S6.

On chip 1 (higher concentrations):

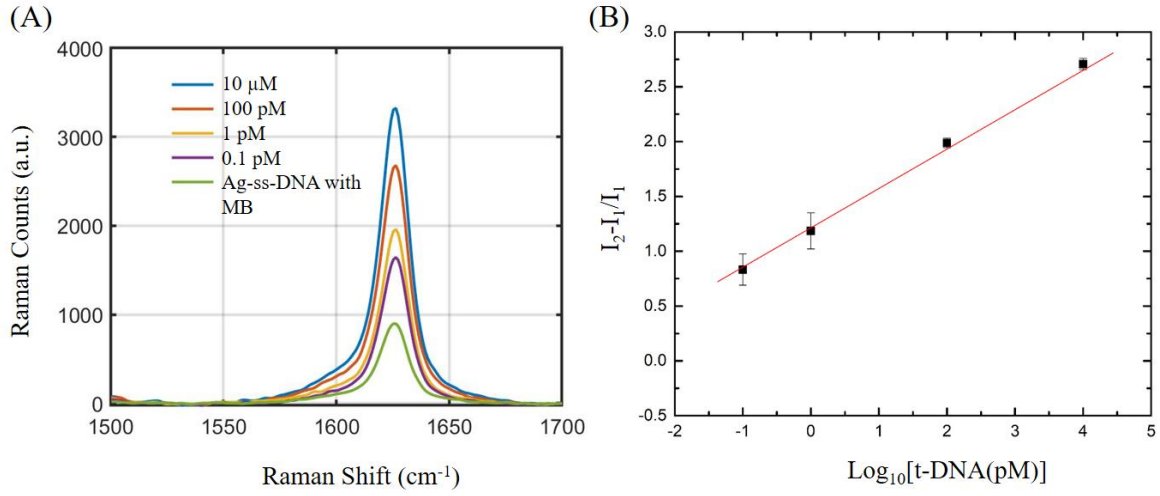

Figure 4.7: Targeted DNA (*stx*2) detection by SERS sensor at higher concentrations (A) MB spectra after hybridization with different target DNA concentrations (i) 0.1 pM, (ii) 1 pM, (iii) 100 pM, (iv) 10 μM. And reference spectra of Ag-ss-DNA SERS substrate with MB (in green). (B) Linear trend for I_1-I_2/I_1 VS Log_{10} ([t-DNA] (in pM)) at different target DNA concentrations for eye guide only. Ten different spectra, taken in ten different random points on the functionalized Ag-ss-DNA SERS substrate are presented for each concentration of targeted ss-DNA, the error bars were the RSD (relative standard deviation) of these ten measurements.

On chip 2 (lower concentrations, 1st repeat experiment for 1 aM ss-DNA detection):

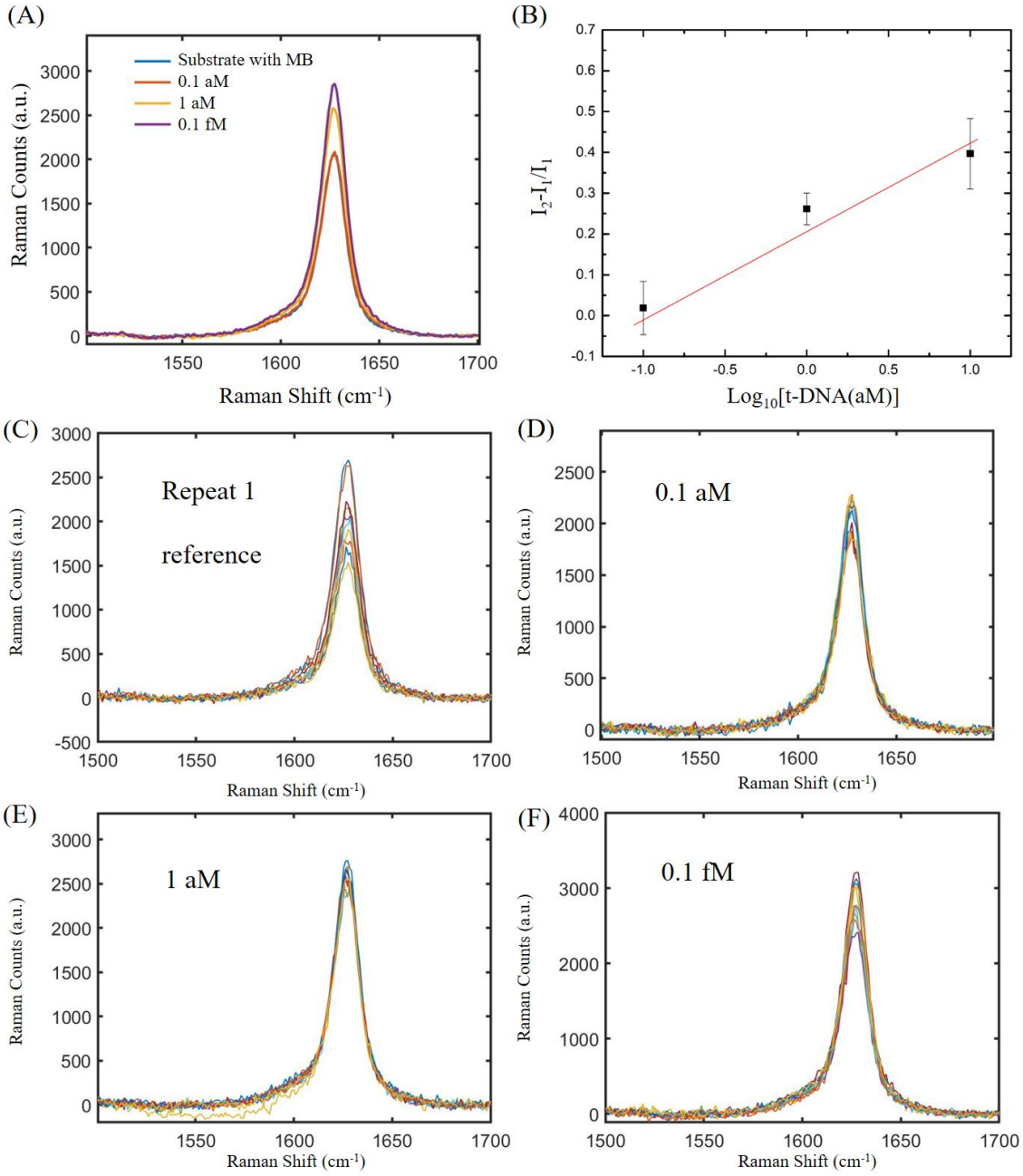

Figure 4.8: Targeted DNA (*stx*2) detection at lower concentrations. (Newly made targeted ss-DNA solutions). (A) MB spectra after hybridization with different target DNA concentrations (i) 0.1 aM, (ii) 1 aM, (iii) 0.1 fM. And reference spectra of Ag-ss-DNA SERS substrate with MB. (B) Linear trend for I_1-I_2/I_1 vs Log_{10} ([t-DNA] (in pM)) at different target DNA concentrations for eye guide only. Ten different spectra, taken in ten different random points on the functionalized Ag-ss-DNA SERS substrate are

presented for each concentration of targeted ss-DNA, the error bars were the RSD (relative standard deviation) of these ten measurements. (C-F) All raw data in (A).

On chip 3 (2nd repeat experiment for 1 aM ss-DNA detection):

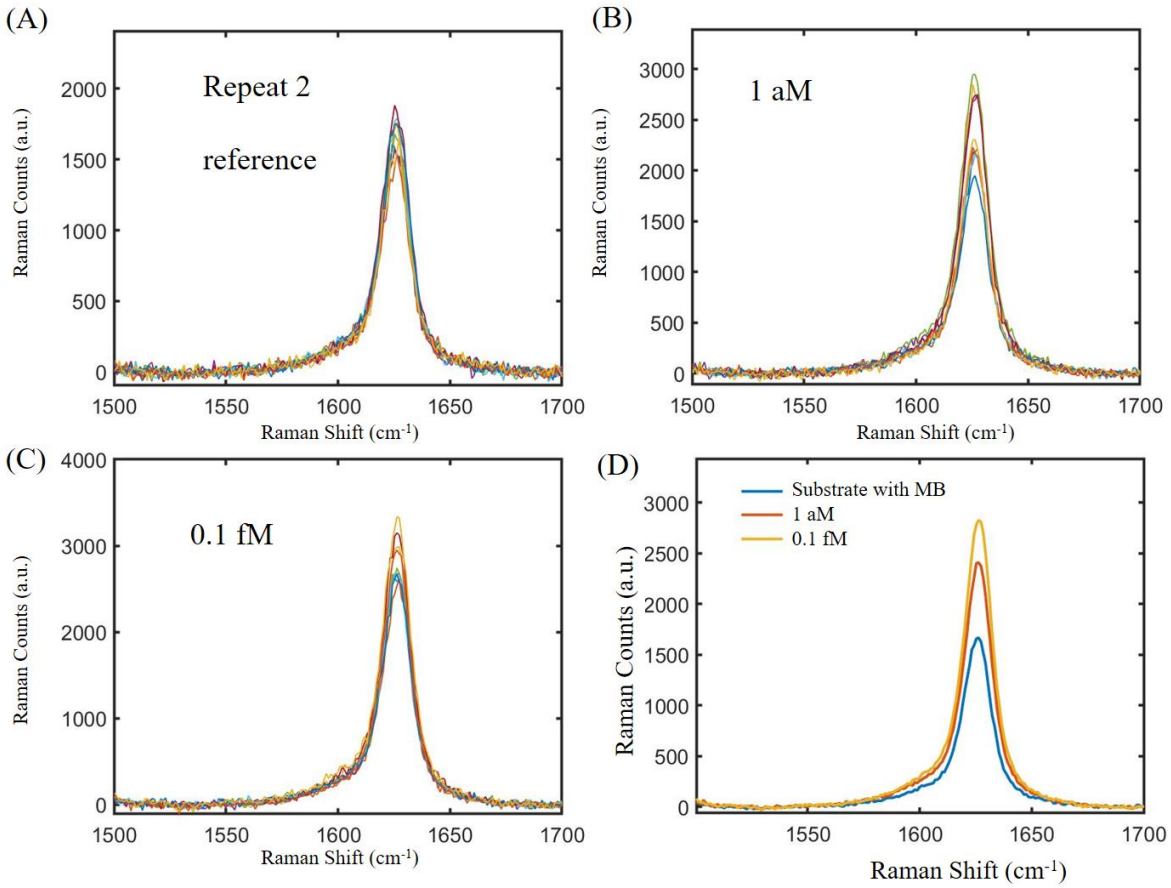

Figure 4.9: Targeted DNA (*stx*2) detection at lower concentrations (Newly made targeted ss-DNA solutions). (A) Reference spectra of Ag-ss-DNA SERS substrate with MB. (B-C) MB spectra after hybridization with different target DNA concentrations (i) 1 aM, (ii) 0.1 fM. (D) MB spectra after hybridization with different target DNA concentrations (i) 1 aM, (ii) 0.1 fM. And reference spectra of Ag-ss-DNA SERS substrate with MB. Ten different spectra, taken in ten different random points on the functionalized Ag-ss-DNA SERS substrate are presented for each concentration of targeted ss-DNA.

On chip 4 (3rd repeat experiment for 1 aM ss-DNA detection):

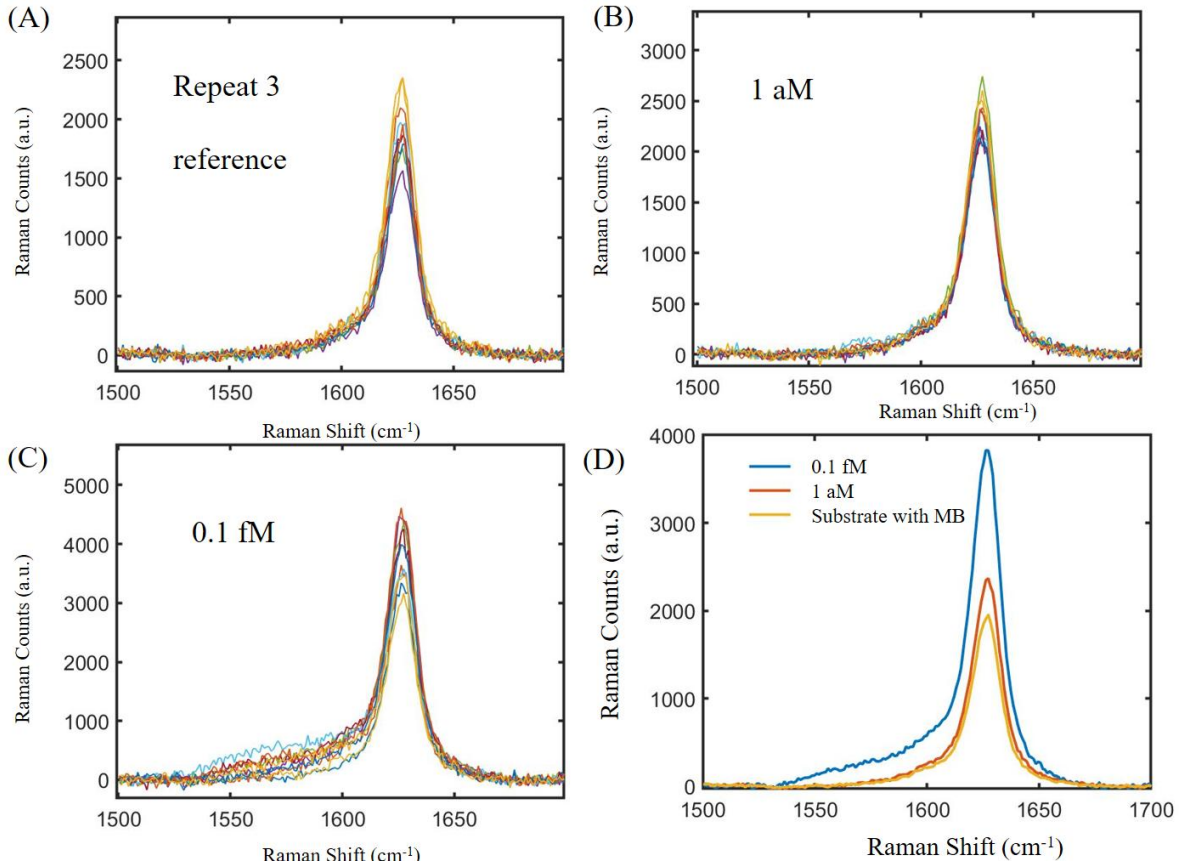

Figure 4.10: Targeted DNA (*stx*2) detection at lower concentrations (Newly made targeted ss-DNA solutions). (A) Reference spectra of substrate with MB. (B-C) MB spectra after hybridization with different target DNA concentrations (i) 1 aM, (ii) 0.1 fM. Ten different spectra, taken in ten different random points on the functionalized Ag-ss-DNA SERS substrate are presented for each concentration of targeted ss-DNA. (D) MB spectra after hybridization with different target DNA concentrations (i) 1 aM, (ii) 0.1 fM. And reference spectra of Ag-ss-DNA SERS substrate with MB. Ten different spectra, taken in ten different random points on the functionalized Ag-ss-DNA SERS substrate are presented for each concentration of targeted ss-DNA.

3.4, Comparison between Ag-MB and Ag-ss-DNA/ds-DNA-MB.

In section 3.2, the experimental LOD for MB, obtained on an Ag SERS substrate, was 0.01 μM (Raman count is around 900 a.u.). With the Ag-thiol-ss-DNA SERS substrate, the Raman count was 600 a.u., but it is important to point out that this was obtained to a different (DNA modified) surface compared to the initial MB experiments. The effective SERS height was around 100 nm, the laser spot size was 1-2 μm. Total MB volume (0.01 μM) that was needed to reach this Raman account was $\pi \times (1)^2$ $\mu m^2 \times 100 \times 10^{-6}$ μm= 3×10^{-4} μL. In the real situation, the length of this thiol-ss-DNA was around several nm,[44] this would help to bring more MB molecules closer to SERS substrate surface with a higher EF (Enhancement Factor) as described by Sharma et al (several orders of magnitude).[45] See Figure 4.11.

After binding with targeted ss-DNA (1 aM), Raman count increased from 600 to 1000 a.u., this arises from both electrostatic attraction and intercalation of MB to ds-DNA (several times more MB molecules bonded to ds-DNA comparing to bond to ss-DNA). ds-DNA folding in space compared to ss-DNA alone after MB application,[46-47] The EF can increase by several orders of magnitude nearer to the Ag surface.[48] Besides, for DNA detection, the experiment was carried out in a dry environment. In theory, only a few targeted ss-DNA needed to hybridize to ss-DNA SERS substrate at 1 aM on a laser spot (30 DNA molecules in 50μL DNA solution) and align with experimental results. In my experiments, Raman measurements and calibrations, the spectra were measured at ten different locations; the final spectrum presented is an average of these ten spectra. This means that in these ten locations, targeted DNAs were able to hybridize and interact with the MB and offer a readable SERS signal increase. See all the raw data in Figures 4.8-4.10 for reference.

In summary, Ag-MB interaction and Ag-ss-DNA/ds-DNA-Ag interaction were two different systems, and the experiments were carried out in different conditions. For Ag-MB, Raman detection happened immediately without incubation (see Figure 4.11 (B)), the distance between the MB molecule and the Ag nano structure surface was limited by the diffusion limit at certain concentrations and surface energies of Ag and MB in a aqueous environment.[49] For MB as a Raman marker in DNA detection, Raman detection happened after 10 minutes of incubation in MB (10 μL, 50 μM) and was carried out in a dry environment. (Figure 4.11 (A, C)). MB binds to ss-DNA through electrostatic force and is bound to ds-DNA by both electrostatic and intercalation. DNA could also change its orientation and space arrangement during hybrization, thus, changing the distance the towards the Ag nano structure surface. The Enhancement Factor of SERS related to the distance between the metal nano structure surface and the molecule. With different bonding mechanisms for these two system, their EF could be several orders of magnitude different. On top of that, ss-DNA can host large numbers of MB molecules after incubation at 50 μM MB and help its SERS signal reading. The Raman signal is usually much higher in a dry detection environment than in a water environment, and this has been demonstrated experimentally in chapters 2 and 3. All statements above explain the LOD differences in sections 3.2 and 3.3., as well as the ultra-low detection ability. On top of this, the repeat experiment for target ss-DNA also confirmed the result. See Figure 4.8-4.10.

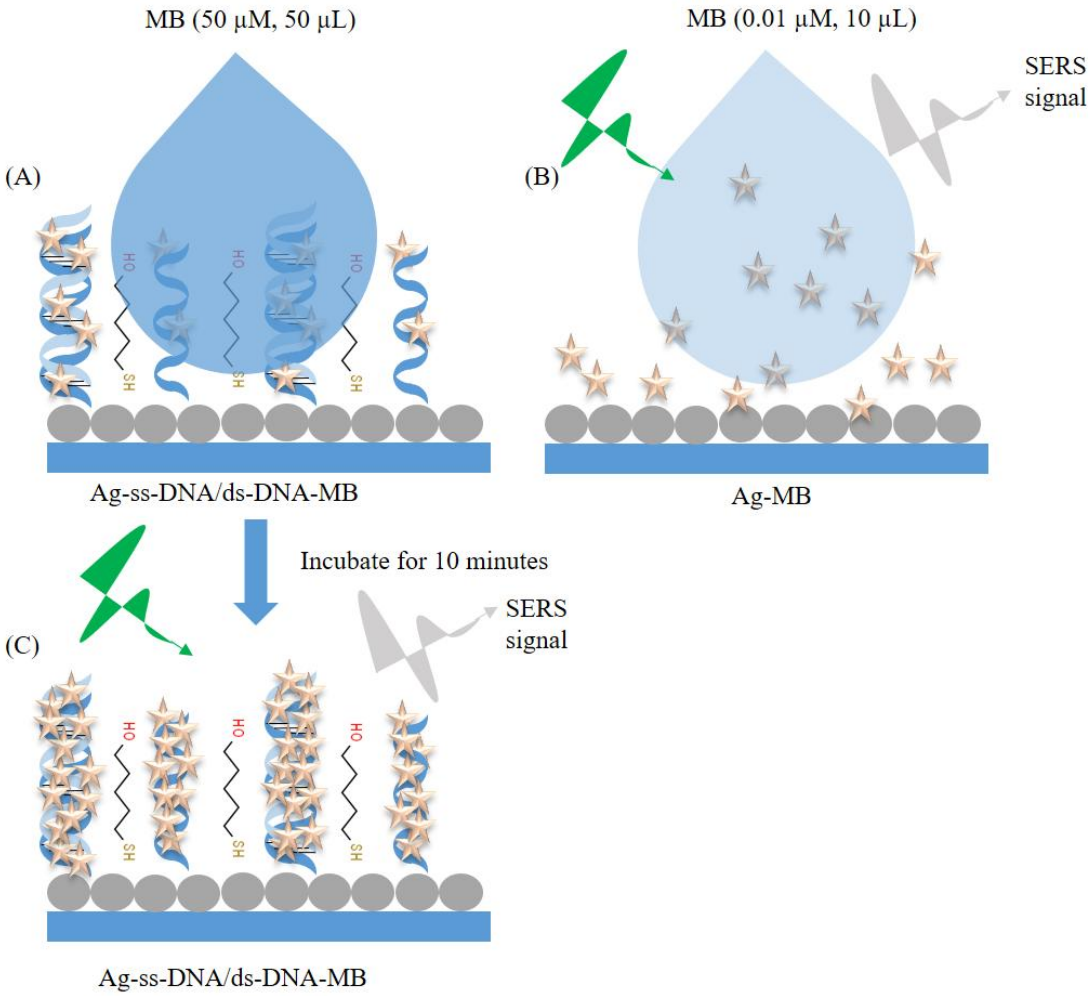

Figure 4.11: Illustration of (A) Ag-ss-DNA/ds-DNA-MB : 50 µL, 50 µM MB applied to SERS sensor (Ag-ss-DNA/ds-DNA) and incubate for 10 minutes. (B) Ag-MB: MB solution (µM) directly contacts with silver surface and gets SERS signal. (C) After 10 minutes of incubation, removing MB solution, Raman measurements were carried out in dry environment.

3.5, Real sample detection by Ag nanostructure SERS substrates.

Chromosomal DNA from different bacterial strains (STEC O157, *Salmonella spp.,* and *Staphylococcus aureus*) extracted from the overnight cultures were used to confirm the selectivity of developed sensors. DNA was first sonicated to break the DNA into

smaller strands and heated to denaturate the double strand. After that, the samples were cooled down immediately and incubated on top of the sensor for 20 minutes and the detection with MB (50 mM, 20 μL, 10 minutes) was performed. Three replicate experiments were done for each bacterial species on three individual SERS sensors. For each experiment, the spectra were normalized at initial Raman peak after MB application to ss-DNA SERS sensor for better data comparison and visualization.

The results showed, for targeted-ss-DNA from STEC containing *stx*2 gene, the Raman intensity changes dramatically, with the intensity increase comparing to ss-DNA. When non-target bacteria were used, such as *Salmonella spp*. and *Staphylococcus aureus*, no obvious change in Raman intensity was observed, as shown in Figure 4.12 (A). The Raman intensities change (I_2-I_1/I_1) for these three bacteria are shown in Figure 4.12 (B), each with three replicates. For STEC O157, the Raman intensity changes in the range from 125% to 274%, with an average intensity of 192%. By contrast, for *Salmonella* and *Staphylococcus*, the average Raman intensity changes stayed within 11%. These results strongly suggest that the two thiols functionalized Ag nanostructure SERS substrate developed in this work is suitable for highly selective and highly sensitive DNA/ bacteria sensor without DNA amplification.

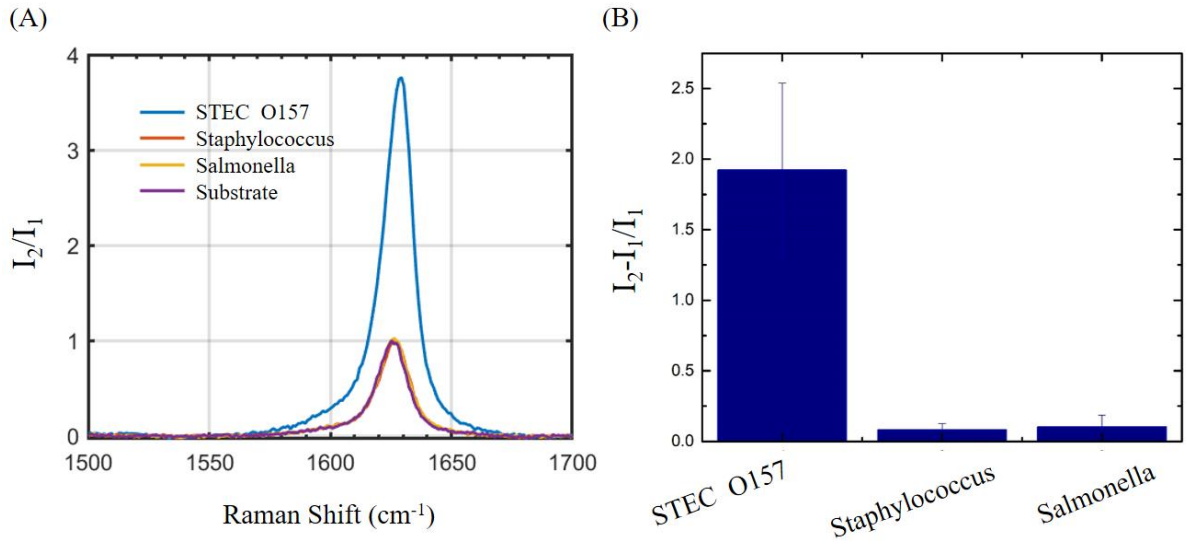

Figure 4.12: Real DNA samples study from different bacteria (STEC O157, *Salmonella spp.* and *Staphylococcus aureus*) on functionalized Ag nanostructure SERS sensors. (A) DNA from different bacteria samples on different SERS substrates (Incubation time: 20 minutes), after binding with 50 μM MB (20 μL) for 10 minutes. Only targeted bacteria STEC O157 showed significant changes in Raman intensity (274%). (B) Bar plot of intensity change for different bacteria DNA extraction, error bars were from three replications; where DNA from STEC O157 shows significant Raman intensity change (average 192%), the other two bacteria DNA do not show that much difference in Raman intensity change (within 11% Raman intensity change in average).

4. Conclusions.

In this research, Ag nanostructure with regularly distributed nano gaps were successfully synthesized through an electrochemical deposition method on a recycled SiO_2/Si chip with a large Pt/Au electrode. Those Ag nanostructures stacked on the SiO_2/Si chip well without lifting off after functionalization steps and DNA detection steps, following two functionalization steps with thiol-ss-DNA and 6-Mercapto-1-hexanol on the Ag nanostructure SERS substrate. This SERS substrate showed good linearity with R^2 = 0.997 in a 1 aM to 100 pM dynamic concentration range, the detection ability was 1 aM from the experimental result. In real sample verification, this SERS substrate showed good selectivity towards target DNA (*stx*2) in STEC O157, while it did not show much Raman intensity change towards other bacteria such as *Salmonella* and *Staphylococcus*. Overall, this study showed proof of principle that the SERS substrate has potential as a cost effective, high selective, high sensitive DNA and bacteria sensor without the aid of PCR DNA amplification. With further development and validation, this methodological approach has the potential for use in the point-of-use detection for instance on a farm or in the food industry.

Reference.

1. Joseph, A.; Cointe, A.; Mariani Kurkdjian, P.; Rafat, C.; Hertig, A., Shiga Toxin-Associated Hemolytic Uremic Syndrome: A Narrative Review. *Toxins (Basel)* **2020,** *12* (2), 67.

2. Yang, X.; Bai, X.; Zhang, J.; Sun, H.; Fu, S.; Fan, R.; He, X.; Scheutz, F.; Matussek, A.; Xiong, Y., Escherichia coli strains producing a novel Shiga toxin 2 subtype circulate in China. *International Journal of Medical Microbiology* **2020,** *310* (1), 151377.

3. Haugum, K.; Brandal, L. T.; Lindstedt, B. A.; Wester, A. L.; Bergh, K.; Afset, J. E., PCR-based detection and molecular characterization of shiga toxin-producing Escherichia coli strains in a routine microbiology laboratory over 16 years. *J Clin Microbiol* **2014,** *52* (9), 3156-3163.

4. TECHNICAL SPECIFICATION ISO/TS 13136:2012(en) : Microbiology of food and animal feed — Real-time polymerase chain reaction (PCR)-based method for the detection of food-borne pathogens — Horizontal method for the detection of Shiga toxin-producing Escherichia coli (STEC) and the determination of O157, O111, O26, O103 and O145 serogroups. **2012**.

5. Liang, W.; Xu, L.; Sui, Z.; Li, Y.; Li, L.; Wen, Y.; Li, C.; Ren, S.; Liu, G., Quantification of plasmid DNA reference materials for Shiga toxin-producing Escherichia coli based on UV, HR-ICP-MS and digital PCR. *Chemistry Central Journal* **2016,** *10* (1), 55.

6. Lisle, J. T.; Hamilton, M. A.; Willse, A. R.; McFeters, G. A., Comparison of fluorescence microscopy and solid-phase cytometry methods for counting bacteria in water. *Appl Environ Microbiol* **2004,** *70* (9), 5343-5348.

7. Pan, X.-T.; Liu, Y.-Y.; Qian, S.-Q.; Yang, J.-M.; Li, Y.; Gao, J.; Liu, C.-G.; Wang, K.; Xia, X.-H., Free-Standing Single Ag Nanowires for Multifunctional Optical Probes. *ACS Applied Materials & Interfaces* **2021,** *13* (16), 19023-19030.

8. Yang, Y.; O'Riordan, A.; Lovera, P., Highly Sensitive Pesticide Detection using Electrochemically Prepared Silver-Gum Arabic Nanocluster SERS Substrates. *Sensors and Actuators B: Chemical* **2022**, 131851.

9. Lee, H. G.; Choi, W.; Yang, S. Y.; Kim, D.-H.; Park, S.-G.; Lee, M.-Y.; Jung, H. S., PCR-coupled Paper-based Surface-enhanced Raman Scattering (SERS) Sensor for Rapid and Sensitive Detection of Respiratory Bacterial DNA. *Sensors and Actuators B: Chemical* **2021,** *326*, 128802.

10. Parnsubsakul, A.; Ngoensawat, U.; Wutikhun, T.; Sukmanee, T.; Sapcharoenkun, C.; Pienpinijtham, P.; Ekgasit, S., Silver nanoparticle/bacterial nanocellulose paper composites for paste-and-read SERS detection of pesticides on fruit surfaces. *Carbohydrate Polymers* **2020,** *235*, 115956.

11. Shi, L.; Zhong, X.; Ding, H.; Yu, Z.; Jin, J.; Zhou, T.; Zhu, Y.; Liu, Z., Continuous separation of microparticles based on optically induced dielectrophoresis. *Microfluidics and Nanofluidics* **2022,** *26* (1), 6.

12. Camargo, P. H. C.; Au, L.; Rycenga, M.; Li, W.; Xia, Y., Measuring the SERS enhancement factors of dimers with different structures constructed from silver nanocubes. *Chemical Physics Letters* **2010,** *484* (4), 304-308.

13. Chen, K.-H.; Lee, S.-H.; Kok, L.-C.; Ishdorj, T.-O.; Chang, H.-Y.; Tseng, F.-G., A 3D-ACEK/SERS system for highly efficient and selectable electrokinetic bacteria concentration/detection/ antibiotic-susceptibility-test on whole blood. *Biosensors and Bioelectronics* **2022,** *197*, 113740.

14. Zhou, Z.; Xiao, R.; Cheng, S.; Wang, S.; Shi, L.; Wang, C.; Qi, K.; Wang, S., A universal SERS-label immunoassay for pathogen bacteria detection based on Fe3O4@Au-aptamer separation and antibody-protein A orientation recognition. *Analytica Chimica Acta* **2021,** *1160*, 338421.

15. Ali, H. T.; Mateen, A.; Ashraf, F.; Javed, M. R.; Ali, A.; Mahmood, K.; Zohaib, A.; Amin, N.; Ikram, S.; Yusuf, M., A new SERS substrate based on Zn2GeO4 nanostructures for the rapid identification of E.Coli and methylene blue. *Ceramics International* **2021,** *47* (19), 27998-28003.

16. Srivastava, S. K.; Hamo, H. B.; Kushmaro, A.; Marks, R. S.; Grüner, C.; Rauschenbach, B.; Abdulhalim, I., Highly sensitive and specific detection of E. coli by a SERS nanobiosensor chip utilizing metallic nanosculptured thin films. *Analyst* **2015,** *140* (9), 3201-3209.

17. Zhou, H.; Yang, D.; Ivleva, N. P.; Mircescu, N. E.; Niessner, R.; Haisch, C., SERS Detection of Bacteria in Water by in Situ Coating with Ag Nanoparticles. *Analytical Chemistry* **2014,** *86* (3), 1525-1533.

18. Bi, L.; Wang, X.; Cao, X.; Liu, L.; Bai, C.; Zheng, Q.; Choo, J.; Chen, L., SERS-active Au@Ag core-shell nanorod (Au@AgNR) tags for ultrasensitive bacteria detection and antibiotic-susceptibility testing. *Talanta* **2020,** *220*, 121397.

19. Díaz-Amaya, S.; Lin, L.-K.; Deering, A. J.; Stanciu, L. A., Aptamer-based SERS biosensor for whole cell analytical detection of E. coli O157:H7. *Analytica Chimica Acta* **2019,** *1081*, 146-156.

20. Macdonald, D.; Smith, E.; Faulds, K.; Graham, D., DNA detection by SERS: hybridisation parameters and the potential for asymmetric PCR. *Analyst* **2020,** *145* (5), 1871-1877.

21. Liu, M.; Wang, Z.; Zong, S.; Zhang, R.; Zhu, D.; Xu, S.; Wang, C.; Cui, Y., SERS-based DNA detection in aqueous solutions using oligonucleotide-modified Ag nanoprisms and gold nanoparticles. *Analytical and Bioanalytical Chemistry* **2013,** *405* (18), 6131-6136.

22. Hamm, L.; Gee, A.; De Silva Indrasekara, A. S., Recent Advancement in the Surface-Enhanced Raman Spectroscopy-Based Biosensors for Infectious Disease Diagnosis. *Applied Sciences* **2019,** *9* (7), 1448.

23. Strelau, K. K.; Kretschmer, R.; Möller, R.; Fritzsche, W.; Popp, J., SERS as tool for the analysis of DNA-chips in a microfluidic platform. *Analytical and Bioanalytical Chemistry* **2010,** *396* (4), 1381-1384.

24. Hering, K.; Cialla, D.; Ackermann, K.; Dörfer, T.; Möller, R.; Schneidewind, H.; Mattheis, R.; Fritzsche, W.; Rösch, P.; Popp, J., SERS: a versatile tool in chemical and biochemical diagnostics. *Analytical and Bioanalytical Chemistry* **2008,** *390* (1), 113-124.

25. Strelau, K. K.; Brinker, A.; Schnee, C.; Weber, K.; Möller, R.; Popp, J., Detection of PCR products amplified from DNA of epizootic pathogens using magnetic nanoparticles and SERS. *Journal of Raman Spectroscopy* **2011,** *42* (3), 243-250.

26. Liu, Y.; Wu, S.-H.; Du, X.-Y.; Sun, J.-J., Plasmonic Ag nanocube enhanced SERS biosensor for sensitive detection of oral cancer DNA based on nicking

endonuclease signal amplification and heated electrode. *Sensors and Actuators B: Chemical* **2021,** *338*, 129854.

27. Seymour, I.; O'Sullivan, B.; Lovera, P.; Rohan, J. F.; O'Riordan, A., Elimination of Oxygen Interference in the Electrochemical Detection of Monochloramine, Using In Situ pH Control at Interdigitated Electrodes. *ACS Sensors* **2021,** *6* (3), 1030-1038.

28. Wahl, A. J. C.; Seymour, I. P.; Moore, M.; Lovera, P.; O'Riordan, A.; Rohan, J. F., Diffusion profile simulations and enhanced iron sensing in generator-collector mode at interdigitated nanowire electrode arrays. *Electrochimica Acta* **2018,** *277*, 235-243.

29. Wasiewska, L. A.; Seymour, I.; Patella, B.; Inguanta, R.; Burgess, C. M.; Duffy, G.; O'Riordan, A., Reagent free electrochemical-based detection of silver ions at interdigitated microelectrodes using in-situ pH control. *Sensors and Actuators B: Chemical* **2021,** *333*, 129531.

30. Daly, R.; Narayan, T.; Shao, H.; O'Riordan, A.; Lovera, P., Platinum-Based Interdigitated Micro-Electrode Arrays for Reagent-Free Detection of Copper. *Sensors* **2021,** *21* (10), 3544.

31. Gillibert, R.; Triba, M.; Chapelle, M., Surface Enhanced Raman Scattering Sensor for Highly Sensitive and Selective Detection of Ochratoxin A. *The Analyst* **2017,** *143*.

32. Ji, J.; Li, P.; Sang, S.; Zhang, W.; Zhou, Z.; Yang, X.; Dong, H.; Li, G.; Hu, J., Electrodeposition of Au/Ag bimetallic dendrites assisted by Faradaic AC-electroosmosis flow. *AIP Advances* **2014,** *4* (3), 031329.

33. Harpster, M. H.; Zhang, H.; Sankara-Warrier, A. K.; Ray, B. H.; Ward, T. R.; Kollmar, J. P.; Carron, K. T.; Mecham, J. O.; Corcoran, R. C.; Wilson, W. C.; Johnson, P. A., SERS detection of indirect viral DNA capture using colloidal gold and methylene blue as a Raman label. *Biosensors and Bioelectronics* **2009,** *25* (4), 674-681.

34. Vu, X. H.; Dien, N. D.; Ha Pham, T. T.; Trang, T. T.; Ca, N. X.; Tho, P. T.; Vinh, N. D.; Van Do, P., The sensitive detection of methylene blue using silver nanodecahedra prepared through a photochemical route. *RSC Advances* **2020,** *10* (64), 38974-38988.

35. Gillibert, R.; Triba, M. N.; Lamy de la Chapelle, M., Surface enhanced Raman scattering sensor for highly sensitive and selective detection of ochratoxin A. *Analyst* **2018,** *143* (1), 339-345.

36. Shokoufi, N.; Abbasgholi Nejad Asbaghi, B.; Nouri Hajibaba, S., Sensitive determination of DNA based on phosphate-dye interaction using photothermal lens technique. *Appl. Opt.* **2019,** *58* (12), 3074-3082.

37. Yang, W.; Ozsoz, M.; Hibbert, D. B.; Gooding, J. J., Evidence for the Direct Interaction Between Methylene Blue and Guanine Bases Using DNA-Modified Carbon Paste Electrodes. *Electroanalysis* **2002,** *14* (18), 1299-1302.

38. Vardevanyan, P. O.; Antonyan, A. P.; Parsadanyan, M. A.; Shahinyan, M. A.; Hambardzumyan, L. A., Mechanisms for Binding between Methylene Blue and DNA. *Journal of Applied Spectroscopy* **2013,** *80* (4), 595-599.

39. Zhu, L.; Zhao, R.; Wang, K.; Xiang, H.; Shang, Z.; Sun, W., Electrochemical behaviors of methylene blue on DNA modified electrode and its application to the detection of PCR product from NOS sequence. *Sensors* **2008,** *8* (9), 5649-5660.

40. Almehmadi, L. M.; Curley, S. M.; Tokranova, N. A.; Tenenbaum, S. A.; Lednev, I. K., Surface Enhanced Raman Spectroscopy for Single Molecule Protein Detection. *Scientific Reports* **2019,** *9* (1), 12356.

41. Farjami, E.; Clima, L.; Gothelf, K. V.; Ferapontova, E. E., DNA interactions with a Methylene Blue redox indicator depend on the DNA length and are sequence specific. *Analyst* **2010,** *135* (6), 1443-1448.

42. Kara, P.; Kerman, K.; Ozkan, D.; Meric, B.; Erdem, A.; Ozkan, Z.; Ozsoz, M., Electrochemical genosensor for the detection of interaction between methylene blue and DNA. *Electrochemistry Communications* **2002,** *4* (9), 705-709.

43. Li, L.; Wang, S.; Yang, T.; Huang, S.; Wang, J., Electrochemical growth of gold nanoparticles on horizontally aligned carbon nanotubes: A new platform for ultrasensitive DNA sensing. *Biosensors and Bioelectronics* **2012,** *33* (1), 279-283.

44. Roth, E.; Glick Azaria, A.; Girshevitz, O.; Bitler, A.; Garini, Y., Measuring the Conformation and Persistence Length of Single-Stranded DNA Using a DNA Origami Structure. *Nano Letters* **2018,** *18* (11), 6703-6709.

45. Radziuk, D.; Moehwald, H., Prospects for plasmonic hot spots in single molecule SERS towards the chemical imaging of live cells. *Physical Chemistry Chemical Physics* **2015,** *17* (33), 21072-21093.

46. Kominami, H.; Kobayashi, K.; Yamada, H., Molecular-scale visualization and surface charge density measurement of Z-DNA in aqueous solution. *Scientific Reports* **2019,** *9* (1), 6851.

47. Rohs, R.; Sklenar, H.; Lavery, R.; Röder, B., Methylene Blue Binding to DNA with Alternating GC Base Sequence: A Modeling Study. *Journal of the American Chemical Society* **2000,** *122* (12), 2860-2866.

48. Keating, M.; Song, S.; Wei, G.; Graham, D.; Chen, Y.; Placido, F., Ordered Silver and Copper Nanorod Arrays for Enhanced Raman Scattering Created via Guided Oblique Angle Deposition on Polymer. *The Journal of Physical Chemistry C* **2014,** *118* (9), 4878-4884.

49. Chernov, S. F.; Fedorov, Y. V.; Zakharov, V. N., Surface tension of silver in different media. *Journal of Physics and Chemistry of Solids* **1993,** *54* (8), 963-966.

Supporting Information.

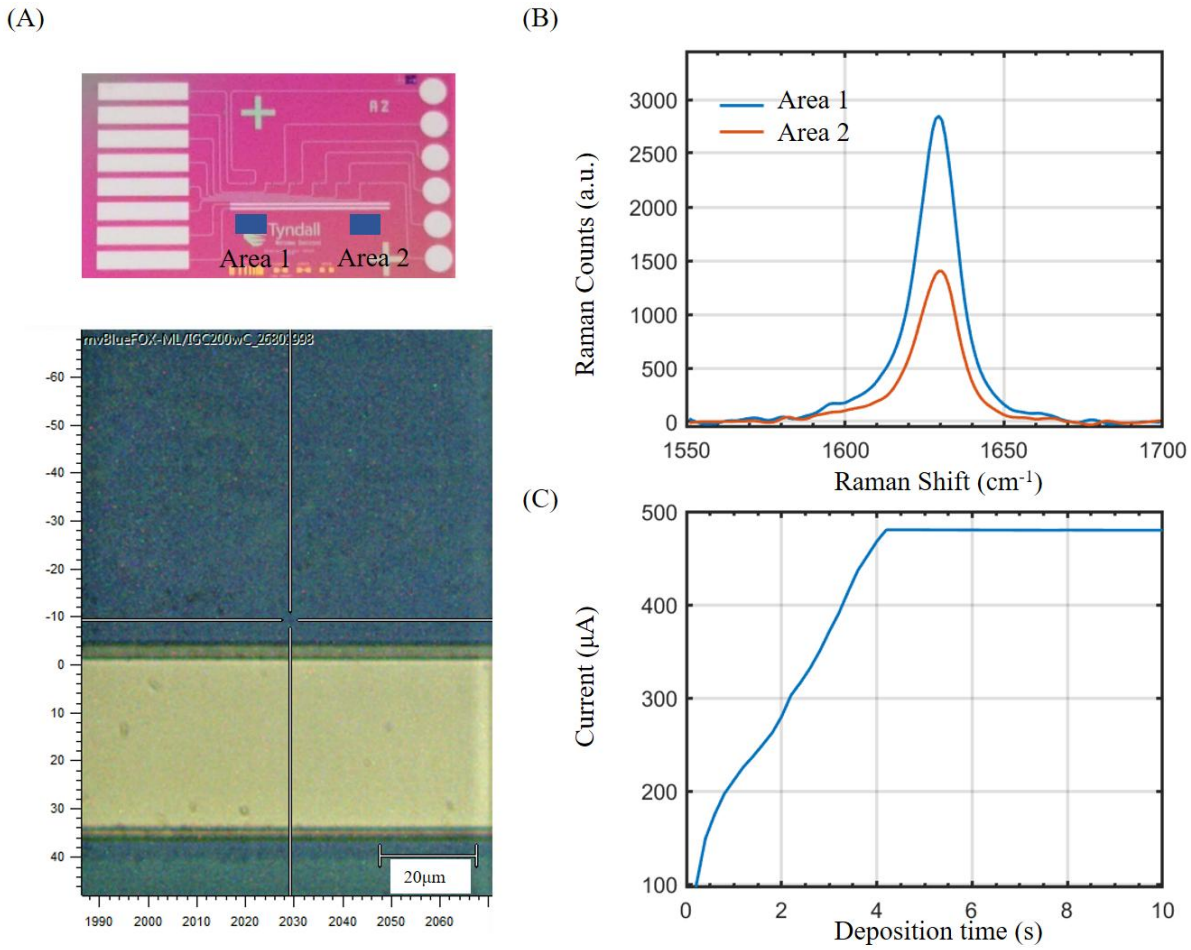

Figure S1 (A) Confined Raman measurement areas on chip and ruler window (x, y) to mark the test area for Raman measurements. (B) Different Raman intensity at different locations (area1 and area2 in (A)). (C) Electrochemical deposition current (µA) VS time (s) plot.

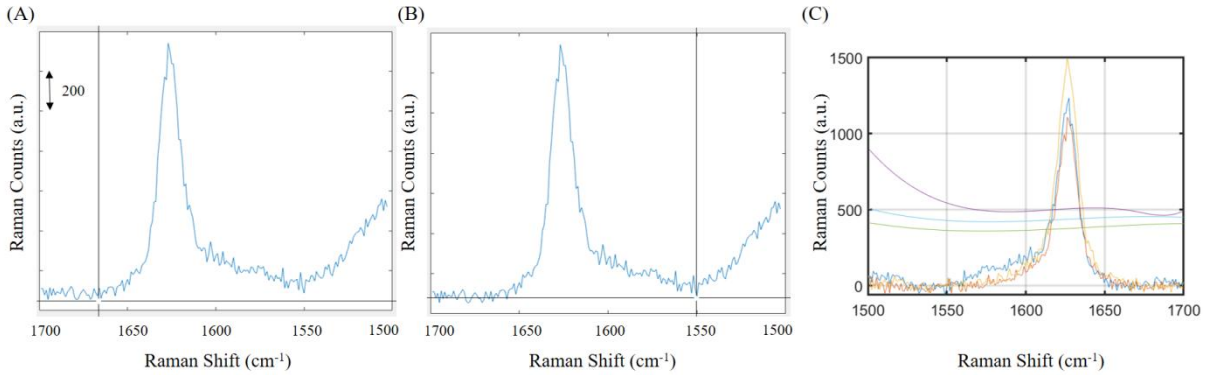

Figure S2 (A-B) catch two point for baseline subtraction for this spectrum range from 1500 cm^{-1} to 1700 cm^{-1}; (C) spectra after the baseline subtraction, the straight lines were the baselines.

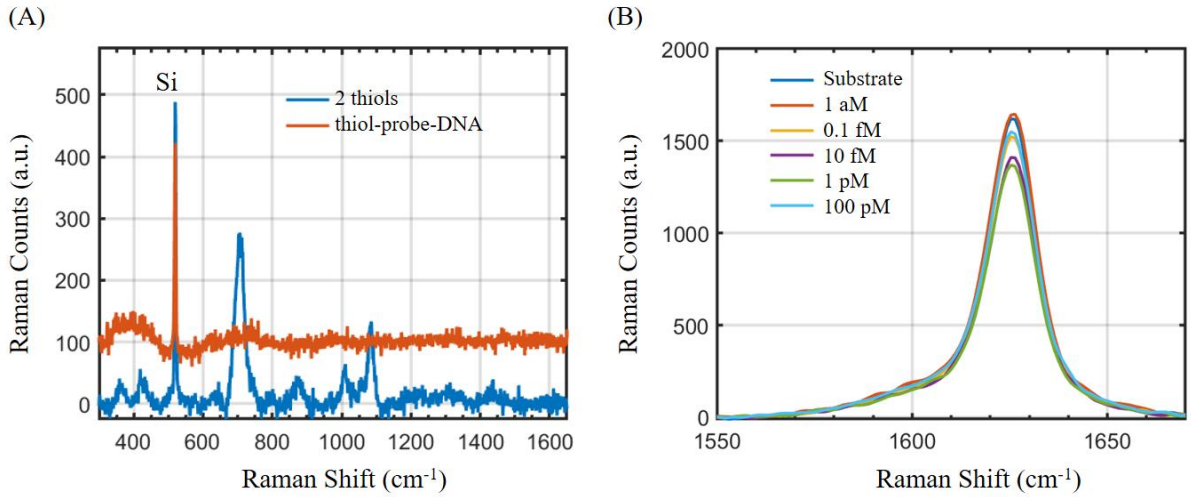

Figure S3 (A) Spectra for Ag NPs SERS substrate functionalization: with thiol-DNA and with two thiols (thiol-DNA+ thiol-OH). Spectra offset for clarity, peak around 520 cm^{-1} is SiO_2. (C) Spectra for non-targeted DNA at different concentrations and spectrum for the functionalized substrate as a reference

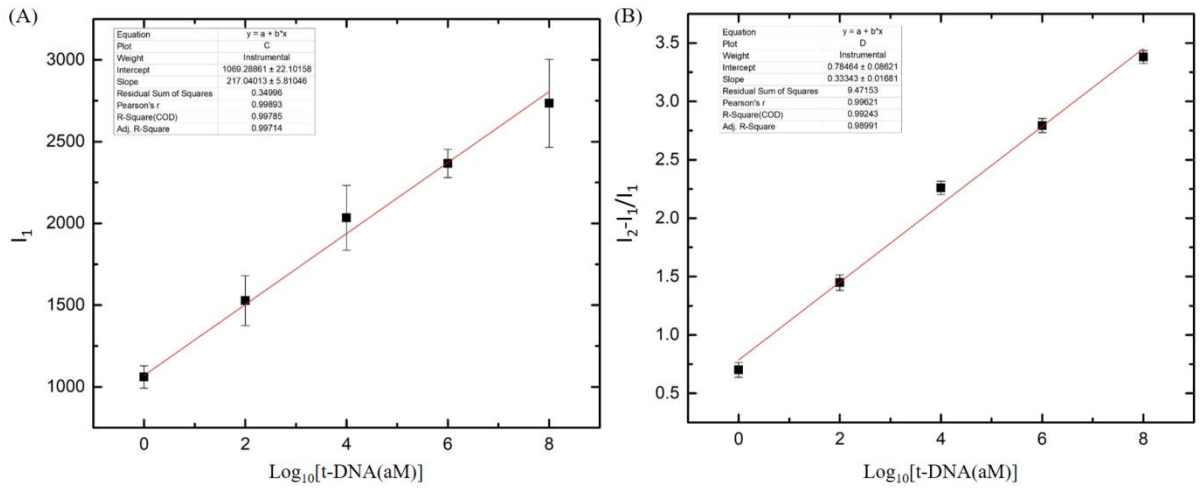

Figure S4 Comparison of two linear fitting method: (A) I_1 VS log $_{10}$ (t-DNA (aM));(B) I_2-I_1/I_1 VS log $_{10}$ (t-DNA (aM)).

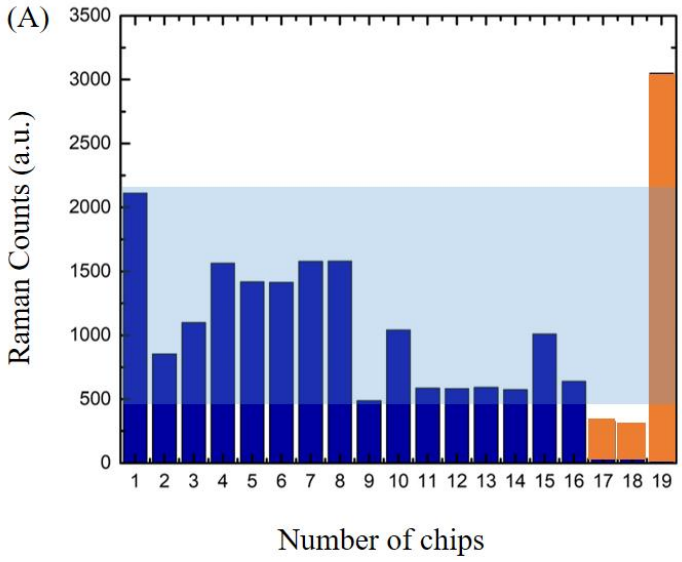

Figure S5 Bar plot of initial Raman counts of 19 SERS sensors after MB application, the success rate is evaluated by Raman counts (a.u.), Raman counts range from 500-2000 are good for DNA detection. The success rate is 16/19 (84.21%).

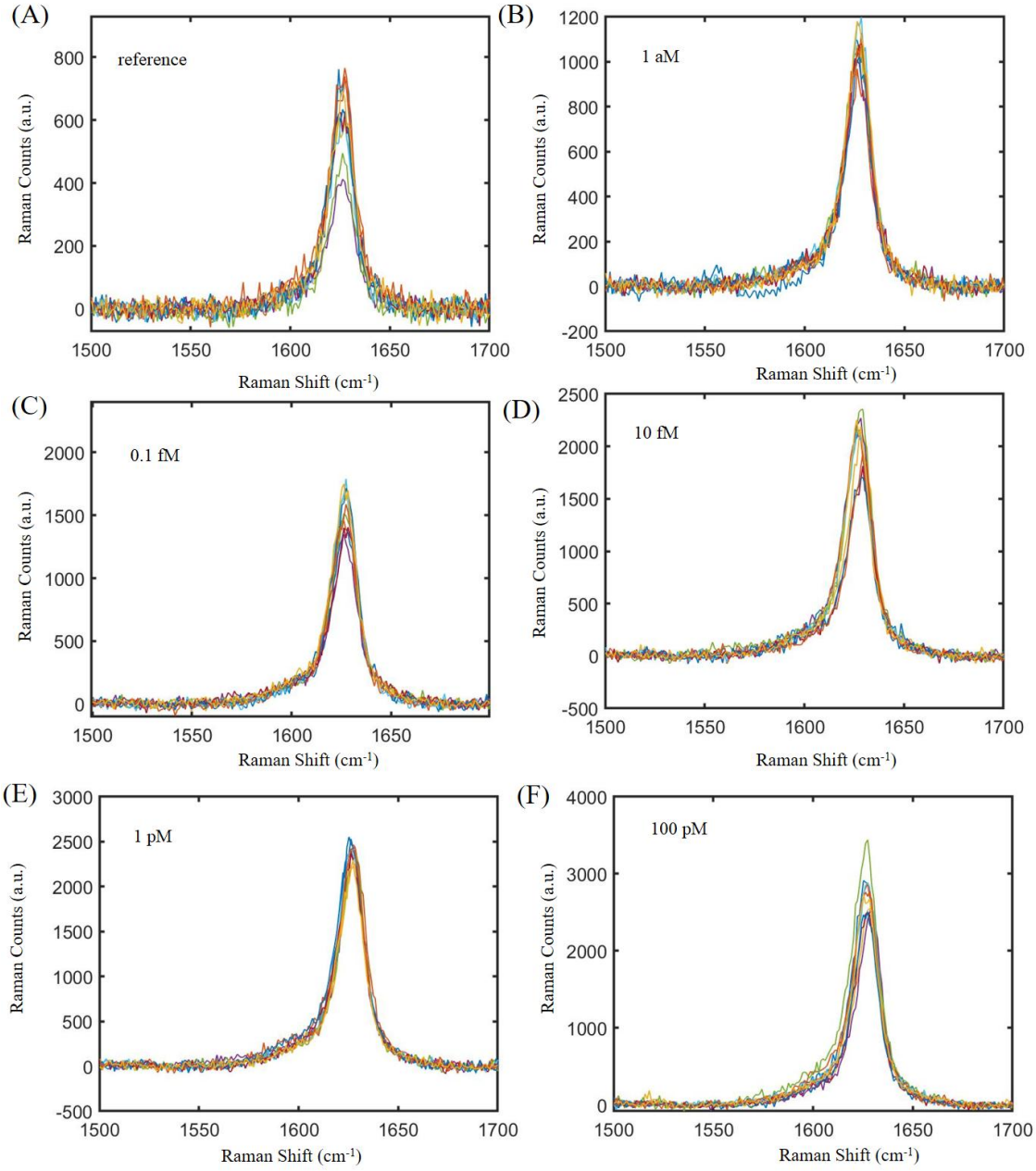

Figure S6: All raw data in Figure 4.7: targeted DNA (*stx*2) detection. (A) Reference spectra of Ag-ss-DNA SERS substrate with MB. (B-F) MB spectra after hybridization with different target DNA concentrations (i) 1 aM, (ii) 0.1 fM, (iii) 10 fM, (iv) 1 pM, and (v) 100 pM. Ten different spectra, taken at ten different random points on the

functionalized Ag-ss-DNA SERS substrate are presented for each concentration of targeted ss-DNA.

$EF = I_{SERS} \cdot N_{bulk} / N_{SERS} \cdot I_{bulk}$

For 0.01 μM MB by SERS:

$I_{SERS} = 868.332$, $N_{SERS} = V_{MB\ effective\ for\ SERS} \cdot [MB]$, $V_{MB\ effective\ for\ SERS} = \pi \cdot r^2 \cdot 10^{-7}$, where r is the laser spot radius (in μm) (total surface area of Ag nano structure was estimated to be equal to laser spot area); 10^{-7} is the estimated SERS effective height for MB solution (100 nm, which is the SERS effective range), even if the total amount of MB that interact with Ag NPs surface could be much smaller;

For normal Raman at 1 mM MB concentration:

$I_{bulk} = 517$, $N_{bulk} = V_{MB\ effective\ for\ Raman} \cdot [MB]$, $V_{MB\ effective\ for\ Raman} = \pi \cdot r^2 \cdot h_{effective}$, where r is the laser spot radius (in μm); $h_{effective}$ is the effective height for MB for Raman measurement and is estimated to be 1 mm.

$EF = 868.332 \cdot \pi \cdot r^2 \cdot 10^{-3}\ m \cdot 10^{-3}\ M / 517 \cdot \pi \cdot r^2 \cdot 10^{-7} m \cdot 0.01 \cdot 10^{-6}\ M = 0.169 \times 10^{10}$

Appendix 1

A.1. Publications:

1, **Yuqing Yang**, Niamh Creedon, Alan O'Riordan, Pierre Lovera. Surface Enhanced Raman Spectroscopy: Applications in Agriculture and Food Safety. *Photonics* 2021, *8*(12), 568;

2, **Yuqing Yang**, Alan O'Riordan, Pierre Lovera. Highly sensitive pesticide detection using electrochemically prepared Silver-Gum Arabic nanocluster SERS substrates. Sensors and Actuators B: Chemical. Volume 364, 1 August 2022, 131851.

3, **Yuqing Yang,** Luiza Adela Wasiewska, Catherine M Burgess, Geraldine Duffy, Pierre Lovera, Alan O'Riordan. Detection of str2 from Shiga toxin-producing Escherichia coli (STEC) by a Surface Enhanced Raman Spectroscopy (SERS) sensor using recycled silicon chips. Sensors and Actuators B: Chemical: Volume 373, 15 December 2022, 132618.

4, **Yuqing Yang**, et al. Sensing Technologies for Real Time Monitoring of Water Quality, **Chapter 4,** Wiley.

A.2. Conferences and Conference papers:

1, **Yuqing Yang**, Alan O'Riordan, Pierre Lovera. Quantitative Detection of Dopamine by SERS in Water Environment. Oral presentation. 21st AISEM (The Italian Association of Sensors and Microsystems) online Conference, 2022, Rome, Italy. http://www.aisem.eu/. This work has submitted to AISEM conference proceeding: SENSORS and MICROSYSTEMS.

2, **Yuqing Yang**, Luiza Adela Wasiewska, Pierre Lovera, Alan O'Riordan. Shiga toxin-producing *E.coli* (STEC) *str*2 ss-DNA detection by Surface Enhanced Raman

Spectroscopy (SERS). Oral presentation. 19th ECASIA (European Association on Applications of Surface and Interface Analisis) conference, 2022, Limerick, Ireland.

Appendix 2

Answers to reviewer's question for chapter 2 publication.

Reviewers' comments:

Reviewer #1: This manuscript describes the fabrication of Silver-Gum Arabic (Ag-GA) SERS substrates by electrochemical deposition for herbicide 2,4-D detection. In this study, Gum Arabic was used to reduce silver ions for substrates fabrication as well as to attract an analyate in the surface of Ag nanostructures for high sensitivity. Authors explained well the control of size and morphology of Ag nanparticles by changing several electrochemical deposition parameters. The data presented in the context are convincing. However, some major issues should be explained for publication.

1. Authors assert a rapid fabrication of Ag-GA SERS substrates where it require less than 10s. However, they must prepare the microelectrode on Si/SiO2 chip via complex and time-consuming steps such as photolithograpy, PVD, metal deposition, and CVD to start electrochemical depostion with Ag precursor and Gum Arabic. Can the authors provide the detailed advantages of their SERS substrates in the aspect of cost and fabrication processes compared to other reliable, simple and cheap SERS substrates such as nanocellulose-based SERS substrates with high performance (Sensors and Actuators B: Chemical 2018, 274, 30-36, Carbohydrate Polymers 2020, 235, 115956)?

We thank the reviewer for the comments.

Regarding the comment on the fabrication time, we understand the point of view of the reviewer. We described our fabrication method as ‘fast’ because we considered the

chips are consumables as they can be fabricated using mass production processes – and therefore only the time for the electrodeposition process was taken in consideration. To avoid any confusion, we have removed 'rapid' and replaced it by 'efficient': 'This electrochemical deposition is based on SiO_2/Si chips that were fabricated following standard photolithography process and can be mass produced in typical microelectronic foundries. Electrochemical method produces large area SERS substrate (40 μm x 20 μm) and requires less than 10 s for electrochemical deposition.....This is an environment friendly, efficient, high throughput and scalable method in comparison to other ways of fabricating SERS substrates.'

We addressed 'SERS sensors were fabricated on four-inch silicon wafer substrates with a 300 nm layer of thermally grown silicon dioxide as previously described.[1] 34 individual SiO_2/Si chips were produced on each silicon wafer, with a chip size 1 cm (width) x 1.7 cm (length) x 0.1 cm (thickness).' in experimental section in Microelectrode Fabrication on Si/SiO_2 chip part. And 'Considering SiO_2/Si chip fabrication allows mass production with high throughput, this electrodeposition process took only 10 seconds, the present approach was efficient, low cost, scalable and environmentally friendly.' in the result and discussion part.

We have added the comparison between different fabrication methods in the introduction part : 'SERS substrates are commonly fabricated through chemical synthesis,[2-3] electron beam (E-beam) lithography,[4] laser assisted fabrication or templating method.[5-7] For chemical methods, though size and morphology controllable nano particles are available, drop casting of the nano particles onto a substrate, paper, glass or silica, etc. is still required.[8-18] So that the distance between the nano particles is hard to control. This in turn leads to difficulties in quantification of target analytes, as

for quantification in SERS, data points for each analytes concentration for linear calibration are the sum average of more than three measurements in more than three locations on a SERS substrate. Another significant issue with the use of nanoparticles is that they are likely to be lifting or moving after application of analytes solvent, again resulting in quantification inaccuracy. Most research papers that reported on chemical synthesis fabrication methods for effective SERS substrates carry out experiments in a dry environment (i.e., the solution was dropped casted and allowed to dry) instead of in a water environment, with the drying time usually lasting for 30 minutes to one hour.[9-10, 12-13, 15] Besides of that, for some research using paper SERS substrate and chemical synthesized nano particles as effective SERS substrates, the background Raman signal from a paper substrate could affect the target analyte Raman signal readout. Laser assisted fabrication methods combining laser etching on glass/ silica substrate for nano pattern and followed by metal layer deposition, it has limited choices for the morphology nano patterns and plasmonic materials.[19-21] Templating method involves several steps and has higher fabrication failure possibility.[6, 22] These methods are either time consuming or involve complex steps. High throughput, low cost and reproducible fabrication of SERS substrates is still elusive.'

Specifically, for cheap paper based SERS substrate, as mentioned above, most of the papers published that are able to quantify analytes carry Raman experiments in a dry environment instead of in aqueous environment, see Table 1 below. Also, the LOD for paper based SERS substrates are usually at the μM level, as the nano gaps in between nano clusters is less controllable compared to electrochemical deposition method, and it is hard to achieve homogeneously distributed nm gaps. In terms of fabrication process, electrochemical deposition method has higher success rate comparing to chemical

synthesis methods, as it involves less chemical reactions, and does not required control over temperature.

Table 3 Paper SERS substrates performance in analytes quantification.

Paper SERS substrates	Analytes	LODs	Linear range	Testing Environment
Ag NPs on paper	Tetracycline in milk9	0.2 μM	0-2.25 M	Dry at room temperature
Ag NCs@SiO2/PMHS modified paper	Adenine13	1 nM	10-8 M-10-4 M	Dry naturally
Au NPs on paper	Thiram12	1 μM	10-6 M-10-4 M	Dry
Au NPs on paper	Methyl parathion15	0.011 μg/cm2	0.018 μg/cm2 to 0.354 μg/cm2	Dry
Ag NPs on paper	Adenine11	0.160 μM	0.5-20 μM	dried for 20 min at 80 °C
Ag NPs on biodegradable bacterial nanocellulose paper	Methomyl pesticide10	36 μM	10-2 to 5 × 10-7 M	complete evaporation of solvent
This work	2,4-D pesticides	1 pM	0.2 mM down to 1 pM	Test in 2,4-D solution directly

2. Authors should study the detection of other pesticides and compare the results of 2,4-D and others.

We thank the reviewer for this comment.

We focused our research on 2,4-D as there are few reports in the literature regarding its detection by SERS methods. These Ag-Gum Arabic (Ag-GA) SERS substrates were

designed for 2,4-D herbicides detection specifically. It is hard to detect 2,4-D directly using only Ag NPs (There is no adsorption between 2,4-D and silver). Unlike other SERS active molecules such as Methylene Blue[23] or 4-ATP,[24] the interaction between Ag NPs and 2,4-D are random physical contact and rather weak, which is challenging for quantification study - See Figure (A) below where three Raman measurements for 2,4-D detection on a Ag NPs SERS substrate at three different locations showed different spectra. A few research papers regarding 2,4-D detection by SERS were based on functionalized SERS substrate instead of detecting it directly by Ag NPs SERS substrates, (SERS substrates based on hollow Au@Ag nano-snowflake particles functionalized with 4-MBA/2,4-D antigen,[25] citrate functionalized AgNPs on cellulose paper,[26] silver NPs with molecular imprint polymers (MIP).[27] Particularly, SERS substrates based on well-ordered AuNPs inside mesostructured silica channels[28] have been used to detect 2,4-D, with the limit of detection (LOD) down to 0.79 ppt (parts per trillion) achieved.[28]), with an equilibrate time for 1 h and further centrifugation time needed. One research paper was published using rough Ag NPs SERS substrate (highly roughened surface flower-like Ag NPs.[29]), but this research detected 2,4-D in a dry environment with a drying time needed.

Rapid detection of 2,4-D is still a challenge without complex functionalization steps, and our research developed a SERS sensor that was able to detect 2,4-D down to 0.001 nM immediately in water environment.

Other pesticides have already been detected at trace level using a variety of functionalized and non-functionalized SERS substrates [30-32] and we do not believe we would advance on the current state of the art with the present methods.

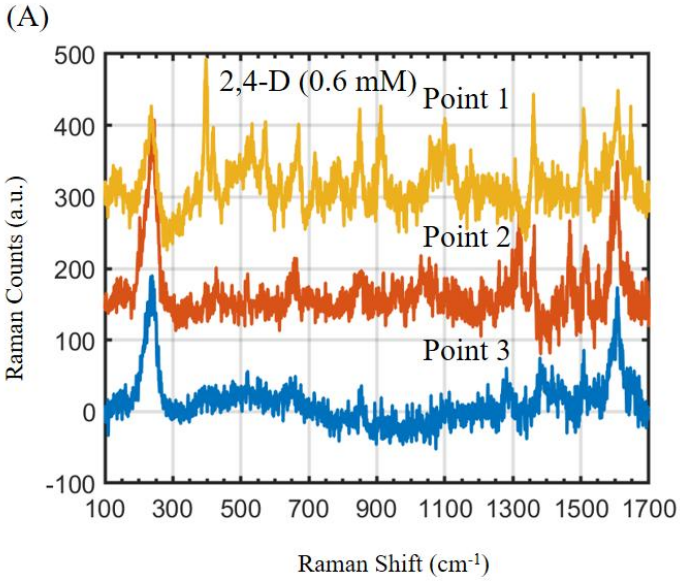

Figure A Spectra of uncoated Ag NPs SERS substrates at three locations for 2,4-D detection (1 pM).

3. How is the stability of the Ag-GA SERS substrate? Could the Ag-GA SERS substrate maintain the high sensitivity several months (days) after fabrication? Fabrication other environment? Isn't there the oxidation of Ag nanoparticles?

Ag NPs can be oxidized to Ag_2O because of oxygen and water in air.[33] One can initially think that a gum Arabic layer acts as a protective layer preventing oxidation. However, Gum Arabic is a micro porous polysaccharides layer that allows air to enter[34-35] and can also absorb water from the air[36]. This aqueous environment and porous structure can accelerate the oxidation of Ag NPs. Therefore, Ag-GA SERS substrate might not be stable without extra protection.

In this work, SERS substrates were freshly deposited prior to undertaking the Raman measurement for 2,4-D study. This was possible because of the short time it takes to prepare the SERS substrates.

Reviewer #3: The authors fabricated a Ag-Gum Arabic nanocluster-based SERS substrates using an electrochemical deposition method. The substrates could detect 2,4-D pesticide in water directly without sample pre-treatment with a detection limit of 1 pM. The detection in mineral or river water was also achieved. Before publication, the following concerns are needed to address.

(1) It is highly suggested to reconsider and highlight the advances of this work. In the introduction section, the authors concluded that the challenges or problems of the previous works included (i) an incubation time of more than 1 h, (ii) a pre-treatment step by mixing the solution with ethanol, or (iii) waiting time to allow 2,4-D solution to dry on the SERS substrate. The authors claimed "This is a time-saving, environment friendly, high throughput and scalable method in comparison to the other ways" based on the "fabrication method produces large area SERS substrate (40 μm x 20 μm) and requires less than 10 s, with 2 μL of a non-toxic solvent." However, the used photolithography and physical vapor deposition process for the substrate fabrication are time-consuming. Additionally, the achieved signal response needs 30 min for sample incubation before spectroscopy measurement.

We thank the reviewer for the comment. Regarding the comment on the fabrication time, we understand the point of view of the reviewer. We described our fabrication method as ‘ fast ’ because we considered the chips are consumables as they can be fabricated using mass production processes – and therefore only the time for the electrodeposition process was taken in consideration. To avoid any confusion, we have removed the mention of ‘rapid’ and replaced it by ‘efficient’.

We have also added the comparison between different SERS fabrication methods in the introduction part and highlighted the advantages of electrochemical deposition methods.

It should be noted that 30 minutes were needed for detection of very low concentration of 1 pM while 2,4-D at 0.1 nM concentration could be detected **immediately** - 0.1 nM is already below the Maximum Residue Limit for the EU legislation (which is 0.1 ppb).

(2) Figure 4 (A) is not clear to show the change of intensity. Moreover, based on the wide and nonuniform distribution of nanostructures shown in SME images, it's challenge to achieve a RSD about 10%.

We thank the reviewer for this comment. We have changed Figure 4 (A) from a black & white waterfall spectrum to a color waterfall spectra. So that the Raman intensity for each spectrum can be showed clearly.

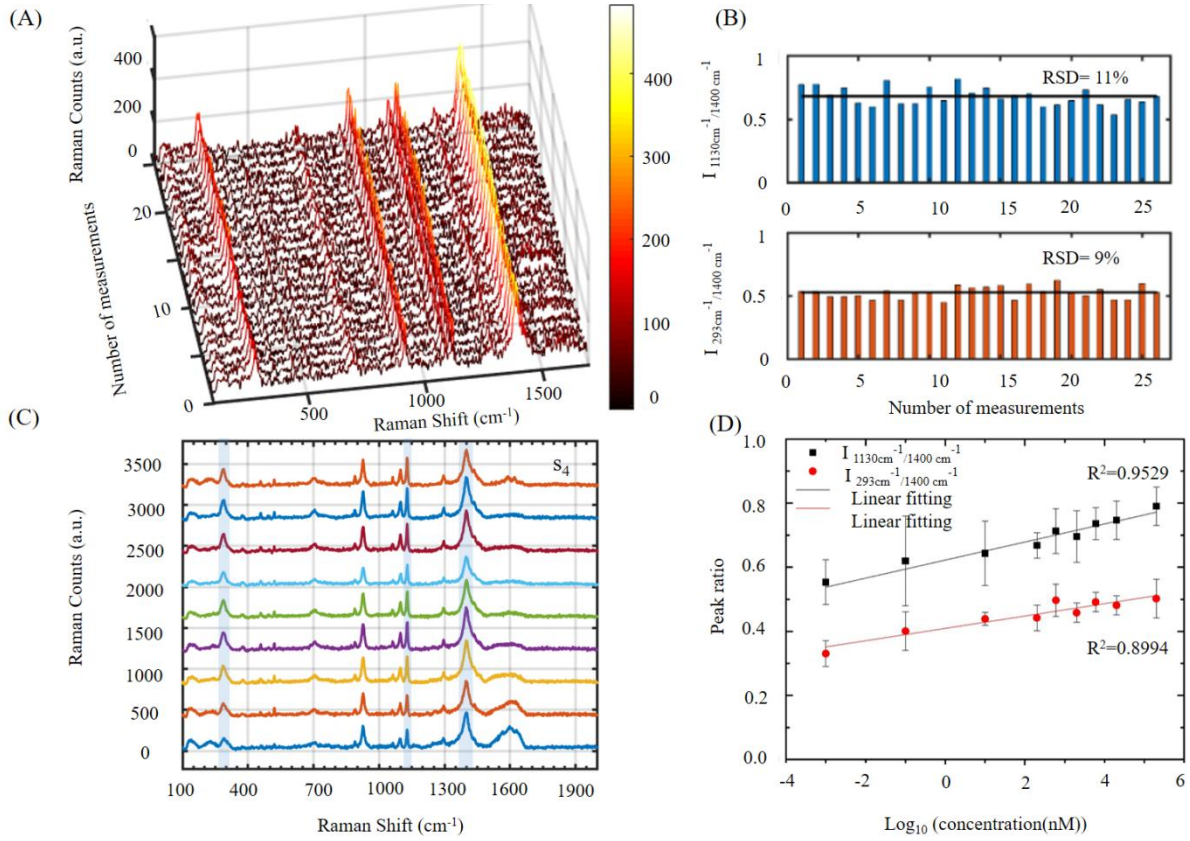

Figure 4 (A) Color waterfall spectra of 25 random points for 2 μM 2,4-D on a S_4 SERS substrate, the color bar stands for Raman intensity (a.u.). (B) Histogram of I_{293} cm^{-1} / I_{1400} cm^{-1}, I_{1130} cm^{-1} / I_{1400} cm^{-1} at 25 different random points; (C) Spectra of 2,4-D concentration from 1 pM to 0.2 mM, offset for clarity. (D) Linear fitting line for I_{1130} cm^{-1} / I_{1400} cm^{-1}, I_{293} cm^{-1} / I_{1400} cm^{-1} VS $\log_{10}$ (concentration) (in nM) for a S_4 substrate. The error bars were obtained from the standard deviation (SD) of ten measurements at random points.

For RSD value and linear calibration,

(1). Peak ratios (I_{1130} cm^{-1} / I_{1400} cm^{-1}, I_{293} cm^{-1} / I_{1400} cm^{-1}) were used rather than single peaks. With single peaks, RSD values were a bit higher than peak ratio values -

13%, 10%, 14% for I_{1130} cm^{-1}, I_{1400} cm^{-1}, and I_{293} cm^{-1} , respectively and 11% and 9 % for I_{1130} cm^{-1} / I_{1400} cm^{-1}, I_{293} cm^{-1} / I_{1400} cm^{-1}, respectively.

(2). As shown in Figure 2 (D), a false color map from SEM image for a structure 4 Ag-GA SERS substrate, with a scale bar five μm, the laser spot size is estimated to be one μm range and is marked in the false color map with a back circle and a '√' mark. Within this one μm area range, Ag NPs distribution is regarded as homogeneous, and the Raman signal is a statistic results gained from Ag NPs in this laser spot area. In conclusion, for each measurement at different SERS substrate locations within the laser spot size range (μm), the areas are homogeneous. Of course, we tried to avoid carrying out Raman measurements at the points where there was an obvious micro gap in between those nano clusters (one example of the obvious gaps are shown in deep blue color in false color map, with a circle and a 'X' mark).

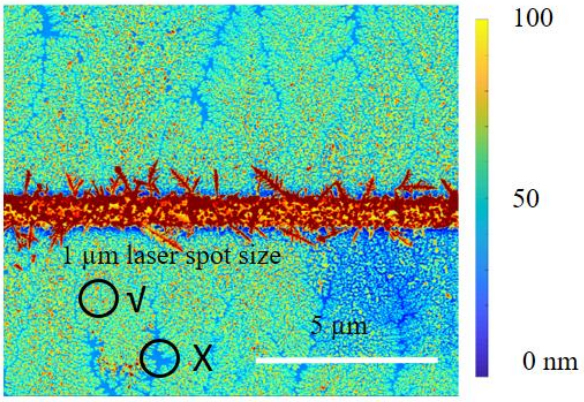

Figure 0.1 (D) False colour map from SEM image for structure four by Matlab, scale bar 5 μm; the color bar at 0 nm is the SiO_2/Si reference surface.

(3) More and clear discussion about the reason for the low slope in linear calibration is

suggested, especially considering the large error bars (it is not about error bar but the slope makes it looks big).

We thank the reviewer for this comment. We added the following discussion about the low slope: 'The error bars for $I_{1130\ cm\text{-}1}$ / $I_{1400\ cm\text{-}1}$ against the logarithm of the concentrations of the 2,4-D solutions linear fitting range from 4-14%, while the linear fitting for $I_{293\ cm\text{-}1}$ / $I_{1400\ cm\text{-}1}$ against the logarithm of the concentrations of the 2,4-D solutions linear fitting range from 2-6%. The adsorption of 2,4-D on the Gum Arabic surface is based on π-π interaction. According to the fitting results, 2,4-D concentration difference does not affect much this adsorption behavior in a time frame of 10 to 20 minutes. Standard addition methods could be used to determine the 2,4-D concentration in unknown samples.'

(4) Why used 3 steps of electrodeposition with different applied potentials?

We thank the reviewer for the comment. In this research, three steps were used mainly for structure 2 Ag-GA SERS substrate, while for structure 1, 3, 4, only two steps electrochemical deposition were used.

(1) First, two seconds at -0.2 V was used to initiate the mass transport boundary layer formation and for Ag-GA core formation.[37] (2) The second stage was for the growth of Ag-GA NPs, because of edge effect and large electric field, Ag-GA NPs formed on SiO_2/Si substrate; (this is the main step for Ag-GA SERS substrate growth as this step lasts longer (8 s) than the other steps (2 s)). And (3) the third stage with a larger voltage applied was intended to be used for changing Ag-GA NPs morphology and decorate Ag-GA NPs that has grown in step two.[38]

What we want to point out is that there are many possibilities to gain different Ag-GA NPs morphologies by applying different deposition parameters and the examples shown in this research paper were sufficient to realize 2,4-D detection reaching the EU restriction requirement.

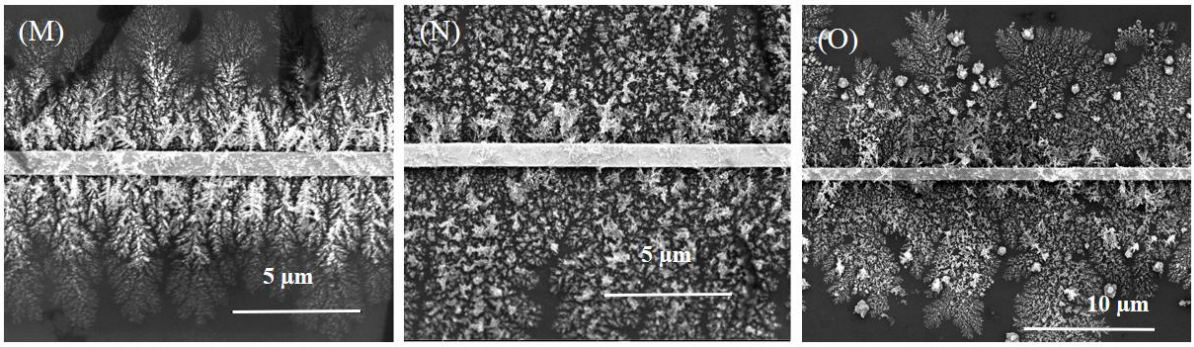

Figure 1: Different voltage combinations at the same concentration of $AgNO_3$ (5 mM) and Gum Arabic (2 g/L). (M) Combination 1: step1: -0.2 V, 2 s; step2: -0.5 V, 8 s; step3: -0.6 V, 2 s; (N) combination 2: step1: -0.2 V, 2 s; E_2: -0.8 V, 8 s; E_3: -1.2 V, 2 s; (O) combination 3: step1: -0.2 V, 2 s; step2: -1.2 V, 8 s; step3: -1.5 V, 2 s. $AgNO_3$: Gum Arabic=1:1 in all the experiments. All the nanostructures had been electrochemical deposited at least 3 times.

(5) Why deposition current went up with the time (under same applied potential)? Especially, the concentration of the Ag ions would decrease with the deposition, resulting in low and less growth of Ag nanostructures.

We thank reviewer for this comments. We agree that in a typical deposition experiment, the current should decrease due to mass transport limitations. However, in the present case, the Ag-GA NPs grows laterally over time under the strong electric field, towards region where there is no depletion of Ag ions. So that the current goes up with time (larger electrode and no diffusion limitation).

Besides, Gum Arabic is a conductive biopolymer.[39] This current increase also related to Ag-GA NPs nucleation and growth on Au electrode surface.[40] There were also Ag-GA nano branches grew on Au electrodes and they connected to the Au electrodes (as shown in Figure 2 (A-D) colored red). Those Ag-GA nano branches enlarged the Au electrode surface so that the total resistance of the electrode decreased, with the same voltage, the current increased.

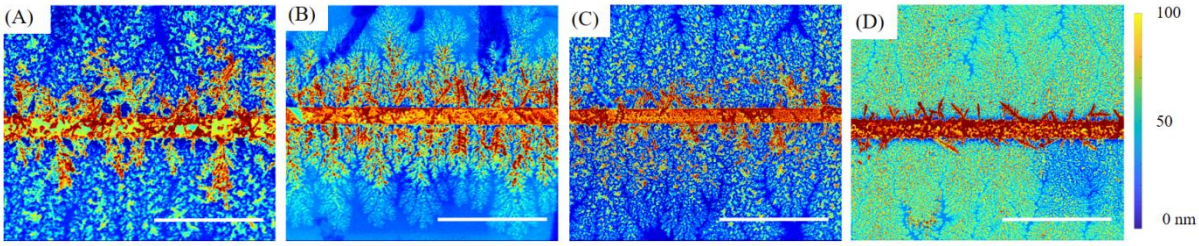

Figure 2 (A - D) False colour map from SEM image for structure one to structure four by Matlab, scale bar 5 μm; the color bar at 0 nm is the SiO_2/Si reference surface.

(6) It is highly suggested to check through the whole manuscript, for there are a lot of typo and format problems. For example, "514 nm Ag ion laser" on page 6; smaller font size for "Step 3: -0.6 V, 2s." in table 1 on page 11; "The mineral composition for the commercial mineral water is shown in table S3 in SI" on page 17 should be "…table S1"; "A direct comparison of the sensor developed herein with those reported in the literature is provided in SI Table 2 and Table 3" on page should be "…Table S2 and Table S3". In supporting information ,"Figure S3" should be "Figure S9" on Page 5 and 6; "Figure 12" should be "Figure S12"; "Table 1", "Table 2" and "Table 3" should be "Table S1", "Table S2" and "Table S3", respectively. Additionally, it is also need to modify and polish the format of the references and supporting information section.

We thank reviewer for this comments. We have gone through the whole manuscript and fixed the typo/format problems, and checked and polished the references

Reviewer #4: Authors prepared a large-area Ag-Gum Arabic nanocluster-based SERS substrates using electrochemical deposition method. The fabricated SERS substrates exhibit a limit of detection as low as 1pM for 2,4-D pesticide detection. However, the novelty and scientific discussion (such as SERS mechanism) of this manuscript is limited, and the review comments are as following:

1. Table 1, Table 2, Table 3 in supplement materials should be Table S1, Table S2, Table S3. And the caption for Figure S11 and Figure S12 could be revised with more detailed information.

We thank reviewer for this comments. We have changed the table label and added detailed information for Figure S11 and Figure S12.

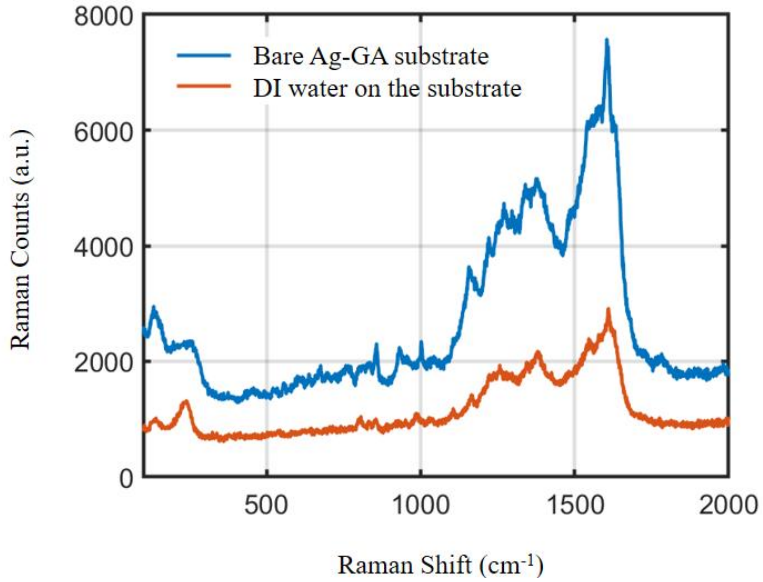

Figure S11 Spectra for the bare SERS substrate in air and the SERS substrate after applying DI water. For Ag-GA substrate, two broad peaks around 1400 cm^{-1} and 1600 cm^{-1} were showed. After application of DI water, Raman intensity (a.u.) of spectrum decrease from around 8000 to around 3000 because of water envoriment and the interaction between Gum Arabic and water.

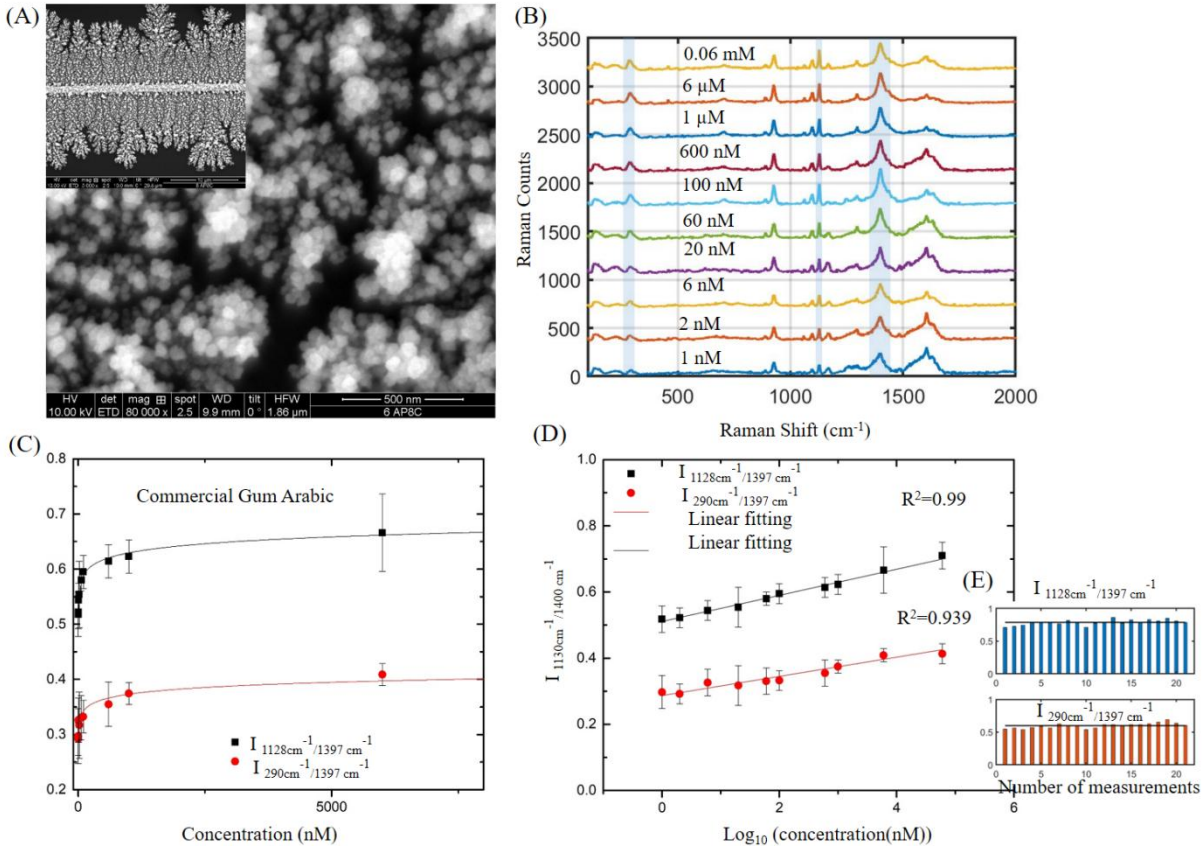

Figure S12 An Ag-GA SERS substrate that was deposited from commercial Gum Arabic for 2,4-D detection. The deposition parameters (-0.2 V, 2 s; -0.8 V, 8 s; -1.2 V, 2 s; 5 mM $AgNO_3$; 20 g/L Gum Arabic). (A) A SEM image for the Ag - GA nano structure; (B) Spectra of 2,4-D at different concentrations on SERS substrate from 1 nM to 0.06 mM. (C) logarithm trend for I_{1130} cm^{-1} / I_{1400} cm^{-1}, I_{293} cm^{-1} / I_{1400} cm^{-1} vs concentration (in nM); (D) Linear fitting for I_{1130} cm^{-1} / I_{1400} cm^{-1}, I_{293} cm^{-1} / I_{1400} cm^{-1} vs $\log_{10}$(concentration) (in nM); The linear relation between I_{1130} cm^{-1} / I_{1400} cm^{-1} (y) and $\log_{10}$ (concentration (in nM)) (x) was $y = 0.51 + 0.04*\log_{10}(x)$ with $R^2 = 0.99$. The linear relation between I_{290} cm^{-1} / I_{1400} cm^{-1} (y) and $\log_{10}$ (concentration (in nM)) (x) and was $y = 0.29 + 0.027*\log_{10}(x)$ with $R^2 = 0.939$. The error bar was from the standard deviation (SD) of ten measurements at random points on a SERS substrate. (E) The

reproducibility of the SERS substrate for 2,4-D at 1 μM at 20 different random points on a SERS substrate.

2. Electrochemical deposition method has been widely applied in SERS substrates fabrication, recent references could be introduced in the manuscripts. The novelty and scientific issues of this work should be further highlighted.

We thank reviewer for this comments, we have added other papers that also used electrochemical deposition method for SERS substrate fabrication, and we further highlighted the novelty and scientific issues.

Electrochemical methods allow morphology, size, nano gap controllable deposition of nano structures and are able to achieve high Enhancement Factor, a number of papers relate to deposition of metallic materials only. For instance, Xia, Y. et al. [41] synthesised Ag nanosheets with a nanogap smaller than 10 nm by environmentally friendly electrochemical deposition and this method achieved high reproducibility; [14] Wang, J. et al. used electrochemically roughened nano-Au film to detect environmental pollutant *p*-nitrophenol (PNP). Chen, S. et al. [42] prepared pyramid-shape silver nanostructures by electrochemical deposition as an effective and reusable SERS substrate. Zong, X. et al.[16] synthesized a gold nanostructure on microelectrodes in micro-chip by gold electroplating and used for SERS characterization by R6G. Cheng, ZQ.et al.[43] electrochemically synthesized branched metallic nanostructures and evaluated them by SERS using DTTCI as the analyte. Those researches demonstrated fabrication of effective SERS substrate by electrochemical method, but none of them used SERS substrates as an analytical sensor, until Dao, T. C. [44] used electrochemical

deposition of Ag nanoparticles on the Si surface to detect and quantify fungicide difenoconazole in dry environment with a LOD = 0.023 ppm (0.56 nM). In our work, we used electrodeposition of composite materials and show their SERS based sensing abilities towards 2,4–D.

3. In "Raman measurements" of "Experimental Section", the preparation process of SERS samples with probe molecules could be added.

Thank reviewer for the comments. The preparation of SERS samples with probe molecules refers to electrochemical deposition of Ag-GA NPs SERS substrate in this research paper; this has been discussed in 'Synthesis of Gum Arabic Coated Ag (Ag-GA) nanoclusters' in 'Experimental section'. Moreover, operation for 2,4-D detection for Raman measurements has been described in 'Raman measurements' also in 'Experiment Section'.

4. The advantages of Gum Arabic on SERS enhancement and 2,4-D pesticide detection is less discussed in the manuscript, compared with other synthesis or substrates. In addition, more detailed discussions on SERS mechanism are suggested.

Thank reviewer for the comments. This SERS sensor is designed for 2,4-D detection, comparing to other SERS platforms for 2,4-D detection, there is a discussion in Introduction part: 'Because of the simplicity of operation and sensitivity in detection, SERS has been used for trace detection of 2,4-D pesticides[45] including: SERS substrates based on hollow Au@Ag nano-snowflake particles functionalized with 4-MBA/2,4-D

antigen,[25] citrate functionalized AgNPs on cellulose paper,[26] silver NPs with molecular imprint polymers (MIP),[27] highly roughened surface flower-like Ag NPs.[29] Particularly, SERS substrates based on well-ordered AuNPs inside mesostructured silica channels[28] have been used to detect 2,4-D, with the limit of detection (LOD) down to 0.79 ppt (parts per trillion) achieved.[28] These methods require either (i) an incubation time of more than 1 h, (ii) a pre-treatment step by mixing the solution with ethanol, or (iii) waiting time to allow 2,4-D solution to dry on the SERS substrate. To rapid determine pesticides such as 2,4-D directly in water samples without any pre-treatment remains a key challenge. ’

We added more detailed discussion for the reason of using Gum Arabic in the Introduction part: ‘Gum Arabic was selected as it is a branched hetero-polysaccharide containing protein and carbohydrate groups, which is a biodegradable, nontoxic, and easily available biopolymer.[46-47] It has been used to act as a biopolymer for removal of heavy metal,[48] pesticides and pollutants in polluted water bodies,[49-50] because of its great adsoption ability towards different chemicals.[51]……Gum Arabic is a conductive biopolymer which is also widely used as raw material for composite conductive materials studies.[39, 52] Besides, its viscosity changes significantly as the change of Gum Arabic solution concentration, this property allow it act as an shape monitoring agent in Ag NPs electrochemical deposition.’

We also added more detailed discussion about SERS mechanism in introduction part: ‘Surface Enhanced Raman Spectroscopy is an ultra-sensitive technology that is capable of providing a spectral fingerprint of the analytes under investigation. SERS is mostly based on the enhanced Raman signal by noble metallic nano structures that can generate strong electromagnetic field with the excitation at certain laser wavelength, such as Ag,

Au and Cu, which also named as Localized Surface Plasmon Resonance (LSPR).[53-54] The excited LSPR generates a large electric field on the surface and this electric field induces dipole moments in a molecule on the surface of nanostructures, and gains an enhanced Raman signal. This strong, localized electromagnetic fields present in nano-gaps between nanostructures are known as “hot spots”.[55] The enhanced Raman signal are from electromagnetic enhancement[56] and chemical enhancement,[57] electromagnetcial enhancement contributes to 10^{11}-10^{13} magnitude of SERS signal while chemical enhancement contributes only a factor of 10^2 for Raman enhancement.[58] The magnitude of the SERS enhancement depends on the morphology,[59] the size of the metallic nano particles,[60] the gap size between the metallic nano particles,[61] the measurement environment, as well as the wavelength of the laser excitation source.[62-65]’

5. It is mentioned in Page 10 that "by adjusting the concentration of AgNO3 and Gum Arabic in the solution as well as the electrochemical deposition parameters such as applied voltage and deposition time, it is possible to engineer the size and morphology of the Ag-GA nano structures and the nano gap patterns in between the nano clusters." Optimization details are in supplement materials. But how to select the optimized SERS substrate for 2,4-D pesticide detection via morphology manipulation? Since size, gap and density might influence the SERS enhancement in complicate way. Corresponding SERS measurements are suggested to support the conclusion.

We thank the reviewer for the comment. As stated in the SERS mechanism introduction section: ‘The magnitude of the SERS enhancement depends on the morphology,[59] the size of the metallic nano particles,[60] the gap size between the metallic nano particles,[61] the measurement environment, as well as the wavelength of the laser

excitation source.[62-65]' Having nano particle and nano gap, is enough to gain enhanced signal. However, when it comes to quantification, SERS substrates have to be homogeneous in a μm range both for nano particles and nano gaps. Because: 'as in quantification steps, data points for each analytes concentration for linear calibration are the sum average of more than three measurements in more than three different SERS substrate locations'. We have added 'homogeneously distributed' in the manuscript: 'The homogeneously distributed, high density of nanostructures and nano gaps made these substrates good candidates for SERS applications' in Electrodeposition process and sample characterization part.

We show in this research in SI Figure S9 and Figure 1 below, how $AgNO_3$ concentration, Gum Arabic concentration, and deposition time and voltage affect the deposition results: 'When the concentration of Gum Arabic larger than 3 g/L, the silver nano particles tend to aggregate, while when the concentration of Gum Arabic was below 3 g/L, the silver nano clusters distributed separately on the SiO_2/Si substrate with nano gap forming in between the silver nano clusters'. 'the deposition time increased, the nano dendrites grow bigger', 'At higher voltage combination (combination 3: step1: -0.2 V, 2 s; step2: -1.2 V, 8 s; step3: -1.5 V, 2 s), irregular growth of the Ag-GA particles occurs, this inhomogeneous growth of Ag-GA particles resulted in dramatically different Raman signal at different points during the 2,4-D detection process. In this electrochemical platform, a voltage below 1.2 V was used.' The trend for how those deposition parameters could affect Ag-GA NP formation is show in Figure 2 below. Based on those trends, we could carefully chose parameters that allow 'the homogeneously distributed, high density of nanostructures and nano gaps'

formation. At the same time, we avoided parameters that lead to irregular aggregation of Ag NPs, which are not suitable for SERS quantification.

Four structures S_1, S_2, S_3, S_4 were chosen and the detection results are compared in table 2 below. The selection of Ag-GA nano structure was based on: response time at certain 2,4-D concentration and the lowest concentration the SERS substrate can detect. In the end., Structure 4 was chosen for more detailed study in the manuscript as it had faster response time.

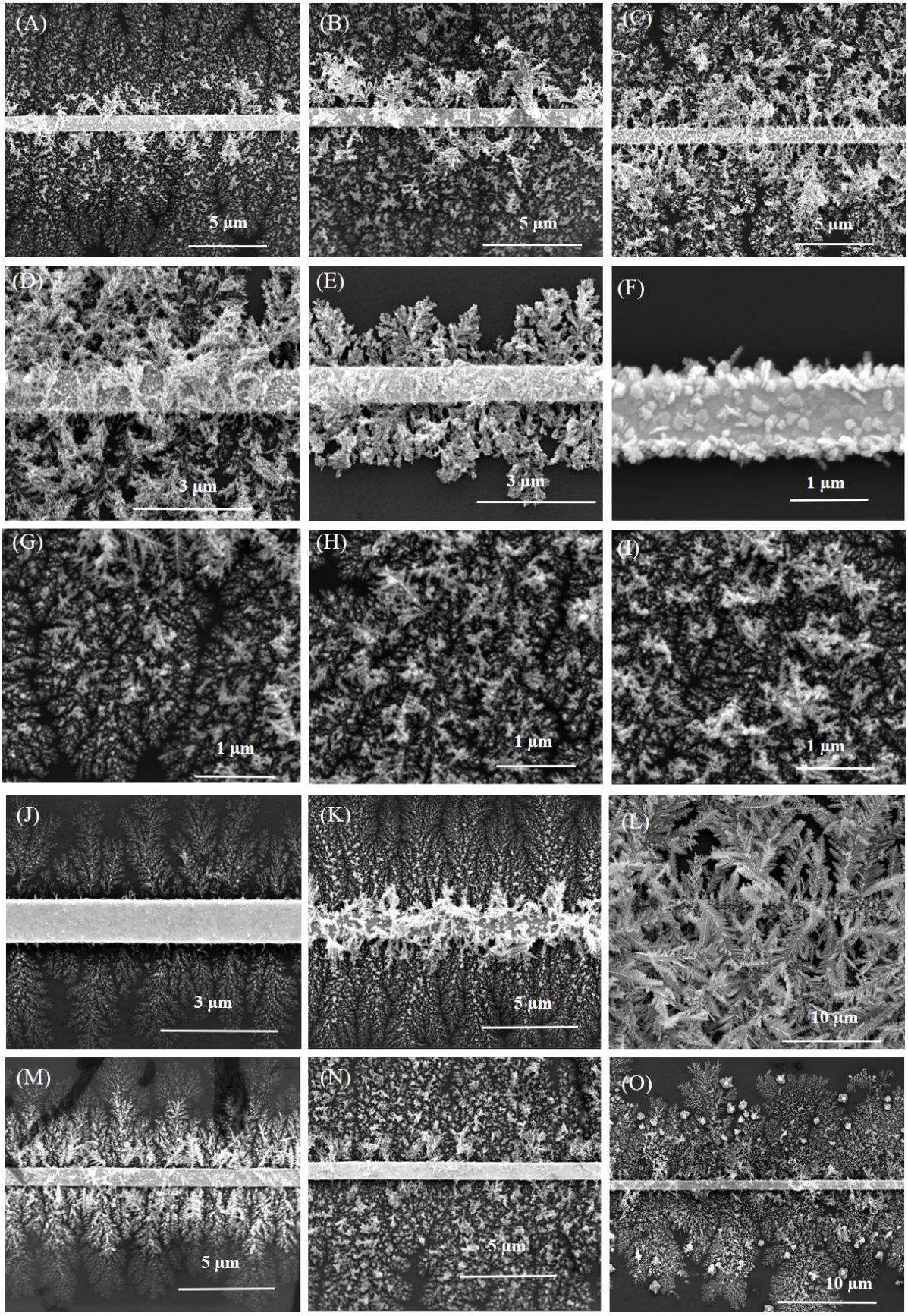
(A)
5 µm
(B)
5 µm
(C)
5 µm
(D)
3 µm
(E)
3 µm
(F)
1 µm
(G)
1 µm
(H)
1 µm
(I)
1 µm
(J)
3 µm
(K)
5 µm
(L)
10 µm
(M)
5 µm
(N)
5 µm
(O)
10 µm

Figure 1: SEM images of different deposition parameters. (A)(B)(C)(D)(E): different Gum Arabic concentration: 1 g/L, 2 g/L, 3 g/L, 10 g/L, 100 g/L; (F) deposition voltage at -0.2 V, 2 s; (G)(H)(I) E: -0.8 V, different deposition time: 8 s, 12 s, 16 s; (J)(K)(L) different $AgNO_3$ concentrations: 1 mM, 5 mM, 0.05 M. (M)(N)(O) different voltage settings which effected the growth pattern of the nano gaps. $AgNO_3$: Gum Arabic=1:1 in all the experiments. All the nanostructures had been electrochemical deposited at least 3 times.

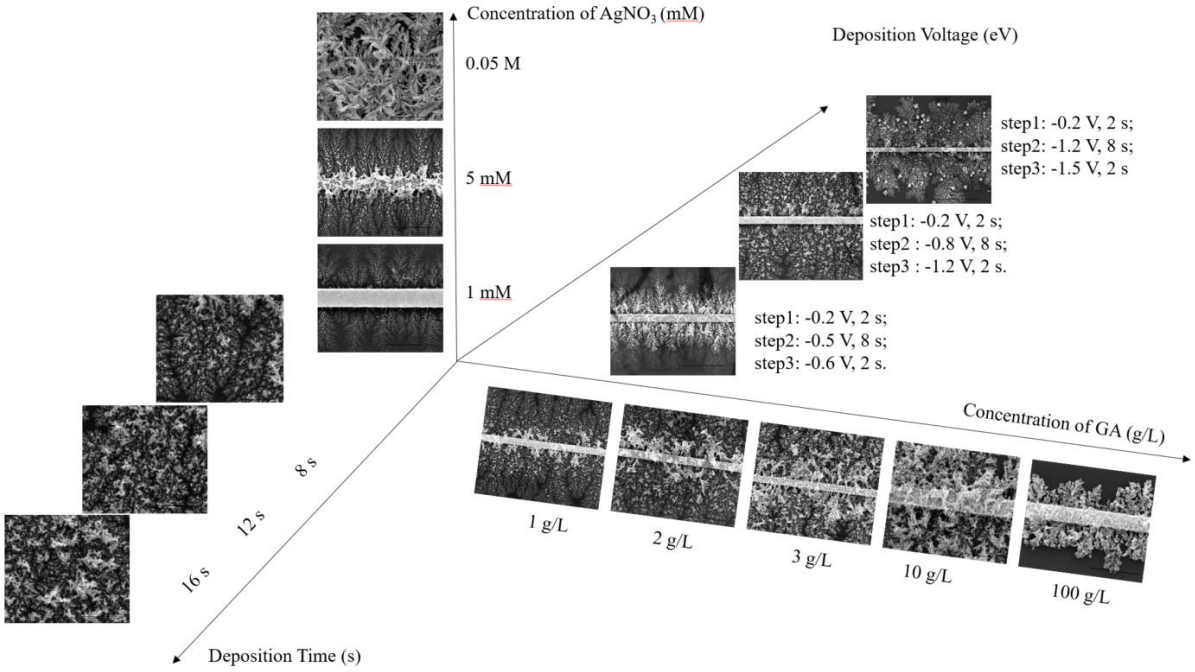

Figure 2 The trend for how those deposition parameters could affect Ag-GA NP deposition.

Table 4 Comparison between the four SERS substrates for 2,4-D detection.

Comparisons	LOD in 30 minutes response time	Response time for 0.1 nM
Structure 1	0.1 nM	30 minutes

Structure 2	0.1 nM	30 minutes
Structure 3	0.1 nM	30 minutes
Structure 4	0.001 nM	Immediately

6. In Page 12 "Gum Arabic polymer layers helped to provide stable SERS signal and facilitated 2,4-D detection using Raman spectroscopy", experimental evidences should be provided.

'Stable' means 'repeatable'. In order not to confuse readers, we changed the word 'stable' to 'repeatable' in the manuscript, and added 'helped to capture 2,4-D' in that sentence. The repeatability study for 2,4-D study using Ag-GA SERS substrate on 20 different random points at concentration of 2 μM actually showed that this SERS substrate provide repeatable SERS signal for 2,4-D detection. See Figure 4 (A-B) in manuscript or Figure blow. In addition, we explained in that paragraph in page 14-15 that : It consists of polysaccharides rich in galactose and arabinose, and a small protein fraction associated with these polysaccharides, see SI Figure S10, and contains a large amount of -OH, -O-, and -CH bonds as well as a small portion of $–NH_2$ and –SH group associated with the protein.[66] Such functional groups may attract 2,4-D to the surface of the Ag-GA nano particles, through hydrogen bonding between -OH / -O- group on Ag-GA surface and the halogen (-Cl) group in 2,4-D moleculars, or π-π interactions between –CH and the benzene ring of 2,4-D.[67], which is why 'Gum Arabic polymer layers **helped to capture 2,4-D** to provide **repeatable** SERS signal and facilitated 2,4-D detection using Raman spectroscopy.'

Combining the data shown in question 9, Ag NPs SERS substrates were not able to provide stable SERS signal as 2,4-D does not have stable interaction with Ag surface.

Instead, Gum Arabic layer is able to capture 2,4-D through π-π interaction and provide repeatable SERS signal, this '**facilitated**' 2,4-D detection.

Furthermore, research papers published about quantitatively detecting 2,4-D mostly used functionalized Ag NPs SERS substrates instead of using Ag NPs directly, except one paper used highly roughed Ag NPs to detect 2,4-D in a dry environment. We also discussed about the drawback of those methods. This has been introduced in the Introduction part: 'Because of the simplicity of operation and sensitivity in detection, SERS has been used for trace detection of 2,4-D pesticides[45] including: SERS substrates based on hollow Au@Ag nano-snowflake particles functionalized with 4-MBA/2,4-D antigen,[25] citrate functionalized AgNPs on cellulose paper,[26] silver NPs with molecular imprint polymers (MIP),[27] highly roughened surface flower-like Ag NPs.[29] Particularly, SERS substrates based on well-ordered AuNPs inside mesostructured silica channels[28] have been used to detect 2,4-D, with the limit of detection (LOD) down to 0.79 ppt (parts per trillion) achieved.[28] These methods require either (i) an incubation time of more than 1 h, (ii) a pre-treatment step by mixing the solution with ethanol, or (iii) waiting time to allow 2,4-D solution to dry on the SERS substrate. To quickly determine pesticides such as 2,4-D directly in water samples without any pre-treatment remains a key challenge.' This further proves the Ag-GA SERS substrate presented in this research paper 'facilitated' 2,4-D detection.

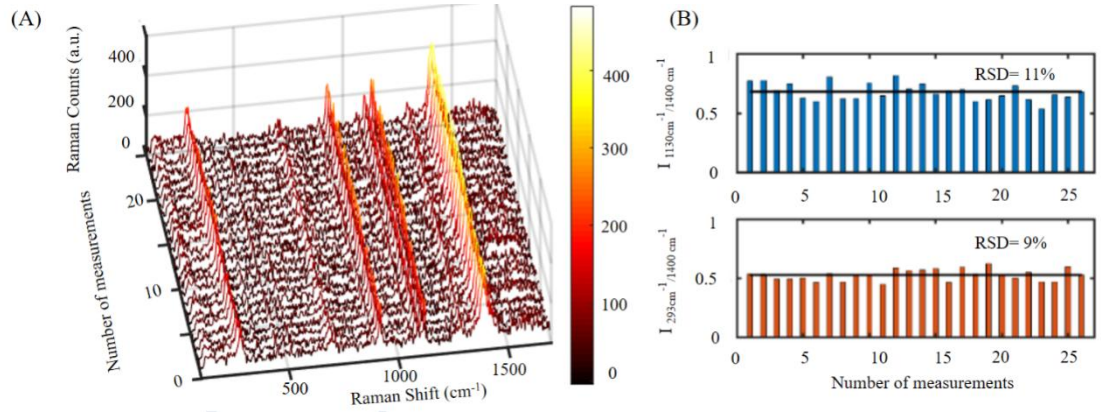

Figure 0.2 (A) Color waterfall spectra of 25 random points for 2 μM 2,4-D on S_4 SERS substrate, the color bar stands for Raman intensity. (B) Histogram of I_{293} cm^{-1} / I_{1400} cm^{-1}, I_{1130} cm^{-1} / I_{1400} cm^{-1} at 25 different random points;

7. In Page 14, it is mentioned that "it was observed that structures S1, S2, S3 were able to detect 0.1 nM (0.0221 ppb) 2,4-D in 30 min; while structure S4 was able to detect as low as 1 pM (0.221 ppt) 2,4-D in the same time frame", corresponding spectra data are not found? Also, a brief explanation on the differences is needed.

We thank the reviewer for the comments. We added spectra for S1, S2 and S3 for 2,4-D detection at 0.1 nM after 30 minutes in SI Figure S12 (reproduced below) to support this statement. While for S4, the spectrum is shown in Figure 3 (B).

There was a brief explanation in the manuscript on the difference: 'The better sensing capabilities of S_4 could be attributed to the morphology and size difference of the Ag-GA nano particles.[60, 68-69]'. We added a few more sentences to explained this: 'As SERS enhancement factor depends on the morphology, size of plasmonic structures, as well as the gap in between those plasmonic structures. Also it depends on the adsorption ability and total adsorption amount towards targeted analytes from SERS substrates. Thus, the nano particles density in one laser spot area also contribute to this detection ability

difference for these four structures.[70] Apart from the morphology and nano particles size difference, S_4 has higher Ag-GA NPs density and narrower nano gap in between nano clusters comparing to the other three, observing from color maps in **Error! Reference source not found.** (A-D).'

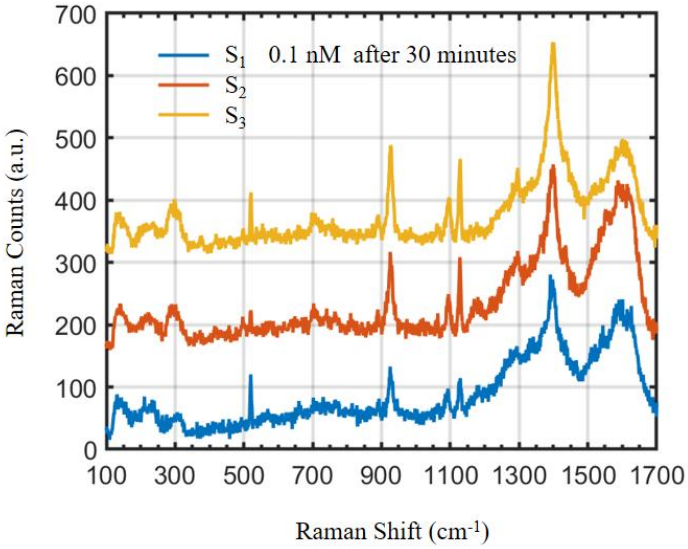

Figure S12 Structure 1, 2 and 3 were able to detect 2,4-D at 0.1 nM after 30 minutes.

8. In "Linear calibration for 2,4-D detection in DI water" section, "The peak ratio I293 cm-1 / I1400 cm-1, I1130 cm-1 / I1400 cm-1 were studied as those peak ratios exhibited a good linear response towards different concentration of 2,4-D." What is the theoretical reason or basis for choosing these peak ratios for linear calibration, except for their linear response?

We thank the reviewer for the comment. We added this discussion in the manuscript : 'While the single peaks intensity $I_{293\ cm\text{-}1}$, $I_{1130\ cm\text{-}1}$, $I_{1400\ cm\text{-}1}$ change with the change of

2,4-D concentrations are show in SI Figure S13, peak 1400 cm^{-1} kept constant with the 2,4-D concentration change, and the R^2 value of the fitting results for $I_{293\ cm-1}$ and $I_{1130\ cm-1}$ against the logarithm of the concentrations of the 2, 4-D solutions were 0.5977 and 0.7366, which is not as good as using peak ratio $I_{293\ cm-1}$ / $I_{1400\ cm-1}$, $I_{1130\ cm-1}$ / $I_{1400\ cm-1}$. Peak 1400 cm^{-1} could be a characteristic peak for Gum Arabic layer,[71] while peaks at 1130 cm^{-1} and 293 cm^{-1} are for 2,4-D, using peak at 1400 cm^{-1} as a reference peak gain a better fitting results.' as shown in Figure 4 (D). This method has also been used in other papers.[72-73]

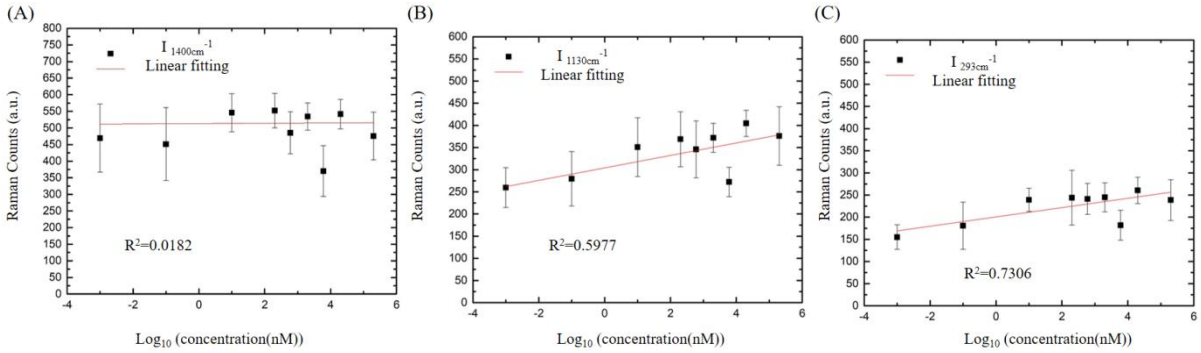

Figure S13: the single Raman peak intensity change (A) $I_{1400\ cm-1}$, (B) $I_{1130\ cm-1}$, (C) $I_{293\ cm-1}$ with the change of the logarithm of the concentrations of the 2, 4-D solutions.

9. "The adsorption of 2,4-D on the gum Arabic surface based on π-π interaction during measurements" is mentioned in Page 17, is there any adsorption or interaction between 2,4-D and Ag?

Additional experiments using pure Ag NPs SERS substrate were undertaken. Figure (A) below shows the Raman spectra after applying 2,4-D solution at 0.6 mM, at three different location. As can be seen, three different spectra were obtained, which makes

2,4-D quantification impractical. For quantification, the SERS signal should be repeatable at different locations on a SERS substrate. This is probably because the surface energy of Ag NPs and 2,4-D do not match with each other to have active physical contact. While one research paper used non functionalised Ag nano structure to detect 2,4-D,[29] they measurement was carried out in the dry and therefore adsorption happened upon solvent evaporation.

To conclude, from this experiment demonstration, there is no adsorption between 2,4-D and silver. Unlike other SERS active molecules such as Methylene Blue[23] or 4-ATP,[24] the interaction between Ag NPs and 2,4-D are random physical contact and rather weak.

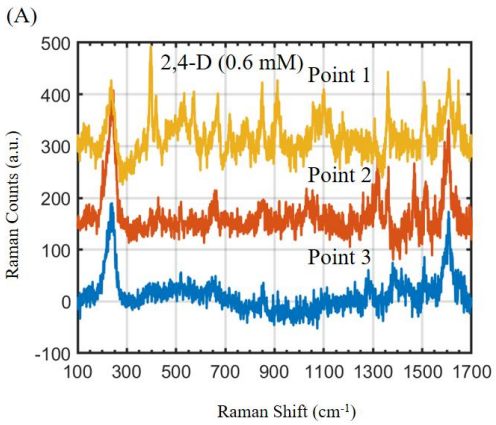

Figure (A) Raman spectra after applying 2,4-D solution at 0.6 mM on a Ag NPs SERS substrate, at three different locations.

Reference.

1. Seymour, I.; O'Sullivan, B.; Lovera, P.; Rohan, J. F.; O'Riordan, A., Elimination of Oxygen Interference in the Electrochemical Detection of Monochloramine, Using In Situ pH Control at Interdigitated Electrodes. *ACS Sensors* **2021,** *6* (3), 1030-1038.

2. Joseph, D.; Kwak, C. H.; Huh, Y. S.; Han, Y.-K., Synthesis of AuAg@Ag core@shell hollow cubic nanostructures as SERS substrates for attomolar chemical sensing. *Sensors and Actuators B: Chemical* **2019,** *281*, 471-477.

3. Medetalibeyoglu, H.; Kotan, G.; Atar, N.; Yola, M. L., A novel sandwich-type SERS immunosensor for selective and sensitive carcinoembryonic antigen (CEA) detection. *Analytica Chimica Acta* **2020,** *1139*, 100-110.

4. Petti, L.; Capasso, R.; Rippa, M.; Pannico, M.; La Manna, P.; Peluso, G.; Calarco, A.; Bobeico, E.; Musto, P., A plasmonic nanostructure fabricated by electron beam lithography as a sensitive and highly homogeneous SERS substrate for bio-sensing applications. *Vibrational Spectroscopy* **2016,** *82*, 22-30.

5. Shi, G.; Wang, M.; Zhu, Y.; Yan, X.; Pan, S.; Zhang, A., Nanoflower-like Ag/AAO SERS platform with quasi-photonic crystal nanostructure for efficient detection of goat serum. *Current Applied Physics* **2019,** *19* (11), 1276-1285.

6. Creedon, N. C.; Lovera, P.; Furey, A.; O'Riordan, A., Transparent polymer-based SERS substrates templated by a soda can. *Sensors and Actuators B: Chemical* **2018,** *259*, 64-74.

7. Lovera, P.; Creedon, N.; Alatawi, H.; Mitchell, M.; Burke, M.; Quinn, A. J.; O'Riordan, A., Low-cost silver capped polystyrene nanotube arrays as super-hydrophobic substrates for SERS applications. *Nanotechnology* **2014,** *25* (17), 175502.

8. Jiang, T.; Wang, X.; Tang, S.; Zhou, J.; Gu, C.; Tang, J., Seed-mediated synthesis and SERS performance of graphene oxide-wrapped Ag nanomushroom. *Scientific Reports* **2017,** *7* (1), 9795.

9. Marques, A.; Veigas, B.; Araújo, A.; Pagará, B.; Baptista, P. V.; Águas, H.; Martins, R.; Fortunato, E., Paper-Based SERS Platform for One-Step Screening of Tetracycline in Milk. *Scientific Reports* **2019,** *9* (1), 17922.

10. Parnsubsakul, A.; Ngoensawat, U.; Wutikhun, T.; Sukmanee, T.; Sapcharoenkun, C.; Pienpinijtham, P.; Ekgasit, S., Silver nanoparticle/bacterial nanocellulose paper composites for paste-and-read SERS detection of pesticides on fruit surfaces. *Carbohydrate Polymers* **2020,** *235*, 115956.

11. Rajapandiyan, P.; Yang, J., Photochemical method for decoration of silver nanoparticles on filter paper substrate for SERS application. *Journal of Raman Spectroscopy* **2014,** *45* (7), 574-580.

12. Siebe, H. S.; Chen, Q.; Li, X.; Xu, Y.; Browne, W. R.; Bell, S. E. J., Filter paper based SERS substrate for the direct detection of analytes in complex matrices. *Analyst* **2021,** *146* (4), 1281-1288.

13. Tegegne, W. A.; Su, W.-N.; Beyene, A. B.; Huang, W.-H.; Tsai, M.-C.; Hwang, B.-J., Flexible hydrophobic filter paper-based SERS substrate using silver nanocubes for sensitive and rapid detection of adenine. *Microchemical Journal* **2021,** *168*, 106349.

14. Wang, J.; Qiu, C.; Mu, X.; Pang, H.; Chen, X.; Liu, D., Ultrasensitive SERS detection of rhodamine 6G and p-nitrophenol based on electrochemically roughened nano-Au film. *Talanta* **2020,** *210*, 120631.

15. Xie, J.; Li, L.; Khan, I. M.; Wang, Z.; Ma, X., Flexible paper-based SERS substrate strategy for rapid detection of methyl parathion on the surface of fruit. *Spectrochimica Acta Part A: Molecular and Biomolecular Spectroscopy* **2020,** *231*, 118104.

16. Zong, X.; Zhu, R.; Guo, X., Nanostructured gold microelectrodes for SERS and EIS measurements by incorporating ZnO nanorod growth with electroplating. *Scientific Reports* **2015,** *5* (1), 16454.

17. Tezcan, T.; Hsu, C.-H., High-sensitivity SERS based sensing on the labeling side of glass slides using low branched gold nanoparticles prepared with surfactant-free synthesis. *RSC Advances* **2020,** *10* (56), 34290-34298.

18. Zhang, J.; He, L.; Chen, P.; Tian, C.; Wang, J.; Liu, B.; Jiang, C.; Zhang, Z., A silica-based SERS chip for rapid and ultrasensitive detection of fluoride ions triggered by a cyclic boronate ester cleavage reaction. *Nanoscale* **2017,** *9* (4), 1599-1606.

19. Liu, X.; Lebedkin, S.; Besser, H.; Pfleging, W.; Prinz, S.; Wissmann, M.; Schwab, P. M.; Nazarenko, I.; Guttmann, M.; Kappes, M. M.; Lemmer, U., Tailored Surface-Enhanced Raman Nanopillar Arrays Fabricated by Laser-Assisted Replication for Biomolecular Detection Using Organic Semiconductor Lasers. *ACS Nano* **2015,** *9* (1), 260-270.

20. Hoffmann, M.; Wackerow, S.; Abdolvand, A.; Zolotovskaya, S. A., High performance SERS platforms via parametric optimization of the laser-assisted photodeposition of silver and gold nanoparticles. *Opt. Mater. Express* **2021,** *11* (9), 3079-3098.

21. MacKenzie, M.; Chi, H.; Varma, M.; Pal, P.; Kar, A.; Paterson, L., Femtosecond laser fabrication of silver nanostructures on glass for surface enhanced Raman spectroscopy. *Scientific Reports* **2019,** *9* (1), 17058.

22. Sammi, H.; Nair, R. V.; Sardana, N., Recent advances in nanoporous AAO based substrates for surface-enhanced raman scattering. *Materials Today: Proceedings* **2021,** *41*, 843-850.

23. Vu, X. H.; Dien, N. D.; Ha Pham, T. T.; Trang, T. T.; Ca, N. X.; Tho, P. T.; Vinh, N. D.; Van Do, P., The sensitive detection of methylene blue using silver nanodecahedra prepared through a photochemical route. *RSC Advances* **2020,** *10* (64), 38974-38988.

24. Zhang, L.; Weng, Y.-j.; Liu, X.; Gu, W.; Zhang, X.; Han, L., Fe(III) Mixed IP6@Au NPs with Enhanced SERS Activity for Detection of 4-ATP. *Scientific Reports* **2020,** *10* (1), 5752.

25. Xu, Y.; Kutsanedzie, F. Y. H.; Hassan, M. M.; Zhu, J.; Li, H.; Chen, Q., Functionalized hollow Au@Ag nanoflower SERS matrix for pesticide sensing in food. *Sensors and Actuators B: Chemical* **2020,** *324*, 128718.

26. Hassan, M. M.; Jiao, T.; Ahmad, W.; Yi, X.; Zareef, M.; Ali, S.; Li, H.; Chen, Q., Cellulose paper-based SERS sensor for sensitive detection of 2,4-D residue levels in tea coupled uninformative variable elimination-partial least squares. *Spectrochimica Acta Part A: Molecular and Biomolecular Spectroscopy* **2021,** *248*, 119198.

27. Hua, M. Z.; Feng, S.; Wang, S.; Lu, X., Rapid detection and quantification of 2,4-dichlorophenoxyacetic acid in milk using molecularly imprinted polymers–surface-enhanced Raman spectroscopy. *Food Chemistry* **2018,** *258*, 254-259.

28. Xu, Y.; Kutsanedzie, F. Y. H.; Hassan, M.; Zhu, J.; Ahmad, W.; Li, H.; Chen, Q., Mesoporous silica supported orderly-spaced gold nanoparticles SERS-based sensor for pesticides detection in food. *Food Chemistry* **2020,** *315*, 126300.

29. Hassan, M. M.; Zareef, M.; Jiao, T.; Liu, S.; Xu, Y.; Viswadevarayalu, A.; Li, H.; Chen, Q., Signal optimized rough silver nanoparticle for rapid SERS sensing of pesticide residues in tea. *Food Chemistry* **2021,** *338*, 127796.

30. Wei, W.; Du, Y.; Zhang, L.; Yang, Y.; Gao, Y., Improving SERS hot spots for on-site pesticide detection by combining silver nanoparticles with nanowires. *Journal of Materials Chemistry C* **2018,** *6* (32), 8793-8803.

31. Pham, T. B.; Hoang, T. H. C.; Pham, V. H.; Nguyen, V. C.; Nguyen, T. V.; Vu, D. C.; Pham, V. H.; Bui, H., Detection of Permethrin pesticide using silver nano-dendrites SERS on optical fibre fabricated by laser-assisted photochemical method. *Scientific Reports* **2019,** *9* (1), 12590.

32. Zhang, D.; Liang, P.; Ye, J.; Xia, J.; Zhou, Y.; Huang, J.; Ni, D.; Tang, L.; Jin, S.; Yu, Z., Detection of systemic pesticide residues in tea products at trace level based on SERS and verified by GC–MS. *Analytical and Bioanalytical Chemistry* **2019,** *411* (27), 7187-7196.

33. Mikhlin, Y. L.; Vishnyakova, E. A.; Romanchenko, A. S.; Saikova, S. V.; Likhatski, M. N.; Larichev, Y. V.; Tuzikov, F. V.; Zaikovskii, V. I.; Zharkov, S. M., Oxidation of Ag nanoparticles in aqueous media: Effect of particle size and capping. *Applied Surface Science* **2014,** *297*, 75-83.

34. Humphreys, M. R.; Castle, E. P.; Andrews, P. E.; Gettman, M. T.; Ereth, M. H., Microporous polysaccharide hemospheres for management of laparoscopic trocar injury to the spleen. *The American Journal of Surgery* **2008,** *195* (1), 99-103.

35. Li, M.; Li, H.; Li, X.; Zhu, H.; Xu, Z.; Liu, L.; Ma, J.; Zhang, M., A Bioinspired Alginate-Gum Arabic Hydrogel with Micro-/Nanoscale Structures for Controlled Drug Release in Chronic Wound Healing. *ACS Applied Materials & Interfaces* **2017,** *9* (27), 22160-22175.

36. White, P. B.; Wang, T.; Park, Y. B.; Cosgrove, D. J.; Hong, M., Water–Polysaccharide Interactions in the Primary Cell Wall of Arabidopsis thaliana from Polarization Transfer Solid-State NMR. *Journal of the American Chemical Society* **2014,** *136* (29), 10399-10409.

37. Lee, S. A.; Yang, J. W.; Choi, S.; Jang, H. W., Nanoscale electrodeposition: Dimension control and 3D conformality. *Exploration* **2021,** *1* (3), 20210012.

38. Wang, X.; Yang, T.; Li, X.; Jiao, K., Three-step electrodeposition synthesis of self-doped polyaniline nanofiber-supported flower-like Au microspheres for high-performance biosensing of DNA hybridization recognition. *Biosensors and Bioelectronics* **2011,** *26* (6), 2953-2959.

39. Bhakat, D.; Barik, P.; Bhattacharjee, A., Electrical conductivity behavior of Gum Arabic biopolymer-Fe3O4 nanocomposites. *Journal of Physics and Chemistry of Solids* **2018,** *112*, 73-79.

40. Choi, S.; Jeong, H.; Choi, K.-h.; Song, J. Y.; Kim, J., Electrodeposition of Triangular Pd Rod Nanostructures and Their Electrocatalytic and SERS Activities. *ACS Applied Materials & Interfaces* **2014,** *6* (4), 3002-3007.

41. Xia, Y.; Wu, Y.; Hang, T.; Chang, J.; Li, M., Electrodeposition of High Density Silver Nanosheets with Controllable Morphologies Served as Effective and Reproducible SERS Substrates. *Langmuir* **2016,** *32* (14), 3385-3392.

42. Chen, S.; Liu, B.; Zhang, X.; Mo, Y.; Chen, F.; Shi, H.; Zhang, W.; Hu, C.; Chen, J., Electrochemical fabrication of pyramid-shape silver microstructure as effective and reusable SERS substrate. *Electrochimica Acta* **2018,** *274*, 242-249.

43. Cheng, Z.-Q.; Li, Z.-W.; Xu, J.-H.; Yao, R.; Li, Z.-L.; Liang, S.; Cheng, G.-L.; Zhou, Y.-H.; Luo, X.; Zhong, J., Morphology-Controlled Fabrication of Large-Scale Dendritic Silver Nanostructures for Catalysis and SERS Applications. *Nanoscale Research Letters* **2019,** *14* (1), 89.

44. Dao, T. C.; Luong, T. Q. N., Fabrication of uniform arrays of silver nanoparticles on silicon by electrodeposition in ethanol solution and their use in SERS detection of difenoconazole pesticide. *RSC Advances* **2020,** *10* (67), 40940-40947.

45. Creedon, N.; Lovera, P.; Moreno, J. G.; Nolan, M.; O'Riordan, A., Highly Sensitive SERS Detection of Neonicotinoid Pesticides. Complete Raman Spectral Assignment of Clothianidin and Imidacloprid. *The Journal of Physical Chemistry A* **2020,** *124* (36), 7238-7247.

46. Street, C. A.; Anderson, D. M. W., Refinement of structures previously proposed for gum arabic and other acacia gum exudates. *Talanta* **1983,** *30* (11), 887-893.

47. Goff, H. D.; Guo, Q., Chapter 1 The Role of Hydrocolloids in the Development of Food Structure. In *Handbook of Food Structure Development*, The Royal Society of Chemistry: 2020; pp 1-28.

48. Banerjee, S. S.; Chen, D. H., Fast removal of copper ions by gum arabic modified magnetic nano-adsorbent. *Journal of hazardous materials* **2007,** *147* (3), 792-9.

49. Sanchez, L. M.; Ollier, R. P.; Pereira, A. E. S.; Fraceto, L. F.; Alvarez, V. A., Chapter 15 - Pesticide removal from industrial effluents using biopolymeric materials. In *Biopolymer Membranes and Films*, de Moraes, M. A.; da Silva, C. F.; Vieira, R. S., Eds. Elsevier: 2020; pp 359-382.

50. Kee, Y. L.; Mukherjee, S.; Pariatamby, A., Effective remediation of phenol,2,4-bis(1,1-dimethylethyl) and bis(2-ethylhexyl) phthalate in farm effluent using Guar gum – A plant based biopolymer. *Chemosphere* **2015,** *136*, 111-117.

51. Riddell, G. L.; Davies, C. W., A Study of Gum Arabic, Part I. Viscosity and Adsorption Measurements. *The Journal of Physical Chemistry* **1931,** *35* (9), 2722-2731.

52. Chabot, V.; Kim, B.; Sloper, B.; Tzoganakis, C.; Yu, A., High yield production and purification of few layer graphene by Gum Arabic assisted physical sonication. *Scientific Reports* **2013,** *3* (1), 1378.

53. Langer, J.; Jimenez de Aberasturi, D.; Aizpurua, J.; Alvarez-Puebla, R. A.; Auguié, B.; Baumberg, J. J.; Bazan, G. C.; Bell, S. E. J.; Boisen, A.; Brolo, A. G.; Choo, J.; Cialla-May, D.; Deckert, V.; Fabris, L.; Faulds, K.; García de Abajo, F. J.; Goodacre, R.; Graham, D.; Haes, A. J.; Haynes, C. L.; Huck, C.; Itoh, T.; Käll, M.; Kneipp, J.; Kotov, N. A.; Kuang, H.; Le Ru, E. C.; Lee, H. K.; Li, J.-F.; Ling, X. Y.; Maier, S. A.; Mayerhöfer, T.; Moskovits, M.; Murakoshi, K.; Nam, J.-M.; Nie, S.; Ozaki, Y.; Pastoriza-Santos, I.; Perez-Juste, J.; Popp, J.; Pucci, A.; Reich, S.; Ren, B.; Schatz, G. C.; Shegai, T.; Schlücker, S.; Tay, L.-L.; Thomas, K. G.; Tian, Z.-Q.; Van Duyne, R. P.; Vo-Dinh, T.; Wang, Y.; Willets, K. A.; Xu, C.; Xu, H.; Xu, Y.; Yamamoto, Y. S.; Zhao, B.; Liz-Marzán, L. M., Present and Future of Surface-Enhanced Raman Scattering. *ACS Nano* **2020,** *14* (1), 28-117.

54. Han, B.; Chen, L.; Jin, S.; Guo, S.; Park, J.; Yoo, H. S.; Park, J. H.; Zhao, B.; Jung, Y. M., Modulating Mechanism of the LSPR and SERS in Ag/ITO Film: Carrier Density Effect. *The Journal of Physical Chemistry Letters* **2021,** *12* (31), 7612-7618.

55. Li, M.; Cushing, S. K.; Zhou, G.; Wu, N., Molecular hot spots in surface-enhanced Raman scattering. *Nanoscale* **2020,** *12* (43), 22036-22041.

56. Ding, S.-Y.; You, E.-M.; Tian, Z.-Q.; Moskovits, M., Electromagnetic theories of surface-enhanced Raman spectroscopy. *Chemical Society Reviews* **2017,** *46* (13), 4042-4076.

57. Yu, X.; Cai, H.; Zhang, W.; Li, X.; Pan, N.; Luo, Y.; Wang, X.; Hou, J. G., Tuning Chemical Enhancement of SERS by Controlling the Chemical Reduction of Graphene Oxide Nanosheets. *ACS Nano* **2011,** *5* (2), 952-958.

58. Le Ru, E. C.; Blackie, E.; Meyer, M.; Etchegoin, P. G., Surface Enhanced Raman Scattering Enhancement Factors: A Comprehensive Study. *The Journal of Physical Chemistry C* **2007,** *111* (37), 13794-13803.

59. Li, M.; Qiu, Y.; Fan, C.; Cui, K.; Zhang, Y.; Xiao, Z., Design of SERS nanoprobes for Raman imaging: materials, critical factors and architectures. *Acta Pharmaceutica Sinica B* **2018,** *8* (3), 381-389.

60. Stamplecoskie, K. G.; Scaiano, J. C.; Tiwari, V. S.; Anis, H., Optimal Size of Silver Nanoparticles for Surface-Enhanced Raman Spectroscopy. *The Journal of Physical Chemistry C* **2011,** *115* (5), 1403-1409.

61. Guo, C.; Chen, X.; Ding, S.-Y.; Mayer, D.; Wang, Q.; Zhao, Z.; Ni, L.; Liu, H.; Lee, T.; Xu, B.; Xiang, D., Molecular Orbital Gating Surface-Enhanced Raman Scattering. *ACS Nano* **2018,** *12* (11), 11229-11235.

62. Mao, P.; Liu, C.; Favraud, G.; Chen, Q.; Han, M.; Fratalocchi, A.; Zhang, S., Broadband single molecule SERS detection designed by warped optical spaces. *Nature Communications* **2018,** *9* (1), 5428.

63. Zhu, W.; Crozier, K. B., Quantum mechanical limit to plasmonic enhancement as observed by surface-enhanced Raman scattering. *Nature Communications* **2014,** *5* (1), 5228.

64. Zhang, Y.; Gu, Y.; He, J.; Thackray, B. D.; Ye, J., Ultrabright gap-enhanced Raman tags for high-speed bioimaging. *Nature Communications* **2019,** *10* (1), 3905.

65. Liu, W.; Bai, H.; Li, X.; Li, W.; Zhai, J.; Li, J.; Xi, G., Improved Surface-Enhanced Raman Spectroscopy Sensitivity on Metallic Tungsten Oxide by the Synergistic Effect of Surface Plasmon Resonance Coupling and Charge Transfer. *The Journal of Physical Chemistry Letters* **2018,** *9* (14), 4096-4100.

66. Mariod, A. A., 6 - Chemical Properties of Gum Arabic. In *Gum Arabic*, Mariod, A. A., Ed. Academic Press: 2018; pp 67-73.

67. Schneider, H.-J., Dispersive Interactions in Solution Complexes. *Accounts of Chemical Research* **2015,** *48* (7), 1815-1822.

68. Shen, X. S.; Wang, G. Z.; Hong, X.; Zhu, W., Nanospheres of silver nanoparticles: agglomeration, surface morphology control and application as SERS substrates. *Physical Chemistry Chemical Physics* **2009,** *11* (34), 7450-7454.

69. Joseph, D.; Huh, Y. S.; Han, Y.-K., A top-down chemical approach to tuning the morphology and plasmon resonance of spiky nanostars for enriched SERS-based chemical sensing. *Sensors and Actuators B: Chemical* **2019,** *288*, 120-126.

70. Solís, D. M.; Taboada, J. M.; Obelleiro, F.; Liz-Marzán, L. M.; García de Abajo, F. J., Optimization of Nanoparticle-Based SERS Substrates through Large-Scale Realistic Simulations. *ACS Photonics* **2017,** *4* (2), 329-337.

71. Vandenabeele, P.; Ortega-Avilès, M.; Castilleros, D. T.; Moens, L., Raman spectroscopic analysis of Mexican natural artists' materials. *Spectrochimica Acta Part A: Molecular and Biomolecular Spectroscopy* **2007,** *68* (4), 1085-1088.

72. Tian, L.; Su, M.; Yu, F.; Xu, Y.; Li, X.; Li, L.; Liu, H.; Tan, W., Liquid-state quantitative SERS analyzer on self-ordered metal liquid-like plasmonic arrays. *Nature Communications* **2018,** *9* (1), 3642.

73. Liu, L.; Shangguan, C.; Guo, J.; Ma, K.; Jiao, S.; Yao, Y.; Wang, J., Ultrasensitive SERS Detection of Cancer-Related miRNA-182 by MXene/MoS2@AuNPs with Controllable Morphology and Optimized Self-Internal Standards. *Advanced Optical Materials* **2020,** *8* (23), 2001214.

Appendix 3

Answers to reviewer's question for chapter 3 publication.

Reviewer #1:

1. The use of recycled silicon chips in this study can effectively save cost, so is this sensor reusable in this paper?

In this work, we used recycled chips which were previously used for electrochemical experiments. This drastically reduced the cost of undertaking this research and reduce the time for new chip fabrication. We also postponed the need for discarding the old chips.

In this work, we did not do experiments regarding reusing the developed DNA Raman sensors. This is typically done by breaking the hydrogen bond of dsDNA using either NaOH or high temperature, those process would also change or destroy the Ag nano particles on SERS sensors. For this reason, we do not reuse the DNA SERS sensor.

2. The author used Methylene Blue (MB) as a Raman marker to quantify targeted-ss-DNA, and hybridization of target DNA. Is any difference about reaction rate between MB-ssDNA and MB-dsDNA.

As state in the paper:

'MB can attach to DNA through electrostatic interaction where the negatively charged phosphate backbone of DNA (weak binding),[35] bind with guanine on single strand DNA[36] or intercalate between the double strand DNA (strong binding).[37] The higher the targeted ss-DNA concentration, the higher concentration of MB that is attached to DNA through electrostatic force; Also, MB shows different binding affinities towards ss-DNA and ds-DNA, as MB binds to ss-DNA by electrostatic force while it binds to ds-

DNA by both intercalations and electrostatic interactions.[38-39] Thus, MB can be used to quantify targeted ss-DNA upon DNA hybridization.'

The amount of MB bonded to ss-DNA or ds-DNA depends on the amount of guanine on ss-DNA, the length of ds-DNA, etc. Hence, it is hard to define the reaction rate between MB-ssDNA and MB-dsDNS as it varies from case to case.

3. The real sample detection part, the author may give some hits about this sensor applying in the food contamination.

Some information has beed added to give some hits about SERS sensor applying in the food contamination:

This SERS sensor has the potential to monitoring STEC in food industry for raw/undercooked meat products,[43] unpasteurized milk[44], fruit juice,[45] and fresh vegetables.[46] In the future, more complex samples, such as naturally contaminated or spiked with bacteria food samples should be tested to confirm a real-life application of the developed sensor.

4. There is some errors and typos in the manuscript, such as Figure 1, the description part should be consistent, and more clear.

The description of Figure 1 was rewritten and the whole manuscript was reviewed to correct all grammar and spelling mistakes.

Appendix 4 1st Revision according to the report

Introduction:

1, Explanation of the Raman effect is weak and needs revising…it's surprising that the word monochromatic does not appear in the thesis anywhere…. Also, some of the other statements about the Raman method are very misleading…this section should be revised and corrected. The annotated thesis contains many individual comments that need to be addressed.

- Raman effect and theory has been revised in Chapter 1, section 2.
- Monochromatic has been added to the introduction.
- Individual comments has been corrected and addressed in the thesis.

2, The introduction fails to adequately discuss or address the shortcomings of the SERS methods.

Shortcomings of SERS including the technology, substrate fabrication, functionalization and application were added in Chapter 1, section 2.4, 3.4, 4.1, 5.2:

2.4 Limitation of SERS technology.

SERS is a non-destructive technique to identify chemicals with good sensitivity and does not have strong a signal for water, so is good for bio applications and applications in the food or environment industries. However, SERS technology itself has its own limitations. Firstly, there are limited SERS-effective materials available. Traditional SERS-effective materials that are noble metal nano particles, e.g. silver nano particle, gold nano particles, or copper nano particles. New SERS effective materials emerged are Mxene,[1] and composite materials such as noble nano particles with graphene.[2] Secondly, Raman instrument will affect the measurement results, including the choice

of laser excitation wavelength and detectors. When the laser wavelength is tuned to the peak of the Plasmon resonance, this would lead to high enhancements and has been approved experimentally. For the detector, a long-pass or notch filter is used to absorb or reflect any Rayleigh scattering while allowing for the transmission of the Raman signal.[3] Hence, it is hard to compare SERS performance for different devices across different laboratories.[4] Finally, high-resolution handheld Raman instruments need more effort to be developed, and this blocks the way for minimized SERS device development.

3.4 Summary of advantages and disadvantages for SERS substrate fabrication.

There are several ways to fabricate SERS substrates, including bottom-up synthesis (a chemical-synthesis related process) and top-down synthesis (electron-beam (E-beam) lithography, laser etching together with film deposition, templating, and inkjet printing). Each of them has its own advantages and disadvantages. For chemical synthesis, it is not easy to control the distance between the nano particles (especially for the self-assembly chemical method), and sometimes nano particles are easy to aggregate. Most of the time, it is needed to shift the nano particles to a supporting substrate for analyte detection with a visual drying process involved. If the distance between the NPs is not controlled, the enhancement factor (EF) from site to site will be different, and this will lead to poor repeatability of SERS signal on a single SERS substrate. The SERS device will show a big error bar in the quantification process. Apart from that, this fabrication method could show poor reproducibility across different SERS substrates. For E-beam lithography or nanoimprint, the fabrication of SERS substrates is quite reproducible; however, the nano gap in between the nano particles is usually large compared to the

other fabrication methods. This large nano gap will lead to a bad detection limit in SERS applications. For the laser-assisted fabrication method, the choices of supporting substrate and SERS active materials are limited. The supporting materials are usually silicon and glass, while the SERS active material is gold. Electrochemical synthesis is a good candidate for SERS sensor and device fabrication, as it enables control of the morphology, size, nano gap of the NPs, by controlling the deposition parameters such as deposition time, voltage, and precursor concentrations. Besides, it does not need a high temperature or high vacuum environment, which will provide a more reproducible fabrication process.

4.1 Summary of advantages and disadvantages for SERS substrate functionalization.

Surface functionalization can improve the selectivity and sometimes sensitivity of a SERS device, especially in real-world application where there are many different chemical species. For some molecules that do not have active interaction with the SERS substrate (noble metal nano particles), surface functionalization could help trap targeted analytes on nano particle surface, thus getting an effective Raman signal and detecting them. For example, a metal-organic frame network is widely used as a functionalization approach.[5] Benzene, nitrobenzene, toluene, or 2,6–di–*tert*–butylpyridine do not have active interactions with nano particles, but metal–organic framework (MOF) films trap targets at the nano particles surface, allowing the unique Raman spectrum of each molecule to be recognized. The choices for SERS surface functionalization are limited. Molecules used for

SERS functionalization are SH-functionalized molecules, 4-Mercaptobenzoic acid, Thiophenol, N, NH*x* functionalized molecules (Adenine), and these molecules form an adsorbate on the metallic surface through S or N binding. Dye molecules, such as methylene blue, crystal violet, or rhodamine 6G have also been used, as they provide very high Raman cross-sections because of resonant enhancement, even if with lower affinity to the surface through electrostatic interaction.[4]

SERS surface functionalization usually takes more than 24 hours to finalize. Functional molecules orientation on SERS substrate surfaces varies and this results in poor repeatability of the SERS signal. Another drawback of functionalization in SERS applications is that SERS signals come from not only analytes but also functional layer, this makes data analysis more difficult. The variation generated in functionalization steps on a SERS device will also lead to variation in quantification for this SERS device, e.g., the variation of thiol bonding or chemical bonding in functionalization steps will lead to different baseline for the developed SERS device.

5.2 Shortcomings and challenges of SERS device development.

SERS device is used to identify or further quantify an unknown sample. All challenges stated in sections 2.4, 3.4, 4.1 for SERS are valid for SERS device development. First, high-resolution handheld or portable Raman instrument development is difficult and limits SERS application in a real outdoor environment; SERS devices with good performance are only available at the laboratory level. Second, SERS substrates with good repeatability and reproducibility are made by E-beam lithography, and such substrates have a lower EF compared to SERS substrates made by other approaches, e.g., chemical synthesis, electrochemical deposition, etc. While

repeatability and reproducibility are important for SERS quantification, usually, ten measurements are recommended and taken on a single SERS substrate for quantification. Reproducibility is essential to retain the same sensitivity/ LOD for the developed SERS device. Reproducibility is an important parameter for application and mass production, though a standard addition method could be used to minimize the difference between different SERS devices. Machine learning and artificial intelligence have been used to help increase the accuracy, reliability, and sensitivity of SERS.[6] In real-world application, cross-contamination is another factor to consider, sample pre-treatments or surface functionalization for SERS substrate can help improve the selectivity of SERS device and avoid the impact of contaminants that appear in the real sample. Last, SERS signal reading and data analysis are important and are one of the most difficult parts of SERS study. As in most the cases, it is hard to precisely determine the adsorption site of analytes on nano particle surface.[7] In summary, although SERS devices are widely studied at lab/research level, compared to MS and HPLC technologies, there are still problems to be solved until SERS devices can be used in industry. SERS devices are good for tracing ultra-low concentration analytes while MS/HPLC can help with accurate quantification.

3, There is a lack of information about how the chemical structure of molecules affects SERS spectra and in particular a lack of discussion about why Nitrogen and Sulfur containing species work well….this explains why the data in Chapter 2 and 3 are unreliable and why their SERS spectra are anomalous.

Chapter 1:

Surface binding of molecule on the SERS surface, molecule orientation on surfaces, adsorption state, etc. will affect the final detection results in SERS application. Different molecule orientation will affect the intensity or spectrum feature of SERS signal.[8-9] Marshall et al. synthesized silver nano particles with different nano gaps and assembled them into an extended silver film, for single–molecule Surface–Enhanced Raman Scattering (SERS) spectroscopy. They found that the SERS signal is strongly dependent on the particle size and the molecule orientation in the nano gap. Finite Difference Time Domain (FDTD) simulations have also been used to support the experimental results in this research.[8] Sun et al. used a molecular template (MT) on the SERS substrates with self-assembly probe molecules on silver nano particles to improve the detection sensitivity. This SERS platform reaches a good limit of detection (LOD) of SERS by controlling molecular orientations.[9] This method is efficient, accurate, and simple. Molecular structure will also result in different EF, for example, Morton et al. found that the enhancement of SERS for the pyridine ring does not increase as more charge is transferred from the pyridine ring to the cluster. However, the magnitude of chemical enhancement is governed by the energy difference between the lowest unoccupied energy level (LUMO) of the molecule and the highest occupied energy level (HOMO) of the metal. This trend has been verified by considering substituted benzenethiols,

small molecules, and silver clusters of different sizes. The results indicate that molecules that show significant stabilization of the HOMO-LUMO gaps (such as those that readily accept π-backbonding) most likely to have strong chemical enhancement. This provided the theory for designing new molecules that exhibit high chemical enhancements. However, it is still very challenging to describe the magnitude of the Raman enhancements using electronic structure methods such as DFT accurately, as they probably underestimate the energy gap.[10] Several molecule such as SH-functionalized molecules,[11-12] 4-MBA,[13] Rhodamine 6G,[14] crystal violet[15] etc. have strong Raman response and are often used as Raman reporter. Marques et al. studied 4-Mercaptobenzoic acid (4-MBA) adsorbate by connecting it to Ag surface through thiolate-Ag bonding and were to trigger a self-assembly process of AgNP. This process is driven by cooperative hydrogen bonds between the carboxylic groups of 4-MBA located in different nanoparticles at pH=4. UV-Vis and DFT-based calculations of the model complex [AgNP-(4-MBA)2-AgNP] help to understand the self-assembled complex formation through the comparison of calculated and experimental SERS spectra.[16] Madzharova et al. obtained surface-enhanced hyper Raman scattering (SEHRS) spectra (excited off-resonance at a wavelength of 1064 nm) and surface-enhanced Raman scattering (SERS) spectra excited at 785 nm or at 633 nm, from thiophenol, benzyl mercaptan, and phenylethyl mercaptan and from the three isomers 2-aminothiophenol (2-ATP), 3-aminothiophenol (3-ATP), and 4-aminothiophenol (4-ATP). The SEHRS spectra show different interactions of thiophenol, benzyl mercaptan, and phenylethyl mercaptan with silver and gold nanostructures with the support of Density functional theory (DFT) calculations. Besides, 2-ATP, 3-ATP, and 4-ATP show

a different interaction with gold nanostructures that were found to depend on pH.[12]

Those SERS reporter molecules contain sulfur atom(s) or nitrogen atom(s), this will help the molecule have better affinity for nano metal particles and gain a better SERS signal. Organophosphates (OP) and neonicotinoids detected by SERS are widely studied,

Organophosphates (matrix)		SERS substrate	LOD (reported)	LOD (converted)
Phosmet 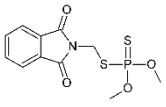	Ooling tea[17]	Ag NPs	0.1 mg/kg	0.3 μmol/L
	fruit or vegetable peels[18]	Snowflake-like Au NPs	0.032 ng/cm^2	\
	fruit[19]	multi-walled carbon nanotubes	0.5 mg/kg	1.5 μmol/L
	paddy water[20]	Au nanorods	0.25mg/L	7.5 μmol/L
	fruit skin[21]	polyurethane-Ag NPs	0.6 μg/mL	1.8

most OP contains sulfur atoms and neonicotinoids contain nitrogen atom (s) or both. Silver/Au and sulfur/nitrogen atoms are larger in size. They have lower charge states and can be easily polarized. Covalent bonds form between Au/Ag and sulfur/nitrogen atoms.

Chemical structures for analytes in Chapter 1 has been addressed in Chapter 1, table 1.

				μmol/L
	Plant Surfaces[22]	polyurethane micelle/ Ag NP	0.08 g/mL	240 μmol/L
	pesticides residue[23]	Au NP coated ZrO_2 nanofiber	10^{-8} M	10^{-8} mol/L
	Orange[24]	Au NPs decorated glycidyl methacrylate-ethylene dimethacrylate material	1 μg/L	3 nmol/L
Parathion-methyl 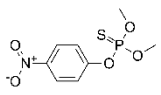	fruit or vegetable peels[25]	Snowflake-like Au NPs	0.026 ng/cm^2	\
	peach[26]	Au@Ag NP	0.001 mg/kg	3.8 nmol/L
	solvent[27]	Ag NP decorated ZnO-nanorods	10^{-8} M	10^{-8} M
Malathion 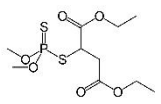	solvent[28]	Au NP	1 ppm	3 μM/L
	solvent[29]	nanoporous structure	12 ppb	36 nMol/L
	solvent[30]	nanostructured Ag	10 nM	10 nM
Chlorpyrifos	tomato surface[31]	Ag colloid	10^{-9} mol/L	10^{-9} mol/L

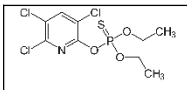	soil[32]	Au NP	10 ppm	28.6 μMol/L
	fruits[33]	Ag NP	10 ng/ml	28.6 nMol/L

4, Experimental details in the thesis are extremely lacking and need to be expanded. These should provide all the necessary information to allow someone to repeat the work..this does not seem to be the case here. The experimental work has been edited down to fit the needs of the papers however, it became very apparent that many critical factors.

Experimental details were included and expanded in each chapter.

5, Thesis claims of very low limits of quantification are questionable in chapters 2, 3, and 4, and should be carefully re-examined. I know that some of this work has been published, but, the authors may want to reconsider carefully what was published in these papers….as the evidence provided in the thesis (and during the viva voce) do not, in the external examiners view, support many of the conclusions, in particular the quantitative aspects. The LOD's claimed in Chapters 2 and 3 are OK (and potentially very good), but the mechanism for achieving this, which is missing from the thesis (and the published papers), needs to be included.

Mechanism added: Chapter 2, section 4.2.

While the single peaks intensity $I_{293\ cm\text{-}1}$, $I_{1130\ cm\text{-}1}$, $I_{1400\ cm\text{-}1}$ change with the change of 2,4-D concentration as shown in SI Figure S19, peak 1400 cm^{-1} kept constant with the 2,4-D concentration change. And the R^2 values of the fitting results for $I_{293\ cm\text{-}1}$ / $I_{1400\ cm\text{-}1}$ and $I_{1130\ cm\text{-}1}$ / $I_{1400\ cm\text{-}1}$ against the logarithm of the concentrations of the 2, 4-D solutions

were 0.5977 and 0.7366, which is not as good as using peak ratios $I_{293\ cm\text{-}1}$ / $I_{1400\ cm\text{-}1}$, $I_{1130\ cm\text{-}1}$ / $I_{1400\ cm\text{-}1}$. Peak 1400 cm^{-1} could be a characteristic peak for Gum Arabic layer,[34] while peaks at 1130 cm^{-1} and 293 cm^{-1} are for 2,4-D, using peak at 1400 cm^{-1} as a reference peak gain a better fitting results. In SI Figure S20, for 2,4-D crystal Raman spectrum, Raman bands at 194, 414, 840 and 1105 cm^{-1}, assigned to in-plane vibrational modes involving C-Cl and C-O-C bonds, are shifted in the enhanced SERS bands to 293, 889 and 1100 cm^{-1} for 2,4-D solution.[35-36] 2,4-D Raman peak in 1159 cm^{-1} is related to C-H_{ring} scissoring and shift to 1130 cm^{-1} in SERS.[37] 1393 cm^{-1} shift to 1297 cm^{-1} for the 2,4-D solution on SERS substrate and is related to -CH_2 wagging, See Table S1. While Raman peaks relate to test environments, PH, etc, for precise Raman peak assignment, theoretic studies such as DFT (density functional theory) modeling are necessary to assist the analysis.[38] …… All raw data, including baselines for each 2,4-D concentration, are shown in SI Figure S21. 2,4-D spectra and background signal subtraction lines were shown in SI Figure S21. The background signal was probably from Gum Arabic.[39] At a lower 2,4-D concentration of 1 pM, the background signal is higher; as 2,4-D concentration increased, the background signal became flatter. This is because of the coverage of 2,4-D molecules on the Ag-GA SERS surface, signal from Gum Arabic decreased. ……. The error bars for $I_{1130\ cm\text{-}1}$ / $I_{1400\ cm\text{-}1}$ against the logarithm of the concentrations of the 2,4-D solutions fitting range from 4-14%, while the fitting for $I_{293\ cm\text{-}1}$ / $I_{1400\ cm\text{-}1}$ against the logarithm of the concentrations of the 2,4-D solutions fitting range from 2-6%. The adsorption of 2,4-D on the Gum Arabic surface is based on the interaction between them. According to the fitting results, the 2,4-D concentration increase does not affect much of this interaction. This can be related to the interaction mechanism between 2,4-D and Gum Arabic, one hypothesis is that 2,4-D adsorbed in

gum Arabic layer and enters its porous structure, the other hypothesis is that 2,4-D interacts with functional groups on the gum Arabic surface. For either hypothesis and from the experimental results in this research, the interaction between 2,4-D and gum Arabic is not sensitive to the change in 2,4-D concentrations in 15 minutes. To further understand the interaction mechanism between 2,4-D and Gum Arabic, Langmuir diffusion model and Raman counts vs time experiments at one concentration can be further studied, but this is not within the scope of this study.[40]

Chapter 3, section 3.4:

MCPA and 2,4-D have similar chemical structure, their SERS spectra share the same peak features. MCPA crystal Raman spectrum is shown in Figure 3.4 (B). However, there are not so many research papers on MCPA peak assignment by using Raman or SERS..…... Peaks 1400 cm^{-1} and 1600 cm^{-1} are related to Cornstarch. According to 2,4-D crystal Raman peak assignment and MCPA Raman peaks, see table 1, peak 291 cm^{-1} is assigned to C-Cl and C-O-C bonds, and peak 1129 cm^{-1} is related to C-H_{ring} scissoring. 1296 cm^{-1} is -CH_2 wagging, and 928 cm^{-1} is related to C-COO^- vibration. Raman spectra are sensitive to test environments, pH, etc. So for precise Raman peak assignment, it is necessary to use theoretic studies such as DFT (density functional theory) modeling to help the analysis.[38] It is possible that MCPA molecules enter Corn Starch porous structure, or that MCPA functional groups interact with Cornstarch functional groups.[41-42] Corn Starch has -OH, -O-, and -CH bonds.[43] Theses bonds helped to trap MCPA.

6, Student/Author contributions are not adequately explained (see below for more details).

Student/Author contributions have added in the first page of each chapter.

7, Some useful refs to consult:

- This paper has to be read: Towards Reliable and Quantitative SERS: from Key Parameters to Good Analytical Practice, S. Schlücker, S. Bell, et al., Angew. Chem. Int. Ed. DOI: 10.1002/anie.201908154
- Surface-enhanced Raman spectroscopy (SERS): progress and trends Dana Cialla & Anne März & René Böhme & Frank Theil & Karina Weber &Michael Schmitt & Jürgen Popp, Anal Bioanal Chem (2012) 403:27–54, DOI 10.1007/s00216-011-5631-x
- Size Effects: J. Phys. Chem. C 2007, 111, 14664-14669. This is for gold NPs but the argument also holds for silver…thus from the SEM analysis particle size is important as it needs to be tweaked for maximum effect according to the excitation wavelength.
- The SERS substrate plays a crucial role as the electromagnetic enhancement is related to the material, size, and shape of the nanostructure.[from ref below].

Citation number of these papers in thesis: 17, 47, 58.

SERS substrate regarding size, shape in chapter 1:

SERS substrate plays a crucial role as the electromagnetic enhancement is related to the material, size, shape, and distance between the nano particles. Solís et al. used [44] state-of-the-art electromagnetic computation methods to produce predictive simulations for varieties of nanoparticle-based SERS substrates with different shapes. ….Particle size and morphology will also affect the final SERS intensity.[45] Peter et al. synthesized a group of gold nano particles with different sizes, and studied their SERS intensity towards MBA detection. They found that the SERS intensity increased with the increase of the nano particles size from 20-100 nm. The SERS intensity of the adsorbed MBAs is

detectable for particle sizes larger than 50 nm, and it increases with particle size, while the SERS signal is not detectable within the detection limit for particle sizes smaller than 50 nm. Njoki et al. studied the correlation between the optical and spectroscopic properties of gold nanoparticles and their diameters (10-100 nm) in solution. They found that the particle size was related to the surface Plasmon (SP) resonance band properties as well as the surface-enhanced Raman scattering (SERS) spectroscopic properties. The wavelength of the SP bands λmax (519 to 569 nm) displays a gradual increase with gold particle size, this trend was fitted by a polynomial cubic curve. This correlation is also compared to the simulation results based on Mie theory, the experimental results agree with the theory studies.[45]

Experimental Issues:

8, **Sampling Issues:** During the viva voce the actual sampling method was explained….this was not done in the thesis or papers, and needs to be explained clearly in a step by step manner for Chapters 2 &3:

Samples were tested from low concentration to high, and the samples were spotted on the same surface after a wicking type cleaning operation. This is not good analytical practice; samples should be tested in a random order and wither a new SERS substrate or a properly cleaned substrate should have been used to be compliant. The amended thesis needs to include a detailed, step-by-step guide to the actual experimental procedure and a critical evaluation of the methodology.

Chapter 2, section 1.5: All spectra were obtained using a laser power of 0.07 mW[4] and an integration time of 10 s with one measurement/spectrum for each spot….. . For calibration experiments, different concentrations of 2,4-D from a lower concentration to a higher concentration, were used on the same SERS sensor. After Raman measurements of previous concentration of 2,4-D finished, this analyte solution was removed with a small piece of cleanroom wipe (SUPERIOR Polycellulose wipes purchased from Sigma-Aldrich (Ireland).) from the edge of the analyte droplet (do not touch the SERS substrate itself) and apply the next concentration of 2,4-D solution.

Chapter 2 section 4.2 paragraph 2:

Different 2,4-D concentrations ranging from 0.2 mM down to 1 pM in DI water were used for the calibration study on the same Ag-GA substrate to minimize the variation from different substrates, see Figure 2.5 (A).

Chapter 3 section 2.5

For calibration experiments, different concentrations of MCPA from a lower concentration to a higher concentration, were used on the same Ag-CS SERS sensor. After Raman measurements at a lower concentration finished, this analyte solution was removed with a small piece of cleanroom wipe (SUPERIOR Polycellulose wipes purchased from Sigma-Aldrich (Ireland)) from the edge of the analyte droplet (do not touch the SERS substrate itself) and apply the next concentration of MCPA solution.

[4] The laser power was checked daily by using a reference Si calibration chip shown in Figure S3.

Experimental method detailed explanation (why not put 2,4-D of different concentration in a random order): As 2,4-D interacts with Ag-GA nano particles, this interaction is not completely reversible (see Figure 1 below: after rinse with DI water for S1 Ag-GA nano structure with 0.1 nM 2,4-D, the spectra features stayed unchanged). If apply pesticides in a random order, higher concentration pesticides will attach to the SERS substrate and cannot be removed, so it is not good to use lower concentration of analytes anymore. In this case, 2,4-D has to be added to a sensor from a lower concentration to a higher concentration. It is the same for MCPA.

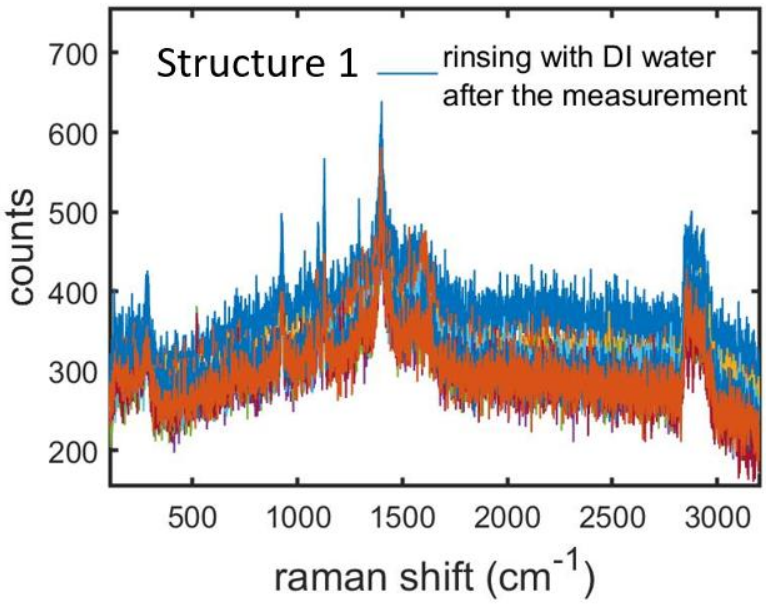

Figure 1 S_1 Ag-GA nano structure with 0.1 nM 2,4-D detetcted: after rinse with DI water, the spectra features stayed unchanged

Removing the previous concentration with a piece of clean room cotton wipe is acceptable as the diffusion and equilibrium of the next (higher) concentration of pesticides can be realized in a few seconds. If I remove the previous analyte solution by DI water rinse and air gun drying, I am risking destroy or change the SERS sensor. I have to test a series of concentrations on the same SERS sensor as it is the same

experiment condition. If I test different concentrations of analytes on different SERS sensors, the variation/error bar will also come from the variation of the SERS sensor besides the concentration change.

9, **Gum Arabic:** Full details of this key ingredient need to be provided….not appropriate just to say one of them came from Amazon.

Chapter 2 SI section 5

5 Gum Arabic from Amazon: purchase information.

- Gum Arabic Powder-100g
- 100% Pure and Natural
- The soothing and anti-inflammatory properties of the gum from African trees, (notably the Acacia Arabica), are extracted to provide the Gum Arabic granules.
- These Gum Arabic granules are used as an emulsifying and thickening ingredient in cosmetics and beauty products.

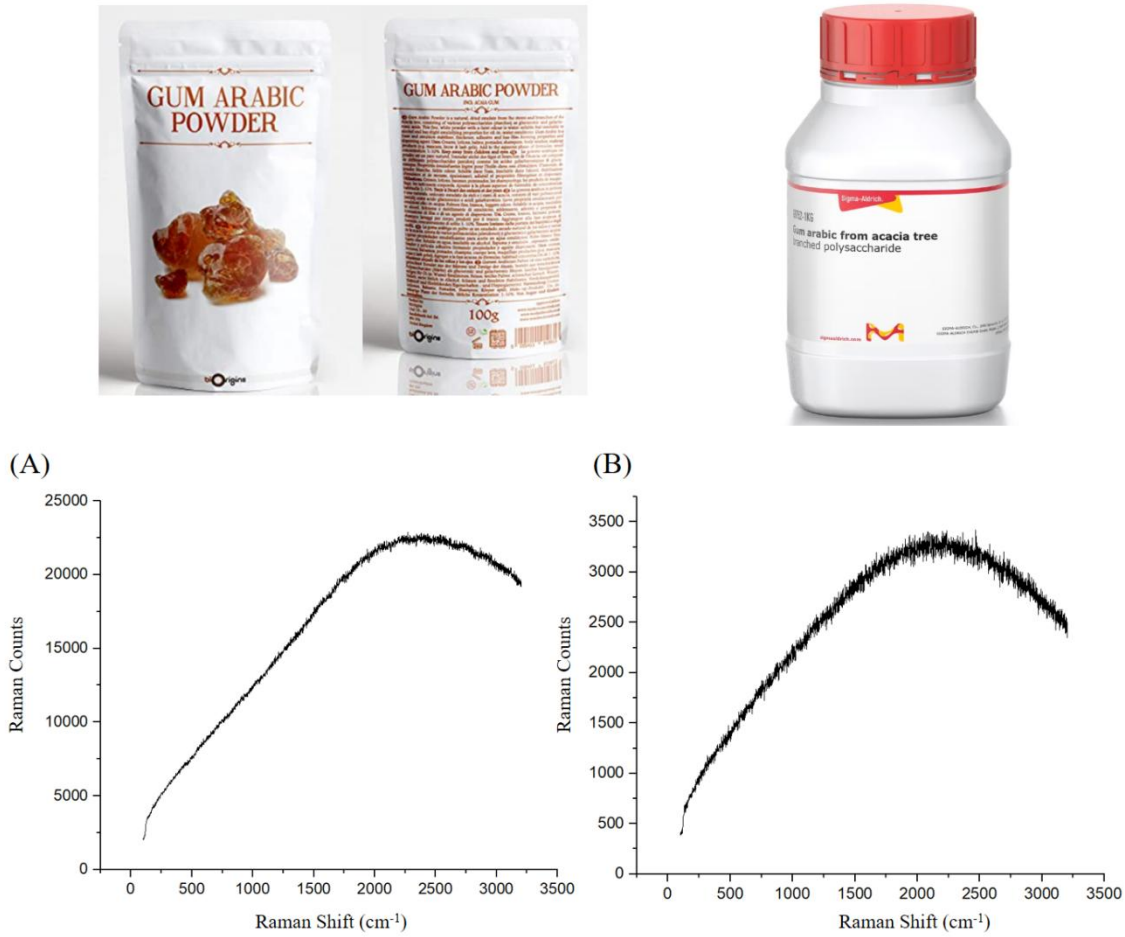

Chapter 2 SI Figure S22: (A) Raman spectrum for Gum Arabic: Mystic Moments from Amazon. (B) Raman spectrum for Gum Arabic from Sigma Aldrich for comparison.

10, **Contamination Control:** No evidence for contamination control presented anywhere…no acid washes of glassware, fresh DI? This needs to be addressed in the experimental sections. All serious practitioners of SERS are very aware of the problems with unwanted contamination generating spurious signals.

Chapter 2 section 1.1:

DI water and 2,4-D analyte used in this research were stored in new colorless Eppendorf AG PCR tubes (mL range) from Sigma-Aldrich (Ireland), $AgNO_3$ solution was contained in a new centrifuge tube from Sigma-Aldrich (Ireland).

Chapter 3 section 2.1:

DI water and MCPA analyte used in this research were stored in new colorless Eppendorf AG PCR tubes (mL range) from Sigma-Aldrich (Ireland), $AgNO_3$ solution was contained in new centrifuge tube from Sigma-Aldrich (Ireland).

Chapter 4 section 2.1: Containers used for dilution are new colorless Eppendorf AG PCR tubes (mL range) from Sigma-Aldrich (Ireland).

11, **Raman Experimental Details:** These need to be written up in much more detail to explain exactly how each set of measurements were made. I am not convinced that the Raman spectra can be repeated with the information presented in the thesis. A lot of the necessary and important information tends to be edited out for publications and in such a case these details should be included in the supplemental information, or more appropriately in an additional section within the thesis. My strong recommendation is for the latter option here. Issues like:

- **Spot size** (axial & lateral) are important to determine where exactly the Raman data is being acquired from. For example, 514 nm, using a 0.4 NA objective in an air sampling mode (as used by you) will give a lateral resolution of ~688 nm and an axial resolution of ~6875 nm (see https://imaging.gurdon.cam.ac.uk/ext/calculator.html)…This means that there should be Si/SiO_2 substrate bands in the Raman spectra of the controls & the lowest conc. samples.

- **Raman system:** Really not enough information provided about the Raman system used…what type of detector, how was it calibrated. The specific type of ×20 and ×50 microscope objectives used…etc.,

This has been added in each chapter in experimental section.

Chapter 2, section 1.5.

Raman spectra were acquired with a Renishaw InVia microscope (confocal, software: Renishaw's WiRE™ 3.4 (Windows®-based Raman Environment), special resolution: 0.3 cm^{-1} (FWHM), special resolution (lateral): 0.25 µm, spatial resolution (axial) < 1 µm) equipped with a 514 nm Ag ion laser (model number: stellar-pro, grating: 2400 l/mm(vis)) and Renishaw CCD detector (1024 pixel × 256 pixel). For the measurements, SERS sensor chips were placed in a dedicated holder, shown in SI Figure S2 (C-D). A 10 µL aliquot of 2,4-D solution was dropped over Ag-GA SERS substrate and covered with a cover glass slide. All measurements were acquired using a 20x lens (LEICA, NA 0.4, lateral resolution of ~688 nm and an axial resolution of ~6875 nm) with the smallest and brightest laser spot adjusted to focus on the measurement surface. All the spectra presented herein were averaged from ten measurements obtained at different random points on the substrate, except for the repeatability study, where 25 measurements were employed. For the first concentration in the calibration experiment, 2,4-D spectrum was gained after half an hour. All spectra were obtained using a laser power of 0.07 mW[5] and an integration time of 10 s with one measurement/spectrum for each spot.

[5] The laser power was checked daily by using a reference Si calibration chip shown in Figure S3.

- No details of an **intensity calibration method** are provided and since these methods are all intensity based this is critical (none of the peaks selected for the ratio method have been demonstrated to be a constant).

Footer: The laser power was checked daily by using a reference Si calibration chip shown in Chapter 2 SI Figure S3.

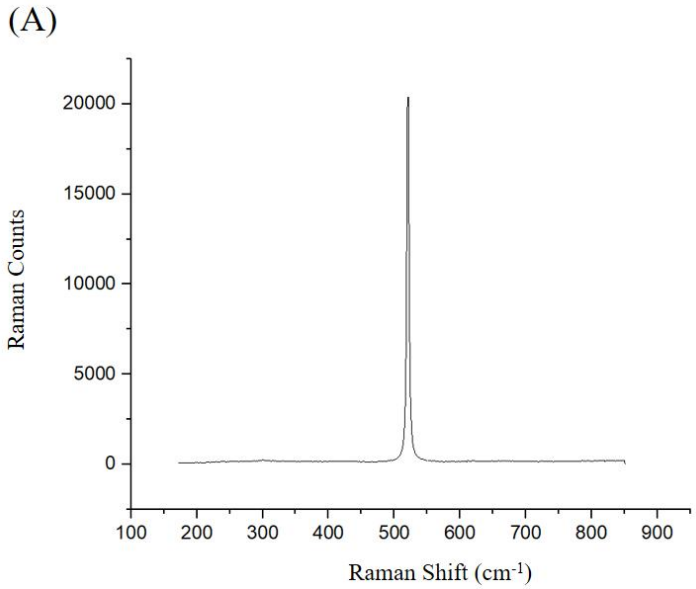

Figure S3: Spectrum of Si chip used for daily laser power calibration by Raman counts (around 20000 a.u.), Raman peak at 520 cm^{-1}. Laser power: 0.7 mW, lens: 50x, exposure time: 1s.

- **Focus Control:** there is no information about how the z-axis focus was controlled to ensure that reproducible data could be acquired. Figure S3.12 clearly shows that the intensity of the Si band is varying hugely…..This is a problem.

Focus control: All measurements were acquired using a 20x lens (LEICA, NA 0.4, lateral resolution of ~688 nm and an axial resolution of ~6875 nm) with the smallest and brightest laser spot adjusted to focus on the measurement surface.

Si band is varying hugely: this is because of the coverage of Ag-GA nano particles and different locations of Raman measurements. At different Raman measurement locations, the nano gaps in between the nano particles is different, the exposed Si area are different, and thus the Raman intensity is different.

- **Raman Library of substrate Materials:** All of the substrates used in the manufacture of the chips (Si, SiO_2, Si_3N_4) and SERS substrates (Both Gum Arabic samples) should have been Raman analysed in the bulk form and their spectra included in the thesis so that you can assign unknown bands in the SERS spectra.

Chapter 2 section 4.1: The Raman peaks of Si/SiO_2 substrate under Ag-GA nano particles are located in 520 cm^{-1} and 950 cm^{-1}.[46] (see SI Figure S3 (B) and Figure 1 below).

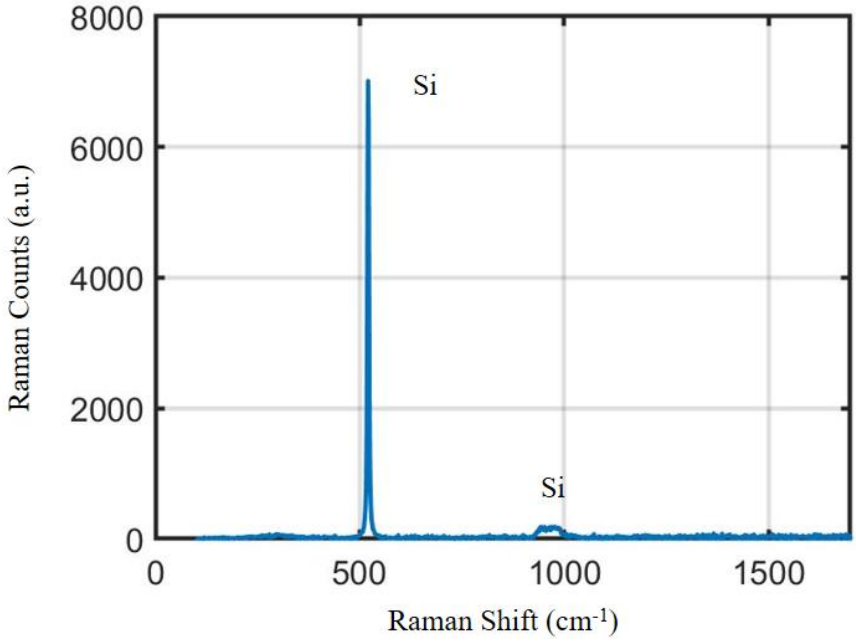

Figure 1: Raman spectra of Si/SiO_2 sensor chip. Si: 520 cm^{-1}, 950 cm^{-1}.

Si_3N_4 is not the supporting substrate of SERS nano particles and does not conclude in Raman signal measured: Plasma-enhanced chemical vapor deposition (PECVD) Si_3N_4 was blanket deposited on the whole wafer, the openings were over the working/counter/reference electrodes and the electrical contacts were defined by lithography and the dry etching process.

Raman Spectra of both Gum Arabic: chapter 2 SI Figure S22 and in point 9.

12, **Matlab:** Version not given etc.,

Chapter 2, section 1.6. : All spectra were corrected using the baseline subtraction algorithm,[47] the false colour map was generated by Matlab R2018b-academic use.

Chapter 3, section 2.6.： The spectra for 4-ATP and MB were corrected based on the baseline subtraction algorithm by Matlab R2018b-academic use.[47]

Chapter 4, section 2.7: All spectra were corrected by subtracting the baseline using Matlab R2018b-academic use.

13, *This suggestions in this paper should have been implemented*: **Towards Reliable and Quantitative SERS: from Key Parameters to Good Analytical Practice**, S. Schlücker, S. Bell, et al., *Angew. Chem. Int. Ed*. DOI: 10.1002/anie.201908154

This paper has been cited and implemented.

chapter 1 reference number 47 with discussion: By tuning the excitation laser wavelength, an optimized SERS signal would be achieved, it is also called surface enhanced resonance Raman spectroscopy (SERRS),[48] where the excitation wavelength matches both the plasmon and the molecular electronic resonance.[4]….. Hence, it is hard to compare SERS performance for different devices across different laboratories.[4]….. Dye molecules, such as methylene blue, crystal violet, or rhodamine 6G have also been used, as they provide very high Raman cross-sections because of resonant enhancement, even if with lower affinity to the surface through electrostatic interaction.[4]

14, **Repeatability & Reproducibility:** This area is very poorly described and is not rigorous….need to have a scientifically valid explanation for why no reproducibility measurements were undertaken on the sensors that were used in the thesis.

The word wrongly used in the thesis regarding these two has been revised.

Reproducibility study in this thesis:

The reproducibility of SERS sensors was accessed in the first step: electrochemical deposition fabrication. With the same electrochemical deposition parameters, the final morphology, size, nano gap etc. were the same for each deposition. This was included in:

Chapter 2 SI S10: All the nanostructures have been electrochemically deposited at least 3 times.

Chapter 3 figure 3.1: All the depositions have been repeated at least 3 times.

Chapter 4: The success rate of SERS sensor fabrication was 84.21% out of 19 sensors as shown in SI bar plot Figure S8.

As well as:

Chapter 2 real sample study, there are three sensors used for each concentration of 2,4-D for both real water samples: Ten measurements were undertaken for each concentration on a substrate, the experiments were repeated three times on three individual SERS substrates using three individual sensor chips. (Section 4.3.)

Analysis & Interpretation

15, Of all the SERS spectra shown where there is a concentration series, the only ones that I have confidence in are the Methylene Blue ones in (Fig 3.2 & 4.4)….in that case you definitely have SERS, for the rest no, it's not clear at all. This is very worrying as there is no comparison made between the obvious SERS spectra for MB and the very weak or non-SERS like spectra in the preceding chapters. During the viva voce it became apparent that the issue had to do with analyte concentrations in the gum Arabic layer reaching a maximum for the lowest concentration..

SERS spectrum for MB (0.05 μM) and the 1mM non-SERS spectrum in Chapter 3 SI Figure S2:

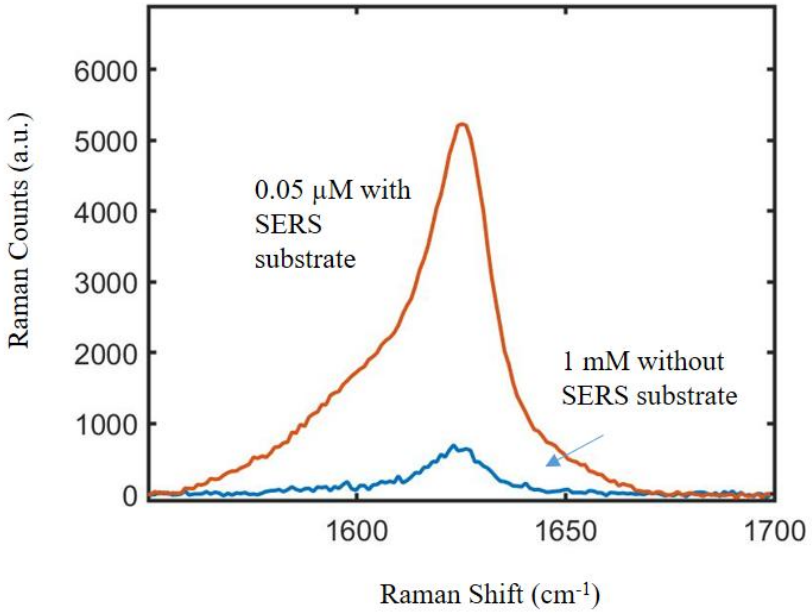

Chapter 3 SI Figure S2: The spectra of MB at 1 mM without SERS substrate and MB at 0.05 µM with SERS substrate.

Saturation explanation:

Figure 2.5 (B) in chapter 2 showed peak ratios vs Concentration (in nM) for a S_4 substrate, peak ratio increased with the increase of concentration and not saturated.

Figure S21 in chapter 2 are the raw data for all concentrations in calibration and as described in Chapter 2 section 4.2 paragraph 2: All raw data, including baselines for each 2,4-D concentration, are shown in SI Figure S21. 2,4-D spectra and background signal subtraction lines were shown in SI Figure S21. The background signal was probably from Gum Arabic.[39] At a lower 2,4-D concentration of 1 pM, the background signal is higher; as 2,4-D concentration increased, the background signal became flatter. This is because of the coverage of 2,4-D molecules on the Ag-GA SERS surface, the signal from Gum Arabic decreased.

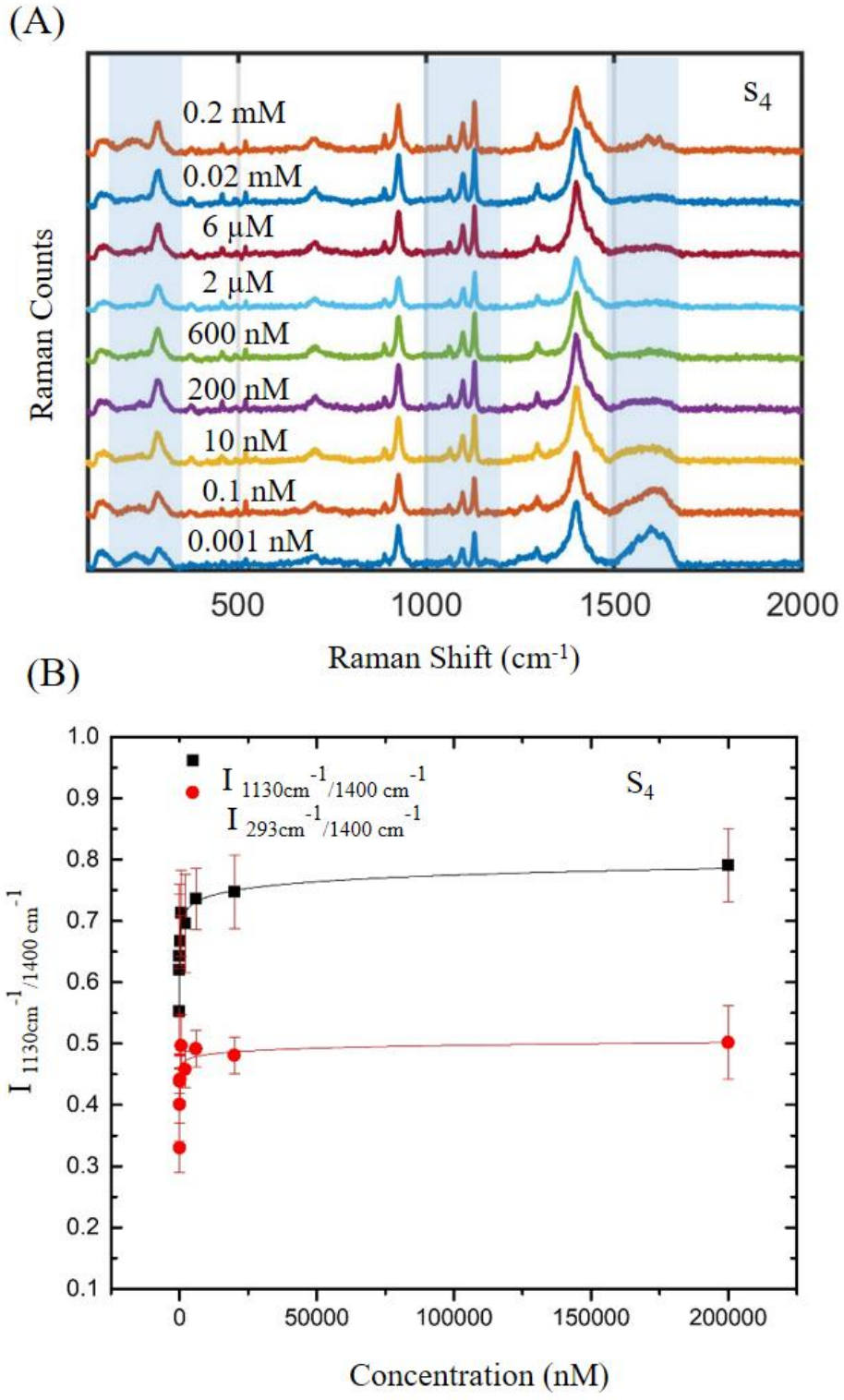

Figure 2.5: (A) Spectra of 2,4-D concentration from 1 pM to 0.2 mM, offset for clarity. (B) I_{1130} cm^{-1} / I_{1400} cm^{-1}, I_{293} cm^{-1} / I_{1400} cm^{-1} vs Concentration (in nM) for a S_4 substrate.

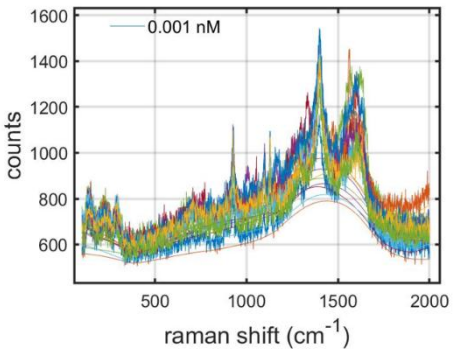
0.001 nM
counts
raman shift (cm-1)

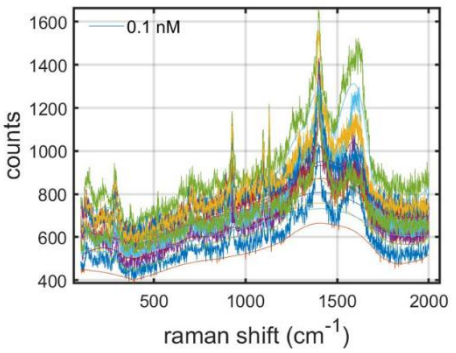
0.1 nM
counts
raman shift (cm-1)

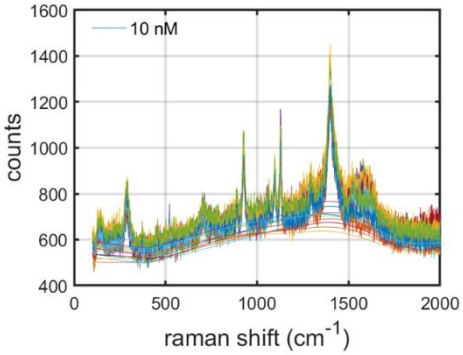
10 nM
counts
raman shift (cm-1)

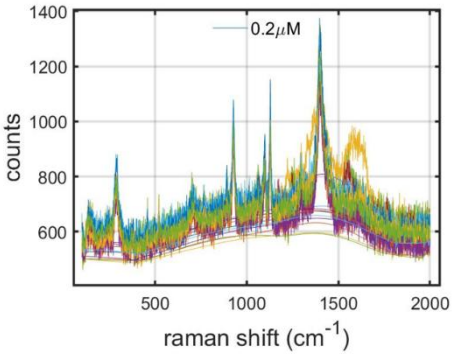
0.2μM
counts
raman shift (cm-1)

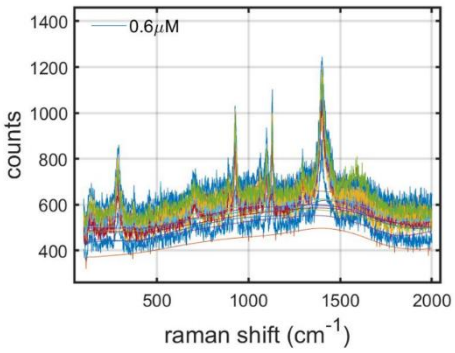
0.6μM
counts
raman shift (cm-1)

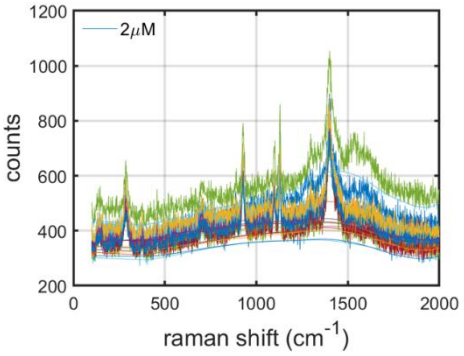
2μM
counts
raman shift (cm-1)

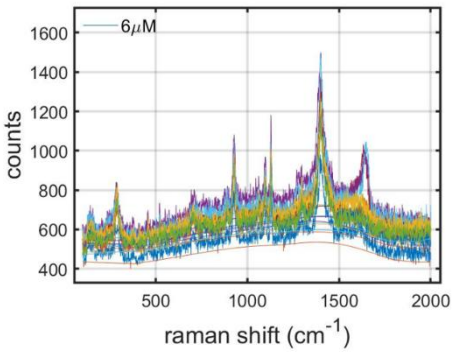
6μM
counts
raman shift (cm-1)

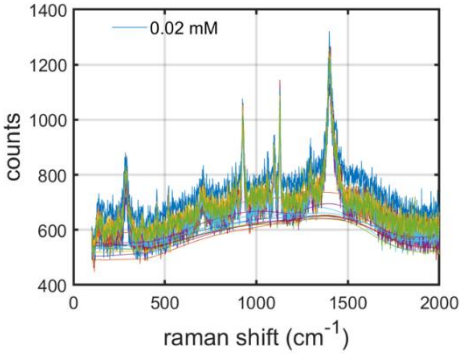
0.02 mM
counts
raman shift (cm-1)

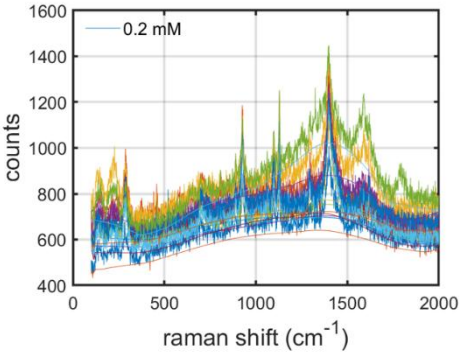
0.2 mM
counts
raman shift (cm-1)

Figure S21: Raw data in Figure 2.4. The spectra were for 2,4-D at different concentrations and the smooth lines were substracted background signal in data analysis. Ten spectra were used for each concentration. At the lowest/first 2,4-D concentration, it took around 30 minutes to get the signal. It took 15 minutes in total to get all data for each concentartions.

16, **Chemical structures:** As far as I can see the only analyte structures included are those of methylene blue and 4-ATP. This is not good enough because SERS is uniquely sensitive to the chemical and physical structure of the analyte molecules. There needs to be a section included showing the molecular structure and how they are likely to bond to the silver surfaces from this you might then be able to explain which vibrational modes are being SERS enhanced and thus explain the differences in the spectra collected from the different analytes.

Chemical structure of 2,4-D is included in chapter 2 Figure 2.3 (B).

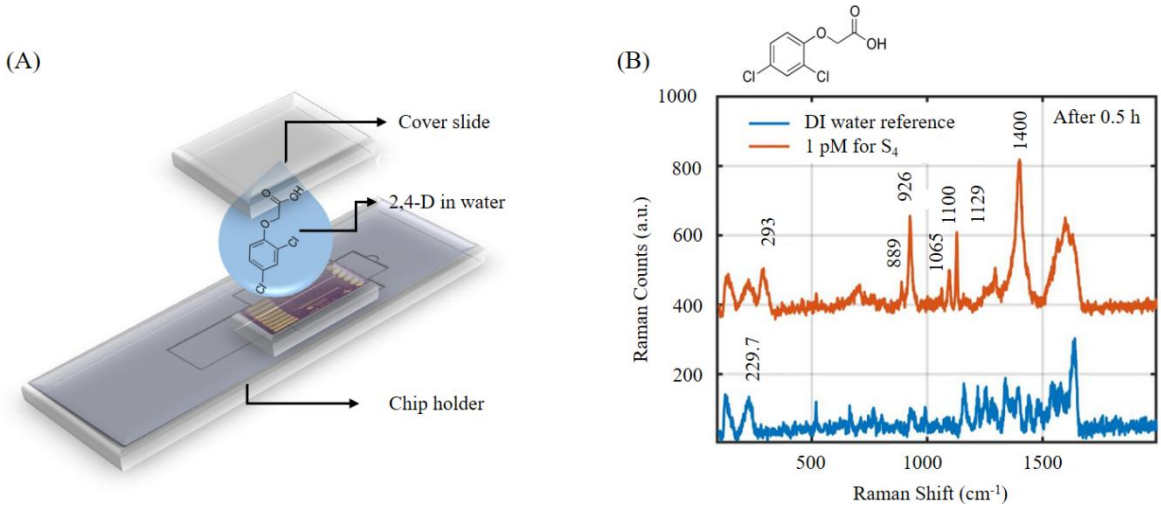

Figure 2.3 (A) Schematic illustration of the SERS measurement setup; (B) Spectrum of 2,4-D at 1 pM on structure four SERS substrate after a detection time of 30 min and

spectrum of deionized water as the reference (background corrected). Spectra offset for clarity.

The possible interaction is explained in chapter 2 section 4.2: The adsorption of 2,4-D on the Gum Arabic surface is based on the interaction between them. According to the fitting results, the 2,4-D concentration increase does not affect much of this interaction. This can be related to the interaction mechanism between 2,4-D and Gum Arabic, one hypothesis is that 2,4-D adsorbed in gum Arabic layer and enters its porous structure, the other hypothesis is that 2,4-D interacts with functional groups on the gum Arabic surface. For either hypothesis and from the experimental results in this research, the interaction between 2,4-D and gum Arabic is not sensitive to the change in 2,4-D concentrations in 15 minutes. To further understand the interaction mechanism between 2,4-D and Gum Arabic, Langmuir diffusion model and Raman counts vs time experiments at one concentration can be further studied, but this is not within the scope of this study.[40]

Chemical structure for MCPA is included in Chapter 3, Figure 3.5:

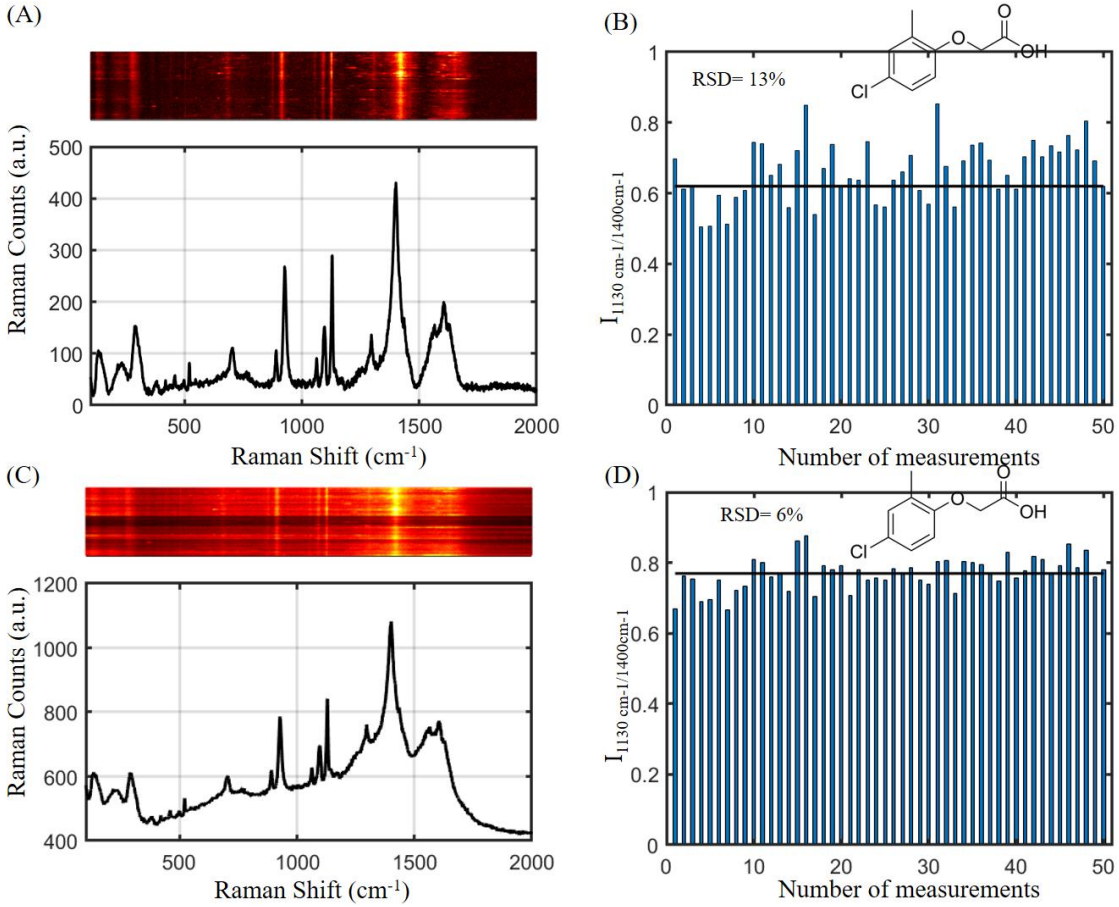

Figure 3.5: Repeatability study of the SERS substrate with 0.285nM MCPA at 50 different random points. (A, C) Raman color maps and spectra; (B, D) Bar plot of 50 Raman measurements, RSD = 13% for (B) and 6% for (D).

Peaks 1400 cm^{-1} and 1600 cm^{-1} are related to Cornstarch. According to 2,4-D crystal Raman peak assignment and MCPA Raman peaks, see table 1, peak 291 cm^{-1} is assigned to C-Cl and C-O-C bonds, and peak 1129 cm^{-1} is related to C-H_{ring} scissoring. 1296 cm^{-1} is -CH_2 wagging, and 928 cm^{-1} is related to C-COO^- vibration. Raman spectra are sensitive to test environments, pH, etc. So for precise Raman peak assignment, it is necessary to use theoretic studies such as DFT (density functional theory) modeling to help the analysis.[38] It is possible that MCPA molecules enter Corn Starch porous

structure, or that MCPA functional groups interact with Cornstarch functional groups.[41-42] Corn Starch has -OH, -O-, and -CH bonds.[43] Theses bonds helped to trap MCPA.

17, **SERS band explanations/assignments:** There is nowhere in the thesis where the origin of the bands used for quantitative analysis are explained (apart from the methylene blue case).

The 1400 cm–1 broad band is ascribed to the substrate…but what type of signal?

1130 cm–1 is called an interference peak..due to interaction of chemicals in the mineral water (page 84).

293 cm–1 used in chapter 3 not identified at all.

The use of two substrate bands for quantitative analysis is very odd….no valid scientific reason given…..this needs to be explained or reconsidered.

Chapter 2 section 4.2:

While the single peaks intensity $I_{293\ cm\text{-}1}$, $I_{1130\ cm\text{-}1}$, $I_{1400\ cm\text{-}1}$ change with the change of 2,4-D concentration as shown in SI Figure S19, peak 1400 cm^{-1} kept constant with the 2,4-D concentration change. And the R^2 values of the fitting results for $I_{293\ cm\text{-}1}$ / $I_{1400\ cm\text{-}1}$ and $I_{1130\ cm\text{-}1}$ / $I_{1400\ cm\text{-}1}$ against the logarithm of the concentrations of the 2, 4-D solutions were 0.5977 and 0.7366, which is not as good as using peak ratios $I_{293\ cm\text{-}1}$ / $I_{1400\ cm\text{-}1}$, $I_{1130\ cm\text{-}1}$ / $I_{1400\ cm\text{-}1}$. Peak 1400 cm^{-1} could be a characteristic peak for Gum Arabic layer,[34] while peaks at 1130 cm^{-1} and 293 cm^{-1} are for 2,4-D, using peak at 1400 cm^{-1} as a reference peak gain a better fitting results. In SI Figure S20, for 2,4-D crystal Raman spectrum, Raman bands at 194, 414, 840 and 1105 cm^{-1}, assigned to in-plane vibrational modes involving C-Cl and C-O-C bonds, are shifted in the enhanced SERS bands to 293, 889 and 1100 cm^{-1} for 2,4-D solution.[35-36] 2,4-D Raman peak in 1159 cm^{-1} is related to C-H_{ring} scissoring and shift to 1130 cm^{-1} in SERS.[37] 1393 cm^{-1} shift to 1297 cm^{-1} for the

2,4-D solution on SERS substrate and is related to -CH_2 wagging, See Table S1. While Raman peaks relate to test environments, PH, etc, for precise Raman peak assignment, theoretic studies such as DFT (density functional theory) modeling are necessary to assist the analysis.[38]

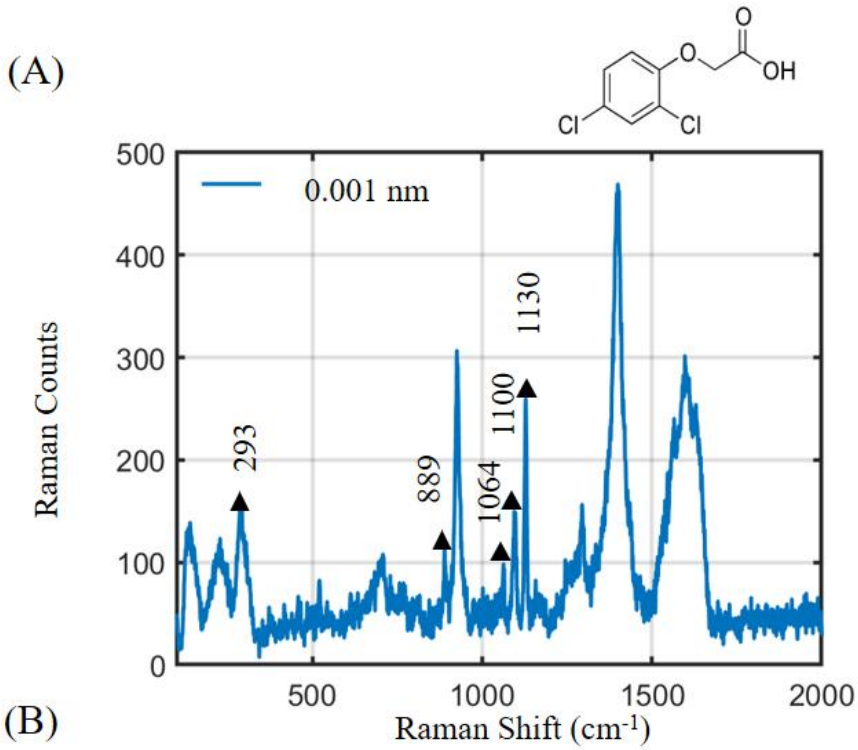

Figure S20: (A) SERS for 0.001 nM 2,4-D; (B) Raman spectrum for 2,4-D crystal. (laser power: 0.35 mW, exposure time: 30 s, 20x.).

Table S1 2,4-D crystal and 2,4-D solution on SERS substrate peak assignment.

2,4-D crystal	2,4-D solution on Ag-GA SERS substrate	vibration modes
194, 414	288	δ(COC) + δ(CCl)
840	889	ν(CC)ring + ν(C–O) + ν(C–Cl)
893	928	ν(C–COO−)
1050	1064	ν(CC)ring + ν(CO) + δ(CH)ring
1105	1110	ν(CC)ring + ν(C–Cl)
1159	1130	δ(CH)ring
1393	1297	ω(CH2)

Chapter 3 section 3.4:

MCPA and 2,4-D have similar chemical structure, their SERS spectra share the same peak features. MCPA crystal Raman spectrum is shown in Figure 3.4 (B). However, there are not so many research papers on MCPA peak assignment using Raman or SERS.. …. Peaks 1400 cm^{-1} and 1600 cm^{-1} are related to Cornstarch. According to 2,4-D crystal Raman peak assignment and MCPA Raman peaks, see table 1, peak 291 cm^{-1} is assigned to C-Cl and C-O-C bonds, and peak 1129 cm^{-1} is related to C-H_{ring} scissoring. 1296 cm^{-1} is -CH_2 wagging, and 928 cm^{-1} is related to C-COO^- vibration. Raman spectra are sensitive to test environments, pH, etc. So for precise Raman peak assignment, it is necessary to use theoretic studies such as DFT (density functional theory) modeling to help the analysis.[38]

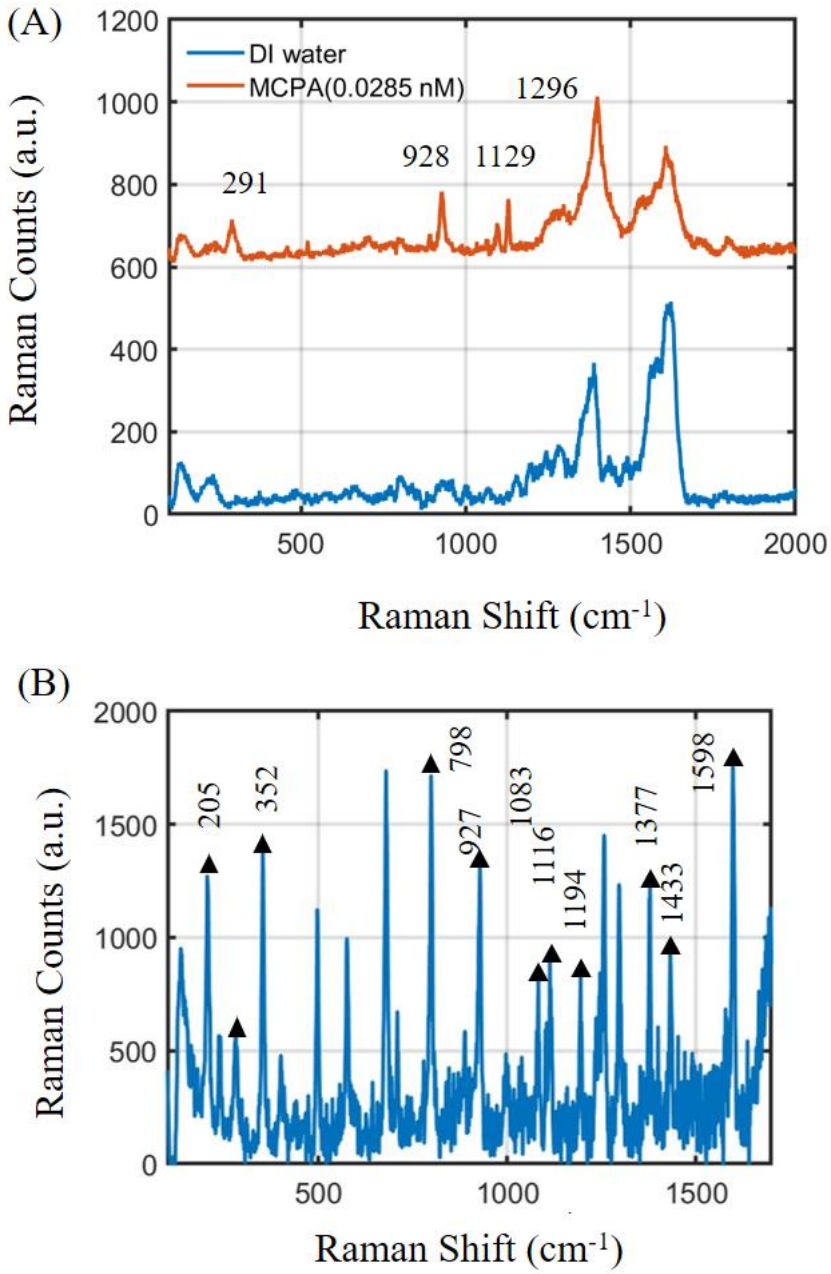

Figure 0.1 Ag-CS SERS sensor after application of DI water as a reference and after application of MCPA (0.0285 nM) solution. (B) MCPA crystal Raman Spectrum (laser power: 0.35 mW, exposure time: 30 s, 20x.).

Table 1: MCPA Raman peak and MCPA solution on SERS substrate peak assignment according to 2,4-D crystal vibration modes.

2,4-D crystal	MCPA crystal	MCPA on Ag-CS substrate	vibration modes
194	205	291	δ(COC) + δ(CCl)
840	798	\	$\nu(CC)_{ring}$ + ν(C–O) + ν(C–Cl)
893	927	928	$\nu(C–COO^-)$
1050	1083	1098	$\nu(CC)_{ring}$ + ν(CO) + $\delta(CH)_{ring}$
1105	1116	1110	$\nu(CC)_{ring}$ + ν(C–Cl)
1159	1194	1129	$\delta(CH)_{ring}$
1393	1377	1296	$\omega(CH_2)$

18, **Raman Spectra:** These are all uniformly too small to make any objective analysis by the reader….in addition the use of waterfall plots is not acceptable…these need to be replaced with mean standard deviation plots to properly show the degree of spectral change induced by the changing concentrations. Furthermore, there are insufficient control spectra of the analyte and substrate materials to use for comparison purposes.

Raman spectra has been adjusted to page wide where possible.

Mean and standard deviation plots were shown in chapter 2 SI 18 for repeatability study, chapter 3 Figure 3.3 for stability study, chapter 4 Figure 4.5 for repeatability study.

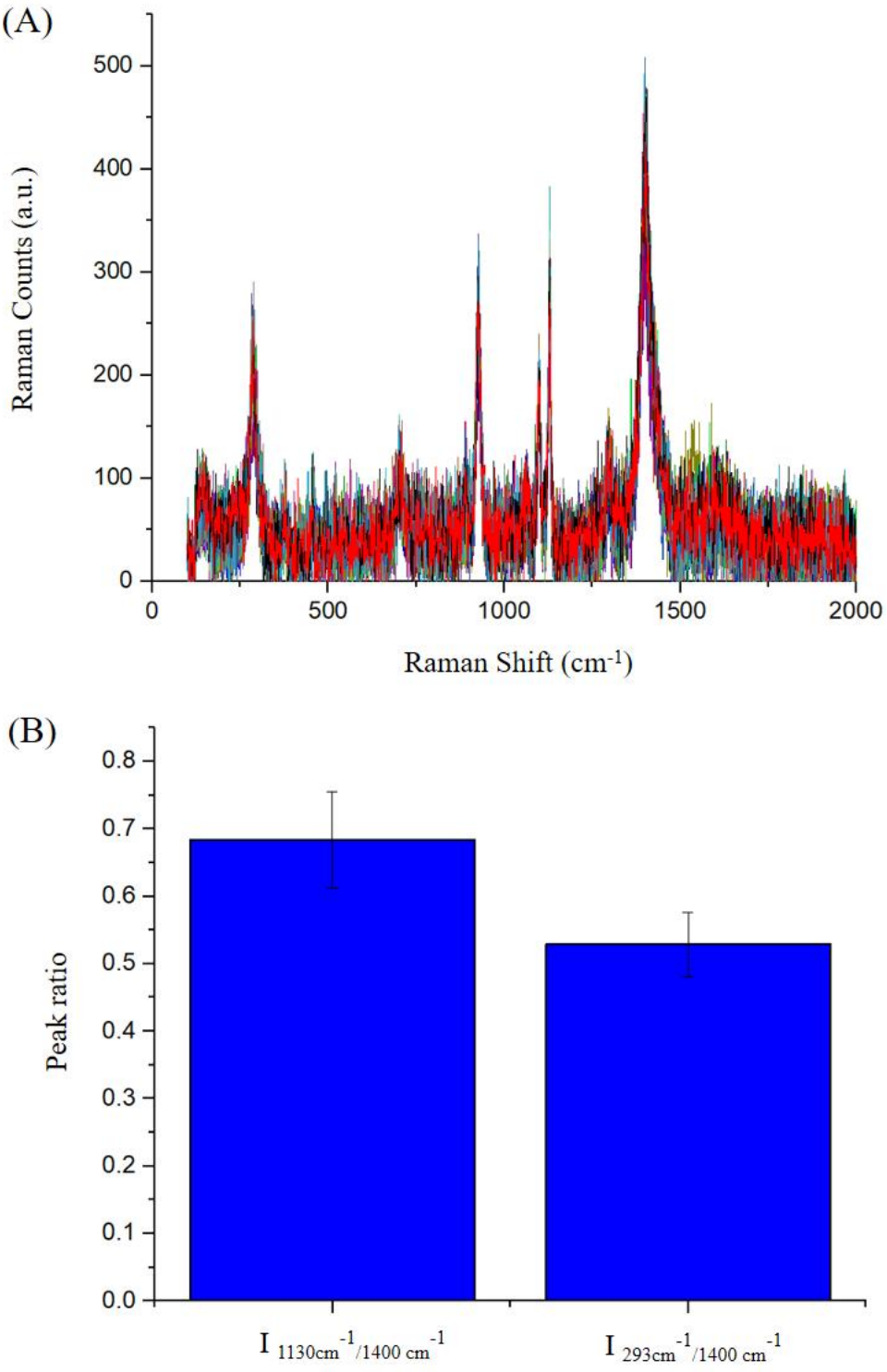

Figure S18: (A) Spectra of 25 random points for 2 μM 2,4-D on a S_4 SERS substrate in Figure 2.4. (B) Mean and SD plot for peak ratio I_{293} cm^{-1} / I_{1400} cm^{-1}, I_{1130} cm^{-1} / I_{1400} cm^{-1} at 25 different random points in (A).

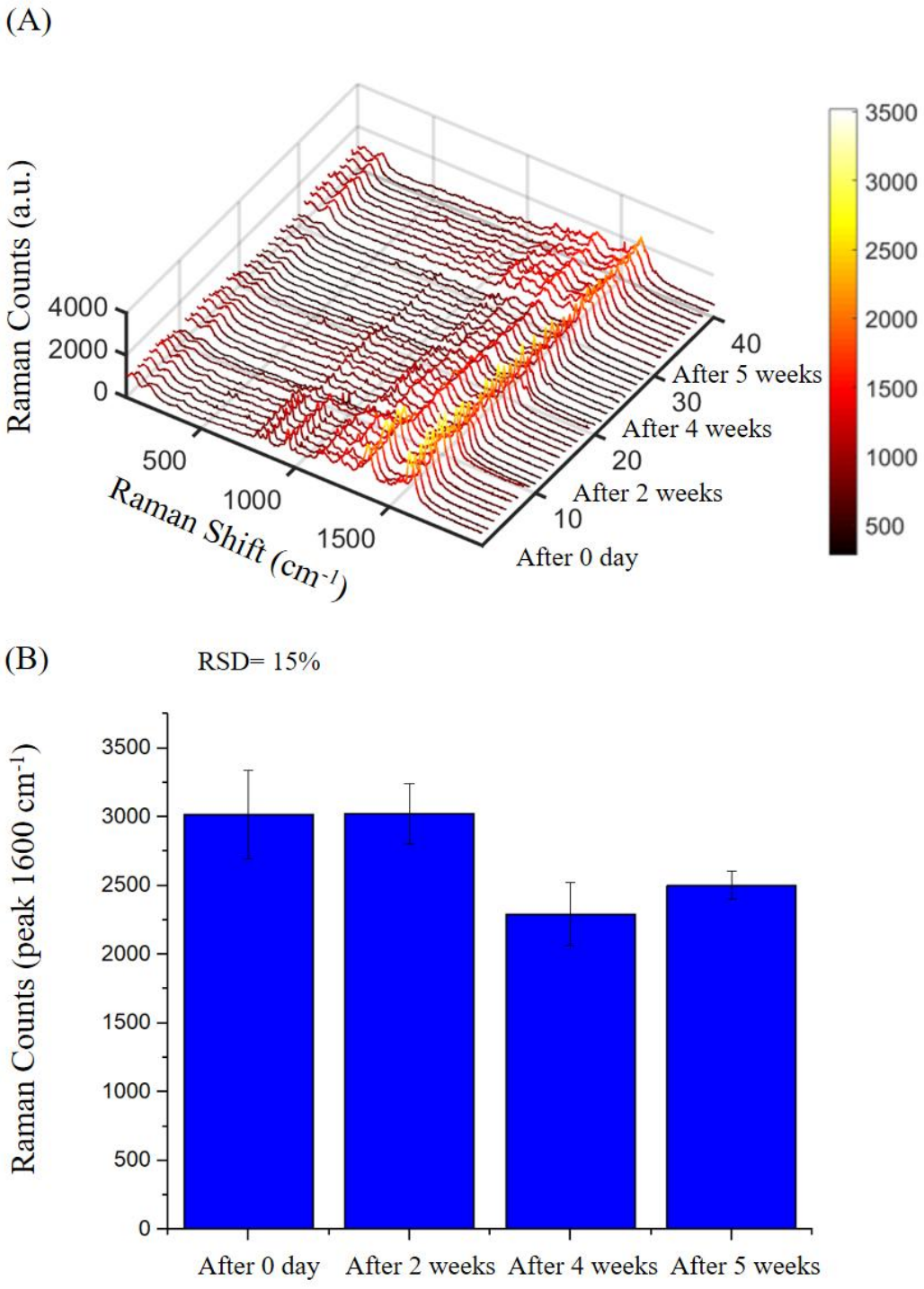

Figure 3.3: Stability study of the SERS substrate after zero days, two weeks, four weeks, and five weeks. (A) 40 spectra of bare Ag-CS SERS sensor after 0/2/4/5 weeks. (B)

Corresponding bar plot at peak 1600 cm^{-1}, the overall RSD of these data was 15%. Ten spectra were taken for each experiment.

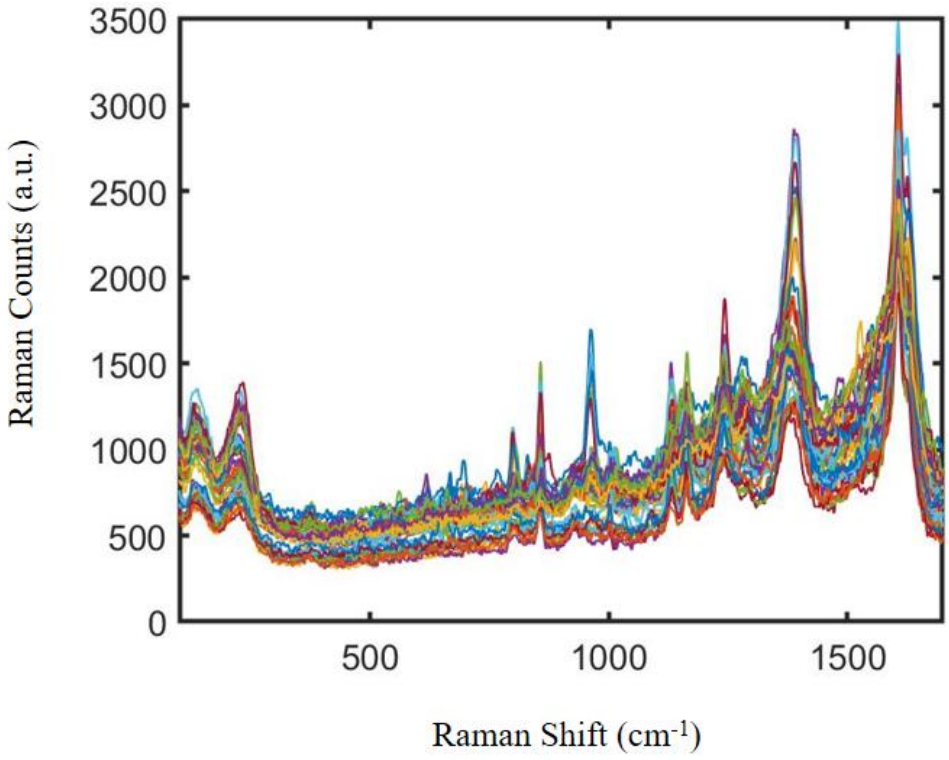

Figure S7: Raw data for stability study in Figure 3.3. Ten spectra was taken each week over five weeks.

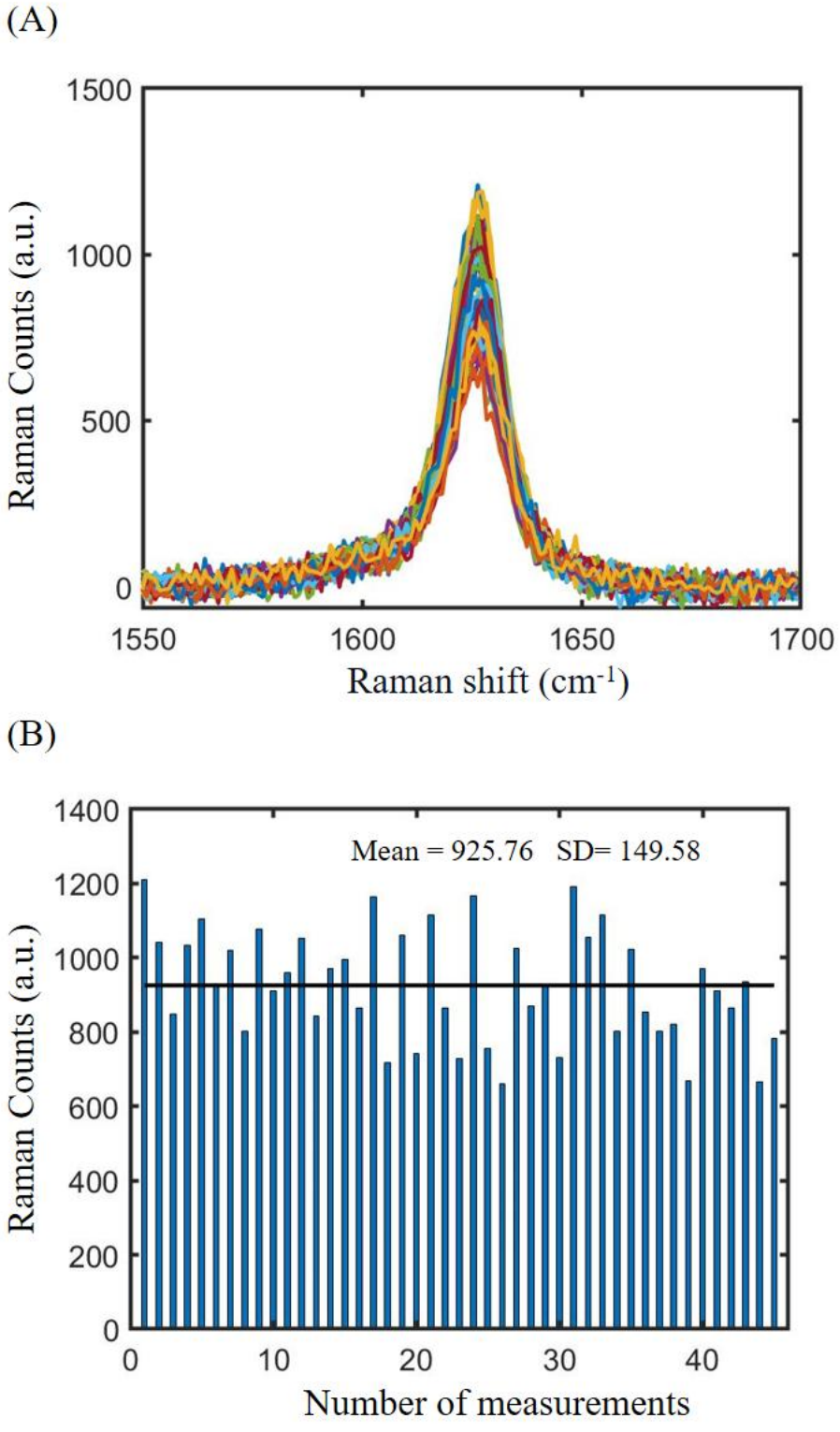

Figure 4.5: Repeatability study of an Ag nanostructure SERS substrate. (A) Spectra of MB at 0.1 μM from 45 different random points on a Ag nanostructure SERS substrate

after baseline subtraction. (B) Bar plot of Raman intensity of the characteristic peak of MB at 1625 cm^{-1} in (A) after baseline subtraction, with SD=149.58 for 45 different random points on an Ag nanostructure SERS substrate.

Control spectra: chapter 2 SI figure S4 (A) SERS subtsrate and after DI water application. Figure 2.3 (B) DI water vs 2,4-D at 1 pM.

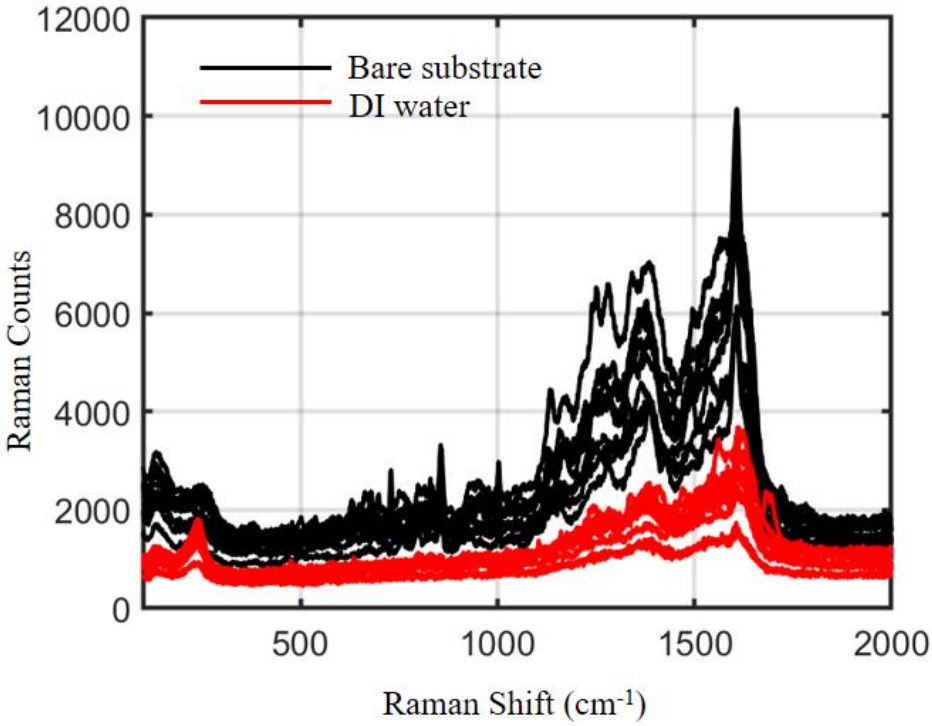

chapter 2 SI Figure S4 (A): bare substrate and substrate after application of DI water; Chapter 3: Figure 3.4: DI water vs MCPA at 0.0285 nM.

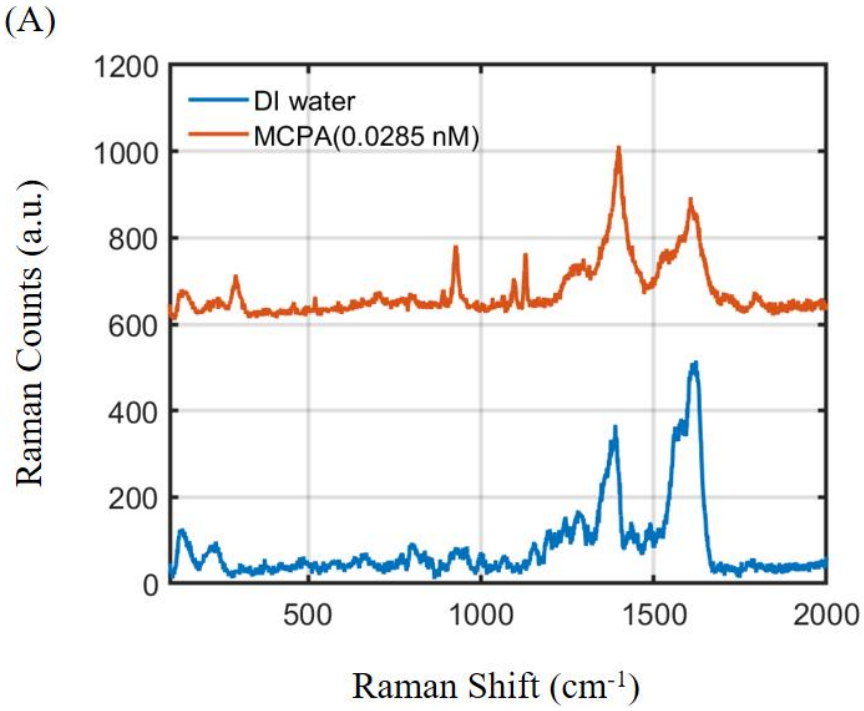

Chapter 3 Figure 3.4: Ag-CS SERS sensor after application of DI water as a reference and after application of MCPA (0.0285 nM) solution.

Control in chapter 4 is non-complementary DNA in the same buffer environment as targeted DNA does, non-targeted bacterial DNA as controls in real sample detection.

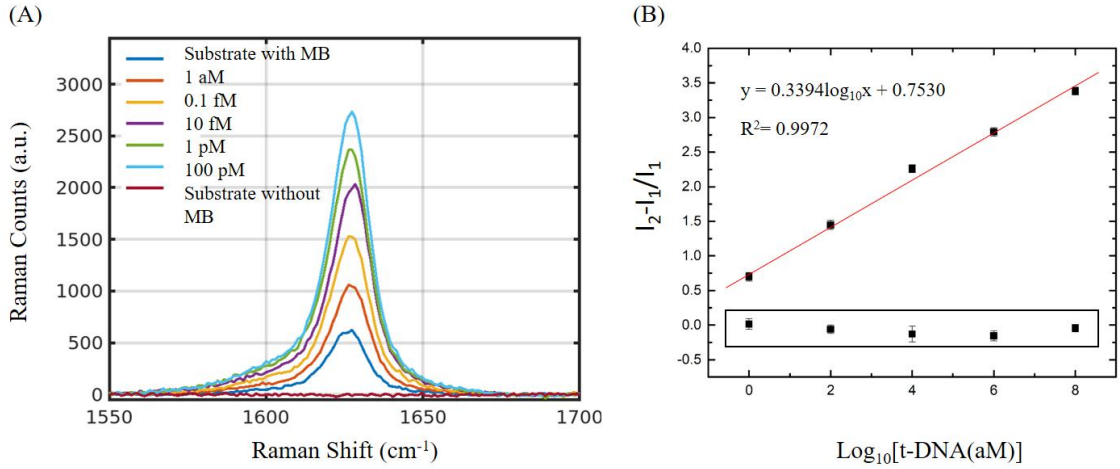

Figure 4.6: Targeted DNA (*stx*2) detection and linear calibration. (A) MB spectra after hybridization with different target DNA concentrations (i) 1 aM, (ii) 0.1 fM, (iii) 10 fM, (iv) 1 pM, and (v) 100 pM. And reference spectra of substrate with/without MB. (B) Linear fitting for I_1-I_2/I_1 vs Log_{10} ([t-DNA] (in aM)) at different target DNA concentrations: $y = 0.3394\log_{10}x + 0.7530$, with $R^2 = 0.9972$. Data points in the box is non-targeted DNA, which do not show Raman intensity change with the change of non-targeted DNA concentrations. The measurements for each targeted/non-targeted DNA concentration were taken in ten different random points on the functionalized Ag nanostructure SERS substrate, the error bars were the SD (standard deviation) of these ten measurements.

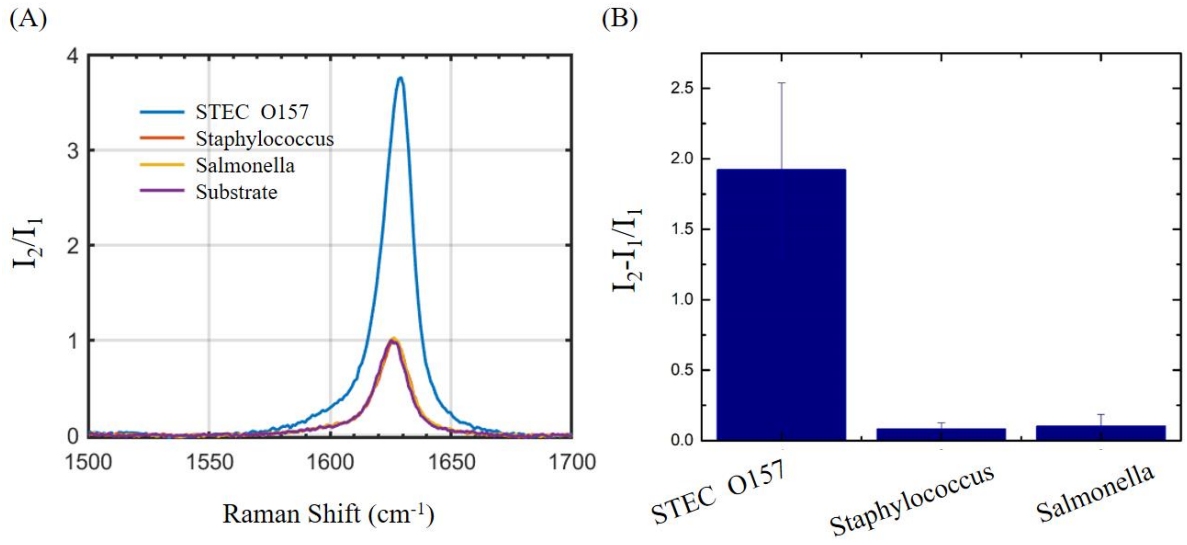

Figure 4.7: Real DNA samples study from different bacteria (STEC O157, *Salmonella spp.* and *Staphylococcus aureus*) on functionalized Ag nanostructure SERS sensors. (A) DNA from different bacteria samples on different SERS substrates (Incubation time: 20 minutes), after binding with 50 μM MB (20 μL) for 10 minutes. Only targeted bacteria STEC O157 showed significant changes in Raman intensity (274%). (B) Bar plot of intensity change for different bacteria DNA extraction, error bars were from three replications; where DNA from STEC O157 shows significant Raman intensity change (average 192%), the other two bacteria DNA do not show that much difference in Raman intensity change (within 11% Raman intensity change in average).

19, Kinetic Data: During the viva voce exam the examiners asked if Raman data were acquired from the analyte spotted SERS substrates in over the first 30 minutes. This data should be included to show the evolution of the SERS signal with time which should give information as to how the analyte is penetrating into the polymer layer and when the signal saturates.

Chapter 2 section 4.1:

Peak ratio $I_{1130\ cm\text{-}1}$ / $I_{1400\ cm\text{-}1}$ used for calibration in sections 4.2 and 4.3 do not show any kinetic trend before the 2,4-D signal at low concentration (1 pM) appeared, as shown in SI Figure S16. But at higher concentration, 2,4-D peaks showed up in the first measurement, see Figure S17. In SI Figure S15, there are many other random peaks other than 2,4-D feature peaks, 2,4-D characteristic peaks have been marked in Figure S15. The value of peak ratio $I_{1130\ cm\text{-}1}$ / $I_{1400\ cm\text{-}1}$ is in the range of 0.3-1 and as a appeared random value before the 2,4-D signal appeared at 1 pM, the peak ratio is only valid after the 2,4-D signal is shown for analysis. From a spectrum feature point of view, the 2,4-D spectrum is shown after around 30 minutes (SI Figure S15) and only random spectra are detected before that. After the application of 2,4-D at 1 pM on Ag-GA SERS substrate, 2,4-D molecules could probably interact with Ag-GA surfaces in different orientations. In different SERS substrate locations, Gum Arabic has many different functional groups (-OH, -COOH, -C-O-C-, and functional groups from proteins in Gum Arabic) on its surface and interacts with water/2,4-D in different ways, these factors all contributed to the random spectrum feature in SI Figure S15. Besides, it needs numbers of 2,4-D molecules on the Ag-GA surface for the SERS signal to show, because of the Enhancement Factor and LOD this Ag-GA SERS sensor has.

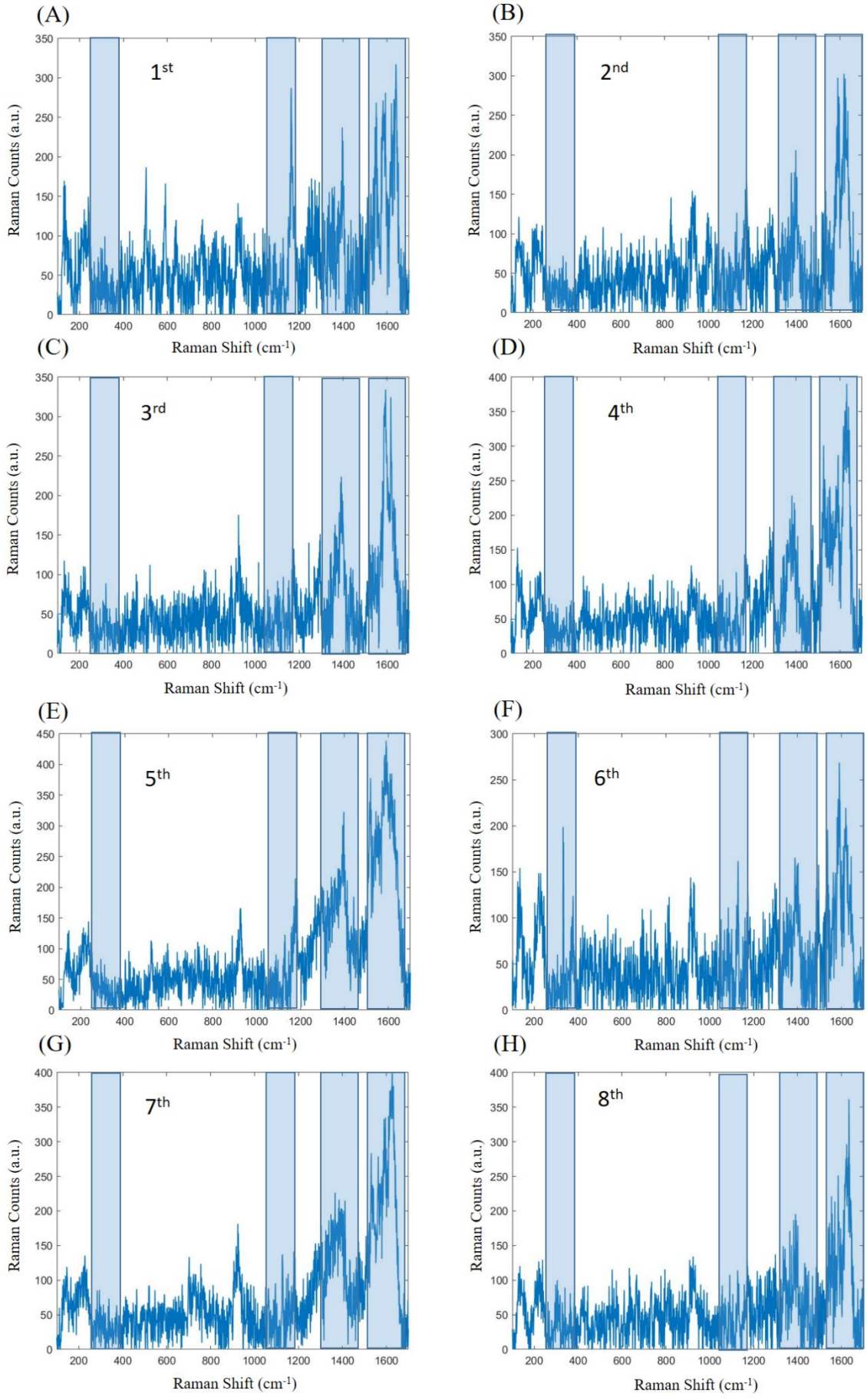
(A)
1st
(B)
2nd
(C)
3rd
(D)
4th
(E)
5th
(F)
6th
(G)
7th
(H)
8th
Raman Counts (a.u.)
Raman Shift (cm-1)

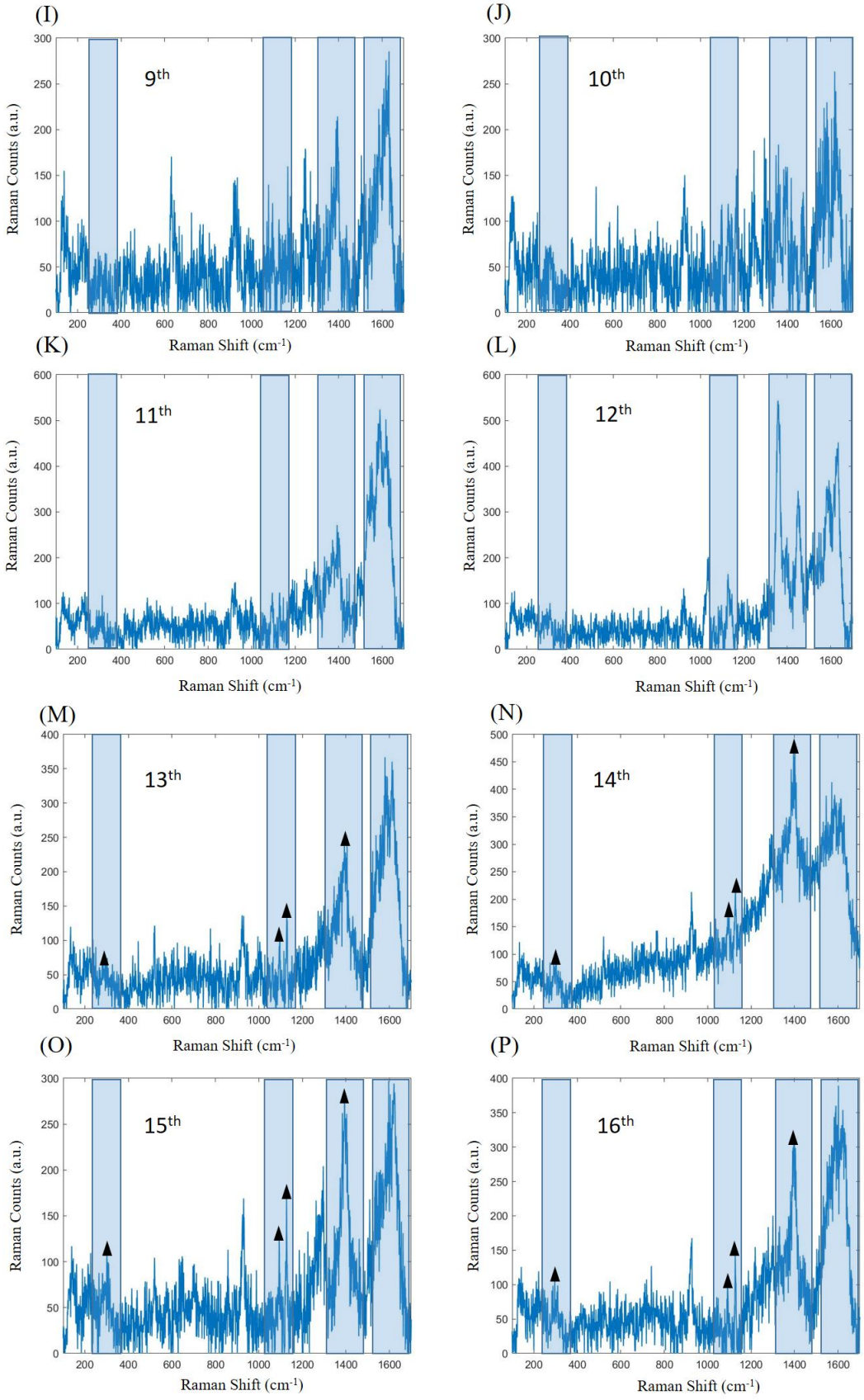
(I)
9th
(J)
10th
(K)
11th
(L)
12th
(M)
13th
(N)
14th
(O)
15th
(P)
16th
Raman Counts (a.u.)
Raman Shift (cm-1)

Figure S15: (A-P) The change of spectra before 2,4-D (1 pM) on Ag-GA structure 4 SERS substrate Raman signal appeared. (A-L) 1st -12th spectra. (M-P) 13th -16th spectra are for 2.4-D at 1 pM after around 30 minutes. Baselines have been subtracted for all spectra.

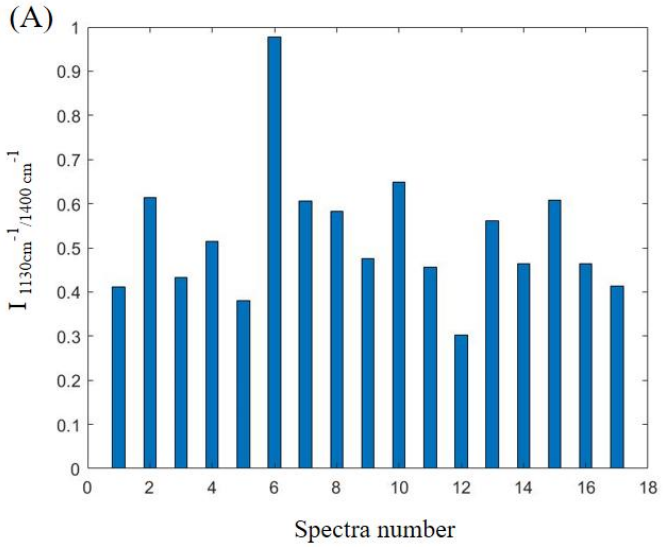

Figure S16: (A) peak ratio $I_{1130\ cm\text{-}1}/I_{1400.}$

Chapter 3 SI Figure S4.

After applying MCPA solution at 0.0285 nM, and new peaks at 293 cm^{-1}, 889 cm^{-1} and three sharp peaks around 1129 cm^{-1}show up at the 2nd measurement; peaks at 926 cm^{-1}, 1400 cm^{-1} becomes sharp. (SI Figure S4 and Figure 3.4 (A))

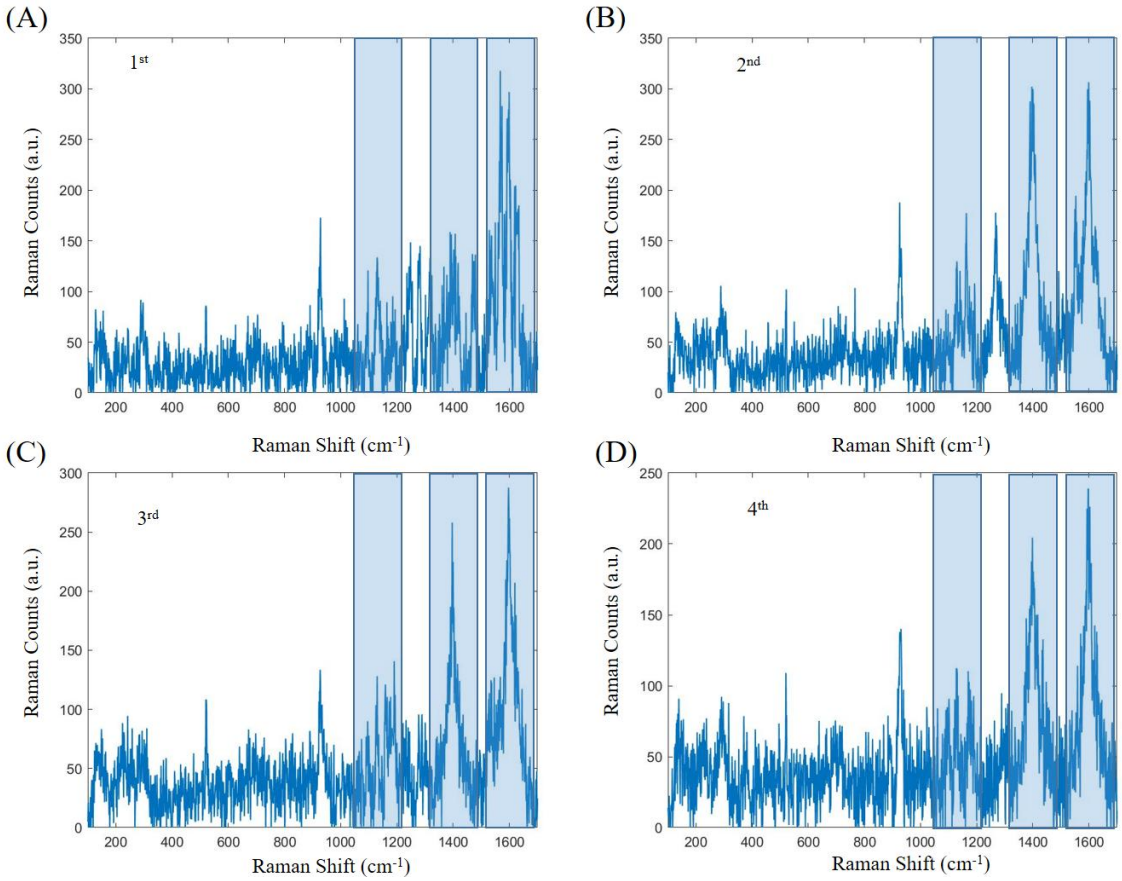

Chapter Figure S4: After the application of MCPA at 28.5 fM. (A-D) 1-4th Raman spectra. MCPA feature peaks shown in the second measurement (B).

20, Overall, the analysis and interpretation is weak because it is neither critical nor objective…It is clear that there is a problem with the spectral data in Chapters 2 and 3 in terms of the SERS spectra….It's obvious that you are not getting substantial increase in SERS as the concentration increased. From questioning in the viva, the most likely explanation is that the 2,4-D or MPCA analytes are being concentrated in the gum Arabic or corn-starch coatings…thus increasing the local concentration enabling a low LOD. However, the subsequent quantitative measurements are not really valid because the layer

close to the silver surface are analyte saturated..so further additions of analyte do not produce a significant increase in Raman signal.

Gum Arabic and corn starch helped trap pesticides 2,4-D and MCPA, subsequent concentrations of 2,4-D and MCPA on SERS sensors got an increased signal but were not good enough for quantification. The word 'quantification' has been removed from the thesis in chapters 2 and 3. The saturation problem has been discussed in point 15.

21, Suggestion: I would strongly suggest that the reviewers' comments and author replies for *all published papers* be included in an appendix at the end of the thesis so one can judge the level and detail of the review process.

These documents are in appendix 2-3.

Supplemental Information: the lack of experimental detail

22, In general, there is a lack of experimental detail/explanatory text provided for each of the three chapters. It looks like the research has been heavily edited down and selected for publication. The SI sections for Chapters 2-4 need to be substantially expanded to include all the relevant experimental details and raw spectra not included in the papers. Additional data/information needs to be included to deal with all the other issues raised. Our suggestion is to add an Appendix for each of chapters 2-4 with all of the corrections/additions included.

Experimental conditions have been expanded in each chapter. All relevant data and discussion has been included in Chapter 2-4 SI. Including:

- Figure S4 (A), S12, S14, S15, S16, S17, S18, S20, S21, S22, S24 in Chapter 2.
- Figure S3, S4, S6, S7, Figure 3,4 in chapter3.

- Figure 4.7-4.11, Figure S6 in chapter4.

23, **Figures S.2/S.3:** Not referenced in the main body text…this needs to be fixed. All figures in a thesis have to be referenced in the text/paper.

All figures have referenced in text/paper.

24, **Figure S3.2:** Scale bars should be provided. Also, images are reproduced are too small to show all the relevant detail.

The dimensions of connector and chip holder were included in Figure S2. Images size have been adjusted.

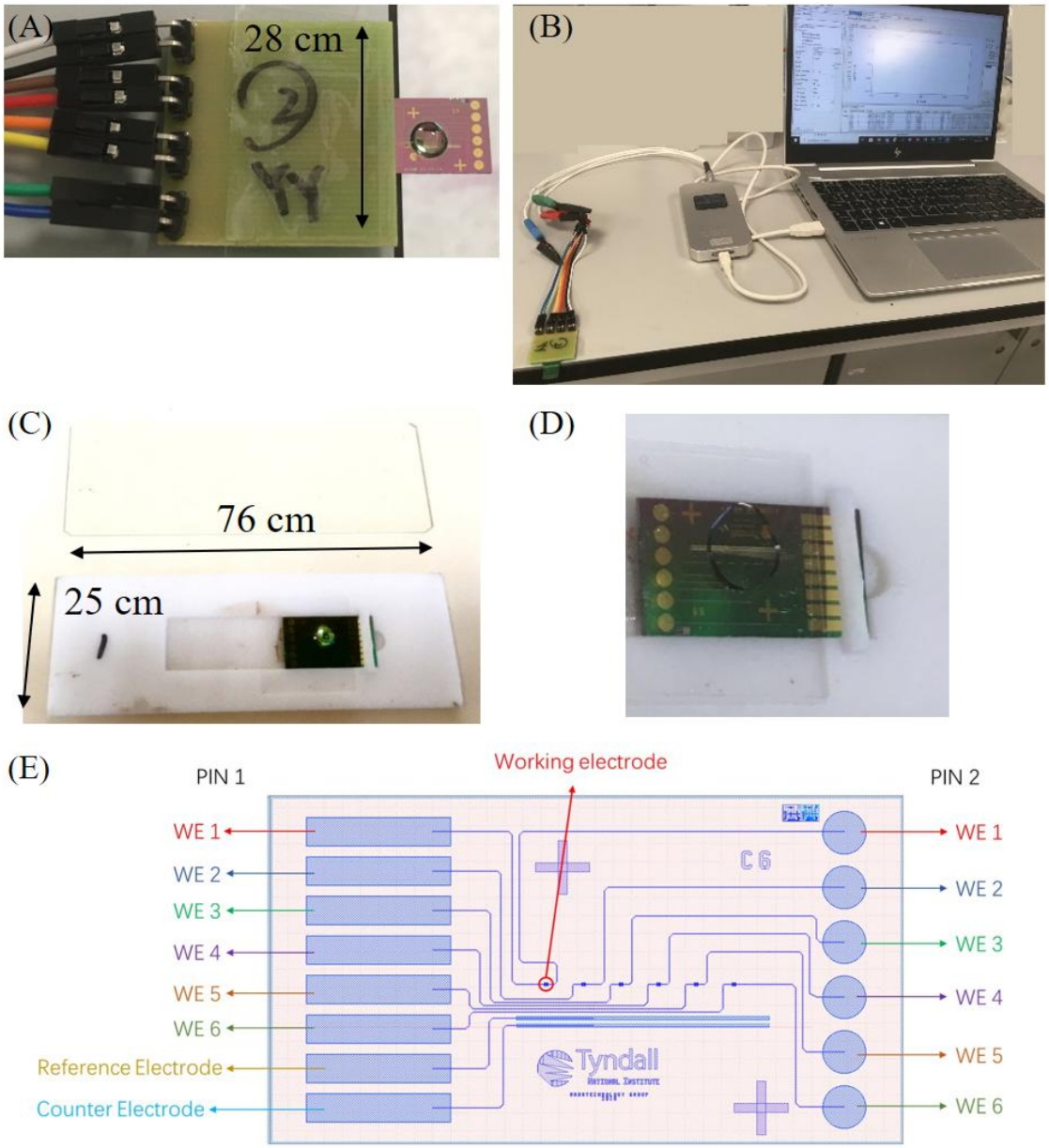

Figure S2: (A) Chip connector; (B) SERS substrate fabrication setup. (C)(D) Chip holder for Raman measurements in water environment. (E) Chip design layout.

Scientific Issues:

25, There is insufficient detail in the thesis with respect to the *reproducibility* of the SERS measurement. This needs to be addressed in the corrected thesis.

The same as point 14.

Reproducibility study:

The reproducibility of SERS sensors was accessed in the first step: electrochemical deposition fabrication. With the same electrochemical deposition parameters, the final morphology, size, nano gap etc. were the same for each deposition.

This was included in chapter 2 SI S10: All the nanostructures had been electrochemically deposited at least three times. Chapter 3 Figure 3.1: All the depositions have been repeated at least three times. Chapter 4: The success rate of SERS sensor fabrication was 84.21% out of 19 sensors as shown in SI bar plot Figure S8.

chapter 2 real sample study, there are three sensors used for each concentration of 2,4-D for both real water samples: Ten measurements were undertaken for each concentration on a substrate, the experiments were repeated three times on three individual SERS substrates using three individual sensor chips. (section 4.3, paragraph 1.)

26, Page 84: Not sufficient to say "*chemicals present in mineral water*", need to explain which anions or cations are most likely to generate a signal….this is known in the literature.

Chapter 2, section 4.3 paragraph 2: The reference spectrum for mineral water is shown in Figure 2.6 (A), the interference peaks near 1000 cm^{-1} are probably due to the interaction between Gum Arabic and SO_4^{2-} present in mineral water.[49]

27, **Page 146:** Repeatability experiment. One might argue that the repeatability is actually worse ...need to have the baseline count known...or subtracted. Cannot tell from the plot on left....looks like it's ~500 counts...then variability is >25%RSD.

- Incorrect to say R^2 = 12.48%.

This has been revised:

(A)

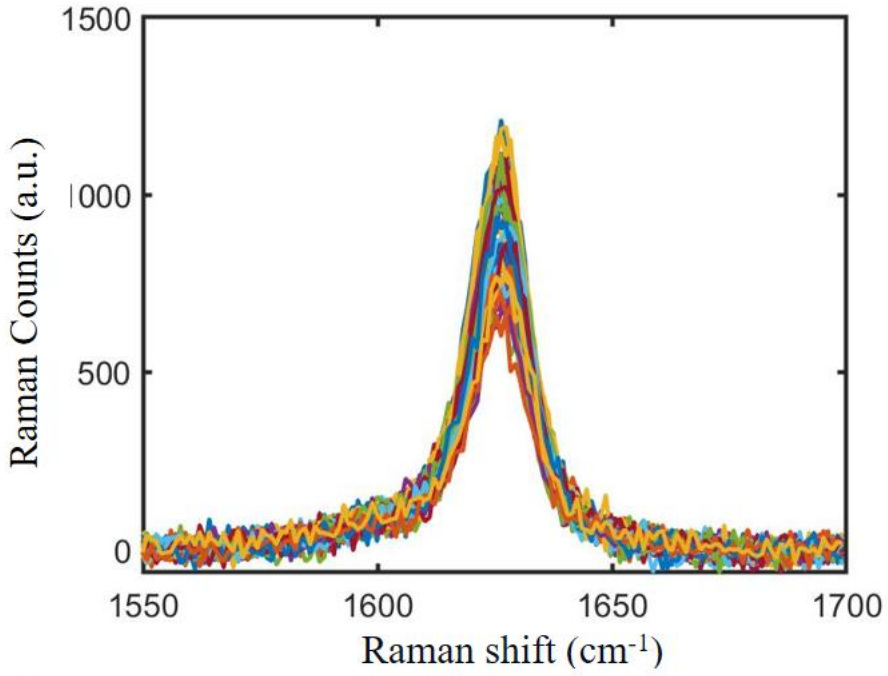
1500
1000
500
0
Raman Counts (a.u.)
1550
1600
1650
1700
Raman shift (cm-1)

(B)

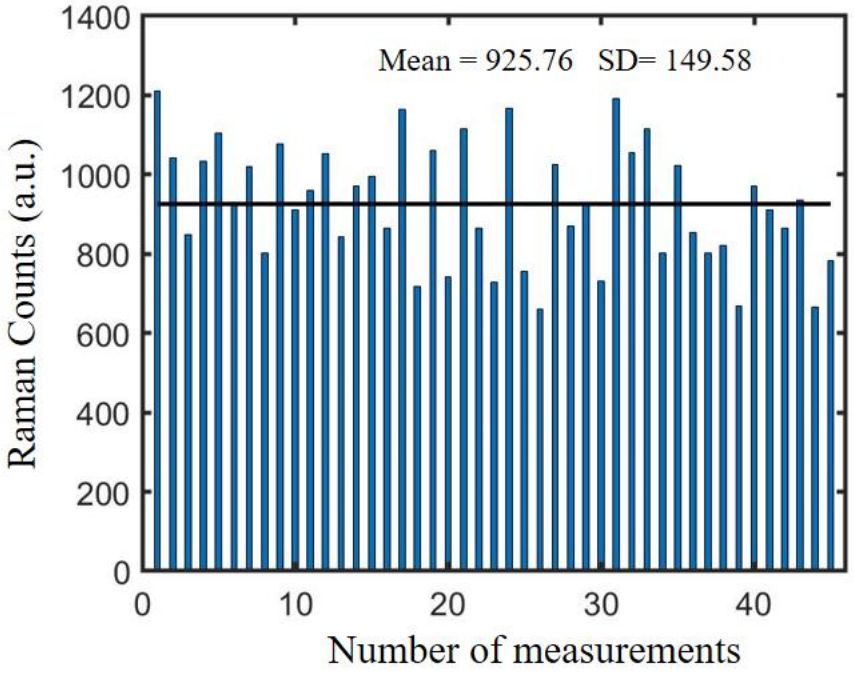
Mean = 925.76 SD= 149.58
1400
1200
1000
800
600
400
200
0
Raman Counts (a.u.)
0
10
20
30
40
Number of measurements

Figure 4.5: Repeatability study of an Ag nanostructure SERS substrate. (A) Spectra of MB at 0.1 μM from 45 different random points on a Ag nanostructure SERS substrate after baseline subtraction. (B) Bar plot of Raman intensity of the characteristic peak of MB at 1625 cm^{-1} in (A) after baseline subtraction, with SD=149.58 for 45 different random points on an Ag nanostructure SERS substrate.

28, Serial Dilutions: The calculations and method used to prepare all the serial dilutions should be explicitly spelt out in the thesis. Claims of ultra-low LOD/LOQ require a lot of supplementary information to validate these claims.

This has been included in chapter 2, section 1.1: For 2,4-D serial concentration preparation, 0.0088 g 2,4-D crystal was dissolved in DI water (20 mL) to a concentration of 2 mM. 2 mM (100 μL) of 2,4-D then diluted in DI water (900 μL) to 0.2 mM in Eppendorf AG PCR tubes (1 mL) from Sigma-Aldrich (Ireland) and diluted to serial concentrations by using the same approach.

Chapter 3: For MCPA solution preparation, 28.5 mg MCPA crystal was dissolved in 500 mL DI water to 0.285 mM, 0.285 mM MCPA (100 μL) then diluted in DI water (900 μL) to 28.5 μM. The other concentrations were prepared by using the same approach.

Chapter 4: Targeted-ss-DNA was prepared by diluting targeted-ss-DNA solution (100 μM, 10 μL) in PBS buffer (990 μL) to 1 μM, and repeating the step to different concentrations.

29, Types of container used: These need to be specified for SERS as leachates from plasticware can cause problems.

Type of container for analytes: new colorless Eppendorf AG PCR tubes (mL range) from Sigma-Aldrich (Ireland).

The other comments:

1, Comment on 'However, lithography based methods, although extremely tuneable and scalable, suffer from high cost, slow throughput and are time consuming', is that true?

Lithography based technology is complex as ‘In E-beam lithography, the photon resist is cross-linked after being exposed to an electron beam. The exposed resist can then be washed away, leaving only the unexposed resist on the substrate. Metal layer is then evaporated onto the whole substrate and the unexposed polymer is then removed together with its metal over-layer, leaving only the metal pattern on the substrate.’ It involves lithography several times and physical vapour deposition step, thus time consuming. The instruments used are expensive and are operated in high vacuum environment, SERS material is usually gold.

Chapter 2.

30, It is not clear from the thesis or paper that the Gum Arabic is being used as a concentrator for the poorly binding pesticide analytes. Also, as the experimental information is very sketchy here, it’s not clear if all of the gum Arabic was being removed during rinsing and if so how did you validate that it was not removed and how thick the layer is. This is critical information related to the performance of the material. Really needed to validate the performance of this substrate with a known molecule with good SERS response.

Function of Gum Arabic: As there is no nitrogen or sulfur atom that has good affinity towards noble metal nano particles as discussed in chapter 1 in 2,4–D chemical structure, it is hard to directly detect 2,4–D using silver or gold nano particles SERS substrates. Sliver–Gum Arabic nano structure used in this study can help attract 2,4–D to the SERS surface to get SERS signal.

Gum Arabic was selected as it is a branched hetero-polysaccharide containing protein and carbohydrate groups that is a biodegradable, nontoxic, and easily available biopolymer.[50-51] It has been used to act as a biopolymer for the removal of heavy metal,[52] pesticides, and pollutants in polluted water bodies,[53-54] because of its great adsorption ability towards different chemicals.[55]…… Gum Arabic is a conductive biopolymer that is also widely used as a raw material for composite conductive materials studies.[56-58] Besides, its viscosity changes significantly with the change in Gum Arabic solution concentration, this property allows it to act as a shape monitoring agent in Ag NPs electrochemical deposition. ……..Gum Arabic has been used for green chemical synthesis of silver nano particles.[59-61] During this process, Gum Arabic acts as a reducing agent to reduce silver ions, then Gum Arabic forms nano structure with Ag atoms, subsequently forming Ag-GA NPs.[61]……. Gum Arabic has previously been used to interact with pesticides[53], however, the interaction mechanism is not well known. Gum Arabic is also known to attract an analyte (such as pesticides that have poor interaction with silver surfaces) in close

proximity to the surface of the GA related nanoparticles. In addition, it has been realized to use Gum Arabic to electrochemically synthesize homogeneous Ag-GA SERS substrates in this research. For this reason, Gum Arabic polymer layers helped capture 2,4-D to provide repeatable SERS signal and facilitated 2,4-D detection using Raman spectroscopy.

High intensity SERS signal with broad background signal in chapter 2 SI Figure S4 (A) below of bare Ag-GA substrate (in black) can also prove the formation of Ag-GA NPs.

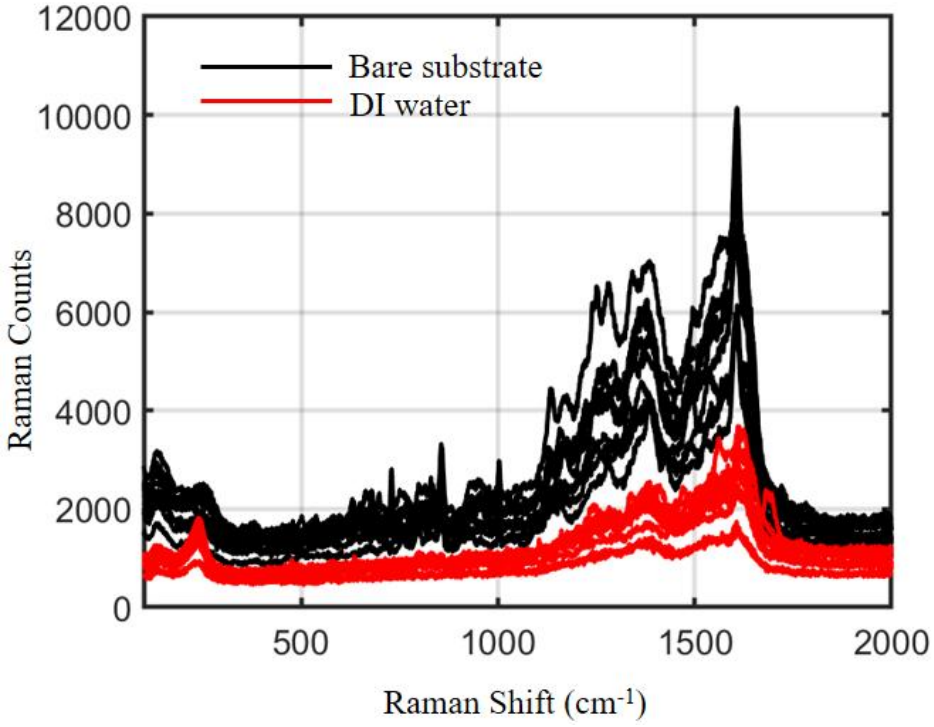

chapter 2 SI Figure S4 (A): bare substrate and substrate after application of DI water;

31,

- **Control spectra:** The fact that no control spectra of the 2,4-D analyte in bulk form or in concentrated solution is very worrying. This needs to be included so that one can compare these spectra with those in Figure 2.3, 2.4,

2.5, and S3.3. The bands selected for quantitative analysis need to be identified …. That is, we need to know what vibrational modes are involved.

- **Band assignments:** Not given for those used for quantification nor the scientific rationale….already made the point above.

Chapter 2, section 4.2: Peak 1400 cm^{-1} could be a characteristic peak for Gum Arabic layer,[34] while peaks at 1130 cm^{-1} and 293 cm^{-1} are for 2,4-D, using peak at 1400 cm^{-1} as a reference peak gain a better fitting results. In SI Figure S20, for 2,4-D crystal Raman spectrum, Raman bands at 194, 414, 840 and 1105 cm^{-1}, assigned to in-plane vibrational modes involving C-Cl and C-O-C bonds, are shifted in the enhanced SERS bands to 293, 889 and 1100 cm^{-1} for 2,4-D solution.[35-36] 2,4-D Raman peak in 1159 cm^{-1} is related to C-H_{ring} scissoring and shift to 1130 cm^{-1} in SERS.[37] 1393 cm^{-1} shift to 1297 cm^{-1} for the 2,4-D solution on SERS substrate and is related to -CH_2 wagging, See Table S1.

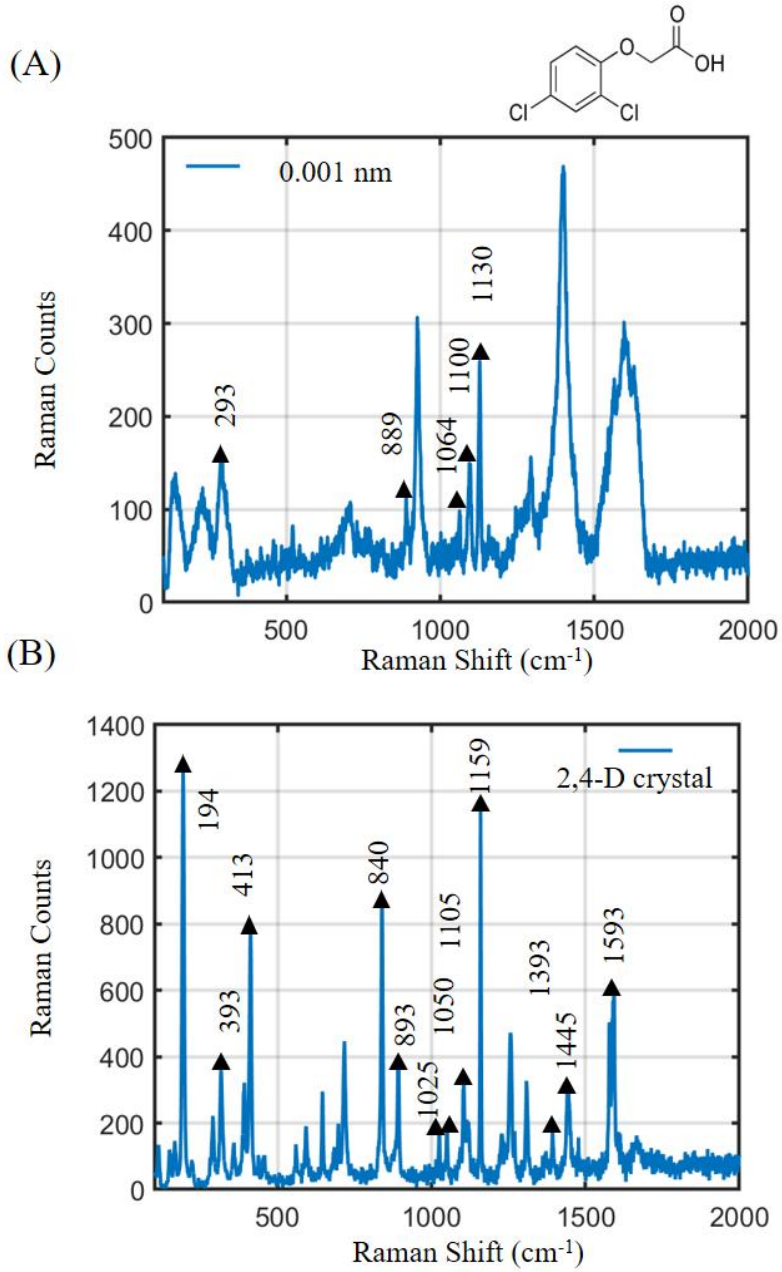

Figure S20: (A) SERS for 0.001 nM 2,4-D; (B) Raman spectrum for 2,4-D crystal.

Table S1 2,4-D crystal and 2,4-D solution on SERS substrate peak assignment.

2,4-D crystal	2,4-D solution on Ag-GA SERS substrate	vibration modes
194	288	δ(COC) + δ(CCl)
840	889	ν(CC)ring + ν(C–O) + ν(C–Cl)
893	928	ν(C–COO−)
1050	1064	ν(CC)ring + ν(CO) + δ(CH)ring
1105	1110	ν(CC)ring + ν(C–Cl)
1159	1130	δ(CH)ring
1393	1297	ω(CH2)

32, Kinetic Spectra: The spectra collected from the SERS substrate with the lowest analyte concentrations should be included to show how the analyte is diffusing through the gum Arabic to the surface….this will better explain what has been done.

The same as point 19.

33, Structures & surface bonding: Need to explain how structures of the analytes actually attached to the surface to give a SERS spectrum.

The same as point 16.

34, Linear Fits: The data presented in chapter 2 is not really believable….have the same SERS spectra over a huge range of concentrations. During the viva voce it became apparent that what has happened is that the gum Arabic layer is becoming saturated with the analyte and there cannot be any further significant increase in signal because of this.

The explanation about saturation is in point 15. ‘Linear’ changed to ‘calibration’ in the main text.

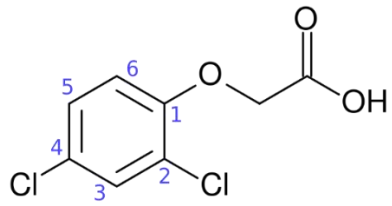

35, 2,4-Dichlorophenoxyacetic acid: Structure…..No nitrogen, no sulfur…..so not likely to be very SERS active…what holds it to the surface? This is why the conventional SERS spectra are so poor and you need a polymer layer to concentrate it at the surface

Chapter 2: Because there is no nitrogen or sulfur atoms that have good affinity for noble metal nano particles as discussed in chapter 1 in 2,4-D chemical structure, it is hard to directly detect 2,4-D using silver or gold nano particles SERS substrates. Sliver-Gum Arabic nano structure used in this study can help attract 2,4-D to the SERS surface to get the signal.

Other additional information included in chapter 2:

To support the statement: While 2,4-D does not have repeatable SERS signal on silver nano particle surface in experiment even at a very high concentration (1 mM), see SI Figure S12.

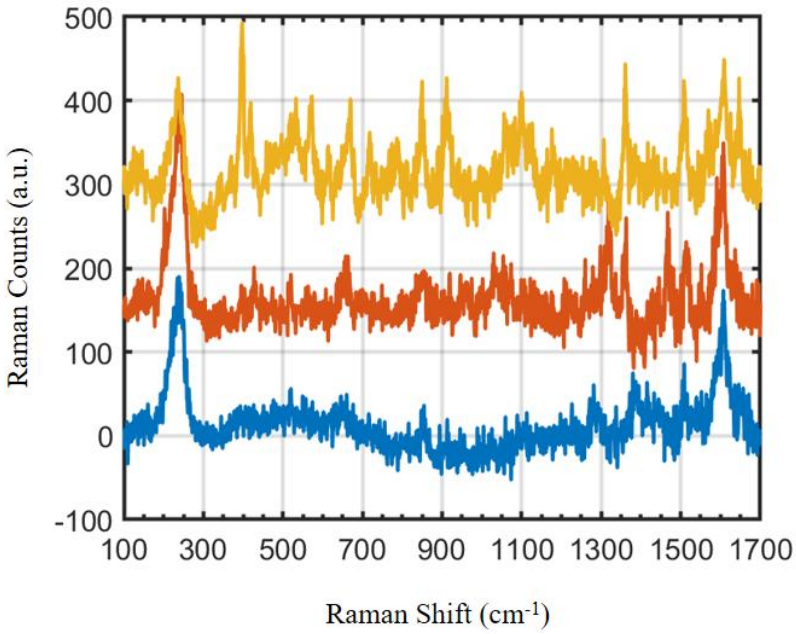

Figure S12: Spectra for 2,4-D at 1mM on bare silver nano particle SERS surface, at three different locations. The silver nano particle was deposited by electrochemical synthesis, the electrochemical deposition curve is shown in Figure S9.

To support that statement in chapter 2: In the initial work, it was observed that structures S_1, S_2, S_3 were able to detect 0.1 nM (0.0221 ppb) 2,4-D in 30 min… and SI Figure S14 (A) of 0.1 nM 2,4-D detection in 30 minutes for S_1-S_3.

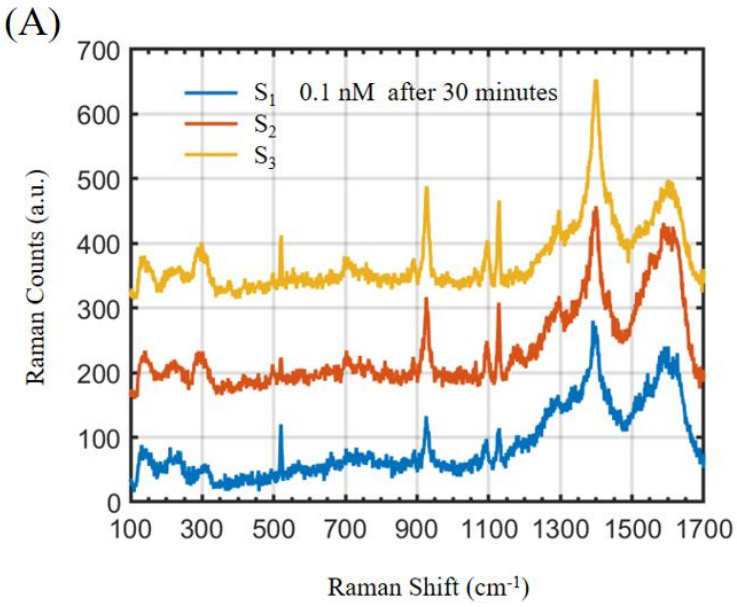

Figure S14 (A) Raman spectra for structure 1, 2 and 3 that were able to detect 2,4-D at 0.1 nM after 30 minutes. Peak around 520 cm^{-1} is from Si sensor substrate under Ag-GA nano structures, because of different coverage/nano gaps of Ag-GA nano structures at different measurement locations, Si peak Raman signal intensity varies.

To support the statement: An immediate response was observed for 0.1 nM 2,4-D (S_4 substrates) which is more than four times lower than the MRL (0.1 ppb) required by EU water framework directive for individual pesticides.[62-63] See SI Figure S17.

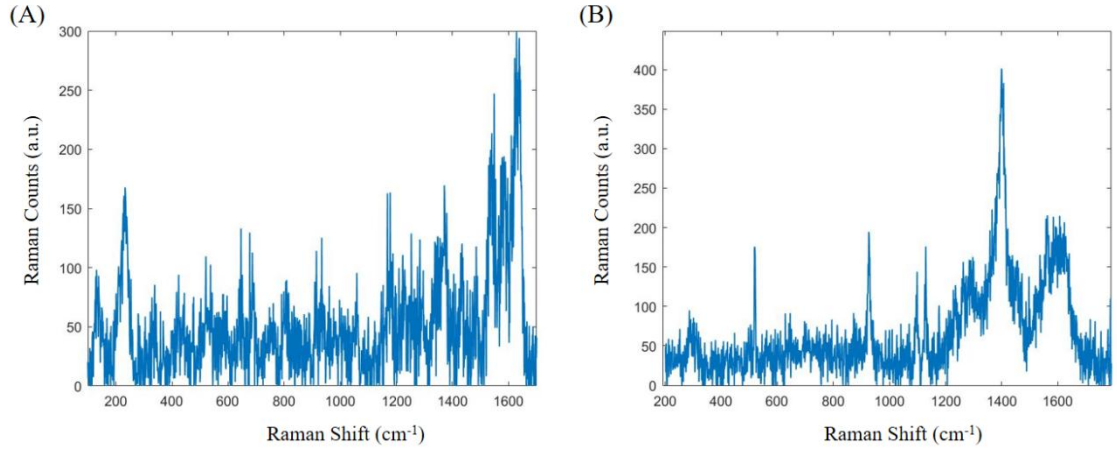

Figure S17: Reference spectrum (A) for DI water; (B) 2,4-D at 0.1 nM for Ag-GA structure S_4.

Section 4.1: At a lower 2,4-D concentration (1 pM), it took 30 minutes to get SERS signal, while at a higher 2,4-D concentration (0.1 nM), the SERS signal showed immediately. At a low concentration of 2,4-D, it took longer for the molecule to reach the SERS hotspot because of diffusion.[64] In the same time window (half an hour), at a higher concentration of 2,4-D, more molecules reached the SERS surface, and it was faster to get the SERS signal.

Raw data for commercial Gum Arabic from Amazon for calibration:

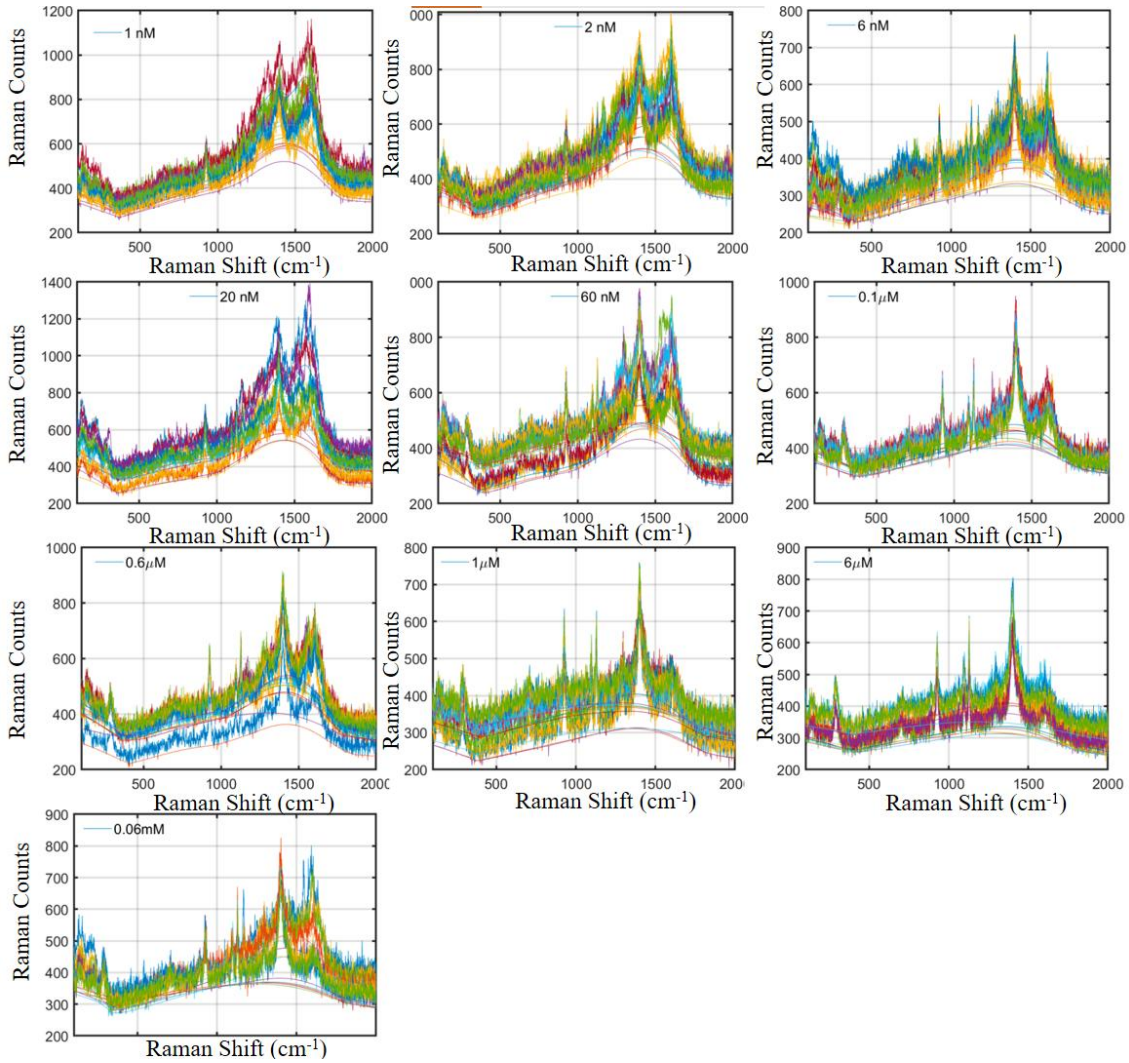

Figure S24: all raw data in Figure S23. The spectra were for 2,4-D at different concentrations and the smooth lines were substracted background signal in data analysis. Ten spectra were used for each concentration. At the lowest/first 2,4-D concentration, it took around 30 minutes to get the signal. It took 15 minutes in total to get all data for each concentartions.

Added more information in introduction: SERS is mostly based on the enhanced Raman signal by noble metallic nano structures that can generate strong electromagnetic field with

the excitation at certain laser wavelength, such as Ag, Au and Cu, which also named as Localized Surface Plasmon Resonance (LSPR).[65-66] The excited LSPR generates a large electric field on the metal surface and this electric field induces dipole moments in a molecule on the surface of nanostructures, and gains an enhanced Raman signal. This strong, localized electromagnetic fields present in nano-gaps between nanostructures are known as "hot spots".[67] The enhanced Raman signal are from electromagnetic enhancement[68] and chemical enhancement,[69] electromagnetic enhancement contributes to 10^{11}-10^{13} magnitude of SERS signal while chemical enhancement contributes only a factor of 10^2 for Raman enhancement.[70]……. For chemical methods, though size and morphology controllable nano particles are available, drop casting of the nano particles onto a substrate, paper, glass or silica, etc. is still required.[71-81] The distance between the nano particles is hard to control. This in turn leads to difficulties in quantification of target analytes, as for quantification in SERS, data points for each analytes concentration for linear calibration are the average of more than three measurements in more than three locations on a SERS substrate (usually ten spectra are measured in ten different locations). Another significant issue with the use of nanoparticles is that they could be removed or lifted after application of analytes solvent, again resulting in quantification inaccuracy. Most research papers that reported on chemical synthesis fabrication methods for effective SERS substrates carry out experiments in a dry environment (i.e., the solution was dropped casted and allowed to dry) instead a water environment, with the drying time usually lasting for 30 minutes to one hour.[72-73, 75-76, 78] Besides that, for some research using paper SERS substrates and chemically synthesized nano particles as effective SERS substrates, the

background Raman signal from a paper substrate could affect the target analyte Raman signal readout. Laser-assisted fabrication methods, combining laser etching on glass/silica substrates for nano pattern and followed by metal layer deposition, have limited choices for the morphology nano patterns and plasmonic materials.[82-84] The templating method entails several steps and has a higher likelihood of fabrication failure.[85-86] These methods are either time-consuming or involve complex steps. High throughput, low cost and reproducible fabrication of SERS substrates are still elusive.

Other comment in Chapter 2:

1, The optimal size for nano particles? how thick Gum Arabic layer is?

I did not do this research. The optimal SERS substrate I conclude in this research was based their homogeneity and their detection ability towards 2,4-D in application. I attach some research that have done size research:

https://doi.org/10.1021/jp106666t.

Journal of Nanoparticle Research volume 19, Article number: 267 (2017).

To determine the gum Arabic layer thickness, TEM characterization should be carried out. However, for this sensor chip, it is hard to prepare the sample. To cut the chip, Ag-GA nano particles would be damaged as they are soft.

2, comments: no humidity control thus we could see drying effects.

Humidity control and dry effect: there is no humidity concern, every measurement used fresh Ag-GA SERS sensor, chapter 2 only showed the effect after application of DI water. The decrease of the Raman signal: water environment reduces Raman signal in general.

compare	LOD in 30 minutes response time	Response time for 0.1 nM
Structure 1	0.1 nM	30 minutes
Structure 2	0.1 nM	30 minutes
Structure 3	0.1 nM	30 minutes
Structure 4	0.001 nM	Immediately

After Ag-GA SERS sensor has dried in air, because of the oxidation of silver, it will lose its SERS enhancement ability.

3, 2,4-D solution did not dry: visually see the solution as I put a drop of analyte solution.

4, What does it mean by optimize through the detection ability?

As shown below, in this research, comparing four structures of SERS substrate by detection ability (response time, detection limit).

5， laser power effect: to check if the thermal effect or other effect of the laser would influence the 2,4-D SERS signal or not within the laser power that is used in the measurement, I studied the dependence of the peak Raman counts at peak 293 cm^{-1}, 1130 cm^{-1}, 1400 cm^{-1} and ratio between 293 cm-1/1400 cm-1, 1130 cm-1/1400 cm-1 on the laser power. For every laser power parameter, the spectrum is the average of 10 measurements. For S4, different laser power (1)1%, (2) 5%, (3) 10% (4) 5%, (5) 1% are used to measure the spectrum of 2,4-D at 0.1 nM on the same type of substrate; For S1-S3, different laser power (1)1%, (2) 5%, (3) 10% (4) 5%, (5) 1% are used to measure the spectrum of 2,4-D at

0.2 μM on the same substrate, total laser power is 7 mW. The Raman spectra is shown in Figure 3 (A).

As the results, the laser power that we used for this experiment is below the threshold to damage the SERS substrate, though the overall Raman intensity increases with the increase of the laser power, then decrease with the deceasing of the laser power (Figure 3 (B)) and the signal to noise ratio (S/N) is higher at the same time. Peak ratio 293 cm-1/1400 cm-1, 1130 cm-1/1400 cm-1 were not depend on laser power. As shown in (Figure 3 (C-D)).

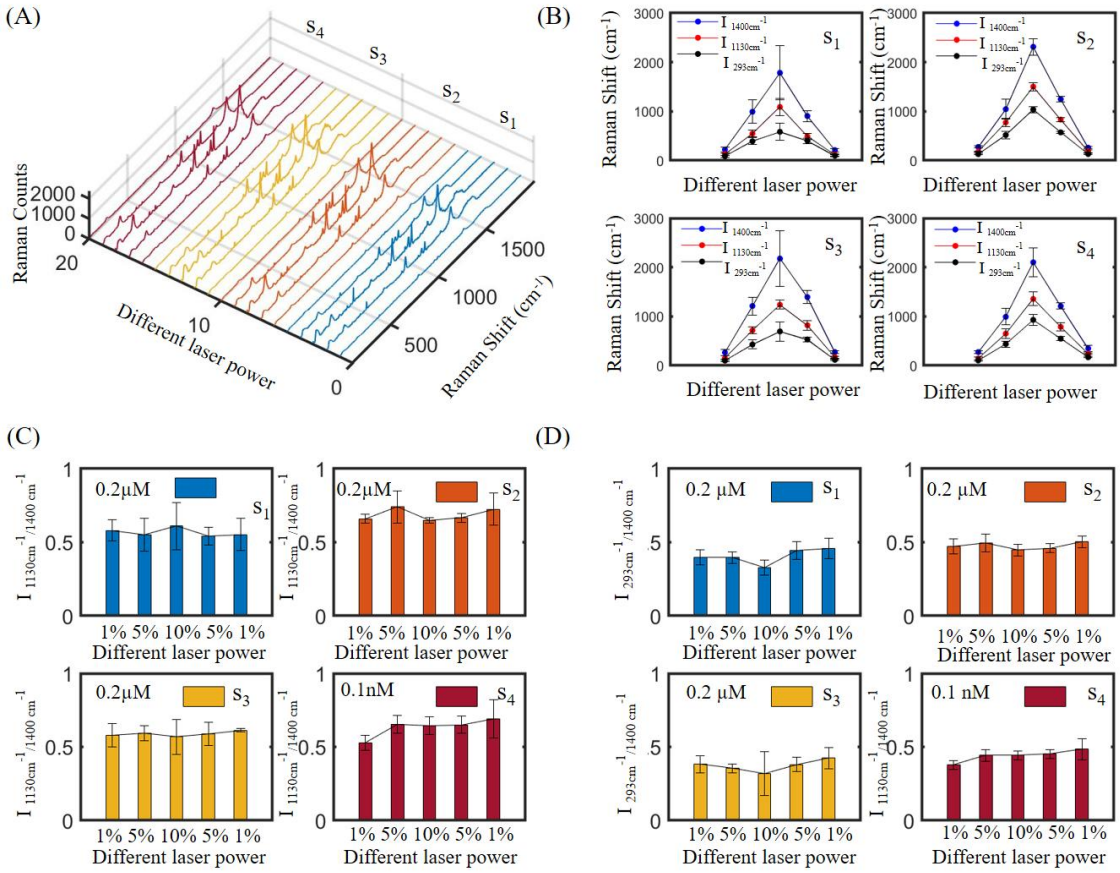

Figure 3: Different laser power ((1)1%, (2) 5%, (3) 10%, (4) 5%, (5) 1%) applied to S1-S3. (A) peak intensity change for each single peak 293 cm^{-1}, 1130 cm^{-1}, 1400 cm^{-1} at different

laser power; (C-D) peak ratios of 293 cm^{-1}/1400 cm^{-1}, 1130 cm^{-1}/1400 cm^{-1} change with the change of laser power.

Chapter 3.

36, Similar to above, the analyte molecule will not bind strongly to the silver surface and thus the SERS effect is going to be weak or non-existent using conventional SERS. It needs to be explicitly clarified that the corn-starch layer serves to concentrate the MPCA in the layer close to the silver surface and thus generate a detectable signal. .

Chapter 3: MCPA molecule does not contain sulfur or nitrogen atoms that have active interactions with silver nano particles surface as discussed in Chapter 1. Cornstarch biopolymer layer helps trap MCPA on the Ag-CS nano structure surface to gain enhanced Raman signal.

37, Reference/ Control spectra: These need to be included for the bulk analytes also…and these spectra compared to good quality SERS spectra.

Chapter 3 section 3.4:

MCPA and 2,4-D have similar chemical structure, their SERS spectra share the same peak features. MCPA crystal Raman spectrum is shown in Figure 3.4 (B). However, there are not so many research papers on MCPA peak assignment by using Raman or SERS.. …. Peaks 1400 cm^{-1} and 1600 cm^{-1} are related to Cornstarch. According to 2,4-D crystal Raman peak assignment and MCPA Raman peaks, see table 1, peak 291 cm^{-1} is assigned to C-Cl and C-O-C bonds, and peak 1129 cm^{-1} is related to C-H_{ring} scissoring. 1296 cm^{-1} is -CH_2 wagging, and 928 cm^{-1} is related to C-COO^- vibration. Raman spectra are sensitive to

test environments, pH, etc. So for precise Raman peak assignment, it is necessary to use theoretic studies such as DFT (density functional theory) modeling to help the analysis.[38]

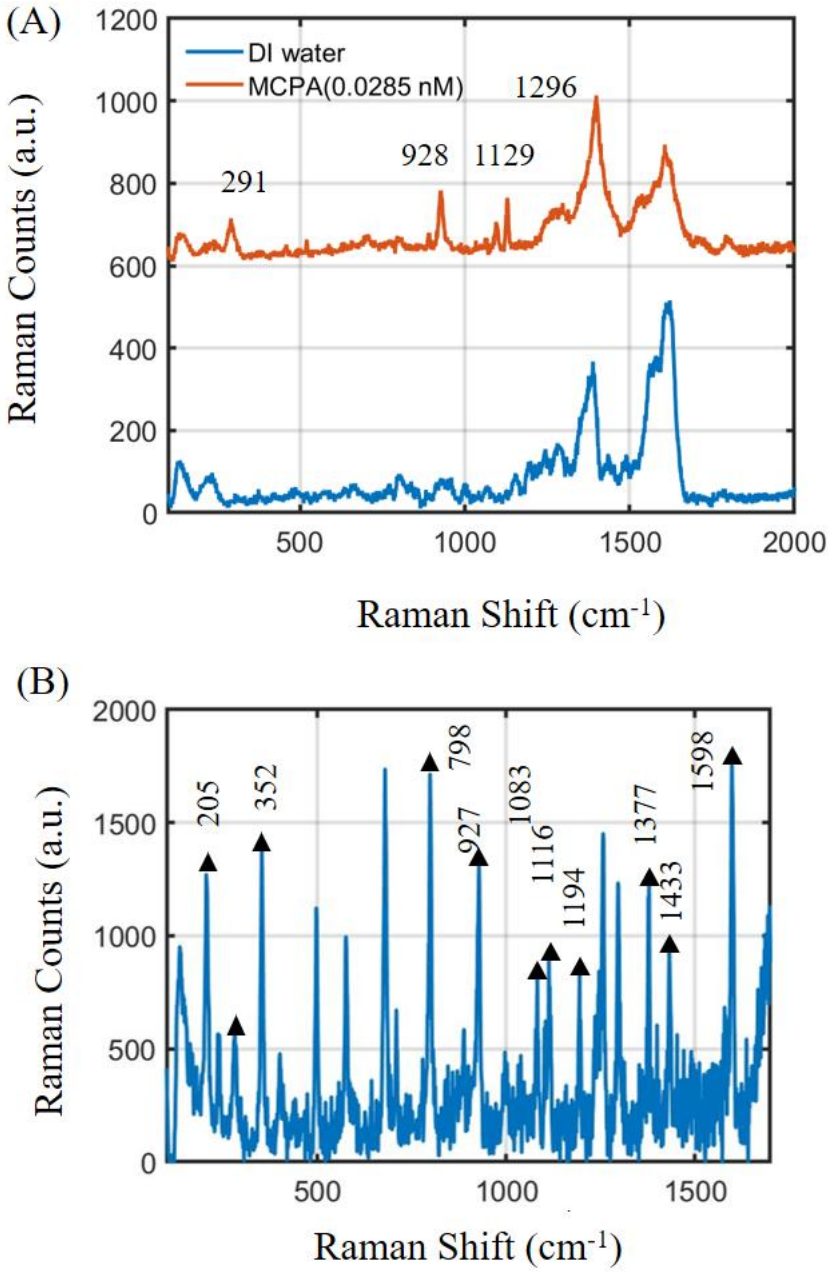

Figure 0.2 Ag-CS SERS sensor after application of DI water as a reference and after application of MCPA (0.0285 nM) solution. (B) MCPA crystal Raman Spectrum (laser power: 0.35 mW, exposure time: 30 s, 20x.).

Table 1: MCPA Raman peak and MCPA solution on SERS substrate peak assignment according to 2,4-D crystal vibration modes.

2,4-D crystal	MCPA crystal	MCPA on Ag-CS substrate	vibration modes
194	205	291	δ(COC) + δ(CCl)
840	798	\	$\nu(CC)_{ring}$ + ν(C–O) + ν(C–Cl)
893	927	928	ν(C–COO^-)
1050	1083	1098	$\nu(CC)_{ring}$ + ν(CO) + $\delta(CH)_{ring}$
1105	1116	1110	$\nu(CC)_{ring}$ + ν(C–Cl)
1159	1194	1129	$\delta(CH)_{ring}$
1393	1377	1296	$\omega(CH_2)$

38, Linear Fits: The data presented in chapter 3 for MCPA (Figure 3.5 & 3.6) is not really believable….have the same SERS spectra over a huge range of concentrations…

The concentration value has been checked and fixed. Figure 3.6 and section about MCPA in river water has been removed.

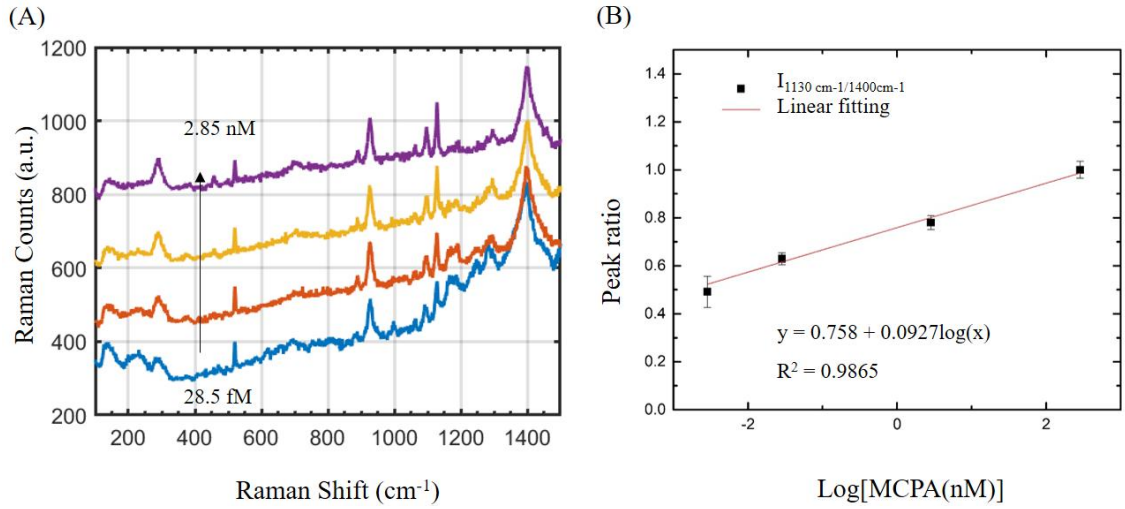

Chapter 3, Figure 3.6: (A) Spectra for MCPA at different concentrations from 28.5 fM to 2.85 nM in DI water. (B) Linear calibration for peak ratio $I_{1130\ cm\text{-}1}$ / $I_{1400\ cm\text{-}1}$ in (A) from 28.5 fM to 2.85 nM.

39, Band assignments: Not given for those used for quantification nor the scientific rationale….already made the point above.

Chapter 3, section 3.4: Peaks 1400 cm^{-1} and 1600 cm^{-1} are related to Cornstarch. According to 2,4-D crystal Raman peak assignment and MCPA Raman peaks, see table 1, peak 291 cm^{-1} is assigned to C-Cl and C-O-C bonds, and peak 1129 cm^{-1} is related to C-H_{ring} scissoring. 1296 cm^{-1} is -CH_2 wagging, and 928 cm^{-1} is related to C-COO^- vibration. Raman spectra are sensitive to test environments, pH, etc. So for precise Raman peak assignment, it is necessary to use theoretic studies such as DFT (density functional theory) modeling to help the analysis.[38]

40, Structures & surface bonding**:** Need to explain how structures of the analytes actually attached to the surface to give a SERS spectrum.

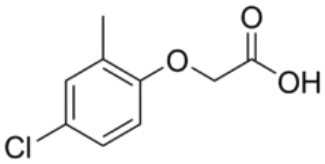

MCPA: Structure…..No nitrogen, no sulfur…..so not likely to be very SERS active…what holds it to the surface?

Chapter 3, section 3.4: It is possible that MCPA molecules enters Corn Starch porous structure, or that MCPA functional groups interact with Corn starch functional groups.[41-42] Corn Starch has -OH, -O-, and -CH bonds.[43] Theses bonds helped to trap MCPA.

Other revision:

For MCPA in Chapter 3, the saturation happened after 4th data point, MCPA concentrations/spectra have been checked and revised:

(A)

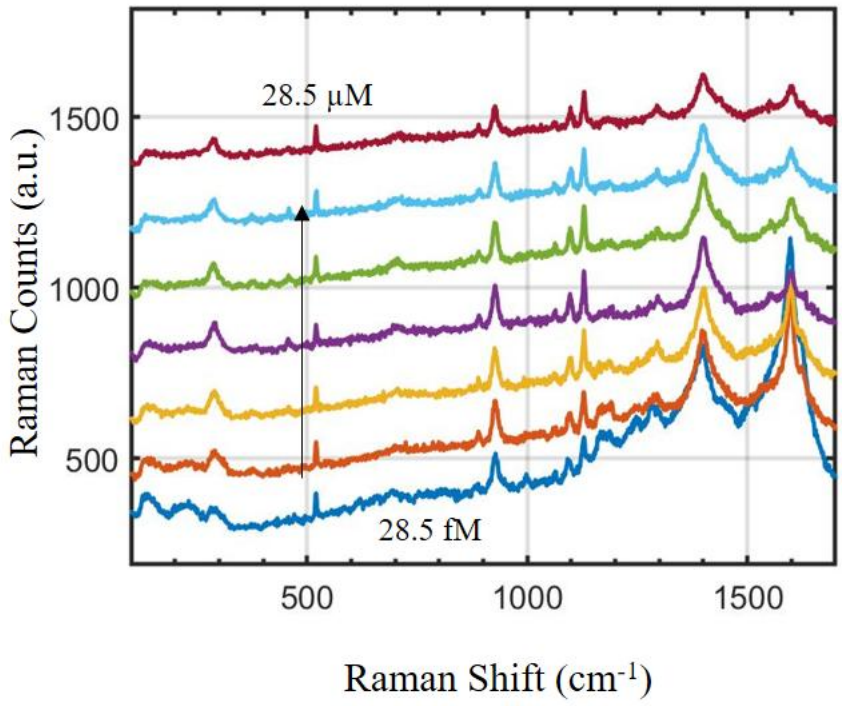
28.5 μM
28.5 fM
Raman Counts (a.u.)
500
1000
1500
500
1000
1500
Raman Shift (cm-1)

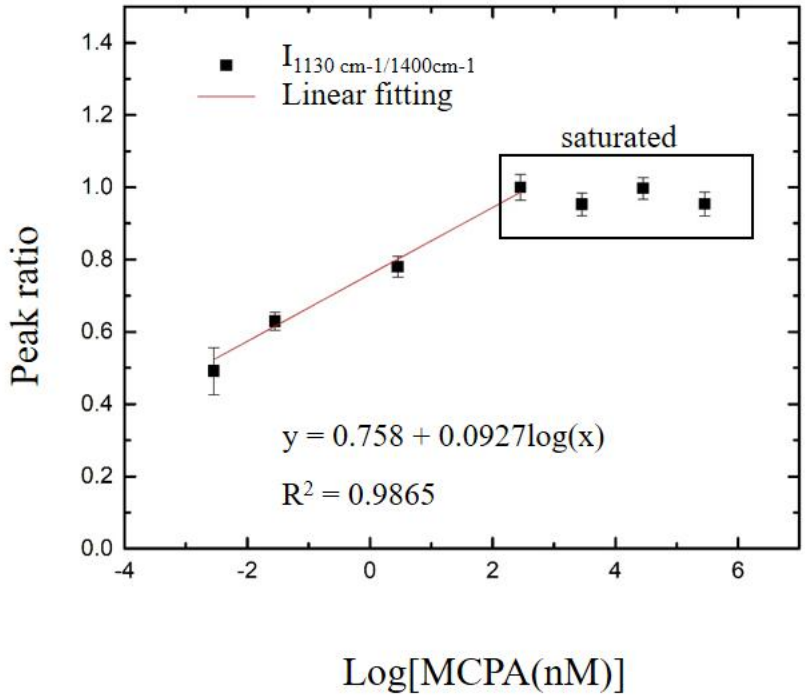
I1130 cm-1/1400cm-1
Linear fitting
saturated
y = 0.758 + 0.0927log(x)
R2 = 0.9865
Peak ratio
0.0
0.2
0.4
0.6
0.8
1.0
1.2
1.4
-4
-2
0
2
4
6
Log[MCPA(nM)]

Chapter 3 Figure S5: MCPA linear calibration in DI water. (A) Raman spectra for different concentration of MCPA from 28.5 fM to 28.5 μM ((28.5 fM, 2.85 pM, 0.285 nM, 2.85 nM, 28.5 nM, 0.285 μM, 28.5 μM). (B) Plot for peak ratio $I_{1130\ cm\text{-}1}$ / $I_{1400\ cm\text{-}1}$ in (A).

Reason for Raman signal change over 5 weeks in stability study section 3.3: The decrease in Raman signal over the five weeks was due to the slight oxidation of the SERS substrate contacting air every time doing the measurements by opening the sealing film and exposing it to air.

Chapter 4.

41, LOD: The LOD of 0.49 aM (10^{-18}) reported in the final chapter is not believable because the LOD for MB on its own is 0.32 μM (10^{-6})….which in essence means the targeted DNA method is 10^{12} times more sensitive!!.....so this says that each DNA strand attached is attracting 10^{12} MB molecules?

- The calculated LOD for MB is 0.3 μM, however, the experimental LOD is 0.01 μM. The calculated LOD=0.3 μM has been removed in thesis and replaced with experimental detection limit.
- Sensors were modified with ss-DNA overnight (24 hours) at a concentration of 1 μM. ss-DNA is well known to interact with MB. Consequently, there is a concentration of MB at the surface of a sensor in excess of the LOD of MB on a silver substrate. This is evident in Figure 4.4 and Figure 4.11, where a clear signal is observed for the ss-DNA prior to hybridization with target DNA. This is the reason why each DNA strand does not need to bind to 10^{12} MB molecules.

- DNA can accumulate MB, in DNA detection experiment section, MB was incubated on top of the SERS sensor for 10 minutes at 50 μM, 50 μL, there was enough time and MB molecule numbers to accumulate to DNA and further get SERS signal. Besides 0.49 aM is targeted ss-DNA, not the concentration of MB.

The explanation of this ultra-low detection ability for this SERS sensor is in section 3.4. Results from literature also proved the possibility of zmol or amol DNA detection. For example, Li et al. synthesized DNA-functionalized single walled carbon nanotube (SWCNT)-Au platform where gold-coated SWCNT acts as an isolated micro electrode, this platform was able to detect lower than 10 zmol complimentary 10-base DNA, this corresponds to having 6 DNA molecules in a 1 mL sample solution.[87] Shi et al. used two-dimensional carbon-coated molybdenum disulfide (2-D MoS_2@C) hollow nano rods combining with nucleic acid signal amplification strategies and a DNA hexahedral nano framework to fabricate a novel self-powered biosensing platform for microRNA-199a detection. The nanomaterial is then applied to carbon cloth. This assay shows an extensive linear range of 0.0001-100 pM with a low detection limit of 4.94 amol/L.[88]

A comparison between Ag-MB and Ag-ss-DNA/ds-DNA-MB was also discussed in section 3.4 and demonstrated in Figure 4.11. Figure 4.7-4.10 show four repeat experiments on four different chips for both higher and lower concentrations (Newly made targeted ss-DNA solutions for each experiments). For higher concentrations of targeted ss-DNA, I_1-I_2/I_1 vs Log_{10} ([t-DNA] (in pM)) showed a linear trend (Figure 4.7). For lower

concentrations (Figure 4.8), there was no signal change for targeted ss-DNA at 0.1 aM and at 1 aM, MB SERS signal increased. Repeat experiments proved the possibility of this ultra-low (1 aM) target ss-DNA detection (Figure 4.8-4.10).

Chapter 4 section 3.4:

In section 3.2, the experimental LOD for MB, obtained on an Ag SERS substrate, was 0.01 μM (Raman count is around 900 a.u.). With the Ag-thiol-ss-DNA SERS substrate, the Raman count was 600 a.u., but it is important to point out that this was obtained to a different (DNA modified) surface compared to the initial MB experiments. The effective SERS height was around 100 nm, the laser spot size was 1-2 μm. Total MB volume (0.01 μM) that was needed to reach this Raman account was $\pi \times (1)^2\ \mu m^2 \times 100 \times 10^{-6}\ \mu m = 3 \times 10^{-4}\ \mu L$. In the real situation, the length of this thiol-ss-DNA was around several nm,[89] this would help to bring more MB molecules closer to SERS substrate surface with a higher EF (Enhancement Factor) as described by Sharma et al. (several orders of magnitude).[90] See Figure 4.11.

After bonding with targeted ss-DNA (1 aM), Raman count increased from 600 to 1000 a.u., this arises from both electrostatic attraction and intercalation of MB to ds-DNA (several times more MB molecules bonded to ds-DNA comparing to bond to ss-DNA). ds-DNA folding in space compared to ss-DNA alone after MB application,[91-92] The EF can increase by several orders of magnitude closer to the Ag surface.[93] Besides, for DNA detection, the experiment was carried out in a dry environment. In theory, only a few targeted ss-DNA needed to hybridize to ss-DNA SERS substrate at 1 aM on a laser spot (30 DNA molecules in 50μL DNA solution) and align with experimental results. In my

experiments, Raman measurements and calibrations, the spectra were measured at ten different locations; the final spectrum was presented is an average of these ten spectra. This means that in these ten locations, targeted DNAs were able to hybridize and interact with the MB and offer a readable SERS signal increase. See all the raw data in Figures 4.8-4.10 for reference.

In summary, Ag-MB interaction and Ag-ss-DNA/ds-DNA-Ag interaction were two different systems, and the experiments were carried out in different conditions. For Ag-MB, Raman detection happened immediately without incubation (see Figure 4.11 (B)), the distance between the MB molecule and the Ag nano structure surface was limited by the diffusion limit at certain concentrations and surface energies of Ag and MB in a aqueous environment.[94] For MB as a Raman marker in DNA detection, Raman detection happened after 10 minutes of incubation in MB (10 μL, 50 μM) and was carried out in a dry environment. (Figure 4.11 (A, C)). MB bonds to ss-DNA through electrostatic force and is bonded to ds-DNA by both electrostatic and intercalation. DNA could also change its orientation and space arrangement during hybrization, thus, changing the distance towards the Ag nano structure surface. The Enhancement Factor of SERS related to the distance between the metal nano structure surface and the molecule. With different bonding mechanisms for these two system, their EF could be several orders of magnitude different. On top of that, ss-DNA can host large numbers of MB molecules after incubation at 50 μM MB and help its SERS signal reading. The Raman signal is usually much higher in a dry detection environment than in a water environment, and this has been demonstrated experimentally in chapters 2 and 3. All statements above explain the LOD differences in

sections 3.2 and 3.3., as well as the ultra-low detection ability. On top of this, the repeat experiment for target ss-DNA also confirmed the result. See Figure 4.8-4.10.

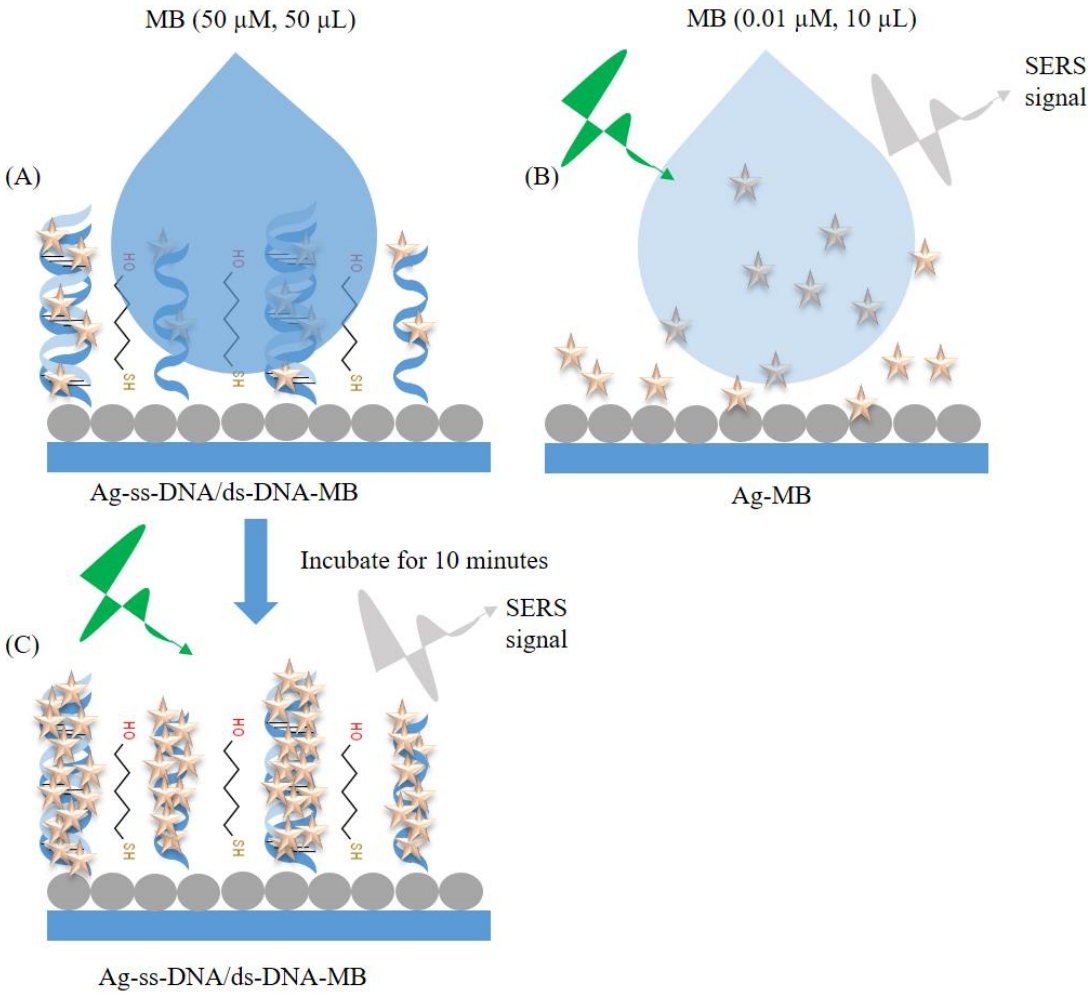

Figure 4.11: Illustration of (A) Ag-ss-DNA/ds-DNA-MB : 50 µL, 50 µM MB applied to SERS sensor (Ag-ss-DNA/ds-DNA) and incubate for 10 minutes. (B) Ag-MB: MB solution (µM) directly contacts with silver surface and gets SERS signal. (C) After 10 minutes of incubation, after removing the MB solution, Raman measurements were carried out in a dry environment.

42, The question has to be asked…was this experiment repeated with different chip, samples, analyst? During the viva voce the student could not provide a sound scientific explanation for how the ultra-low detection is being achieved…this needs to be done.

For higher concentrations of targeted ss-DNA, I_1-I_2/I_1 vs Log_{10} ([t-DNA] (in pM)) showed linear trend (Figure 4.7). For lower concentrations (Figure 4.8), there was no signal change for targeted ss-DNA at 0.1 aM and at 1 aM, MB SERS signal increased. Repeat experiments proved the possibility of this ultra-low (1 aM) target ss-DNA detection (Figure 4.8-4.10).

One chipe 1 (higher concentrations):

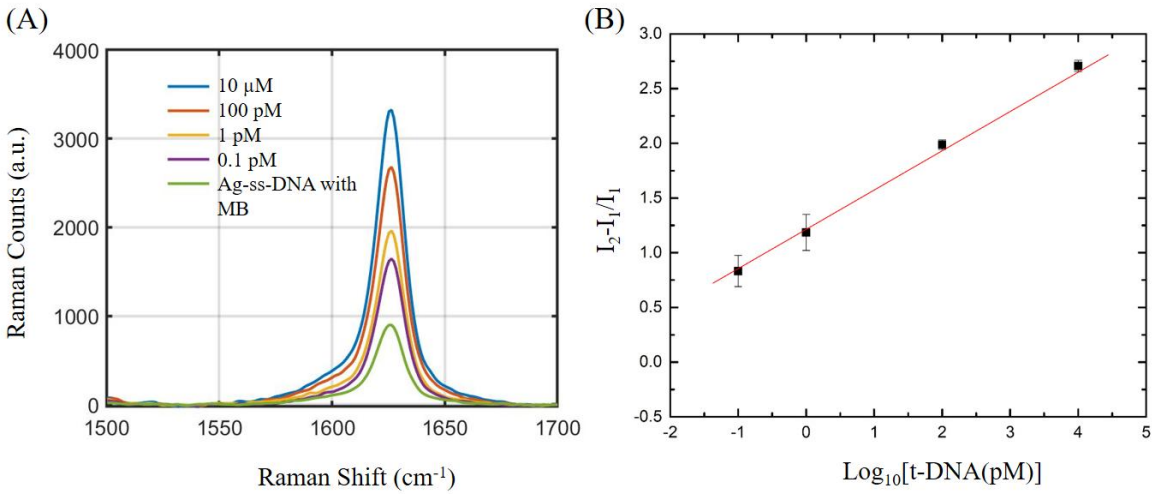

Figure 4.7: Targeted DNA (*stx*2) detection by SERS sensor at higher concentrations (A) MB spectra after hybridization with different target DNA concentrations (i) 0.1 pM, (ii) 1 pM, (iii) 100 pM, (iv) 10 µM. And reference spectra of Ag-ss-DNA SERS substrate with MB (in green). (B) Linear trend for I_1-I_2/I_1 vs Log_{10} ([t-DNA] (in pM)) at different target DNA concentrations for eye guide only. Ten different spectra, taken at ten different random

points on the functionalized Ag-ss-DNA SERS substrate are presented for each concentration of targeted ss-DNA, the error bars are the RSD (relative standard deviation) of these ten measurements.

On chip 2 (lower concentrations, 1st repeat experiment for 1 aM ss-DNA detection):

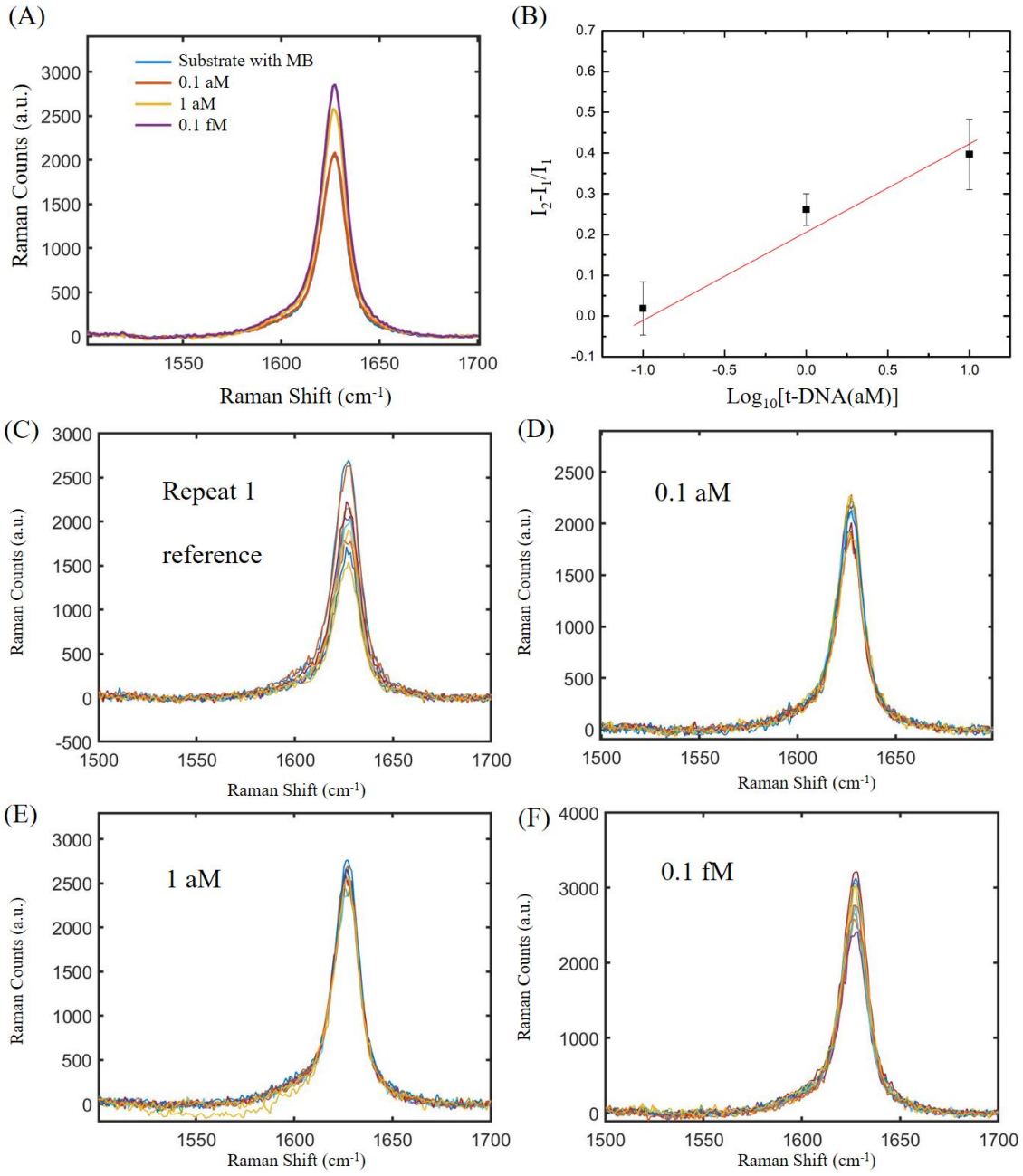

Figure 4.8: Targeted DNA (*stx*2) detection at lower concentrations. (Newly made targeted ss-DNA solutions). (A) MB spectra after hybridization with different target DNA concentrations (i) 0.1 aM, (ii) 1 aM, (iii) 0.1 fM. And reference spectra of Ag-ss-DNA SERS substrate with MB. (B) Linear trend for I_1-I_2/I_1 vs Log_{10} ([t-DNA] (in pM)) at

different target DNA concentrations for eye guide only. Ten different spectra, taken at ten different random points on the functionalized Ag-ss-DNA SERS substrate are presented for each concentration of targeted ss-DNA, the error bars are the RSD (relative standard deviation) of these ten measurements. (C-F) All raw data in (A).

On chip 3 (2nd repeat experiment for 1 aM ss-DNA detection):

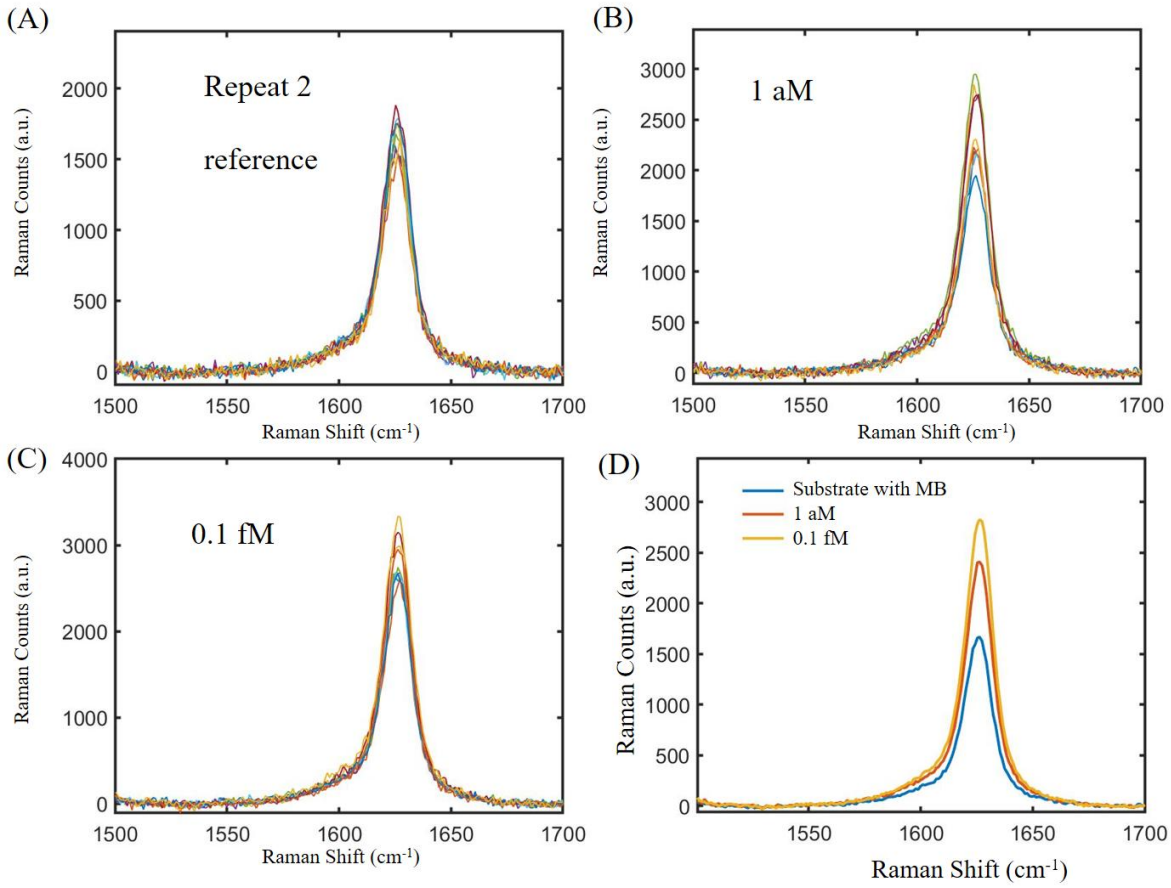

Figure 4.9: Targeted DNA (*stx*2) detection at lower concentrations (Newly made targeted ss-DNA solutions). (A) Reference spectra of Ag-ss-DNA SERS substrate with MB. (B-C) MB spectra after hybridization with different target DNA concentrations (i) 1 aM, (ii) 0.1

fM. (D) MB spectra after hybridization with different target DNA concentrations (i) 1 aM, (ii) 0.1 fM. And reference spectra of Ag-ss-DNA SERS substrate with MB. Ten different spectra, taken at ten different random points on the functionalized Ag-ss-DNA SERS substrate are presented for each concentration of targeted ss-DNA.

On chip 4 (3rd repeat experiment for 1 aM ss-DNA detection):

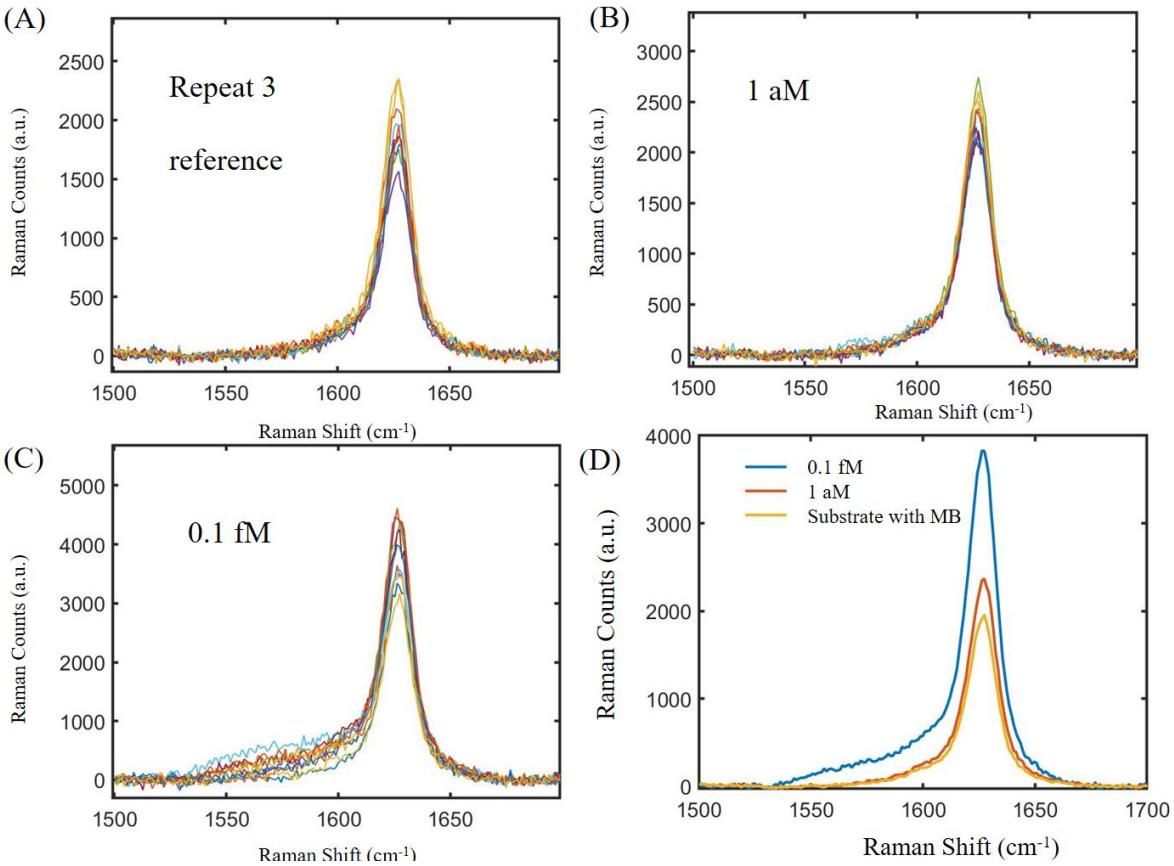

Figure 4.10: Targeted DNA (*stx*2) detection at lower concentrations (Newly made targeted ss-DNA solutions). (A) Reference spectra of substrate with MB. (B-C) MB spectra after hybridization with different target DNA concentrations (i) 1 aM, (ii) 0.1 fM. Ten different spectra, taken in ten different random points on the functionalized Ag-ss-DNA SERS substrate are presented for each concentration of targeted ss-DNA. (D) MB spectra after hybridization with different target DNA concentrations (i) 1 aM, (ii) 0.1 fM. And reference spectra of Ag-ss-DNA SERS substrate with MB. Ten different spectra, taken at ten different random points on the functionalized Ag-ss-DNA SERS substrate are presented for each concentration of targeted ss-DNA.

43, The required corrections are to include a sound scientific explanation for the huge increase in sensitivity reported here. It has already been noted in multiple places that the experimental details are deficient. Here, the details of all serial dilutions used to make these incredibly dilute solutions need to be included here…*I would also double check all calculations*.

The explanation is stated in point 41.

More experimental details has been included in chapter 4 SI and in point 42. All calculations have been checked.

44, Control experiments: These are lacking and should be included…..for example all 6 steps shown in Figure 4.1 should have Raman data….I would even have a second set of controls using deionised water included….

Chapter 4, section 2,5:

After the application of thiol ss-DNA, SERS surface was covered and only Si Raman signal shown; peaks at around 707 cm^{-1} (O-H out of plane bending), 1011 cm^{-1} (C-C-C stretching) and 1086 cm^{-1} (C-O stretching) for 6-Mercapto-1-hexanol[95] were shown in Figure 4.1 (C) after the second thiol application; There is no MB peak at 1625 cm^{-1} in Figure 4.1 (C), while the peak emerged after MB application in Figure 4.1 (D). In Figure 4.1 (F), after applying targeted ss-DNA, its signal increased.

The control used in this research is non-complementary DNA strands and DNA from non-targeted bacterial in section 3.3 and section 3.5 which do not have the Str 2 gene. Hybridization was undertaken in buffer solution (in agreement with literature approaches), using both targeted and non-targeted DNA.

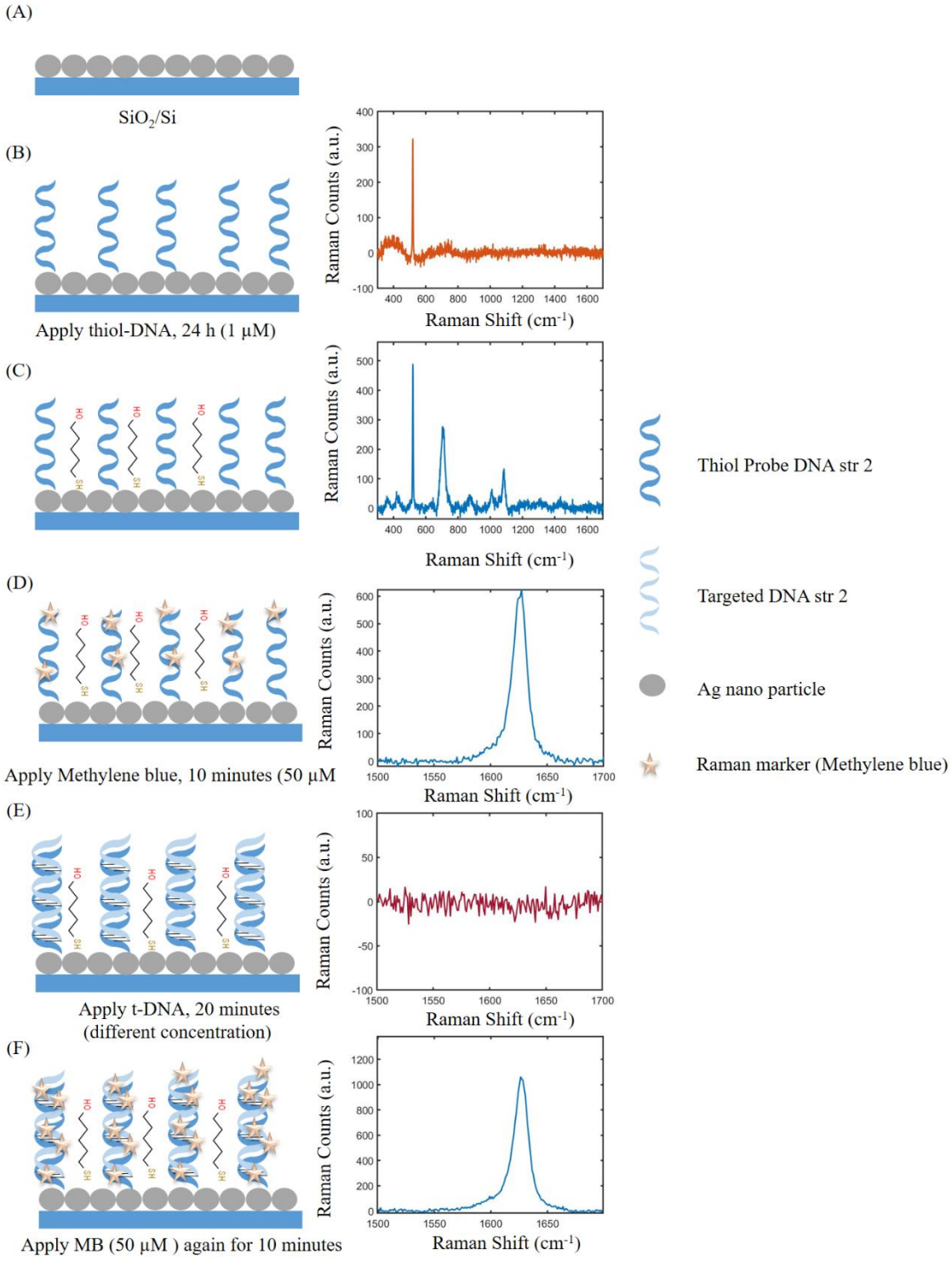
(A)
SiO_2/Si
(B)
Apply thiol-DNA, 24 h (1 µM)
(C)
(D)
Apply Methylene blue, 10 minutes (50 µM
(E)
Apply t-DNA, 20 minutes
(different concentration)
(F)
Apply MB (50 µM) again for 10 minutes
Raman Counts (a.u.)
Raman Shift (cm^{-1})
Thiol Probe DNA str 2
Targeted DNA str 2
Ag nano particle
Raman marker (Methylene blue)

Figure 4.1: Illustration of the DNA sensor development process and the corresponding Raman spectra (A) Ag nanostructure electrodeposition on SiO_2/Si substrate; (B) Immobilization of thiol modified probe DNA (50µL, 1µM) onto a SERS substrate and incubating for 24 hours. (C) Immobilization of 6-Mercapto-1-hexanol (50µL, 5mM) in the free spaces between probe DNA; (D) MB binding ss-DNA on a functionalized SERS substrate (incubation time: 10 minutes); (E) Hybridization of target DNA to the ss-DNA modified SERS substrate for 20 minutes; (F) MB intercalation between the dsDNA (incubation time: 10 minutes).

45, Full Raman Spectra: Again, the full Raman spectra should be included here……

Full Raman spectra for thiol functional steps has been included above and in chapter 4 Figure 4.1. For MB related experiment, spectra were only measured from 1500-1700 cm^{-1}. Its highest characteristic peak is located in 1625 cm^{-1}. And there was no 1625 cm^{-1} peak show in SERS substrate surface before MB application in Figure 4.1.

Other Raw data:

Figure S6 shows the Raw data for Figure 4.6. Again ten different spectra, taken in ten different random points on the functionalized Ag-ss-DNA SERS substrate are presented for each concentration of targeted ss-DNA:

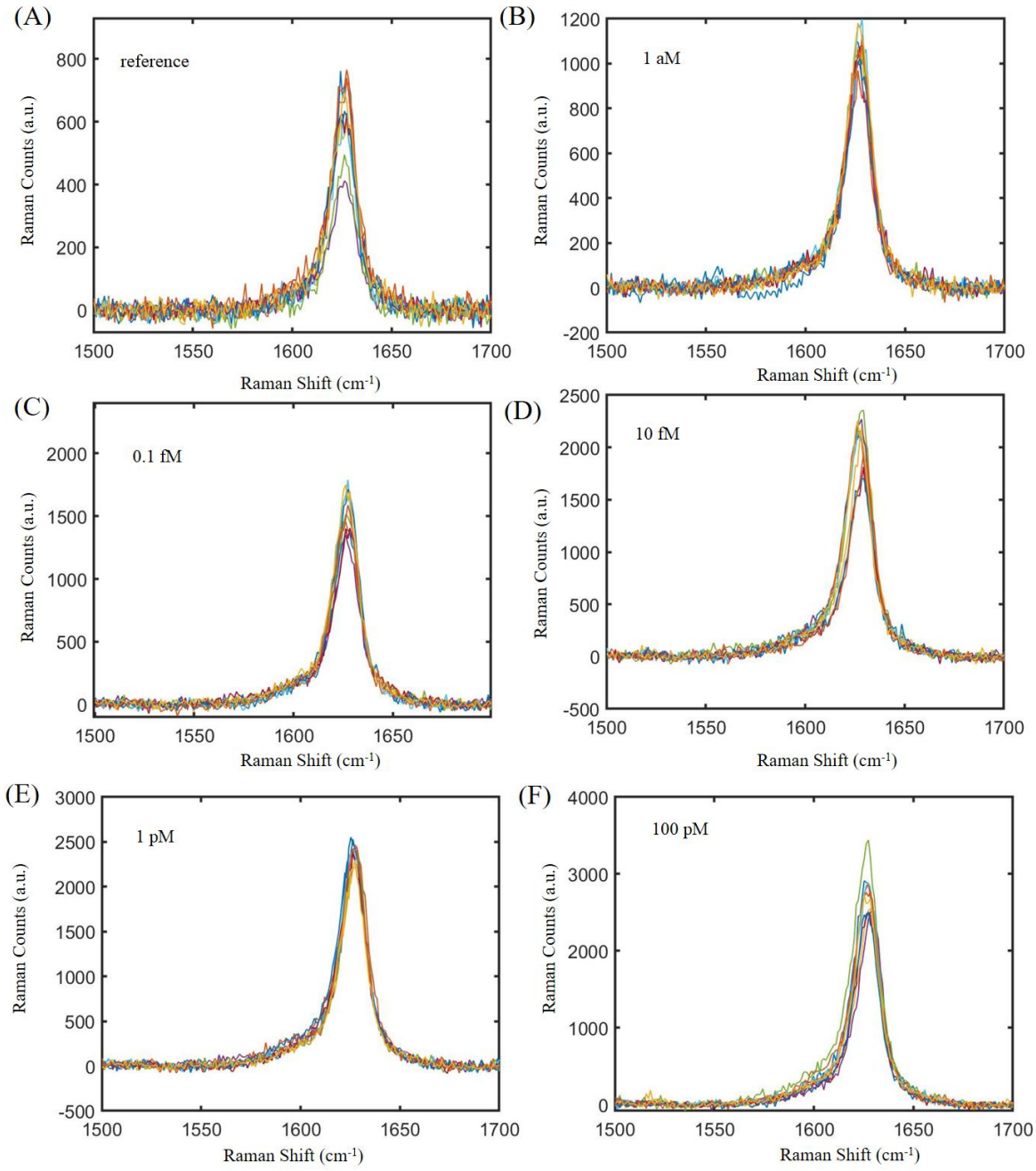

Figure S6: All raw data in Figure 0.3: targeted DNA (*stx*2) detection. (A) Reference spectra of Ag-ss-DNA SERS substrate with MB. (B-F) MB spectra after hybridization with different target DNA concentrations (i) 1 aM, (ii) 0.1 fM, (iii) 10 fM, (iv) 1 pM, and (v)

100 pM. Ten different spectra, taken at ten different random points on the functionalized Ag-ss-DNA SERS substrate are presented for each concentration of targeted ss-DNA.

Other Required corrections.

46, Each paper chapter "should contain a short introductory chapter, explanation of the research question, relevant literature and methodology and a concluding chapter. The student's contribution to each article must be made explicit". This is our criterion in Galway, and is similar to UCC's requirements, and is similar to author contributions in papers…..

There is an abstract (introductory chapter) for each chapter:

Chapter 1:

Abstract: Recent global warming has resulted in shifting of weather patterns and led to intensification of natural disasters and upsurges in pests and diseases. As a result, global food systems are under pressure and need adjustments to meet the change-often by pesticides. Unfortunately, such pesticides are harmful for human and the environment, and they need to be controlled. Traditional detection methods currently used are time consuming in terms of sample preparation, are high cost, and devices are typically not portable. Surface Enhanced Raman Scattering (SERS) has emerged as an attractive candidate for rapid, high sensitivity and high selectivity detection of contaminants relevant to the food industry and environmental monitoring. In this review, the principles of SERS as well as recent SERS substrate fabrication methods are first discussed. Following this, their development and applications for agrifood safety is reviewed, with focus on detection

of dye molecules, melamine in food products, and the detection of different classes of pesticides such as organophosphate and neonicotinoids.

Chapter 2:

Abstract: Surface Enhanced Raman is a promising analytical method for harmful pesticides detection. Herein, we demonstrate a rapid method to directly monitor 2,4-D pesticide in water environment without the need of sample pre-treatment by using Silver-Gum Arabic (Ag-GA) electrochemically co-deposited SERS substrates. This electrochemical synthesis of high nano particle density, and homogeneous SERS substrates (area: 40 μm x 20 μm) needs as little as 2 μL $AgNO_3$ and Gum Arabic mixed solution by a portable potentiostat. Different morphologies including Ag-GA spherical nanoparticles and nano dendrites were synthesized by tuning the deposition parameters. This study therefore offers a novel way to fabricate SERS substrates for determination of 2,4-D pesticides down to 1 pM in half hour and down to 0.1 nM immediately in deionized water, 0.15 nM in commercial bottled and also river water samples. This Ag-GA SERS sensor showed linear response towards 2,4-D detection in a wide linear range.

Chapter 3:

Abstract: Surface Enhanced Raman Spectroscopy (SERS) has been widely used in analytical sensing field. However, SERS substrate fabrication in large scale for analytical application is still a challenge. In this research, electrochemical deposition method was used for Ag-Cornstarch SERS substrate fabrication, which took three seconds for each SERS substrate deposition with precursors of $AgNO_3$ and cornstarch. After Ag-Cornstarch

nano structure optimization by changing electrochemical deposition parameters, one Ag-Cornstarch nano structure was used for further SERS characterization and study. It was found that this Ag-Cornstarch nano structure were still active for SERS after five weeks with RSD = 15% in SERS signal change. Enhancement Factor (EF) of this Ag-CS SERS substrate was estimated to be at 10^9 level by using methylene blue. In the end, this Ag-CS SERS sensor was used for MCPA pesticides detection. For MCPA in DI water, the relative standard deviation (RSD) of 50 spectra at peak 1600 cm^{-1} for certain MCPA concentration was 6%, with a LOD = 2 fM according to the calibration. Besides, river water was also used for MCPA detection study to check the interference from a real sample, experimental results showed that Ag-CS SERS sensor could also be used for river water sample study. This Ag-CS SERS sensor thus showed high EF, good detection limit towards several chemicals, and could be reserved for weeks.

Chapter 4:

Abstract: In this research, a selective, cost-efficient, highly sensitive Ag nanostructure Surface Enhanced Raman Spectroscopy (SERS) sensor was developed as a methodological approach to rapidly detect a targeted-ss-DNA (*stx*2) in STEC (Shiga toxin-producing *Escherichia coli*). The Ag nanostructure-based SERS substrate was functionalized by two type of thiols: thiol-ss-DNA for bonding targeted-ss-DNA and 6-Mercapto-1-hexanol ($HS(CH_2)_6OH$) for blocking the Ag nanostructure surface. Methylene Blue (MB) was used as a Raman marker to quantify targeted-ss-DNA, as well as a model molecule to characterize the electrodeposited Ag nanostructure SERS substrate. Ag nanostructure SERS

substrates showed good sensitivity and repeatability towards MB detection, with a LOD = 0.3 μM, RSD = 12.48% (at 45 different random points). More importantly, the Ag nanostructure/ss-DNA SERS substrate showed good selectivity towards STEC O157 *stx*2 targeted DNA, as well as good linearity and sensitivity towards its detection in a buffer solution. A limit of detection of 0.49 aM in a quantification range from 1 aM to 100 pM was demonstrated. The SERS sensors were able to identify target DNA (*stx*2) in an STEC strain and the study showed proof of principle that SERS substrate has potential as a cost effective, highly selective, highly sensitive DNA and bacteria sensor without the aid of DNA amplification. With further development and validation, this methodological approach has the potential for use in the point-of-use detection for instance on a farm or in the food industry.

This needs to be implemented and the expectation is that it should detail exactly what the student did experimentally and in terms of the write up. The contributions of the other authors to the papers should also be included in this section which should precede each paper.

Contributions have added for each chapter.

Chapter 1: Contribution: Conceptualization, Y.Y. and N.C.; data curation, Y.Y. and N.C.; writing-original draft preparation, Y.Y. and N.C.; writing-review and editing, A.O. and P.L.; visualization, Y.Y. and N.C.; supervision, A.O. and P.L.; project administration, A.O. and P.L.; funding acquisition, A.O. and P.L. All authors have read and agreed to the published version of the manuscript.

Chapter 2: Author Contributions: Y.Y. (Yuqing Yang) undertake experimental results including the Raman data analysis and manuscript preparation. P.L. (Pierre Lovera) responsible for supervising and data analysis & manuscript preparation and A. O'R. (Alan O'Riordan) responsible for supervising and manuscript preparation.

Chapter 3: Author Contributions: Y.Y. (Yuqing Yang) undertake experimental results including the Raman data analysis and manuscript preparation. P.L. (Pierre Lovera) and A. O'R. (Alan O'Riordan) responsible for supervising and manuscript preparation.

Chapter 4: Author Contribution: Y.Y. (Yuqing Yang) and L.A.W. (Luiza Adela Wasiewska) contribute equally to this research. Y.Y. responsible for SERS experiments, analyze the data and writes the manuscript, L.A.W. responsible for DNA part and contributed to intelligent suggestions, C.M.B (Catherine M. Burgess) and G.D (Geraldine Duffy) responsible for DNA part and supervising, P.L. (Pierre Lovera) responsible for supervising and SERS data analysis and A.O. (Alan O'Riordan) responsible for supervising.

Reference.

1. He, Z.; Rong, T.; Li, Y.; Ma, J.; Li, Q.; Wu, F.; Wang, Y.; Wang, F., Two-Dimensional TiVC Solid-Solution MXene as Surface-Enhanced Raman Scattering Substrate. *ACS Nano* **2022,** *16* (3), 4072-4083.
2. Srichan, C.; Ekpanyapong, M.; Horprathum, M.; Eiamchai, P.; Nuntawong, N.; Phokharatkul, D.; Danvirutai, P.; Bohez, E.; Wisitsoraat, A.; Tuantranont, A., Highly-Sensitive Surface-Enhanced Raman Spectroscopy (SERS)-based Chemical Sensor using 3D Graphene Foam Decorated with Silver Nanoparticles as SERS substrate. *Scientific Reports* **2016,** *6* (1), 23733.
3. Sharma, B.; Frontiera, R. R.; Henry, A.-I.; Ringe, E.; Van Duyne, R. P., SERS: Materials, applications, and the future. *Materials Today* **2012,** *15* (1), 16-25.
4. Bell, S. E. J.; Charron, G.; Cortés, E.; Kneipp, J.; de la Chapelle, M. L.; Langer, J.; Procházka, M.; Tran, V.; Schlücker, S., Towards Reliable and Quantitative Surface-Enhanced Raman Scattering (SERS): From Key Parameters to Good Analytical Practice. *Angewandte Chemie International Edition* **2020,** *59* (14), 5454-5462.
5. Kreno, L. E.; Greeneltch, N. G.; Farha, O. K.; Hupp, J. T.; Van Duyne, R. P., SERS of molecules that do not adsorb on Ag surfaces: a metal–organic framework-based functionalization strategy. *Analyst* **2014,** *139* (16), 4073-4080.
6. Zhou, H.; Xu, L.; Ren, Z.; Zhu, J.; Lee, C., Machine learning-augmented surface-enhanced spectroscopy toward next-generation molecular diagnostics. *Nanoscale Advances* **2023,** *5* (3), 538-570.
7. Brem, S.; Schlücker, S., Surface-Enhanced Raman Spectroscopy and Density Functional Theory Calculations of a Rationally Designed Rhodamine with Thiol Groups at the Xanthene Ring. *The Journal of Physical Chemistry C* **2017,** *121* (28), 15310-15317.
8. Marshall, A. R. L.; Stokes, J.; Viscomi, F. N.; Proctor, J. E.; Gierschner, J.; Bouillard, J.-S. G.; Adawi, A. M., Determining molecular orientation via single molecule SERS in a plasmonic nano-gap. *Nanoscale* **2017,** *9* (44), 17415-17421.

9. Sun, C.; Chen, T.; Ruan, W.; Zhao, B.; Cong, Q., Controlling the orientation of probe molecules on surface-enhanced Raman scattering substrates: A novel strategy to improve sensitivity. *Analytica Chimica Acta* **2017,** *994*, 65-72.

10. Morton, S. M.; Jensen, L., Understanding the Molecule−Surface Chemical Coupling in SERS. *Journal of the American Chemical Society* **2009,** *131* (11), 4090-4098.

11. Hong, Y.; Wang, R.; Jiang, Z.; Cong, Z.; Song, H., Rapid SERS Detection of Thiol-Containing Natural Products in Culturing Complex. *International journal of analytical chemistry* **2020,** *2020*, 9271236.

12. Madzharova, F.; Heiner, Z.; Kneipp, J., Surface-Enhanced Hyper Raman Spectra of Aromatic Thiols on Gold and Silver Nanoparticles. *The Journal of Physical Chemistry C* **2020,** *124* (11), 6233-6241.

13. Wang, K.; Li, J., Reliable SERS detection of pesticides with a large-scale self-assembled Au@4-MBA@Ag nanoparticle array. *Spectrochimica Acta Part A: Molecular and Biomolecular Spectroscopy* **2021,** *263*, 120218.

14. de Barros, A.; Shimizu, F. M.; de Oliveira, C. S.; Sigoli, F. A.; dos Santos, D. P.; Mazali, I. O., Dynamic Behavior of Surface-Enhanced Raman Spectra for Rhodamine 6G Interacting with Gold Nanorods: Implication for Analyses under Wet versus Dry Conditions. *ACS Applied Nano Materials* **2020,** *3* (8), 8138-8147.

15. Chen, H.; You, T.; Jiang, L.; Gao, Y.; Yin, P., Creating dynamic SERS hotspots on the surface of pH-responsive microgels for direct detection of crystal violet in solution. *RSC Advances* **2017,** *7* (52), 32743-32748.

16. Marques, F. C.; Alves, R. S.; dos Santos, D. P.; Andrade, G. F. S., Surface-enhanced Raman spectroscopy of one and a few molecules of acid 4-mercaptobenzoic in AgNP enabled by hot spots generated by hydrogen bonding. *Physical Chemistry Chemical Physics* **2022,** *24* (44), 27449-27458.

17. Chen, X.; Wang, D. H.; Li, J.; Xu, T. T.; Lai, K. Q.; Ding, Q.; Lin, H. T.; Sun, L.; Lin, M. S., A spectroscopic approach to detect and quantify phosmet residues in Oolong tea by surface-enhanced Raman scattering and silver nanoparticle substrate. *Food Chemistry* **2020,** *312*.

18. He, D. Y.; Wu, Z. Z.; Cui, B.; Xu, E. B., Aptamer and gold nanorod-based fumonisin B1 assay using both fluorometry and SERS. *Microchimica Acta* **2020,** *187* (4).

19. Jiang, L.; Gu, K. J.; Liu, R. Y.; Jin, S. Z.; Wang, H. Q.; Pan, C. P., Rapid detection of pesticide residues in fruits by surface-enhanced Raman scattering based on modified QuEChERS pretreatment method with portable Raman instrument. *Sn Applied Sciences* **2019,** *1* (6).

20. Weng, S. Z.; Zhu, W. X.; Dong, R. L.; Zheng, L.; Wang, F., Rapid Detection of Pesticide Residues in Paddy Water Using Surface-Enhanced Raman Spectroscopy. *Sensors* **2019,** *19* (3).

21. Kang, Y.; Wu, T.; Chen, W. C.; Li, L.; Du, Y. P., A novel metastable state nanoparticle-enhanced Raman spectroscopy coupled with thin layer chromatography for determination of multiple pesticides. *Food Chemistry* **2019,** *270*, 494-501.

22. Kang, Y.; Li, L.; Chen, W. C.; Zhang, F. Y.; Du, Y. P.; Wu, T., Rapid In Situ SERS Analysis of Pesticide Residues on Plant Surfaces Based on Micelle Extraction of Targets and Stabilization of Ag Nanoparticle Aggregates. *Food Analytical Methods* **2018,** *11* (11), 3161-3169.

23. Lee, H.; Liao, J. D.; Sivashanmugan, K.; Liu, B. H.; Fu, W. E.; Chen, C. C.; Chen, G. D.; Juang, Y. D., Gold Nanoparticle-Coated ZrO2-Nanofiber Surface as a SERS-Active Substrate for Trace Detection of Pesticide Residue. *Nanomaterials* **2018,** *8* (6).

24. Wang, X.; Du, Y. P.; Zhang, H.; Xu, Y.; Pan, Y. C.; Wu, T.; Hu, H. L., Fast enrichment and ultrasensitive in-situ detection of pesticide residues on oranges with surface-enhanced Raman spectroscopy based on Au nanoparticles decorated glycidyl methacrylate-ethylene dimethacrylate material. *Food Control* **2014,** *46*, 108-114.

25. Huang, D. D.; Zhao, J. C.; Wang, M. L.; Zhu, S. H., Snowflake-like gold nanoparticles as SERS substrates for the sensitive detection of organophosphorus pesticide residues. *Food Control* **2020,** *108*.

26. Yaseen, T.; Pu, H. B.; Sun, D. W., Rapid detection of multiple organophosphorus pesticides (triazophos and parathion-methyl) residues in peach by SERS based on core-shell bimetallic Au@Ag NPs. *Food Additives and Contaminants Part a-Chemistry Analysis Control Exposure & Risk Assessment* **2019,** *36* (5), 762-778.

27. Tang, F.; Zhang, M. Z.; Li, Z. B.; Du, Z. F.; Chen, B. S.; He, X.; Zhao, S. Y., Hexagonally arranged arrays of urchin-like Ag-nanoparticle decorated ZnO-nanorods grafted on PAN-nanopillars as surface-enhanced Raman scattering substrates. *Crystengcomm* **2018,** *20* (25), 3550-3558.

28. Dowgiallo, A. M., Trace level pesticide detection utilizing gold nanoparticles and surface enhanced Raman spectroscopy (SERS). In *Synthesis and Photonics of Nanoscale Materials Xvi*, Kabashin, A. V.; Dubowski, J. J.; Geohegan, D. B., Eds. 2019; Vol. 10907.

29. Yazdi, S. H.; White, I. M., A nanoporous optofluidic microsystem for highly sensitive and repeatable surface enhanced Raman spectroscopy detection. *Biomicrofluidics* **2012,** *6* (1).

30. Fathi, F.; Lagugne-Labarthet, F.; Pedersen, D. B.; Kraatz, H. B., Studies of the interaction of two organophosphonates with nanostructured silver surfaces. *Analyst* **2012,** *137* (19), 4448-4453.

31. Ma, P.; Wang, L. Y.; Xu, L.; Li, J. Y.; Zhang, X. D.; Chen, H., Rapid quantitative determination of chlorpyrifos pesticide residues in tomatoes by surface-enhanced Raman spectroscopy. *European Food Research and Technology* **2020,** *246* (1), 239-251.

32. Dowgiallo, A. M.; Guenther, D. A., Determination of the Limit of Detection of Multiple Pesticides Utilizing Gold Nanoparticles and Surface-Enhanced Raman Spectroscopy. *Journal of Agricultural and Food Chemistry* **2019,** *67* (46), 12642-12651.

33. Tang, J. S.; Chen, W. W.; Ju, H. X., Rapid detection of pesticide residues using a silver nanoparticles coated glass bead as nonplanar substrate for SERS sensing. *Sensors and Actuators B-Chemical* **2019,** *287*, 576-583.

34. Vandenabeele, P.; Ortega-Avilès, M.; Castilleros, D. T.; Moens, L., Raman spectroscopic analysis of Mexican natural artists' materials. *Spectrochimica Acta Part A: Molecular and Biomolecular Spectroscopy* **2007,** *68* (4), 1085-1088.

35. Hua, M. Z.; Feng, S.; Wang, S.; Lu, X., Rapid detection and quantification of 2,4-dichlorophenoxyacetic acid in milk using molecularly imprinted polymers–surface-enhanced Raman spectroscopy. *Food Chemistry* **2018,** *258*, 254-259.

36. Santos Costa, J. C.; Ando, R. A.; Sant'Ana, A. C.; Rossi, L. M.; Santos, P. S.; Temperini, M. L. A.; Corio, P., High performance gold nanorods and silver nanocubes in

surface-enhanced Raman spectroscopy of pesticides. *Physical Chemistry Chemical Physics* **2009,** *11* (34), 7491-7498.

37. Jia, J.; Jin, X.-Y.; Liu, Q.-L.; Liang, W.; Lin, M.-S.; Xu, H.-H., Preparation, Characterization and Intracellular Imaging of 2,4-Dichlorophenoxyacetic Acid Conjugated Gold Nanorods. *Journal of Nanoscience and Nanotechnology* **2016,** *16*, 4936-4942.

38. Cañamares, M. V.; Chenal, C.; Birke, R. L.; Lombardi, J. R., DFT, SERS, and Single-Molecule SERS of Crystal Violet. *The Journal of Physical Chemistry C* **2008,** *112* (51), 20295-20300.

39. Vandenabeele, P.; Ortega, M.; Tenorio, D.; Moens, L., Raman spectroscopic analysis of Mexican natural artists' materials. *Spectrochimica acta. Part A, Molecular and biomolecular spectroscopy* **2008,** *68*, 1085-8.

40. Zhao, X.; Zhang, H.; Li, W.; Li, X.; Fan, W.; Zhang, Y., Langmuir-diffusion model: Its modification and further application to glutinous rice flour particles. *Journal of Food Process Engineering* **2020,** *43* (9), e13470.

41. Wu, W.; Jiao, A.; Xu, E.; Chen, Y.; Jin, Z., Effects of Extrusion Technology Combined with Enzymatic Hydrolysis on the Structural and Physicochemical Properties of Porous Corn Starch. *Food and Bioprocess Technology* **2020,** *13* (3), 442-451.

42. Davoudi, Z.; Azizi, M. H.; Barzegar, M., Porous corn starch obtained from combined cold plasma and enzymatic hydrolysis: Microstructure and physicochemical properties. *International Journal of Biological Macromolecules* **2022,** *223*, 790-797.

43. Mariod, A. A., Chemical Properties of Gum Arabic. In *Gum Arabic*, Mariod, A. A., Ed. Academic Press: 2018; pp 67-73.

44. Solís, D. M.; Taboada, J. M.; Obelleiro, F.; Liz-Marzán, L. M.; García de Abajo, F. J., Optimization of Nanoparticle-Based SERS Substrates through Large-Scale Realistic Simulations. *ACS Photonics* **2017,** *4* (2), 329-337.

45. Njoki, P. N.; Lim, I. I. S.; Mott, D.; Park, H.-Y.; Khan, B.; Mishra, S.; Sujakumar, R.; Luo, J.; Zhong, C.-J., Size Correlation of Optical and Spectroscopic Properties for Gold Nanoparticles. *The Journal of Physical Chemistry C* **2007,** *111* (40), 14664-14669.

46. Narayanan, S.; Kalidindi, S.; Schadler, L., Determination of unknown stress states in silicon wafers using microlaser Raman spectroscopy. *Journal of Applied Physics* **1997,** *82*.

47. Schulze, H. G.; Foist, R. B.; Okuda, K.; Ivanov, A.; Turner, R. F. B., A Small-Window Moving Average-Based Fully Automated Baseline Estimation Method for Raman Spectra. *Appl. Spectrosc.* **2012,** *66* (7), 757-764.

48. Nicolson, F.; Jamieson, L. E.; Mabbott, S.; Plakas, K.; Shand, N. C.; Detty, M. R.; Graham, D.; Faulds, K., Surface enhanced resonance Raman spectroscopy (SERRS) for probing through plastic and tissue barriers using a handheld spectrometer. *Analyst* **2018,** *143* (24), 5965-5973.

49. Niaura, G.; Malinauskas, A., Surface-enhanced Raman spectroscopy of ClO4- and SO42- anions adsorbed at a Cu electrode. *Journal of the Chemical Society, Faraday Transactions* **1998,** *94* (15), 2205-2211.

50. Street, C. A.; Anderson, D. M. W., Refinement of structures previously proposed for gum arabic and other acacia gum exudates. *Talanta* **1983,** *30* (11), 887-893.

51. Goff, H. D.; Guo, Q., The Role of Hydrocolloids in the Development of Food Structure. In *Handbook of Food Structure Development*, The Royal Society of Chemistry: 2020; pp 1-28.

52. Banerjee, S. S.; Chen, D. H., Fast removal of copper ions by gum arabic modified magnetic nano-adsorbent. *J Hazard Mater* **2007,** *147* (3), 792-9.

53. Sanchez, L. M.; Ollier, R. P.; Pereira, A. E. S.; Fraceto, L. F.; Alvarez, V. A., Pesticide removal from industrial effluents using biopolymeric materials. In *Biopolymer Membranes and Films*, de Moraes, M. A.; da Silva, C. F.; Vieira, R. S., Eds. Elsevier: 2020; pp 359-382.

54. Kee, Y. L.; Mukherjee, S.; Pariatamby, A., Effective remediation of phenol,2,4-bis(1,1-dimethylethyl) and bis(2-ethylhexyl) phthalate in farm effluent using Guar gum – A plant based biopolymer. *Chemosphere* **2015,** *136*, 111-117.

55. Riddell, G. L.; Davies, C. W., A Study of Gum Arabic, Part I. Viscosity and Adsorption Measurements. *The Journal of Physical Chemistry* **1931,** *35* (9), 2722-2731.

56. Bhakat, D.; Barik, P.; Bhattacharjee, A., Electrical conductivity behavior of Gum Arabic biopolymer-Fe3O4 nanocomposites. *Journal of Physics and Chemistry of Solids* **2018,** *112*, 73-79.

57. A, I.; K.S, S.; S, M.; K.S, R., Viscosity and thermal conductivity of dispersions of gum arabic capped MWCNT in water: Influence of MWCNT concentration and temperature. *Journal of the Taiwan Institute of Chemical Engineers* **2013,** *44* (3), 474-479.

58. Chabot, V.; Kim, B.; Sloper, B.; Tzoganakis, C.; Yu, A., High yield production and purification of few layer graphene by Gum Arabic assisted physical sonication. *Scientific Reports* **2013,** *3* (1), 1378.

59. Chen, Z.; Ye, H.; Chen, Y.; Xu, J., Tuning the dispersity and sphericity of silver particles by wrapping mechanism using Arabic gum. *Materials Letters* **2021,** *293*, 129665.

60. Anwar, A.; Masri, A.; Rao, K.; Rajendran, K.; Khan, N. A.; Shah, M. R.; Siddiqui, R., Antimicrobial activities of green synthesized gums-stabilized nanoparticles loaded with flavonoids. *Scientific Reports* **2019,** *9* (1), 3122.

61. Song, J. E., et al., Hydrophobic Interactions Increase Attachment of Gum Arabic- and PVP-Coated Ag Nanoparticles to Hydrophobic Surfaces. *Environmental Science & Technology* **2011,** *45* (14), 5988-5995.

62. Communities, E., EU Policy for a sustainable use of pesticides

The story behind the Strategy. **2007**.

63. Establishing a framework for Community action in the field of water policy. *Official Journal of the European Communities* **2000**.

64. Rodriguez-Ruiz, V.; Maksimenko, A.; Salzano, G.; Lampropoulou, M.; Lazarou, Y.; Agostoni, V.; Couvreur, P.; Gref, R.; Yannakopoulou, K., Positively charged cyclodextrins as effective molecular transporters of active phosphorylated forms of gemcitabine into cancer cells. *Scientific Reports* **2017,** *7*.

65. Langer, J., et al., Present and Future of Surface-Enhanced Raman Scattering. *ACS Nano* **2020,** *14* (1), 28-117.

66. Han, B.; Chen, L.; Jin, S.; Guo, S.; Park, J.; Yoo, H. S.; Park, J. H.; Zhao, B.; Jung, Y. M., Modulating Mechanism of the LSPR and SERS in Ag/ITO Film: Carrier Density Effect. *The Journal of Physical Chemistry Letters* **2021,** *12* (31), 7612-7618.

67. Peng, Y. S.; Cai, P.; Yang, L. L.; Liu, Y. Y.; Zhu, L. F.; Zhang, Q. Q.; Liu, J. J.; Huang, Z. R.; Yang, Y., Theoretical and Experimental Studies of Ti3C2 MXene for Surface-Enhanced Raman Spectroscopy-Based Sensing. *ACS Omega* **2020,** *5* (41), 26486-26496.

68. Ding, S.-Y.; You, E.-M.; Tian, Z.-Q.; Moskovits, M., Electromagnetic theories of surface-enhanced Raman spectroscopy. *Chemical Society Reviews* **2017,** *46* (13), 4042-4076.

69. Yu, X.; Cai, H.; Zhang, W.; Li, X.; Pan, N.; Luo, Y.; Wang, X.; Hou, J. G., Tuning Chemical Enhancement of SERS by Controlling the Chemical Reduction of Graphene Oxide Nanosheets. *ACS Nano* **2011,** *5* (2), 952-958.

70. Le Ru, E. C.; Blackie, E.; Meyer, M.; Etchegoin, P. G., Surface Enhanced Raman Scattering Enhancement Factors: A Comprehensive Study. *The Journal of Physical Chemistry C* **2007,** *111* (37), 13794-13803.

71. Jiang, T.; Wang, X.; Tang, S.; Zhou, J.; Gu, C.; Tang, J., Seed-mediated synthesis and SERS performance of graphene oxide-wrapped Ag nanomushroom. *Scientific Reports* **2017,** *7* (1), 9795.

72. Marques, A.; Veigas, B.; Araújo, A.; Pagará, B.; Baptista, P. V.; Águas, H.; Martins, R.; Fortunato, E., Paper-Based SERS Platform for One-Step Screening of Tetracycline in Milk. *Scientific Reports* **2019,** *9* (1), 17922.

73. Parnsubsakul, A.; Ngoensawat, U.; Wutikhun, T.; Sukmanee, T.; Sapcharoenkun, C.; Pienpinijtham, P.; Ekgasit, S., Silver nanoparticle/bacterial nanocellulose paper composites for paste-and-read SERS detection of pesticides on fruit surfaces. *Carbohydrate Polymers* **2020,** *235*, 115956.

74. Rajapandiyan, P.; Yang, J., Photochemical method for decoration of silver nanoparticles on filter paper substrate for SERS application. *Journal of Raman Spectroscopy* **2014,** *45* (7), 574-580.

75. Siebe, H. S.; Chen, Q.; Li, X.; Xu, Y.; Browne, W. R.; Bell, S. E. J., Filter paper based SERS substrate for the direct detection of analytes in complex matrices. *Analyst* **2021,** *146* (4), 1281-1288.

76. Tegegne, W. A.; Su, W.-N.; Beyene, A. B.; Huang, W.-H.; Tsai, M.-C.; Hwang, B.-J., Flexible hydrophobic filter paper-based SERS substrate using silver nanocubes for sensitive and rapid detection of adenine. *Microchemical Journal* **2021,** *168*, 106349.

77. Wang, J.; Qiu, C.; Mu, X.; Pang, H.; Chen, X.; Liu, D., Ultrasensitive SERS detection of rhodamine 6G and p-nitrophenol based on electrochemically roughened nano-Au film. *Talanta* **2020,** *210*, 120631.

78. Xie, J.; Li, L.; Khan, I. M.; Wang, Z.; Ma, X., Flexible paper-based SERS substrate strategy for rapid detection of methyl parathion on the surface of fruit. *Spectrochimica Acta Part A: Molecular and Biomolecular Spectroscopy* **2020,** *231*, 118104.

79. Zong, X.; Zhu, R.; Guo, X., Nanostructured gold microelectrodes for SERS and EIS measurements by incorporating ZnO nanorod growth with electroplating. *Scientific Reports* **2015,** *5* (1), 16454.

80. Tezcan, T.; Hsu, C.-H., High-sensitivity SERS based sensing on the labeling side of glass slides using low branched gold nanoparticles prepared with surfactant-free synthesis. *RSC Advances* **2020,** *10* (56), 34290-34298.

81. Zhang, J.; He, L.; Chen, P.; Tian, C.; Wang, J.; Liu, B.; Jiang, C.; Zhang, Z., A silica-based SERS chip for rapid and ultrasensitive detection of fluoride ions triggered by a cyclic boronate ester cleavage reaction. *Nanoscale* **2017,** *9* (4), 1599-1606.

82. Liu, X.; Lebedkin, S.; Besser, H.; Pfleging, W.; Prinz, S.; Wissmann, M.; Schwab, P. M.; Nazarenko, I.; Guttmann, M.; Kappes, M. M.; Lemmer, U., Tailored Surface-Enhanced Raman Nanopillar Arrays Fabricated by Laser-Assisted Replication for Biomolecular Detection Using Organic Semiconductor Lasers. *ACS Nano* **2015,** *9* (1), 260-270.

83. Hoffmann, M.; Wackerow, S.; Abdolvand, A.; Zolotovskaya, S. A., High performance SERS platforms via parametric optimization of the laser-assisted photodeposition of silver and gold nanoparticles. *Opt. Mater. Express* **2021,** *11* (9), 3079-3098.

84. MacKenzie, M.; Chi, H.; Varma, M.; Pal, P.; Kar, A.; Paterson, L., Femtosecond laser fabrication of silver nanostructures on glass for surface enhanced Raman spectroscopy. *Scientific Reports* **2019,** *9* (1), 17058.

85. Creedon, N. C.; Lovera, P.; Furey, A.; O'Riordan, A., Transparent polymer-based SERS substrates templated by a soda can. *Sensors and Actuators B: Chemical* **2018,** *259*, 64-74.

86. Sammi, H.; Nair, R. V.; Sardana, N., Recent advances in nanoporous AAO based substrates for surface-enhanced raman scattering. *Materials Today: Proceedings* **2021,** *41*, 843-850.

87. Li, L.; Wang, S.; Yang, T.; Huang, S.; Wang, J., Electrochemical growth of gold nanoparticles on horizontally aligned carbon nanotubes: A new platform for ultrasensitive DNA sensing. *Biosensors and Bioelectronics* **2012,** *33* (1), 279-283.

88. Shi, J.; Qin, W.; Lin, Y.; Li, M.; Wu, Y.; Luo, H.; Yan, J.; Huang, K.-J.; Tan, X., Enhancing biosensing with fourfold amplification and self-powering capabilities: MoS2@C hollow nanorods-mediated DNA hexahedral framework architecture for amol-level liver cancer tumor marker detection. *Analytica Chimica Acta* **2023,** *1271*, 341413.

89. Roth, E.; Glick Azaria, A.; Girshevitz, O.; Bitler, A.; Garini, Y., Measuring the Conformation and Persistence Length of Single-Stranded DNA Using a DNA Origami Structure. *Nano Letters* **2018,** *18* (11), 6703-6709.

90. Radziuk, D.; Moehwald, H., Prospects for plasmonic hot spots in single molecule SERS towards the chemical imaging of live cells. *Physical Chemistry Chemical Physics* **2015,** *17* (33), 21072-21093.

91. Kominami, H.; Kobayashi, K.; Yamada, H., Molecular-scale visualization and surface charge density measurement of Z-DNA in aqueous solution. *Scientific Reports* **2019,** *9* (1), 6851.

92. Rohs, R.; Sklenar, H.; Lavery, R.; Röder, B., Methylene Blue Binding to DNA with Alternating GC Base Sequence: A Modeling Study. *Journal of the American Chemical Society* **2000,** *122* (12), 2860-2866.

93. Keating, M.; Song, S.; Wei, G.; Graham, D.; Chen, Y.; Placido, F., Ordered Silver and Copper Nanorod Arrays for Enhanced Raman Scattering Created via Guided Oblique

Angle Deposition on Polymer. *The Journal of Physical Chemistry C* **2014,** *118* (9), 4878-4884.

94. Chernov, S. F.; Fedorov, Y. V.; Zakharov, V. N., Surface tension of silver in different media. *Journal of Physics and Chemistry of Solids* **1993,** *54* (8), 963-966.

95. Gillibert, R.; Triba, M.; Chapelle, M., Surface Enhanced Raman Scattering Sensor for Highly Sensitive and Selective Detection of Ochratoxin A. *The Analyst* **2017,** *143*.

Appendix 5 2nd Revision according to the report

External Examiners Report on the Revised Thesis:

There are several main technical concerns from external examiner's comments:

1, Experimental method was flawed and LOD wrongly claimed in chapter 2 and 3;

2, No SERS for 2,4-D and MCPA, no concentration dependence, no noise/signal change for analyte concentration change, not a good linear fit over a wide range.

3, Similarity of 2,4-D and MCPA spectra in Chapter 2 and 3, because of possible contamination.

External examiner also suggest rewriting the parts that used unsuitable scientific word such as "quantification over a wide range", making extension in conclusion part to address the drawback of Ag-GA/Ag-CS NPs SERS based sensors for pesticides detection. The result, discussion and conclusion parts have been completely rewritten for Chapter 2 and 3 according to external examiner's comments.

Appendix 5 has addressed all the comments, as well as reflected in the main text.

1, **Analysis & Interpretation**: This was improved by inclusion of text explaining the effect of S and N atoms on SERS. However, critical analysis and interpretation of the data in Chapter 2 and 3 was not done.

- Figure 2.4 demonstrated the possible interaction between 2,4-D and Ag-GA SERS substrate in chapter 2. And explained the possible interaction in page 87. Chapter 3, Figure 3.7, page 180, explanation in page 179.

Question 2-4: sampling issue and LOD.

2, **Experimental details**: Additional information was provided in the revised thesis to better explain the experimental work undertaken. This encompassed most of the suggestions from the EE, however, these updates also raised some significant issues, both of which had been mentioned in the viva voce examination:

Sampling Issue: The sampling issue for C2 and C3 identified in the viva voce was more clearly explained in the thesis…but the student did not adequately explain the negative consequences of this method….that is the reported LOD's are not true…. This should have been obvious to the candidate that this approach tends to invalidate the claims of very low detection and quantification in C2 and C3. On page 259 the figure shows that the signal remains the same after DI rinsing…. This is a good indication that whatever material is generating the signal remains. The wicking away procedure used therefore does not remove the first deposited sample and thus for each addition the candidate is just adding more material……This alone should have resulted in an extensive revision of the two chapters.

- The sampling issue is discussed in both experimental section and the conclusion section:
- Chapter 2, section 1.6, page 81. And page 106, the 2nd paragraph.
- Chapter 3, section 2.5, page 167.
- The term 'LODs' has been removed, and replaced with 'detection ability' and the experimental data.

3, In summary, the claims for ultra-low quantification of this analyte by SERS are not proven by the data presented in the revised thesis chapter. The student did not address these

issues in the conclusions and still incorrectly maintains that a 1 pM detection limit was achieved.

1 pM is the experimental data, incubation time is also important for the detection.

4, In summary, the claims for ultra-low quantification of this analyte by SERS are not proven by the data presented in the revised chapter. The student did not address these issues in the conclusions and still incorrectly maintains that a 2 fM detection limit was achieved. The Conclusions section (p155-156, marked thesis) do not reflect or deal with the very serious issues raised here.

2 fM (calculated data) has been replaced by 28.5 fM (experimental data). Detection limit data has been removed in conclusion.

Question 5-7: Contamination concern and similarity of 2,4-D and MCPA.

5, **Contamination**: It was mentioned during the viva that the use of plastic containers is not good practice in SERS work. In the revised thesis it was stated that all of the liquid samples were held in new colourless Eppendorf AG PCR tubes (mL range) and AgNO3 solution was contained in a new centrifuge tube from Sigma-Aldrich (Ireland). Most practitioners of SERS will use acid washed glassware to ensure that there are no issues with leachate. It is the external examiners view that the data presented in several chapters (C2 and C3) shows evidence that the Raman signals being generated are very, very similar.

- For contamination in detection section:

The initial detection of 2,4-D and MCPA pesticides in Chapter 2 section 4.1, Figure 2.6 and in Chapter 3 section 3.4, Figure 3.6., showing that the signal were from the analytes. The observed signal was indeed from 2,4-D was discussed in page 92-94.

- For container discussion:

See Chapter 2, section 1.1., the last paragraph.

- The spectra for 2,4-D and MCPA were the same:

Similar chemical structure has the same SERS spectra has been proved in literature. This is discussed in Chapter 3, section 3.4, page 180-181.

6, It is also clear from Chapter 2 and 3 that the SERS spectra and behaviour are very similar in both cases. The top row shows that the solid state Raman spectra of the two analytes are very different, which would suggest a very different SERS spectrum….although neither of these molecules are SERS active.

See question 5.

7, The distinctive triplet of bands at ~1100 cm–1 and doublet at ~900 cm–1 are the same in each set of spectra. Allowing for the difference between the SERS substrates, one could say that they are uncommonly similar. The plots below illustrate this again..….

See question 5.

8, **Intensity calibration method**: This was not provided in the revised thesis, the image (Chapter 2, Figure S3) only shows a single Si Raman spectrum but does not show how this was used to generate an intensity calibration.

This has been revised in chapter 2 SI, page 110:

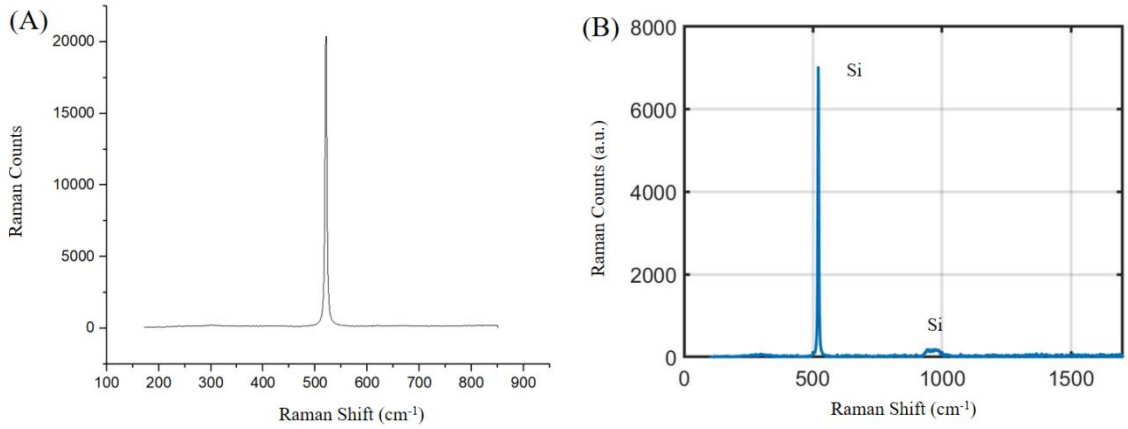

Figure S4: (A) Spectrum of Si chip used for daily laser power calibration by Raman counts (around 20000 a.u.), Raman peak at 520 cm^{-1}. Laser power: 0.7 mW, lens: 50x, exposure time: 1s. For laser power calibration, a daily check of this Si chip was carried out before

experiments. The intensity should be tuned to remain around 20000 a.u and the peak should stay near 520 cm^{-1}. (B) Raman spectra of Si/SiO_2 sensor chip. Si: 520 cm^{-1}, 950 cm^{-1}. Laser power: 0.07 mW, exposure time: 10s, lens: 20x.

Question 9-16: No SERS for 2,4-D and MCPA, no concentration dependence, no noise/signal change for different analytes concentrations, not a good linear fit over a wide range.

9, Lack of SERS: It was obvious when one compares the spectra collected in the three chapters that neither the 2,4-D nor the MPCA analytes generated a SERS signal….and the corrected thesis does not say this.

- The raw data used for calibration plots are all essentially the same…and the candidate has not recognised or acknowledged this in the revised thesis.
- 2,4-D and MCPA do not generate SERS signal directly: Chapter 2 section 4.1 and Chapter 3 section 3.4 and 4.
- Raw data comment: chapter 2 section 4.1, page 86. Chapter 3, section 3.4, the 3rd paragraph.

10, Overall, the analysis and interpretation in the corrected thesis is weak because it is neither critical nor objective…It is clear that there is a problem with the spectral data in Chapters 2 and 3 in terms of the spectra presented….It's obvious that the candidate is not getting any significant increase in SERS (if there is any in the first place) as the analyte concentration increased. From questioning in the viva, the most likely explanation is that the 2,4-D or MPCA analytes are being physically concentrated in the gum Arabic or corn-starch coatings…thus increasing the local concentration and generating a change in

signal….but to use this as the basis of an analytical method based on Raman spectroscopy is inherently flawed (see below).

- Experimental sampling issue: see question 2.
- Discussion about the low slope is in chapter 2, page 104-106, and chapter 3 section 3.4.2, the last paragraph.

A research that has low slope and large error bar using peak ratio[1]:

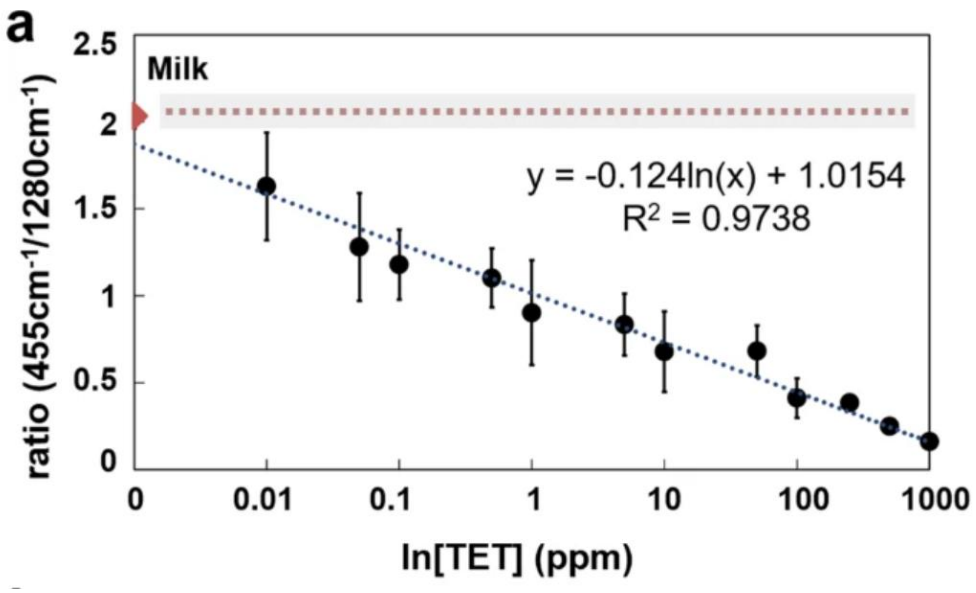

Figure 2: Dependence of SERS signal intensity ratio and TET concentration (n = 3). (a) Correlation between ratio 455 cm-1/1280 cm-1 versus analyte concentration in logarithmic scale. Linear correlation y = -0.124ln(x) + 1.0154; R2 = 0.9738).

On top of this, Ag-GA or Ag-CS SERS substrate in chapter 2 and 3 was NIP (non-molecular imprint) method, this method was much less sensitive comparing to MIP, see example below:

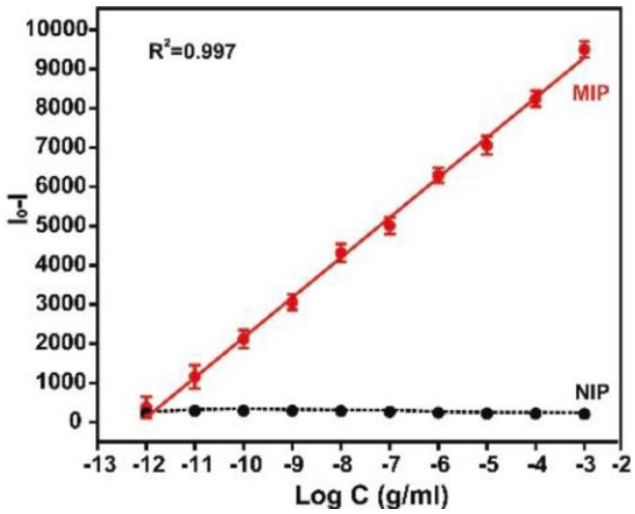

Figure 3: Calibration curve of SERS signal intensity at 1175 cm^{-1} for NDKB in the concentration range of 1 pg/mL ~ 1 mg/mL.[2]

Not only for NIP (non-molecular imprint) SERS sensor, the sensitivity is not as good as MIP (molecular imprint) ones; for electrochemical sensors, it is the same, see Figure 4 and 5; and Fluorescence sensor, see Figure 6.

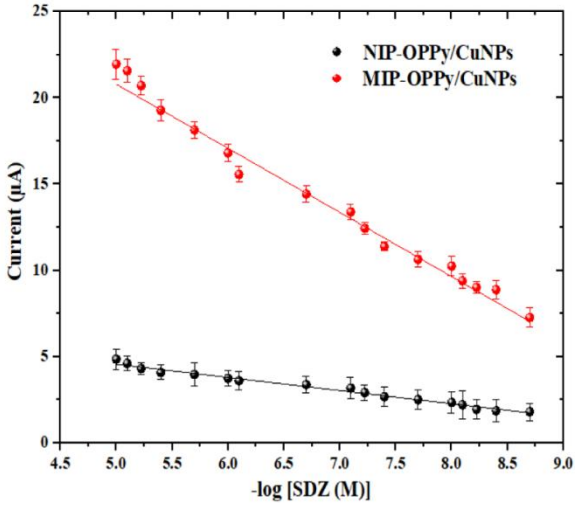

Figure 4: the corresponding calibration curves for MIP and NIP sensors: DPV peak current versus the logarithm of SDZ concentration.[3]

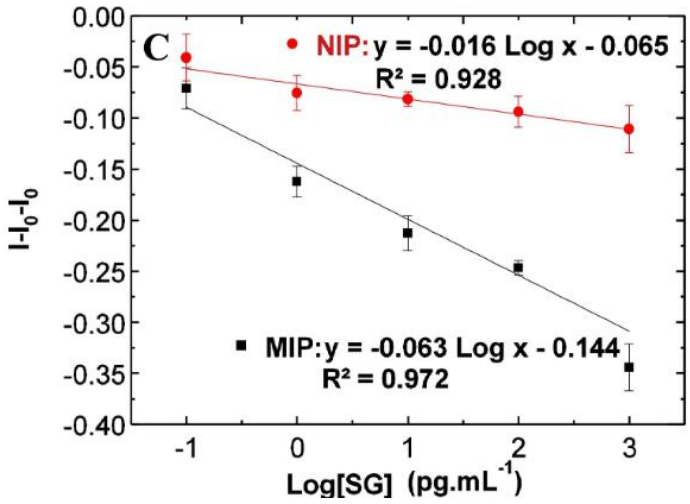

Figure 5: Differential pulse voltammograms obtained after SG detection at different concentrations on calibration curves corresponding to MIP and NIP sensors.[4]

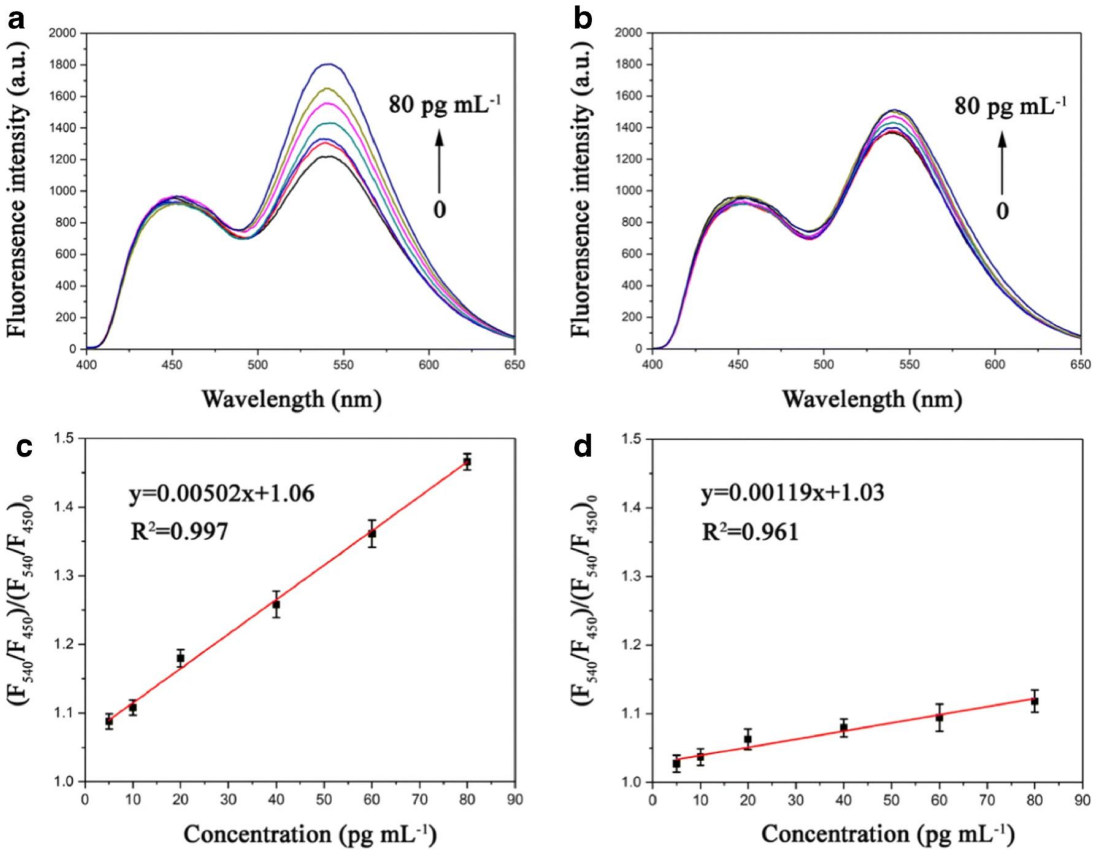

Figure 6: Fluorescence spectra of **a** SiO_2@CDs&NBD@MIP and **b** SiO_2@CDs&NBD@NIP with addition of the indicated concentrations of CNP; relationships between fluorescence ratios and different concentrations of CNP for **c** SiO_2@CDs&NBD@MIP and **d** SiO_2@CDs&NBD@NIP.[5]

11, **Not SERS, no conc. dependence**: Figure S21 (2,4-D samples) clearly shows that there is no substantial change in the Raman spectra from the 0.001 nM to the 0.2 mM samples. The signal intensities and noise levels are similar in all plots which is clear evidence that this is largely spontaneous Raman. This in essence invalidates the claims for chapter 2. [The same situation pertains with chapter 3]

See question 9, 10.

Peak ratio was used for data analysis. See Figure 2.9 in Chapter 2 and figure below, peak ratio increased with [2,4-D].

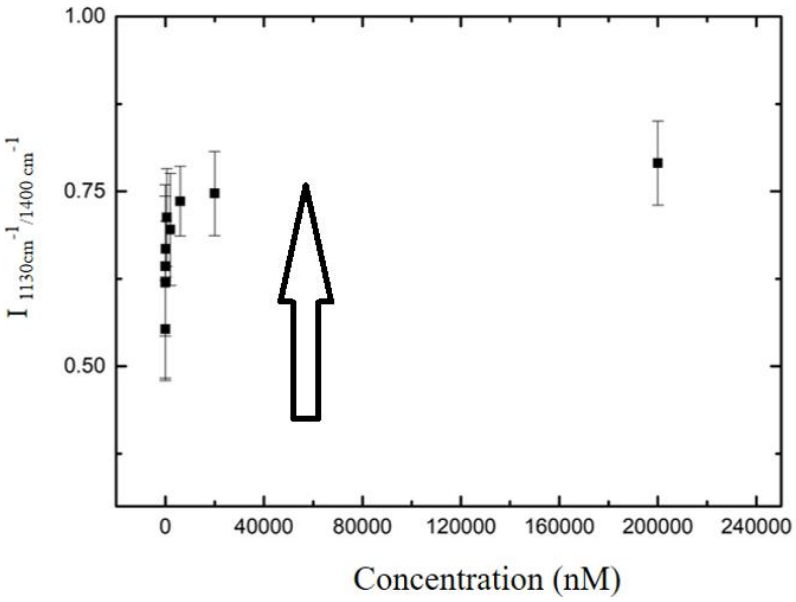

12, Similar to above, the analyte molecule will not bind strongly to the silver surface and thus the SERS effect is going to be weak or non-existent using conventional SERS. It needed to be explicitly clarified that the corn-starch layer serves to concentrate the MPCA in the layer close to the silver surface and thus generate a detectable signal. This was done to a certain degree, but the candidate failed to address the fact that the spectra provided show no evidence for substantial SERS, nor do they show any kind of acceptable concentration dependence. The student failed to look critically at the data being presented…but what is more serious is that they failed to correct this in the revised thesis when offered the chance to do so.

- Address the concern: Chapter 3, page 187, the 1st paragraph.
- The reason for this low slope is in question 10.
- Data analysis has been checked and revised: Chapter 3 section 3.4.

13, **Not SERS, no conc. dependence**: Figure S6 (MPCA samples) and Figure 3.6 (bottom right) clearly shows that there is no substantial change in the Raman spectra from the 28.5 fM to the 28.5 µM samples. If anything all we see is a reduction in signal intensity from the first lowest concentration sample to the final highest concentration sample. The signal intensities and noise levels are similar in all plots. This in essence invalidates the claims for chapter 3. [The same situation pertains with chapter 2] If one compares the spectra above with the spectra of the substrate (Figure S3 below) one can clearly see that there is something amiss.

See question 9, 10 and 12. Again, peak ratio was used for data analysis instead of single peaks.

14, Linear Fits: The data presented in chapter 2 is not really believable….have the same spectra over a huge range of concentrations. During the viva voce it became apparent that what has happened is that the gum Arabic layer was becoming saturated with the analyte and there cannot be any further significant increase in signal because of this. There is little to no SERS being observed either. This was not addressed satisfactorily in the revised thesis.

See question 9, 10, 11, 12 and appendix 4 saturation explanation.

The reason for such low slope has been discussed in question 10.

In Chapter 2, Structure 1-4 Ag-GA SERS sbstrate have the same SERS detetcion behavior towards 2,4-D, except the detection limite and response time. See page 140-149.

15, In both cases there is no substantial increase in signal intensity with increasing analyte concentration. This means no SERS in either case from the analyte molecules.

This is the same question for saturation and sensitivity. See question 9, 10, 11, 12.

16, Finally, one needs to address the linear plots displayed in the thesis, and look sensibly at what is being displayed. The band ratios being used for quantification vary from ~0.55 to ~0.75 and ~0.5 to 1.0 over a huge concentration range and the error bars are also significant in the first case. The fit equations show that the slope is tiny (<0.1), and as such to talk about LOD's in the fM and pM range is not sensible. This is very obvious when one compares these plots to those of C4 (e.g. Figure 4.4) where there is an actual SERS signal from Methylene Blue.

The term 'LOD' has been removed, 'detection ability' was replaced to indicate the lowest concentration that the research has claimed from experimental data.

Reason for such low slope and signal change with the change of concentration was discussed in question 10.

17, In summary, there was a failure to recognize that the chapter 2 and 3 conclusions were not supported by the data provided…and this can be explained by the fact that the analytes are not SERS active, the sampling methodology is flawed, and there is potential contamination via the use of plasticware for storage of materials in solution form. If the candidate had recognised this and rewritten the chapter to show all these clearly it would have been acceptable, however, as provided in the revised thesis it is not clear that these are in essence failed SERS assays. I know that this is not a very palatable conclusion, but scientifically, one needs to address this.

Conclusion has been rewritten and extended, as well as sampling issue, see question 2.

The contamination issues is in question 2-4.

Chapter 2 and 3 has been rewritten to address these issues.

18, However, this also largely invalidates the original thesis claims that the analyte 2,4-D was generating a SERS signal and that the analyte could be quantified over a wide concentration range. One would have expected a complete rewrite of the results & discussion and conclusions sections to deal with this and correct these obvious problems.

The statement has already been removed.

The the results & discussion and conclusions sections were rewrote to deal with this and correct these obvious problems.

19, **Data does not match**: It is also clear that the spectra shown in Figure 3.5 does not match the corresponding spectrum in figure S6.

Figure 3.5 and Figure S6 were two different experiment. Figure 3.5 was for repeatability study on a SERS substrate while Figure S6 was another experiment for different MCPA concentration study. The peak at 1600 cm^{-1} was not always present the same sharp feature and this has been discussed in Chapter 3, page 183, the last paragraph and page 184, the 1st paragraph.

20, However, for completeness, Figure 4.1 needs to be revised to ensure that this methodology is correct. The Raman spectra for panels D, E, and F need to be plotted with the same spectral range as for B and C, so that we can see the other Raman bands and verify that all is in order. It would also be important to note the exposure times used for each of these spectra.

For MB related experiment, spectra were only measured from 1500-1700 cm^{-1}. Its highest characteristic peak is located in 1625 cm^{-1}. And there was no 1625 cm^{-1} peak show in SERS substrate surface before MB application in Figure 4.1.

The exposure time has been noted.

To conclude, EE's comments are valuable for the thesis completion and for scientific expression, especially for chapter 2 and 3. The drawback of chapters is the drawback of the feature of the SERS sensors for 2,4-D/MCPA detection.

It has to connect to its detection principle and the fact that the interaction between 2,4-D/MCPA with SERS substrate were irreversible by NIP method, what is more important, the analytes concentration does not have significate effect to the SERS signal in the measurement time window. In the conclusion section, I have included possible approach to

improve the sensitivity/selectivity of these SERS sensors, e.g. by using MIP. Nevertheless, this research offered a new insight for pesticides detection, which are not possible to detect directly in water environment by only noble metal nano particles.

Reference.

1. Marques, A.; Veigas, B.; Araújo, A.; Pagará, B.; Baptista, P. V.; Águas, H.; Martins, R.; Fortunato, E., Paper-Based SERS Platform for One-Step Screening of Tetracycline in Milk. *Scientific Reports* **2019,** *9* (1), 17922.
2. Lu, Y.; Liu, Q.; Fu, B.; Li, P.; Xu, W., Label-free MIP-SERS biosensor for sensitive detection of colorectal cancer biomarker. *Talanta* **2023,** *258*, 124461.
3. Elamin, M. B.; Ali, S. M. A.; Essousi, H.; Chrouda, A.; Alhaidari, L. M.; Jaffrezic-Renault, N.; Barhoumi, H., An Electrochemical Sensor for Sulfadiazine Determination Based on a Copper Nanoparticles/Molecularly Imprinted Overoxidized Polypyrrole Composite. *Sensors* **2023,** *23* (3), 1270.
4. El Alami El Hassani, N.; Llobet, E.; Popescu, L.-M.; Ghita, M.; Bouchikhi, B.; El Bari, N., Development of a highly sensitive and selective molecularly imprinted electrochemical sensor for sulfaguanidine detection in honey samples. *Journal of Electroanalytical Chemistry* **2018,** *823*, 647-655.
5. He, H.; Cao, M.; Hu, J.; Zhu, L.; Su, C.; Du, S.; Yang, J.; Tang, Y.; Chen, L., Fluorescent turn-on assay of C-type natriuretic peptide using a molecularly imprinted ratiometric fluorescent probe with high selectivity and sensitivity. *Microchimica Acta* **2020,** *187*.

Appendix 6 External Examiners 2nd Report on the Revised Thesis:

Student: Yuqing Yang, Tyndall Institute, UCC.

External Examiner: Prof. Alan G. Ryder, University of Galway

Summary: In my opinion the corrected thesis (ver. 2) as supplied to me, still requires some changes to how the material in Chapter 2 and 3, is presented and explained. The explanation and discussion needs to be clearer and less ambiguous. Basically, both the external and internal examiner still have reservations about the Raman signals presented in C2 and C3 being presented as SERS signals.

The conventional SERS signal is considered significant, with an enhancement factor (EF) of up to 10^9, particularly in research involving only noble metal nanoparticles (NPs). However, with the emergence of various SERS substrates, including molecularly imprinted polymer (MIP)-based substrates or non-metal nanomaterial substrates such as pure MXene or other 2D materials, the definition of SERS has broadened. For organic molecules, detection can be achieved using molecularly imprinted SERS sensors, where the signal arises not from the molecule itself but from interactions between the analytes and the polymer layer.

I am not opposed to the reviewers' perspective and would prefer to avoid the term 'SERS' where possible in Chapter 2 to maintain stricter scientific terminology. Nevertheless, this study utilizes the SERS effect and aligns with similar studies on NIP (non-imprinted polymer)-SERS sensors, as mentioned in Appendix 5, page xxx and in C2. In Chapter 3, the EF was calculated using 4-ATP and MB, confirming that Ag-CS functions as a SERS substrate with a high EF of 10^9. However, its ability to detect MCPA is limited due to the molecular features of MCPA and other factors.

To avoid disputes over defining a scientific term not found in textbooks, I am happy to follow the reviewers' suggestion and avoid using 'SERS' where possible.

DETAILS OF MINOR CORRECTIONS REQUIRED

Abstract.

The statement here is ambiguous and still a bit misleading as it suggests that SERS is taking place whereas, the data presented in C2 and C3, in my opinion does not really support a SERS based detection of these two analytes.

"For the detection of pesticides 2,4-D and MCPA, Ag-Gum Arabic and Ag-Corn Starch nanoparticles were electrochemically deposited as efficient SERS substrates. The principle behind the detection of these compound lies in the local concentration of the pesticides by the polysaccharide polymer layers of Gum Arabic and Corn Starch. These sensors were capable of detecting - but not quantifying - pesticides at concentrations lower than the threshold limit (0.1 ppb) set in EU's Water Framework Directive."

We have made this change in page 3-4 to reflect this comment.

The fabricated sensors were based on Ag-Gum Arabic nanostructures for detection of 2,4-D in chapter 2, Ag-Corn starch for MCPA in chapter 3 and Ag/ss-DNA in chapter 3. The nanoparticles were synthesized using the electrochemical deposition method, which allows for tailoring of nanoparticle structure by adjusting deposition parameters such as deposition time, precursor concentrations, and applied voltage. This electrochemical deposition method is simple and repeatable, making this approach of fabricating sensors reproducible.

For chapter 2 and 3, no significant changes in the Raman signal intensities were recorded as the concentration of the analytes increased, as would have been expected with SERS effects. Instead, a small increase in the ratio between two peaks of the Raman spectra could be observed. This may be attributed to the local increase in the concentration of the

pesticides by the polysaccharide polymer layers of Gum Arabic and Corn Starch. While changes in the ratio between two peaks could be detected as concertation increased, quantification was not possible because of the low slope obtained and the inadequate experimental procedure chosen, based on over sampling. Also, the recorded spectra were very similar for the two pesticides, effectively making selectivity impossible.

For the bacteria E. coli O157 ss- DNA SERS sensor, neither Gum Arabic nor Corn Starch was used. Instead, a two-thiol functionalization method was employed for Ag nanoparticle SERS ss-DNA sensor development. This ss-DNA SERS sensor exhibited good linearity, selectivity, and relatively fast detection compared to other sensors or methods for ss-DNA detection

Chapter 2.

While we acknowledge the corrections made by the student, we do have to point out that the chapter as written is still a bit ambiguous and misleading in places. It still suggests that SERS due to the analyte is present…..

For example: Abstract is still highly misleading as it does not clearly describe the revised chapter...gives the impression that it worked...should be rewritten to reflect the current state of the chapter/knowledge. The abstract/chapter/conclusion needs to be rewritten from the point of view that SERS was not achieved and thus quantification was not possible (I do not thank that the detected signal is that of the analyte either…).

The candidate has more than enough data and material, but it needs to be accurately interpreted and presented throughout the thesis.

The correct approach here is to start at the outset and say it didn't work as intended and then explain in detail why….that will make it a much better piece of scientific literature, and also fulfils the thesis requirement. Please note, the substrate fabrication and discussion is very good and OK, it's just the attempted SERS of the analyte that is the problem. I would suggest that if Methylene Blue

was tested on this substrate it would have worked very well…and SERS would have been demonstrated….

We have made this change in page 75 to reflect this comment.

P75, C2: **Abstract:** .....However, no significant change in peak intensity was observed as the analyte concentration increased, contrary to what is typically expected with SERS. Consequently, the sensor did not perform as designed. A change in the peak ratio was observed over a wide range of 2,4-D concentrations, but the slope was very low. This suggests that the detection principle might rely on the local concentration of 2,4-D within the Gum Arabic layer, as more material accumulates with increasing concentrations. It should be noted that the experimental method involved oversampling, a flawed analytical practice that rendered quantification of 2,4-D impossible.

Note p96: Figure 2.8 shows clearly that there is no significant change in Raman signal intensity as one goes from 0.001 nM to 0.2 mM. This needs to be unambiguously described as a problem…..One would expect a big change in signal like that observed in C4 if SERS were present…. There is no point doing data analysis on this when it's obvious that something is not right….

We have made this change in page 99-100 to reflect this comment.

P100 "However, when plotting the intensity of these peaks against Log[2,4-D], **no strong correlation was observed**, as shown in SI Figure S17. "

Peak ratio was studied based on the detection principle, the interaction between 2,4-D and pesticides. It is still worth to see the change of the peak ratio VS. Raman intensity change based on the detection principle:

"The peak at 1400 cm^{-1} could be related to the characteristic peak for the Gum Arabic layer, [95] while the peaks at 1130 cm^{-1} and 293 cm^{-1} can be related to 2,4-D (Peak 1130 cm^{-1}

is related to ν(CC)ring + ν(C–Cl), and peak 293 cm^{-1} is δ(COC) + δ(CCl), see table 2). The peak ratio could thus reflect the interaction between 2,4-D and GA. Using the peak at 1400 cm^{-1} as a reference peak could yield better fitting results."

Note on p98 it is said that the peak at 1400 cm^{-1} is due to Gum Arabic…but elsewhere it's attributed to the analyte (Table 2 on p.91).

Peak at 1400 cm^{-1} has been deleted in table 2.

Page 106: The discussion on the method used, i.e., one substrate with analyte being over spotted is not acceptable…it seeks to regularise a bad experimental design, and one which has contributed to a lot of the problems with this thesis. The student should say clearly that this was not an acceptable practice for a SERS substrate/assay.

We have made this change in page106, and page 109 to reflect this comment.

P106 "This calibration approach, however, **is not a good analytical practice in general.** In most of the situations, a single substrate was used for a single concentration. The sampling method has been discussed also in experimental section 1.6."

P109"In this sense, **using the same substrate for calibration is a bad analytical practice**. "

Page 110: This statement is not proven, or backed up by any of the data provided. If there were an irreversible interaction I would have expected a very strong SERS signal….and we don't see that:

The interaction between 2,4-D and the Ag-GA SERS substrate was found to be irreversible. After

This statement has been removed.

Page 110: This statement is misleading as no form of data analysis will improve the spectral data that is presented. The raw data is suspect and doesn't show SERS…you cannot fix bad or non-existent data by this route.

Other data processing approach could also been used for this study such as uninformative variable elimination-partial least squares (UVE-PLS) method, but this is not the scope of this research.105-106

These statement has been deleted.

Chapter 3.

The exact same point hold for C3 as for C2, the attempted SERS assay failed…and the chapter should be revised to explain why. Again, the substrates are fine, I expect with MB or another good SERS analyte you would have gotten real SERS…but here no it's not there. So as above for C2, he correct approach here is to start at the outset and say it didn't work as intended and then explain in detail why….

We have made this change in page 166, page 190, and page 191 to reflect this comment.

P166 C3: **Abstract**: ...Similar to Chapter 2, no change in Raman peak intensity was observed as the concentration of MCPA increased, suggesting that its detection was not based on strong SERS effects. As with 2,4-D, a slight increase in the peak ratio was observed with increasing concentrations. However, the experiment faced the same shortcomings as in Chapter 2 regarding the experimental protocol, rendering quantification impossible. Additionally, the spectra were very similar to those recorded in Chapter 2 for 2,4-D, making it impossible to discriminate between the two analytes due to a lack of selectivity.

P190 "However, **quantification is not possible a**s the starting values are different for the same MCPA concentration on different Ag-CS substrates, this is related to fabrication variation. Also, adding more MCPA on the Ag-CS substrate will make the Raman signal increase regardless of the concentration. "

P190 "The peak ratio reflects the interaction between MCPA and CS. Each -OH site in the carbon ring of CS can interact with more than one MCPA molecule, and the signal

increases with addition of MCPA to the substrate.....Similar to Chapter 2, this research used Ag-CS to attract MCPA to close to the silver surface and it constitute an indirect detection of MCPA where the CS layer helped capture and concentrate MCPA to gain an increased Raman signal. This approach can be viewed as non-molecular imprint (NIP) and not molecular imprint (MIP), the latter method helps to gain better sensitivity and selectivity as discussed in Chapter 2."

P191 "MCPA does not contain a -S or -N atom and as such does not have strong interaction with silver nanoparticles. Cornstarch on the other side may assist in attracting and concentrating MCPA closing to the Ag-CS surface. The detection principle is based on the interaction between MCPA and the cornstarch function layer, similar to non-molecular imprint method. This Ag-CS sensor cannot quantify MCPA due to the sensor surface's low capacity to host MCPA and the experimental approach."

Besides, in P175-177 There were SERS test for MB and 4-ATP in C3 section 3.2:

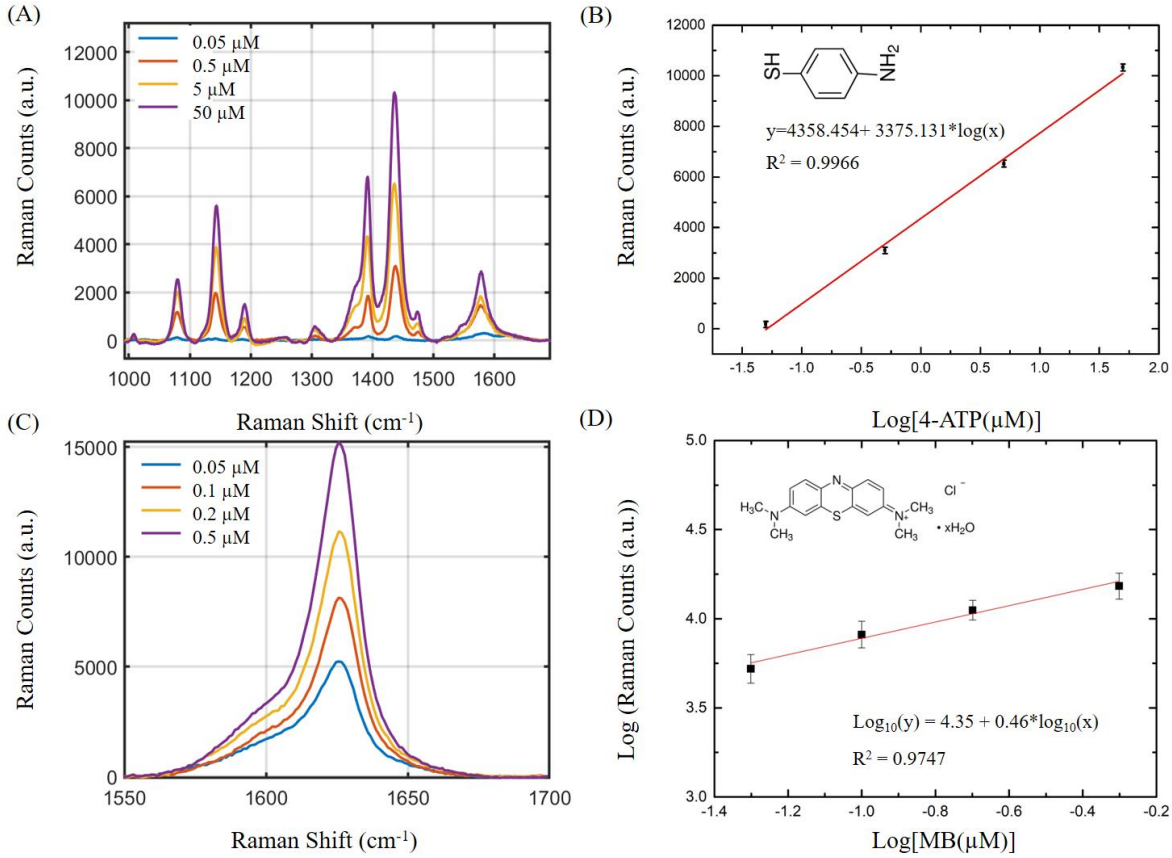

Figure 3.2: Ag-CS SERS sensor characterization by Raman reporter 4-ATP and Methylene Blue (MB). (A) Spectra for 4-ATP at different concentrations: 0.05 µM, 0.5 µM, 5µM, 50 µM; (B) Linear calibration for 4-ATP for the highest peak at 1440 cm^{-1}; (C) Spectra for Methylene Blue (MB) at different concentrations: 0.05 µM, 0.1 µM, 0.2 µM, 0.5 µM; (D) Linear calibration for 4-ATP for the highest peak at 1625 cm^{-1}.

Critical issue for C2 and C3.

It is still also clear from Chapter 2 and 3 that the SERS spectra and behaviour are very similar in both cases. The top row shows that the solid state Raman spectra of the two analytes are very different, which would suggest a very different SERS spectrum….although neither of these molecules are SERS active.

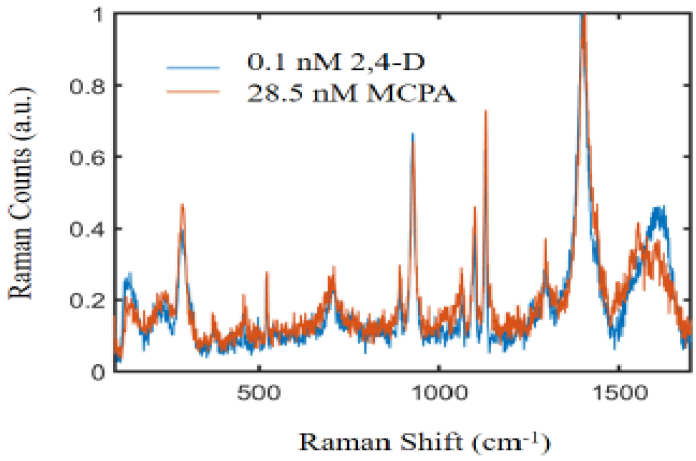

Figure S7: Comparison of the spectra of 2,4-D and MCPA.

It was and is my contention that the "SERS" data presented in both C2 and C3 are the same. The figure S7 provided by the candidate in the revised thesis proves this. This in conjunction with the solid state Raman spectra below, proves that there is a major problem with the data being presented in C2 and C3.

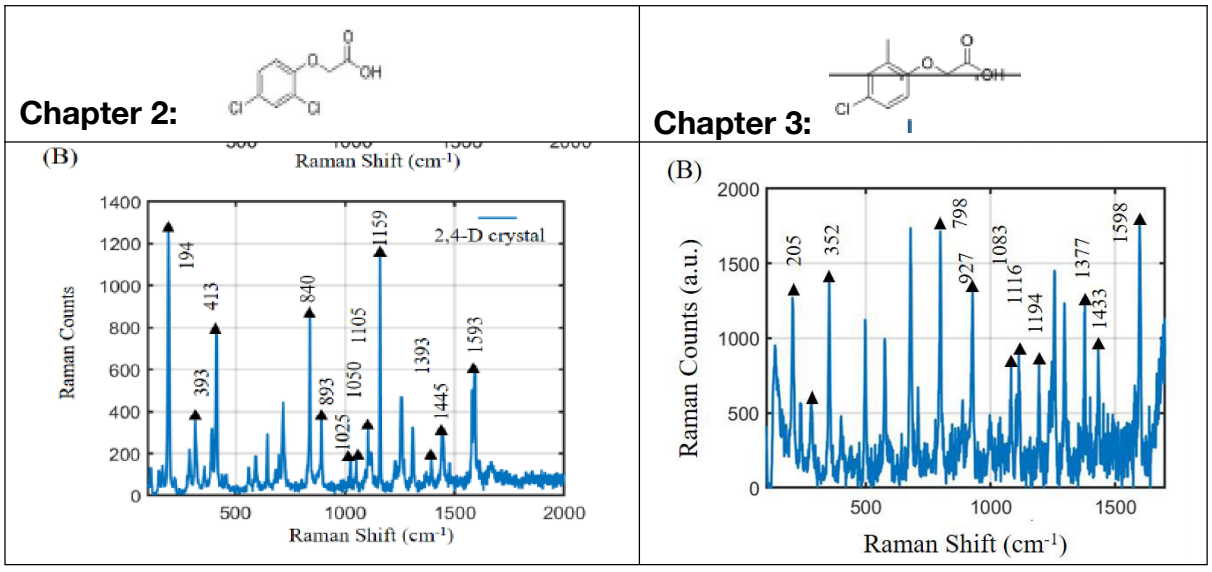

The simplest explanation is that this is a contaminant signal….but in any event, it makes it impossible to claim with any certainty that:

"The sensing capabilities of the developed SERS substrate were tested for 2,4-D pesticide. The sensors provided a spectral response after incubation for 30 minutes in a 1pM 2,4-D solution. They exhibited a response to 0.1 nM 2,4-D in DI water immediately, and they were also able to respond to 0.15 nM 2,4-D in both commercial bottled and river water samples."

OR…

"Detection of herbicide MCPA was undertaken using these substartes. While direct quanitifcation was not possible with the methodology used, it was possible to get Raman signals for concentartion down to 28.5 fM based on the experimental data."

Here is a really important point: If this is a contaminant, and I'm pretty sure it is….this is where you have achieved very low level detection….what it is, is not knowable here….but I suspect that it's a contaminant from the plastic containers that you have used. It's a leachate of some kind or another… I say this because the signals are essentially the same for C2 and C3, the tiny changes in signal may be due to accumulation of this contaminant in the layers along with the analytes. In any event, it's not proven that the detected signals are definitely from the two different analytes.

The spectra in C2 and C3 are indeed very similar, and this has been highlighted in the thesis (abstract and in chapter 3). We have also emphasised that because of this, it is not possible to distinguish the two molecules (lack of selectivity). Raman contribution from a common contaminant from the plastic container is possible. However, if this was the case, it would be expected to obtain the same spectrum for DI water only (stored in the same type of containers and acquired under the same experimental conditions) and this was not observed as shown in Figure 2.6 and 3.6.

1, P93 &P181 C2&3: using DI water that contained in the same type of container under the same experimental conditions (same substrate and same Raman measurement parameters), the spectra of DI water vs. MCPA/2,4-D were different. This suggested that this signal were related to the presence of 2,4-D/ MCPA.

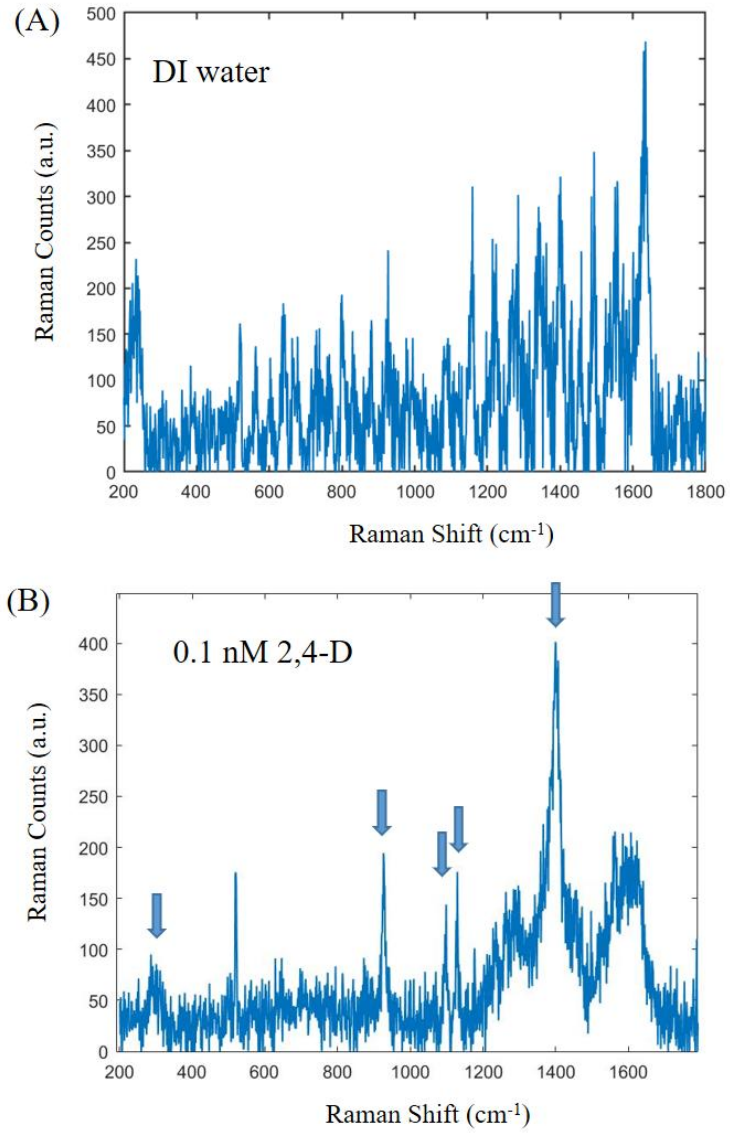

Figure 2.6: (A) Spectrum of deionized water as the reference (background corrected); (B) Spectrum of a 0.1 nM solution of 2,4-D on a S_4 SERS substrate.

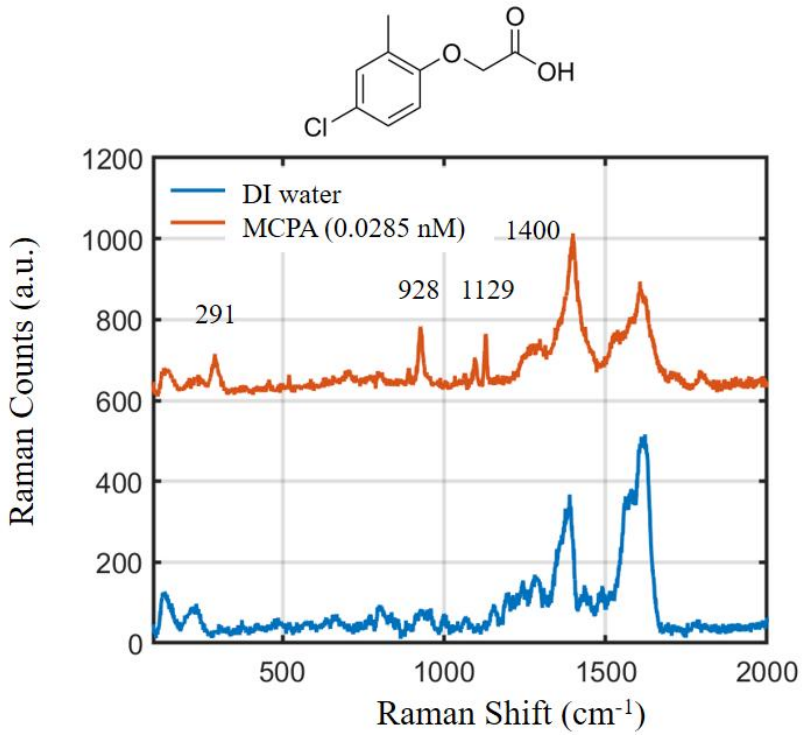

Figure 3.6: Raman spectra of Ag-CS substrate after application of DI water (bottom) and (top) after application of MCPA (0.0285 nM) solution.

P93 C2: "Figure 2.6 (A) shows the Raman spectra of DI water and a 0.1nM 2,4-D solution after baseline correction. There are no clear peak features in the DI water spectrum of the Ag-GA substrate. On the contrary, after the application of the 2,4-D solution on the Ag-GA substrate, the spectrum shown in Figure 2.6 (B) immediately appeared, and clear peaks at 293 cm^{-1}, ~900 cm^{-1}, ~1098 cm^{-1}, ~1129 cm^{-1}, and 1400 cm^{-1} can be observed. These peaks were not observed in DI water, suggesting that the signal was generated because of the 2,4-D analyte."

P181 C3: The Raman spectrum after application of DI water is also shown in Figure 3.6 for reference. For the spectrum acquired in MCPA solution, new peaks at ~291 cm^{-1} and sharp peaks around ~928 cm^{-1}, ~1129 cm^{-1} and 1400 cm^{-1} show up after the 2nd Raman measurement. In DI water, these peaks did not show, suggesting they were related to MCPA.

Aside from the point above, a time dependence was observed when analysing solution of different concentration. For example, under the same experimental conditions, it took 30 minutes to obtain the typical spectrum for a concentration of 0.001nM while the spectrum could be seen immediately when using a 0.1nM solution. No time dependence would be expected if the spectra were originating from a contaminant.

2, there is time dependence to get the signal when detecting 2,4-D in C2 table 3, P97.

"The difference in response time between lower and higher 2,4-D concentrations suggests that the observed peaks are indeed related to 2,4-D."

Table 3: Comparison of response time and detection ability of S_4 under the same experimental condition.

Structure 4	Detection of 0.001 nM 2,4-D in 30 minutes	detection of 0.1 nM immediately

The time to get readable Raman signal varies depended on the concentration, the Raman siganl was related to 2,4-D presence. If the signal is from container, no time dependence would be expected.

4, similiar to NIP or MIP SERS sensors, the spectra was not from the analytes themselves, but based on the interaction between the analytes and the polymer layer.

We acknowledge that the substrates can't distinguish 2,4-D or MCPA and is the shortcoming of this type of sensors.

P197, "Although some analytes such as MB or 4-ATP have their own characteristic peaks, there are other contaminants in the real world, resulting in the SERS signal originating from other chemicals. This sensor does not have selectivity. A possible way to overcomce this problem is to use MIP functional layers."

Other small corrections:

- There are numerous spelling and grammatical errors in the text. It should be spellchecked before final submission.

Spelling and grammar have been checked.